UNIVERSIDAD AUTÓNOMA METROPOLITANA
UNIDAD IZTAPALAPA
DEPARTAMENTO DE QUÍMICA

DQ.0215.2025

Julio 3, 2025

Dr. Román Linares Romero
Presidente del Consejo Divisional
de la División de Ciencias Básicas e Ingeniería
PRESENTE

A través de este medio le solicito incluir en el orden del día de la próxima sesión del Consejo Divisional, la discusión, y en su caso la aprobación, el informe de actividades del profesor visitante Dr. Ricardo Atahualpa Peralta Ávila comprendido entre el 03 de octubre de 2024 y el 02 de octubre de 2025.

De acuerdo al informe que entrega el Dr. Ricardo Atahualpa Peralta Ávila lo encuentro satisfactorio.

Agradezco su atención a la presente y le envío un cordial saludo.

Atentamente
Casa abierta al tiempo

[redacted]
Dr. Juan Marcos Esparza Schulz
Jefe del Departamento de Química

UNIDAD IZTAPALAPA
División de Ciencias Básicas e Ingeniería
Departamento de Química
Ave. Ferrocarril San Rafael Atlixco 186. Col. Leyes de Reforma 1A Sección. Iztapalapa C.P. 09310. CdMx, México.
Apartado Postal 55-534.

INFORME DE ACTIVIDADES 2024-2025

Profesor visitante: Dr. Ricardo A. Peralta Ávila

Periodo de informe: 10/Agosto/2024 – 19/Junio/2025

Institución receptora: Universidad Autónoma Metropolitana – Iztapalapa

Adscripción: Área de Catálisis, Departamento de Química, CBI



Dr. Ricardo A. Peralta Ávila

Ciudad de México, 19/Junio/2025

Contenido

Docencia....2
NIVEL: LICENCIATURA....2
NIVEL: POSGRADO....3
Formación de recursos humanos....4
DIRECCIÓN DE SERVICIO SOCIAL....4
ASESOR DE ESTUDIANTES DE POSGRADO....4
MIEMBRO DE COMITÉ TUTORIALES....4
Investigación....4
RESULTADOS DEL PROYECTO DE INVESTIGACIÓN....4
CONFERENCIAS IMPARTIDAS....6
Difusión de la ciencia....6
CONFERENCIAS IMPARTIDAS....6
ARTÍCULOS DE DIVULGACIÓN....6
PARTICIPACIONES EN ACTIVIDADES DE DIFUSIÓN....7
Gestión de recursos financieros....7
PROYECTOS FINANCIADOS....7
Otras actividades académicas....8

Durante el periodo que comprende el presente informe (10/Agosto/2024–19/Junio/2025) se realizaron actividades de docencia, formación de recursos humanos, investigación, divulgación, extensión, gestión de recursos financieros y otras actividades académicas, las cuales se describen de forma resumida en el siguiente informe de actividades.

Docencia

NIVEL: LICENCIATURA

UEA: Estructura de la materia para Tronco General (TG), División de Ciencias Básicas e Ingeniería, Universidad Autónoma Metropolitana-Iztapalapa (15/Julio/2024-04/Octubre/2024). 48 horas, 18 alumnos, *Trimestre* 24-P.

UEA: Estructura de la materia para Tronco General (TG), División de Ciencias Básicas e Ingeniería, Universidad Autónoma Metropolitana-Iztapalapa (21/Octubre/2024-24/Enero/2025). 48 horas, 41 alumnos, *Trimestre* 24-O.

UEA: Estructura de la materia para Tronco General (TG), División de Ciencias Básicas e Ingeniería, Universidad Autónoma Metropolitana-Iztapalapa (21/Octubre/2024-24/Enero/2025). 48 horas, 36 alumnos, *Trimestre* 24-O.

UEA: Proyecto terminal I-Fisicoquímica para Licenciatura en Química, División de Ciencias Básicas e Ingeniería, Universidad Autónoma Metropolitana-Iztapalapa (21/Octubre/2024-24/Enero/2025). 48 horas, 1 alumnos, *Trimestre* 24-O.

UEA: Química Inorgánica I para Licenciatura en Química, División de Ciencias Básicas e Ingeniería, Universidad Autónoma Metropolitana-Iztapalapa (10/Febrero/2025-09/Mayo/2025). 48 horas, 17 alumnos, *Trimestre* 25-I.

UEA: Química Inorgánica avanzada para Licenciatura en Química, División de Ciencias Básicas e Ingeniería, Universidad Autónoma Metropolitana-Iztapalapa (10/Febrero/2025-09/Mayo/2025). 48 horas, 7 alumnos, *Trimestre* 25-I.

UEA: Proyecto terminal I-Fisicoquímica para Licenciatura en Química, División de Ciencias Básicas e Ingeniería, Universidad Autónoma Metropolitana-Iztapalapa (10/Febrero/2025-09/Mayo/2025). 48 horas, 1 alumnos, *Trimestre* 25-I.

UEA: Proyecto terminal II-Fisicoquímica para Licenciatura en Química, División de Ciencias Básicas e Ingeniería, Universidad Autónoma Metropolitana-Iztapalapa (10/Febrero/2025-09/Mayo/2025). 48 horas, 1 alumnos, *Trimestre* 25-I.

NIVEL: POSGRADO

UEA: Química del Estado Sólido para Posgrado en Química, División de Ciencias Básicas e Ingeniería, Universidad Autónoma Metropolitana-Iztapalapa (15/Julio/2024-04/Octubre/2024). 48 horas, 2 alumnos, *Trimestre* 24-P.

UEA: Introducción a la investigación II para Posgrado en Química, División de Ciencias Básicas e Ingeniería, Universidad Autónoma Metropolitana-Iztapalapa (15/Julio/2024-04/Octubre/2024). 48 horas, 1 alumnos, *Trimestre* 24-P.

UEA: Química del Estado Sólido para Posgrado en Química, División de Ciencias Básicas e Ingeniería, Universidad Autónoma Metropolitana-Iztapalapa (21/Octubre/2024-24/Enero/2025). 48 horas, 2 alumnos, *Trimestre* 24-O.

UEA: Introducción a la investigación III para Posgrado en Química, División de Ciencias Básicas e Ingeniería, Universidad Autónoma Metropolitana-Iztapalapa (21/Octubre/2024-24/Enero/2025). 48 horas, 1 alumnos, *Trimestre* 24-O.

Formación de recursos humanos

DIRECCIÓN DE SERVICIO SOCIAL

Alumno: Christian Daniel Jiménez Zaragoza, (Licenciatura en Química, UAM-I): Síntesis de ligantes para sintetizar materiales porosos. (10 marzo del 2025 – 10 octubre del 2025)

ASESOR DE ESTUDIANTES DE POSGRADO

Director del alumno: Pablo Marín Rosas, (Doctorado en Ciencias Químicas, UAM-I): Grado: Doctorado. Síntesis de Redes Metal Orgánicas (MOF) y sus posibles aplicaciones.

Codirector del alumno: Jorge Daniel Ávila Monroy, (Doctorado en Ciencias Químicas, UAM-I): Grado: Doctorado. Comprensión del estudio de la interacción de iones metálicos en materiales de Azul de Prusia para aplicaciones de energía y remoción a través de XPS visto desde un enfoque sistémico.

MIEMBRO DE COMITÉ TUTORIALES

Alumno: Aguayo Tabares David,. Nacionalidad: mexicano. Grado: Maestría. Proyecto de tesis: ""Síntesis de pirrolo[3,4- b]piridin-5-onas vía Reacciones de Multicomponentes tipo Ugi-Zhu catalizadas con óxidos metálicos". UAM-Iztapalapa. (mayo/2025-continua)

Investigación

RESULTADOS DEL PROYECTO DE INVESTIGACIÓN

1) ***Metal–organic frameworks (MOFs) toward SO_2 detection***

Juan L Obeso, Catalina V Flores, **Ricardo A Peralta**, Margarita Viniegra, N Martín-Guaregua, Michael T Huxley, Diego Solis-Ibarra, Ilich A Ibarra, Christoph Janiak. *Chemical Society Reviews*, **2025**. DOI: 10.1039/D4CS00997E.

2) ***Achieving Sub-ppm Sensitivity in SO_2 Detection with a Chemically Stable Covalent Organic Framework***

Wei Zhao, Juan L. Obeso, Valeria B. López-Cervantes, Mounib Bahri, Elí Sánchez-González, Yoarhy A. Amador-Sánchez, Junyu Ren, Nigel D. Browning, **Ricardo A. Peralta**, Giovanni

Barcaro, Susanna Monti, Diego Solis-Ibarra, Ilich A. Ibarra, Dan Zhao, *Angew. Chem. Int. Ed*. **2024**. DOI: 10.1002/anie.202415088.

3) Record-Breaking H_2S Capture and ppm-level Sensing with a Chemically Stable Porous Organic Cage

Juan L. Obeso, Dingyue Hu, Valeria B. López-Cervantes, Catalina V. Flores, Enrique Lima, Aída Gutiérrez-Alejandre, Marco A. Vera, **Ricardo A. Peralta**, José Antonio de los Reyes, Diego Solis-Ibarra, Ilich A. Ibarra, Ming Liu. *Small*. **2024**. DOI: 10.1002/smll.202408155.

4) (Hf)Pcn-224(Co) as an Efficient Ppm-Level Sensor for Toxic SO_2

Sergio Carrasco, Marco L Martínez, Yoarhy A Amador-Sánchez, Valeria B López Cervantes, Elí Sánchez-González, Nora S Portillo-Vélez, **Ricardo A Peralta**, Ariel Guzmán-Vargas, Patricia Horcajada, Diego Solís-Ibarra, Ilich A Ibarra. *Materials Today*. **2025**. DOI: 10.1016/j.mtadv.2025.100579.

5) ***CO_2 Hydrogenation over Ni–Co/$Ce_{0.6}Zr_{0.4}O_2$ Catalysts for Light Hydrocarbons under Mild Conditions***

Víctor Martínez-Jiménez, J Gabriel Flores, Bettina Baumgartner, Juan L Obeso, Catalina V Flores, Bert M Weckhuysen, JR Rosas-Cedillo, Pablo Marín-Rosas, Raul Perez Hernandez, Aida Gutierrez-Alejandre, Eduardo González-Zamora, Ilich A Ibarra,* **Ricardo A Peralta,*** Jose Antonio de los Reyes*. *ACS Applied Engineering Materials*, **2025**. DOI: 10.1021/acsaenm.5c00055.

6) *Formation of polysulfides as a smart strategy to selectively detect H_2S in a Bi (III)-based MOF material*

Valeria B López-Cervantes, Juan L Obeso, J Gabriel Flores, Aida Gutierrez-Alejandre, Raul A Marquez, J de los Reyes, Catalina V Flores, NS Portillo-Vélez, Pablo Marín-Rosas, Christian A Celaya, Eduardo González-Zamora, Diego Solis-Ibarra,* **Ricardo A Peralta,*** Ilich A Ibarra*. *Chem. Sci.*, **2025**. DOI:10.1039/D4SC07144A.

7) ***Gas-flow activation of MOFs: unlocking efficient catalysis through dynamic bonding***

Mariana L. Díaz-Ramírez, Sun Ho Park, Marcos Rivera-Almazo, Erika Medel, **Ricardo A. Peralta**, Ilich A. Ibarra, Rubicelia Vargas, Jorge Garza, Nak Cheon Jeong, *Chem. Sci.*, **2025**. DOI: 10.1039/D4SC07011A.

8) *Benefits and Complexity of Defects in Metal-Organic Frameworks*

N. S. Portillo-Vélez, Juan L. Obeso, José Antonio de los Reyes, **Ricardo Peralta,*** Ilich A. Ibarra,* Michael T Huxley*. Commun. Mater. **2024.** DOI: 10.1038/s43246-024-00691-1.

9) UTSA-16(Zn) for SO_2 detection: elucidating the fluorescence mechanism

Valeria B. López-Cervantes, Marco L. Martínez, Juan L. Obeso, Celene García-Carvajal, Nora S. Portillo-Vélez, Ariel Guzmán-Vargas, **Ricardo A. Peralta,** Eduardo González-Zamora, Ilich A. Ibarra, Diego Solis-Ibarra, John Luke Woodliffe and Yoarhy A. Amador-Sánchez. *Dalton Transactions*, **2024**. DOI: 10.1039/D4DT02852J.

10) Effective BPA degradation from water: the integration of bimetallic UiO-66 Ce-Zr

Leidy Marcela Gallo, Juan L. Obeso, Nora S. Portillo-Vélez, Carlos E. Garduño-Albino, Catalina V. Flores, Leonardo Herrera-Zuñiga, Alejandro Islas-Jácome, **Ricardo A. Peralta,*** Carolina Leyva*. *RSC Advances*, **2024**. DOI: 10.1039/d4ra06460g.

11) ***Dual-state emission of pyrazolyl-pyrrolo [3, 4-b] pyridin-5-ones via excited-state intramolecular proton transfer (ESIPT): multicomponent synthesis and optical characterization***

Julio C Flores-Reyes, Yoarhy A Amador-Sánchez, Alejandro Valderrama-Celestino, Bertha D Barrios-Campos, **Ricardo A Peralta**, Michael T Huxley, Ilich A Ibarra, Alejandro Islas-Jácome, Diego Solis-Ibarra, Eduardo González-Zamora. *Organic Chemistry Frontiers,* **2025**. DOI: 10.1039/D4QO02256D.

12) Low-toxicity metal–organic frameworks: Sustainable solutions for versatile applications

Juan L Obeso, Catalina V Flores, Aldo G Gutiérrez, Carolina Leyva, Juan Carlos Valdivia-Corona, Leonardo D Herrera-Zúñiga, José Antonio de los Reyes, **Ricardo A Peralta,*** Ilich A Ibarra*. *Bulletin of the Korean Chemical Society,* **2025**. DOI: 10.1002/bkcs.70005.

13) The Use of Porous Materials in Heterogeneous Catalysis

Pablo Marín-Rosas, Nora S Portillo-Veléz, J Gabriel Flores, Eduardo González-Zamora, Alejandro Islas-Jácome, Leonardo D Herrera-Zúñiga, Ilich A Ibarra, Margarita Viniegra, N Martín-Guaregua,* **Ricardo A Peralta,*** Julia Aguilar-Pliego*. *Journal of the Mexican Chemical Society,* **2025**. DOI: 10.29356/jmcs.v69i1.2270.

CONFERENCIAS IMPARTIDAS

1) Ciclo de seminarios en Cinvestav-IPN. CDMX (México) 22 de agosto 2024. Oral presentation. “Heterogenización de complejos catalíticamente activos soportados en sólidos con alta área superficial”.

Difusión de la ciencia

CONFERENCIAS IMPARTIDAS

1) Participación en ponencia de divulgación en el evento encuentro de divulgación COLBACH plantel 11 – UAMI 2024. Presentación “La química del estado sólido ¿es útil?, 19 de noviembre del 2024.
2) Participación en ponencia de divulgación en el evento encuentro de divulgación COLBACH plantel 12 – UAMI 2025. Presentación “La química del estado sólido ¿es útil?, 22 de julio del 2025.

ARTÍCULOS DE DIVULGACIÓN

1) ***Contactos, Revista de Educación en Ciencias e Ingeniería, UAM-I,*** No. 136. "La química detrás de los MOFs" p.p. 69-76, **2024**.
2) ***Contactos, Revista de Educación en Ciencias e Ingeniería, UAM-I,*** No. 135. "Nanopartículas metálicas soportadas como catalizadores" p.p. 58-69, **2024**.

PARTICIPACIONES EN ACTIVIDADES DE DIFUSIÓN

1) Organizador en las actividades del "Instituto Carlos Graef 2024, Jóvenes hacia la Ciencia y la Ingeniería", 18 de mayo del 2024.
2) Editor en jefe del Podcast del Departamento de Química Q-UAM-I. (7 de junio del 2023 – Continua). Mis principales responsabilidades son:
   I. Promover el podcast
   II. Recibir los escritos de los posibles podcasts.
   III. Hacer una revisión para ver si es adecuado el contenido y el lenguaje usado.
   IV. Enviar a dos colegas que revisen el escrito.
   V. Generar una versión final de acuerdo a los comentarios de revisores y autores.
   VI. Grabar la lectura del texto.
   VII. Musicalizar la grabación.
   VIII. Publicarlo en anchor y de ahí se va a varias emisoras.

Gestión de recursos financieros

PROYECTOS FINANCIADOS

1) Convocatoria para la postulación de Proyectos de Investigación relacionados con Desafíos Actuales. Proyecto: "Bio-MOFs: Hacia la erradicación selectiva de contaminantes emergentes en aguas". Monto financiado: 500,000 MXN. Vigencia: 01 de mayo del 2024 – 30 de noviembre del 2025.
2) Convocatoria 2024 para presentar proyectos científicos, de desarrollo tecnológico e innovación y divulgación para la atención de problemas específicos de la Ciudad de México" Monto financiado: 930,646.06 MXN. Vigencia: 02 de septiembre del 2024 – 31 de enero del 2026.

Otras actividades académicas

1) Reconocimiento PRODEP a profesores de tiempo completo. Vigencia del reconocimiento es de 3 años 2025-2028.
2) Organizador en las actividades del “Instituto Carlos Graef 2025, Jóvenes hacia la Ciencia y la Ingeniería”. 08 de marzo 2025 – 05 de abril 2025.
3) Talleres colaborativos entre profesores del Colegio de Bachilleres y la UAM Iztapalapa”, con una duración de 30 horas, realizado los días 4, 6 y 7 de febrero de 2025 en la Casa de la Primera Imprenta de América.
4) Evaluador del Informe Técnico Etapa 2 de un proyecto, apoyado en el marco de la convocatoria Ciencia de Frontera 2023”. SECIHTI, México. 23 de mayo de 2025.
5) Tutor de 10 estudiantes de licenciatura por parte del a CODDAA del División de CBI.
6) Videos para ingreso al posgrado en el Departamento de Química en el tema de “Cinética Química”.
7) Evaluador de 15 artículos de investigación en revistas de Alto impacto como ”Applied Organometallic Chemistry”, entre otras.

DOCUMENTOS PROBATORIOS

3er año Profesor Visitante

Profesor visitante: Dr. Ricardo A. Peralta Ávila

Periodo de informe: 10/Agosto/2024 – 19/Junio/2025

Institución receptora: Universidad Autónoma Metropolitana – Iztapalapa

Adscripción: Área de Catálisis, Departamento de Química, CBI



Dr. Ricardo A. Peralta Ávila

Ciudad de México, 19/Junio/2025

1. Docencia

Casa abierta al tiempo
UNIVERSIDAD AUTÓNOMA METROPOLITANA
Unidad Iztapalapa

Fecha 25/11/2024
Folio 18523
Página 1

Constancia de Cursos Impartidos

Profesor: 45029 PERALTA AVILA RICARDO ATAHUALPA

No.	UEA	GRUPO	Insc.	NOMBRE	Cred.	H.T.	H.L	TRIM.
1	2141073	CF51	16	QUIMICA INORGANICA (ING.)	12	5.0	2.0	22O
2	2141091	CE51	11	QUIMICA INORGANICA I	7	3.0	1.0	23I
3	2141158	CK05	1	PROYECTO TERMINAL I QUIMICA ORGANICA	15	0.0	15.0	23I
4	2141092	CF01	20	QUIMICA INORGANICA II	7	3.0	1.0	23P
5	2141152	CK04	1	PROYECTO TERMINAL I FISICOQUIMICA	15	0.0	15.0	23P
6	2141159	CL05	1	PROYECTO TERMINAL II QUIMICA ORGANICA	15	0.0	15.0	23P
7	2141093	CG01	28	QUIMICA INORGANICA III	7	3.0	1.0	23O
8	2141094	CG01	8	LABORATORIO DE QUIMICA INORGANICA	5	0.0	5.0	24I
9	2141107	CM01	17	INTRODUCCION A LA CIENCIA DE LOS NANOMATERIALES	9	3.0	3.0	24I
10	2146039	CO13	2	QUIMICA DEL ESTADO SOLIDO	9	4.5	0.0	24I
11	2146069	CO13J	1	INTRODUCCION A LA INVESTIGACION I	20	0.0	0.0	24I
12	2140009	CB52	18	ESTRUCTURA DE LA MATERIA	9	3.0	3.0	24P
13	2146039	CQ13	4	QUIMICA DEL ESTADO SOLIDO	9	4.5	0.0	24P
14	2146070	CP13I	1	INTRODUCCION A LA INVESTIGACION II	20	0.0	0.0	24P

La información que aparece en este documento es copia fiel de la contenida en los archivos que obran en poder de la Coordinación de Sistemas Escolares.

Atentamente
Casa abierta al tiempo

[redacted]

LIC. MARTHA X. GONZÁLEZ GUERRERO
Coordinadora de Sistemas Escolares

Casa abierta al tiempo
UNIVERSIDAD AUTÓNOMA
METROPOLITANA
UNIDAD IZTAPALAPA
COORDINACIÓN DE SISTEMAS ESCOLARES

CamScanner

Instrumento de Opinión del alumnado
Trimestre: 22O

Nombre del profesor: RICARDO ATAHUALPA PERALTA AVILA

Clave UEA: 2141073 **UEA:** QUIMICA INORGANICA (ING.)

Alumnos inscritos: 16 **Alumnos que realizaron encuesta:** 3 **Nivel:** Licenciatura

Organización de la UEA

1. La o el profesor presentó y entregó el programa de la UEA en la primera semana de clase o antes.

No	0
Si	3

2. El programa incluyó: objetivos, contenidos temáticos, estrategias de enseñanza aprendizaje, bibliografía, otros apoyos didácticos, formas de evaluación y cronograma de actividades.

Totalmente en desacuerdo	0
En desacuerdo	0
De acuerdo	0
Totalmente de acuerdo	3
No aplica	0

3. El programa incluyó actividades realizadas en modalidad sincrónica (tiempo real) y asincrónica (sin interacción simultánea).

Totalmente en desacuerdo	0
En desacuerdo	0
De acuerdo	0
Totalmente de acuerdo	3

No aplica	0

4. Se acordaron normas, criterios de convivencia armónica y respetuosa, así como mecanismos de comunicación en el grupo.

Totalmente en desacuerdo	0
En desacuerdo	0
De acuerdo	1
Totalmente de acuerdo	2
No aplica	0

Práctica docente

5. En general, las actividades se han realizado conforme a lo programado.

Totalmente en desacuerdo	0
En desacuerdo	0
De acuerdo	0
Totalmente de acuerdo	3
No aplica	0

6. La o el profesor muestra conocimiento amplio sobre los temas del programa.

Totalmente en desacuerdo	0
En desacuerdo	0
De acuerdo	0
Totalmente de acuerdo	3
No aplica	0

7. Se favorece la participación individual y colectiva para el desarrollo de los conocimientos.

Totalmente en desacuerdo	0
En desacuerdo	0

De acuerdo	0
Totalmente de acuerdo	3
No aplica	0

8. Se favorece la participación individual y colectiva para el desarrollo de las habilidades (comunicación, uso de lenguaje, pensamiento crítico, resolución de problemas, trabajo en equipo).

Totalmente en desacuerdo	0
En desacuerdo	0
De acuerdo	0
Totalmente de acuerdo	3
No aplica	0

9. Se promueve tu aprendizaje autónomo con base en la implementación de actividades, recursos y apoyos didácticos.

Totalmente en desacuerdo	0
En desacuerdo	0
De acuerdo	0
Totalmente de acuerdo	3
No aplica	0

10. Las actividades prácticas se han realizado conforme a las necesidades de la UEA y contribuyen al logro de los aprendizajes y experiencias.

Totalmente en desacuerdo	0
En desacuerdo	0
De acuerdo	0
Totalmente de acuerdo	3
No aplica	0

11. Se resuelven las dudas con base en explicaciones compresibles y fortalecen los aprendizajes sobre los contenidos abordados.

Totalmente en desacuerdo	0
En desacuerdo	0

De acuerdo	0
Totalmente de acuerdo	3
No aplica	0

12. Se incentiva el desarrollo de prácticas de investigación para el fortalecimiento de los aprendizajes.

Totalmente en desacuerdo	0
En desacuerdo	0
De acuerdo	0
Totalmente de acuerdo	3
No aplica	0

13. Se impulsa la aplicación práctica y/o analítica de los conocimientos adquiridos.

Totalmente en desacuerdo	0
En desacuerdo	0
De acuerdo	0
Totalmente de acuerdo	3
No aplica	0

14. Se promueve un ambiente de respeto, confianza y colaboración.

Totalmente en desacuerdo	0
En desacuerdo	0
De acuerdo	0
Totalmente de acuerdo	3
No aplica	0

15. En general, todas las actividades se han realizado con pleno respeto a los derechos universitarios, como son, entre otros, la igualdad, diversidad y pluralidad de la comunidad universitaria en general, y del alumnado del grupo en particular.

Totalmente en desacuerdo	0
En desacuerdo	0

De acuerdo	0
Totalmente de acuerdo	3
No aplica	0

16. La o el profesor imparte asesorías cuando le son solicitadas.

Totalmente en desacuerdo	0
En desacuerdo	0
De acuerdo	0
Totalmente de acuerdo	3
No aplica	0

17. Los criterios y formas de evaluación establecidas en el programa se han respetado.

Totalmente en desacuerdo	0
En desacuerdo	0
De acuerdo	0
Totalmente de acuerdo	3
No aplica	0

18. Recibes retroalimentación de las modalidades de evaluación implementadas durante el curso.

Totalmente en desacuerdo	0
En desacuerdo	0
De acuerdo	0
Totalmente de acuerdo	3
No aplica	0

Autoevaluación

19. Me he presentado puntualmente a clases y he permanecido la duración total de las sesiones.

Totalmente en desacuerdo	0
En desacuerdo	0
De acuerdo	1
Totalmente de acuerdo	2
No aplica	0

20. He participado en clase expresando dudas, aportando ejemplos, respondiendo preguntas y trabajando en equipo.

Totalmente en desacuerdo	0
En desacuerdo	0
De acuerdo	0
Totalmente de acuerdo	3
No aplica	0

21. He cumplido con los requisitos y actividades académicas establecidas en el programa.

Totalmente en desacuerdo	0
En desacuerdo	0
De acuerdo	0
Totalmente de acuerdo	3
No aplica	0

22. Hasta el momento he logrado los aprendizajes esperados de acuerdo con los objetivos del programa.

Totalmente en desacuerdo	0
En desacuerdo	0
De acuerdo	0
Totalmente de acuerdo	3
No aplica	0

Evaluación global

23. Tomaría otro de los cursos que imparte la o el profesor.

Totalmente en desacuerdo	0
En desacuerdo	0
De acuerdo	0
Totalmente de acuerdo	3
No aplica	0

24. El profesor mostró especial interés en el desarrollo de la UEA.

Totalmente en desacuerdo	0
En desacuerdo	0
De acuerdo	0
Totalmente de acuerdo	3
No aplica	0

25. Con base en lo anterior, califica del 1 al 10 el desempeño del profesor en el trimestre: (donde 1 es nada satisfactorio y 10 es muy satisfactorio).

1	2	3	4	5	6	7	8	9	10
0	0	0	0	0	0	0	0	0	3

26. Comentarios y sugerencias a tu profesor

Comentarios
Excelentísimo trabajo
Tomaría clases de nuevo con él, es un gran profesor, a pesar de ser nuevo, mostró gran interés y disciplina en la forma de enseñarnos, no muchos profesores te dan retroalimentación, ya dan por hecho que sabes las cosas, pero este profe es otra cosa ya que si nos vuelve a explicar cosas pasadas y el ambiente en cuanto a la enseñanza es grato, más profesores como él, no lo dejen ir.

Instrumento de Opinión del alumnado
Trimestre: 24O

Nombre del profesor: RICARDO ATAHUALPA PERALTA AVILA

Clave UEA: 2141152 **UEA:** PROYECTO TERMINAL I FISICOQUIMICA

Alumnos inscritos: 1 **Alumnos que realizaron encuesta:** 1 **Nivel:** Licenciatura

Organización de la UEA

1. La o el profesor presentó y entregó el programa de la UEA en la primera semana de clase o antes.

No	0
Si	1

2. El programa incluyó: objetivos, contenidos temáticos, estrategias de enseñanza aprendizaje, bibliografía, otros apoyos didácticos, formas de evaluación y cronograma de actividades.

Totalmente en desacuerdo	0
En desacuerdo	0
De acuerdo	0
Totalmente de acuerdo	1
No aplica	0

3. El programa incluyó actividades realizadas en modalidad sincrónica (tiempo real) y asincrónica (sin interacción simultánea).

Totalmente en desacuerdo	0
En desacuerdo	0
De acuerdo	0
Totalmente de acuerdo	1

No aplica	0

4. Se acordaron normas, criterios de convivencia armónica y respetuosa, así como mecanismos de comunicación en el grupo.

Totalmente en desacuerdo	0
En desacuerdo	0
De acuerdo	0
Totalmente de acuerdo	1
No aplica	0

Práctica docente

5. En general, las actividades se han realizado conforme a lo programado.

Totalmente en desacuerdo	0
En desacuerdo	0
De acuerdo	1
Totalmente de acuerdo	0
No aplica	0

6. La o el profesor muestra conocimiento amplio sobre los temas del programa.

Totalmente en desacuerdo	0
En desacuerdo	0
De acuerdo	0
Totalmente de acuerdo	1
No aplica	0

7. Se favorece la participación individual y colectiva para el desarrollo de los conocimientos.

Totalmente en desacuerdo	0
En desacuerdo	0

De acuerdo	0
Totalmente de acuerdo	1
No aplica	0

8. Se favorece la participación individual y colectiva para el desarrollo de las habilidades (comunicación, uso de lenguaje, pensamiento crítico, resolución de problemas, trabajo en equipo).

Totalmente en desacuerdo	0
En desacuerdo	0
De acuerdo	0
Totalmente de acuerdo	1
No aplica	0

9. Se promueve tu aprendizaje autónomo con base en la implementación de actividades, recursos y apoyos didácticos.

Totalmente en desacuerdo	0
En desacuerdo	0
De acuerdo	0
Totalmente de acuerdo	1
No aplica	0

10. Las actividades prácticas se han realizado conforme a las necesidades de la UEA y contribuyen al logro de los aprendizajes y experiencias.

Totalmente en desacuerdo	0
En desacuerdo	0
De acuerdo	0
Totalmente de acuerdo	1
No aplica	0

11. Se resuelven las dudas con base en explicaciones compresibles y fortalecen los aprendizajes sobre los contenidos abordados.

Totalmente en desacuerdo	0
En desacuerdo	0

De acuerdo	0
Totalmente de acuerdo	1
No aplica	0

12. Se incentiva el desarrollo de prácticas de investigación para el fortalecimiento de los aprendizajes.

Totalmente en desacuerdo	0
En desacuerdo	0
De acuerdo	0
Totalmente de acuerdo	1
No aplica	0

13. Se impulsa la aplicación práctica y/o analítica de los conocimientos adquiridos.

Totalmente en desacuerdo	0
En desacuerdo	0
De acuerdo	0
Totalmente de acuerdo	1
No aplica	0

14. Se promueve un ambiente de respeto, confianza y colaboración.

Totalmente en desacuerdo	0
En desacuerdo	0
De acuerdo	0
Totalmente de acuerdo	1
No aplica	0

15. En general, todas las actividades se han realizado con pleno respeto a los derechos universitarios, como son, entre otros, la igualdad, diversidad y pluralidad de la comunidad universitaria en general, y del alumnado del grupo en particular.

Totalmente en desacuerdo	0
En desacuerdo	0

De acuerdo	0
Totalmente de acuerdo	1
No aplica	0

16. La o el profesor imparte asesorías cuando le son solicitadas.

Totalmente en desacuerdo	0
En desacuerdo	0
De acuerdo	0
Totalmente de acuerdo	1
No aplica	0

17. Los criterios y formas de evaluación establecidas en el programa se han respetado.

Totalmente en desacuerdo	0
En desacuerdo	0
De acuerdo	0
Totalmente de acuerdo	1
No aplica	0

18. Recibes retroalimentación de las modalidades de evaluación implementadas durante el curso.

Totalmente en desacuerdo	0
En desacuerdo	0
De acuerdo	0
Totalmente de acuerdo	1
No aplica	0

Autoevaluación

19. Me he presentado puntualmente a clases y he permanecido la duración total de las sesiones.

Totalmente en desacuerdo	0
En desacuerdo	0
De acuerdo	1
Totalmente de acuerdo	0
No aplica	0

20. He participado en clase expresando dudas, aportando ejemplos, respondiendo preguntas y trabajando en equipo.

Totalmente en desacuerdo	0
En desacuerdo	0
De acuerdo	0
Totalmente de acuerdo	1
No aplica	0

21. He cumplido con los requisitos y actividades académicas establecidas en el programa.

Totalmente en desacuerdo	0
En desacuerdo	0
De acuerdo	1
Totalmente de acuerdo	0
No aplica	0

22. Hasta el momento he logrado los aprendizajes esperados de acuerdo con los objetivos del programa.

Totalmente en desacuerdo	0
En desacuerdo	0
De acuerdo	1
Totalmente de acuerdo	0
No aplica	0

Evaluación global

23. Tomaría otro de los cursos que imparte la o el profesor.

Totalmente en desacuerdo	0
En desacuerdo	0
De acuerdo	0
Totalmente de acuerdo	1
No aplica	0

24. El profesor mostró especial interés en el desarrollo de la UEA.

Totalmente en desacuerdo	0
En desacuerdo	0
De acuerdo	0
Totalmente de acuerdo	0
No aplica	1

25. Con base en lo anterior, califica del 1 al 10 el desempeño del profesor en el trimestre: (donde 1 es nada satisfactorio y 10 es muy satisfactorio).

1	2	3	4	5	6	7	8	9	10
0	0	0	0	0	0	0	0	0	1

26. Comentarios y sugerencias a tu profesor

Comentarios

Instrumento de Opinión del alumnado
Trimestre: 24O

Nombre del profesor: RICARDO ATAHUALPA PERALTA AVILA

Clave UEA: 2146039 **UEA:** QUIMICA DEL ESTADO SOLIDO

Alumnos inscritos: 2 **Alumnos que realizaron encuesta:** 1 **Nivel:** Licenciatura

Organización de la UEA

1. La o el profesor presentó y entregó el programa de la UEA en la primera semana de clase o antes.

No	0
Si	1

2. El programa incluyó: objetivos, contenidos temáticos, estrategias de enseñanza aprendizaje, bibliografía, otros apoyos didácticos, formas de evaluación y cronograma de actividades.

Totalmente en desacuerdo	0
En desacuerdo	0
De acuerdo	0
Totalmente de acuerdo	1
No aplica	0

3. El programa incluyó actividades realizadas en modalidad sincrónica (tiempo real) y asincrónica (sin interacción simultánea).

Totalmente en desacuerdo	0
En desacuerdo	0
De acuerdo	0
Totalmente de acuerdo	1

No aplica	0

4. Se acordaron normas, criterios de convivencia armónica y respetuosa, así como mecanismos de comunicación en el grupo.

Totalmente en desacuerdo	0
En desacuerdo	0
De acuerdo	0
Totalmente de acuerdo	1
No aplica	0

Práctica docente

5. En general, las actividades se han realizado conforme a lo programado.

Totalmente en desacuerdo	0
En desacuerdo	0
De acuerdo	0
Totalmente de acuerdo	1
No aplica	0

6. La o el profesor muestra conocimiento amplio sobre los temas del programa.

Totalmente en desacuerdo	0
En desacuerdo	0
De acuerdo	0
Totalmente de acuerdo	1
No aplica	0

7. Se favorece la participación individual y colectiva para el desarrollo de los conocimientos.

Totalmente en desacuerdo	0
En desacuerdo	0

De acuerdo	0
Totalmente de acuerdo	1
No aplica	0

8. Se favorece la participación individual y colectiva para el desarrollo de las habilidades (comunicación, uso de lenguaje, pensamiento crítico, resolución de problemas, trabajo en equipo).

Totalmente en desacuerdo	0
En desacuerdo	0
De acuerdo	0
Totalmente de acuerdo	1
No aplica	0

9. Se promueve tu aprendizaje autónomo con base en la implementación de actividades, recursos y apoyos didácticos.

Totalmente en desacuerdo	0
En desacuerdo	0
De acuerdo	0
Totalmente de acuerdo	1
No aplica	0

10. Las actividades prácticas se han realizado conforme a las necesidades de la UEA y contribuyen al logro de los aprendizajes y experiencias.

Totalmente en desacuerdo	0
En desacuerdo	0
De acuerdo	0
Totalmente de acuerdo	1
No aplica	0

11. Se resuelven las dudas con base en explicaciones compresibles y fortalecen los aprendizajes sobre los contenidos abordados.

Totalmente en desacuerdo	0
En desacuerdo	0

De acuerdo	0
Totalmente de acuerdo	1
No aplica	0

12. Se incentiva el desarrollo de prácticas de investigación para el fortalecimiento de los aprendizajes.

Totalmente en desacuerdo	0
En desacuerdo	0
De acuerdo	0
Totalmente de acuerdo	1
No aplica	0

13. Se impulsa la aplicación práctica y/o analítica de los conocimientos adquiridos.

Totalmente en desacuerdo	0
En desacuerdo	0
De acuerdo	0
Totalmente de acuerdo	1
No aplica	0

14. Se promueve un ambiente de respeto, confianza y colaboración.

Totalmente en desacuerdo	0
En desacuerdo	0
De acuerdo	0
Totalmente de acuerdo	1
No aplica	0

15. En general, todas las actividades se han realizado con pleno respeto a los derechos universitarios, como son, entre otros, la igualdad, diversidad y pluralidad de la comunidad universitaria en general, y del alumnado del grupo en particular.

Totalmente en desacuerdo	0
En desacuerdo	0

De acuerdo	0
Totalmente de acuerdo	1
No aplica	0

16. La o el profesor imparte asesorías cuando le son solicitadas.

Totalmente en desacuerdo	0
En desacuerdo	0
De acuerdo	0
Totalmente de acuerdo	1
No aplica	0

17. Los criterios y formas de evaluación establecidas en el programa se han respetado.

Totalmente en desacuerdo	0
En desacuerdo	0
De acuerdo	0
Totalmente de acuerdo	1
No aplica	0

18. Recibes retroalimentación de las modalidades de evaluación implementadas durante el curso.

Totalmente en desacuerdo	0
En desacuerdo	0
De acuerdo	0
Totalmente de acuerdo	1
No aplica	0

Autoevaluación

19. Me he presentado puntualmente a clases y he permanecido la duración total de las sesiones.

Totalmente en desacuerdo	0
En desacuerdo	0
De acuerdo	1
Totalmente de acuerdo	0
No aplica	0

20. He participado en clase expresando dudas, aportando ejemplos, respondiendo preguntas y trabajando en equipo.

Totalmente en desacuerdo	0
En desacuerdo	0
De acuerdo	1
Totalmente de acuerdo	0
No aplica	0

21. He cumplido con los requisitos y actividades académicas establecidas en el programa.

Totalmente en desacuerdo	0
En desacuerdo	0
De acuerdo	1
Totalmente de acuerdo	0
No aplica	0

22. Hasta el momento he logrado los aprendizajes esperados de acuerdo con los objetivos del programa.

Totalmente en desacuerdo	0
En desacuerdo	0
De acuerdo	0
Totalmente de acuerdo	1
No aplica	0

Evaluación global

23. Tomaría otro de los cursos que imparte la o el profesor.

Totalmente en desacuerdo	0
En desacuerdo	0
De acuerdo	0
Totalmente de acuerdo	1
No aplica	0

24. El profesor mostró especial interés en el desarrollo de la UEA.

Totalmente en desacuerdo	0
En desacuerdo	0
De acuerdo	0
Totalmente de acuerdo	1
No aplica	0

25. Con base en lo anterior, califica del 1 al 10 el desempeño del profesor en el trimestre: (donde 1 es nada satisfactorio y 10 es muy satisfactorio).

1	2	3	4	5	6	7	8	9	10
0	0	0	0	0	0	0	0	0	1

26. Comentarios y sugerencias a tu profesor

Comentarios

Instrumento de Opinión del alumnado
Trimestre: 24O

Nombre del profesor: RICARDO ATAHUALPA PERALTA AVILA

Clave UEA: 2146071 **UEA:** INTRODUCCION A LA INVESTIGACION III

Alumnos inscritos: 1 **Alumnos que realizaron encuesta:** 1 **Nivel:** Licenciatura

Organización de la UEA

1. La o el profesor presentó y entregó el programa de la UEA en la primera semana de clase o antes.

No	0
Si	1

2. El programa incluyó: objetivos, contenidos temáticos, estrategias de enseñanza aprendizaje, bibliografía, otros apoyos didácticos, formas de evaluación y cronograma de actividades.

Totalmente en desacuerdo	0
En desacuerdo	0
De acuerdo	0
Totalmente de acuerdo	1
No aplica	0

3. El programa incluyó actividades realizadas en modalidad sincrónica (tiempo real) y asincrónica (sin interacción simultánea).

Totalmente en desacuerdo	0
En desacuerdo	0
De acuerdo	0
Totalmente de acuerdo	1

No aplica	0

4. Se acordaron normas, criterios de convivencia armónica y respetuosa, así como mecanismos de comunicación en el grupo.

Totalmente en desacuerdo	0
En desacuerdo	0
De acuerdo	0
Totalmente de acuerdo	1
No aplica	0

Práctica docente

5. En general, las actividades se han realizado conforme a lo programado.

Totalmente en desacuerdo	0
En desacuerdo	0
De acuerdo	0
Totalmente de acuerdo	1
No aplica	0

6. La o el profesor muestra conocimiento amplio sobre los temas del programa.

Totalmente en desacuerdo	0
En desacuerdo	0
De acuerdo	0
Totalmente de acuerdo	1
No aplica	0

7. Se favorece la participación individual y colectiva para el desarrollo de los conocimientos.

Totalmente en desacuerdo	0
En desacuerdo	0

De acuerdo	0
Totalmente de acuerdo	1
No aplica	0

8. Se favorece la participación individual y colectiva para el desarrollo de las habilidades (comunicación, uso de lenguaje, pensamiento crítico, resolución de problemas, trabajo en equipo).

Totalmente en desacuerdo	0
En desacuerdo	0
De acuerdo	0
Totalmente de acuerdo	1
No aplica	0

9. Se promueve tu aprendizaje autónomo con base en la implementación de actividades, recursos y apoyos didácticos.

Totalmente en desacuerdo	0
En desacuerdo	0
De acuerdo	0
Totalmente de acuerdo	1
No aplica	0

10. Las actividades prácticas se han realizado conforme a las necesidades de la UEA y contribuyen al logro de los aprendizajes y experiencias.

Totalmente en desacuerdo	0
En desacuerdo	0
De acuerdo	0
Totalmente de acuerdo	1
No aplica	0

11. Se resuelven las dudas con base en explicaciones compresibles y fortalecen los aprendizajes sobre los contenidos abordados.

Totalmente en desacuerdo	0
En desacuerdo	0

De acuerdo	0
Totalmente de acuerdo	1
No aplica	0

12. Se incentiva el desarrollo de prácticas de investigación para el fortalecimiento de los aprendizajes.

Totalmente en desacuerdo	0
En desacuerdo	0
De acuerdo	0
Totalmente de acuerdo	1
No aplica	0

13. Se impulsa la aplicación práctica y/o analítica de los conocimientos adquiridos.

Totalmente en desacuerdo	0
En desacuerdo	0
De acuerdo	0
Totalmente de acuerdo	1
No aplica	0

14. Se promueve un ambiente de respeto, confianza y colaboración.

Totalmente en desacuerdo	0
En desacuerdo	0
De acuerdo	0
Totalmente de acuerdo	1
No aplica	0

15. En general, todas las actividades se han realizado con pleno respeto a los derechos universitarios, como son, entre otros, la igualdad, diversidad y pluralidad de la comunidad universitaria en general, y del alumnado del grupo en particular.

Totalmente en desacuerdo	0
En desacuerdo	0

De acuerdo	0
Totalmente de acuerdo	1
No aplica	0

16. La o el profesor imparte asesorías cuando le son solicitadas.

Totalmente en desacuerdo	0
En desacuerdo	0
De acuerdo	0
Totalmente de acuerdo	1
No aplica	0

17. Los criterios y formas de evaluación establecidas en el programa se han respetado.

Totalmente en desacuerdo	0
En desacuerdo	0
De acuerdo	0
Totalmente de acuerdo	1
No aplica	0

18. Recibes retroalimentación de las modalidades de evaluación implementadas durante el curso.

Totalmente en desacuerdo	0
En desacuerdo	0
De acuerdo	0
Totalmente de acuerdo	1
No aplica	0

Autoevaluación

19. Me he presentado puntualmente a clases y he permanecido la duración total de las sesiones.

Totalmente en desacuerdo	0
En desacuerdo	0
De acuerdo	0
Totalmente de acuerdo	1
No aplica	0

20. He participado en clase expresando dudas, aportando ejemplos, respondiendo preguntas y trabajando en equipo.

Totalmente en desacuerdo	0
En desacuerdo	0
De acuerdo	0
Totalmente de acuerdo	1
No aplica	0

21. He cumplido con los requisitos y actividades académicas establecidas en el programa.

Totalmente en desacuerdo	0
En desacuerdo	0
De acuerdo	0
Totalmente de acuerdo	1
No aplica	0

22. Hasta el momento he logrado los aprendizajes esperados de acuerdo con los objetivos del programa.

Totalmente en desacuerdo	0
En desacuerdo	0
De acuerdo	0
Totalmente de acuerdo	1
No aplica	0

Evaluación global

23. Tomaría otro de los cursos que imparte la o el profesor.

Totalmente en desacuerdo	0
En desacuerdo	0
De acuerdo	0
Totalmente de acuerdo	1
No aplica	0

24. El profesor mostró especial interés en el desarrollo de la UEA.

Totalmente en desacuerdo	0
En desacuerdo	0
De acuerdo	0
Totalmente de acuerdo	1
No aplica	0

25. Con base en lo anterior, califica del 1 al 10 el desempeño del profesor en el trimestre: (donde 1 es nada satisfactorio y 10 es muy satisfactorio).

1	2	3	4	5	6	7	8	9	10
0	0	0	0	0	0	0	0	0	1

26. Comentarios y sugerencias a tu profesor

Comentarios
Un gran mentor para proyecto, ha estado pendiente de mi y mis avances diario. Me explica y da retroalimentaciones oportunas. La mejor eleccion para proyectos

Instrumento de Opinión del alumnado
Trimestre: 24O

Nombre del profesor: RICARDO ATAHUALPA PERALTA AVILA

Clave UEA: 2140009 **UEA:** ESTRUCTURA DE LA MATERIA

Alumnos inscritos: 36 **Alumnos que realizaron encuesta:** 9 **Nivel:** Licenciatura

Organización de la UEA

1. La o el profesor presentó y entregó el programa de la UEA en la primera semana de clase o antes.

No	0
Si	9

2. El programa incluyó: objetivos, contenidos temáticos, estrategias de enseñanza aprendizaje, bibliografía, otros apoyos didácticos, formas de evaluación y cronograma de actividades.

Totalmente en desacuerdo	0
En desacuerdo	0
De acuerdo	1
Totalmente de acuerdo	8
No aplica	0

3. El programa incluyó actividades realizadas en modalidad sincrónica (tiempo real) y asincrónica (sin interacción simultánea).

Totalmente en desacuerdo	0
En desacuerdo	0
De acuerdo	2
Totalmente de acuerdo	6

No aplica	1

4. Se acordaron normas, criterios de convivencia armónica y respetuosa, así como mecanismos de comunicación en el grupo.

Totalmente en desacuerdo	0
En desacuerdo	0
De acuerdo	3
Totalmente de acuerdo	6
No aplica	0

Práctica docente

5. En general, las actividades se han realizado conforme a lo programado.

Totalmente en desacuerdo	0
En desacuerdo	0
De acuerdo	1
Totalmente de acuerdo	8
No aplica	0

6. La o el profesor muestra conocimiento amplio sobre los temas del programa.

Totalmente en desacuerdo	0
En desacuerdo	0
De acuerdo	3
Totalmente de acuerdo	6
No aplica	0

7. Se favorece la participación individual y colectiva para el desarrollo de los conocimientos.

Totalmente en desacuerdo	0
En desacuerdo	0

De acuerdo	2
Totalmente de acuerdo	7
No aplica	0

8. Se favorece la participación individual y colectiva para el desarrollo de las habilidades (comunicación, uso de lenguaje, pensamiento crítico, resolución de problemas, trabajo en equipo).

Totalmente en desacuerdo	0
En desacuerdo	1
De acuerdo	1
Totalmente de acuerdo	7
No aplica	0

9. Se promueve tu aprendizaje autónomo con base en la implementación de actividades, recursos y apoyos didácticos.

Totalmente en desacuerdo	0
En desacuerdo	0
De acuerdo	1
Totalmente de acuerdo	8
No aplica	0

10. Las actividades prácticas se han realizado conforme a las necesidades de la UEA y contribuyen al logro de los aprendizajes y experiencias.

Totalmente en desacuerdo	0
En desacuerdo	0
De acuerdo	2
Totalmente de acuerdo	7
No aplica	0

11. Se resuelven las dudas con base en explicaciones compresibles y fortalecen los aprendizajes sobre los contenidos abordados.

Totalmente en desacuerdo	0
En desacuerdo	0

De acuerdo	3
Totalmente de acuerdo	6
No aplica	0

12. Se incentiva el desarrollo de prácticas de investigación para el fortalecimiento de los aprendizajes.

Totalmente en desacuerdo	0
En desacuerdo	0
De acuerdo	3
Totalmente de acuerdo	5
No aplica	1

13. Se impulsa la aplicación práctica y/o analítica de los conocimientos adquiridos.

Totalmente en desacuerdo	0
En desacuerdo	0
De acuerdo	1
Totalmente de acuerdo	7
No aplica	1

14. Se promueve un ambiente de respeto, confianza y colaboración.

Totalmente en desacuerdo	0
En desacuerdo	0
De acuerdo	2
Totalmente de acuerdo	7
No aplica	0

15. En general, todas las actividades se han realizado con pleno respeto a los derechos universitarios, como son, entre otros, la igualdad, diversidad y pluralidad de la comunidad universitaria en general, y del alumnado del grupo en particular.

Totalmente en desacuerdo	0
En desacuerdo	0

De acuerdo	3
Totalmente de acuerdo	6
No aplica	0

16. La o el profesor imparte asesorías cuando le son solicitadas.

Totalmente en desacuerdo	0
En desacuerdo	0
De acuerdo	4
Totalmente de acuerdo	5
No aplica	0

17. Los criterios y formas de evaluación establecidas en el programa se han respetado.

Totalmente en desacuerdo	0
En desacuerdo	0
De acuerdo	3
Totalmente de acuerdo	6
No aplica	0

18. Recibes retroalimentación de las modalidades de evaluación implementadas durante el curso.

Totalmente en desacuerdo	0
En desacuerdo	0
De acuerdo	3
Totalmente de acuerdo	6
No aplica	0

Autoevaluación

19. Me he presentado puntualmente a clases y he permanecido la duración total de las sesiones.

Totalmente en desacuerdo	0
En desacuerdo	0
De acuerdo	3
Totalmente de acuerdo	6
No aplica	0

20. He participado en clase expresando dudas, aportando ejemplos, respondiendo preguntas y trabajando en equipo.

Totalmente en desacuerdo	0
En desacuerdo	1
De acuerdo	3
Totalmente de acuerdo	4
No aplica	1

21. He cumplido con los requisitos y actividades académicas establecidas en el programa.

Totalmente en desacuerdo	0
En desacuerdo	0
De acuerdo	3
Totalmente de acuerdo	6
No aplica	0

22. Hasta el momento he logrado los aprendizajes esperados de acuerdo con los objetivos del programa.

Totalmente en desacuerdo	0
En desacuerdo	1
De acuerdo	4
Totalmente de acuerdo	4
No aplica	0

Evaluación global

23. Tomaría otro de los cursos que imparte la o el profesor.

Totalmente en desacuerdo	1
En desacuerdo	1
De acuerdo	1
Totalmente de acuerdo	6
No aplica	0

24. El profesor mostró especial interés en el desarrollo de la UEA.

Totalmente en desacuerdo	0
En desacuerdo	0
De acuerdo	3
Totalmente de acuerdo	6
No aplica	0

25. Con base en lo anterior, califica del 1 al 10 el desempeño del profesor en el trimestre: (donde 1 es nada satisfactorio y 10 es muy satisfactorio).

1	2	3	4	5	6	7	8	9	10
0	0	0	0	0	1	1	4	0	3

26. Comentarios y sugerencias a tu profesor

Comentarios
Es un gran profesor, sin embargo su forma de evaluar es un poco estricta y puede generar desconfianza a uno mismo, aunque es de aceptar que es mejor a comparación de otros casos abusivos que he tenido. Por otro lado, se entienden los temas a la perfección y me agrada que de apoyo con ejercicios y muestre interés en el aprendizaje de los alumnos por lo que su forma de evaluar se justifica, aunque no estaría mal hacer un leve ajuste para dar más seguridad al conocimiento de los alumnos.
buen profe no me gusta que use diapositivas pero al menos si las explica y no solo las lee, ademas debe fuera de eso deben quitar lo del examen departamental es basura no sirve y se pierden clases por ese chistecito mejor dejen que los profes hagan sus exámenes son mas capaces de hacer un mejor examen que todo el consejo junto, incluso si un profe e del consejo el sólito haria un mejor examen que todos juntos

Comentarios
Es buen maestro, aveces me gustaría que vaya un poco mas lento pero entiendo que en trimestres es difícil
Pues realmente me desagrada que estructura este seriada con electrónica y no sea magnetismo,siendo que tiene más relacion directa con la electrónica .En relación al profesor no tengo nada que decirEs bueno sin embargo las formas de evaluación no me agradan Porque si no eres bueno en química o no vas a estudiar química ,o peor aún si no eres de cbi. la forma de evaluación se vuelve tediosa y estresante Me gustaría que evaluarán sin tener que aprobar dos departamentales o un global .Y quiénes si estudien química pues se profundice totalmente Siento que los planes de estudio tienen muchas materias de relleno
Es un buen profesor, que explica muy bien las dudas que uno tiene y lleva un ritmo adecuado para comprender el tema

Instrumento de Opinión del alumnado
Trimestre: 24P

Nombre del profesor: RICARDO ATAHUALPA PERALTA AVILA

Clave UEA: 2140009 **UEA:** ESTRUCTURA DE LA MATERIA

Alumnos inscritos: 18 **Alumnos que realizaron encuesta:** 12 **Nivel:** Licenciatura

Organización de la UEA

1. La o el profesor presentó y entregó el programa de la UEA en la primera semana de clase o antes.

No	0
Si	12

2. El programa incluyó: objetivos, contenidos temáticos, estrategias de enseñanza aprendizaje, bibliografía, otros apoyos didácticos, formas de evaluación y cronograma de actividades.

Totalmente en desacuerdo	2
En desacuerdo	0
De acuerdo	4
Totalmente de acuerdo	6
No aplica	0

3. El programa incluyó actividades realizadas en modalidad sincrónica (tiempo real) y asincrónica (sin interacción simultánea).

Totalmente en desacuerdo	0
En desacuerdo	0
De acuerdo	4
Totalmente de acuerdo	6

No aplica	2

4. Se acordaron normas, criterios de convivencia armónica y respetuosa, así como mecanismos de comunicación en el grupo.

Totalmente en desacuerdo	2
En desacuerdo	0
De acuerdo	4
Totalmente de acuerdo	6
No aplica	0

Práctica docente

5. En general, las actividades se han realizado conforme a lo programado.

Totalmente en desacuerdo	2
En desacuerdo	0
De acuerdo	4
Totalmente de acuerdo	6
No aplica	0

6. La o el profesor muestra conocimiento amplio sobre los temas del programa.

Totalmente en desacuerdo	2
En desacuerdo	0
De acuerdo	2
Totalmente de acuerdo	8
No aplica	0

7. Se favorece la participación individual y colectiva para el desarrollo de los conocimientos.

Totalmente en desacuerdo	2
En desacuerdo	0

De acuerdo	8
Totalmente de acuerdo	2
No aplica	0

8. Se favorece la participación individual y colectiva para el desarrollo de las habilidades (comunicación, uso de lenguaje, pensamiento crítico, resolución de problemas, trabajo en equipo).

Totalmente en desacuerdo	2
En desacuerdo	0
De acuerdo	4
Totalmente de acuerdo	6
No aplica	0

9. Se promueve tu aprendizaje autónomo con base en la implementación de actividades, recursos y apoyos didácticos.

Totalmente en desacuerdo	2
En desacuerdo	0
De acuerdo	4
Totalmente de acuerdo	6
No aplica	0

10. Las actividades prácticas se han realizado conforme a las necesidades de la UEA y contribuyen al logro de los aprendizajes y experiencias.

Totalmente en desacuerdo	2
En desacuerdo	0
De acuerdo	4
Totalmente de acuerdo	6
No aplica	0

11. Se resuelven las dudas con base en explicaciones compresibles y fortalecen los aprendizajes sobre los contenidos abordados.

Totalmente en desacuerdo	2
En desacuerdo	0

De acuerdo	2
Totalmente de acuerdo	8
No aplica	0

12. Se incentiva el desarrollo de prácticas de investigación para el fortalecimiento de los aprendizajes.

Totalmente en desacuerdo	2
En desacuerdo	0
De acuerdo	4
Totalmente de acuerdo	4
No aplica	2

13. Se impulsa la aplicación práctica y/o analítica de los conocimientos adquiridos.

Totalmente en desacuerdo	2
En desacuerdo	0
De acuerdo	4
Totalmente de acuerdo	6
No aplica	0

14. Se promueve un ambiente de respeto, confianza y colaboración.

Totalmente en desacuerdo	2
En desacuerdo	0
De acuerdo	2
Totalmente de acuerdo	8
No aplica	0

15. En general, todas las actividades se han realizado con pleno respeto a los derechos universitarios, como son, entre otros, la igualdad, diversidad y pluralidad de la comunidad universitaria en general, y del alumnado del grupo en particular.

Totalmente en desacuerdo	2
En desacuerdo	0

De acuerdo	4
Totalmente de acuerdo	6
No aplica	0

16. La o el profesor imparte asesorías cuando le son solicitadas.

Totalmente en desacuerdo	2
En desacuerdo	0
De acuerdo	4
Totalmente de acuerdo	6
No aplica	0

17. Los criterios y formas de evaluación establecidas en el programa se han respetado.

Totalmente en desacuerdo	2
En desacuerdo	0
De acuerdo	4
Totalmente de acuerdo	6
No aplica	0

18. Recibes retroalimentación de las modalidades de evaluación implementadas durante el curso.

Totalmente en desacuerdo	2
En desacuerdo	0
De acuerdo	4
Totalmente de acuerdo	6
No aplica	0

Autoevaluación

19. Me he presentado puntualmente a clases y he permanecido la duración total de las sesiones.

Totalmente en desacuerdo	2
En desacuerdo	2
De acuerdo	4
Totalmente de acuerdo	4
No aplica	0

20. He participado en clase expresando dudas, aportando ejemplos, respondiendo preguntas y trabajando en equipo.

Totalmente en desacuerdo	2
En desacuerdo	0
De acuerdo	4
Totalmente de acuerdo	4
No aplica	2

21. He cumplido con los requisitos y actividades académicas establecidas en el programa.

Totalmente en desacuerdo	2
En desacuerdo	4
De acuerdo	2
Totalmente de acuerdo	4
No aplica	0

22. Hasta el momento he logrado los aprendizajes esperados de acuerdo con los objetivos del programa.

Totalmente en desacuerdo	2
En desacuerdo	0
De acuerdo	4
Totalmente de acuerdo	6
No aplica	0

Evaluación global

23. Tomaría otro de los cursos que imparte la o el profesor.

Totalmente en desacuerdo	2
En desacuerdo	0
De acuerdo	2
Totalmente de acuerdo	8
No aplica	0

24. El profesor mostró especial interés en el desarrollo de la UEA.

Totalmente en desacuerdo	2
En desacuerdo	0
De acuerdo	4
Totalmente de acuerdo	4
No aplica	2

25. Con base en lo anterior, califica del 1 al 10 el desempeño del profesor en el trimestre: (donde 1 es nada satisfactorio y 10 es muy satisfactorio).

1	2	3	4	5	6	7	8	9	10
0	0	0	0	0	0	0	2	8	2

26. Comentarios y sugerencias a tu profesor

Comentarios
Un excelente profesor, es muy bueno resolviendo dudas y en el manejo de la información
Muy satisfecho con su clase. Mi favorita del trimestre. Aprendí mucho y me gustó la forma en la que distribuye conocimiento. Demuestra demasiado conocimiento y es muy bueno. No hace ver menos a nadie y nos trata como sus iguales.
Retroalimentar un poco más al grupo con los temas antes de una evaluación departamental, en este caso aplicar más ejercicios, pero fuera de todo bastante claro.
Un excelente profesor, es muy bueno resolviendo dudas y en el manejo de la información

Comentarios
Muy satisfecho con su clase. Mi favorita del trimestre. Aprendí mucho y me gustó la forma en la que distribuye conocimiento. Demuestra demasiado conocimiento y es muy bueno. No hace ver menos a nadie y nos trata como sus iguales.
Retroalimentar un poco más al grupo con los temas antes de una evaluación departamental, en este caso aplicar más ejercicios, pero fuera de todo bastante claro.

UNIVERSIDAD AUTÓNOMA METROPOLITANA
Casa abierta al tiempo
Unidad Iztapalapa

Ciencias Básicas e Ingeniería CBI

FORMATO DE INICIO Y REGISTRO DE SERVICIO SOCIAL

TRIMESTRE LECTIVO 25-I

FECHA 17 03 2025
DÍA / MES / AÑO

DATOS DEL ALUMNO

NOMBRE COMPLETO: Christian Daniel Jiménez Zaragoza MATRÍCULA: 221300114

LICENCIATURA: Química

DOMICILIO: Sor Juana Inés de la Cruz 105 3ra manzana, Tepetitlán, Hgo.

TELÉFONO: 7731211144 CORREO ELECTRÓNICO: daniel23zaragoza24@gmail.com

DATOS DEL SERVICIO SOCIAL

TIPO DE SERVICIO SOCIAL ☑ INTERNO ☐ EXTERNO

NOMBRE DEL PROYECTO: " Síntesis de ligantes para sintetizar materiales porosos"

ASESOR RESPONSABLE: Ricardo Atahualpa Peralta Ávila no. económico 45029
*proyecto interno

CARGO: Profesor visitante TELÉFONO: 1050481888

CORREO ELECTRÓNICO: rperalta@izt.uam.mx

LUGAR DE REALIZACIÓN: (Dependencia): Laboratorio R201, R212, Departamento de Química, UAM Iztapalapa

DOMICILIO: Av. Ferrocarril San Rafael Atlixco, Núm. 186, Col. Leyes de Reforma 1 A Sección, Alcaldía Iztapalapa, C.

FECHA DE INICIO: 24/03/2025 FECHA DE TERMINACIÓN: 24/10/2025

[redacted]
FIRMA DEL ALUMNO

[redacted]
FIRMA DEL ASESOR

FIRMA DEL COORDINADOR DE LICENCIATURA

FIRMA DE APROBACIÓN

Lic. Luis Fernando Castro Careaga
Secretario Académico de la División de Ciencias Básicas e Ingeniería, UAM-I
P R E SE N T E

Asunto: Carta de aceptación para realizar servicio social

Estimado Lic. Castro, por este conducto le informo que acepto al estudiante de la Licenciatura en Química **Christian Daniel Jimenez Zaragoza** con matrícula **2213008114** para que realice el **Servicio Social** bajo mi asesoría en el laboratorio R-201 del área de Química Inorgánica del Departamento de Química de la División de Ciencias Básicas e Ingeniería de la Universidad Autónoma Metropolitana Unidad Iztapalapa.

El proyecto lleva por título **"Síntesis de ligantes para sintetizar materiales porosos"** y está planeado a realizarse del **24 de marzo de 2025** al **24 octubre de 2025.**

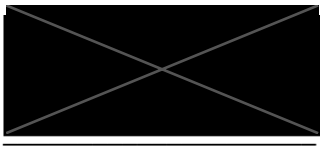
Las actividades para realizar involucran la Síntesis y optimización para la síntesis de materiales porosos, para su posterior uso en catálisis o adsorción. Es importante mencionar que el laboratorio en que se realiza la parte experimental del Servicio Social cuenta con los reactivos, espacio e instrumental necesario para el desarrollo del proyecto y su terminación en tiempo y forma. Además, cabe resaltar que se cuenta con el equipo necesario para la caracterización del material sintetizado (Espectrómetros de RMN, FTIR, Difracción de polvos, Equipos de adsorción).

Para cualquier información adicional y/o aclaración, por favor no dude en contactarme vía email (rperalta@izt.uam.mx)

Agradeciendo de antemano la atención prestada a este documento, aprovecho para enviarle cordiales saludos.

A t e n t a m e n t e

"Casa abierta al tiempo"



Dr. Ricardo Atahualpa Peralta Ávila

ASESOR

Laboratorio R-212 Área de Catálisis, Departamento de Química, División de Ciencias Básicas e Ingeniería. Universidad Autónoma Metropolitana – Iztapalapa. San Rafael Atlíxco 186, Col. Vicentina, Del. Iztapalapa, CP 09340, CDMX. Tel. (+52) 55-5804-4913

Casa abierta al tiempo

Constancia No. 1

CONSTANCIA DE CREDITOS

A quien corresponda:

La Universidad Autónoma Metropolitana, Unidad IZTAPALAPA, hace constar que para concluir el plan de estudios de **LICENCIATURA EN QUIMICA** de la División de CIENCIAS BASICAS E INGENIERIA, con área de concentración en **********, es requisito cubrir 467 (cuatrocientos sesenta y siete) créditos.

El alumno **JIMENEZ ZARAGOZA CHRISTIAN DANIEL** con matrícula **2213008114** se encuentra cursando la Licenciatura antes indicada y tiene 377 (trescientos setenta y siete) créditos contabilizados a la fecha.

Los créditos contabilizados corresponden al 80.72% (ochenta punto setenta y dos por ciento) de los créditos totales de la Licenciatura.

A petición y para los fines que estime conveniente, se extiende la presente en a los cinco días del mes de marzo del año dos mil veinticinco.

Atentamente
Casa abierta al tiempo

[redacted]

LIC. JUAN ROGELIO HERN NDEZ ORTEGA
Jefe de la Sección de Registro Académico

Casa abierta al tiempo
UNIVERSIDAD AUTÓNOMA
METROPOLITANA
UNIDAD IZTAPALAPA
COORDINACIÓN DE SISTEMAS ESCOLARES

Síntesis de ligantes para sintetizar materiales porosos

Reporte inicial

Christian Daniel Jiménez Zaragoza
2213008114
Licenciatura en Química

Justificación

El proyecto “Síntesis de ligantes para sintetizar materiales porosos” se justifica por la creciente necesidad de desarrollar materiales innovadores con aplicaciones en áreas estratégicas como la catálisis, el almacenamiento de gases, la separación de moléculas y la liberación controlada de fármacos. Los materiales porosos, debido a su alta superficie específica y versatilidad estructural, han demostrado ser fundamentales en el avance de la ciencia de materiales y la química aplicada. Sin embargo, la síntesis de estos materiales requiere de ligantes específicos que permitan controlar su porosidad, estabilidad y funcionalidad.

Este proyecto busca contribuir al conocimiento científico en este campo, proporcionando herramientas químicas para la creación de nuevos materiales con propiedades mejoradas. Además, representa una oportunidad para que el estudiante aplique los conocimientos teóricos adquiridos en su formación universitaria, desarrolle habilidades prácticas en el laboratorio y se involucre en investigación de vanguardia, lo que fortalecerá su perfil académico y profesional.

Objetivos

- Sintetizar y caracterizar ligantes orgánicos que permitan la obtención de materiales porosos con propiedades específicas para su aplicación en áreas como la catálisis y el almacenamiento de gases.
- Diseñar y optimizar rutas sintéticas para la obtención de ligantes con funcionalidades específicas.
- Caracterizar los ligantes sintetizados mediante técnicas analíticas como espectroscopía de infrarrojo (IR), resonancia magnética nuclear (RMN) y espectrometría de masas (MS).
- Evaluar la eficiencia de los ligantes en la formación de materiales porosos mediante técnicas de difracción de rayos X y análisis de superficie (BET).
- Analizar las propiedades fisicoquímicas de los materiales obtenidos y su potencial aplicación en procesos de interés industrial o ambiental.

Lugar de realización:

Laboratorio R-212 y R-201 Área de Catálisis, Departamento de Química, División de Ciencias Básicas e Ingeniería. Universidad Autónoma Metropolitana – Iztapalapa. Av. Ferrocarril San Rafael Atlixco, Núm. 186, Col. Leyes de Reforma 1 A Sección, Alcaldía Iztapalapa, C.P. 09310, Ciudad de México.

Duración y etapas

Se realizará del 24 de marzo de 2025 al 24 de octubre de 2025. Las etapas por ligante comprenden investigación, planeación, síntesis, purificación, caracterización, aplicación y observación de los resultados.

Licenciaturas que comprende
Licenciatura en Química
Participantes
Christian Daniel Jiménez Zaragoza
Asesor responsable
Ricardo A. Peralta Ávila, profesor visitante, área de catálisis, rperalta@izt.uam.mx
Tiempo de dedicación
5 horas diarias
Criterios de evaluación
Para garantizar que el proyecto se desarrolle de manera efectiva y que se cumplan los objetivos planteados, se establecerán los siguientes criterios de evaluación:

a) **Desempeño en el Laboratorio:**

- Habilidad para seguir protocolos de seguridad y manejar equipos y reactivos de manera adecuada.
- Capacidad para realizar las síntesis de ligantes de manera eficiente y reproducible.
- Organización y limpieza en el área de trabajo.

b) **Calidad de los Resultados:**

- Pureza y rendimiento de los ligantes sintetizados, verificados mediante técnicas analíticas (IR, RMN, MS).
- Caracterización exitosa de los materiales porosos obtenidos (porosidad, superficie específica, estabilidad térmica, etc.).
- Cumplimiento de los parámetros establecidos en el diseño experimental.

c) **Análisis y Interpretación de Datos:**

- Capacidad para analizar e interpretar los resultados obtenidos mediante técnicas analíticas.
- Uso adecuado de software y herramientas para el procesamiento de datos (espectros, difracción de rayos X, etc.).
- Conclusiones claras y fundamentadas a partir de los resultados experimentales.

d) **Cumplimiento de Plazos:**

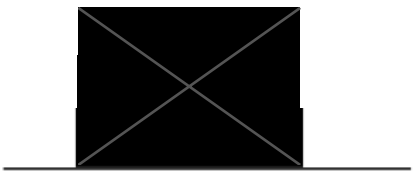
- Entrega oportuna de avances y reportes parciales del proyecto.
- Conclusión del proyecto dentro del tiempo establecido.

e) **Participación y Colaboración:**

- Actitud proactiva y colaborativa en el equipo de trabajo.
- Asistencia puntual y participación activa en reuniones y discusiones del proyecto.



FIRMA DEL ALUMNO



FIRMA DEL ASESOR

FIRMA DEL COORDINADOR
DE LICENCIATURA

Casa abierta al tiempo

UNIVERSIDAD AUTÓNOMA METROPOLITANA
Unidad-Iztapalapa

CBI.AP.268. 2025
Ciudad de México a 26 de marzo de 2025

Dr. Ricardo Atahualpa Peralta Ávila
Departamento de Química
UAM - Iztapalapa

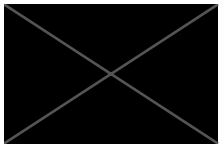
P r e s e n t e

Estimado Dr. Peralta:

La Comisión de Posgrado en Química le agradece su participación como director, en la modalidad de coasesoría, de la tesis de Maestría **"Síntesis de pirrolo [3,4-b] piridin-5-onas vía la reacción Ugi-Zhu catalizada por SU-101",** que defendió el **Lic. Pablo Marín Rosas** (CVU # 1277642) en el examen de grado sustentado el día 26 de marzo de 2025.

Sin otro particular y agradeciendo sus atenciones, quedo de usted.

A t e n t a m e n t e
Casa abierta al tiempo



Dr. Francisco Javier Tzompantzi Morales
Coordinador del Posgrado en Química

División de Ciencias Básicas e Ingeniería
Av. Ferrocarril San Rafael Atlixco No. 186, Col. Leyes de Reforma 1ª. Sección,
Alcaldía Iztapalapa, 09310 Ciudad de México
Tel. 55 5804 4600 ext. 4669, E-mail: pquim@xanum.uam.mx

8:27

Por tal motivo dicha comisión les proporciona la:

LISTA DE ACEPTADOS AL DOCTORADO EN INGENIERIA DE SISTEMAS CON SUS RESPECTIVOS ASESORES ACADÉMICOS.

No.	Aspirante ACEPTADO PERIODO B-2025	Maestría realizada	ASESOR ACADÉMICO
1	**ÁVILA MONROY JORGE DANIEL**	MAESTRÍA EN TECNOLOGÍA AVANZADA CICATA-IPN	**DR. MIGUEL ANGEL MARTÍNEZ CRUZ** DR. RICARDO ATAHUALPA PERALTA AVILA
2	**RASGADO ROMERO ANA MARIA**	MAESTRÍA EN INGENIERÍA ESTRUCTURAL UAM-AZCAPOTZALCO	**DRA. CLAUDIA HERNÁNDEZ AGUILAR** DRA. JUANA ISABEL MÉNDEZ GARDUÑO
3	**CORTÉS LAGUNA CARLA JESSICA**	MAESTRÍA EN TECNOLOGÍA DE COMPUTO UPICSA-IPN	**DR. JUAN BORY REYES** DR. VICTOR MANUEL SILVA GARCÍA
4	**GALLO GUERRERO LEIDY MARCELA**	MAESTRÍA EN TECNOLOGÍA AVANZADA CICATA - IPN	**DR. MIGUEL ANGEL MARTÍNEZ CRUZ** DR. LEONARDO DAVID HERRERA ZUÑIGA
5	**ALBARRÁN CARMONA ISABEL**	MAESTRÍA EN CIENCIAS EN SISTEMAS ESIME-IPN	**DRA. ROSALBA ZEPEDA BAUTISTA** DR. JAIME ROBLES GARCÍA
6	**ÁLVAREZ RUIZ YAIR**	MAESTRÍA EN CIENCIAS EN SISTEMAS ESIME-IPN	**DRA. ROSALBA ZEPEDA BAUTISTA** DR. JAIME ROBLES GARCÍA

De este modo tengo el gusto de darles la **mas**

Responder
Responder a todos
Reenviar

Casa abierta al tiempo
UNIVERSIDAD AUTÓNOMA METROPOLITANA

QUÍMICA
UAM IZTAPALAPA

Departamento de Química
División de Ciencias Básicas e Ingeniería

DIVISIÓN DE CIENCIAS BÁSICAS E INGENIERÍA

DEPARTAMENTO DE QUÍMICA

EVALUACIÓN DEL COMITÉ DE POSGRADO EN QUÍMICA

TRIMESTRE 25I

En el salón VIRTUAL DE ZOOM de la UAM-Iztapalapa, siendo las 15:00 horas del día _07_ de Mayo del 2025, se presentó el alumno: ***Aguayo Tabares David***, inscrito a la UEA: **Introducción a la Investigación II**, correspondiente a la maestría en Ciencias (Química). El alumno presentó los avances en la investigación relacionados con su tema de tesis titulada: *"Síntesis de pirrolo[3,4- b]piridin-5-onas vía Reacciones de Multicomponentes tipo Ugi-Zhu catalizadas con óxidos metálicos"*.
Presidente: Dr. Eduardo González Zamora
Secretario:Dr. Ricardo A. Peralta Ávila
Vocal: Dr. Carlos Cortes García

Ante el Comité de seguimiento integrado por los Profesores:

Presidente: Dr. Eduardo González Zamora Firma _____
Secretario:Dr. Ricardo A. Peralta Ávila Firma_____
Vocal: Dr. Carlos Cortes García Firma_____

Quienes después de revisar el documento escrito, atender y cuestionar la exposición oral del alumno, emitieron las calificaciones siguientes:

Escrito	NA	S	B	MB
Presentación Oral	NA	S	B	MB
Respuesta a los Cuestionamientos	NA	S	B	MB
Avances	NA	S	B	MB
Calificación Integral Recomendada	NA	S	B	MB

Comentarios, sugerencias y observaciones del Comité:

Con base al escrito enviado, se recomienda replantear el resumen. Revisar el formato de la bibliografía. Evitar el uso de libros para bibliografía. La introducción debe de ser fluida y tratar de no poner subcapítulos. Las páginas deben de ser enumeradas. Reestructurar el escrito que tenga: Introducción, antecedentes, justificación, hipótesis, objetivos, esquema general de síntesis, resultados y discusión, parte experimental, anexos y bibliografía. En los antecedentes hablar mas de los catalizadores utilizados en las RMC-I. añadir esquemas de reacción. Reescribir la parte de resultados, ya que parece mas metodología. Describir los RMN y mecanismo de reacción asi como la influencia de los catalizadores en los rendimientos. El estudiante no justifica el uso de los óxidos por lo que debe de profundizar la química. Reescribir las conclusiones. El estudiante debe de repasar profundamente los conceptos de todos los procesos one-pot, química de isonitrilos, mejorar la estética de sus presentaciones.

NOMBRE DEL EVALUADOR Dr. Carlos Jesús Cortés García
INSTITUCIÓN Universidad Michoacana de San Nicolás de Hidalgo

2.Investigación

Review

J. Mex. Chem. Soc. **2025**, *69*(1)
Special Issue
©2025, Sociedad Química de México
ISSN-e 2594-0317

The Use of Porous Materials in Heterogeneous Catalysis

Pablo Marín-Rosas[1], Nora S. Portillo-Veléz[1], J. Gabriel Flores[2], Eduardo González-Zamora[1], Alejandro Islas-Jácome[1], Leonardo D. Herrera-Zúñiga[1], Ilich A. Ibarra[3,4], Margarita Viniegra[1], N. Martín-Guaregua[1*], Ricardo A. Peralta[1*], Julia Aguilar-Pliego[2*]

[1]Departamento de Química, División de Ciencias Básicas e Ingeniería, Universidad Autónoma Metropolitana-Iztapalapa, 09340, Ciudad de México, México.
[2]Área de Química Aplicada, Departamento de Ciencias Básicas, Universidad Autónoma Metropolitana-Azcapotzalco, 02200, Ciudad de México, México.
[3]Laboratorio de Fisicoquímica y Reactividad de Superficies (LaFReS), Instituto de Investigaciones en Materiales, Universidad Nacional Autónoma de México, Circuito Exterior s/n, CU, Coyoacán, 04510, Ciudad de México, Mexico.
[4]On sabbatical as "Catedra Dr. Douglas Hugh Everett" at Departamento de Química, Universidad Autónoma Metropolitana-Iztapalapa, San Rafael Atlixco 186, Col. Vicentina, Iztapalapa, C.P. 09340, Ciudad de México, Mexico.

***Corresponding author:** N. Martín-Guaregua, email: nmartin@izt.uam.mx; Ricardo A. Peralta, email: rperalta@izt.uam.mx; Julia Aguilar-Pliego, email: apj@azc.uam.mx

Received May 2nd, 2024; Accepted September 25th, 2024.

DOI: http://dx.doi.org/10.29356/jmcs.v69i1.2270

Abstract. Heterogeneous catalysis, a cornerstone of the industry, offers the practical advantage of easy recovery and multiple reuses, leading to significant process cost reduction. The catalytic activity of porous materials, such as silica-based, zeolites, and MOFs, has proven to be not just interesting, but also superior to conventional heterogeneous systems. In this paper, we highlight the practical importance of these materials, their advances and modifications through the years, and their use as catalysts or support for other materials to enhance their catalytic properties.
Keywords: MOFs; zeolites; silicates; catalysts; heterogeneous systems.

Resumen. La catálisis heterogénea ha sido de mucha importancia en la industria; estos sistemas se pueden recuperar de manera sencilla y reutilizar varias veces, lo que tiene un impacto importante en la reducción de costos en el proceso. Los materiales porosos han demostrado una actividad catalítica interesante y han superado a los sistemas heterogéneos convencionales. En este estudio resumimos la importancia de materiales basados en sílice, zeolitas y MOFs. En este artículo, destacamos la importancia de materiales como los basados en sílice, las zeolitas y los MOF, sus avances y modificaciones a través de los años a medida que se utilizan como catalizadores o soporte de otros materiales para potenciar sus propiedades catalíticas.
Palabras clave: MOFs; zeolitas; silicatos; catalizadores; sistemas heterogéneos.

Introduction

Catalysis became crucial with the growth of the chemical industry through the last decades; 85 %–90 % of these processes include at least one catalytic step to achieve them in a more sustainable way [1-3]. A catalyst is defined as a substance that increases the rate of a particular reaction under mild or soft reaction conditions without being part of the product. One of the most important aims for scientists who study this field is to design catalysts with highly active catalytic sites. These sites normally define whether the desired reaction

J. Mex. Chem. Soc. **2025**, *69*(1)
Special Issue
©2025, Sociedad Química de México
ISSN-e 2594-0317

will proceed with a higher rate and/or selectivity to avoid the formation of unwanted sub-products and under relatively mild conditions in comparison with a non-catalyzed reaction [3,4].

The catalyzed reactions can be carried out in a homogeneous manner where the reactants and the catalyst are in the same phase, usually in the liquid phase. Homogeneous catalysis has the advantage of allowing precise control of reaction conditions, which is very important in organic chemistry and the pharmaceutic industry [5]. Li and coworkers presented the synthesis of γ- Valerolactone using $Sc(OTf)_3$ as an efficient homogeneous catalyst, obtaining yields over 90 % in this compound that is key in some industries related to green chemistry and biomass refinery [6]. However, this catalysis is less stable at high temperatures, and the catalyst is difficult to recover from the reaction mixture and, thereby, can elevate the cost of the process [5].

Heterogeneous catalysts are systems that present the property of being in a different phase as the reactants. In heterogeneous catalysis, the reactants (liquid, gas) adsorb onto the surface of a solid catalyst [5]. The advantages of these types of systems are the stability to high temperatures and easy removal from the reaction medium, reducing the overall cost, which is of great importance for industries such as oil and gas refining and wastewater, among others [7]. Thus, heterogeneous catalysis plays an integral role in producing over 80 % of chemical products worldwide. These catalysts can be synthesized with the control of important properties like particle size and morphology. However, a key feature in these systems is controlling the porosity because of the intimate relationship between the activity and product selectivity. The pore dimensions of solid catalysts can directly influence the diffusion properties of reactive species during a chemical process [8,9].

Metal nanoparticles have been used in catalysis since the 1940´s to the date, starting with precious metals like gold, silver, platinum or palladium and changing to the use of less expensive metals like nickel, cobalt or iron. Although these precious materials have been used for important reactions like the hydrogenation of polyvinyl alcohols [10], degradation of dyes in water like xylenol orange [11] or the oxidation of CO to CO_2 [12]; and some of these nanoparticles are stabilized by weak linkers [13], an alternative to improve the activity of these materials and the use of less precious metals was presented when the catalyst was supported in other materials (solid matrix). The support can be chemically inert or active [14], resulting in interest when is catalytically active because it can take advantage of the inherent properties of the material, such as high surface area to interact and easy separation and reuse [13]. Traditional heterogeneous catalysts, such as metal oxides supported on a surface, are systems susceptible to dissolution and ion release, which can lead to environmental problems. 15 Furthermore, they possess lower turnover frequencies than homogeneous systems due to the non-homogeneous distribution of the catalytic sites [16]. Thus, a new wave of porous catalytic solids has been developed, such as silica-based materials, zeolites, and metal–organic frameworks (MOFs). Due to their predictable and designable long-range ordered structures, guest-accessible pores, and easily functionalized channels by pre- or post-modifications, decades of research on these materials have furnished numerous porous catalysts that are of substantial scientific and industrial interest [17,18]. In this review, we highlight some of these porous materials and their applications in heterogeneous catalysis. These materials have been studied for decades with promising results, presenting an alternative to conventional unsupported catalysts. Although there are some reviews related to this topic in the literature, we focus on the important contributions of research groups at the "Universidad Autónoma Metropolitana" (UAM) in this field over the years.

Silica-based materials in heterogeneous catalysis

In the 1990s, there was a great impulse in the investigation of mesoporous materials as heterogeneous catalysts, the synthesis of mesoporous silicate and aluminosilicate molecular sieves opened new possibilities for preparing catalysts with uniform pores 19, confinement of the catalyst within mesopores provided a means of introducing size and/or shape selectivity and greater specificity to reactions [20]. Later in the '90s, specifically in 1997, it was reported the possibility of generating Brønsted acid sites on the surface of the mesoporous structures, opening new possibilities for producing monofunctional acid as well as acid/metal oxide bifunctional catalysts. These molecular sieves presented very high surface areas, which were of great utility because they can act as support for catalytically active phases such as metal oxide complexes, among others [21].

A widely employed material is the hexagonal MCM-41 (Mobil Composition of Matter), which became the focus for scientists due to its potential applications, both as a catalyst and as support [22]. In 2002, the

J. Mex. Chem. Soc. **2025**, *69*(1)
Special Issue
©2025, Sociedad Química de México
ISSN-e 2594-0317

encapsulation of copper complexes within MCM-41 and the partial oxidation of phenol was reported. The system demonstrated to be a good support and an excellent selective catalyst to produce catechol. Moreover, the absence of leaching copper through the process was observed [23]. A major limitation of this catalyst is its use in acidic conditions, as silica materials have low intrinsic stability in this environment. To overcome this problem, scientists studied the incorporation of strong acidic functional groups, like alkyl- or aryl-sulfonic acid, on the silica surface. It has been reported that these groups produce higher numbers of improved acid centres and enhance the activity in reactions catalyzed by the acid function. In 2005, Boveri and collaborators reported a method to prepare HSO_3-functionalized MCM-41, as shown in Fig. 1; the materials were tested as catalysts for the reaction of benzene alkylation with 1-dodecane with moderate activity and good selectivity to 2-phenyl dodecane [24]. This methodology was also evaluated in the catalysis of stearic acid with glycerol, presenting interesting results like the selectivity to monoglyceride and the inhibition of di- and triglycerides, and the relation between the pore size and the increment of the activity in the reaction [25]. In 2010, the incorporation of Brønsted acid sites from HSO_3 to Co-Mo/MCM-41 catalyst was presented in the treatment of heavy oil, performing sulfur removal and improving the properties of the expected products [26].

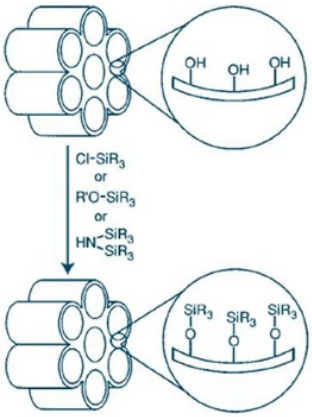


Fig. 1. Functionalization of mesoporous silicates by grafting [20].

A further method to improve the acidity of the material is the incorporation of metals such as Al^{+3} or Ga^{+3} in the material MCM-41 tested with the isomerization of α-pinene reaction where the main products were camphene and limonene, and the selectivity to one product or the other could be varied depending on the content of Al or Ga ions [27]. Recently, these systems have been used in many different potential industrial applications, such as the production of biodiesel, where the basicity or acidity of these materials should play an important role in this process. These materials can also be used to immobilize enzymes or magnetic nanoparticles for the catalytic degradation of organic dyes in contaminated water. A novel application for silica-based materials is their use as support for anti-cancer drugs; for instance, some of these materials have been functionalized with different drugs or active proteins, and these systems showed good results in the elimination of the infected cells and presented null toxicity for the healthy ones [28,29].

Silica-based materials were one of the first porous materials studied in catalysis due to their large surface area reported in the 90´s decade, especially MCM-41, which was evaluated in several reactions presenting good results in the catalytic activity. Modifications were made in the material to overcome acidity problems; the addition of metal nanoparticles is another way to expand the activity of the catalyst. These materials were the pioneers in these applications and landed the foundations for other materials to be studied as heterogeneous catalysts, such as zeolites and Metal-organic Frameworks (MOFs) that we will discuss in the next topics.

J. Mex. Chem. Soc. **2025**, *69*(1)
Special Issue
©2025, Sociedad Química de México
ISSN-e 2594-0317

Zeolites in heterogeneous catalysis

Zeolites are porous crystalline oxides consisting of TO_4 tetrahedra, where T is generally Si, but it can be substituted for Al or other heteroatoms [17,30,31]. The tridimensional networks of well-defined micropores act as reactor vessels whose activity and selectivity can be enhanced by introducing catalytic active sites [32]. The success of these catalysts is related to their specific properties that rely on their surface area and adsorption capacity. Zeolites can be modified to control their adsorption properties, they can be varied from hydrophobic to hydrophilic type materials and active sites [21,32].

The control of acid strength, as well as the density of acid sites, has also led these materials to be successful catalysts; doping these materials with other atoms like aluminum can create protons that have Brønsted acidity and demonstrate unique properties for adsorption and catalysis [33]. Furthermore, in catalysis, it is of special importance for catalyzing reactions involving strong bases such as NH_3 or pyridines [32]. The use of Zn has been reported in the methanol conversion to aromatics, showing great selectivity to aromatic compounds like benzene, toluene and xylene. The introduction of Zn particles in zeolites like ZSM-5 (Zeolite Socony Mobil) [34,35], MCM-22, TNU- 9 (Taejon National University) and MCM-68 [36], has shown the generation of strong acid sites while maintaining stability at high temperatures.

It is also possible to generate basic sites within the pores of zeolites to use them as catalytic active sites. The basic sites are of the Lewis type and correspond to framework oxygens, or they can also be exchanged with alkali metals. These systems have been reported to efficiently catalyze a variety of reactions, including Knoevenagel condensation, amide hydroxylation, one- pot multicomponent reactions (MCRs) and cycloaddition reactions [37]. An interesting feature of basic zeolites is that they are useful catalysts for some reactions that require acid-base pairs. In this situation, the Lewis acidity of the cation and the basicity of the oxygen can be balanced [32]. The use of Ni particles in zeolite ZSM-5 has been applied in CO_2 methanation (conversion of carbon monoxide and carbon dioxide to methane through hydrogenation), presenting 99 % conversion related to weak and medium basic sites within the material [38].

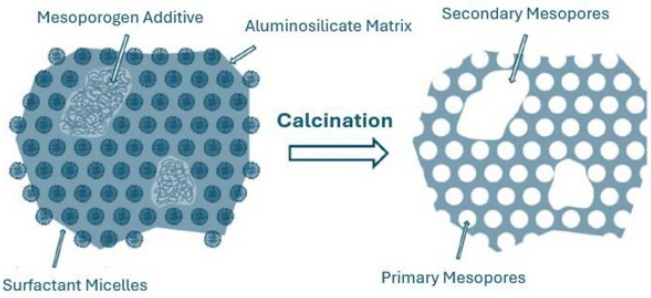


Fig. 2. Sketch of the dual mesopore system templating in mesoporous aluminosilicates [39].

Controlling the size of the pores is a property that can be useful when the molecules cannot access or leave the pores of the zeolite. A reported strategy is to produce mesopores within the channels of these systems with the addition of agents that can generate mesopores in the zeolites (mesoporogenic agents), as shown in Fig. 2 [40]. In 2014, a study presented the synthesis of zeolite ZSM-5 with the addition of carbon nanoparticles and chitosan (biopolymer derived from crustacean shells); these additives changed the Si/Al ratio in the material and improved the pore sizes and volumes compared to the pure zeolite. The materials showed an interesting route for the catalytic cracking of low-density polyethylene (LDPE) to fuel [39].

Commonly, bulky molecules are of interest in catalysis; the reaction takes place only on the surface of the material, limiting the interaction with the reactants [41-43]. Another inconvenience is the irreversible adsorption of heavy secondary products or bulky molecules of products that may be trapped inside the cavities and lead to the deactivation of the catalyst [44]. New investigations are in progress to develop large pores zeolites; however, the synthesis of these materials is costly due to the use of expensive templates or multistep

J. Mex. Chem. Soc. **2025**, *69*(1)
Special Issue
©2025, Sociedad Química de México
ISSN-e 2594-0317

procedures [45]. More importantly, the chemical compositions for zeolites are limited to aluminosilicates, which can accommodate only marginal amounts of transition metals, primarily as defects [46]. Studies have shown us that zeolites can be competitive catalysts thanks to their properties. Nevertheless, more investigations and modifications must be performed on these materials so they can be applied to other industrial processes. The advances in technology can help them to play an interesting role in the transition to better technologies.

MOFs in heterogeneous catalysis

Metal-organic frameworks (MOFs) have attracted immense attention during the last two decades due to their potential to produce a wide variety of structures [47]. MOFs are constructed from metal cations (or clusters of metal cations) linked to one another by bridging organic linkers. The wide variety of these materials motivated research groups to seek a broad spectrum of applications such as gas storage, gas separation, and catalysis [48], among many others. There is continuous interest in seeking new MOF materials because these systems possess many outstanding features that commend them as catalysts, such as their large surface areas, adjustable pore sizes, and tunable properties [49,50].

MOFs have shown advantages over other porous materials, for instance, their crystalline morphology, unlike siliceous mesoporous materials which cannot be investigated by crystallographic techniques. MOFs can be modified using organic synthesis, and their pores may be decorated with catalytic sites, unlike some zeolites whose structures are fixed and unalterable. MOF materials show a balanced mix of crystallinity, porosity, and tunability, and there is significant potential for the commercial application of such materials in heterogeneous catalysis [51]. Some of the modifications can occur when the ligand is used to attach other active groups, such as Brønsted acid centres (sulfonic acid), basic centres (amino) or appropriate binding sites, which may engage in the development of metal complexes at lateral sites and implement some unique catalytic performance [52].

Another approach is to use the metal nodes of the MOF framework, as normally, these metal complexes possess solvent labile molecules coordinated, which can be removed to produce unsaturated metal sites. A common activation method is to expose the material to a vacuum at a certain temperature. Nevertheless, it has been reported that more methods, such as chemical activation, succeed in this task [53]. In several other instances, structural defects and imperfections might also insert certain coordinately unsaturated sites across the metal centres [52].

In 2023 several studies were made to demonstrate that these open metal sites could work in the alcoholysis of cyclohexene oxide using MOFs as catalysts. SU-101 (Stockholm University) presented conversion over 99 % with methanol, over 96 % with ethanol and over 24 % with propanol; the material presented retention of the catalytic activity over 5 cycles and a mechanism was proposed involving the Bi^{+3} open metal sites in the MOF [54], MOF-74 presented over 90 % conversion using methanol at 50 °C in less than 2 days, presenting no degradation, leaching or loss in the catalytic activity over 3 cycles [55] the mechanism is shown in Fig. 3. MOF-74 has also been used as a catalyst with different metal sites in the oxidation of styrene to benzaldehyde using peroxides as oxidants, where Cu-MOF-74 reported the highest yield, and Zn-MOF-74 acted as an inhibitor rather than as a real catalyst [56].

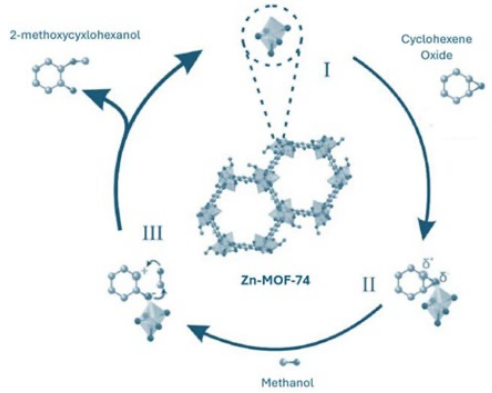


Fig. 3. Steps proposed for the alcoholysis of cyclohexene oxide with methanol catalyzed by Zn-MOF-74 55.

J. Mex. Chem. Soc. **2025**, *69*(1)
Special Issue
©2025, Sociedad Química de México
ISSN-e 2594-0317

One of the most challenging processes in the industry is the production of vanillin; only 1 % corresponds to natural extraction, and the rest of the production is obtained by chemical synthesis. In the effort to facilitate the production of this molecule, the use of catalysts such as MOFs to produce vanillin by the transformation of trans-ferulic acid has been reported in this process. HKUST-1 (Hong Kong University of Science and Technology) was one of the first materials to be tested in this synthesis; the results showed that this material can be used for the effective conversion to vanillin with 95 % yield using hydrogen peroxide 57; later, a Cu(II) metal-organic polyhedron was tested, presenting a 60 % yield, but the material lost its crystallinity; however, no copper leaching in the reaction was presented [58]. Finally, Cu-MOF-74 presented yields between 71 and 97 % for vanillin production though the reaction presented copper leaching and the disruption of the framework structure [59]. This demonstrates that vanillin can be successfully synthesized using MOFs for this reaction; however, the reaction conditions and solvents need to be established before scaling up the reaction.

On the other hand, there can be semi-open metal sites where the linker offers the ability to switch on or switch off the active sites on the MOF. A good example is the use of MOF MFM-300(Sc) (Manchester Framework Material) as a catalyst for the Strecker reaction between N- Benzylideneaniline and trimethylsilyl cyanide (TMSCN) to form 2-phenyl-2-(phenylamino)acetonitrile, reported in 2022 by Peralta and collaborators. It was demonstrated that the material showed retention of the crystalline structure and catalytic activity over 5 cycles [60]. This same strategy was used by López-Olvera and collaborators with the MFM-300(Sc) material as a catalyst to transform H_2S into polysulfides, compounds that can be used in other fields like battery electrodes [61].

One thing to take into consideration is the thermal stability of the material; under certain conditions, the structural integrity of MOFs can be compromised; such processes include amorphization or framework collapse. That changes the physical and chemical properties of a material, making it inappropriate for catalytic applications [62,63]. The election of the organic linker and metal plays a key role in the stability of the framework [62]; therefore it is crucial for the catalytic process. The design of new MOFs that can tolerate high temperatures should be considered an area of opportunity for many applications, not only catalysis.

Overall, research on MOFs in catalysis has continuously increased in the last decade thanks to their inherent properties. A salient feature of MOFs is their large surface area and their relationship with the catalytic activity, along with the robustness of the systems. For instance, gas adsorption and separation are classic MOF applications due to the pore size and stability. This last property depends on the strength of the metal−linker bond; the research of new MOFs with more robust frameworks could present a solution. Nevertheless, the structural and compositional complexity is a challenge that must be considered.

On the other hand, the challenge for heterogeneous catalysts is the loss of reactivity or selectivity; MOFs can present a solution with their open-metal sites that can act as acid or basic sites. Encapsulation of enzymes could be another solution to this problem. However, these systems have been barely studied, and considerations must be realized, such as the enzyme leaching within the framework due to a large pore of the MOF. It is worth mentioning that encapsulation could also lead to a decrease in porosity and thereby generate mass transport problems [46]. Porous materials could be a solution to the difficulties of the industry in the coming years, and the present review intends to show their importance and potential applications.

Conclusions

Porous materials have shown interesting advances in catalytic applications. Pre- and post-synthetic modifications can improve the selectivity in some reactions; these materials can also work as supports for other catalysts, improving their activity, which makes them perfect candidates for this type of application.

Silica-based materials were one of the first porous materials used in catalysts. Their activity was tested in important reactions, and modifications were made in their structure to overcome important problems in their use. Zeolites presented an improvement in porous materials with the presence of acid or basic sites, leading to interesting catalytic applications. Finally, MOFs have been one of the most studied porous materials in the last two decades thanks to their high crystallinity, large surface area, tuneable properties and adjustable pores. The catalytic process can occur within the pores of the MOFs thanks to the open metal sites or functional groups that act as acids or basic centres.

J. Mex. Chem. Soc. **2025**, *69*(1)
Special Issue
©2025, Sociedad Química de México
ISSN-e 2594-0317

These materials have many possible applications, like gas adsorption, which is one of the most common since many industrial processes produce gases such as CO_2 and H_2S, which are harmful to the environment. Porous materials can also be applied to catalytically degrade contaminants, organic dyes, or other emergent pollutants like plastic and drug residues. Some of the other applications investigated for these materials are energy storage, drug delivery, and the sensing or detection of contaminants.

It is important to mention that there is still a lot of work to do before this can be applied in the industrial field; reaction conditions and solvent issues need to be tested so the materials can retain their structure and the catalyst can be easily recovered to be used again. Another alternative is the synthesis of new and more robust materials that can endure the harsh conditions that the industrial field presents. Understanding these materials is important to gain perspective on their significance in possible real-world applications.

Acknowledgements

This work was supported by the Universidad Autónoma Metropolitana "Proyectos de Investigación relacionados con Desafíos Actuales" P. M-R. thanks CONAHCyT - México for his MSc scholarship (1277642). N. S. P-V (CVU) thanks CONAHCyT for the scholarship "Estancias Posdoctorales 2022(2).

References

1. Poovan, F.; Chandrashekhar, V. G.; Natte, K.; Jagadeesh, R. V. *Catal. Sci. Technol.* **2022**, *12*, 6623-6649. DOI: http://dx.doi.org/10.1039/d2cy00232a.
2. Friend, C. M.; Xu, B. *Acc. Chem. Res.* **2017**, *50*, 517-521. DOI: 10.1021/acs.accounts.6b00510 From NLM PubMed-not-MEDLINE.
3. Védrine, J. C. *Chin. J. Catal.* **2019**, *40*, 1627-1636. DOI: http://dx.doi.org/10.1016/s1872-2067(18)63162-6.
4. Rogge, S. M. J.; Bavykina, A.; Hajek, J.; Garcia, H.; Olivos-Suarez, A. I.; Sepulveda-Escribano, A.; Vimont, A.; Clet, G.; Bazin, P.; Kapteijn, F.; et al. *Chem. Soc. Rev.* **2017**, *46*, 3134-3184. DOI: http://dx.doi.org/10.1039/c7cs00033b From NLM PubMed-not-MEDLINE.
5. Álvarez, M. S.; Longo, M. A.; Rodríguez, A.; Deive, F. J. *J. Ind. Eng. Chem.* **2024**, *132*, 36-49. DOI: http://dx.doi.org/10.1016/j.jiec.2023.11.030.
6. Li, F.; Yang, R.; Du, Z.; Dai, J.; Wang, X.; Li, N.; Zhang, J.; Zhang, X.; Liu, Y.; Gong, H.; et al. *Mol. Catal.* **2023**, 535. DOI: http://dx.doi.org/10.1016/j.mcat.2022.112863.
7. Schlogl, R. *Angew Chem. Int. Ed. Engl.* **2015**, *54*, 3465-3520. DOI: http://dx.doi.org/10.1002/anie.201410738.
8. Alsudairy, Z.; Brown, N.; Campbell, A.; Ambus, A.; Brown, B.; Smith-Petty, K.; Li, X. *Mater. Chem. Front.* **2023**, *7*, 3298-3331. DOI: http://dx.doi.org/10.1039/d3qm00188a.
9. Sudarsanam, P.; Peeters, E.; Makshina, E. V.; Parvulescu, V. I.; Sels, B. F. *Chem. Soc. Rev.* **2019**, *48*, 2366-2421. DOI: http://dx.doi.org/10.1039/c8cs00452h.
10. Louis D. Rampino, F. F. N. *J. Ame. Chem. Soci.* **1941**, *63*, 2745 – 2749. DOI: http://dx.doi.org/10.1021/ja01855a070.
11. Chen, Y.-N.; Liu, T.; Zhang, Q.; Shang, C.; Wang, H. *RSC Advances.* **2017**, *7*, 758-763. DOI: http://dx.doi.org/10.1039/c6ra24926d.
12. Masatake Haruta, T. K.; Sano, H.; Yamada, N. *Chem. Lett.* **1987**, *16*, 405–408. DOI: 10.1246/CL.1987.405.
13. Astruc, D. *Chem. Rev.* **2020**, *120*, 461-463. DOI: http://dx.doi.org/10.1021/acs.chemrev.8b00696.
14. Shinde, P. S.; Suryawanshi, P. S.; Patil, K. K.; Belekar, V. M.; Sankpal, S. A.; Delekar, S. D.; Jadhav, S. A. *J. Compos. Sci.* **2021**, *5*. DOI: http://dx.doi.org/10.3390/jcs5030075.
15. Manuja, A.; Kumar, B.; Kumar, R.; Chhabra, D.; Ghosh, M.; Manuja, M.; Brar, B.; Pal, Y.; Tripathi, B. N.; Prasad, M. *Toxicol. Rep.* **2021**, *8*, 1970-1978. DOI: http://dx.doi.org/10.1016/j.toxrep.2021.11.020.

J. Mex. Chem. Soc. **2025**, *69*(1)
Special Issue
©2025, Sociedad Química de México
ISSN-e 2594-0317

16. Mabate, T. P.; Maqunga, N. P.; Ntshibongo, S.; Maumela, M.; Bingwa, N. *SN Appl. Sci.* **2023**, *5*. DOI: http://dx.doi.org/10.1007/s42452-023-05416-6.
17. Ou, Z.; Li, Y.; Wu, W.; Bi, Y.; Xing, E.; Yu, T.; Chen, Q. *Chem. Eng. J.* **2022**, 430. DOI: http://dx.doi.org/10.1016/j.cej.2021.132925.
18. Qiao, L.; Kang, Z.; Li, Z.; Feng, Y.; Sun, D. *Fuel.* **2024**, 359. DOI: http://dx.doi.org/10.1016/j.fuel.2023.130477.
19. Beck, J. S.; J. C. V.; Roth, W. J.; Leonowicz, M. E.; Kresge, C. T.; Schmitt, K. D.; Chu, C. T. W.; D. H. *J. Ame. Chem. Soc*. **1992**, 92.
20. Stein, A.; Melde, B. J.; Schroden, R. C. *Adv. Mater.* **2000**, *12*, 1403-1419.
21. Corma, A. *Chem. Rev.* **1997**, *97*, 2373-2419.
22. Aguilar-Pliego, P. B. J.; Zicovich-Wilson, C.; Herrera-Perez, G.; Lara, V. H. *Open Catal. J.* **2012**, *5*, 66-71.
23. Noreña-Franco, I. H.-P. L.; Aguilar-Pliego, J.; Maubert-Franco, A. *Catal. Today*. **2002**, *75*, 189-195.
24. Boveri, M.; Aguilar-Pliego, J.; Pérez-Pariente J.; Sastre, E. *Catal. Today.* **2005**, 107-108, 868-873.
25. Boveri, J. A.-P. M.; Márquez-Alvarez, C.; Pérez-Pariente, J.; Sastre, E. *Stud. Surf. Sci. Catal.* **2005**, *158*, 1549-1556.
26. Persi Schacht, J. A.-P.; Ramírez-Garnica, M.; Ramírez, S.; Abu, I.; Noreña-Franco, L. *J. Mex. Chem. Soc.* **2010**, *54*, 175-181.
27. Díaz-García, M.; Aguilar-Pliego, J.; Herrera-Pérez, G.; Guzmán, L.; Schachat, P.; Noreña-Franco, L. E.; Aguilar-Elguezabal, A.; Gutierrez-Arzaluz, M. *Adv. Mater. Res.* **2010**, *132*, 162-173.
28. Fatimah, I.; Fadillah, G.; Sagadevan, S.; Oh, W.-C.; Ameta, K. L. *ChemEngineering*. **2023**, 7.
29. Nayl, A. A.; Abd-Elhamid, A. I.; Aly, A. A.; Brase, S. *RSC Adv*. **2022**, *12*, 13706-13726.
30. Van Speybroeck, V.; Hemelsoet, K.; Joos, L.; Waroquier, M.; Bell, R. G.; Catlow, C. R. *Chem. Soc. Rev.* **2015**, *44*, 7044-7111.
31. Meng, X.; Xiao, F. S. *Chem. Rev.* **2014**, *114*, 1521-1543.
32. Corma, A. *J. Catal.* **2003**, *216*, 298-312.
33. Khivantsev, K.; Derewinski, M. A.; Szanyi, J. *Microporous Mesoporous Mater.* **2023**, 358.
34. Ruiz, M. G.; Casados, D. A. S.; Pliego, J. A.; Álvarez, C. M.; de Andrés, E. S.; Tartalo, D. S.R.; Vaque, S.; Casas, M. G. *React. Kinet., Mech. Catal.* **2020**, *129*, 471-490.
35. Ruiz, M. G.; Solís Casados, D. A.; Pliego, J. A.; Álvarez, C. M.; de Andrés, E. S. *Catal. Lett.* 2022, 153, 2493-2503.
36. García-Ruiz, M.; Solís-Casados, D. A.; Aguilar-Pliego, J.; Márquez-Álvarez, C.; Sastre-de Andrés, E.; Sanjurjo-Tartalo, D.; Sáinz-Vaque, R.; Grande-Casas, M. *Top. Catal.* **2020**, *63*, 451-467.
37. Mendoza-Castro, M. J.; Linares, N.; García-Martínez, J. *Catal. Today.* **2023**, 419.
38. Guo, X.; Traitangwong, A.; Hu, M.; Zuo, C.; Meeyoo, V.; Peng, Z.; Li, C. *Energy Fuels*. **2018**, *32*, 3681-3689.
39. Juárez-Hernández, L.; Pérez-Pariente, J.; Aguilar-Pliego, J.; Múgica-Álvarez, V.; Gutiérrez-Arzaluz, M.; Grande, M. S.; Márquez-Álvarez, C.; Sastre, E. *J. Porous Mater.* **2014**, *22*, 269-281.
40. Kadja, G. T. M.; Mukti, R. R.; Liu, Z.; Rilyanti, M.; Ismunandar; Marsih, I. N.; Ogura, M.; Wakihara, T.; Okubo, T. *Microporous Mesoporous Mater.* **2016**, *226*, 344-352.
41. Bingre, R.; Louis, B.; Nguyen, P. *Catalysts.* **2018**, *8*.
42. Zhang, H.; Samsudin, I. b.; Jaenicke, S.; Chuah, G.-K. *Catal. Sci. Technol.* **2022**, *12*, 6024-6039.
43. Derbe, T.; Temesgen, S.; Bitew, M.; Fedel, M. *Adv. Mater. Sci. Eng.* **2021**, *2021*, 1-17.
44. Perot, M. G. G. *J. Mol. Catal.* **1990**, *61*, 173-196.
45. Čejka, J.; Centi, G.; Perez-Pariente, J.; Roth, W. J. *Catal. Today.* **2012**, *179*, 2-15.
46. Hendon, C. H.; Rieth, A. J.; Korzynski, M. D.; Dinca, M. *ACS Cent Sci*. **2017**, *3*, 554-563.
47. Stock, N.; Biswas, S. *Chem. Rev.* **2012**, *112*, 933-969.

J. Mex. Chem. Soc. **2025**, *69*(1)
Special Issue
©2025, Sociedad Química de México
ISSN-e 2594-0317

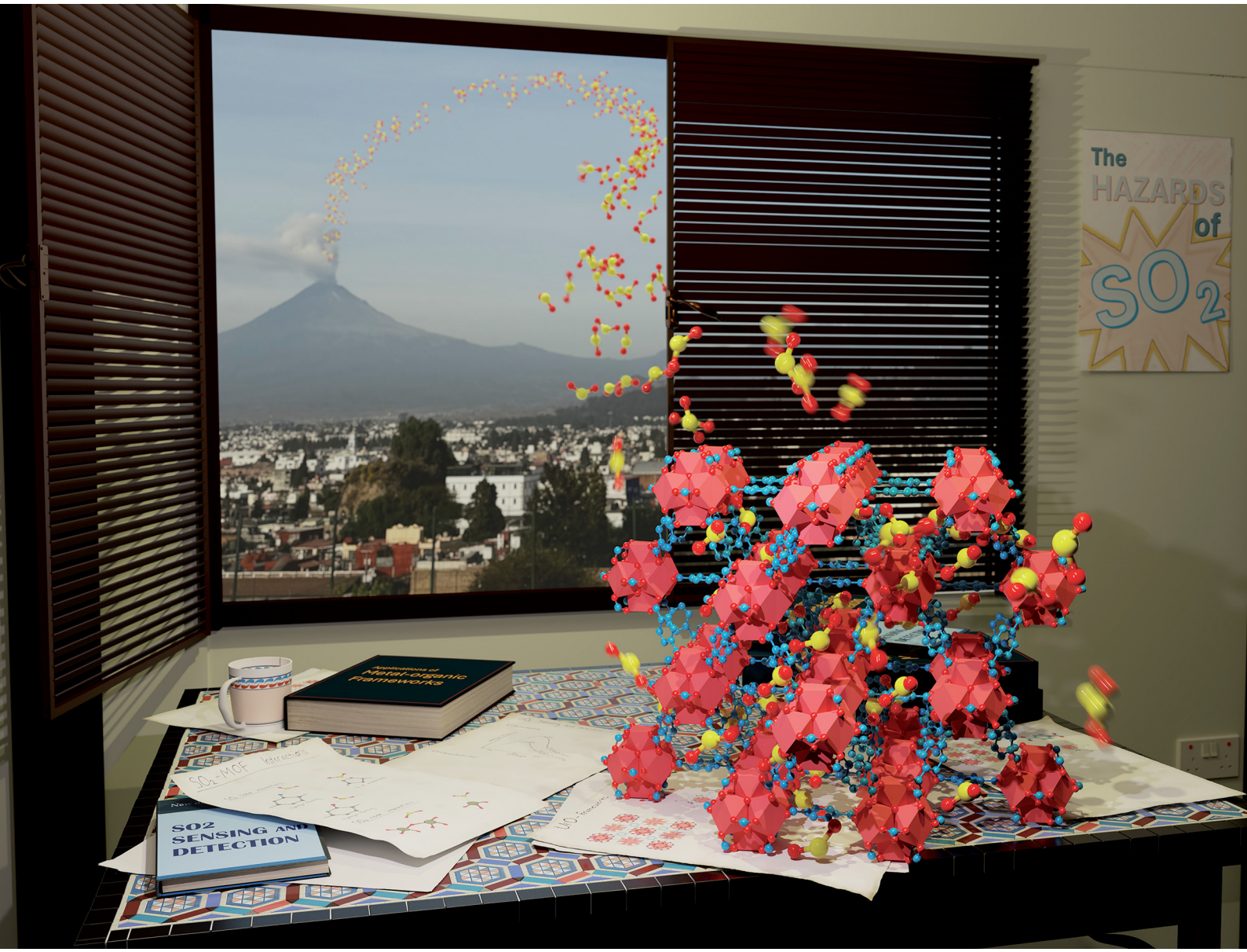
48. Yang, D.; Gates, B. C. *ACS Catal.* **2019**, *9*, 1779-1798.
49. Liu, X.; Valentine, H. L.; Pan, W.-P.; Cao, Y.; Yan, B. *Inorg. Chim. Acta*. **2016**, *447*, 162-167.
50. Gangu, K. K.; Maddila, S.; Mukkamala, S. B.; Jonnalagadda, S. B. *Inorg. Chim. Acta.* **2016**, *446*, 61-74.
51. Pascanu, V.; Gonzalez Miera, G.; Inge, A. K.; Martin-Matute, B. *J. Am. Chem. Soc.* **2019**, *141*, 7223-7234.
52. Alhumaimess, M. S. *J. Saudi Chem. Soc.* **2020**, *24*, 461-473.
53. Park, S. H.; Peralta, R. A.; Moon, D.; Jeong, N. C. *J. Mater. Chem. A.* **2022**, *10*, 23499-23508.
54. Obeso, J. L.; Gabriel Flores, J.; Flores, C. V.; Rios-Escobedo, R.; Aguilar-Pliego, J.; Ken Inge, A.; Antonio de los Reyes, J.; Peralta, R. A.; Ibarra, I. A.; Leyva, C. *ChemCatChem.* **2023**, 15.
55. Flores, J. G.; Obeso, J. L.; Martinez-Jimenez, V.; Martin-Guaregua, N.; Islas-Jacome, A.; Gonzalez-Zamora, E.; Serrano-Espejel, H.; Mondragon-Rodriguez, B.; Leyva, C.; Solis-Casados, D. A.; Ibarra, I. A.; Peralta, R. A.; Aguilar-Pliego, J.; Antonio de Los Reyes, J. *RSC Adv*. **2023**, *13*, 27174-27179.
56. Flores, J. G.; Díaz-García, M.; Ibarra, I. A.; Aguilar-Pliego, J.; Sánchez-Sánchez, M. *J. Solid State Chem.* **2021**, 298.
57. Yepez, R.; Illescas, J. F.; Gijon, P.; Sanchez-Sanchez, M.; Gonzalez-Zamora, E.; Santillan, R.; Alvarez, J. R.; Ibarra, I. A.; Aguilar-Pliego, J. *J. Vis. Exp.* **2016**, 113.
58. Sánchez-González, E.; López-Olvera, A.; Monroy, O.; Aguilar-Pliego, J.; Gabriel Flores, J.; Islas-Jácome, A.; Rincón-Guevara, M. A.; González-Zamora, E.; Rodríguez-Molina. B.: Ibarra, I. A. *CrystEngComm*. **2017**, *19*, 4142-4146.
59. Flores, J. G.; Sanchez-Gonzalez, E.; Gutierrez-Alejandre, A.; Aguilar-Pliego, J.; Martinez, A.; Jurado-Vazquez, T.; Lima, E.; Gonzalez-Zamora, E.; Diaz-Garcia, M.; Sanchez-Sanchez, M.; Ibarra, I. A. *Dalton Trans*. **2018**, *47*, 4639-4645.
60. Peralta, R. A.; Lyu, P.; Lopez-Olvera, A.; Obeso, J. L.; Leyva, C.; Jeong, N. C.; Ibarra, I. A.; Maurin, G. *Angew Chem. Int. Ed. Engl*. **2022**, *61*, e202210857.
61. López-Olvera, A.; Flores, J. G.; Aguilar-Pliego, J.; Brozek, C. K.; Gutiérrez-Alejandre, A. ; Ibarra, I. A.; *Chem. Mater.* **2021**, *33*, 6269-6276.
62. Healy, C.; Patil, K. M.; Wilson, B. H.; Hermanspahn, L.; Harvey-Reid, N. C.; Howard, B. I.; Kleinjan, C.; Kolien, J.; Payet, F.; Telfer, S. G.; Kruger, P. E.; Bennett, T. D. *Coord. Chem. Rev.* **2020**, 419.
63. Escobar-Hernandez, H. U.; Pérez, L. M.; Hu, P.; Soto, F. A.; Papadaki, M. I.; Zhou, H.-C.; Wang, Q. *Ind. Eng. Chem. Res.* **2022**, *61*, 5853-5862.

Volume 54
Number 9
7 May 2025
Pages 4089–4618

Chem Soc Rev

Chemical Society Reviews

rsc.li/chem-soc-rev



ISSN 0306-0012

ROYAL SOCIETY OF CHEMISTRY

REVIEW ARTICLE

Michael T. Huxley, Diego Solis-Ibarra, Ilich A. Ibarra, Christoph Janiak *et al.*

Metal–organic frameworks (MOFs) toward SO_2 detection

Chem Soc Rev

REVIEW ARTICLE

View Article Online
View Journal | View Issue

Check for updates

Cite this: *Chem. Soc. Rev.*, 2025, **54**, 4135

Metal–organic frameworks (MOFs) toward SO_2 detection

Juan L. Obeso, [ab] Catalina V. Flores, [ab] Ricardo A. Peralta, [c] Margarita Viniegra, [c] N. Martín-Guaregua,[c] Michael T. Huxley,*[d] Diego Solis-Ibarra, *[a] Ilich A. Ibarra *[a] and Christoph Janiak *[e]

Received 29th October 2024

DOI: 10.1039/d4cs00997e

rsc.li/chem-soc-rev

Developing technology that can precisely monitor specific air pollutants in diverse settings is essential to control emissions and ensure safe exposure limits are not exceeded. Metal–organic frameworks (MOFs) are crystalline organic–inorganic hybrid materials, which are promising candidates for SO_2 detection. Their chemically mutable periodic structure confers outstanding surface area, thermal stability, and a well-defined pore distribution. Moreover, MOFs have exhibited extraordinary performance for SO_2 capture. Therefore, research has focused on their possible applications for SO_2 sequestration due to the selective and robust chemical and physical interactions of SO_2 molecules within MOFs. The variable SO_2 affinity presented by MOFs enables the adsorption mechanism and preferential adsorption sites to be resolved. However, for MOF-based SO_2 detection, selective SO_2 capture at shallow partial pressure (0.01–0.1 bar) is required. Thus, capturing SO_2 at low concentration is crucial for SO_2 detection, where textural properties of MOFs, mainly the pore-limiting diameter, are essential to achieve selective detection. In this review, we discuss the fundamental aspects of SO_2 detection in MOFs, providing a step-by-step methodology for SO_2 detection in MOFs. We hope this review can provide valuable background around SO_2 detection in MOFs and inspire further research within this new and exciting field.

Open Access Article. Published on 10 March 2025. Downloaded on 6/30/2025 11:42:55 PM.
This article is licensed under a Creative Commons Attribution 3.0 Unported Licence.

1. Introduction

The environmental and health implications of volatile pollutants pose major technological and economic challenges to modern society. The role of anthropogenic CO_2 and methane emissions in promoting an enhanced greenhouse effect is no doubt the most publicized example, yet lesser known pollutants such as carbon monoxide (CO), tropospheric ozone (O_3), ammonia (NH_3), volatile organic compounds, hydrogen sulfide (H_2S), and sulfur dioxide (SO_2) are harmful and prevalent in their own right.[1] These toxic gases contribute to poor health outcomes, crop damage, acidification of soils and waters, and the loss of biodiversity.[2,3] Therefore, targeting emissions and remediating contaminated areas remains a principal goal of governments worldwide.

The developed world's accelerating demand for energy,[4] which is still predominantly satisfied by fossil fuels, represents the major anthropogenic source of volatile pollutants.[5] Natural sources, such as volcanic activity, are a further contributing factor.[6] For example, México hosts several of the world's largest and most frequently active volcanoes. Volcanic gas emissions from these and other volcanoes are damaging to both the environment and human health in localized areas.[7,8]

Of the pollutants identified above, SO_2 is particularly hazardous due to a combination of toxicity and its ubiquity in flu gas emissions and various industrial settings. SO_2 is a colourless, irritating, and non-flammable gas with a strong odor that can be absorbed through the respiratory system or dermal contact.[9] It is classified as one of the most hazardous gases: exposure can to concentrations exceeding 100 ppm can be fatal in minutes.[10] However, even at lower concentrations, inhalation can cause severe respiratory complications.[11,12] The maximum daily average concentration for human exposure to SO_2 is 20 μg m^{-3} (8 ppb). Therefore, based on environmental and human health considerations, it is necessary to enforce stringent SO_2 emission regulations and prioritize the detection of SO_2 in both ecological and workplace settings.[13]

[a] *Laboratorio de Fisicoquímica y Reactividad de Superficies (LaFReS), Instituto de Investigaciones en Materiales, Universidad Nacional Autónoma de México, Circuito Exterior s/n, CU, Coyoacán, 04510 Ciudad de México, Mexico. E-mail: diego.solis@unam.mx, argel@unam.mx*

[b] *Instituto Politécnico Nacional, Centro de Investigación en Ciencia Aplicada y Tecnología Avanzada, Legaria 694, Col. Irrigación, Miguel Hidalgo, 11500 Ciudad de México, Mexico*

[c] *Departamento de Química, División de Ciencias Básicas e Ingeniería. Universidad Autónoma Metropolitana (UAM-I), 09340, Mexico*

[d] *School of Physics, Chemistry and Earth Sciences, Faculty of Sciences, Engineering and Technology, The University of Adelaide, Adelaide, South Australia 5005, Australia. E-mail: michael.huxley@adelaide.edu.au*

[e] *Institut für Anorganische Chemie und Strukturchemie, Heinrich-Heine-Universität Düsseldorf, 40204 Düsseldorf, Germany. E-mail: janiak@uni-duesseldorf.de*

Open Access Article. Published on 10 March 2025. Downloaded on 6/30/2025 11:42:55 PM. This article is licensed under a Creative Commons Attribution 3.0 Unported Licence.

1.1 Physicochemical properties of SO_2

To understand the challenges associated with the capture and detection of SO_2, the chemical and physical properties of the compound must be considered.[14,15] Valence shell electron pair repulsion theory predicts SO_2 to possess a bent geometry with an approximately 120° angle between the central sulfur and peripheral oxygen atoms (Fig. 1a). The bonding in SO_2 can be described with mesomeric bonds: a covalent S═O double bond and an ionic S^+–O^- bond (Fig. 1b). The molecule is polar (dipole moment 1.63305 D or 5.4473×10^{-30} C m) and is therefore soluble in water (Fig. 1c).[16] The S–O bond length in SO_2 is 1.43 Å, commensurate with the bonding models described above.[17]

1.2 Sources of SO_2 pollution

The SO_2 pollution is directly related to industrial activities associated with burning fossil fuels and biomass by power plants and chemical industries. This can include metal extraction from mines, locomotives, vehicles, and volcanos.[18] In general, power plants generate electricity *via* combustion, which releases SO_2 because the feedstocks contain sulfur compounds.

Therefore, industrial cities are confronted with an SO_2 pollution problem. Jion *et al.*[19] reported that 27.6% of SO_2 emissions in Asian countries arise from coal burning, while industry accounts for 20.7%, fossil fuel and biomass burning 13.8%, power plants and brick kilns 10.3%, and domestic production 3.4%. The increase in SO_2 pollution is related to industrialization, urbanization, and economic development. Specifically, the SO_2 concentration observed in several Asian countries is relatively high. For example, at Langkawi Island, Malaysia, the concentration is 14 ppb (data from 1999–2011)[20] while in Lahore City, Pakistan, it is 19.11 ± 6.18 ppb.[21] For Longfengshan, Shangdianzi, Houma, Huaian, Lin'an, kaili,



Juan L. Obeso

Juan L. Obeso was born in Sinaloa, Mexico. He obtained a BSc in chemical engineering at Universidad Autónoma de Sinaloa in 2019 and an MS at Instituto Politécnico Nacional in 2021. He is currently a PhD student at Instituto Politécnico Nacional and Universidad Nacional Autónoma de México under the supervision of Prof. Ilich Ibarra. His research interests mainly focus on MOF synthesis, catalysis, adsorption, and detecting water and toxic pollutants.



Margarita Viniegra

She earned her PhD in Chemistry from the Universidad Autónoma Metropolitana (UAM) and completed a postdoctoral fellowship at the Institute of Physics at the Universidad Nacional Autónoma de México. Since 1982, she has served as a professor at UAM. Her research interests in heterogeneous catalysis focus primarily on transition metals and their oxides. In recognition of her teaching excellence, she was awarded the UAM-I Teaching Award in 2010. She has held several leadership roles, including Head of the Department of Chemistry, Coordinator of both Undergraduate and Graduate Studies, President of the Academy of Catalysis A.C., and President of the National Council for the Evaluation of Chemical Sciences Programs.



Michael T. Huxley

Michael Huxley was born in Adelaide, South Australia. He completed his undergraduate studies at The University of Adelaide, completing a PhD in Chemistry under the supervision of Prof. Christian Doonan and Prof. Christopher Sumby in 2018. Michael's research interests focus on catalysis in MOFs and elucidation of chemical processes within MOF matrices. He is presently an Associate Lecturer in chemistry at The University of Adelaide.



Diego Solis-Ibarra

Diego Solis-Ibarra obtained his Chemistry degree from UNAM in 2008 and completed his PhD in 2012 under the supervision of Prof. Vojtech Jancik. He conducted research stays at UC Santa Barbara and MIT before joining Stanford University as a postdoctoral researcher in Prof. Hemamala Karunadasa's group. In 2015, he returned to UNAM, where he is now an Associate Professor and serves as the Director of the Institute for Materials Research. His research focuses on hybrid materials for sensing, photovoltaics, and optoelectronics.

 This journal is © The Royal Society of Chemistry 2025

Open Access Article. Published on 10 March 2025. Downloaded on 6/30/2025 11:42:55 PM. This article is licensed under a Creative Commons Attribution 3.0 Unported Licence.

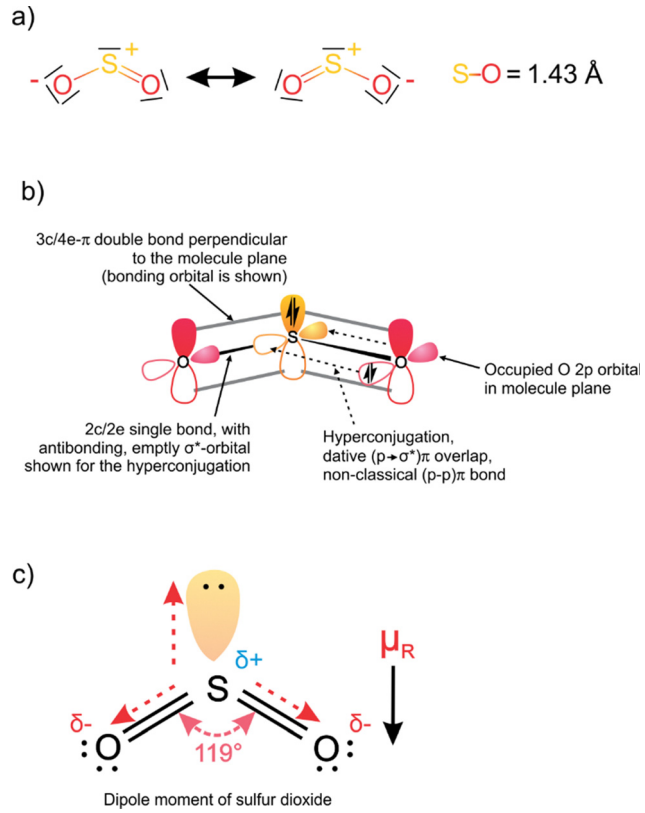


Fig. 1 (a) Valence bond resonance SO_2 structure, (b) scheme displaying the molecular orbital bonding model for SO_2, (c) SO_2 dipole moment.

Chenzhou, Meixian, Dianbai of China is 23.59 ± 23.97 ppb (data from 2010).[22] In rural sites in China is 21.06 ± 9.23 ppb (data from 2007–2008).[23] Furthermore, Mousavi *et al.*[24] reported an analysis of the SO_2 concentration arising from flares at the Maroon gas refinery located in the suburb of Ahvaz, Iran. It was found that the SO_2 concentration rises to 82.1 ppb during the cold season.

1.3 Industrial uses for SO_2 and existing capture technologies

SO_2 finds multifarious industrial uses. For example, the remarkable antiseptic and antioxidant properties of SO_2 have led to its frequent use as a food and beverage preservative,[25] particularly in winemaking, where it acts as an antimicrobial agent during the aging and storage of wine.[26] In the chemical industry, SO_2 is an intermediate in the production of sulfuric acid (H_2SO_4). The industrial synthesis of H_2SO_4 takes place by first transforming sulfur into SO_2 using O_2 as an oxidant, followed by the conversion of SO_2 into sulfur trioxide (SO_3) using vanadium and alkali oxides.[27] The resulting SO_3 is dissolved in 98 wt% H_2SO_4 solution to generate a 99.7 vol% H_2SO_4 solution.[28] SO_2 is also employed as a bleaching agent[29] and was a first-generation refrigerant due to its high heat of evaporation.[30]

Indeed, industrial demand for SO_2 and inadvertent emission from coal-fired power stations necessitates strict control for safety and environmental reasons. Considering the need to limit anthropogenic SO_2 emissions, significant investment has been expended toward SO_2 capture at point sources such as coal-fired power stations. The first SO_2 capture system, the spiral-tile packed tower, was developed in the early 1930s[31–33] but is highly inefficient due to the consumption of vast quantities of water during its operation. The process also produces large quantities of sulfuric acid contaminated water.[34]

SO_2 scrubbing, also known as flue-gas desulfurization (FGD).[35] FGD is employed using either a once-through or regenerative process. In the former, the spent sorbent (which is calcium sulfate) can be used in the construction industry or otherwise disposed. The regenerative process is more desirable because the sorbent is re-activated, and SO_2 is recovered for use in chemical industries. Despite this process being widely applied and largely successful in mitigating the worst impacts of acid rain, FGD systems still release significant quantities of SO_2 into the atmosphere.[36] Therefore, interest has been garnered by alternative processes such as the use of ceramic



Ilich A. Ibarra

Ilich Ibarra was born in Mexico City, Mexico in 1981. He completed a BSc in chemistry at UAM (Mexico) in 2005. In 2010 he obtained his PhD in Chemistry at Nottingham University (UK). He then took a postdoctoral position, in 2010, at UT Austin (USA). In 2013 he was awarded as a Wenner-Gren researcher at SU (Sweden). In 2020 he was awarded with the Young Investigators Award in Exact Sciences by the Mexican Academy of Sciences. In 2024 he was promoted as Full Professor at UNAM.



Christoph Janiak

Christoph Janiak is full professor for Nanoporous and Nanoscale Materials at the Heinrich Heine University of Düsseldorf since 2010, with research interests in the synthesis and properties of metal and porous organic frameworks (MOFs, COFs), mixed matrix membranes, metal nanoparticles, ionic liquids, and catalysis. He is currently an honorary professor at Wuhan University of Technology and guest professor at the Hoffmann Institute of Advanced Materials at Shenzhen Polytechnic University in China. He has (co-)authored about 730 research papers (H index 91) and is a Fellow of the Royal Society of Chemistry (FRSC).

Open Access Article. Published on 10 March 2025. Downloaded on 6/30/2025 11:42:55 PM. This article is licensed under a Creative Commons Attribution 3.0 Unported Licence.

hollow fiber membranes filled with various aqueous solutions to capture SO_2.[37–40] Finally, various 'wet-sulfuric acid' processes have been used extensively for sulfur removal since the 1980s,[41] motivated in part by the generation of valuable byproducts.[42]

1.4 Emerging technologies for SO_2 capture

The aforementioned processes generate large quantities of wastewater, corrode pipelines, impose significant economic costs, and leave residual traces of SO_2.[43] Thus, as an alternative, solid-state adsorbents have received growing interest. For example, zeolites and metal oxides have been investigated for SO_2 uptake.[44,45] Zeolites are widely used as adsorptive materials, ion exchangers, and catalysts.[46] Zeolites present attractive qualities in adsorption applications, including low-cost synthesis, relatively high surface area, microporosity, and thermal and mechanical stability.[47] However, zeolites exhibit drawbacks associated with their regeneration process. In some cases, the strong host–guest interaction between a zeolite and gas molecule invokes chemical bonding,[48] necessitating thermal activation (200 °C) under vacuum to regenerate the adsorbent and increasing operating costs.[49] Similarly, metal-oxides offer advantageous properties for adsorption applications but often form non-reversible interactions with gases of interest.[50]

Therefore, new porous materials have been investigated with a focus on sustainable development and real-world applications.[51,52] This includes a new generation of organic or hybrid organic–inorganic adsorbent materials such as metal–organic cages (MOCs),[53] porous organic cages (POCs),[54] and metal–organic frameworks (MOFs).[55] The latter are crystalline, typically microporous materials constructed from metal ions interconnected by organic linkers, forming two or three-dimensional coordination networks.[56,57] MOFs feature tunable physicochemical properties due to reticular design principles, narrow pore size distributions, high surface areas, and in some instances, chemical and thermal stability.[58,59] Their metal and linker building blocks allow the design of a tremendous range of different MOFs which can be tuned *via* reticular synthesis to suite specific applications. These properties have conferred significant advantages in adsorption,[60–63] catalysis,[64–66] drug delivery,[67,68] separation,[69,70] and proton conductivity[71,72] applications.

Only a limited number of chemically stable MOFs have so-far exhibited promising SO_2 adsorption properties. This paucity reflects the often-poor stability of coordination clusters – central to the structural integrity of MOFs – towards SO_2 exposure.[73] During adsorption, SO_2 molecules interact with MOFs *via* chemical or physical adsorption, depending on the nature of the binding sites available in the framework. The stability of MOFs towards SO_2 is dependent on the strength of the metal–ligand coordination bond (ranging between 300 kJ mol^{-1} to 600 kJ mol^{-1} for carboxylate linkers) and coordination number of the metal node.[74,75] Displacement of metal-linker bonds by SO_2 leads to decomposition of the MOF sorbent. Since linkers are classified as electron-donating species and metal ions are electron-accepting species,[76] Pearson's hard-soft acid–base (HSAB) concept provides a rationale for the stability of MOFs. Hard bases establish stronger bonds with hard acids and soft acids with soft bases.[77]

Based on these principles, a range of chemically stable MOFs have been synthesized and found to exhibit high SO_2 uptakes.[78] Chemical stability is, however, only one of the challenges facing chemists as they work to establish an industrial role for MOFs. Criticism frequently centers around the high cost of MOF linkers as well as the scalability of MOF synthesis, leading to questions about the economic feasibility of industrial-scale SO_2 capture (and that of other gases such as CO_2) using MOFs.[79] Indeed, the feasibility of adsorptive SO_2 capture with MOFs at scale remains uncertain. However, laboratory scale results for MOF-based SO_2 removal suggest that other applications that require smaller quantities of adsorbent, particularly SO_2 detection rather than capture, are promising avenues for MOF research.

1.5 Principals for SO_2 detection

Detecting a specific molecule relies on stimulating a specific response in the sensor, which, when measured, gives either a quantitative or qualitative measure of the concentration (or presence) of the analyte.[80,81] Since MOFs are naturally suited to sensing applications due to their intrinsic porosity and functional versatility, a wide range of MOF based sensing techniques have been envisaged.[82] These include MOF-based chemiresistive sensors,[83] luminescent sensors,[84] colourimetric sensors,[85] and magnetic sensors.[86] MOF-based chemo resistive materials are based on the change in resistance in response to a chemical surface reaction or adsorption of a guest molecule.[87] Sensors based on luminescence response employ the change in luminescence properties of certain MOFs, which generate a turn-on or, more often, turn-off fluorescence response.[88,89] Furthermore, some MOFs exhibit a characteristic shift in their emission wavelength(s) when exposed to specific molecules such as ammonia.[90] Colourimetric detection is used for simplicity and can be performed *via* visual analysis.[91] Additionally, the spin-crossover (SCO) effect has gained interest in the scientific community for its applications in magnetic sensors. In MOFs for instance, exposure to external stimuli such as temperature, pressure or magnetic field can induce measurable changes in the spin state of framework metal ions (typically Fe(II) framework nodes).[92,93] However, guest molecules can also induce a spin transition, which can be exploited for the purpose of detection.[94] These techniques have been combined to detect various small molecules, including organic solvents,[95] aqueous pollutants,[96] greenhouse gases,[97] and acidic solvents.[98] However, SO_2 detection has received limited attention.

Presently available SO_2 detectors employ an electrochemical system based on a solid polymer, usually polycarbonate. In such devices, an electrochemical reaction occurs, generating an electron in the working electrode, which produces an electrical current that is proportional to the SO_2 concentration. The SO_2 detection range is from 0 to 20 ppm with a response time of 30 s.[99,100] Such devices are frequently used in coal mines and the petroleum and chemical industries where SO_2 is encountered. However, drawbacks associated with existing SO_2 detectors,

 This journal is © The Royal Society of Chemistry 2025

Open Access Article. Published on 10 March 2025. Downloaded on 6/30/2025 11:42:55 PM.
This article is licensed under a Creative Commons Attribution 3.0 Unported Licence.

including interference from other gases, and sensitivity towards temperature and humidity fluctuations which lead to low sensitivity and accuracy.[101–103]

SO_2 detectors can be improved by introducing new solid-state materials with increased selectivity towards SO_2. Therefore, considering the promising SO_2 adsorption properties of MOFs, SO_2 detection is a logical next step. SO_2 tolerant MOFs have shown moderate to high SO_2 uptake. Intuitively, materials with a high SO_2 affinity – interpreted as evidence for an enhanced interaction between SO_2 and the MOF framework – could be promising candidates for detection applications.[104] To exploit this potential, it is necessary to understand the fundamental interactions between SO_2 molecules and the MOF. By transforming these host–guest interactions into measurable signals, the presence and, in some cases, concentration of SO_2 can be reliably determined. To meet this goal, researchers must draw on the vast wealth of research which has characterized the structure–property relationships of MOFs and optimized their mechanical and chemical stability – both crucial properties for real-world applications where MOFs are incorporated into functional devices. The accelerated development of MOFs to improve their properties for gas detection is crucial for building functional devices.

Thus, this review provides a comprehensive summary and analysis of MOF-based SO_2 detection strategies. To provide a suitable background, seminal examples of MOF-based detection of sulfur compounds other than SO_2 (and also in solution) are also provided. We emphasize the relationship between specific characteristics of porous materials (*i.e.*, surface area, pore volume, pore diameter, and functionalisation), which combine with the molecular properties of SO_2 to provide a means for reliable detection. The primary techniques with which SO_2 detection is studied in MOFs are discussed in detail. We aim to encourage further investigation into the exciting field of MOF-based environmental remediation and sensing applications.

2. MOFs for SO_2 capture

One of the primary purposes of this review is to explore existing – and postulate promising – MOF candidates for detecting SO_2. Therefore, the characteristic properties shared by MOFs that exhibit a high affinity towards SO_2 must be examined so that these desirable properties can be refined for SO_2 detection applications.

2.1 Main interactions of the SO_2 molecule within MOFs

The host–guest interaction between SO_2 molecules and MOFs provides a fundamental basis for understanding the application of MOFs in SO_2 detection. Considering the chemical diversity of MOF pores, it is necessary to establish the potential modes by which SO_2 can interact with adsorbents.

The adsorption of gases on surfaces is divided into two limiting processes: (i) physisorption, that is, physical adsorption, which displays weak gas–sorbent interactions comprising van der Waals forces, reversibility and a low heat of adsorption (<50 kJ mol^{-1}); and (ii) chemisorption, that is, chemical adsorption, which exhibits comparatively strong interactions characteristic of chemical bonding, a high heat of adsorption (>50 kJ mol^{-1}), and less facile reversibility.[105] From this point of view, SO_2 adsorption processes are governed by the chemistry of available adsorption sites within a MOF, which determines the type and strength of interactions.

Preferential adsorption sites within MOF structures (Fig. 2a) can include hydroxyl/amino groups, open metal sites (including defects and missing linkers), and halogen/methyl groups.[106] Thus, the extraordinary chemical diversity available in MOFs gives rise to a range of possible interactions with polar SO_2 molecules (Fig. 2b), including hydrogen bonding, direct coordination to framework metal ions, sulfur–halogen bonding, S–π interactions, and other electrostatic interactions.[107–109]

When coordinating to metal centres, such as open metal sites in MOFs, an SO_2 molecule can exhibit multiple binding modes that employ both oxygen and sulfur donors. Typical SO_2 coordination modes are summarized in Fig. 2c and include (i) η^1-SO_2, planar and S-bonded, (ii) η^1-SO_2, pyramidal and S-bonded, (iii) η^2-SO_2, both S and O-bonded, and (iv) η^1-SO_2, O-bonded.[111] These metal–SO_2 coordination modes have been exploited to improve SO_2 adsorption in MOFs at open metal centres.

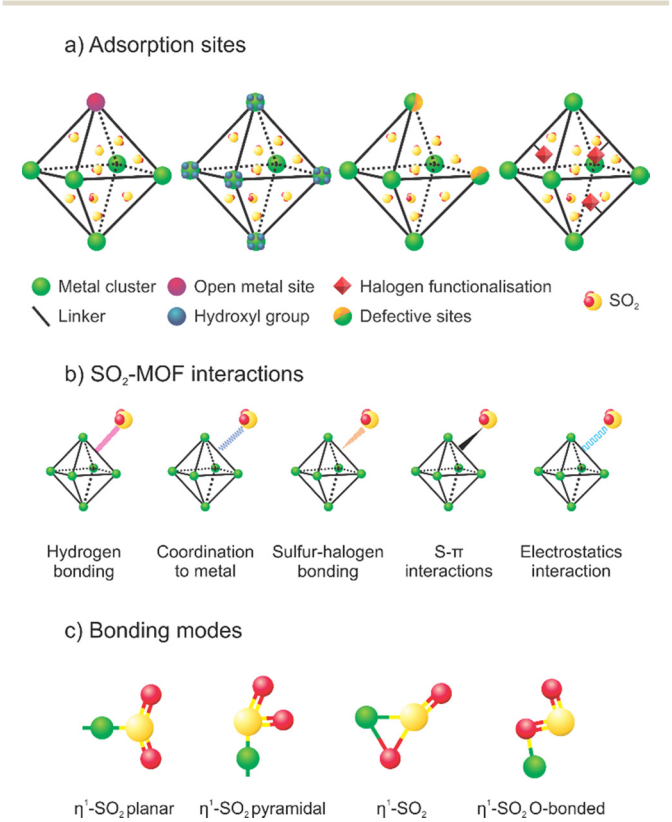


Fig. 2 (a) Main adsorption sites in MOF, (b) summary of possible SO_2–MOF interactions, and (c) metal bonding modes of the SO_2 molecule depicted schematically. Based on ref. 106,110.

Open Access Article. Published on 10 March 2025. Downloaded on 6/30/2025 11:42:55 PM. This article is licensed under a Creative Commons Attribution 3.0 Unported Licence.

Metal centres do not comprise the only sites with which SO_2 can interact within MOFs. Hydrogen bond donors are a common preferential adsorption site in MOFs, particularly in the form of hydroxyl and amine moieties. The hydroxido, hydroxo, or hydroxy group is an intrinsic characteristic of numerous MOFs bearing cluster-based SBUs, where, for instance, the μ-OH moieties bridge two or three metal centers.[112] Amino groups on the other hand are provided *via* suitably functionalized organic linkers.[113] The interaction between SO_2 molecules and hydroxy sites in a MOF was first directly identified in 2012 by Yang *et al.*[114] in NOTT-300(Al) (later renamed MFM-300(Al), linker BPTC)[115] using *in situ* powder X-ray diffraction (PXRD), inelastic neutron scattering, and grand canonical Monte Carlo (GCMC) simulations. The NOT-300(Al) structure features μ-OH groups, which bridge between Al(III) ions to form infinite 1D chains that extend along the MOF pores and are bridged by BPTC moieties. Comprehensive analysis revealed that SO_2 molecules engage in hydrogen bonds ($SO_2(O)\cdots H(OH)$ = 2.376(13) Å) with μ-OH sites (Fig. 3a), supported by complementary interactions with aromatic C–H sites of adjacent linkers. Five hydrogen bond interactions were observed between the host framework and bound SO_2. Furthermore, the SO_2 molecules bound to the framework interact *via* dipole–dipole $S\cdots O$ interactions ($S\cdots O$ = 3.34(7) Å) with secondary SO_2 molecules located within the MOF pore (Fig. 3b). A follow-up study published in 2020 established the long-term stability of NOT-300(Al) towards SO_2, NH_3, and NO_2. This study highlighted the capacity of diffraction techniques to precisely elucidate the interaction mechanisms behind SO_2 adsorption in robust, crystalline adsorbents.

MFM-300(Sc), which is isostructural to MFM-300(Al) (previously named NOT-300(Al) as described above), exhibits infinite 1D [Sc_2(μ-OH)] chains interconnected by BPTC moieties. SO_2 interactions were elucidated using GCMC simulations, which revealed that SO_2 molecules engage in hydrogen bonding with μ-OH sites situated along the inorganic node.[116] The indium analog MFM-300(In) displayed high selectivity for SO_2 over N_2, CH_4, and CO_2. *In situ* PXRD revealed similar behavior to that observed in MFM-300(Al): SO_2 occupies two adsorption sites. One molecule interacts with a bridging hydroxyl group [$SO_2(O)\cdots H(OH)$ = 3.17 Å] while at the same time, a second SO_2 molecule is supported in the MOF pore *via* dipole–dipole $S\cdots O$ interactions with the bound SO_2 molecule. Inelastic neutron scattering experiments probed the interaction between N_2, CO_2, and SO_2 gas molecules and μ-OH sites. A substantial shift in signals associated with wagging/bending modes of aromatic C–H bonds and bridging μ-OH sites was observed upon exposure to SO_2. A less significant shift was observed upon CO_2 adsorption, confirming that SO_2 adsorption is associated with stronger hydrogen bonding interactions with these framework sites.[117] Further spectroscopic evidence for the hydrogen bonding interaction was provided by monitoring the ν(OH) band at 3657 cm^{-1}. These studies validate the role of hydrogen bonding between SO_2 and inorganic hydroxyl sites and intermolecular SO_2–SO_2 interactions in stabilizing adsorbed SO_2 in robust MOFs.

Similar interactions have been described for various μ-OH bearing MOFs. For example, rigid MIL-53(Al)-TDC (TDC = 2,5-thiophenedicarboxylate) and the flexible MIL-53(Al)-BDC displayed this characteristic interaction.[118] DFT simulations were employed to probe the SO_2/MOF host–guest chemistry. SO_2 was observed to interact through hydrogen bonding with the μ-OH group of both MIL-53(Al)-TDC and MIL-53(Al)-BDC (with a mean $SO_2(O)\cdots H(OH)$ separation distance of 2.05 Å and 1.78 Å, respectively). The shorter hydrogen bonding interactions observed in the more flexible framework were related to adsorption-induced decrease in pore size in the flexible framework, facilitating stronger hydrogen bonding interactions. Multiple steps in the SO_2 adsorption isotherm supported this flexible behavior. Furthermore, the strong affinity for SO_2 molecules at the μ-OH site leads to a remarkable selectivity over a wide range of gases. Another framework bearing bridging μ-OH groups, DUT-4[119] (with the linker NDC), displays relatively high SO_2 adsorption (13.6 mmol g^{-1} – compared to 8.9 mmol g^{-1} for MIL-53(Al)-TDC and 0.8 mmol g^{-1} for MIL-53(Al)-BDC) at 298 K and 1 bar).[118] DFT studies show that SO_2 interacts with the μ-OH group and the linker (distance of 2.9 and 2.7 Å, respectively). The affinity towards the μ-OH group contributed to selective adsorption of SO_2 over CH_4. Furthermore, the μ-OH bearing framework, Mn-CUK with the linker PDCA = 2,4-pyridinedicarboxylate, contains a [$Mn_3(\mu_3\text{-OH})_2$] cluster and displays moderate SO_2 adsorption capacity (5.51 mmol g^{-1}) at 298 K and 1 bar.[120] Variable-temperature SCXRD studies suggested that SO_2 binds *via* hydrogen bonding with the μ_3-OH sites.

MIL-160 (with the linker FDCA = 2,5-furandicarboxylate) is a furan-based MOF with a moderate SO_2 uptake (7.2 mmol g^{-1}) at 293 K and 0.97 bar.[121] However, the framework displays high selectivity towards SO_2 over CO_2, CH_4, N_2, and H_2. The feasible binding sites for SO_2 in MIL-160 were identified by DFT calculations using geometry optimization of SO_2 within the pores (Fig. 4a–c). Three main interactions were found to occur between MIL-60 and SO_2: dipole–dipole bonding at furan oxygen sites ($SO_2(S)\cdots O$(furan) distance 3.27 Å), hydrogen

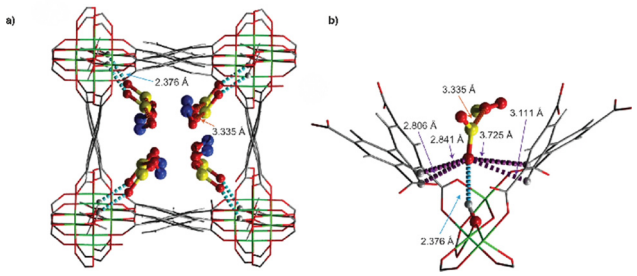


Fig. 3 (a) View of the crystal structure of NOTT-300·4.0-SO_2 obtained from Rietveld refinement of data on SO_2-loaded material at 1.0 bar. The adsorbed SO_2 molecules in the void are highlighted using a ball-and-stick representation. The sulfur atom of the second site of SO_2 is highlighted in blue. (b) Detailed view of the OH and CH contact with SO_2 molecules in a distorted pocket-like cavity. (Aluminum, green; carbon, grey; oxygen, red; hydrogen, white; sulfur, yellow.) (Reprinted (adapted) with permission from ref. 114 Copyright (2012) Springer Nature).

This journal is © The Royal Society of Chemistry 2025

Open Access Article. Published on 10 March 2025. Downloaded on 6/30/2025 11:42:55 PM. This article is licensed under a Creative Commons Attribution 3.0 Unported Licence.

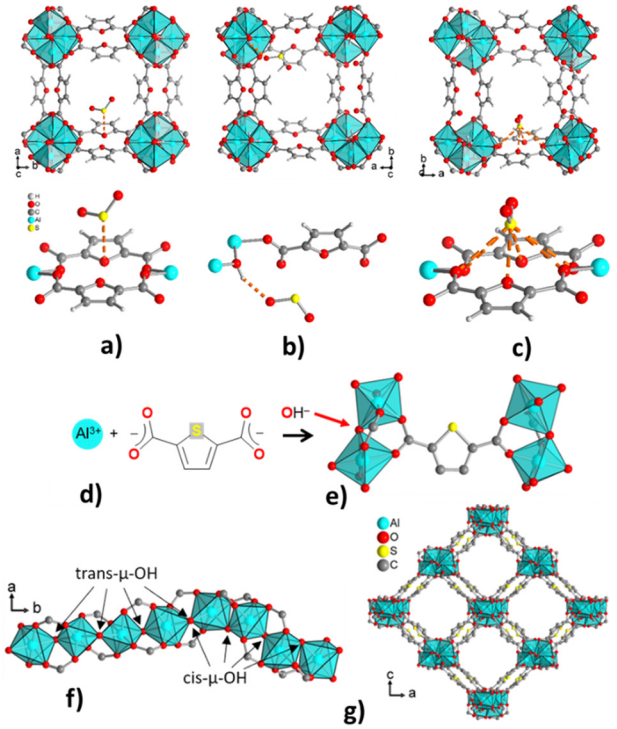


Fig. 4 DFT-simulated binding sites of SO_2 in MIL-160. (a) $O_{furan}\cdots S_{SO_2}$ interaction, (b) $OH_{Al\text{-}chain}\cdots O_{SO_2}$ interaction, and (c) $O_{furan/carboxylate}\cdots S_{SO_2}$ interaction. (Reprinted with permission from ref. 121 Copyright (2019) American Chemical Society). Crystal structure of CAU-23: (d) Al^{3+}, 2,5-thiophenedicarboxylate (TDC^{2-}) and hydroxide ions as building blocks, (e) TDC^{2-} linker coordination to {AlO_6} octahedra, (f) chains composed of alternating segments of four helical *cis*- and four *trans*-corner sharing {AlO_6} octahedra, (g) section of the packing diagram with the {AlO_6} chains connected by the TDC^{2-} linkers to yield square-shaped channels. (Reprinted with permission from ref. 122 Copyright (2022) with permission from John Wiley & Sons).

bonding at μ-OH ($SO_2(O)\cdots H(OH)$ distance 2.10 Å), and finally, dipole–dipole bonding between SO_2 and two furan units (distances of 3.15 and 3.36 Å). The short $SO_2(O)\cdots H(OH)$ hydrogen bond contact implies a high affinity between SO_2 and the hydroxyl sites which contributes to the outstanding selectivity toward SO_2.

Similarly, CAU-23 (with the linker TDC) displays *cis* and *trans*-μ-OH sites in the inorganic building unit (Fig. 4d–g) and has been evaluated for gas sorption properties.[122] CAU-23 shows a relatively high SO_2 adsorption capacity (8.4 mmol g^{-1}, at 1 bar and 293 K) and low CO_2 and CH_4 adsorption capacity (3.97 mmol g^{-1} and 0.89 mmol g^{-1}, respectively, all at 1 bar and 293 K). Moreover, the presence of *cis* and *trans*-μ-OH groups imparts a high affinity towards polar SO_2 molecules over CO_2, H_2, and CH_4. Further to the behavior described above, adsorbed SO_2 can also interact favorably with the π-system and S atom from the linker.

Coordinatively unsaturated sites can be generated in MOFs at the framework nodes when coordinated solvent (*i.e.*, water) is dissociated during thermal activation, leaving behind an accessible Lewis acidic metal site.[123,124] This attribute has drawn considerable interest in the adsorption and catalysis fields.[125,126] M-MOF-74 (with the linker DHTP = 2, 5-dihydroxyterephthalate) (M = Zn and Mg) is one such material and displays strong interactions between adsorbed SO_2 and open metal sites generated during activation.[127] Using *in situ* infrared spectroscopy and *ab initio* DFT calculations, the first preferential adsorption site was identified as a direct $SO_2(O)$–M interaction. Another MOF, MFM-170, features well-defined Cu(II) sites which also interact directly with SO_2. MFM-70 consists of a $[Cu_2(O_2CR)_4]$ (O_2CR = 4′,4‴-(pyridine-3,5-diyl)bis([1,1′-biphenyl]-3,5-dicarboxylate) dimer with four linker carboxylate moieties occupying the equatorial sites and one linker *N*-pyridyl donor coordinating to one of the two axial sites of the dimer (the second being available for guest coordination).[128] This available Cu(II) coordination site facilitates reversible SO_2 capture, while the structure remains stabile even towards exposure to wet SO_2. Using *in situ* SCXRD, FTIR microspectroscopy, and inelastic neutron scattering, the open Cu(II) sites were confirmed to act as $SO_2(O)$–Cu adsorption sites. The Cu(II) framework, MFM-190 (linker: 5,5′-(pyridine-2,5-diyl)diisophthalate), also exhibits open Cu^{2+} sites which form the primary adsorption site for SO_2.[129] Furthermore, an S–π interaction was observed between SO_2 and delocalized π systems of the two neighboring phenyl rings. *In situ* neutron powder diffraction, inelastic neutron scattering, and synchrotron infrared microspectroscopy studies revealed the location of host–guest binding. The MOF MIL-101(Cr)-4F(1%) is a partially fluorinated MOF from the MIL-101(Cr) family. This Cr(III)-based MOF was synthesised by mixing BDC and 2,3,5,6-tetrafluoro-1,4-benzenedicarboxylate (BDC-4F), thereby doping the structure with fluorine (MIL-101(Cr)-4F(1%) = $[Cr_3O(BDC)_{2.91}(BDC\text{-}F4)_{0.09}]Cl$).[130] The presence of fluorine modulates the pore-surface electron density leading to considerably improved SO_2 capture due to the enhanced dipole–dipole interactions with the pore surface.

Defect sites in MOFs – such as missing linker or missing cluster defects, which are prominent in Zr(IV) frameworks, among many others[131,132] – are correlated with a decrease in the chemical stability of the framework but provide new interaction sites for adsorbate molecules, including SO_2.[133] The MOF $[Ni_8(OH)_4(H_2O)_2(BDP_X)_6]$,[134] (where H_2BDP_X = 1,4-bis(pyrazol-4-yl)benzene-X with X = H (1), OH (2), NH_2 (3)) (Fig. 5a), was post-synthetically modified by placing the material in ethanolic solutions of potassium hydroxide to generate the defect rich frameworks $K[Ni_8(OH)_3(EtO)_3(BDP_X)_{5.5}]$ (1@KOH, 3@KOH) and $K_3[Ni_8(OH)_3(EtO)(BDP_O)_5]$ (2@KOH). The defective frameworks were soaked in aqueous $Ba(NO_3)_2$, leading to exchange of extra-framework potassium ions for Ba(II), giving $Ba_{0.5}[Ni_8(OH)_3(EtO)_3(BDP_X)_{5.5}]$ (1@$Ba(OH)_2$, X = H; 3@$Ba(OH)_2$, X = NH_2), and $Ba_{1.5}[Ni_8(OH)_3(EtO)(BDP_O)_5]$ (2@$Ba(OH)_2$). The logical basis for this extensive post-synthetic modification was to imbue the defective frameworks with a greater capacity to interact with SO_2. Possible SO_2 interactions were evaluated by DFT calculations (Fig. 5b–e). The preferential SO_2 adsorption sites in 1@$Ba(OH)_2$ are the crystal defects where SO_2 coordinates in a bidentate fashion with Ba(II) ions. This is contrasted with 1@KOH wherein SO_2 coordinates through a

Open Access Article. Published on 10 March 2025. Downloaded on 6/30/2025 11:42:55 PM. This article is licensed under a Creative Commons Attribution 3.0 Unported Licence.

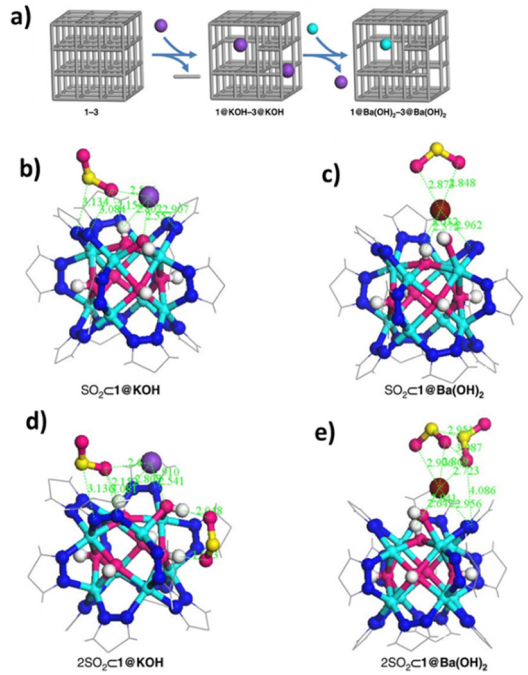


Fig. 5 (a) Schematic representation of the successive post-synthetic modifications, from pristine nickel pyrazolate $[Ni_8(OH)_4(H_2O)_2(BDP_X)_6]$ (H_2BDP_X = 1,4-bis(pyrazol-4-yl)benzene-4-X with X = H (1), OH (2), NH_2 (3)) frameworks to yield the missing linker defective $K[Ni_8(OH)_3(EtO)_3(BDP_X)_{5.5}]$ (1@KOH, 3@KOH) and $K_3[Ni_8(OH)_3(EtO)(BDP_O)_5]$ (2@KOH) and subsequently, the ion-exchanged $Ba_{0.5}[Ni_8(OH)_3(EtO)_3(BDP_X)_{5.5}]$ (1@$Ba(OH)_2$, X = H; 3@$Ba(OH)_2$, X = NH_2), and $Ba_{1.5}[Ni_8(OH)_3(EtO)(BDP_O)_5]$ (2@$Ba(OH)_2$) materials. Organic linker (grey bar), potassium (purple), barium (cyan). Sulfur dioxide interaction with crystal defect sites. DFT structure minimization of the molecular configuration of one (b) and (c) and two (d) and (e) adsorbed SO_2 molecules on 1@KOH (left) and 1@$Ba(OH)_2$ (right) materials. (Reprinted (adapted) with permission from ref. 134 Copyright (2017) Springer Nature under a Creative Commons CC BY license).

less favourable monodentate mode with potassium ions. Ba(II) ions are therefore associated with enhanced interactions between SO_2 and the framework. The formation of missing linker defects, where hydroxide displaces framework linkers, also contributes since the hydroxyl moieties interact favorably with SO_2. Thus, this novel defect engineering methodology facilitated improved adsorption performance by producing defect sites with a high affinity towards SO_2 and improving the accessibility of the framework to sorbate due to the presence of missing linker defects.[134,135]

Finally, the installation of halogen atoms on organic linkers can enhance the gas capture performance of MOFs. For example, the HHU-2-X (X = Cl, I, and Br) family are halogen functionalized MOF-801 derivatives, which are composed of halofumarate linkers which bridge 12-connected $[Zr_6O_4(OH)_4]$ clusters.[136] These materials display moderate SO_2 uptake compared to pristine MOF-801 which shares the same *fcu* topology but an unfunctionalized fumarate linker. HHU-2-Cl for instance displayed an SO_2 adsorption capacity of 9.69 mmol g^{-1} at 296 K and 1 bar, while MOF-801 reaches only 8.00 mmol g^{-1} at 296 K and 1 bar. Halogen functionalisation increases the polarity of the MOF pores, improving the affinity towards polar SO_2 molecules over CO_2.

Thus, it is evident that the chemical functionality of MOFs directly affects their SO_2 affinity by modulating the SO_2 interaction mechanism. Preferential SO_2 adsorption sites range from μ-OH moieties involved in hydrogen bonding to coordinatively unsaturated metal centres where coordination chemistry can take place.[117,120] The studies highlighted so far have focused on SO_2 adsorption at relatively high pressure (1 bar). However, systems that detect SO_2 must possess strong and selective affinity towards the gas at much lower pressures.

2.2 Selective capture of SO_2 in MOFs

An important consideration for the effective MOF-based detection of SO_2 is high selectivity. The modular nature of MOFs provides opportunities to tune their frameworks *via* the incorporation of specific functional groups that preferentially interact with SO_2 over other molecules. One of the earliest investigations into selective SO_2 adsorption in MOFs was reported in 2008 by Britt *et al.*[137] Using kinetic breakthrough measurements the authors calculated the dynamic SO_2 adsorption capacity of MOF-5, IRMOF-3, MOF-74, MOF-177, MOF-199, and IRMOF-62. Remarkably, the pore functionality (*i.e.*, unsaturated metal sites and amino functionality) was found to play a dominant role in determining the dynamic SO_2 adsorption performance. Later, it was reported that the incorporation of urea within Zn(II)-based MOFs (achieved using the linker 6-oxo-6,7-dihydro-5*H*-dibenzo[*d*,*f*][1,3]diazepine-3,9-dicarboxylate),[138] provided enhanced hydrogen-bonding interactions with SO_2 over other gas molecules such as CO_2.

Savage *et al.*[117] demonstrated the utility of the hydroxo functional group (–OH) in promoting high SO_2 selectivity in MFM-300(In). The material exhibited remarkable selectivity (SO_2/CO_2 60, SO_2/CH_4 425, and SO_2/N_2 5000) under ambient conditions (*i.e.*, 50 : 50 mixture at 1 bar and 298 K). The origin of this behavior was investigated by combining crystallographic and spectroscopic techniques including inelastic neutron scattering; which revealed that enhanced supramolecular binding interactions – especially hydrogen bonding by the –OH functional group – are directly responsible for observed affinity towards SO_2. Using *in situ* synchrotron X-ray diffraction experiments, the same authors established the role of μ_3-O and μ_3-OH functional groups in the remarkable SO_2/CO_2 and SO_2/N_2 selectivity observed in MFM-601 (with the linker PPTA = 4,4′,4″,4‴-(1,4-phenylenebis(pyridine-4,2,6-triyl))tetrabenzoate).[139] The dipole moment of SO_2 interacts favorably with the μ_3-O and μ_3-OH groups within the pores of MFM-601, which explains the affinity between MFM-601 and polar SO_2 over non-polar CO_2 or N_2. MIL-160 is an Al(III)-based MOF which also exhibits high SO_2 uptakes at low pressures ($p < 0.01$ bar) and a remarkable selectivity towards SO_2 over CO_2 due to the presence of furan moieties which provide preferential binding sites for SO_2(O(furan)$\cdots$S(SO_2)).[121] Recently, the SO_2/CO_2 selectivity of NH_2-MIL-101(Cr), Basolite F300 (Fe-1,3,5-BTC), HKUST-1, ZIF-8 and ZIF-67 was evaluated in comparison to non-MOF

 This journal is © The Royal Society of Chemistry 2025

Open Access Article. Published on 10 March 2025. Downloaded on 6/30/2025 11:42:55 PM. This article is licensed under a Creative Commons Attribution 3.0 Unported Licence.

adsorbents Zeolite Y, SAPO-34, silica gel 60 and CTF-1,[140] concluding that Zeolite Y and CTF-1(600) showed the most promising SO_2/CO_2 selectivity results with an ideal adsorbed solution theory selectivity in the range of 265–149 and 63–43 with a mole fraction of 0.01–0.5 SO_2 at 293 K and 1 bar.

Using solid-state cationexchange, Mon *et al.*[141] post-synthetically modified a Ni(II)-based MOF (with the linker MPBA = *N*,*N*′-2,4,6-trimethyl-1,3-phenylenebis(oxamate)) to increase its N_2/SO_2 selectivity considerably. By soaking the MOF crystals in a saturated aqueous solution of $Ba(NO_3)_2$ for 48 hours, Ni(II) ions hosted within the framework were exchanged for hydrated Ba(II) ions. Using X-ray crystallography and theoretical calculations the authors identified that the hydrated barium cations act as preferential adsorption sites for SO_2. Then, Chen *et al.*[142] observed high SO_2/CO_2 selectivity (325) and ultrahigh selectivities for SO_2/N_2 ($>1.0 \times 10^4$) and SO_2/CH_4 ($>1.0 \times 10^4$) in M-gallate MOFs, which was attributed to particularly favourable pore apertures and chemical functionality. In a similar vein, excellent SO_2/CO_2 selectivities have been achieved by optimising the pore aperture to approximate the size of SO_2. For instance, by modulating methyl group densities at the benzenedicarboxylate linker in $[Ni_2(BDC\text{-}X)_2DABCO]$ (BDC-X = mono-, di-, and tetramethyl-1,4-benzenedicarboxylate/terephthalate; DABCO = 1,4-diazabicyclo[2,2,2]octane) the pore size can be precisely tuned.[143] Indeed, the highly selective SO_2 adsorption by these methyl-functionalized DMOFs was accredited to the numerous non-covalent interactions between the small methyl-functionalized pore and SO_2 molecules, which was revealed by DFT calculations (this work is described in further detail below). This strategy was also investigated in ECUT-77, a Co(II)-based MOF composed of 4-(4*H*-1,2,4-triazol-4-yl)benzoate linkers, which exhibits a SO_2/CO_2 selectivity of 44 due to its small pore aperture (approximately 3 Å).[144]

Thus, as outlined above, by tuning the MOF pore aperture and allocating appropriate chemical functionality to the molecular components,[145] high SO_2 selectivities can be achieved.[146] Indeed, SO_2 adsorption based applications benefit significantly from the modular and chemically mutable nature of MOFs.[147]

2.3 Low-pressure capture of SO_2 in MOFs

Considering that concentration intervals for SO_2 detection are at the ppm level (or sometimes even the ppb level depending on the application), it is SO_2 adsorption in the low-partial pressure range that is of interest. Thus, total SO_2 uptake at ambient pressure becomes irrelevant. Instead, the most important metric for MOFs intended for SO_2 detection applications is SO_2 adsorption capacity at low pressure ($p \ll 0.1$ bar). For example, after scrubbing, SO_2 concentrations in flu gas lie between 150–450 ppm, corresponding to a shallow partial pressure (0.0005 bar)[148] and trace concentrations in the atmosphere can be considered to be under 1000 ppm. That is, SO_2 exerts a partial pressure of around 0.001 bar.[149] Ideally, a MOF should exhibit high SO_2 adsorption and affinity in a pressure range from 0.001 to 0.05 bar to be considered a candidate for SO_2 detection. Furthermore, high selectivity towards SO_2 over other atmospheric gases such as O_2, NO_x, CH_4, and CO_2 is vital. This low-pressure range could be ideal for SO_2 detection since only a few SO_2 molecules interact with the adsorption sites within the material.[60]

Some specific factors which influence SO_2 uptake in MOFs at low pressure include the SO_2 interaction mechanism and affinity (as described above) and the physical properties of MOFs, particularly the pore diameter. Indeed, the pore limiting diameter (PLD), the smallest diameter of a pore or window present in a framework, pore volume, and chemical functionalization thereof can directly influence the low-pressure SO_2 adsorption capacity. These effects can be elucidated experimentally by comparing the adsorption behavior of MOFs with diverse physicochemical properties.

In a comparative study the MOF-based (NH_2-MIL-101(Cr), Basolite F300(Fe-1,3,5-BTC), HKUST-1, ZIF-8 and ZIF-67) non-MOF-based adsorbents (Zeolite Y, SAPO-34, silica gel 60 and CTF-1, and Basolite F300) were investigated on account of their small pore diameters.[140] The prototypical MOFs listed above possess a robust structure and high chemical stability, which make them feasible for real-world applications, including gas adsorption/detection. However, ZIF-8 and ZIF-67 show low SO_2 adsorption capacity under the same conditions, which was attributed to their pore window diameter (3.4 Å) being smaller than the kinetic diameter of SO_2 (4.1 Å).[140] Thus, below the gate-opening pressure (0.3 bar), SO_2 cannot enter the pore, which significantly retards the low-pressure adsorption capacity. At 0.01 bar, the highest uptakes were 5.0 mmol g^{-1} for Zeolite Y, 2.2 mmol g^{-1} for CTF-1(400), 2.0 mmol g^{-1} for HKUST-1, and 1.9 mmol g^{-1} for SAPO-34. HKUST-1 displays the highest SO_2 adsorption at 0.1 bar among these materials (10.1 mmol g^{-1} at 293 K).[140] The outstanding performance of HKUST-1 is attributed to the presence of open metal sites in combination with an optimal PLD (5–11 Å).[123,150] The highest affinity towards and uptake of SO_2 at low partial pressures (0.01–0.1 bar) were registered for materials featuring pore diameters of ≈4–8 Å (Fig. 6) and aromatic nitrogen atoms (*i.e.*, CTF frameworks).[140]

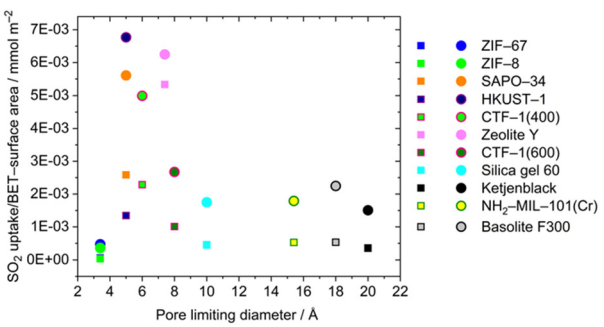


Fig. 6 Surface specific SO_2 at 0.01 bar (squares) and 0.1 bar (circles) *vs.* the pore limiting diameter. For silica gel 60, CTF-1, and Ketjenblack, only the smallest pore diameter is indicated, and these materials have a broad pore size distribution. (Reprinted with permission from the author of ref. 140 Copyright (2021) John Wiley & Sons under the Creative Commons CC-BY-NC-ND license).

Open Access Article. Published on 10 March 2025. Downloaded on 6/30/2025 11:42:55 PM. This article is licensed under a Creative Commons Attribution 3.0 Unported Licence.

Dispersion forces between a gas molecule and the pore surface are optimized when the pore diameter (defined by the Connolly surface, which is the accessible surface for a probe molecule of given size) approximates the length of the gas molecule. As alluded to above, an optimal pore aperture for SO_2 at low pressure is in a range from ≈4–8 Å. The upper limit of this range (∼8 Å = 2 × 4 Å) is approximately double the length of an SO_2 molecule and arises due to favorable dipole–dipole interactions between two SO_2 molecules bound to adjacent pore walls.[151]

Data presented in Table 1 substantiates these points. These findings support the prioritization of frameworks that feature an optimal PLD (4–8 Å), which can significantly improve SO_2 uptake at low pressure range pertinent to detection applications.

The family of isostructural M-gallate MOFs (M = Mg, Co, and Ni) exhibit record SO_2 adsorption at low pressure (0.002 bar).[142] The pore structure within these MOFs displays three-dimensional interconnected zigzag channels with a size again approximating the kinetic diameter of SO_2 (Fig. 7a–g), leading to solid confinement of SO_2. The Co, Mg, and Ni derivatives exhibit SO_2 adsorption capacities of 3.99, 4.65, and 2.67 mmol g^{-1}, respectively, at 0.002 bar and 298 K. DFT calculations indicate that the synergistic combination of hydrogen bonding interactions involving SO_2 and the unique microstructure of the MOF pores directly contribute to the high SO_2 uptake observed at low pressure.

Based on the idea that an ideal PLD can significantly enhance low-pressure SO_2 capture, the pore environment of a Ni(II)-based MOF, Ni_2(BDC-X)$_2$DABCO (X = mono-, di- and tetramethyl) was systematically modified *via* methylation to modulate the low-pressure SO_2 adsorption properties (Fig. 8).[143] In this case, four homologous MOFs were compared, where different methyl functionalization was introduced: the parent MOF (DMOF) as well as reticular frameworks composed of BDC based linkers substituted with one (M), two (DM) or four (TM) methyl groups. The BDC-TM framework (DMOF-TM) displayed the greatest low pressure SO_2 uptake (3.79 mmol g^{-1} at 293 K and 0.01 bar). This was attributed to increased steric hindrance and hydrophobicity arising from the extensive methyl substitution, leading to changes in the physicochemical properties of the framework, particularly the pore aperture.[143] Notably, the SO_2 capacity at 0.97 bar decreased with greater methyl substitution due to the systematic decrease in pore volume and BET (Brunauer–Emmett–Teller) surface area. The excellent low-pressure SO_2 adsorption capacity conforms to the expected relationship between PLD and low-pressure adsorption capacity since DMOF-TM exhibits a PLD value of ≈4.5 Å (close to the kinetic diameter of SO_2) and high uptake at low pressure (in contrast to the other methyl-DMOFs). When confined within pores that approximate the SO_2 kinetic diameter, the SO_2 molecules engage in extensive dispersion interactions with the pore surface, leading to enhanced uptake.[187,188]

2.4 Relationship between low and high-pressure SO_2 adsorption and in the textual properties of MOFs

As mentioned above, different framework properties influence SO_2 capture at low and high pressures. The results described so far indicate that BET surface area and the pore volume are the main factors contributing to high SO_2 adsorption capacity at high pressure. Fig. 9 presents the relationship between BET surface area (Fig. 9a) and pore volume (Fig. 9b) with total SO_2 uptake at 1 bar. The data indicates that MOF-808, MIL-100(Al), and NH_2-MIL-101(Al) display high SO_2 uptakes in this pressure regime due to their high surface areas. This effect is related to their micro and mesopore distribution, which improves the SO_2 uptake for MIL-100(Al) and NH_2-MIL-101(Al), associated with the large BET surface area.[151] The framework NU-1000 exhibits a mixture of micro and mesopores (∼12 and ∼29 Å) and is an outlier in the surface area/pore volume relationship observed in other frameworks (Fig. 9b). It is known that saturation is not achieved under these experimental conditions (at 1 bar and room temperature).[154] The pore volume represents a limit for the maximum SO_2 capacity for a MOF.[189] Zr-fum and NH_2-MIL-53(Al) show a low SO_2 uptake associated with the low surface area and pore volume. These results clearly illustrate the effect of surface area and pore volume on SO_2 uptake at higher pressures.

However, unlike high-pressure SO_2 adsorption, SO_2 uptake within the low-pressure range is unrelated to surface area and pore volume. Instead, the uptake at low pressure correlates with the affinity between SO_2 and the MOF pore surface. This can be mediated by chemical functionalization and/or by tuning the pore diameter using reticular synthesis techniques. Pore diameters only slightly larger than the 4.1 Å kinetic diameter of the SO_2 molecule afford high-affinity interactions at low pressure. A clear correlation can be observed by plotting the surface-specific uptake at 0.1 bar divided by the BET surface area against PLD (Fig. 9c).[190] As discussed above, pore diameter in the ∼4 and 8 Å range is optimal for high SO_2 uptake at low pressure, which correlates well with the SO_2 kinetic diameter (4.1 Å) and is supported by GCMC simulations. A PLD size within this range optimizes dispersive interactions between adsorbed SO_2 molecule and the pore surface.

To supplement this discussion, SO_2 adsorption capacities at pressure increments between 0.01 and 1 bar are summarized in Table 1 in conjunction with crucial framework metrics, including surface area, pore diameter, and pore volume. As expected from the points elaborated on above, this data confirms a relationship between the physical metrics of MOF pores and the observed SO_2 uptake. For example, as the BET surface area (Fig. 10a) and pore volume (Fig. 10b) increase, so does SO_2 adsorption capacity at 1 bar. For instance, MFM-101 exhibits a high BET surface area (2300 m^2 g^{-1}) and an outstanding adsorption capacity (18.7 mmol g^{-1}) at 1 bar and 298 K.[129] UR3-MIL-101(Cr) shows a BET surface area of 1900 m^2 g^{-1} and SO_2 capture of 13.9 mmol g^{-1} at 1 bar and 293 K.[158] MFM-422 shows a BET surface area of 3296 m^2 g^{-1} and SO_2 capture of 13.6 mmol g^{-1} at 1 bar and 298 K.[171] Ni(BDC)(TED)$_{0.5}$ displays a BET surface area of 1783 m^2 g^{-1} and SO_2 capture of 9.97 mmol g^{-1} at 1 bar and 293 K.[183] In the case of pore volume, CB6@MIL-101-Cl displays a high pore volume of 1.0 cm^3 g^{-1} with the uptake of 17.0 mmol g^{-1} at 1 bar and 298 K.[157] MIL-53(Al) with a high volume of 0.706 cm^3 g^{-1} and uptake of 10.5 mmol g^{-1} at 1 bar, and

 This journal is © The Royal Society of Chemistry 2025

Open Access Article. Published on 10 March 2025. Downloaded on 6/30/2025 11:42:55 PM. This article is licensed under a Creative Commons Attribution 3.0 Unported Licence.

Table 1 Comparison of SO_2 adsorption in MOFs

Material	BET SA ($m^2\ g^{-1}$)	V_p ($cm^3\ g^{-1}$)	Pore diameter (Å)	SO_2 uptake (mmol g^{-1}) at different pressure (bar) 0.01	0.05	0.1	1	T (K)	Ref.
NH_2-MIL-101(Cr)	2290	1.16	15.4	1.2	2.9$^+$	4.1	16.7	293	140
Fe(BTC)	1070	0.49	18	0.6	1.5$^+$	2.4	9.5	293	
ZIF-8	1820	0.80	3.4	0.1	0.4$^+$	0.7	8.2	293	
ZIF-67	1980	0.69	3.4	0.1	0.5$^+$	0.9	11.0	293	
HKUST-1	1490	0.61	5	2.0	7.2$^+$	10.1	13.8	293	
HKUST-1	1400					3.86	8.4	298	152
$YIL_{0.5}$@HKUST-1						5.10	7.54	298	
$PIL_{0.5}$@HKUST-1						5.15	7.73	298	
$HIL_{0.5}$@HKUST-1						5.45	8.06	298	
HIL_1@HKUST-1	600					5.71	8.33	298	
MOF-177	4100	1.51	10.6	0.3	0.5$^+$	1.0	25.7*	293	121
NH_2-MIL-125(Ti)	1560	0.651	5	3.0	4.95$^+$	7.9	10.8	293	
MIL-160	1170	0.460	5	4.2	4.8$^+$	5.5	7.2	293	
Zr-Fum	600	0.290	4.8	1.2	2.4$^+$	3.1	4.9	293	151
MOF-808	1990	0.749	4.8	2.1	2.9$^+$	3.6	14.6	293	
DUT-67(Zr)	1260	0.544	8.8	0.7	1.55$^+$	2.3	9.0	293	
NH_2-MIL-53(Al)	620	0.358	7.3	2.0	3.7$^+$	4.3	8.0	293	
Al-Fum	970	0.447	5.8	1.0	3.1$^+$	4.1	7.5	293	
CAU-10-H	600	0.258	6	1.2	3.1$^+$	3.7	4.8	293	
MIL-96(Al)	530	0.237		1.2	2.2$^+$	3.7	6.5	293	
MIL-100(Al)	1890	0.824	25	0.4	1.4$^+$	2.5	16.3	293	
NH_2-MIL-101(Al)	1770	1.001	25	1.5	2.7$^+$	3.6	17.3	293	
NU-1000	1740	1.196	12	0.6	1.5$^+$	2.6	12.2	293	
NU-1000	1970					2.1	10.9	298	153
[Ir]@NU-1000.	1842					2.4	10.6	298	
[RuGa]@NU-1000	1796			0.5		2.2	7.5	298	154
MIL-53(Al)-BDC	1450	0.706	8.5	0.4	2.45$^+$	3.3	10.5	293	151
MIL-53(Al)-BDC	1210	0.51	8.5		0.65	0.95	10.8	298	118
MIL-53(Al)-TDC	1000	0.415	8	0.6	3.6$^+$	5.0	6.9	293	151
MIL-53(Al)-TDC	1260	0.45	8		4.7		8.9	298	118
DUT-67-HCl	1349	0.509	6			3.0$^+$	9.3	298	155
DMOF	1956	0.76	7	0.25	0.9$^+$	7.21	13.09	293	143
DMOF-M	1557	0.63	7	0.46	1.8$^+$	6.40	12.15	293	
DMOF-DM	1343	0.52	7	1.0	3.0$^+$	5.70	10.40	293	
DMOF-TM	900	0.43	6	3.79	5.1$^+$	6.43	9.68	293	
HHU-2-Cl	852	0.41		2.9$^+$	3.6$^+$	4.5$^+$	9.69	293	136
HHU-2-Br	620	0.31		1.7$^+$	2.3$^+$	3.0$^+$	6.07	293	
MOF-801	939	0.43		2.1$^+$	2.9$^+$	3.9$^+$	8.00	293	
nanoCB6-H	441	0.22	6	2.3$^+$	2.9$^+$	3.4$^+$	4.98	293	156
MIL-101	3217	1.54	29	0.6	1.5$^+$	4.4$^+$	24.4	298	157
CB6@MIL-101-Cl	2077	1.0		2.0	3.0$^+$	5.2$^+$	17.0	298	
UR1-MIL-101(Cr)	1700	0.98		0.9$^+$	1.8$^+$	2.7$^+$	8.2	293	158
UR2-MIL-101(Cr)	1360	0.82		1.3$^+$	1.7$^+$	2.4$^+$	6.9	293	
UR3-MIL-101(Cr)	1900	0.96		1.8$^+$	2.9$^+$	4.0$^+$	13.9	293	
UR4-MIL-101(Cr)	1340	0.68		1.3$^+$	2.4$^+$	3.3$^+$	11.0	293	
CAU-23	1176	0.51	7.6	0.9$^+$	4.5$^+$	6.0$^+$	8.4	293	122
CCIQS-1	398		4.2				1.3	298	159
Bz@InOF-1						5.4	6.3	298	160
CAU-10	630	0.25	7			3.9	4.47	298	161
Co-URJC-5	233		8.9		0.8		1.48*	298	162
DUT-4	1348	0.71	8		2.4	5.1	13.6	298	119
SU-101	412		6.8				2.2	298	163
MFM-300(Sc)	1360	0.56	8.1		7.0		9.4	298	116
UNAM-1	522		7.3		1.1		3.5	298	164
MIL-101(Cr)-4F(1%)	2176	1.19				4.6	18.4	298	130
NiBDP	1220		9	1.52			8.48	298	165
IL/MIL-0.7	3	0.14		1.68		4.87	13.17	298	166
HBU-23	384.2		6.8				2.42	298	167
HBU-20	1551.1		7.0				6.71	298	145
ECUT-100	688	0.27	5.5				4.95	298	168
DUT-5	1611	0.9	11		2.17			298	169
PCN-250 (Fe)	1495	0.48				7.93	11.21	298	170
PCN-250 (Fe_2Co)	1583	0.51				8.06	11.92	298	
PCN-250 (Fe_2Ni)	1619	0.52				8.64	12.44	298	
PCN-250 (Fe_2Mn)	1483	0.47				7.70	11.14	298	
PCN-250 (Fe_2Zn)	1560	0.50				8.21	12.11	298	
Zr-bptc	960	0.34	4.5	2.5$^+$	5.1$^+$	6.2	7.8	298	171
UiO-66-Cu(II)	1068	0.54	7.3	0.6$^+$	2.1$^+$	3.0	8.2	298	
UiO-66-NH_2	1037	0.52	7.3	0.8$^+$	2.9$^+$	3.7	8.8	298	

Open Access Article. Published on 10 March 2025. Downloaded on 6/30/2025 11:42:55 PM. This article is licensed under a Creative Commons Attribution 3.0 Unported Licence.

Table 1 (*continued*)

Material	BET SA ($m^2\ g^{-1}$)	V_p ($cm^3\ g^{-1}$)	Pore diameter (Å)	SO_2 uptake (mmol g^{-1}) at different pressure (bar) 0.01	0.05	0.1	1	T (K)	Ref.
Zr-DMTDC	1345	0.68	7.3	0.8$^+$	2.4$^+$	3.1	9.6	298	
UiO-66	1221	0.55	7.3	0.3$^+$	1.7$^+$	2.1	8.6	298	
MFM-133	2156	0.96	10.4	0.1$^+$	0.8$^+$	1.2	8.9	298	
MFM-422	3296		7.7	0.2$^+$	1.0$^+$	1.8	13.6	298	
MFM-190(F)	2538	1.041	11	1.6$^+$	3.4$^+$	6.0$^+$	18.3	298	129
MFM-190(NO_2)	2304	0.962	11	1.8$^+$	7.1$^+$	10.0$^+$	12.7	298	
MFM-190(CH_3)	2550	1.011	11	0.6$^+$	3.1$^+$	6.9$^+$	15.9*	298	
MFM-100	1445	0.68	6	1.0$^+$	2.8$^+$	4.5$^+$	7.6*	298	
MFM-101	2300	0.885	11	2.4$^+$	3.1$^+$	8.1$^+$	18.7	298	
MFM-102	2873	1.138	15	1.0$^+$	2.2$^+$	3.8$^+$	12.1*	298	
MFM-126	965	0.47	12	2.0$^+$	4.8$^+$	5.3$^+$	7.3	298	
MFM-300(Cr)	1360					7.0	7.9	298	172
MFM-300($Al_{0.67}Cr_{0.33}$)	1305					8.5	9.5	298	
MFM-170	2408	0.87	15.9		4.9$^+$	6.2$^+$	17.5	298	128
MFM-305	779	0.373	6.2				6.99	298	173
MFM-305-CH_3	256	0.181	5.2				5.16	298	
MFM-600	2281		9			3.0	5.0	298	139
MFM-601	3644		12			7.9	12.3	298	
MFM-300(In)	1071	0.419	7.5		5.9	7.1$^+$	8.28	298	117
MFM-300(Al)	1370	0.375	6.5	4.65		7.03	7.69	293	114
Ni-gallate	455	0.154	4.85	3.37		3.79	4.49	298	142
Co-gallate	494	0.186	4.85	4.16		4.51	5.30	298	
Mg-gallate	576	0.213	4.85	4.87		5.19	5.81	298	
SIFSIX-1-Cu	1178		8.0	3.43		8.74	11.1	298	174
SIFSIX-2-Cu-i	503		5.2	4.16		6.01	6.90	298	
SIFSIX-3-Zn	250		4.2	1.68		1.89	2.10	298	
SIFSIX-3-Ni	368		4.2	2.43		2.55	2.74	298	
SNFSIX-Cu-TPA	1169			3.33			8.09	298	175
MAF-66	1226					6		308	176
F-Ce-MOF-SC-18.1@1.0PA	52.1	0.11				8.9	15.3	298	177
NbOFFIVECu-TPA	1179	0.50		2.0		3.8	6.3	298	178
TaOFFIVECu-TPA	1041	0.43		1.43		3.5	6.0	298	
ELM-12	706	0.26	4.3	0.72		1.95	2.73	298	146
CPL-1	335	0.125	4.1	0.47		1.06	2.0	298	179
Zr-TPA-HAc	2150						19.6	298	180
Zr-TPA-FA	2190						22.7	298	
men-MIL-101(Cr)	2377	1.2	2.1	3.0				298	181
18-UiO-66-cyanoacetic acid	1375	0.76					11.91	298	182
Ni(BDC)(TED)$_{0.5}$	1783	0.74	7.8			4.54	9.97	298	183
Zn(BDC)(TED)$_{0.5}$	1888	0.84	7.8				4.41	298	
DZU-17	1307.9	0.68	4				14.11	298	184
Co_6-MOF-3	1905.4	0.99	5				16.40	298	
CPL-11	1182		6.7				5.29	298	185
BUT-78	2031		15				13.8	298	186

BET SA: BET surface area, V_p: pore volume, T: temperature, $^+$taken from isotherm *structure collapse after SO_2 uptake.

293 K.[151] DUT-4 shows a high pore volume of 0.71 $cm^3\ g^{-1}$ with the uptake of 13.6 mmol g^{-1} at 1 bar and 298 K.[119] MFM-133 shows a high pore volume of 0.96 $cm^3\ g^{-1}$ with an uptake of 8.9 mmol g^{-1} at 1 bar and 298 K.[171]

We note that for studies whose sole ambition is to contend the MOF SO_2 adsorption record, a high BET surface area and high pore volume is optimal. However, such characteristics are largely irrelevant to detecting low concentrations of SO_2. Instead, selectivity and adsorption capacity at low pressure must be prioritised.

When optimizing the low-pressure SO_2 adsorption capacity, the pore diameter becomes arguably the most essential property of MOF. At 0.01 bar, high SO_2 adsorption (3–5 mmol g^{-1}) is strongly correlated to a pore diameter between 4 to 10 Å (Fig. 11), which is in good agreement with the above discussion. For example, SIFSIX-2-Cu-I with the linker 4,4′-dipyridylacetylene possesses a narrow pore diameter (5.2 Å) and a high SO_2 adsorption (4.16 mmol g^{-1}) at 0.01 bar and 298 K.[174] This is because the kinetic diameter of the SO_2 molecule (4.1 Å) is close to the pore diameter, thereby maximizing dispersion forces between SO_2 and the pore walls. In the case of SO_2 adsorption experiments, to increase the intermolecular interactions, the adequate diffusion of the SO_2 gas through the MOF pores is necessary to achieve adsorption successfully.[191]

3. MOFs applied in SO_2 detection

Although the detection of SO_2 using MOFs remains poorly explored, various techniques that leverage the advantageous features of MOFs are currently under investigation for this purpose. In principle, the presence of an analyte can be

 This journal is © The Royal Society of Chemistry 2025

Open Access Article. Published on 10 March 2025. Downloaded on 6/30/2025 11:42:55 PM. This article is licensed under a Creative Commons Attribution 3.0 Unported Licence.

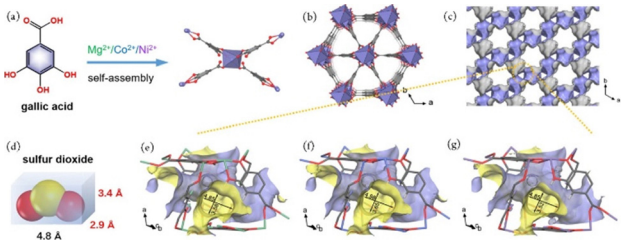


Fig. 7 (a) Illustration of the preparation process and local coordination environments of metal atoms and the ligands. (b) The structure along the *c* axis displaying the main channels and the periodic branched channels leaning against the main channels. (c) Accessible Connolly surface determined by using a probe with a radius of 1.0 Å. (d) Molecular size of the sulfur dioxide molecule. (e) 3.58 × 4.85 Å^2 for Mg-gallate, (f) 3.68 × 4.95 Å^2 for Co-gallate, and (g) 3.52 × 4.85 Å^2. (Reprinted with permission from ref. 142 Copyright (2021) American Chemical Society).

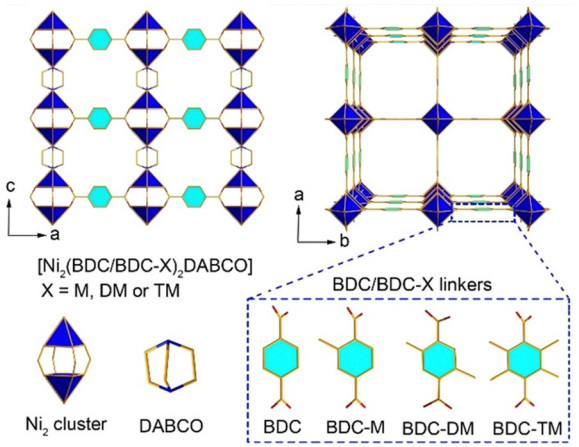


Fig. 8 Top row: Sections of the packing diagram of DMOF showing the channel structures along the *b*- (and identical *a*-) axis and along the *c*-axis. Bottom row: The building blocks of the Ni_2 cluster, DABCO, and BDC/BDC-X in DMOF/DMOF-X. X represents the monomethyl (M), 2,5 dimethyl (DM), or 2,3,5,6 tetramethyl (TM) substituents. (Reprinted from ref. 143 Copyright 2021 with permission from John Wiley & Sons under the Creative Commons CC-BY-NC-ND license).

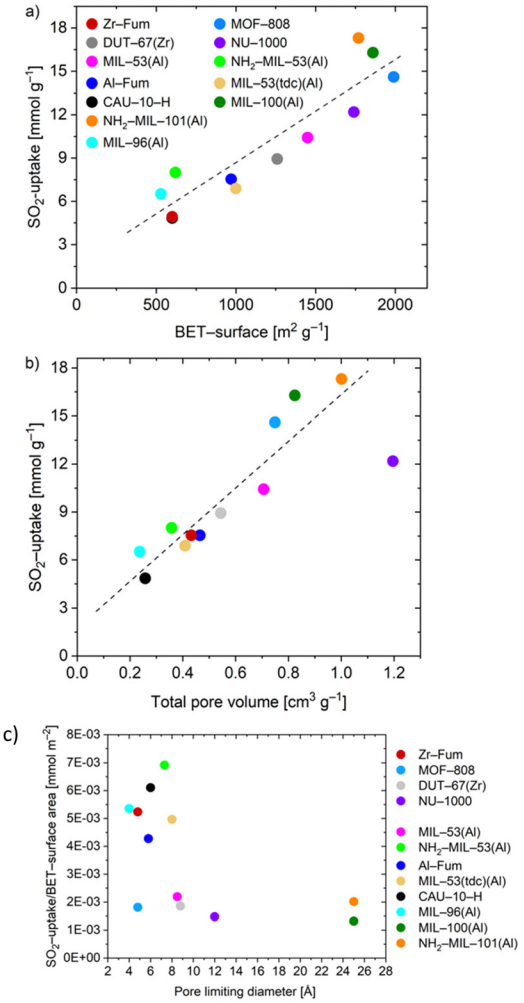


Fig. 9 SO_2 uptake (1 bar, 293 K) *vs.* (a) BET-surface area and (b) total pore volume. The dashed line is a trend line as a guide to the eye, (c) surface-specific SO_2 uptake at 0.1 bar (293 K), which is the uptake at this pressure divided by the BET-surface area *vs.* the pore limiting diameter (PLD). (Reprinted with permission from ref. 151 Copyright (2021) American Chemical Society).

confirmed by monitoring characteristic MOF properties that are altered after an external stimulus (in this case, the SO_2 interaction). This is the fundamental principle upon which MOF-based sensors are premised. The response to the host–guest interaction provides a probe for qualitative and quantitative sensing or detection applications. Only a few MOFs have been employed for SO_2 detection and these have been based on (i) analyte-induced changes in their luminescent properties (generating an energy transfer), (ii) changes in the electrochemical properties (changes in electrical resistance), (iii) changes in spin-crossover (SCO) behavior (change in the spin state), and (iv) a change in the sample mass. To supplement this discussion, the MOF-based materials applied for SO_2 detection are summarized in Table 2 in conjunction with crucial parameters, including sensing technique, sensitivity, and selectivity.

3.1 MOFs for luminescent SO_2 detection

Luminescence behavior has been extensively studied in the MOF field.[215] Generally, such materials are called luminescent metal–organic frameworks (LMOFs) and have been used in optical, medical, and detection applications.[216–218] Different strategies have been developed to construct luminescent MOFs, which are based on the "signal-off" or "signal-on" response strategies (in other words, the so-called turn-on and turn-off effect).[219] The emission centers in such materials may constitute the metal ions, organic linkers, and guest species. The organic linkers typically present π-conjugated systems, facilitating a fluorescence response due to accessible π–π* transitions.[220] In the case of metal centers, the lanthanide family – particularly Tb^{3+} and Eu^{3+} – are frequently employed due to the accessible transitions between $^5D_0$–^7F_j states.[221] Considering these properties, MOFs are excellent candidates for the detection of not only SO_2 but also multiple analytes

Open Access Article. Published on 10 March 2025. Downloaded on 6/30/2025 11:42:55 PM.
This article is licensed under a Creative Commons Attribution 3.0 Unported Licence.

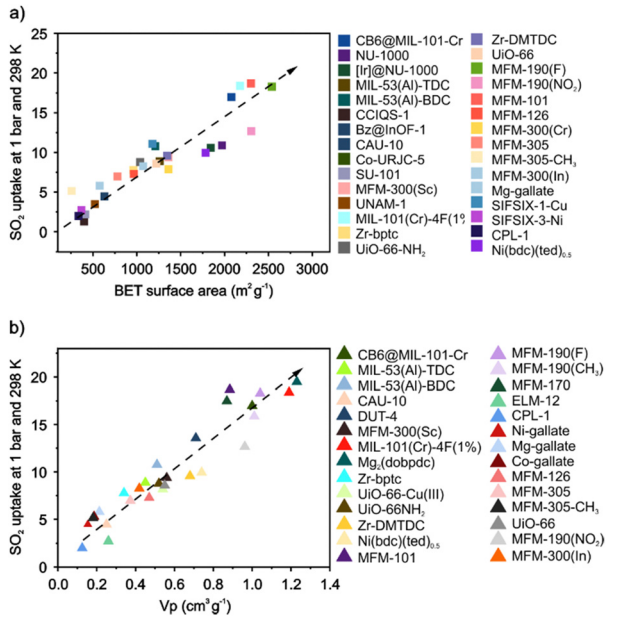


Fig. 10 Relation between SO_2 uptake at 1 bar and 298 K and (a) BET surface area and (b) pore volume. For references to the individual MOFs, see Table 1.

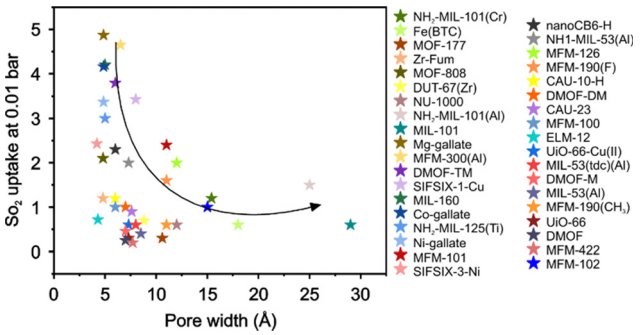


Fig. 11 Relation between SO_2 uptake at 0.01 bar with PLD. For references to the individual MOFs, see Table 1.

using luminescent properties.[96] Notably, the rational construction of LMOFs that exhibit energy transfer properties can tune the luminescence.[222,223]

LMOFs can be synthesized with a tremendous diversity of organic linkers and metal clusters (including pristine MOFs or with linker modifications), providing a wide range of energy transfer LMOFs (ET-LMOFs),[224] affording multiple detection options depending on the target analyte.[225] Additionally, chromophores can be regularly aligned and carefully ordered inside the crystalline LMOF lattice, providing a basis for understanding the short- and long-distance energy transfer mechanisms.[226] The high crystallinity and periodicity of MOFs are advantageous for computational models and calculations that aim to elucidate the luminescence mechanism of LMOFs.[227,228]

LMOFs have been intensely studied for solar cells,[229] photocatalysis,[230] scintillators,[231] X-ray and NMR imaging,[232] and for detecting analytes pertinent to gas pollution.[84] The possible luminescent centers and charge transfer processes in LMOFs (Fig. 12) are classified as (Fig. 12a) linker-centered emission, guest-centered emission, and metal-centered emission, and (Fig. 12b) linker-to-linker, metal-to-metal, metal-to-linker, the linker-to-metal, guest to host, and host to guest.[233] Herein, we will not specifically discuss each case since this would constitute a significant departure from the stated aim of this contribution. However, we provide a brief description when necessary and encourage readers to consider several relevant contributions.[234,235] Aside from possessing suitable luminescent behavior, the first essential requirement for an LMOF to be considered for SO_2 detection applications is demonstrable chemical stability towards SO_2 under ambient conditions (including humidity), as previously mentioned (*vide supra*).

For example, Chen and Wang reported a Ce^{4+}/Tb^{3+} MOF, Ce–PA–Tb MOF, with the linker PA = *m*-phthalate, with promising attributes for SO_2 detection.[195] The design of this novel MOF was inspired by the advantages of lanthanide luminescent properties, which include a long luminescence lifetime.[236] The MOF is a bimetallic material with Ce^{4+} and Tb^{3+} centers coordinated with PA linkers. To assess the detection prowess of the material, the authors generated SO_2 gas *in situ* using 'Kipp's device' – a chamber wherein sodium sulfite (Na_2SO_3) is combined with sulfuric acid (H_2SO_4) under a N_2 atmosphere to generate the SO_2 gas (Fig. 13). Samples containing SO_2 were analyzed using three separate methods: Ce–PA–Tb MOF probed by luminescence, Ce–PA–Tb MOF incorporated into a test strip, and formaldehyde absorbing pararosaniline spectrophotometry (FAPA). The limit of detection (LOD) was found to be 0.006 μg mL^{-1} (0.093 μM), 0.5 μg mL^{-1} (7.8 μM), and 0.05 μg mL^{-1} (0.78 μM) for the respective detection methods. Notably, the luminescence-based measurement is ten times more sensitive to SO_2 than the Ce–PA–Tb-MOF test strip method or FAPA. The mechanism involves the SO_2-induced reduction of Ce^{4+} to Ce^{3+}; subsequent irradiation with 250 nm photons induces an energy transfer from Ce^{3+} to the adjacent Tb^{3+} ion. An electronic transition within the Tb^{3+} ion leads to emission at 545 nm, which is measured. Crucially, the energy transfer does not occur from Ce^{4+} to Tb^{3+}. The presence of Ce^{3+} was confirmed using XPS spectroscopy. It was not stated if the sensor is re-usable.

The use of luminescent MOF-based SO_2 sensors was recently expanded with the development of a DNA-based Tb-MOF composite for SO_2 detection.[196] Briefly, single-stranded DNA (ssDNA) was combined with Tb^{3+} to form ssDNA-Tb^{3+} which was combined with IR-MOF-3 MOF in an ethanol suspension to form a composite. A test strip was fabricated using the DNA-based Tb-MOF composite in this case. The authors used Kipp's device to generate SO_2 for the purpose of assessing the performance of the composite sensor. The results indicate a LOD value of 0.02 ppm of SO_2, a low value which confirms that the material provides a promising platform for SO_2 detection. The DNA-based Tb-MOF composite exhibits a weak PL emission and displays an apparent turn-on effect after interaction with SO_2 and analogues thereof. The authors suggested that the material operates *via* a charge transfer mechanism: the amino

 This journal is © The Royal Society of Chemistry 2025

Open Access Article. Published on 10 March 2025. Downloaded on 6/30/2025 11:42:55 PM. This article is licensed under a Creative Commons Attribution 3.0 Unported Licence.

Table 2 Comparison of SO_2 detection in MOFs

Material	Method	Matrix	Selectivity	SO_2 concentration range	SO_2 detection level	Mechanism	Ref.
Eu-BDC-NH_2 film	Luminescence	MOF film	Over N_2, CO_2, O_2, NH_3, HCHO, H_2O, and H_2S	0–200 ppm	0.65 ppm	Turn-off effect by energy transfer	192
MOF-303	Luminescence	Solid state (powder)	Over CO_2, CH_4, and H_2O	Up to 0.1 bar		Turn-on effect	193
CYCU-3	Luminescence	Solid state (powder)	Over CO_2, and H_2O	Up to 0.1 bar		Turn-on effect by energy transfer	194
Ce–PA–Tb	Luminescence	Solid state (powder)		0–70.4 ppm	0.093 μM	Turn-on effect by energy transfer	195
DNA–Tb-MOF	Luminescence	Test paper		0.2–1.6 ppm	0.02 ppm	Turn-on effect by energy transfer	196
MOP-CDC	Luminescence	Solid state (powder)		Up to 0.1 bar		Turn-off effect	197
Mg_2DOBPDC	Luminescence	Solid state (powder)		Up to 0.1 bar		Turn-on effect	198
Ni_2(dobpdc)	Luminescence	Solid state (powder)	Over CO_2, and H_2O	Up to 0.1 bar		Turn-on effect	199
MIL-53(Cr)-Br	Luminescence	Solid state (powder)	Over CO_2, and H_2O	Up to 0.1 bar		Turn-on effect	200
MUF-16	Luminescence	Solid state (powder)	Over NO_2, CO_2, H_2O, H_2S, O_2, N_2, and CH_4	Up to 0.1 bar		Turn-on effect	201
		THF suspension		1–250 mM	80.72 ppm		
MOF-5-NH_2	Luminescence	Test paper	Over NO_2, NH_3, N_2, CO_2, H_2S, and CS_2	0–3 ppm	0.05 ppm	Turn-on effect	202
UTSA-16(Zn)	Luminescence	THF suspension		1–5 mM	114.6 ppm	Turn-off effect	203
Ni_3BTC_2/OH-SWNTs	Electrochemical	Microelectrode	Over NO_2, CH_4, CO, and C_2H_2	4–20 ppm	4 ppm	Electron transfer	204
CoZn-NCNTs	Electrochemical	Solid state (powder)	Over NO_2, MeOH, acetone, NH_3, CO, H_2, and EtOH	0.5–30 ppm	0.5 ppm	Increase of hole density	205
Ni-MOF/-OH-SWNTs	Electrochemical	Solid state (powder)	Over NO_2, NH_3, and CO	0.5–15 ppm	0.5 ppm	Electron transfer	206
UiO-66-NH_2/PVDF NM	Electrochemical	Nanofibers membrane		1–150 ppm		Interaction with NH_2 groups	207
PAN@UiO-66-NH_2 NM	Electrochemical	Nanofibers membrane	Over CO, CH_4O, C_2H_6O, C_3H_8O, and C_3H_6O	1–125 ppm		Interaction with NH_2 groups	208
UiO-66-THB/PAN-based	Electrochemical	Electrode	Over CO_2, H_2S, NO_2, NO, CO, NH_3, C_3H_6O, and C_2H_6O	1–125 ppm	0.1 ppm	Hydrogen bonding	209
TM-Ag@NU-901	Electrochemical	MOF film		10–200 μM	0.1 ppm	Interaction with C=C groups	210
UiO-66-NH_2	Electrochemical	Solid state (powder)		1–10 ppm	1 ppm	Formation of a charge-transfer complex	211
MFM-300(In)	Electrochemical	Electrode	Over CH_4, H_2, CO_2, C_3H_8, C_7H_8, and NO_2	75–1000 ppb	75 ppb	Capacitance	212
Fe(PZ)[Pt(CN)$_4$]	Magnetism	Solid state (powder)	Over CO_2, and CS_2			Stabilization of the LS state	213
KAUST-7	Gravimetric	QCM	Over H_2O	0–500 ppm	5 ppm	Mass change	214

groups present in DNA–Tb-MOF function as electron-donors from the perspective of the Tb^{3+} ions. When SO_2 and its analogues such as HSO_3^- interact with the amino group, it negates the typical energy transfer between the amino group and Tb^{3+} ions, generating a PL turn-on effect at 491, 546, 585, and 620 nm upon irradiation at 290 nm. These investigations confirm that Tb-MOFs exhibit luminescent properties which form a promising basis for SO_2 detection.

Interestingly, apart from the mechanisms already discussed, changes in luminescence may also be induced by the interaction between SO_2 and the structural linkers. A Cu(II)–metal–organic polyhedron (MOP-CDC, CDC = 9*H*-carbazole-3,6-dicarboxylate) displays a turn-off effect in its fluorescence after SO_2 adsorption.[197] At low pressure (0.05 bar), MOP-CDC exhibits an SO_2 uptake of 1.0 mmol g^{-1} at 298 K. Under 440 nm excitation, MOP-CDC exhibits strong fluorescence emission at 540 and 639 nm. After the SO_2 exposure, these bands are quenched, providing a convenient probe for the presence of SO_2. DFT calculations demonstrate that the SO_2 molecule interacts with the carbazole NH site through hydrogen-bonding [N–H···O=S=O]. Due to this strong host–guest interaction, SO_2 adsorption induces fluorescence quenching. Notably, CO_2 adsorption (a potential interfering gas) had no apparent effect on fluorescence intensity.

However, in some cases, energy transfer processes involving the organic linker result in a turn-on effect. For instance, Mg_2DOBPDC (DOBPDC = 4,4-dioxidobiphenyl-3,3-dicarboxylate), which shows high SO_2 adsorption at low pressure (0.05 bar, 6 mmol g^{-1} at 298 K).[198] At an even lower pressure of 0.002 bar, the material displays an SO_2 uptake of approximately 2.4 mmol g^{-1}.

Open Access Article. Published on 10 March 2025. Downloaded on 6/30/2025 11:42:55 PM.
This article is licensed under a Creative Commons Attribution 3.0 Unported Licence.

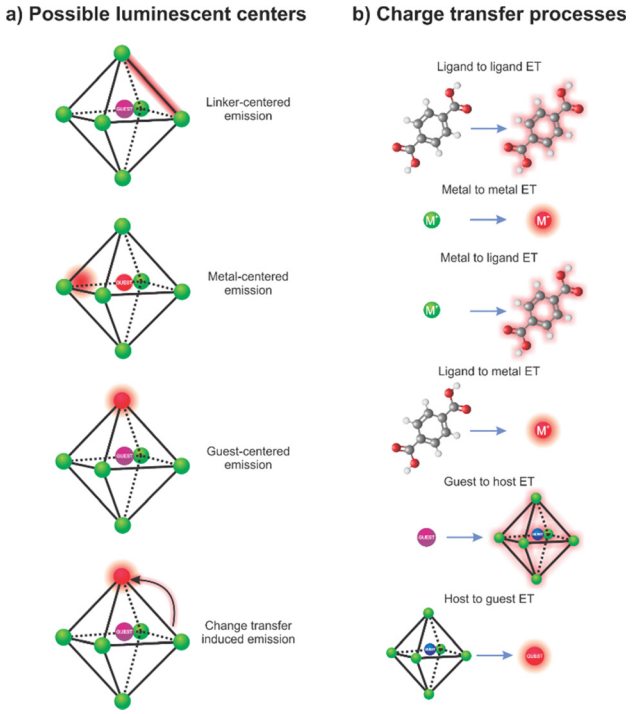


Fig. 12 Schematization of (a) possible luminesce centers and (b) charge transfer processes. Based on ref. 233.

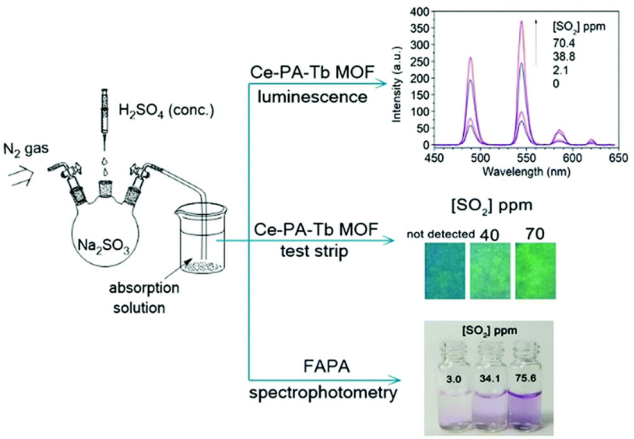


Fig. 13 Determination of SO_2 gas by the methods of standard formaldehyde absorbing pararosaniline (FAPA) spectrophotometry, Ce–PA–Tb luminescence and Ce–PA–Tb test strip with a 254 nm UV lamp. (Reprinted from ref. 195 Copyright 2020 with permission from Royal Society of Chemistry).

This value is comparable to record low pressure SO_2 adsorption exhibited by M-gallate MOFs[142] and several frameworks listed in Table 1. GCMC simulations revealed that SO_2 preferentially adsorbs at open Mg^{2+} coordination sites in a monodentate fashion (SO_2(O)–Mg = 2.17 Å). Nevertheless, the coordinated SO_2 also engages in hydrogen bonding with the adjacent DOBPDC linker, thereby modulating the luminescent properties of the material. Thus, during SO_2 exposure under 320 nm irradiation, the broad

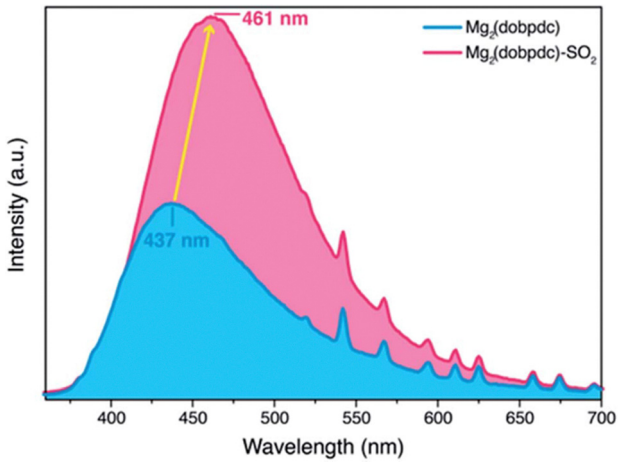


Fig. 14 Emission spectra of Mg_2(dobpdc) before (blue) and after (pink) exposure to SO_2. Both samples were excited with 320 nm UV light. (Reproduced from ref. 198 Copyright 2022 with permission from Royal Society of Chemistry).

photoluminescence band at 437 nm shifts to 461 nm, concomitantly increasing the band's intensity (Fig. 14).

In addition, the isostructural framework Ni_2(DOBPDC) was investigated for application in SO_2 detection.[199] Under 350 nm irradiation, Ni_2(DOBPDC) exhibits a broad emission band at 450 nm. After the sample is exposed to SO_2, the emission peak shifts to 405 nm with a 61% increase in emission intensity. This behavior was observed even at low SO_2 pressure (0.1 bar). To investigate the luminescent mechanism, a time-resolved photoluminescence (TRPL) experiment was performed using a 340 nm picosecond-pulsed LED as the excitation source. The results revealed that the average decay lifetime increases from 2.14 to 2.47 ns upon SO_2 exposure. This suggests that interaction between the SO_2 and Ni^{2+} centers within the framework nullifies the organic linker's molecular motion, minimizing the non-radiative decay pathways available and thereby causing the fluorescence lifetime to increase.

MOF-303 is composed of Al(III) centers which are interconnected by PZDC linkers (PZDC = 1*H*-pyrazole-3,5-dicarboxylate) and was recently evaluated for SO_2 detection.[193] MOF-303 displays one of the highest low pressure SO_2 adsorption capacities so-far reported (6.21 mmol g^{-1} at 298 K and 0.1 bar). At 298 K, the first adsorption step occurs at 0.05 bar and corresponds to 5.44 mmol g^{-1} of SO_2, confirming a high affinity between SO_2 and MOF-303. *In situ* diffuse reflectance infrared Fourier transform spectroscopy (DRIFTS) experiments revealed the preferential adsorption sites to be μ_2-OH and linker N–H sites, which interact with SO_2 through hydrogen bonding. In this material, a hydrogen-bonded dimer forms *via* adjacent pyrazole groups within the pore, generating hydrophilic pockets that bind small molecules, here SO_2. Considering the fluorescent properties of the PZDC linker in several coordination compounds, the luminescent properties of MOF-303 were investigated. However, in MOF-303, the linker fluorescence is quenched because the absorbed energy is released through non-radiative pathways. However, exposure to SO_2 under 248 nm irradiation resulted in

 This journal is © The Royal Society of Chemistry 2025

Open Access Article. Published on 10 March 2025. Downloaded on 6/30/2025 11:42:55 PM.
This article is licensed under a Creative Commons Attribution 3.0 Unported Licence.

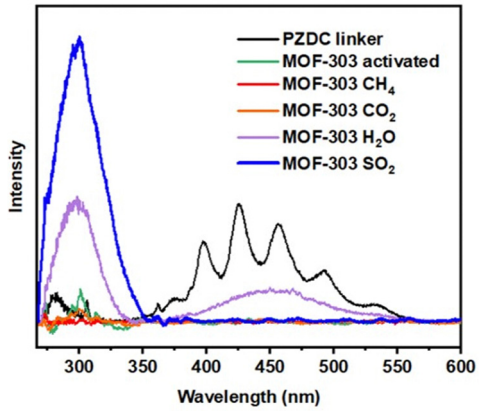


Fig. 15 Solid-state emission spectra of PZDC linker (black line), activated MOF-303 (green line), after exposure to: CH_4 (red line); CO_2 (orange line); H_2O (purple line); and SO_2 (blue line). The excitation wavelength was set at 248 nm. (Reproduced from ref. 193 Copyright 2022 with permission from American Chemical Society).

a fluorescence turn-on effect with emission at 299 nm (Fig. 15). This represents an approximately 125 nm shift in emission relative to that of the linker. No apparent change in emission was observed in the presence of the common interfering gases CH_4 or CO_2. The authors suggest that the physisorption of SO_2 within MOF-303 leads to a rigidification of the structure which suppresses non-radiative decay pathways, thereby intensifying emission.

Similarly, CYCU-3, also an Al(III)-based MOF but composed with SDC linkers (SDC = 4,4′-stilbenedicarboxylate), was assessed for SO_2 detection and capture applications.[194] CYCU-3 shows a total uptake of 11.03 mmol g^{-1} at 1 bar and 298 K. The interaction between SO_2 and the pore surface was elucidated using *in situ* DRIFTS experiments and theoretical calculations. Bridging hydroxyl moieties within the inorganic cluster were identified as preferential interaction sites for SO_2. The fluorescence spectra of both CYCU-3 and solid H_2SDC were recorded. Under 343 nm irradiation, H_2SDC produces a fluorescence emission peak at 450 nm. However, the fluorescent emission from CYCU-3 is blue shifted and less intense than that of the free ligand due to charge transfer between the organic linker and Al(III) centres. After the sample is exposed to SO_2 under irradiation at 343 nm, the emission at 450 nm increased in intensity. This performance was attributed to an enhanced ligand-centered $\pi^* \rightarrow \pi$ electronic transition.

Cr(III)-MOFs have also been applied for SO_2 adsorption and detection, including MIL-53(Cr) (linker: BDC) and the novel reticular analogs MIL-53(Cr)-Br and MIL-53(Cr)-NO_2 with the linkers BDC-Br and BDC-NO_2 respectively.[200] In the presence of SO_2, these MOFs show a turn-off effect under irradiation at 300, 360, and 350 nm, respectively, corresponding to a decrease in the emission intensity at 415, 420, and 507 nm, respectively. The intensity decrease was associated with a charge transfer process involving the organic linker. MIL-53(Cr) displays a slight red shift, suggesting metal-to-linker charge transfer while MIL-53(Cr)-Br shows a change in the emission peak from 450 to 436 nm.

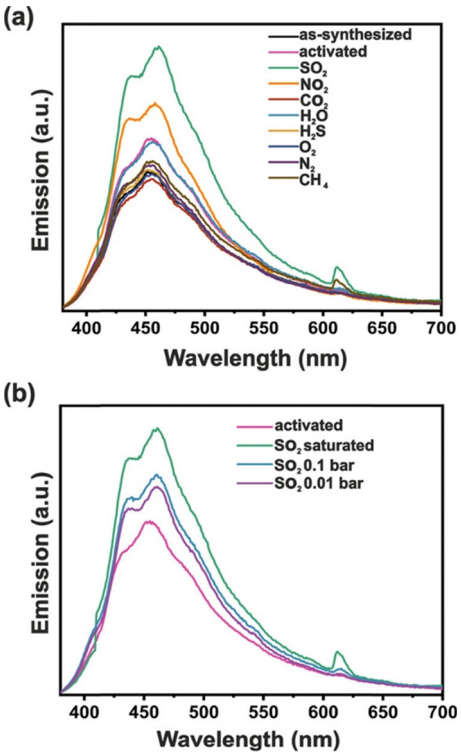


Fig. 16 (a) Comparison of solid-state emission spectra of MUF-16 exposed to different gases, and (b) comparison of solid-state emission spectra of MUF-16 exposed to different SO_2 pressures (Reproduced from ref. 201 Copyright 2024 with permission from American Chemical Society Under CC-BT 4.0 license).

MUF-16 is a Co(II) based framework composed of 5-aminoisophthalate (AIP) linkers, formula [Co(AIP)$_2$], which was explored for the selective detection and capture of SO_2.[201] The SO_2 adsorption isotherm shows an uptake of 2.2 mmol g^{-1} at 298 K and 1 bar. Employing FTIR, DFT calculations, and GCMC simulations, SO_2 was found to engage in favorable hydrogen bonding interactions with the amino groups which decorate the framework. An increased fluorescence response is observed in the presence of SO_2 compared to the other common gases such as CO_2, NO_2, N_2, O_2, CH_4, and water vapor (Fig. 16a and b). The LOD was calculated using a THF solution of SO_2 and was found to be 1.26 mM ($\sim$81 ppm). A fluorescence mechanism was proposed using TRPL analysis.[201]

The amino-functionalized derivative of MOF-5, IR-MOF-3, was incorporated into a test strip for rapid and selective sensing of SO_2 and its derivatives *via* a luminescence enhancement turn-on effect.[202] The test strip offers real-time detection of SO_2 with a detection limit of 0.05 ppm. Within IR-MOF-3 the amino groups donate electron density to the metal centres which quenches the luminescence. However, when SO_2 (or HSO_3^{2-}) interacts with the amino group, a complex is formed which disrupts the linker-to-metal charge transfer process, turning on the characteristic luminescence of the linker. XPS spectroscopy confirms the formation of N–S interactions between amino groups within IR-MOF-3 and SO_3^{2-}. Test strips containing MOF-5 and IR-MOF-3 were exposed to SO_2 gas generated using

Open Access Article. Published on 10 March 2025. Downloaded on 6/30/2025 11:42:55 PM. This article is licensed under a Creative Commons Attribution 3.0 Unported Licence.

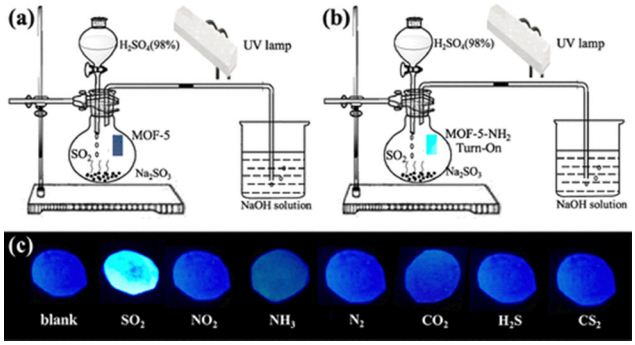


Fig. 17 (a) and (b) Schematic diagrams of the device for detecting SO_2 gas using MOF-5 and MOF-5-NH_2 luminescent test paper, respectively. (c) Luminescence response photographs of MOF-5-NH_2 luminescent test paper after exposure to various gas species under a 365 nm UV lamp. The final concentrations of SO_2, NO_2, NH_3, N_2, CO_2, and H_2S were 2 ppm, while CS_2 gas was saturated vapor of liquid-state CS_2. (Reproduced from ref. 202 Copyright 2018 with permission from American Chemical Society).

a Kipp apparatus (Fig. 17a–c). Notably, unfunctionalized MOF-5 exhibits no response to SO_2. The test strip impregnated with MOF-5-NH_2 was found to be stable after exposure to SO_2, suggesting that the system is reusable for detecting SO_2 with a particularly short 15-second response time. The LOD was calculated to be 0.05 ppm for the test paper. It is worth mentioning that the chemical stability of MOF-5 should be considered when evaluating its suitability for SO_2 detection. The material has for instance proven unstable to water.[237]

A technique, named *in situ* secondary growth, allows MOFs to be deposited on membranes. Qian *et al.*[192] reported a MOF film based on a Eu(III) MOF with BDC-NH_2 linkers. First, the authors prepared a hydroxyl functionalized glass surface using 'piranha' solution (H_2SO_4/H_2O_2 solution). Then, UiO-66-NH_2 was synthesized *in situ* on the functionalized glass. Subsequently, the Eu-MOF was grown by solvothermal synthesis to form a layer which acts as a fluorescence probe for SO_2. Exposure to SO_2 leads to quenching of the fluorescent solid emission due to the $^5D_0 \rightarrow {}^7F_2$ transition of Eu^{3+}. The decay curves for N_2 and SO_2 indicate a reduced emission lifetime of 381.8 μs in 1% SO_2, suggesting the involvement of a charge transfer process between the linker and SO_2 molecules. The LOD value was reported to be 0.65 ppm with a response time of as short as 6 s.

3.2 MOFs for electrochemical SO_2 detection

Besides the luminescence-based sensors described above, electrochemical processes have also been widely used for small molecule detection and quantification. The operation of electrochemical sensors depends on electron transfer events that occur during interactions between the surface of the material and analyte gas molecules.[238] The transfer of electrons accompanying analyte interactions leads to a change in resistance, which can be measured. This change in resistance, and therefore the sensor's sensitivity, depends to a considerable extent on the nature of the material with which the analyte interacts.[239] Materials commonly employed in electrochemical sensors include metal oxides, carbons, nitrides, sulfides, and – to a growing extent – MOFs. The most important parameters to consider in achieving optimal performance are selectivity, response and recovery speed, and stability.[240] The surface area and the reactivity of the surface towards the analyte strongly influence the response. A high response factor can be accompanied by a low LOD, the minimum analyte concentration to which the sensor is sensitive. Various interfering species may be present in the environment besides the analyte of interest. Thus, selectivity is crucial for accurate and reliable detection and is usually evaluated by cross-sensitivity comparison wherein the senor is exposed to various interfering species at fixed concentrations. Selectivity is affected by many factors related to the environment, such as humidity and temperature, the nature and composition of the sensor, the affinity between the gas molecules, and the properties of the sensor material.[241]

Electrochemical techniques are now being implemented for SO_2 detection using MOFs. For example, a composite based on nickel benzene-tricarboxylate (Ni_3BTC_2) and OH-functionalized single-walled carbon nanotubes (OH-SWNTs) was investigated for this purpose.[204] After the composite was exposed to SO_2, the measured change in voltage was successfully related to the SO_2 concentration. A response time of 4.59 s with a recovery time of 11.04 s was achieved with a low SO_2 concentration (15 ppm). This behavior was attributed to an electron transfer from the composite to the SO_2 molecule. In this case, the composite is a p-type material, where a transfer of electrons from the composite to the SO_2 molecule (an electron acceptor) occurs. The selectivity of the composite sensor is maintained in the presence of NO_2, CH_4, CO, and C_2H_2, typical interfering gases in nature.

Moreover, the relative change in electrical resistance can also be leveraged for small molecule sensing. For example, in 2018 Li *et al.*[205] reported a composite material derived from pyrolysis of Zn/Co bimetallic ZIF-67 which undergoes a 53% change in resistance in the presence of SO_2 (100 ppm). A cross-selectivity test was performed using NO_2, MeOH, acetone, NH_3, CO, H_2, and EtOH vapor. The material shows high selectivity over these gases even at low SO_2 concentrations (30 ppm). The response and recovery times are reportedly 88 and 900 s, respectively, with a limit of detection for SO_2 equal to 0.5 ppm.

The changes in the electrical resistance of a Ni-MOF composite (Ni-MOF/-OH-SWNTs) allowed a rapid response time of 10 s with a fast recovery time of 30 s for SO_2 (1 ppm).[206] This function is maintained even in the presence of NO_2, NH_3, and CO. It is known that holes form the major charge carrier within the Ni-MOF composite in the absence of SO_2. However, since SO_2 acts as an electron donor it acts to reduce the population of holes *via* recombination. Because holes are the major carrier within the composite the presence of SO_2 leads to a quantifiable increase in resistance.

Building on these developments, Zhang *et al.*[207] reported a capacitive sensor composed of UiO-66-NH_2 incorporated into a nanofiber membrane composed of polyvinylidene fluoride and carbon nanotubes. The composite material was employed as a sensing layer for real-time monitoring of SO_2. The amine

 This journal is © The Royal Society of Chemistry 2025

Open Access Article. Published on 10 March 2025. Downloaded on 6/30/2025 11:42:55 PM.
This article is licensed under a Creative Commons Attribution 3.0 Unported Licence.

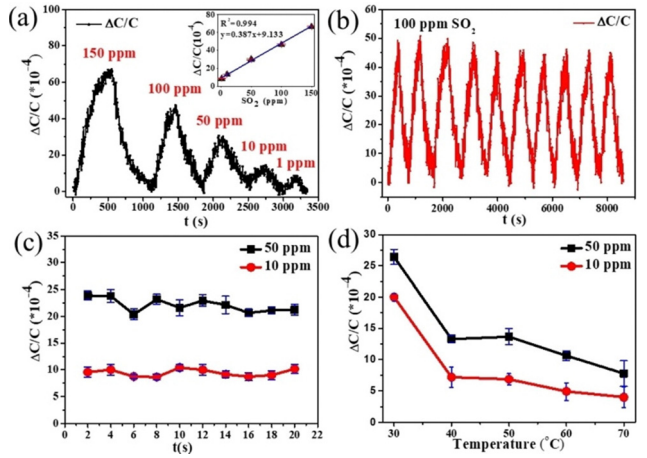


Fig. 18 (a) Detection of SO_2 in the range of 1 to 150 ppm concentration and linear response for the testing range of the inset; (b) reproducibility for the detection of 100 ppm SO_2; (c) response ability for the sensor at 10 and 50 ppm SO_2 within 20 days; (d) temperature influence on the sensor performance. (Reproduced from ref. 207 Copyright 2021 with permission from John Wiley & Sons).

functional groups interact strongly with SO_2 inside the sensor, leading to a change in conductivity (Fig. 18a–d). The detection response time was reportedly 435 s and 185 s towards 150 ppm and 1 ppm SO_2, respectively. Importantly, the SO_2 concentration and change in capacitance are strongly correlated, which was attributed to the adsorption capacity of UiO-66-NH_2. The sensor also shows high reproducibility for 100 ppm SO_2 over ten consecutive cycles. A long-term study was conducted over the course of 20 days in which 10 and 50 ppm SO_2 samples were measured, the change in conductivity was retained ~89% of its original value over this time. The SO_2 sensing performance is stable towards moderate temperature changes, dropping only 22% in going from 30 to 70 °C.

To improve the response time of the nanofiber membrane, the authors also designed a new flexible gas sensor in which UiO-66-NH_2 was incorporated into electrospun polyacrylonitrile (PAN) nanofibers.[208] The device was equipped with carbon nanotube electrodes. The high surface area and porosity of UiO-66-NH_2 make it particularly useful in an electrochemical detection device since the analyte can rapidly diffuse into the MOF. Crucially, the well-established flexibility of the membrane provides exceptional long-term stability.[242] The sensor reportedly to operates with a 1 ppm LOD for SO_2, and the porous MOF platform facilitates rapid SO_2 diffusion within the material with a fast response time of 255 s.

In a separate investigation from the same research group, the MOF UiO-66-NH_2 was incorporated into a nanofiber membrane which was modified to improve SO_2 adsorption and thereby improve the limit of detection.[209] UiO-66-NH_2 was loaded onto a PAN nanofiber membrane and modified with 2,3,4-trihydroxybenzaldehyde (THBA). The composite was synthesized by using imine condensation to cross-link the amine and aldehyde groups to form a Schiff base and obtain a UiO-66-N═C-THB/PAN-based capacitive gas sensor. This design achieved a lower SO_2 detection limit of 0.1 ppm. Based on DFT calculations, hydrogen bonding between SO_2 and the THB hydroxyl groups resulted in a high adsorption affinity. Considering the potential of MOF-based membranes in SO_2 detection applications, NU-901 (with the linker TBAPy = 4,4′,4″,4‴-(pyrene-1,3,6,8-tetrayl)tetrabenzoate) was embedded in a silica film.[210] This film was modified with thiol-magenta (TM) and Ag nanoparticles (TM-Ag@NU-901). SO_2 was detected by surface-enhanced Raman scattering, a new alternative strategy for detecting SO_2.

The UiO-66 analogs UiO-66-NH_2 and UiO-66-OH were employed as chemoresistive sensors for SO_2, NO_2, and CO_2.[211] Archetypal UiO-66 does not exhibit a change in resistance after exposure to any of the acidic gases listed above. However, UiO-66-NH_2 responds with a 22 ± 3% change in resistance to the presence of 10 ppm SO_2, with a 1 ppm LOD (corresponding to a 3.2 ± 0.2% response). This performance was attributed to the formation of a charge-transfer complex when SO_2 interacts with the amine-functionalized linker.

As discussed already, MFM-300(In) exhibits outstanding properties for SO_2 sorption and sensing applications due to a high SO_2 uptake at low pressure and excellent stability. Building on previous work, MFM-300(In) was applied as an electrode for SO_2 detection.[212] The In(III)-based MOF was coated on interdigitated electrodes, and the capacitance changes that occur in response to SO_2 were measured. This sensor displays one of the highest sensitivities to SO_2 and excellent selectivity over interfering gases such as methane, hydrogen, carbon dioxide, nitrogen dioxide, propane, and toluene at 1000 ppb. SO_2 concentration was successfully measured from 75 to 1000 ppb with a detection limit of 5 ppb. The electrochemical response was attributed to the interaction between SO_2 and the μ_2-OH groups in the MOF node (through hydrogen bonds), with further dipole–dipole interactions between adsorbed SO_2 molecules. The resulting electrostatic changes perturb the capacitance of the electrode.

3.3 Other detection techniques

In addition, MOFs have been employed in alternative SO_2 detection systems that use magnetic and mass change sensors. These provide an opportunity to exploit the diverse physicochemical properties of MOFs that do not find utility in the sensing techniques explored so-far. However, only a few examples have been reported, and we therefore emphasize the opportunity these methodologies present for future sensing applications.

In general, for magnetic gas sensors involve analyte-induced changes to the magnetic properties of the sensing material. Such changes can be measured through a range of sophisticated techniques that are beyond the scope of this review.[243] Magnetic gas sensors offer advantages over other gas sensors; for example, they can be designed to operate in a wide temperature range, do not require an electrical current source (therefore, the risk of explosion or fire is reduced), and the response time is much reduced compared to chemosensitivity sensors.[244,245] Various materials are employed as sensing

Open Access Article. Published on 10 March 2025. Downloaded on 6/30/2025 11:42:55 PM. This article is licensed under a Creative Commons Attribution 3.0 Unported Licence.

materials in magnetic gas sensors, recently this has included MOFs.[246,247]

Spin-crossover has emerged as an essential chemical phenomenon upon which magnetic gas sensors can be designed. Recently, MOFs that exhibit spin-crossover behavior have been studied. These typically exhibit structural nodes with $3d^4$–$3d^7$ transition metals in an octahedral coordination geometry. The spin-crossover phenomenon involves stimuli-induced switching between a low-spin and high-spin electronic configuration.[248,249] Of relevance in gas sensors, this change can be induced by the interaction between an analyte gas and the sensing material.

For example, Pham *et al.*[213] undertook a highly explorative study to demonstrate in principal that spin-crossover (SCO) behavior in a MOF can be exploited for SO_2 detection. {Fe(PZ)[Pt(CN)$_4$]} (PZ = pyrazine) was used to explore how adsorption of SO_2 affects the population of high and low spin states. Differences between the SCO properties of {Fe(PZ)[Pt(CN)$_4$]} during the adsorption of various gases point to specific guest–framework interactions, which appear to be sensitive to the physicochemical properties of the guest molecule. In this case, the gas molecules stabilized the LS state of the framework. The material was exposed to CO_2, SO_2, and CS_2 during the heating process in both experimental and simulated settings (Fig. 19). The SO_2 molecule was found to stabilize the LS state, leading to a 20 K shift in temperature caused by changes in the Fe–N bonds within the framework.

Mass change gas sensors which employ a quartz crystal microbalance (QCM) are popular and widely used in industry. QCM sensors exploit the quantitative relationship between the change in frequency of a quartz crystal resonator and the mass change resulting from the adsorption of analyte gas molecules on the QCM.[250] Crucially, the quartz surface can be coated with an appropriate film to enhance the sensitivity and selectivity of the sensor.[251,252] The advantage of QCM sensors is that they are susceptible to mass changes in the nano-gram range. However, fragility can present challenges.[253] Porous materials such as silicas and MOFs have been used as coatings on the quartz surface to improve the performance of QCM sensors.[234] However, it is worth mentioning that gravimetric detection exhibits drawbacks related to low selectivity.

For example, the isostructural fluorinated MOFs KAUST-7 ([Ni(NbOF$_5$)(pyrazine)$_2$]·2H$_2$O) and KAUST-8 ([Ni(AlF$_5$(OH$_2$))-(pyrazine)$_2$]·2H$_2$O) were employed as coatings on QCM based SO_2 sensors.[214] The difference between these materials is the presence of $(NbOF_5)^{2-}$ *versus* $(AlF_5(OH_2))^{2-}$ within the framework. The authors noted that KAUST-7 exhibits a high affinity for SO_2, SCXRD confirms that SO_2 interacts with two electronegative fluorine atoms of the adjacent $(NbOF_5)^{2-}$ moiety *via* the electropositive sulfur atom, while four C–H···O contacts stabilize the interaction. Meanwhile, in KAUST-8, the SO_2 molecule only interacts with four C–H···O from two neighboring pyrazines. Based on these properties, the materials were studied for SO_2 detection in the presence and absence of humidity to mimic atmospheric conditions. Following the change in frequency of the quartz crystal resonator, SO_2 was successfully detected at concentrations between 0 and 500 ppm in balance with nitrogen. The system exhibited with high stability and reproducibility. Both MOF-coated materials show a nonlinear decrease in sensitivity with the increased SO_2 concentration. The lowest detection limit was estimated to be about 100 ppb with noise drift in the resonance frequency of ±1.5 Hz. However, the experimental lowest detection limit was 5 ppm.

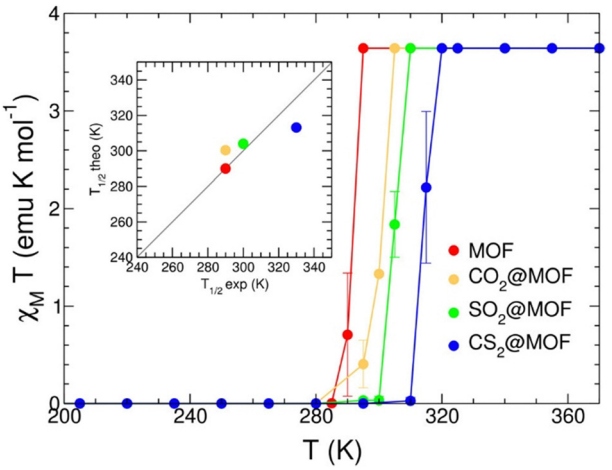


Fig. 19 Temperature dependence of $\chi_M T$ calculated from MC/MD simulations of {Fe(PZ)[Pt(CN)$_4$]} with no adsorbed guest molecules (MOF) as well as upon adsorption of CO_2 (CO_2@MOF), SO_2 (SO_2@MOF), and CS_2 (CS_2@MOF). The theoretical values of the SCO temperature ($T_{1/2}$) are compared in the inset with the experimental values. (Reproduced from ref. 213 Copyright 2018 with permission from American Chemical Society).

4. Overview of SO_2 detection methodology

Considering the discussion above, it is evident that metal–organic frameworks and coordination polymers are well suited for application in gas sensors and detectors. Notably, and unlike many other applications proposed for MOFs, high surface area or elevated gas uptake is not imperative for sensing. Thus, materials deemed unsuitable for "traditional" adsorption applications may find utility in sensing and detection processes where chemical robustness and functionality are prized over uptake capacity. As discussed in this review, the ideal MOF for sensing is stable under relevant working conditions and exhibits a precise and reproducible physical response upon interaction with the analyte at environmental concentrations. Considering these metrics, various devices designed for SO_2 detection were discussed (Fig. 20). These were primarily based on (i) nanofiber membranes, (ii) electrodes, and (iii) test strips.

Below (Fig. 21), the most relevant characterization techniques are evaluated for their potential in gas sensing applications.

(a) Fluorescence measurements: given the broad applicability, high selectivity, and potential for use in super-resolution experiments, fluorescence is one of the most commonly used

 This journal is © The Royal Society of Chemistry 2025

Open Access Article. Published on 10 March 2025. Downloaded on 6/30/2025 11:42:55 PM.
This article is licensed under a Creative Commons Attribution 3.0 Unported Licence.

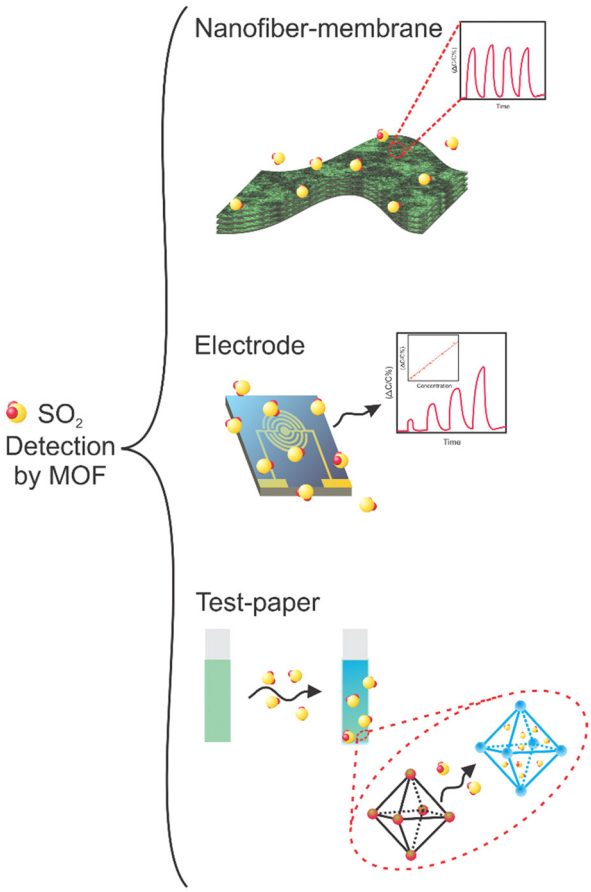


Fig. 20 MOFs applied in different assembled devices for SO_2 detection.

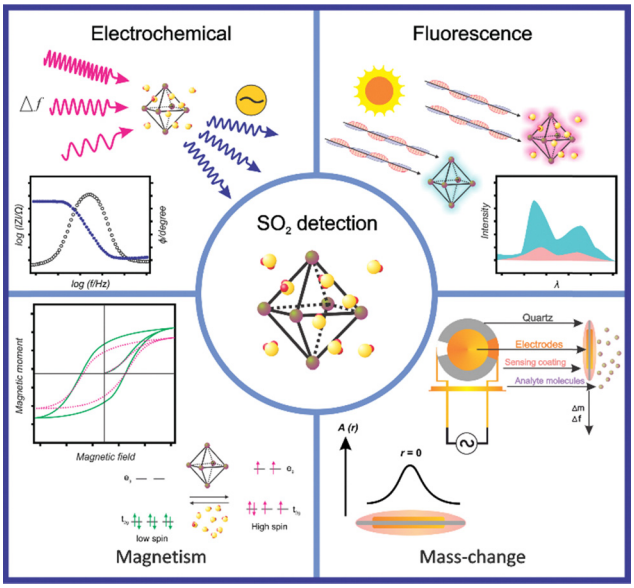


Fig. 21 MOFs applied in different characterization techniques for SO_2 detection.

chemo-sensing techniques.[254] Some fluorescence measurement techniques which are frequently encountered include:

(i) Fluorescence spectroscopy: this technique involves measuring the emission spectrum of a MOF before and after gas adsorption. The change in fluorescence intensity or wavelength can be used to detect and quantify the presence of gas molecules and determine the selectivity of the MOF towards the analyte of interest.[255]

(ii) Time-resolved fluorescence spectroscopy: this technique involves measuring the decay time of the fluorescence emission of a MOF after excitation. The change in decay time upon gas adsorption can be used to detect and quantify the presence of gas molecules and determine the selectivity of the MOF towards the analyte of interest.[196]

(b) Electrochemical measurements: another possible physical response that can be used to sense or detect gaseous molecules is the change in the material's conductivity (or resistivity). The sorption of gas molecules can alter the electrical conductivity of MOFs, which can be measured to detect (and even quantify the concentration of) specific gas molecules. MOFs provide an ideal platform for gas sensing and detection using this technique.[256] However, it must be noted that most MOFs and coordination polymers have very high resistivity and, thus, are not amenable to this kind of measurement. Some of the commonly used conductivity measurements are:

(i) Two and four-point probe measurements: this technique involves applying a voltage to the MOF and measuring the current flowing through it. Thus, the resistivity and conductivity of the MOF can be calculated from the measured values. The measurement can be performed in single crystals, films, or pellets of polycrystalline materials. However, special care must be taken to ensure that the contacts do not interfere with gas sorption and that a reproducible contact is made between the sample and electrodes.[257,258]

(ii) Impedance spectroscopy: this technique involves applying an AC voltage to the MOF and measuring the impedance of the MOF as a function of frequency. The frequency-dependent impedance can provide information about the charge transport properties of the MOF. Similarly, the measurement can be performed in single crystals, thin films, or press pellets. Once again, changes in these properties can be induced by the sorption of the analyte, providing a probe for the detection and quantification of analyte gases.[259,260]

(iii) Field effect transistors (FETs): when a MOF is used as the active material in a FET, changes in the conductivity of the framework upon gas adsorption can be measured using the FET. However, unlike the previous techniques, this measurement is not amenable to polycrystalline samples; instead, MOF single crystals or films are required, which, depending on the material, could pose a synthetic bottleneck.[261,262]

(c) Magnetism measurements: this technique is premised on the fact that the magnetic properties of certain materials will change during sorption of analyte molecules. Changes in magnetic properties can be measured using a variety of sophisticated techniques and related to the concentration of analyte gas.[263,264]

(d) Mass-change: the change of mass that a material, such as a MOF, experiences after the adsorption of a specific gas can be used to evaluate the presence and/or concentration of that gas.

Open Access Article. Published on 10 March 2025. Downloaded on 6/30/2025 11:42:55 PM. This article is licensed under a Creative Commons Attribution 3.0 Unported Licence.

(e) Other techniques: other techniques are used case-by-case to evaluate, study, and apply MOFs as sensors. Some examples are UV-vis absorption, calorimetry, and many others.[265,266]

A comprehensive understanding of these techniques is essential to designing and optimizing MOF-based gas sensors and detectors.

Conclusions

A select class of Metal–organic Frameworks possess high surface area, well-defined pore distribution, and high thermal and chemical stability. In light of these properties, it is not surprising that MOFs have recently garnered significant interest in detection and sensing research. Of particular interest is the detection of SO_2, a hazardous gas to which several chemically stable MOFs have demonstrated promising compatibility. Most SO_2 related MOF research has concentrated on SO_2 adsorption capacity, emphasizing the highest uptake capacity. This is typically reported in conjunction with comprehensive computational and experimental studies that aim to elucidate the specific chemical and physical interactions between SO_2 and the framework with a view to identifying the preferential adsorption sites. This approach has been successfully used for a wide range of materials, yielding valuable insight into the nature of SO_2 adsorption in porous materials. However, in the context of SO_2 detection, both the SO_2 affinity of the framework and the SO_2 adsorption capacity at low pressure must be considered – rather than overall uptake at high pressure. Thus, it is necessary to explore characteristics of MOFs pertinent to SO_2 detection, which typically diverge from those that promote large SO_2 uptake at high pressure. Higher SO_2 uptake at low pressure reflects stronger SO_2 interactions within the framework; this is critical to the operation of SO_2 detectors under environmental conditions since relatively low SO_2 concentrations of $\leq$5000 ppm are typically relevant for sensing. Analysis of the most effective MOFs for SO_2 capture has demonstrated a clear correlation between SO_2 capture at low pressure (0.01 bar) and the pore-limiting diameter.

We have provided an overview of techniques used to perform SO_2 detection in MOFs and evaluated which MOF candidates are likely to perform best. In addition to a high adsorption capacity at low pressure and requisite chemical stability, MOFs require distinct characteristics to selectively detect specific analytes such as SO_2. MOF-based analyte detection is predicated on quantitative (or, in some cases, qualitative) measurement of the response to a particular environmental stimulus (*i.e.*, SO_2 adsorption). As we have outlined, the response typically consists of changes in luminescence, electrochemical properties, or magnetism. Examples of MOF based SO_2 detection using these methodologies have been reported and outlined in detail in the main text. Cruicially, advancement in materials processing combined with excellent chemical stability allow select MOFs to be incorporated into detectors based on nanofiber membranes, electrodes, and test strips.

This review provides a broad overview of the significant role that chemically stable MOFs will play in the expanding field of SO_2 detection. The extraordinary diversity of physiochemical properties displayed by MOFs provides space for chemists to further refine MOF-SO_2 interactions, guided by new characterisation techniques and supported by advanced computational tools. The insights garnered from this process will inform the design of future MOF-based detectors for SO_2 and other volatile compounds.

List of abbreviations

AIP	5-Aminoisophthalate
ATT	3-Amino-1,2,4-triazole-5-thiol
ADC	Acetylenedicarboxylate
BET	Brunauer–Emmett–Teller
BTC	Benzene-1,3,5-tricarboxylate, trimesate
BDC	1,4-Benzenedicarboxylate, terephthalate
BDC-Br	2-Bromoterephthalate
BDC-NH_2	2-Aminoterephthalate
BDC-CH$=$$CH_2$	2-Vinylterephthalate
BDC-NO_2	2-Nitroterephthalate
BDC-4F	2,3,5,6-Tetrafluoro-1,4-benzenedicarboxylate
BPDC	4,4′-Biphenyldicarboxylate
BPTC	Biphenyl-3,3′,5,5′-tetracarboxylate
BTEC	1,2,4,5-Benzenetetracarboxylate
BDP	1,4-Bis(4-pyrazolyl)benzene
CPE	Carbon paste electrode
CDC	9*H*-Carbazole-3,6-dicarboxylate
CD	Carbon dot
CYCU	Chung-Yuan Christian University
CAU	Christian-Albrechts-University
CUK	Cambridge-University-KRICT
CNT	Carbon nanotubes
DFT	Density functional theory
DUT	Dresden University of Technology
DOBPDC	4,4-Dioxidobiphenyl-3,3-dicarboxylate
DABCO	1,4-Diazabicyclo[2,2,2]octane
DHTP	2,5-Dihydroxyterephthalate
DRIFTS	Diffuse reflectance infrared Fourier transform spectroscopy
ETTA	4,4′,4″,4‴-(Ethene-1,1,2,2-tetrayl)tetrabenzoicate
ET-LMOF	Energy transfer LMOFs
GCMC	Grand canonical Monte Carlo
GAL	Gallate
FTIR	Fourier transform infrared
FDCA	2,5-Furandicarboxylate
Fum	Fumarate
FGD	Flue-gas desulfurization
HS	High-spin
HSAB	Pearson's hard-soft acid–base theory
HHTP	2,3,5,6,10,11-Hexahydroxytriphenylene
HATP	2,3,6,7,10,11-Hexaaminotriphenylene
HKUST	Hong Kong University of Science and Technology

 This journal is © The Royal Society of Chemistry 2025

Open Access Article. Published on 10 March 2025. Downloaded on 6/30/2025 11:42:55 PM. This article is licensed under a Creative Commons Attribution 3.0 Unported Licence.

LMOFs	Luminescent metal–organic frameworks
LOD	Limit of detection
NDC-$(NO_2)_2$	4,8-Dinitronaphthalene-2,6-dicarboxylate
NDC	1,4-Naphthalenedicarboxylate
NOTT	Nottingham University
NU	Northwestern University
IRMOF	Isoreticular metal–organic framework
MOCs	Metal–organic cages
MOFs	Metal–organic frameworks
MIL	Matériaux de l' Institut Lavoisier
MFM	Manchester framework material
MUF	Massey University Framework
MPBA	*N*,*N*′-2,4,6-Trimethyl-1,3-phenylenebis(oxamate)
OTf	Trifuoromethanesulfonate
THBA	2,3,4-Trihydroxybenzaldehyde
TBAPy	4,4′,4″,4‴-(Pyrene-1,3,6,8-tetrayl)tetrabenzoate
TCPP	*meso*-Tetrakis(4-carboxylphenyl)porphyrin
TDC	2,5-Thiophenedicarboxylate
TBA	4-(4*H*-1,2,4-Triazol-4-yl)benzoate
TRPL	Time-resolved photoluminescence
LS	Low-spin
LOD	Limit of detection
TATB	2,4,6-Tris(4-carboxyphenyl)-1,3,5-triazine
TDC	2,5-Thiophenedicarboxylate
SDC	4,4′-Stilbenedicarboxylate
SCO	Spin-crossover
ppm	Parts per million
ppb	Parts per billion
POCs	Porous organic cages
PAN	Polyacrylonitrile
PAC	*meso*-Tetrakis(4-carboxylphenyl)porphyrin
PA	*m*-Phthalate
PDDB	4,4′-(Pyridine-2,6-diyl)dibenzoate
PHEN	1,10-Phenanthroline
PBTA	4,4′4″,4‴-(4,4′-(1,4-Phenylene)bis (pyridine-6,4,2-triyl))-tetrabenzoate
PCN	Porous coordination network
PPTA	4,4′,4″,4‴-(1,4-Phenylenebis(pyridine-4,2,6-triyl))tetrabenzoate
PXRD	Powder X-ray diffraction
PDCA	2,4-Pyridinedicarboxylate
PLD	Pore limiting diameter
PVDF	Polyvinylidene fluoride
PTBA	4,4′,4″,4‴-(1,4-Phenylenebis(azanetriyl))tetrabenzoate
PZDC	1*H*-Pyrazole-3,5-dicarboxylate
UiO	Universitetet i Oslo
SCXRD	Single-crystal X-ray diffraction
ZIF	Zeolitic imidazolate framework

Data availability

All data is available in the main text.

Conflicts of interest

There are no conflicts to declare.

Acknowledgements

J. L. O. and C. V. F. thanks CONAHCYT for the PhD fellowship (1003953 and 1040318). I. A. I. thanks PAPIIT-UNAM (IN201123), México, for financial support. We thank U. Winnberg (Euro Farmacos EIR) for scientific discussions and G. Ibarra-Winnberg for scientific encouragement. C. J. thanks the DFG for funding within the Priority Program SPP 1928/2 COORNETs (grant Ja466/43-1).

References

1 L. Bai, J. Wang, X. Ma and H. Lu, *Int. J. Environ. Res. Public Health*, 2018, **15**, 780.
2 M. Höök and X. Tang, *Energy Policy*, 2013, **52**, 797–809.
3 B. Zhang and G. Chen, *Process Saf. Environ. Prot.*, 2010, **88**, 253–262.
4 N. Abas, A. Kalair and N. Khan, *Futures*, 2015, **69**, 31–49.
5 F. Perera, *Int. J. Environ. Res. Public Health*, 2017, **15**, 16.
6 M. E. Quesada-Valverde and A. Quesada-Román, *Geosciences*, 2023, **13**, 39.
7 A. N. Torres, A. L. M. Del Pozzo, G. Groppelli and M. Del Carmen Jaimes Viera, *J. Volcanol. Geotherm. Res.*, 2023, **433**, 107733.
8 S. Valade, D. Coppola, R. Campion, A. Ley, T. Boulesteix, N. Taquet, D. Legrand, M. Laiolo, T. R. Walter and S. De La Cruz-Reyna, *Nat. Commun.*, 2023, **14**, 3254.
9 B. Divol, M. Du Toit and E. Duckitt, *Appl. Microbiol. Biotechnol.*, 2012, **95**, 601–613.
10 E. Calabrese, C. Sacco, G. Moore and S. DiNardi, *Med. Hypotheses*, 1981, **7**, 133–145.
11 P. Amoatey, H. Omidvarborna, M. S. Baawain and A. Al-Mamun, *Process Saf. Environ. Prot.*, 2019, **123**, 215–228.
12 R. J. Melia, C. D. Florey and A. V. Swan, *J. Epidemiol. Community Health*, 1981, **35**, 161–167.
13 W. Van Roy, B. Van Roozendael, L. Vigin, A. Van Nieuwenhove, K. Scheldeman, J.-B. Merveille, A. Weigelt, J. Mellqvist, J. Van Vliet, D. Van Dinther, J. Beecken, F. Tack, N. Theys and F. Maes, *Commun. Earth Environ.*, 2023, **4**, 391.
14 V. Jonas, G. Frenking and M. T. Reetz, *J. Am. Chem. Soc.*, 1994, **116**, 8741–8753.
15 T. P. Cunningham, D. L. Cooper, J. Gerratt, P. B. Karadakov and M. Raimondi, *J. Chem. Soc., Faraday Trans.*, 1997, **93**, 2247–2254.
16 D. Patel, D. Margolese and T. R. Dykea, *J. Chem. Phys.*, 1979, **70**, 2740–2747.
17 I. Jana, S. Naskar and D. Nandi, *J. Phys.:Conf. Ser.*, 2020, **1412**, 052005.
18 Y. Qu, J. An, Y. He and J. Zheng, *J. Environ. Sci.*, 2016, **44**, 13–25.
19 M. M. M. F. Jion, J. N. Jannat, M. Y. Mia, M. A. Ali, M. S. Islam, S. M. Ibrahim, S. C. Pal, A. Islam, A. Sarker,

Open Access Article. Published on 10 March 2025. Downloaded on 6/30/2025 11:42:55 PM. This article is licensed under a Creative Commons Attribution 3.0 Unported Licence.

G. Malafaia, M. Bilal and A. R. M. T. Islam, *Sci. Total Environ*, 2023, **876**, 162851.
20 N. D. Abdul Halim, M. T. Latif, F. Ahamad, D. Dominick, J. X. Chung, L. Juneng and M. F. Khan, *Heliyon*, 2018, **4**, e01054.
21 M. Ali and M. Athar, *Environ. Monit. Assess.*, 2010, **171**, 353–363.
22 Z.-Y. Meng, X.-B. Xu, T. Wang, X.-Y. Zhang, X.-L. Yu, S.-F. Wang, W.-L. Lin, Y.-Z. Chen, Y.-A. Jiang and X.-Q. An, *Atmos. Environ.*, 2010, **44**, 2625–2631.
23 C. Mallik and S. Lal, *Environ. Monit. Assess.*, 2014, **186**, 1295–1310.
24 S. S. Mousavi, G. Goudarzi, S. Sabzalipour, M. M. Rouzbahani and E. Mobarak Hassan, *Environ. Sci. Pollut. Res.*, 2021, **28**, 56996–57008.
25 B. J. Freedman, *Br. J. Dis. Chest*, 1980, **74**, 128–134.
26 S. Giacosa, S. Río Segade, E. Cagnasso, A. Caudana, L. Rolle and V. Gerbi, *Red Wine Technology*, Elsevier, 2019, pp. 309–321.
27 P. Mars, *J. Catal.*, 1968, **10**, 1–12.
28 F. García-Labiano, L. F. De Diego, A. Cabello, P. Gayán, A. Abad, J. Adánez and G. Sprachmann, *Appl. Energy*, 2016, **178**, 736–745.
29 A. S. Milev, G. S. K. Kannangara and M. A. Wilson, in *Kirk-Othmer Encyclopedia of Chemical Technology*, ed. Kirk-Othmer, Wiley, 1st edn, 2005.
30 R. Saidur, M. Sattar, H. H. Masjuki and M. Y. Jamaluddin, *Energy Environ.*, 2009, **20**, 533–551.
31 S. Piché, F. Larachi and B. P. A. Grandjean, *Ind. Eng. Chem. Res.*, 2001, **40**, 476–487.
32 F. W. Adams, *Ind. Eng. Chem.*, 1933, **25**, 424–428.
33 B. Hanley and C. Chen, *AIChE J.*, 2012, **58**, 132–152.
34 M. Reda and G. R. Carmichael, *Atmos. Environ.*, 1982, **16**, 151–159.
35 R. K. Srivastava, W. Jozewicz and C. Singer, *Environ. Prog.*, 2001, **20**, 219–228.
36 D. B. Gingerich, E. Grol and M. S. Mauter, *Environ. Sci.: Water Res. Technol.*, 2018, **4**, 909–925.
37 P. Luis, A. Garea and A. Irabien, *J. Membr. Sci.*, 2009, **330**, 80–89.
38 Y. Sun, J. Xie, W. Huang, G. Li, S. Li, P. Cui, H. Xu, Z. Qu and N. Yan, *Fuel*, 2021, **288**, 119714.
39 Q. Xin, C. Zhang, Y. Zhang, Q. Liang, L. Zhang, S. Wang, H. Ye, X. Ding and Y. Zhang, *Sep. Purif. Technol.*, 2021, **259**, 118222.
40 P. Luis, A. Garea and A. Irabien, *J. Chem. Technol. Biotechnol.*, 2008, **83**, 1570–1577.
41 H.-K. Lee, B. R. Deshwal and K.-S. Yoo, *Korean J. Chem. Eng.*, 2005, **22**, 208–213.
42 Y. A. Husnil, R. Andika and M. Lee, *J. Process Control*, 2019, **74**, 147–159.
43 W. Liu, R. D. Vidic and T. D. Brown, *Environ. Sci. Technol.*, 2000, **34**, 154–159.
44 H. Yi, H. Deng, X. Tang, Q. Yu, X. Zhou and H. Liu, *J. Hazard. Mater.*, 2012, **203–204**, 111–117.
45 H. Fu, X. Wang, H. Wu, Y. Yin and J. Chen, *J. Phys. Chem. C*, 2007, **111**, 6077–6085.
46 Y. Li, L. Li and J. Yu, *Chem*, 2017, **3**, 928–949.
47 S. Beyaz Kayiran and F. Lamari Darkrim, *Surf. Interface Anal.*, 2002, **34**, 100–104.
48 E. Pérez-Botella, S. Valencia and F. Rey, *Chem. Rev.*, 2022, **122**, 17647–17695.
49 Y. Tao, H. Kanoh, L. Abrams and K. Kaneko, *Chem. Rev.*, 2006, **106**, 896–910.
50 N. K. Gupta, E. J. Kim, S. Baek, J. Bae and K. S. Kim, *Sci. Rep.*, 2022, **12**, 15387.
51 C. Petit, *Curr. Opin. Chem. Eng.*, 2018, **20**, 132–142.
52 J. L. Obeso, D. R. Amaro, C. V. Flores, A. Gutiérrez-Alejandre, R. A. Peralta, C. Leyva and I. A. Ibarra, *Coord. Chem. Rev.*, 2023, **485**, 215135.
53 A. Carné-Sánchez, J. Martínez-Esaín, T. Rookard, C. J. Flood, J. Faraudo, K. C. Stylianou and D. Maspoch, *ACS Appl. Mater. Interfaces*, 2023, **15**, 6747–6754.
54 E. Martínez-Ahumada, D. He, V. Berryman, A. López-Olvera, M. Hernandez, V. Jancik, V. Martis, M. A. Vera, E. Lima, D. J. Parker, A. I. Cooper, I. A. Ibarra and M. Liu, *Angew. Chem., Int. Ed.*, 2021, **60**, 17556–17563.
55 J. L. Obeso, A. López-Olvera, C. V. Flores, E. Martínez-Ahumada, R. Paz, H. Viltres, A. Islas-Jácome, E. González-Zamora, J. Balmaseda, S. López-Morales, M. A. Vera, E. Lima, I. A. Ibarra and C. Leyva, *J. Mol. Liq.*, 2022, **368**, 120758.
56 S. R. Batten, N. R. Champness, X.-M. Chen, J. Garcia-Martinez, S. Kitagawa, L. Öhrström, M. O'Keeffe, M. Paik Suh and J. Reedijk, *Pure Appl. Chem.*, 2013, **85**, 1715–1724.
57 S. R. Batten, N. R. Champness, X.-M. Chen, J. Garcia-Martinez, S. Kitagawa, L. Öhrström, M. O'Keeffe, M. P. Suh and J. Reedijk, *CrystEngComm*, 2012, **14**, 3001.
58 S. L. James, *Chem. Soc. Rev.*, 2003, **32**, 276.
59 H.-C. Joe Zhou and S. Kitagawa, *Chem. Soc. Rev.*, 2014, **43**, 5415–5418.
60 N. K. Gupta, A. López-Olvera, E. González-Zamora, E. Martínez-Ahumada and I. A. Ibarra, *ChemPlusChem*, 2022, **87**, e202200006.
61 J. L. Obeso, H. Viltres, C. V. Flores, A. López-Olvera, A. R. Rajabzadeh, S. Srinivasan, I. A. Ibarra and C. Leyva, *J. Environ. Chem. Eng.*, 2023, **11**, 109872.
62 J. L. Obeso, V. B. López-Cervantes, C. V. Flores, H. Viltres, C. Serrano-Fuentes, L. Herrera-Zuñiga, N. S. Portillo-Vélez, R. A. Peralta, D. Solis-Ibarra, I. A. Ibarra and C. Leyva, *ACS Sustainable Resour. Manage.*, 2024, **1**, 661–669.
63 C. V. Flores, J. L. Obeso, H. Viltres, R. A. Peralta, I. A. Ibarra and C. Leyva, *Environ. Sci.: Water Res. Technol.*, 2024, **10**, 2142–2147.
64 J. L. Obeso, J. G. Flores, C. V. Flores, V. B. López-Cervantes, V. Martínez-Jiménez, J. A. De Los Reyes, E. Lima, D. Solis-Ibarra, I. A. Ibarra, C. Leyva and R. A. Peralta, *Dalton Trans.*, 2023, **52**, 12490–12495.
65 J. G. Flores, J. L. Obeso, V. Martínez-Jiménez, N. Martín-Guaregua, A. Islas-Jácome, E. González-Zamora, H. Serrano-Espejel, B. Mondragón-Rodríguez, C. Leyva, D. A. Solís-Casados, I. A. Ibarra, R. A. Peralta, J. Aguilar-Pliego and J. Antonio De Los Reyes, *RSC Adv.*, 2023, **13**, 27174–27179.

 This journal is © The Royal Society of Chemistry 2025

Open Access Article. Published on 10 March 2025. Downloaded on 6/30/2025 11:42:55 PM. This article is licensed under a Creative Commons Attribution 3.0 Unported Licence.

66 V. Pascanu, G. González Miera, A. K. Inge and B. Martín-Matute, *J. Am. Chem. Soc.*, 2019, **141**, 7223–7234.
67 S. Rojas, I. Colinet, D. Cunha, T. Hidalgo, F. Salles, C. Serre, N. Guillou and P. Horcajada, *ACS Omega*, 2018, **3**, 2994–3003.
68 E. Medel, J. L. Obeso, C. Serrano-Fuentes, J. Garza, I. A. Ibarra, C. Leyva, A. K. Inge, A. Martínez and R. Vargas, *Chem. Commun.*, 2023, **59**, 8684–8687.
69 S. Bügel, Q.-D. Hoang, A. Spieß, Y. Sun, S. Xing and C. Janiak, *Membranes*, 2021, **11**, 795.
70 H. B. Tanh Jeazet, C. Staudt and C. Janiak, *Dalton Trans.*, 2012, **41**, 14003.
71 B. Gil-Hernández, S. Millan, I. Gruber, M. Quirós, D. Marrero-López, C. Janiak and J. Sanchiz, *Inorg. Chem.*, 2022, **61**, 11651–11666.
72 B. Gil-Hernández, P. Gili, J. K. Vieth, C. Janiak and J. Sanchiz, *Inorg. Chem.*, 2010, **49**, 7478–7490.
73 X. Han, S. Yang and M. Schröder, *Nat. Rev. Chem.*, 2019, **3**, 108–118.
74 S. Han, Y. Huang, T. Watanabe, S. Nair, K. S. Walton, D. S. Sholl and J. Carson Meredith, *Microporous Mesoporous Mater.*, 2013, **173**, 86–91.
75 G. Mouchaham, S. Wang and C. Serre, in *Metal-Organic Frameworks*, ed. H. García and S. Navalón, Wiley, 1st edn, 2018, pp. 1–28.
76 K. O. Kirlikovali, S. L. Hanna, F. A. Son and O. K. Farha, *ACS Nanosci. Au*, 2023, **3**, 37–45.
77 R. G. Pearson, *J. Am. Chem. Soc.*, 1963, **85**, 3533–3539.
78 Y. Jin, H. Liu, M. Feng, Q. Ma and B. Wang, *Adv. Funct. Mater.*, 2023, 2304773.
79 I. Senkovska and S. Kaskel, *Chem. Commun.*, 2014, **50**, 7089.
80 J. Valdes-García, L. D. Rosales-Vázquez, I. J. Bazany-Rodríguez and A. Dorazco-González, *Chem. – Asian J.*, 2020, **15**, 2925–2938.
81 C. Bargossi, M. C. Fiorini, M. Montalti, L. Prodi and N. Zaccheroni, *Coord. Chem. Rev.*, 2000, **208**, 17–32.
82 H.-Y. Li, S.-N. Zhao, S.-Q. Zang and J. Li, *Chem. Soc. Rev.*, 2020, **49**, 6364–6401.
83 Y. Jian, W. Hu, Z. Zhao, P. Cheng, H. Haick, M. Yao and W. Wu, *Nano-Micro Lett.*, 2020, **12**, 71.
84 G. Yang, X. Jiang, H. Xu and B. Zhao, *Small*, 2021, **17**, 2005327.
85 Y. Wang, Y. Zhu, A. Binyam, M. Liu, Y. Wu and F. Li, *Biosens. Bioelectron.*, 2016, **86**, 432–438.
86 Y. T. Azar, M. S. Lakmehsari, S. M. Kazem Manzoorolajdad, V. Sokhanvaran, Z. Ahadi, A. Shahsavani and P. K. Hopke, *Mater. Chem. Phys.*, 2020, **239**, 122105.
87 W.-T. Koo, J.-S. Jang and I.-D. Kim, *Chem*, 2019, **5**, 1938–1963.
88 Y. Li, S. Zhang and D. Song, *Angew. Chem., Int. Ed.*, 2013, **52**, 710–713.
89 R. Lin, S. Liu, J. Ye, X. Li and J. Zhang, *Adv. Sci.*, 2016, **3**, 1500434.
90 N. B. Shustova, A. F. Cozzolino, S. Reineke, M. Baldo and M. Dincă, *J. Am. Chem. Soc.*, 2013, **135**, 13326–13329.
91 X. Li, B. Liu, K. Ye, L. Ni, X. Xu, F. Qiu, J. Pan and X. Niu, *Sens. Actuators, B*, 2019, **297**, 126822.
92 Z.-P. Ni, J.-L. Liu, Md. N. Hoque, W. Liu, J.-Y. Li, Y.-C. Chen and M.-L. Tong, *Coord. Chem. Rev.*, 2017, **335**, 28–43.
93 A. Tissot, X. Kesse, S. Giannopoulou, I. Stenger, L. Binet, E. Rivière and C. Serre, *Chem. Commun.*, 2019, **55**, 194–197.
94 P. D. Southon, L. Liu, E. A. Fellows, D. J. Price, G. J. Halder, K. W. Chapman, B. Moubaraki, K. S. Murray, J.-F. Létard and C. J. Kepert, *J. Am. Chem. Soc.*, 2009, **131**, 10998–11009.
95 N. Kau, G. Jindal, R. Kaur and S. Rana, *Results Chem.*, 2022, **4**, 100678.
96 P. Samanta, S. Let, W. Mandal, S. Dutta and S. K. Ghosh, *Inorg. Chem. Front.*, 2020, **7**, 1801–1821.
97 H. Zhou, X. Hui, D. Li, D. Hu, X. Chen, X. He, L. Gao, H. Huang, C. Lee and X. Mu, *Adv. Sci.*, 2020, **7**, 2001173.
98 G. Ji, T. Zheng, X. Gao and Z. Liu, *Sens. Actuators, B*, 2019, **284**, 91–95.
99 W.-J. Ju, L.-M. Fu, R.-J. Yang and C.-L. Lee, *Lab Chip*, 2012, **12**, 622–626.
100 T. R. Khan and J. C. Meranger, *Environ. Int.*, 1983, **9**, 195–206.
101 P. Popp and G. Oppermann, *J. Chromatogr. A*, 1981, **207**, 131–137.
102 W. L. Crider, *Anal. Chem.*, 1965, **37**, 1770–1773.
103 M. S. Yogendra Kumar, M. D. Gowtham, Mahadevaiah and G. Nagendrappa, *Anal. Sci.*, 2006, **22**, 757–761.
104 Y. Wen, P. Zhang, V. K. Sharma, X. Ma and H.-C. Zhou, *Cell Rep.*, 2021, **2**, 100348.
105 O. D. Agboola and N. U. Benson, *Front. Environ. Sci.*, 2021, **9**, 678574.
106 E. Martínez-Ahumada, M. L. Díaz-Ramírez, M. D. J. Velásquez-Hernández, V. Jancik and I. A. Ibarra, *Chem. Sci.*, 2021, **12**, 6772–6799.
107 A. J. Rieth, A. M. Wright and M. Dincă, *Nat. Rev. Mater.*, 2019, **4**, 708–725.
108 Q. Zhang, H. Yang, T. Zhou, X. Chen, W. Li and H. Pang, *Adv. Sci.*, 2022, **9**, 2204141.
109 X.-D. Song, S. Wang, C. Hao and J.-S. Qiu, *Inorg. Chem. Commun.*, 2014, **46**, 277–281.
110 E. Martínez-Ahumada, A. López-Olvera, V. Jancik, J. E. Sánchez-Bautista, E. González-Zamora, V. Martis, D. R. Williams and I. A. Ibarra, *Organometallics*, 2020, **39**, 883–915.
111 G. J. Kubas, *Inorg. Chem.*, 1979, **18**, 182–188.
112 D. Kim, M. Kang, H. Ha, C. S. Hong and M. Kim, *Coord. Chem. Rev.*, 2021, **438**, 213892.
113 Y. Lin, C. Kong and L. Chen, *RSC Adv.*, 2016, **6**, 32598–32614.
114 S. Yang, J. Sun, A. J. Ramirez-Cuesta, S. K. Callear, W. I. F. David, D. P. Anderson, R. Newby, A. J. Blake, J. E. Parker, C. C. Tang and M. Schröder, *Nat. Chem.*, 2012, **4**, 887–894.
115 J. H. Carter, C. G. Morris, H. G. W. Godfrey, S. J. Day, J. Potter, S. P. Thompson, C. C. Tang, S. Yang and M. Schröder, *ACS Appl. Mater. Interfaces*, 2020, **12**, 42949–42954.
116 J. A. Zárate, E. Sánchez-González, D. R. Williams, E. González-Zamora, V. Martis, A. Martínez, J. Balmaseda, G. Maurin and I. A. Ibarra, *J. Mater. Chem. A*, 2019, **7**, 15580–15584.

Open Access Article. Published on 10 March 2025. Downloaded on 6/30/2025 11:42:55 PM. This article is licensed under a Creative Commons Attribution 3.0 Unported Licence.

117 M. Savage, Y. Cheng, T. L. Easun, J. E. Eyley, S. P. Argent, M. R. Warren, W. Lewis, C. Murray, C. C. Tang, M. D. Frogley, G. Cinque, J. Sun, S. Rudić, R. T. Murden, M. J. Benham, A. N. Fitch, A. J. Blake, A. J. Ramirez-Cuesta, S. Yang and M. Schröder, *Adv. Mater.*, 2016, **28**, 8705–8711.
118 A. López-Olvera, J. A. Zárate, E. Martínez-Ahumada, D. Fan, M. L. Díaz-Ramírez, P. A. Sáenz-Cavazos, V. Martis, D. R. Williams, E. Sánchez-González, G. Maurin and I. A. Ibarra, *ACS Appl. Mater. Interfaces*, 2021, **13**, 39363–39370.
119 A. López-Olvera, S. Pioquinto-García, J. Antonio Zárate, G. Diaz, E. Martínez-Ahumada, J. L. Obeso, V. Martis, D. R. Williams, H. A. Lara-García, C. Leyva, C. V. Soares, G. Maurin, I. A. Ibarra and N. E. Dávila-Guzmán, *Fuel*, 2022, **322**, 124213.
120 S. G. Dunning, N. K. Gupta, J. E. Reynolds, M. Sagastuy-Breña, J. G. Flores, E. Martínez-Ahumada, E. Sánchez-González, V. M. Lynch, A. Gutiérrez-Alejandre, J. Aguilar-Pliego, K.-S. Kim, I. A. Ibarra and S. M. Humphrey, *Inorg. Chem.*, 2022, **61**, 15037–15044.
121 P. Brandt, A. Nuhnen, M. Lange, J. Möllmer, O. Weingart and C. Janiak, *ACS Appl. Mater. Interfaces*, 2019, **11**, 17350–17358.
122 C. Jansen, N. Tannert, D. Lenzen, M. Bengsch, S. Millan, A. Goldman, D. N. Jordan, L. Sondermann, N. Stock and C. Janiak, *Z. Anorg. Allg. Chem.*, 2022, **648**, e202200170.
123 Ü. Kökçam-Demir, A. Goldman, L. Esrafili, M. Gharib, A. Morsali, O. Weingart and C. Janiak, *Chem. Soc. Rev.*, 2020, **49**, 2751–2798.
124 L. Tao, C.-Y. Lin, S. Dou, S. Feng, D. Chen, D. Liu, J. Huo, Z. Xia and S. Wang, *Nano Energy*, 2017, **41**, 417–425.
125 A. Yadav, S. Kumari, P. Yadav, A. Hazra, A. Chakraborty and P. Kanoo, *Dalton Trans.*, 2022, **51**, 15496–15506.
126 J. H. Choe, H. Kim and C. S. Hong, *Mater. Chem. Front.*, 2021, **5**, 5172–5185.
127 K. Tan, S. Zuluaga, H. Wang, P. Canepa, K. Soliman, J. Cure, J. Li, T. Thonhauser and Y. J. Chabal, *Chem. Mater.*, 2017, **29**, 4227–4235.
128 G. L. Smith, J. E. Eyley, X. Han, X. Zhang, J. Li, N. M. Jacques, H. G. W. Godfrey, S. P. Argent, L. J. McCormick McPherson, S. J. Teat, Y. Cheng, M. D. Frogley, G. Cinque, S. J. Day, C. C. Tang, T. L. Easun, S. Rudić, A. J. Ramirez-Cuesta, S. Yang and M. Schröder, *Nat. Mater.*, 2019, **18**, 1358–1365.
129 W. Li, J. Li, T. D. Duong, S. A. Sapchenko, X. Han, J. D. Humby, G. F. S. Whitehead, I. J. Victórica-Yrezábal, I. Da Silva, P. Manuel, M. D. Frogley, G. Cinque, M. Schröder and S. Yang, *J. Am. Chem. Soc.*, 2022, **144**, 13196–13204.
130 E. Martínez-Ahumada, M. L. Díaz-Ramírez, H. A. Lara-García, D. R. Williams, V. Martis, V. Jancik, E. Lima and I. A. Ibarra, *J. Mater. Chem. A*, 2020, **8**, 11515–11520.
131 O. V. Gutov, M. G. Hevia, E. C. Escudero-Adán and A. Shafir, *Inorg. Chem.*, 2015, **54**, 8396–8400.
132 M. Szufla, J. A. R. Navarro, K. Góra-Marek and D. Matoga, *ACS Appl. Mater. Interfaces*, 2023, **15**, 28184–28192.
133 W. Xiang, Y. Zhang, Y. Chen, C. Liu and X. Tu, *J. Mater. Chem. A*, 2020, **8**, 21526–21546.
134 L. M. Rodríguez-Albelo, E. López-Maya, S. Hamad, A. R. Ruiz-Salvador, S. Calero and J. A. R. Navarro, *Nat. Commun.*, 2017, **8**, 14457.
135 S. Li, W. Han, Q. An, K. Yong and M. Yin, *Adv. Funct. Mater.*, 2023, **33**, 2303447.
136 T. Matemb Ma Ntep, H. Breitzke, L. Schmolke, C. Schlüsener, B. Moll, S. Millan, N. Tannert, I. El Aita, G. Buntkowsky and C. Janiak, *Chem. Mater.*, 2019, **31**, 8629–8638.
137 D. Britt, D. Tranchemontagne and O. M. Yaghi, *Proc. Natl. Acad. Sci. U. S. A.*, 2008, **105**, 11623–11627.
138 S. Glomb, D. Woschko, G. Makhloufi and C. Janiak, *ACS Appl. Mater. Interfaces*, 2017, **9**, 37419–37434.
139 J. H. Carter, X. Han, F. Y. Moreau, I. Da Silva, A. Nevin, H. G. W. Godfrey, C. C. Tang, S. Yang and M. Schröder, *J. Am. Chem. Soc.*, 2018, **140**, 15564–15567.
140 P. Brandt, A. Nuhnen, S. Öztürk, G. Kurt, J. Liang and C. Janiak, *Adv. Sustainable Syst.*, 2021, **5**, 2000285.
141 M. Mon, E. Tiburcio, J. Ferrando-Soria, R. Gil San Millán, J. A. R. Navarro, D. Armentano and E. Pardo, *Chem. Commun.*, 2018, **54**, 9063–9066.
142 F. Chen, D. Lai, L. Guo, J. Wang, P. Zhang, K. Wu, Z. Zhang, Q. Yang, Y. Yang, B. Chen, Q. Ren and Z. Bao, *J. Am. Chem. Soc.*, 2021, **143**, 9040–9047.
143 S. Xing, J. Liang, P. Brandt, F. Schäfer, A. Nuhnen, T. Heinen, I. Boldog, J. Möllmer, M. Lange, O. Weingart and C. Janiak, *Angew. Chem., Int. Ed.*, 2021, **60**, 17998–18005.
144 Y. L. Fan, H. P. Zhang, M. J. Yin, R. Krishna, X. F. Feng, L. Wang, M. B. Luo and F. Luo, *Inorg. Chem.*, 2021, **60**, 4–8.
145 Y.-B. Ren, H.-Y. Xu, S.-Q. Gang, Y.-J. Gao, X. Jing and J.-L. Du, *Chem. Eng. J.*, 2022, **431**, 134057.
146 Y. Zhang, P. Zhang, W. Yu, J. Zhang, J. Huang, J. Wang, M. Xu, Q. Deng, Z. Zeng and S. Deng, *ACS Appl. Mater. Interfaces*, 2019, **11**, 10680–10688.
147 K. Vellingiri, A. Deep and K.-H. Kim, *ACS Appl. Mater. Interfaces*, 2016, **8**, 29835–29857.
148 J.-Y. Lee, T. C. Keener and Y. J. Yang, *J. Air Waste Manage. Assoc.*, 2009, **59**, 725–732.
149 Y. Igarashi, Y. Sawa, K. Yoshioka, H. Matsueda, K. Fujii and Y. Dokiya, *J. Geophys. Res.*, 2004, **109**, 2003JD004428.
150 S. D. Worrall, M. A. Bissett, P. I. Hill, A. P. Rooney, S. J. Haigh, M. P. Attfield and R. A. W. Dryfe, *Electrochim. Acta*, 2016, **222**, 361–369.
151 P. Brandt, S.-H. Xing, J. Liang, G. Kurt, A. Nuhnen, O. Weingart and C. Janiak, *ACS Appl. Mater. Interfaces*, 2021, **13**, 29137–29149.
152 P. Liu, K. Cai, K. Wang, T. Zhao and D.-J. Tao, *Green Energy Environ.*, 2023, S2468025723001309.
153 S. Gorla, M. L. Díaz-Ramírez, N. S. Abeynayake, D. M. Kaphan, D. R. Williams, V. Martis, H. A. Lara-García, B. Donnadieu, N. Lopez, I. A. Ibarra and V. Montiel-Palma, *ACS Appl. Mater. Interfaces*, 2020, **12**, 41758–41764.

 This journal is © The Royal Society of Chemistry 2025

Open Access Article. Published on 10 March 2025. Downloaded on 6/30/2025 11:42:55 PM. This article is licensed under a Creative Commons Attribution 3.0 Unported Licence.

154 J. García Ponce, M. L. Díaz-Ramírez, S. Gorla, C. Navarathna, G. Sanchez-Lecuona, B. Donnadieu, I. A. Ibarra and V. Montiel-Palma, *CrystEngComm*, 2021, **23**, 7479–7484.
155 X.-H. Xiong, Z.-W. Wei, W. Wang, L.-L. Meng and C.-Y. Su, *J. Am. Chem. Soc.*, 2023, **145**, 14354–14364.
156 J. Liang, S. Xing, P. Brandt, A. Nuhnen, C. Schlüsener, Y. Sun and C. Janiak, *J. Mater. Chem. A*, 2020, **8**, 19799–19804.
157 Y. Sun, J. Liang, P. Brandt, A. Spieß, S. Öztürk and C. Janiak, *Nanoscale*, 2021, **13**, 15952–15962.
158 N. Tannert, Y. Sun, E. Hastürk, S. Nießing and C. Janiak, *Z. Anorg. Allg. Chem.*, 2021, **647**, 1124–1130.
159 M. D. J. Velásquez-Hernández, V. B. López-Cervantes, E. Martínez-Ahumada, M. Tu, U. Hernández-Balderas, D. Martínez-Otero, D. R. Williams, V. Martis, E. Sánchez-González, J.-S. Chang, J. S. Lee, J. Balmaseda, R. Ameloot, I. A. Ibarra and V. Jancik, *Chem. Mater.*, 2022, **34**, 669–677.
160 L. J. Barrios-Vargas, J. G. Ruiz-Montoya, B. Landeros-Rivera, J. R. Álvarez, D. Alvarado-Alvarado, R. Vargas, A. Martínez, E. González-Zamora, L. M. Cáceres, J. C. Morales and I. A. Ibarra, *Dalton Trans.*, 2020, **49**, 2786–2793.
161 J. A. Zárate, E. Domínguez-Ojeda, E. Sánchez-González, E. Martínez-Ahumada, V. B. López-Cervantes, D. R. Williams, V. Martis, I. A. Ibarra and J. Alejandre, *Dalton Trans.*, 2020, **49**, 9203–9207.
162 A. López-Olvera, H. Montes-Andrés, E. Martínez-Ahumada, V. B. López-Cervantes, R. D. Martínez-Serrano, E. González-Zamora, A. Martínez, P. Leo, C. Martos, I. A. Ibarra and G. Orcajo, *Eur. J. Inorg. Chem.*, 2021, 4458–4462.
163 E. S. Grape, J. G. Flores, T. Hidalgo, E. Martínez-Ahumada, A. Gutiérrez-Alejandre, A. Hautier, D. R. Williams, M. O'Keeffe, L. Öhrström, T. Willhammar, P. Horcajada, I. A. Ibarra and A. K. Inge, *J. Am. Chem. Soc.*, 2020, **142**, 16795–16804.
164 R. Domínguez-González, I. Rojas-León, E. Martínez-Ahumada, D. Martínez-Otero, H. A. Lara-García, J. Balmaseda-Era, I. A. Ibarra, E. G. Percástegui and V. Jancik, *J. Mater. Chem. A*, 2019, **7**, 26812–26817.
165 J. L. Obeso, K. Gopalsamy, M. Wahiduzzaman, E. Martínez-Ahumada, D. Fan, H. A. Lara-García, F. J. Carmona, G. Maurin, I. A. Ibarra and J. A. R. Navarro, *J. Mater. Chem. A*, 2024, **12**, 10157–10165.
166 H. Zhao, X. Gu, T. Yan, G. Han and D. Liu, *AIChE J.*, 2023, **69**, e17942.
167 S.-Q. Gang, Z.-Y. Liu, Y.-N. Bian, R. Wang and J.-L. Du, *Sep. Purif. Technol.*, 2024, **335**, 126153.
168 L. J. Guo, X. F. Feng, Z. Gao, R. Krishna and F. Luo, *Inorg. Chem.*, 2021, **60**, 1310–1314.
169 A. López-Olvera, J. A. Zárate, J. L. Obeso, E. Sánchez-González, J. A. De Los Reyes, R. A. Peralta, E. González-Zamora and I. A. Ibarra, *Inorg. Chem.*, 2023, **62**, 20901–20905.
170 J. Yao, Z. Zhao, L. Yu, J. Huang, S. Shen, S. Zhao, Y. Wu, X. Tian, J. Wang and Q. Xia, *J. Mater. Chem. A*, 2023, **11**, 14728–14737.
171 J. Li, G. L. Smith, Y. Chen, Y. Ma, M. Kippax-Jones, M. Fan, W. Lu, M. D. Frogley, G. Cinque, S. J. Day, S. P. Thompson, Y. Cheng, L. L. Daemen, A. J. Ramirez-Cuesta, M. Schröder and S. Yang, *Angew. Chem., Int. Ed.*, 2022, **61**, e202207259.
172 L. Briggs, R. Newby, X. Han, C. G. Morris, M. Savage, C. P. Krap, T. L. Easun, M. D. Frogley, G. Cinque, C. A. Murray, C. C. Tang, J. Sun, S. Yang and M. Schröder, *J. Mater. Chem. A*, 2021, **9**, 7190–7197.
173 L. Li, I. Da Silva, D. I. Kolokolov, X. Han, J. Li, G. Smith, Y. Cheng, L. L. Daemen, C. G. Morris, H. G. W. Godfrey, N. M. Jacques, X. Zhang, P. Manuel, M. D. Frogley, C. A. Murray, A. J. Ramirez-Cuesta, G. Cinque, C. C. Tang, A. G. Stepanov, S. Yang and M. Schroder, *Chem. Sci.*, 2019, **10**, 1472–1482.
174 X. Cui, Q. Yang, L. Yang, R. Krishna, Z. Zhang, Z. Bao, H. Wu, Q. Ren, W. Zhou, B. Chen and H. Xing, *Adv. Mater.*, 2017, **29**, 1606929.
175 W. Li, C. Cheng, G. Gao, H. Xu, W. Huang, Z. Qu and N. Yan, *Mater. Horiz.*, 2024, **11**, 1889–1898.
176 N. Aboosedgh and S. Fatemi, *J. Environ. Chem. Eng.*, 2024, **12**, 112042.
177 X. Kan, G. Zhang, J. Ma, F. Liu, Y. Tang, F. Liu, X. Yi, Y. Liu, A. Zheng, L. Jiang, F. Xiao and S. Dai, *Adv. Funct. Mater.*, 2024, **34**, 2312044.
178 W. Xu, L. Li, M. Guo, F. Zhang, P. Dai, X. Gu, D. Liu, T. Liu, K. Zhang, T. Xing, M. Wang, Z. Li and M. Wu, *Angew. Chem., Int. Ed.*, 2023, **62**, e202312029.
179 Y. Zhang, Z. Chen, X. Liu, Z. Dong, P. Zhang, J. Wang, Q. Deng, Z. Zeng, S. Zhang and S. Deng, *Ind. Eng. Chem. Res.*, 2020, **59**, 874–882.
180 W. Gong, Y. Xie, A. Yamano, S. Ito, X. Tang, E. W. Reinheimer, C. D. Malliakas, J. Dong, Y. Cui and O. K. Farha, *J. Am. Chem. Soc.*, 2023, **145**, 26890–26899.
181 Z. Zhang, B. Yang and H. Ma, *Sep. Purif. Technol.*, 2021, **259**, 118164.
182 Y. Ma, A. Li and C. Wang, *Chem. Eng. J.*, 2023, **455**, 140687.
183 K. Tan, P. Canepa, Q. Gong, J. Liu, D. H. Johnson, A. Dyevoich, P. K. Thallapally, T. Thonhauser, J. Li and Y. J. Chabal, *Chem. Mater.*, 2013, **25**, 4653–4662.
184 X.-D. Zhang, N. Wang, Y. Liu, M.-K. Yang, W. Gao, Y.-Z. Zhang, L. Geng, D.-S. Zhang, S. Zhuang and X. Zhang, *Inorg. Chem. Commun.*, 2024, **170**, 113174.
185 L.-Z. Yang, W. Xie, L. Yan, Q. Fu, X. Yuan, Q. Zheng and X. Zhao, *Sep. Purif. Technol.*, 2024, **346**, 127513.
186 G.-R. Si, X.-J. Kong, T. He, Z. Zhang and J.-R. Li, *Nat. Commun.*, 2024, **15**, 7220.
187 M. Thommes, K. Kaneko, A. V. Neimark, J. P. Olivier, F. Rodriguez-Reinoso, J. Rouquerol and K. S. W. Sing, *Pure Appl. Chem.*, 2015, **87**, 1051–1069.
188 R. Vaidhyanathan, S. S. Iremonger, K. W. Dawson and G. K. H. Shimizu, *Chem. Commun.*, 2009, 5230.
189 W. Liu, Y. Zhang, S. Wang, L. Bai, Y. Deng and J. Tao, *Molecules*, 2021, **26**, 5267.
190 J.-R. Li, R. J. Kuppler and H.-C. Zhou, *Chem. Soc. Rev.*, 2009, **38**, 1477.

Open Access Article. Published on 10 March 2025. Downloaded on 6/30/2025 11:42:55 PM. This article is licensed under a Creative Commons Attribution 3.0 Unported Licence.

191 F. Elwinger, P. Pourmand and I. Furó, *J. Phys. Chem. C*, 2017, **121**, 13757–13764.
192 J. Zhang, T. Xia, D. Zhao, Y. Cui, Y. Yang and G. Qian, *Sens. Actuators, B*, 2018, **260**, 63–69.
193 J. L. Obeso, E. Martínez-Ahumada, A. López-Olvera, J. Ortiz-Landeros, H. A. Lara-García, J. Balmaseda, S. López-Morales, E. Sánchez-González, D. Solis-Ibarra, C. Leyva and I. A. Ibarra, *ACS Appl. Energy Mater.*, 2023, **6**, 9084–9091.
194 J. L. Obeso, V. B. López-Cervantes, C. V. Flores, A. Martínez, Y. A. Amador-Sánchez, N. S. Portillo-Velez, H. A. Lara-García, C. Leyva, D. Solis-Ibarra and R. A. Peralta, *Dalton Trans.*, 2024, **53**, 4790–4796.
195 L. Wang and Y. Chen, *Chem. Commun.*, 2020, **56**, 6965–6968.
196 Y. Xie, H. Ma, F. L. He, J. Chen, Y. Ji, S. Han and D. Zhu, *Analyst*, 2020, **145**, 4772–4776.
197 E. Martínez-Ahumada, A. López-Olvera, P. Carmona-Monroy, H. Díaz-Salazar, M. H. Garduño-Castro, J. L. Obeso, C. Leyva, A. Martínez, M. Hernández-Rodríguez, D. Solis-Ibarra and I. A. Ibarra, *Dalton Trans.*, 2022, **51**, 18368–18372.
198 E. Martínez-Ahumada, D. W. Kim, M. Wahiduzzaman, P. Carmona-Monroy, A. López-Olvera, D. R. Williams, V. Martis, H. A. Lara-García, S. López-Morales, D. Solis-Ibarra, G. Maurin, I. A. Ibarra and C. S. Hong, *J. Mater. Chem. A*, 2022, **10**, 18636–18643.
199 V. B. López-Cervantes, D. W. Kim, J. L. Obeso, E. Martínez-Ahumada, Y. A. Amador-Sánchez, E. Sánchez-González, C. Leyva, C. S. Hong, I. A. Ibarra and D. Solis-Ibarra, *Nanoscale*, 2023, **15**, 12471–12475.
200 V. B. López-Cervantes, D. Bara, A. Yañez-Aulestia, E. Martínez-Ahumada, A. López-Olvera, Y. A. Amador-Sánchez, D. Solis-Ibarra, E. Sánchez-González, I. A. Ibarra and R. S. Forgan, *Chem. Commun.*, 2023, **59**, 8115–8118.
201 V. B. López-Cervantes, A. López-Olvera, J. L. Obeso, I. K. Torres, E. Martínez-Ahumada, P. Carmona-Monroy, E. Sánchez-González, D. Solís-Ibarra, E. Lima, E. Jangodaz, R. Babarao, I. A. Ibarra and S. G. Telfer, *Chem. Mater.*, 2024, **36**, 2735–2742.
202 M. Wang, L. Guo and D. Cao, *Anal. Chem.*, 2018, **90**, 3608–3614.
203 V. B. López-Cervantes, M. L. Martínez, J. L. Obeso, C. García-Carvajal, N. S. Portillo-Vélez, A. Guzmán-Vargas, R. A. Peralta, E. González-Zamora, I. A. Ibarra, D. Solis-Ibarra, J. L. Woodliffe and Y. A. Amador-Sánchez, *Dalton Trans.*, 2025, **54**, 1646–1654.
204 N. Ingle, S. Mane, P. Sayyad, G. Bodkhe, T. AL-Gahouari, M. Mahadik, S. Shirsat and M. D. Shirsat, *Front. Mater.*, 2020, **7**, 93.
205 Q. Li, J. Wu, L. Huang, J. Gao, H. Zhou, Y. Shi, Q. Pan, G. Zhang, Y. Du and W. Liang, *J. Mater. Chem. A*, 2018, **6**, 12115–12124.
206 N. Ingle, P. Sayyad, M. Deshmukh, G. Bodkhe, M. Mahadik, T. Al-Gahouari, S. Shirsat and M. D. Shirsat, *Appl. Phys. A: Mater. Sci. Process.*, 2021, **127**, 157.
207 X. Zhang, Z. Zhai, J. Wang, X. Hao, Y. Sun, S. Yu, X. Lin, Y. Qin and C. Li, *ChemNanoMat*, 2021, **7**, 1117–1124.
208 Z. Zhai, X. Zhang, J. Wang, H. Li, Y. Sun, X. Hao, Y. Qin, B. Niu and C. Li, *Chem. Eng. J.*, 2022, **428**, 131720.
209 Z. Zhai, J. Wang, Y. Sun, X. Hao, B. Niu, H. Xie and C. Li, *Appl. Surf. Sci.*, 2023, **613**, 155772.
210 N. Huo, D. Li, S. Zheng and W. Deng, *Chem. Eng. J.*, 2022, **432**, 134317.
211 M. E. DMello, N. G. Sundaram, A. Singh, A. K. Singh and S. B. Kalidindi, *Chem. Commun.*, 2019, **55**, 349–352.
212 V. Chernikova, O. Yassine, O. Shekhah, M. Eddaoudi and K. N. Salama, *J. Mater. Chem. A*, 2018, **6**, 5550–5554.
213 C. H. Pham and F. Paesani, *Inorg. Chem.*, 2018, **57**, 9839–9843.
214 M. R. Tchalala, P. M. Bhatt, K. N. Chappanda, S. R. Tavares, K. Adil, Y. Belmabkhout, A. Shkurenko, A. Cadiau, N. Heymans, G. De Weireld, G. Maurin, K. N. Salama and M. Eddaoudi, *Nat. Commun.*, 2019, **10**, 1328.
215 M. Pamei and A. Puzari, *Nano-Struct. Nano-Objects*, 2019, **19**, 100364.
216 Z. Liao, T. Xia, E. Yu and Y. Cui, *Crystals*, 2018, **8**, 338.
217 M. Runowski, D. Marcinkowski, K. Soler-Carracedo, A. Gorczyński, E. Ewert, P. Woźny and I. R. Martín, *ACS Appl. Mater. Interfaces*, 2023, **15**, 3244–3252.
218 W. P. Lustig, S. Mukherjee, N. D. Rudd, A. V. Desai, J. Li and S. K. Ghosh, *Chem. Soc. Rev.*, 2017, **46**, 3242–3285.
219 Y. Liu, X.-Y. Xie, C. Cheng, Z.-S. Shao and H.-S. Wang, *J. Mater. Chem. C*, 2019, **7**, 10743–10763.
220 C. Yuan, S. Saito, C. Camacho, S. Irle, I. Hisaki and S. Yamaguchi, *J. Am. Chem. Soc.*, 2013, **135**, 8842–8845.
221 Y. Zheng, Y. Zhou, J. Yu, Y. Yu, H. Zhang and W. P. Gillin, *J. Phys. D: Appl. Phys.*, 2004, **37**, 531–534.
222 D. E. Williams and N. B. Shustova, *Chem. – Eur. J.*, 2015, **21**, 15474–15479.
223 S. Xing and C. Janiak, *Chem. Commun.*, 2020, **56**, 12290–12306.
224 M. Zeng, A. Ren, W. Wu, Y. Zhao, C. Zhan and J. Yao, *Chem. Sci.*, 2020, **11**, 9154–9161.
225 L. Chen, Y. Song, W. Liu, H. Dong, D. Wang, J. Liu, Q. Liu and X. Chen, *J. Alloys Compd.*, 2022, **893**, 162322.
226 L. Yu, H. Wang, W. Liu, S. J. Teat and J. Li, *Cryst. Growth Des.*, 2019, **19**, 6850–6854.
227 J. L. Mancuso, A. M. Mroz, K. N. Le and C. H. Hendon, *Chem. Rev.*, 2020, **120**, 8641–8715.
228 M. Ji, X. Lan, Z. Han, C. Hao and J. Qiu, *Inorg. Chem.*, 2012, **51**, 12389–12394.
229 M. Shen, Y. Zhang, H. Xu and H. Ma, *iScience*, 2021, **24**, 103069.
230 F. Ahmadijokani, H. Molavi, S. Tajahmadi, M. Rezakazemi, M. Amini, M. Kamkar, O. J. Rojas and M. Arjmand, *Coord. Chem. Rev.*, 2022, **464**, 214562.
231 J. Perego, I. Villa, A. Pedrini, E. C. Padovani, R. Crapanzano, A. Vedda, C. Dujardin, C. X. Bezuidenhout, S. Bracco, P. E. Sozzani, A. Comotti, L. Gironi, M. Beretta, M. Salomoni,

 This journal is © The Royal Society of Chemistry 2025

Open Access Article. Published on 10 March 2025. Downloaded on 6/30/2025 11:42:55 PM. This article is licensed under a Creative Commons Attribution 3.0 Unported Licence.

N. Kratochwil, S. Gundacker, E. Auffray, F. Meinardi and A. Monguzzi, *Nat. Photonics*, 2021, **15**, 393–400.
232 M. A. Chowdhury, *ChemBioEng Rev.*, 2017, **4**, 225–239.
233 J.-X. Wang, J. Yin, O. Shekhah, O. M. Bakr, M. Eddaoudi and O. F. Mohammed, *ACS Appl. Mater. Interfaces*, 2022, **14**, 9970–9986.
234 L. E. Kreno, K. Leong, O. K. Farha, M. Allendorf, R. P. Van Duyne and J. T. Hupp, *Chem. Rev.*, 2012, **112**, 1105–1125.
235 A. Mallick, A. M. El-Zohry, O. Shekhah, J. Yin, J. Jia, H. Aggarwal, A.-H. Emwas, O. F. Mohammed and M. Eddaoudi, *J. Am. Chem. Soc.*, 2019, **141**, 7245–7249.
236 K. Miyata, T. Nakagawa, R. Kawakami, Y. Kita, K. Sugimoto, T. Nakashima, T. Harada, T. Kawai and Y. Hasegawa, *Chem. – Eur. J.*, 2011, **17**, 521–528.
237 Y. Ming, N. Kumar and D. J. Siegel, *ACS Omega*, 2017, **2**, 4921–4928.
238 I.-D. Kim, A. Rothschild and H. L. Tuller, *Acta Mater.*, 2013, **61**, 974–1000.
239 M. G. Campbell, D. Sheberla, S. F. Liu, T. M. Swager and M. Dincă, *Angew. Chem., Int. Ed.*, 2015, **54**, 4349–4352.
240 V. Schroeder, S. Savagatrup, M. He, S. Lin and T. M. Swager, *Chem. Rev.*, 2019, **119**, 599–663.
241 L. Torsi, M. Magliulo, K. Manoli and G. Palazzo, *Chem. Soc. Rev.*, 2013, **42**, 8612.
242 Z. Hu, J. Miu, X. Zhang, M. Jia and J. Yao, *J. Appl. Polym. Sci.*, 2022, **139**, e52810.
243 P. V. Shinde and C. S. Rout, *Nanoscale Adv.*, 2021, **3**, 1551–1568.
244 A. Punnoose, K. M. Reddy, A. Thurber, J. Hays and M. H. Engelhard, *Nanotechnology*, 2007, **18**, 165502.
245 A. Punnoose, K. M. Reddy, J. Hays, A. Thurber and M. H. Engelhard, *Appl. Phys. Lett.*, 2006, **89**, 112509.
246 A. A. Bagade, V. V. Ganbavle, S. V. Mohite, T. D. Dongale, B. B. Sinha and K. Y. Rajpure, *J. Colloid Interface Sci.*, 2017, **497**, 181–192.
247 H. Goesmann and C. Feldmann, *Angew. Chem., Int. Ed.*, 2010, **49**, 1362–1395.
248 O. Kahn and C. J. Martinez, *Science*, 1998, **279**, 44–48.
249 C. Bartual-Murgui, A. Akou, C. Thibault, G. Molnár, C. Vieu, L. Salmon and A. Bousseksou, *J. Mater. Chem. C*, 2015, **3**, 1277–1285.
250 L. Wang, Z. Wang, Q. Xiang, Y. Chen, Z. Duan and J. Xu, *Sens. Actuators, B*, 2017, **248**, 820–828.
251 R. Paolesse, C. Di Natale, A. Macagnano, F. Davide, T. Boschi and A. D'Amico, *Sens. Actuators, B*, 1998, **47**, 70–76.
252 L. Zhang, Q. Yang and Z. Zhu, *Foods*, 2024, **13**, 1936.
253 X. Wang, J. Zhang, Z. Zhu and J. Zhu, *Appl. Surf. Sci.*, 2007, **253**, 3168–3173.
254 Y. Cui, Y. Yue, G. Qian and B. Chen, *Chem. Rev.*, 2012, **112**, 1126–1162.
255 C. Wu, H. Xu, Y. Li, R. Xie, P. Li, X. Pang, Z. Zhou, B. Gu, H. Li and Y. Zhang, *Talanta*, 2019, **200**, 78–83.
256 M.-S. Yao, W.-H. Li and G. Xu, *Coord. Chem. Rev.*, 2021, **426**, 213479.
257 R.-M. Neubieser, J.-L. Wree, J. Jagosz, M. Becher, A. Ostendorf, A. Devi, C. Bock, M. Michel and A. Grabmaier, *Micro Nano Eng.*, 2022, **15**, 100126.
258 M. Gupta, H. Hawari, P. Kumar and Z. Burhanudin, *Crystals*, 2022, **12**, 264.
259 H. S. Magar, R. Y. A. Hassan and A. Mulchandani, *Sensors*, 2021, **21**, 6578.
260 V. Balasubramani, S. Sureshkumar, T. S. Rao and T. M. Sridhar, *ACS Omega*, 2019, **4**, 9976–9982.
261 B. Zong, Q. Li, X. Chen, C. Liu, L. Li, J. Ruan and S. Mao, *ACS Appl. Mater. Interfaces*, 2020, **12**, 50610–50618.
262 A. Paghi, S. Mariani and G. Barillaro, *Small*, 2023, **19**, 2206100.
263 J. Park, H. Kim and Y. Jung, *J. Phys. Chem. Lett.*, 2013, **4**, 2530–2534.
264 M. Mukoyoshi, M. Maesato, S. Kawaguchi, Y. Kubota, K. Cho, Y. Kitagawa and H. Kitagawa, *Inorg. Chem.*, 2022, **61**, 7226–7230.
265 C. Zhai, Q. Zhao, K. Gu, D. Xing and M. Zhang, *J. Alloys Compd.*, 2019, **784**, 660–667.
266 H. Yuan, J. Tao, N. Li, A. Karmakar, C. Tang, H. Cai, S. J. Pennycook, N. Singh and D. Zhao, *Angew. Chem., Int. Ed.*, 2019, **58**, 14089–14094.

Check for updates

Zitierweise: *Angew. Chem. Int. Ed.* **2025**, *64*, e202415088
doi.org/10.1002/anie.202415088

COFs Hot Paper

Achieving Sub-ppm Sensitivity in SO_2 Detection with a Chemically Stable Covalent Organic Framework

Wei Zhao[+], Juan L. Obeso[+], Valeria B. López-Cervantes[+], Mounib Bahri, Elí Sánchez-González, Yoarhy A. Amador-Sánchez, Junyu Ren, Nigel D. Browning, Ricardo A. Peralta, Giovanni Barcaro, Susanna Monti, Diego Solis-Ibarra,* Ilich A. Ibarra,* and Dan Zhao**

Abstract: We report the inaugural experimental investigation of covalent organic frameworks (COFs) to address the formidable challenge of SO_2 detection. Specifically, an imine-functionalized COF (SonoCOF-9) demonstrated a modest and reversible SO_2 sorption of 3.5 mmol g^{-1} at 1 bar and 298 K. At 0.1 bar (and 298 K), the total SO_2 uptake reached 0.91 mmol g^{-1} with excellent reversibility for at least 50 adsorption-desorption cycles. An isosteric enthalpy of adsorption (ΔH_{ads}) for SO_2 equaled −42.3 kJ mol^{-1}, indicating a relatively strong interaction of SO_2 molecules with the COF material. Also, molecular dynamics simulations and Møller–Plesset perturbation theory calculations showed the interaction of SO_2 with π density of the rings and lone pairs of the N atoms of SonoCOF-9. The combination of experimental data and theoretical calculations corroborated the potential use of this COF for the selective detection and sensing of SO_2 at the sub-ppm level (0.0064 ppm of SO_2).

Introduction

Sulfur dioxide (SO_2), an irritant, colorless, and non-flammable gas with a pungent odor, is cataloged by the World Health Organization as a highly venomous chemical to humans. Exposures exceeding 100 ppm of SO_2 can be fatal in only a few minutes because it can be easily absorbed by dermal contact and the respiratory system.[1,2] Even at concentrations lower than 100 ppm, SO_2 can be responsible for bronchoconstriction and impair lung function. For example, exposure to just 1.5 ppm of SO_2 for a few minutes can induce temporary respiratory impairment.[3] Chronic bronchitis, laryngitis, and severe respiratory tract infections can be caused in healthy individuals at SO_2 concentrations

[*] W. Zhao,[+] J. Ren, Prof. D. Zhao
Department of Chemical and Biomolecular Engineering, National University of Singapore
4 Engineering Drive 4, Singapore, 117585, Singapore
E-mail: chezhao@nus.edu.sg

J. L. Obeso,[+] V. B. López-Cervantes,[+] E. Sánchez-González, Y. A. Amador-Sánchez, Prof. D. Solis-Ibarra, Prof. I. A. Ibarra
Laboratorio de Fisicoquímica y Reactividad de Superficies (LaFReS)
Instituto de Investigaciones en Materiales, Universidad Nacional Autónoma de México
Circuito Exterior s/n, CU, Coyoacán, 04510, Ciudad de México, Mexico
E-mail: diego.solis@unam.mx
argel@unam.mx

J. L. Obeso[+]
Instituto Politécnico Nacional, CICATA U. Legaria
11500, Miguel Hidalgo, CDMX, Mexico

M. Bahri, Prof. N. D. Browning
Albert Crewe Centre for Electron Microscopy, University of Liverpool
Liverpool L69 3GL, United Kingdom

Prof. R. A. Peralta
Departamento de Química, División de Ciencias Básicas e Ingeniería
Universidad Autónoma Metropolitana-Iztapalapa
Av. San Rafael Atlixco,186, Col. Vicentina, 09340, Ciudad de México, Mexico

Prof. G. Barcaro
CNR-IPCF, Institute for Chemical and Physical Processes
CNR Research Area, Via Moruzzi 1, 56124, Pisa, Italy

Prof. S. Monti
CNR-ICCOM, Institute of Chemistry of Organometallic Compounds
CNR Research Area, Via Moruzzi 1, 56124, Pisa, Italy
E-mail: susanna.monti@pi.iccom.cnr.it

Prof. I. A. Ibarra
Sabbatical as "Catedra Dr. Douglas Hugh Everett" at Departamento de Química
Universidad Autónoma Metropolitana-Iztapalapa
Avenida San Rafael Atlixco 186, Leyes de Reforma 1ra Sección, Iztapalapa, Ciudad de México 09310, Mexico

[+] These authors contributed equally to this manuscript.

© 2024 The Authors. Angewandte Chemie published by Wiley-VCH GmbH. This is an open access article under the terms of the Creative Commons Attribution Non-Commercial NoDerivs License, which permits use and distribution in any medium, provided the original work is properly cited, the use is non-commercial and no modifications or adaptations are made.

© 2024 The Authors. Angewandte Chemie published by Wiley-VCH GmbH

higher than 1.5 ppm.[4] Thus, air quality guidelines recommend limiting human exposure to SO_2 to 500 $\mu g\,m^{-3}$ (175 ppb) over a 10-minute period and 20 $\mu g\,m^{-3}$ (8 ppb) for daily averages.[5] SO_2 serves as a precursor to particulate matter (PM), which is toxic to humans as well.[6] Additionally, SO_2 is highly soluble in water, forming sulfurous acid, which can further oxidize to sulfuric acid, a major contributor to acid rain. This damages aquatic environments and hampers the growth of forests and crops.[7] In urban areas, acid rain can accelerate metal corrosion and deteriorate materials like limestone, marble, and mortar.[8] Hence, it is crucial to not only enhance air quality by diminishing emissions or augmenting SO_2 capture but also monitor potentially polluted environments with SO_2. Such measures are essential for averting severe health repercussions for individuals laboring in various urban settings. However, up to now, the vast majority of technological efforts toward SO_2 have been focused on the capture of this toxic gas from scrubbers (based on aqueous alkaline solutions and wet-sulfuric-acid processes), with apparent drawbacks, including huge quantities of wastewater, pipeline corrosion, and high operational and recovery costs.[9] Current solid-state materials for SO_2 capture, e.g., metal oxides[10] and zeolites,[11] have considerable disadvantages like high activation temperatures (above 250 °C) and reduced porosity over multiple cycles. Consequently, there is a pressing need for materials capable of effectively detecting SO_2, exhibiting both high responsiveness and chemical stability.

Porous materials, notably metal–organic frameworks (MOFs), have garnered attention for their potential in SO_2 capture and sensing due to their high porosity.[12] Some promising results from selected examples demonstrate remarkable SO_2 capture,[13] even under humid conditions.[14] Nonetheless, many MOFs have relatively poor chemical stability to SO_2/water[15] and low detection limits to SO_2.[16] In contrast, covalent organic frameworks (COFs), an emerging class of porous materials synthesized through reticular chemistry with building blocks containing light elements (e.g., C, H, O, N, and B) interconnected by covalent bonds, have exhibited elevated stability.[17] Their intrinsic stability, rooted in the covalent nature of their bonds, imparts greater stiffness to their structures, enhancing thermal and chemical stability and rendering them resilient to adverse conditions.[18] Apart from high stability, the functional diversity and structural adjustability of COFs find significant applications in several areas, including gas storage and separation,[19] heterogeneous catalysis,[20] drug delivery,[21] and electronic devices.[22] However, to our knowledge, no studies have specifically addressed the use of COFs for SO_2 detection despite the considerable potential demonstrated by COFs in this field.

Here, we present the first example of a robust and crystalline COF, SonoCOF-9 (Figure 1),[23] that addresses SO_2 detection and sensing effectively. SonoCOF-9 exhibits chemical stability to SO_2, maintaining consistent capture capacity over 50 adsorption–desorption cycles without losing its crystallinity and porosity. Fluorescence experiments further revealed SonoCOF-9 as a promising and effective selective detector and sensor for SO_2 at the ppm level.

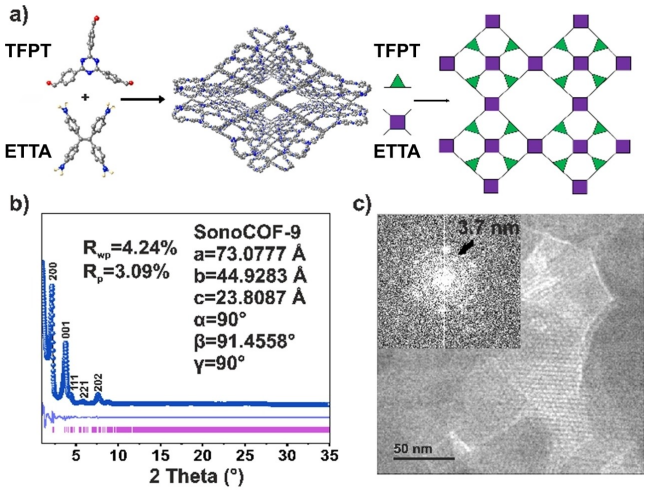


Figure 1. a) Structure of SonoCOF-9. b) PXRD of SonoCOF-9. c) HR-TEM image of SonoCOF-9 (insert shows the FFT pattern, where 3.7 nm is the d-spacing of (200) reflection).

Results and Discussion

Powder X-ray diffraction (PXRD) confirms the phase purity of SonoCOF-9 (Figure 1b). It showed an excellent crystallinity with two strong diffraction signals at 2.16° and 3.79°, and relatively weak signals at 4.38°, 5.81°, and 7.61°, which correspond to the (200), (001), (111), (221), and (202) reflections, respectively. Structural simulation (Figure S1) reveals that sonoCOF-9 shows a monoclinic structure with the **ffc** net, together with the Pawley refinement profile (blue dots) aligning closely with the experimental pattern (Figure 1b, R_{wp} of 4.24 % and R_p of 3.09 %). High-resolution transmission electron microscopy (HR-TEM) images (Figure 1c and Figure S2) depict well-defined and highly crystalline SonoCOF-9 crystallites. N_2 sorption test at 77 K (Figure S3) demonstrates a Brunauer–Emmet–Teller (BET) surface area of 1147 $m^2\,g^{-1}$ and a pore volume of 0.52 $cm^3\,g^{-1}$. The pore size distribution of SonoCOF-9 centers around 18 Å (Figure S4), which agrees with the pore width on the crystalline structure (19.5 Å).

Based on the SO_2 isotherm of this COF (Figure 2a), an SO_2 uptake of approximately 0.91 $mmol\,g^{-1}$ was obtained at 0.1 bar. The SO_2 adsorption isotherm exhibits an approximately linear increase from 0.1 to 0.5 bar, reaching a total uptake of ca. 2.9 $mmol\,g^{-1}$. Finally, a relatively flat trend of SO_2 sorption was observed from 0.5 to 1.0 bar, with a total SO_2 uptake of 3.5 $mmol\,g^{-1}$. This total SO_2 uptake is comparable to several typical chemically stable porous materials.[24,25] For example, CTF-CSU41 shows a higher SO_2 uptake of 6.7 $mmol\,g^{-1}$ at 298 K and 0.11 bar under kinetic conditions over a 360-minute period.[26] For an amine-functionalized COF, PI-COF-m60 displays 4.74 $mmol\,g^{-1}$ at 298 K during a 60-minute kinetic test.[27] At similar conditions, ICTF-SCN exhibits 9.22 $mmol\,g^{-1}$ at 298 K and 1 bar over a 60-minute kinetic test.[28] Under static conditions, TAM-POF shows 9.45 $mmol\,g^{-1}$ at 298 K and 1 bar.[29]

© 2024 The Authors. Angewandte Chemie published by Wiley-VCH GmbH

15213757, 2025, 3, Downloaded from https://onlinelibrary.wiley.com/doi/10.1002/ange.202415088 by Universidad Autonoma Metropolitana, Wiley Online Library on [30/06/2025]. See the Terms and Conditions (https://onlinelibrary.wiley.com/terms-and-conditions) on Wiley Online Library for rules of use; OA articles are governed by the applicable Creative Commons License

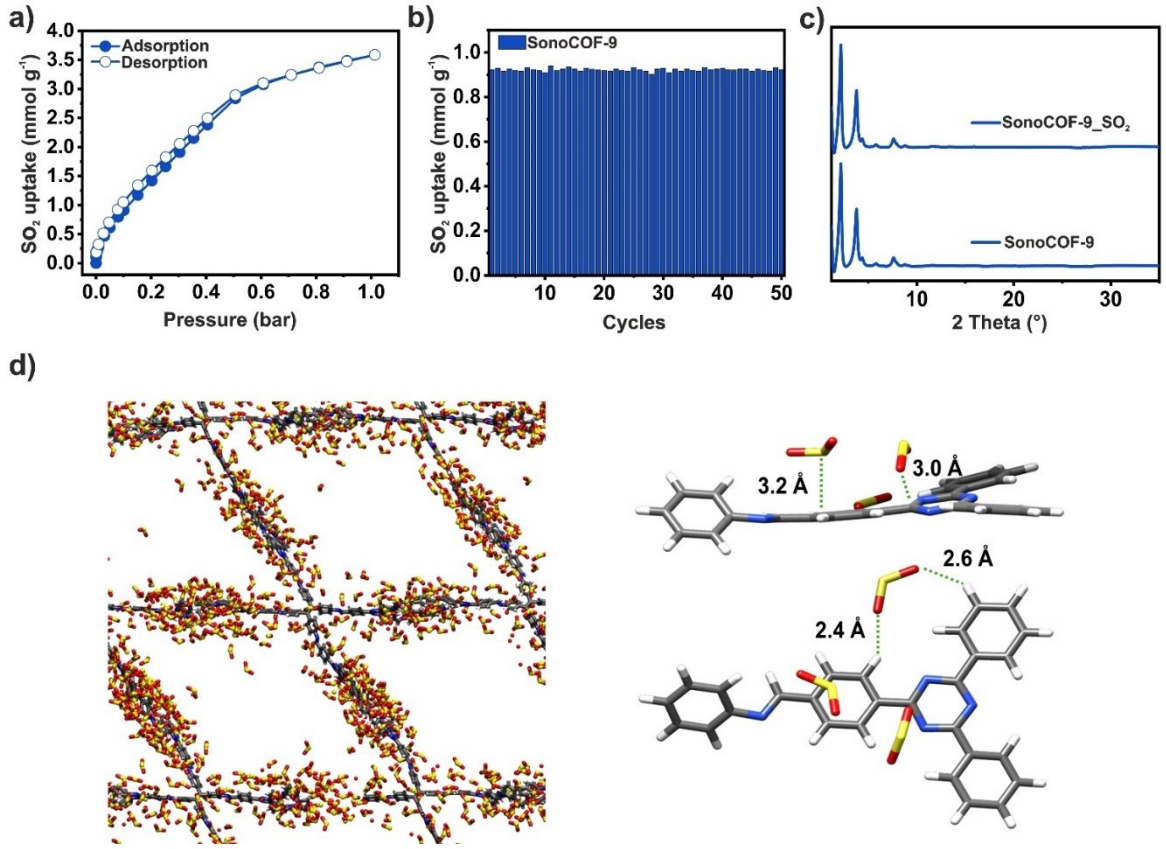


Figure 2. a) The SO_2 isotherm of SonoCOF-9 at 298 K and 1 bar. b) Adsorption–desorption cycles of SO_2 in SonoCOF-9 at 298 K and 0.1 bar. c) PXRD before and after SO_2 sorption performance. d) SO_2 interaction with SonoCOF-9.

A slight hysteresis was observed in the SO_2 desorption isotherm of SonoCOF-9, indicating a relatively strong SO_2/COF interaction energy. A key characteristic of a chemically stable material for SO_2 detection is a relatively high interaction of SO_2 with particular functional groups of the material.[30] Such interactions are most evident at the low pressures ($P < 0.1$ bar). Since SO_2 detection typically focuses on concentrations at the ppm level, these concentrations correspond to the low-pressure range. For instance, flue gas shows SO_2 concentrations up to 10,000 ppm, equivalent to pressures below 0.05 bar.[31]

Cycling experiments with SO_2 at 298 K and 0.1 bar were conducted to assess the stability of the SO_2 sorption performance. The results showed that the SO_2 capture performance remained consistent over 50 adsorption–desorption cycles with a capacity of 0.92 ± 0.11 mmol g^{-1} (Figure 2b). This SO_2 cyclability corroborates that SO_2 can be fully released during subsequent desorption cycles. Additionally, PXRD and Fourier-transform infrared spectroscopy (FTIR) analyses of sonoCOF-9 following 50 adsorption–desorption cycles verified retained crystallinity and stability (Figure 2c and Figure S5).

The host–guest interaction (SonoCOF-9···SO_2) was estimated by calculating the isosteric enthalpy of adsorption (ΔH_{ads}) for SO_2 at low coverage using a fully activated sample of SonoCOF-9 at 298 and 308 K (Figure S7).[32] The calculated ΔH_{ads} (-42.3 kJ mol^{-1}) indicates stable adsorbed SO_2 layers on the COF's walls. This ΔH_{ads} value is coherent with the observed SO_2 isotherm hysteresis, which can be associated with a strong interaction of SO_2 molecules with the π density of the rings and lone pairs of the N atoms from the ETTA building block, as disclosed by the classical reactive molecular dynamics simulations (ReaxFF MD) results and Møller–Plesset perturbation theory calculations (MP2) on reduced model systems of the COF. We also demonstrated that the decrease of ΔH_{ads} as the SO_2 adsorption increased (Figure S8) was probably due to the addition of the weaker binding species that laid on the ring plane connected to the COF structure through unconventional hydrogen bonds between the SO_2 oxygen and the hydrogen of the benzylic ring (Figure 2d). However, being only a small percentage (around 25 %), these configurations had an almost undetectable effect on the total binding values, which were estimated from the MP2-optimized models after grouping the adsorbates into families (i.e., stacked and hydrogen bonded).

The binding energy and enthalpy are displayed in Tables S1 and S2. The binding tendencies are clearly displayed in Figure S10, where a snapshot of the RMD trajectory is depicted. There, the occupation of the various regions of the COF framework is highlighted by the spatial distribution contours (dark yellow areas). It is apparent that

© 2024 The Authors. Angewandte Chemie published by Wiley-VCH GmbH

15213757, 2025, 3, Downloaded from https://onlinelibrary.wiley.com/doi/10.1002/ange.202415088 by Universidad Autonoma Metropolitana, Wiley Online Library on [30/06/2025]. See the Terms and Conditions (https://onlinelibrary.wiley.com/terms-and-conditions) on Wiley Online Library for rules of use; OA articles are governed by the applicable Creative Commons License

the higher occupation densities are around the circular ten-ring bands of the COF, where the molecules are preferentially accommodated on top of the ring planes, interacting with the framework but also with each other. To give an idea of the typical locations, we examined the atom-atom radial distribution functions of S and O in relation to the carbon and hydrogen atoms of the COF. The position of the peak at short distances (lower than 3 Å, Figure S11) suggests that SO_2 tends to stay connected to the framework but remains slightly further from the nitrogen sites (approximately 3.2 Å), which is most probably due to self-intermolecular interactions that mitigated the adsorption distances.[33] Indeed, the evaluation of the binding energy on reduced model systems revealed that, on the one hand, these self-interactions weakened the binding energy of each single molecule but, on the other hand, improved the stability of the formed SO_2 shells.

In the dominant adsorption mode (75 % population), where the molecules were on top of the ring systems, the strongest binding was around $-42\,kJ\,mol^{-1}$, whilst the weakest was approximately $-20\,kJ\,mol^{-1}$. A representative geometry (extracted from the RMDs and optimized at the MP2 level, Figure S12) used for estimating the binding energy is displayed in Figure 2d. There, both characteristic adsorptions, namely in-plane and out-of-plane, are shown. The average binding energy estimated considering the populations and the correction for the enthalpic contribution was approximately $-30\,kJ\,mol^{-1}$. The trend of the evolution of the adsorption enthalpy as a function of the COF uptake (Figure S8) indicates that this estimate corresponds to a scenario of intermediate coverage (Figure 2d), where the most interacting sites are occupied, and the other approaching guest molecules have a weaker interaction with the COF framework.

N_2 sorption isotherm at 77 K showed that the surface area of this COF after SO_2 sorption did not decrease significantly (from 1147 to $1053\,m^2\,g^{-1}$, Figure S13). Moreover, the pore size distribution of SonoCOF-9 centers after SO_2 exposures is around 16 Å (Figure S14), which agrees with the value of the pristine material. These results demonstrate that SO_2 can be fully released during SO_2 cycle experiments without affecting the crystallinity and porosity of SonoCOF-9. Scanning electron microscopy (SEM) analyses of the pristine COF after SO_2 saturation and after SO_2 adsorption-desorption cycles revealed no significant changes in the submicrometric crystallite morphology and particle size of the material, supporting its stability and recyclability in the presence of SO_2 (Figure S15).

Thus far, we have successfully demonstrated the reversible SO_2 capture by SonoCOF-9, particularly at low pressure (0.1 bar), identified the preferential adsorption sites of SO_2, and evaluated the extraordinary chemical stability of this COF to SO_2 uptake. Both reversible adsorption and stability are indeed ideal for SO_2 detection. Selectivity is another crucial aspect of any detector. To compare the SO_2/CO_2 selectivity, CO_2 sorption isotherm was collected at 298 K up to 1 bar (Figure S16). The SO_2 uptake in SonoCOF-9 surpassed the CO_2 uptake across the entire pressure range. Subsequently, the selectivity of SO_2 over CO_2 at varying compositions (SO_2/CO_2) was calculated using the Python package (Table S3), pyIAST.[34] Our result indicates a remarkable SO_2/CO_2 selectivity by SonoCOF-9, especially at low SO_2 concentrations; e.g., a selectivity of 25.44 was estimated for a 1:99 SO_2/CO_2 mixture and 12.93 for a 10:90 mixture. These values are higher than or comparable to some representative porous materials, such as CPL-1 (8.7 at 10:90 SO_2/CO_2),[35] Ni-gallate (25 at 10:90 SO_2/CO_2),[36] NaX zeolite (3.2 at 10:90 SO_2/CO_2),[11] and MFM-300 (31 at 10:90 SO_2/CO_2).[37]

Upon systematically establishing the promising SO_2 adsorption characteristics of SonoCOF-9, we explored the potential utilization of this COF material as a fluorescent SO_2 detector. Due to the highly conjugated crystalline structure, COF displays multiple identical binding sites across the framework. Therefore, the signal can be effectively measured when the sample is stimulated, which can be related to fluorescence change.[38]

Initially, under visible light irradiation at $\lambda_{ex} = 527$ nm (Figure S19), an activated sample of SonoCOF-9 exhibited a broad photoluminescence signal centered at $\lambda_{max} = 622$ nm (Figure 3a). Another activated sample of SonoCOF-9 was exposed to 0.1 bar of SO_2 using our homemade in situ adsorption system (Figure S17) to assess its photoluminescence absorption properties. Remarkably, the photoluminescence was almost wholly quenched (Figure 3a). This turn-off effect at low pressure could be associated with the high interaction between SO_2 molecules and SonoCOF-9. A set of control experiments was carried out to evaluate the selectivity of SonoCOF-9. The fluorescence of SonoCOF-9 when exposed to air and CO_2 (saturated) was measured. Notably, these exposures did not induce significant changes in the shape or intensity of the photoluminescence relative to the spectrum of activated SonoCOF-9 (Figure 3a). Thus, the lack of substantial alterations in the emission shape or intensity during exposures to air and CO_2 supports the selectivity of SonoCOF-9 for SO_2. This suggests that the observed fluorescence change is solely attributable to SO_2 adsorption and is not influenced by the inclusion of other gases. The spectrum of a SonoCOF-9 sample saturated with H_2S was also carried out to test the effect of another acid gas on the material (Figure S20). Although H_2S generated a change in the fluorescence of the material, this was not identical to that generated with SO_2, since the quenching was not as pronounced as with SO_2, confirming that the fluorescence response is more specific and sensitive to SO_2.

Later, five independent exposition cycles were carried out (Figure S21). An activated SonoCOF-9 sample was exposed to 0.1 bar of SO_2, revealing a consistent absorption spectrum with an average decrease in emission intensity of 87 ($\pm$2) %. Up to this point, the results, while not directly translatable to SO_2 sensing, consistently demonstrated a reduction in emission intensity upon re-exposure to SO_2 and re-activation of theSonoCOF-1 at 0.1 bar SO_2 and air, which holds promise for the transition to the next stage: SO_2 sensing. It is worth mentioning that we tested another working temperature of detection (308 K), finding a non-temperature dependence (Figure S22).

© 2024 The Authors. Angewandte Chemie published by Wiley-VCH GmbH

15213757, 2025, 3, Downloaded from https://onlinelibrary.wiley.com/doi/10.1002/ange.202415088 by Universidad Autonoma Metropolitana, Wiley Online Library on [30/06/2025]. See the Terms and Conditions (https://onlinelibrary.wiley.com/terms-and-conditions) on Wiley Online Library for rules of use; OA articles are governed by the applicable Creative Commons License

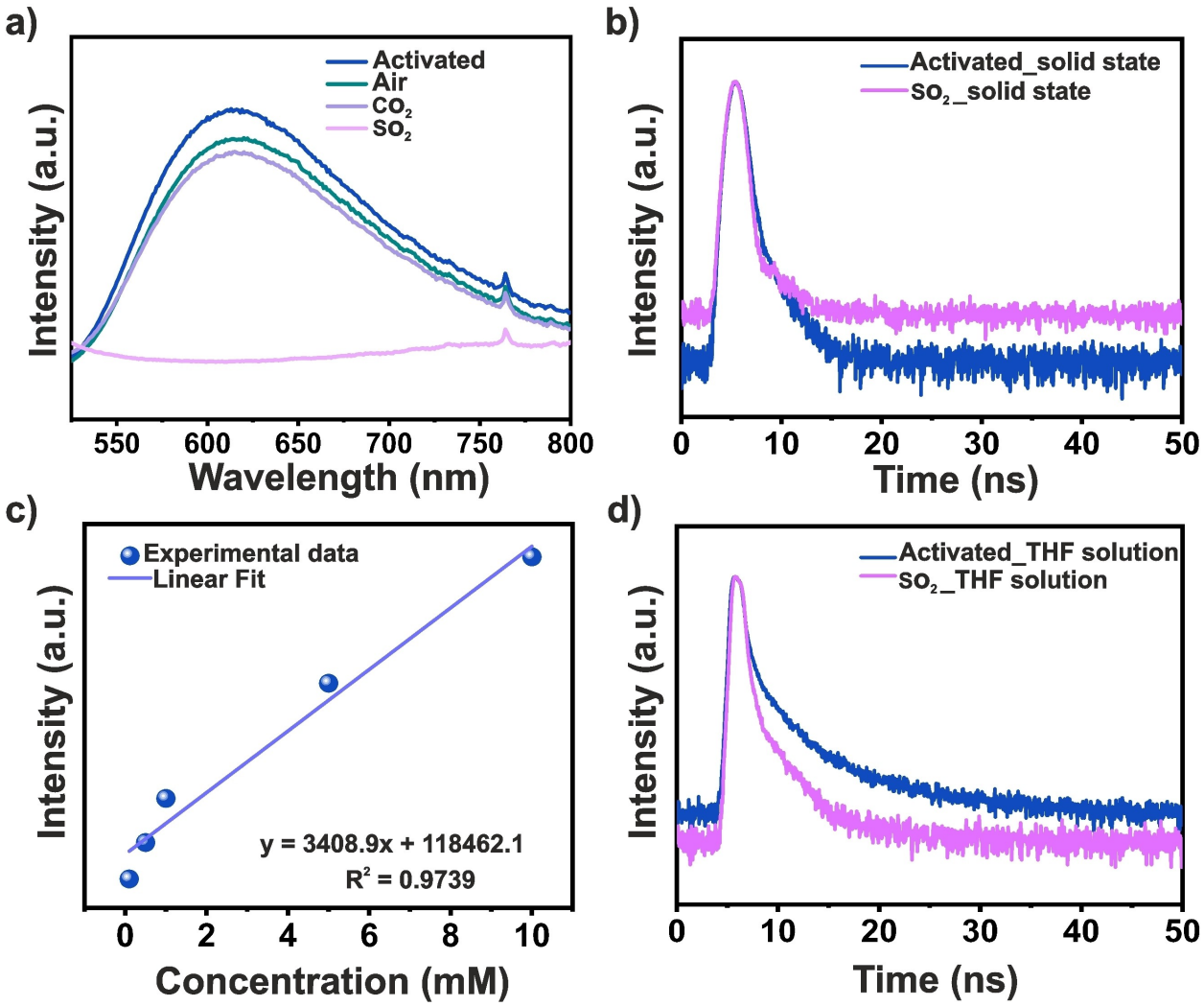


Figure 3. a) Solid-state photoluminescent emission of SonoCOF-9 with air, CO_2, and SO_2. b) Time-resolved photoluminescence (TRPL) of SonoCOF-9 before (activated) and after SO_2 sorption in the solid state. c) Linear fit, and d) TRPL of SonoCOF-9 before (activated) and after SO_2 sorption in THF solution.

To probe the possible mechanism of SO_2 detection by SonoCOF-9, we conducted time-resolved photoluminescence (TRPL) experiments through a 375 nm picosecond-pulsed laser for excitation (Figure 3b). TRPL analyses were performed on both an activated SonoCOF-9 and a sample exposed to 0.1 bar of SO_2. Photoluminescence decay was recorded at 622 nm. The average decay lifetime decreased moderately upon SO_2 exposure (Table S4). Specifically, the average fluorescence lifetime of activated SonoCOF-9 (at $\lambda_{emission} = 622$ nm) was 0.41 ns, whereas that of SonoCOF-9 exposed to 0.1 bar of SO_2 (at $\lambda_{emission} = 622$ nm) was 0.24 ns. Considering that the decrease in half-life is minimal (from 0.41 ns to 0.24 ns) and the turn-off effect is very significant, we postulate that the drastic decrease in emission intensity ($\approx 87\,\%$) is due to a static quenching,[39,40] indicating that the electronic transition $\pi^* \rightarrow \pi$ centered on the building blocks of the SonoCOF-9 structure could be avoided due to the formation of a non-fluorescent "complex" in the basal state due to the previously discussed intermolecular interactions occurring between SonoCOF-9 and SO_2.[41]

Once the selective SO_2 detection properties of SonoCOF-9 at 0.1 bar of SO_2 were established, we aimed to explore its potential for sensing applications at very low SO_2 concentrations (sub-ppm level). It is worth mentioning that 0.1 bar of SO_2 equals approximately 20,000 ppm (considering our experimental setup at 0.2 L and 298 K, Figure S17). This concentration is deemed high, far exceeding the ppm regime.[42] Although SonoCOF-9 consistently showed a significant fluorescence change (turn-off effect) upon exposure to 0.1 bar of SO_2, accurately quantifying the precise amount of SO_2 remains challenging. Additionally, the most pertinent SO_2 concentration regime for a sensing material is at the sub-ppm level. Thus, solutions of SO_2 in THF were used to investigate the sensing properties of SonoCOF-9 by luminescence. First, we measured the photoluminescence absorption properties of 2.5 mg of pristine SonoCOF-9 suspended in 3 mL anhydrous THF, which is equivalent to a

© 2024 The Authors. Angewandte Chemie published by Wiley-VCH GmbH

15213757, 2025, 3, Downloaded from https://onlinelibrary.wiley.com/doi/10.1002/ange.202415088 by Universidad Autonoma Metropolitana, Wiley Online Library on [30/06/2025]. See the Terms and Conditions (https://onlinelibrary.wiley.com/terms-and-conditions) on Wiley Online Library for rules of use; OA articles are governed by the applicable Creative Commons License

concentration of 327.8 μM SonoCOF-9 in THF. The shape of the fluorescence spectrum agreed with the spectrum of the solid-state material with an emission maximum at 622 nm (Figure S23). Later, a solution with a concentration of 1×10^{-4} mM (0.0001 mM = 0.0064 ppm = 6.4 ppb) of SO_2 (in anhydrous THF) was prepared, and the fluorescence emission was measured on the resultant suspension (Figure S24). Upon immersion of the SonoCOF-9 in the SO_2 solution, the photoluminescence emission intensity increased by 70.05 %. Six independent experiments of suspensions (1×10^{-4} mM) with SonoCOF-9 were prepared and analyzed by luminescence. Consistently, the same emission spectra were observed with an approximate 70 % increase in emission intensity (Figure S25), showcasing remarkable reproducibility. It is noteworthy that the change in fluorescence response was observed immediately after the immersion of the COF material in the SO_2 solution, and the response remained stable for up to 12 hours (Figure S26). Table S6 gives a brief review of different materials that have been tested for SO_2 detection. To the best of our knowledge, this is the first study to evaluate the SO_2 detection capability of a COF material.

The high affinity of SonoCOF-9 for SO_2 enables us to estimate the limit of detection (LOD) by measuring fluorescence emission intensity as a function of the SO_2 concentration. The LOD was calculated with the formula: $LOD = 3\sigma/m$, where σ is the standard deviation of the initial intensity of pristine SonoCOF-9, and m represents the slope of the linear fit from the experimental data (Figure 3c).[43] The resulting LOD value for SO_2 sensing in a THF solution was estimated to be 1.36 mM. Additionally, the Stern–Volmer plot (Figure S27) affords a quenching parameter (Ksv) of 7.6×10^{-6} M^{-1}. This relatively low value corroborates the high affinity of SonoCOF-9 for SO_2.[44] The value agrees with the detection of acid compounds (3.12×10^{-7} M^{-1}).[45]

We performed TRPL experiments (Figure 3d) on THF suspensions of a pristine sample of SonoCOF-9 and a sample exposed to 1×10^{-4} mM of SO_2, where measurements were performed at $\lambda_{em} = 622$ nm. Herein, an apparent decrease in photoluminescence half-life times was obtained after SO_2 exposure (Table S5), going from 5.25 ns for the pristine sample suspension to 1.23 ns for the sample exposed to 1×10^{-4} mM SO_2. This apparent decrease in the half-life times suggests that a small amount of SO_2 is enough to stiffen SonoCOF-9, which in turn results in a consistent photoluminescence turn-on effect of ca. 70 %. These results again confirm the propensity of SO_2 molecules to interact favorably with the COF framework.

At a very low concentration of SO_2 (0.0064 ppm), there is an effective interaction between SonoCOF-9 and SO_2 molecule, which enhances the stiffness of the structural molecular motions, hindering the non-radiative decay pathways of the excited state.[46,47] In other words, vibrational relaxations with half-lives of 10^{-12} s or less lead to an increased fluorescence lifetime, and the increased number of excited species undergoing radiatively decay contributes to enhanced photoluminescence. On the other hand, at high SO_2 concentrations (20,000 ppm), after the continuous interaction of SO_2 with the COF, the preferential adsorption sites of the COF became saturated, and the interactions between SO_2 molecules, $SO_2\cdots SO_2$, occurred as previously reported,[48] leading to a quenching effect. More specifically, our current hypothesis is that at high SO_2 concentrations, the predominant interactions and exchange dynamics within the pores of the COF are governed by $SO_2\cdots SO_2$ interactions rather than $COF\cdots SO_2$ interactions. This preference for $SO_2\cdots SO_2$ interactions leads to minimizing the stiffening effects and additional beneficial electronic effects arising from the $COF\cdots SO_2$ interaction, thereby quenching the fluorescence in favor of non-radiative processes (vibrational relaxation).[49,50]

Conclusion

In conclusion, we report the first experimental investigation on the sorption and detection of SO_2 on a COF (SonoCOF-9). While the SO_2 uptake of 3.5 mmol g^{-1} (298 K and 1 bar) does not rival the leading MOF materials and polymers, SonoCOF-9 demonstrates outstanding chemical stability toward SO_2 and maintains excellent cyclability over a minimum of 50 sorption/desorption cycles without compromising its crystalline structure. Notably, the combination of imine functionalities and aromatic moieties of SonoCOF-9 was demonstrated to be the key for the selective detection of SO_2 with the relatively high energy of interaction (-42.3 kJ mol^{-1}), which also provided the ability to sense SO_2 at the sub-ppm level (0.0064 ppm), making SonoCOF-9 promising for practical SO_2 sensing.

Acknowledgements

This work was supported by the Ministry of Education - Singapore (MOE-T2EP10122-0002), the Energy Market Authority of Singapore (EMA-EP009-SEGC-020), the Agency for Science, Technology and Research (U2102d2004, U2102d2012), and the National Research Foundation Singapore (NRF-CRP26-2021RS-0002, NRF-NRFI08-2022-0008). I.A.I thank PAPIIT-UNAM (Grant IIN201123), Mexico, for financial support. V. B. L.-C. and J. L. O. thank CONAHCYT for the Ph.D. fellowship (1005649, 1003953). Y.A.A.-S. acknowledges the support from the DGAPA-UNAM postdoctoral fellowship. The authors thank Dr. Omar Novelo and Dr. Lourdes Bazán-Díaz from the University Laboratory of Electron Microscopy of the UNAM (LUME) for SEM analysis. The TEM analysis was performed in the Albert Crewe Centre for Electron Microscopy, a University of Liverpool Shared Research Facility. The authors thank U. Winnberg (Euro Farmacos EIR) for scientific discussions and G. Ibarra-Winnberg for conceptualizing the design of this contribution.

Conflict of Interest

There are no conflicts to declare.

© 2024 The Authors. Angewandte Chemie published by Wiley-VCH GmbH

15213757, 2025, 3, Downloaded from https://onlinelibrary.wiley.com/doi/10.1002/ange.202415088 by Universidad Autonoma Metropolitana, Wiley Online Library on [30/06/2025]. See the Terms and Conditions (https://onlinelibrary.wiley.com/terms-and-conditions) on Wiley Online Library for rules of use; OA articles are governed by the applicable Creative Commons License

Data Availability Statement

The data that support the findings of this study are available from the corresponding author upon reasonable request.

Keywords: covalent organic frameworks · SO_2 adsorption · SO_2 detection · fluorescence · chemical stability

[1] Z. Meng, Y. Liu, D. Wu, *Inhalation Toxicol.* **2005**, *17*, 303–307.
[2] J. A. Bernstein, N. Alexis, C. Barnes, I. L. Bernstein, A. Nel, D. Peden, D. Diaz-Sanchez, S. M. Tarlo, P. B. Williams, J. A. Bernstein, *J. Allergy Clin. Immunol.* **2004**, *114*, 1116–1123.
[3] A. L. Reno, E. G. Brooks, B. T. Ameredes, *Environ. Health Insights* **2015**, *9s1*, EHI.S15671.
[4] T.-Y. Chiang, T.-H. Yuan, R.-H. Shie, C.-F. Chen, C.-C. Chan, *Environ. Int.* **2016**, *96*, 1–7.
[5] H. Zhang, R. Srinivasan, *Sustainability* **2020**, *12*, 9045.
[6] C. K. Chan, X. Yao, *Atmos. Environ.* **2008**, *42*, 1–42.
[7] A. Kavian, A. Alipour, K. Soleimani, L. Gholami, P. Smith, J. Rodrigo-Comino, *Hydrol. Process.* **2019**, *33*, 261–270.
[8] Z. Shi, J. Zhang, Z. Xiao, T. Lu, X. Ren, H. Wei, *J. Environ. Manage.* **2021**, *297*, 113213.
[9] R. K. Srivastava, W. Jozewicz, C. Singer, *Environ. Prog.* **2001**, *20*, 219–228.
[10] E. J. Romano, K. H. Schulz, *Appl. Surf. Sci.* **2005**, *246*, 262–270.
[11] H. Yi, H. Deng, X. Tang, Q. Yu, X. Zhou, H. Liu, *J. Hazard. Mater.* **2012**, *203*, 111–117.
[12] J. L. Obeso, V. B. López-Cervantes, C. V. Flores, A. Martínez, Y. A. Amador-Sánchez, N. S. Portillo-Velez, H. A. Lara-García, C. Leyva, D. Solis-Ibarra, R. A. Peralta, *Dalton Trans.* **2024**, *53*, 4790–4796.
[13] N. K. Gupta, A. López-Olvera, E. González-Zamora, E. Martínez-Ahumada, I. A. Ibarra, *ChemPlusChem* **2022**, *87*, e202200006.
[14] E. Martínez-Ahumada, D. W. Kim, M. Wahiduzzaman, P. Carmona-Monroy, A. López-Olvera, D. R. Williams, V. Martis, H. A. Lara-García, S. López-Morales, D. Solis-Ibarra, G. Maurin, I. A. Ibarra, C. S. Hong, *J. Mater. Chem. A* **2022**, *10*, 18636–18643.
[15] P. Brandt, A. Nuhnen, M. Lange, J. Möllmer, O. Weingart, C. Janiak, *ACS Appl. Mater. Interfaces* **2019**, *11*, 17350–17358.
[16] M. R. Tchalala, P. M. Bhatt, K. N. Chappanda, S. R. Tavares, K. Adil, Y. Belmabkhout, A. Shkurenko, A. Cadiau, N. Heymans, G. De Weireld, G. Maurin, K. N. Salama, M. Eddaoudi, *Nat. Commun.* **2019**, *10*, 1328.
[17] L. Gilmanova, V. Bon, L. Shupletsov, D. Pohl, M. Rauche, E. Brunner, S. Kaskel, *J. Am. Chem. Soc.* **2021**, *143*, 18368–18373.
[18] B. Shi, X. Pang, S. Li, H. Wu, J. Shen, X. Wang, C. Fan, L. Cao, T. Zhu, M. Qiu, Z. Yin, Y. Kong, Y. Liu, M. Zhang, Y. Liu, F. Pan, Z. Jiang, *Nat. Commun.* **2022**, *13*, 6666.
[19] Y. Zeng, R. Zou, Y. Zhao, *Adv. Mater.* **2016**, *28*, 2855–2873.
[20] M. Lu, M. Zhang, J. Liu, Y. Chen, J. Liao, M. Yang, Y. Cai, S. Li, Y. Lan, *Angew. Chem. Int. Ed.* **2022**, *61*, e202200003.
[21] H. Guo, Y. Liu, N. Wu, L. Sun, W. Yang, *ChemistrySelect* **2022**, *7*, e202202538.
[22] W. Wang, W. Zhao, H. Xu, S. Liu, W. Huang, Q. Zhao, *Coord. Chem. Rev.* **2021**, *429*, 213616.
[23] W. Zhao, P. Yan, H. Yang, M. Bahri, A. M. James, H. Chen, L. Liu, B. Li, Z. Pang, R. Clowes, N. D. Browning, J. W. Ward, Y. Wu, A. I. Cooper, *Nat. Synth.* **2022**, *1*, 87–95.
[24] E. Martínez-Ahumada, A. López-Olvera, P. Carmona-Monroy, H. Díaz-Salazar, M. H. Garduño-Castro, J. L. Obeso, C. Leyva, A. Martínez, M. Hernández-Rodríguez, D. Solis-Ibarra, I. A. Ibarra, *Dalton Trans.* **2022**, *51*, 18368–18372.
[25] V. B. López-Cervantes, D. Bara, A. Yañez-Aulestia, E. Martínez-Ahumada, A. López-Olvera, Y. A. Amador-Sánchez, D. Solis-Ibarra, E. Sánchez-González, I. A. Ibarra, R. S. Forgan, *Chem. Commun.* **2023**, *59*, 8115–8118.
[26] Y. Fu, Z. Wang, S. Li, X. He, C. Pan, J. Yan, G. Yu, *ACS Appl. Mater. Interfaces* **2018**, *10*, 36002–36009.
[27] G.-Y. Lee, J. Lee, H. T. Vo, S. Kim, H. Lee, T. Park, *Sci. Rep.* **2017**, *7*, 557.
[28] H. Zhu, W. Lin, Q. Li, Y. Hu, S. Guo, C. Wang, F. Yan, *ACS Appl. Mater. Interfaces* **2020**, *12*, 8614–8621.
[29] S. Chen, Y. Wu, W. Zhang, S. Wang, T. Yan, S. He, B. Yang, H. Ma, *Chem. Eng. J.* **2022**, *429*, 132480.
[30] X. Zhang, Z. Zhai, J. Wang, X. Hao, Y. Sun, S. Yu, X. Lin, Y. Qin, C. Li, *ChemNanoMat* **2021**, *7*, 1117–1124.
[31] Y. Liu, T. M. Bisson, H. Yang, Z. Xu, *Fuel Process. Technol.* **2010**, *91*, 1175–1197.
[32] A. Nuhnen, C. Janiak, *Dalton Trans.* **2020**, *49*, 10295–10307.
[33] P. Brandt, S.-H. Xing, J. Liang, G. Kurt, A. Nuhnen, O. Weingart, C. Janiak, *ACS Appl. Mater. Interfaces* **2021**, *13*, 29137–29149.
[34] C. M. Simon, B. Smit, M. Haranczyk, *Comput. Phys. Commun.* **2016**, *200*, 364–380.
[35] Y. Zhang, Z. Chen, X. Liu, Z. Dong, P. Zhang, J. Wang, Q. Deng, Z. Zeng, S. Zhang, S. Deng, *Ind. Eng. Chem. Res.* **2020**, *59*, 874–882.
[36] F. Chen, D. Lai, L. Guo, J. Wang, P. Zhang, K. Wu, Z. Zhang, Q. Yang, Y. Yang, B. Chen, Q. Ren, Z. Bao, *J. Am. Chem. Soc.* **2021**, *143*, 9040–9047.
[37] J. A. Zárate, E. Sánchez-González, D. R. Williams, E. González-Zamora, V. Martis, A. Martínez, J. Balmaseda, G. Maurin, I. A. Ibarra, *J. Mater. Chem. A* **2019**, *7*, 15580–15584.
[38] L. Guo, L. Yang, M. Li, L. Kuang, Y. Song, L. Wang, *Coord. Chem. Rev.* **2021**, *440*, 213957.
[39] A. S. Tanwar, R. Parui, R. Garai, M. A. Chanu, P. K. Iyer, *ACS Meas. Sci. Au* **2022**, *2*, 23–30.
[40] J. R. Lakowicz, Ed., in *Principles of Fluorescence Spectroscopy*, Springer US, Boston, MA, **2006**, pp. 277–330.
[41] A. Sharma, D. Kim, J.-H. Park, S. Rakshit, J. Seong, G. H. Jeong, O.-H. Kwon, M. S. Lah, *Commun. Chem.* **2019**, *2*, 39.
[42] M. A. Hanif, N. Ibrahim, A. Abdul Jalil, *Environ. Sci. Pollut. Res. Int.* **2020**, *27*, 27515–27540.
[43] A. Das, S. Das, V. Trivedi, S. Biswas, *Dalton Trans.* **2019**, *48*, 1332–1343.
[44] N. Rajendiran, *Polyhedron* **2002**, *21*, 951–957.
[45] S. Kadian, G. Manik, *Lumin.* **2020**, *35*, 763–772.
[46] P. Srujana, T. P. Radhakrishnan, *Mater. Chem. Front.* **2018**, *2*, 632–634.
[47] Y. Cai, L. Du, K. Samedov, X. Gu, F. Qi, H. H. Y. Sung, B. O. Patrick, Z. Yan, X. Jiang, H. Zhang, J. W. Y. Lam, I. D. Williams, D. Lee Phillips, A. Qin, B. Z. Tang, *Chem. Sci.* **2018**, *9*, 4662–4670.
[48] S. Chen, Y. Wu, W. Zhang, S. Wang, T. Yan, S. He, B. Yang, H. Ma, *Chem. Eng. J.* **2022**, *429*, 132480.
[49] J. Gierschner, J. Shi, B. Milián-Medina, D. Roca-Sanjuán, S. Varghese, S. Park, *Adv. Opt. Mater.* **2021**, *9*, 2002251.
[50] K. Rurack, U. Resch-Genger, *Chem. Soc. Rev.* **2002**, *31*, 116–127.

Manuscript received: August 7, 2024
Accepted manuscript online: September 19, 2024
Version of record online: November 6, 2024

© 2024 The Authors. Angewandte Chemie published by Wiley-VCH GmbH

15213757, 2025, 3, Downloaded from https://onlinelibrary.wiley.com/doi/10.1002/ange.202415088 by Universidad Autonoma Metropolitana, Wiley Online Library on [30/06/2025]. See the Terms and Conditions (https://onlinelibrary.wiley.com/terms-and-conditions) on Wiley Online Library for rules of use; OA articles are governed by the applicable Creative Commons License

Check for updates

RESEARCH ARTICLE

NANO · MICRO small
www.small-journal.com

Record-Breaking H_2S Capture and ppm-Level Sensing with a Chemically Stable Porous Organic Cage

Juan L. Obeso, Dingyue Hu, Valeria B. López-Cervantes, Yoarhy A. Amador-Sánchez, Catalina V. Flores, J. Gabriel Flores, Sanliang Ling, Enrique Lima, Aída Gutiérrez-Alejandre, Marco A. Vera, Ricardo A. Peralta, José Antonio de los Reyes, Diego Solis-Ibarra,* Ilich A. Ibarra,* and Ming Liu**

The first experimental investigation of a porous organic cage (POC) for the challenging task of H_2S capture is reported. The N-containing cage molecular material, a tertiary amine POC (6FT-RCC3), demonstrates the highest H_2S (hydrogen sulfide) capture (record capacity) for a porous material at room temperature and atmospheric pressure (20.6 mmol H_2S g^{-1}; 25 H_2S molecules per cage) combined with excellent reversibility for at least five adsorption–desorption cycles. In situ FTIR spectroscopy, solid-state ^{13}C, and ^{15}N CP MAS NMR spectroscopy experiments are applied to investigate the adsorption mechanism, identifying relatively weak interactions via hydrogen bonding. In addition, the fluorescence performances of this POC material are evaluated for the detection and sensing of H_2S, where a clear H_2S selectivity is observed over other gases. Remarkably, the limit of detection (LOD) is calculated to be 0.13 mM (≈4.43 ppm) in a tetrahydrofuran (THF) solution of H_2S.

1. Introduction

To date, society has faced energy shortages worldwide since high quantities of energy are required. Primarily, the indiscriminate combustion of fossil fuels to supply energy demands has generated the release of highly toxic pollutants into the atmosphere. The negative impact of these emissions is related to health complications and ecosystem deterioration (acidification of the oceans, decrease of biodiversity, and crop damage).[1] Thus, to tackle this problem, the reduction and adequate control of air pollution must be solved in the upcoming years.[2] In general, CO_2, CO, O_3, SO_x, NO_x, NH_3, PM_{10}, $PM_{2.5}$, and VOCs are enlisted

J. L. Obeso, V. B. López-Cervantes, Y. A. Amador-Sánchez, C. V. Flores, E. Lima, D. Solis-Ibarra, I. A. Ibarra
Laboratorio de Fisicoquímica y Reactividad de Superficies (LaFReS)
Instituto de Investigaciones en Materiales
Universidad Nacional Autónoma de México
Circuito Exterior s/n, CU, Coyoacán, Ciudad de México 04510, Mexico
E-mail: diego.solis@unam.mx; argel@unam.mx

J. L. Obeso, C. V. Flores
Laboratorio Nacional de Ciencia
Tecnología y Gestión Integrada del Agua (LNAgua)
Instituto Politécnico Nacional
CICATA U. Legaria
Legaria 694 Irrigación, Miguel Hidalgo, CDMX 11500, Mexico

D. Hu, M. Liu
Department of Chemistry & ZJU-Hangzhou Global Scientific and Technological Inovation Center
Zhejiang University
Zhejiang 311215, China
E-mail: mingliu@zju.edu.cn

J. G. Flores, J. A. de los Reyes
Departamento de Ingeniería de Procesos e Hidráulica
División de Ciencias Básicas e Ingeniería
Universidad Autónoma Metropolitana-Iztapalapa
Ciudad de México 09340, Mexico

The ORCID identification number(s) for the author(s) of this article can be found under https://doi.org/10.1002/smll.202408155

DOI: 10.1002/smll.202408155

J. G. Flores
Área de Química Aplicada
Departamento de Ciencias Básicas
Universidad Autónoma Metropolitana-Azcapotzalco
Ciudad de México 02200, Mexico

S. Ling
Advanced Materials Research Group
Faculty of Engineering
University of Nottingham
Nottingham NG7 2RD, UK

A. Gutiérrez-Alejandre
UNICAT
Departamento de Ingeniería Química
Facultad de Química
Universidad Nacional Autónoma de México (UNAM)
Ciudad de México 04510, Mexico
E-mail: aidag@unam.mx

M. A. Vera, R. A. Peralta
Departamento de Química
División de Ciencias Básicas e Ingeniería
Universidad Autónoma Metropolitana-Iztapalapa
Av. San Rafael Atlixco, 186, Col. Vicentina, Ciudad de México 09340, México

I. A. Ibarra
On sabbatical as "Catedra Dr. Douglas Hugh Everett" at Departamento de Química
Universidad Autónoma Metropolitana-Iztapalapa
Avenida San Rafael Atlixco 186, Leyes de Reforma 1ra Sección, Iztapalapa, Ciudad de México 09310, Mexico

 © 2024 Wiley-VCH GmbH

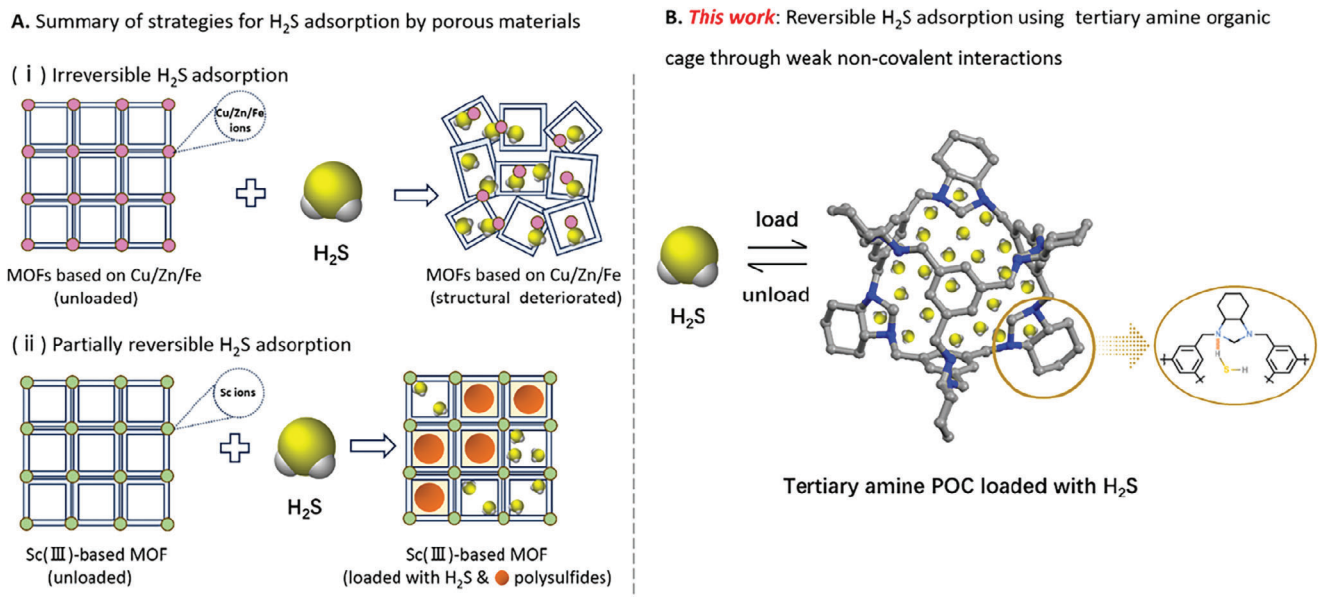


Figure 1. H_2S capture: status quo and challenge.

as highly abundant and risky pollutants. However, one of the most extremely toxic gases is hydrogen sulfide (H_2S). It is classified as a flammable, colorless gas with a distinctive rotten egg stench. The inhalation at concentrations above 700 ppm in the air could be lethal to humans since it is absorbed into the bloodstream, limiting O_2 uptake at the cellular level.[3]

Furthermore, the effective removal of H_2S is crucial for environmental remediation and industrial purposes. Mostly, different approaches have been used for H_2S remediation. It emphasizes the application of ionic liquids, alkanol amines, membrane separation, cryogenic distillation, and adsorption in zeolites, activated carbons, and metal oxides.[4–6] When referring to the adsorption processes, in the majority, these materials exhibit a clear drawback since irreversible structure transformation (chemisorption) is involved, which avoids their effective regeneration.[7] The copper/zinc/iron center of some porous absorbents enhances the hydrogen sulfide reactive adsorption, but the formation of metal sulfide leads to the structural deterioration of porous materials (**Figure 1**A, irreversible H_2S adsorption).[8–10] The chemical stability and the recyclability of the Sc-centered MOF for H_2S are improved, but the irreversibly chemisorbed polysulfides gradually block the pores of the adsorbents. After repeated adsorption-desorption processes, the H_2S adsorption capacities of these adsorbents gradually weaken (Figure 1A, partially reversible H_2S adsorption).[11] Consequently, more porous materials have been developed, displaying suitable H_2S adsorption capacities with facile regeneration conditions.[12] For example, metal–organic frameworks (MOFs) have been explored to capture H_2S. Consisely, MIL-53(Al)-TDC,[13] Mg-CUK-1,[14] Ni-CPO-27,[15] and MIL-47(V)[16] demonstrated outstanding H_2S adsorption capacities. However, MOF materials show high costs for the synthesis of organic ligands and the use (in some cases) of toxic metals, leading to industrial scalability challenges. Undoubtedly, MOF materials for H_2S removal at the industrial scale show a fundamental barrier for real applications.[17]

As an alternative, porous organic cages (POCs) have successfully emerged. Interestingly, the groups of Atwood[18] and Copper[19] independently reported the first shape-persistent organic cage material. Essentially, POCs are discrete organic cages formed by molecular ditopic, tritopic, and tetratopic building blocks (BBs) units. The material forms an intrinsic nano-sized cavity bonded covalently, with extrinsic voids caused by packing in the solid state.[20] Moreover, 12 organic cage topologies, such as Platonic and Archimedean solids, could be synthesized to embrace polyhedral. However, the diversity of topologies has remained to be reported, leading to a high opportunity to search for new porous materials.[21]

In addition, POC materials exhibit the desirable simple synthesis, scalability, functionalization, and regeneration. Based on their outstanding microporosity nature, POCs have been applied for gas adsorption and storage,[22] molecular separation,[23] encapsulation,[24] and sensing/detection.[25] In contrast with metal-based materials, using only organic porous materials embodies an effective alternative to avoid the formation of metal sulfides, which is the case of some MOF materials.[26] Furthermore, POCs offer the opportunity to maximize host-guest interactions due to both intrinsic and extrinsic porosity, which can be exploited to increase the amount of adsorbate uptake. Furthermore, POC materials have been reported to be highly stable under acidic conditions. Copper and co-workers reported a tertiary amine POC (6FT-RCC3), displaying extraordinary chemical stability toward acid and basic conditions (pH 1.7–12.3).[27] This cage was evaluated for SO_2 adsorption under static conditions. It has been suggested that due to the high affinity of SO_2 gas for this cage (6FT-RCC3), SO_2 molecules could be accommodated inside the porous structure until they fill all the holes in the crystalline phase, which eventually disrupts the regular packing of the structure, as observed in the resulting diffractogram.[28] For the SO_2 adsorption application, triazine-based multicomponent metal cages were used, displaying an N-rich structure to increase the SO_2 selectivity.[29] Polymeric amines using POCs as

© 2024 Wiley-VCH GmbH

16136829, 2025, 2, Downloaded from https://onlinelibrary.wiley.com/doi/10.1002/smll.202408155 by Universidad Autonoma Metropolitana, Wiley Online Library on [30/06/2025]. See the Terms and Conditions (https://onlinelibrary.wiley.com/terms-and-conditions) on Wiley Online Library for rules of use; OA articles are governed by the applicable Creative Commons License

molecular porous supports were applied for SO_2 removal at low concentrations (200 ppm).[30] Also, diverse nitrogen-functionalized porous organic polymers were used for the adsorption of H_2S due to their high selectivity, porosity, and long-term chemical stability.[31–33]

Herein, we demonstrate for the first time how a tertiary amine POC (6FT-RCC3) can be used for the efficient and effective capture of H_2S, with good cyclability, easy regeneration, and the highest H_2S adsorption value reported so far for an adsorbent through weak host-host interaction (Figure 1B). Also, the detection and sensing properties for H_2S of 6FT-RCC3 were investigated.

2. Results and Discussion

2.1. H_2S Adsorption Performance

The synthesis of the cage 6FT-RCC3 was conducted as previously reported.[27] The mass spectra corroborate the formation of the cage (Figure S15, Supporting Information). Based on the N_2 adsorption-desorption isotherm at 77 K (Figure S16, Supporting Information), the BET surface area was calculated to be 339 $m^2\ g^{-1}$. For comparison, the cages CC3 and RCCR were also synthesized and evaluated. Thus, based on the outstanding results for SO_2 adsorption capture of these materials,[28] the dynamic H_2S adsorption experiments were investigated. In this case, a series of breakthrough tests were carried out on an activated 6FT-RCC3 sample (80 °C for 2 h under a flow of dry N_2 gas) at 25 °C using a concentration of 5 vol% H_2S and 95 vol% N_2. The breakthrough curves of H_2S adsorption (**Figure 2a**) show a remarkable 21.7 mmol $H_2S\ g^{-1}$ uptake. The cages CC3 and RCCR show an H_2S uptake of 3.61 and 12.6 mmol $H_2S\ g^{-1}$, respectively (Figures S2 and S3, Supporting Information). Therefore, the exceptional H_2S adsorption capacity for 6FT-RCC3 is by far the highest value reported at 25 °C and 1 bar for any adsorbent material, to the best of our knowledge. Interestingly, this uptake is higher than the record reported using the Al(III)-based MOF material MIL-53(Al)-TDC (18.1 mmol $H_2S\ g^{-1}$).[13] The experimental H_2S breakthrough system was validated by performing H_2S adsorption experiments on previously reported MOF materials: Mg-CUK-1 (1.5 mmol $H_2S\ g^{-1}$),[14] MIL-101(Cr) (0.4 mmol $H_2S\ g^{-1}$)[34] and MIL-53(Al)-TDC (18.3 mmol $H_2S\ g^{-1}$).[13] These H_2S adsorptions were in good correlation with the reported values, which corroborated the reliability of our breakthrough measurements. Furthermore, the H_2S regeneration capacity of 6FT-RCC3 was investigated. A total of 5 cycles of H_2S breakthrough experiments (5 vol% H_2S and 95 vol% N_2) on the same 6FT-RCC3 sample was measured. In fact, for the reactivation of the sample between each cycle, only a flow of dry N_2 was necessary at room temperature. Cycling adsorption-desorption results (Figure 2a, inset) demonstrated that the H_2S adsorption capacity remained constant (20.6 mmol $H_2S\ g^{-1} \pm 1$ mmol g^{-1}), highlighting the high stability of 6FT-RCC3 toward H_2S. Also, the superior chemical stability of 6FT-RCC3 after the H_2S cycles was analyzed by PXRD (Figure 2b). It is observed that 6FT-RCC3 retains its crystal structure after the five consecutive H_2S breakthrough experiments. The crystalline structure was also maintained in the case of CCR and RCC3 (Figure S4, Supporting Information). Conversely, it was previously reported the loss of crystallinity for 6FT-RCC3 upon the adsorption of SO_2, was attributed to the relatively strong interaction of the material with SO_2 molecules, and this was demonstrated by FTIR and NMR spectroscopies.[28] Then, the primary hypothesis is based on the possibility that the interaction of H_2S molecules with 6FT-RCC3 is considerably weak. To gain further insights into the structure stability, an activated 6FT-RCC3 sample (80 °C for 2 h under a flow of dry N_2 gas) was exposed for 24 h to concentrated H_2S generated in a home-designed setup (Figure S1, Supporting Information). The PXRD

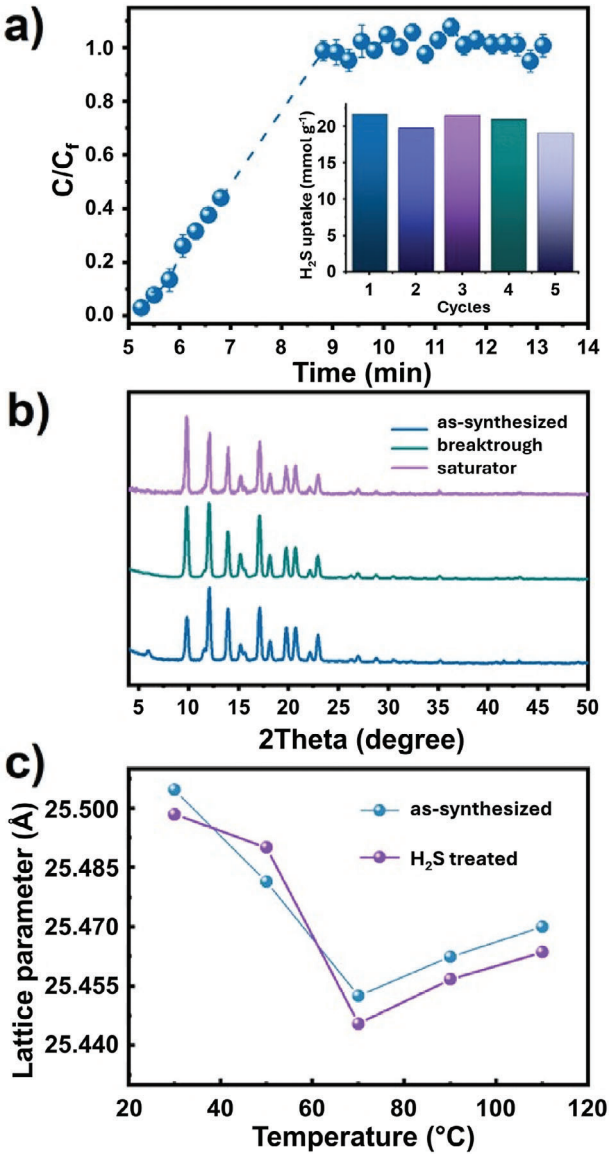


Figure 2. a) Breakthrough curves of H_2S adsorption by 6FT-RCC3 obtained at 25 °C and 1 bar using a feed gas H_2S concentration of 5% vol. The total H_2S/N_2 rate flow was 25 $cm^3\ min^{-1}$. The inset shows the comparative H_2S adsorption capacities for each cycle. b) Comparison of PXRD patterns for 6FT-RCC3 as-synthesized (blue line), after H_2S adsorption-desorption cycles (green line), and after H_2S homemade saturator for 3 days (purple line). c) The lattice parameter plot of Rietveld refinement based on XRD data of as-synthesized (blue dots) and H_2S-treated (purple dots) 6FT-RCC3 at 30–110 °C.

© 2024 Wiley-VCH GmbH

16136829, 2025, 2, Downloaded from https://onlinelibrary.wiley.com/doi/10.1002/smll.202408155 by Universidad Autonoma Metropolitana, Wiley Online Library on [30/06/2025]. See the Terms and Conditions (https://onlinelibrary.wiley.com/terms-and-conditions) on Wiley Online Library for rules of use; OA articles are governed by the applicable Creative Commons License

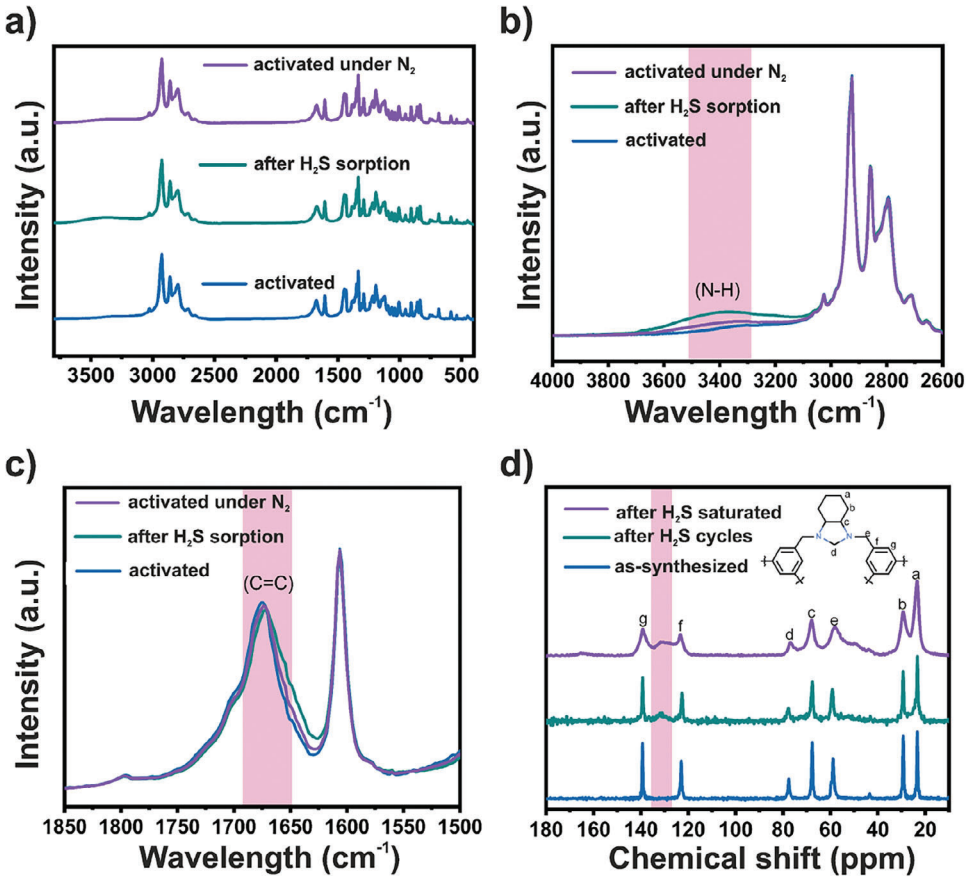


Figure 3. a) FT-IR spectra of activated 6FT-RCC3, after H_2S adsorption and after the reactivation in N_2 flow, b) 2600–4000 cm^{-1} region, c) 1500–1850 cm^{-1} region, and d) 13C CP MAS NMR spectra of 6FT-RCC3 as-synthesized, after cycles of H_2S and after H_2S homemade saturator for 3 days.

of the H_2S-saturated 6FT-RCC3 sample showed the complete retention of its crystallinity (Figure 2b).

2.2. Proposal H_2S Adsorption Interaction

The H_2S saturation adsorbed 6FT-RCC3 were heated from 30 to 110 °C with a heating rate of 1 °C min^{-1} while the lattice parameters were collected by synchrotron radiation X-ray diffraction (SR-XRD) to observe the lattice changes for 6FT-RCC3 during the H_2S gas desorption process. The 6FT-RCC3 were loaded with pure H_2S and sealed in cylindrical quartz capillary tubes. The corresponding SR-XRD data indicate that even in a pure H_2S atmosphere, 6FT-RCC3 could maintain the complete retention of its crystallinity with similar lattice parameters compared to as-synthesized 6FT-RCC3 (Figure S5, Supporting Information). The refined lattice parameters of both as-synthesized and H_2S-treated 6FT-RCC3 were decreased with temperature increasing from 30 to 70 °C, which may refer to the desorption process of the remaining gas within the 6FT-RCC3 crystalline structure. Then, the lattice parameters of as-synthesized 6FT-RCC3 and H_2S increased with temperature increasing from 70 to 110 °C, suggesting the temperature effect becomes dominant after adsorbed H_2S was released (Figure 2c).

Then, in situ DRIFT experiments were performed at 25 °C to confirm this behavior. **Figure** 3a exhibits the IR spectra for 6FT-RCC3 samples: before (activated sample), after H_2S adsorption, and after the reactivation in N_2 flow. The activated 6FT-RCC3 sample shows specific bands in different regions related to stretching vibration modes of the aromatic ring (1600–1400 cm^{-1}), C—H (3050–3020 cm^{-1}), and C—N (1310–1360 cm^{-1}). After the interaction with H_2S, the S—H stretching vibration mode of the H_2S molecule is absent. However, some changes in the main bands of 6FT-RCC3 are clear. It was observed that a new broadband appeared at 3390 cm^{-1} (Figure 3b). This band is assigned to ν(N—H) stretching vibration. It is worth mentioning that in the activated 6FT-RCC3, the N—H bonds are absent since the POC is functionalized with a tertiary amine. Furthermore, this change could be related to the H_2S interaction with 6FT-RCC3 via hydrogen bond. An H-atom from H_2S molecule interacts with the basic amine group, forming an H_2S-amine complex, which requires two molecules to interact with one H_2S, leading to the formation of an N—H bond.[35–37].

It is also possible that H_2S–H_2S interactions inside the cages also contribute to the hydrogen bonding formation, and the

© 2024 Wiley-VCH GmbH

16136829, 2025, 2, Downloaded from https://onlinelibrary.wiley.com/doi/10.1002/smll.202408155 by Universidad Autonoma Metropolitana, Wiley Online Library on [30/06/2025]. See the Terms and Conditions (https://onlinelibrary.wiley.com/terms-and-conditions) on Wiley Online Library for rules of use; OA articles are governed by the applicable Creative Commons License

broadband at 3390 cm^{-1} is formed by both contributions. Therefore, the band with a maximum of 1678 cm^{-1} is lightly red-shifted (Figure 3c).

This indicates that H_2S molecules also perturb the aromatic ring of the 6FT-RCC3 structure. Then, it is observed that after reactivation under N_2 flow, the H_2S molecules were desorbed entirely, and the sample was restored almost completely. SO_2 is a polar molecule with a higher acidity in comparison to H_2S. Thus, it is more likely that H_2S strongly interacts with the basic sites (tertiary amine groups) in 6FT-RCC3. These interactions are characterized by the formation of N→SO_2 adducts, which are relatively strong, as evidenced by the higher binding energy for SO_2 (68.6 kJ mol^{-1}).[28] This strong binding can saturate the active sites within the POC, reducing the availability of these sites for H_2S adsorption, which, although it is also polar, H_2S is a weaker acid and it is expected to weakly interact with the same sites. Thus, H2S is more susceptible to being outcompeted by SO_2. Consequently, in an environment where both gases are present, the higher affinity of SO_2 by 6FT-RCC3 may lead to a significant reduction in the material's capacity to adsorb H_2S. This competition and the potential displacement of H_2S by SO_2 underscore the importance of understanding and quantifying these interactions, especially when considering the application of 6FT-RCC3 in environments where both gases coexist. In fact, in situ DRIFT demonstrated a relatively weak interaction between H_2S and the material.

Moreover, solid-state NMR was conducted to verify the H_2S interactions. ^{13}C CP MAS NMR experiments (Figure 3d) were performed on an activated sample after H_2S cycles and after H_2S homemade saturator for 3 days. The activated sample shows narrow NMR peaks of aliphatic carbons at 22.9, 29.1, 59.0, 67.9, and 77.9 ppm and aromatic carbons at 122.9 and 139.1 ppm. After the consecutive H_2S adsorption cycles, it is possible to observe some minor modifications in the spectrum. The NMR peaks became broader, consistent with a dipolar interaction between the amine group of 6FT-RCC3 and H_2S molecules. Further, a very broad peak is observed at 132 ppm, suggesting that the H_2S molecule can interact with the aromatic ring. These observations are in good agreement with the in situ DRIFT spectroscopy results. The broadness of NMR peaks due to the H_2S adsorption is more evident in the spectrum of the H_2S-saturated 6FT-RCC3 sample. In general, the NMR signals are broad, which is complicated from these spectra to precisely identify the functionalized carbon that functions as a hydrogen acceptor in forming hydrogen bonding. However, from this NMR spectrum, it is possible to propose that H_2S is adsorbed close to the aromatic carbons, which is in good agreement with the in situ DRIFT results.

In addition, ^{15}N solid-state NMR experiments were performed to confirm the interaction between H_2S modules and the tertiary amine groups on the cage which favors the absorption of H_2S.[6] Taking account of the availability of the starting materials, we synthesized the ^{15}N-labeled 6FT-RCC1 which has a very close cage structure and bears the same tertiary amine groups (ESI), as the model compound of 6FT-RCC3.[27] The synthesis of ^{15}N-labeled amine cage 6FT-RCC1 is described in detail in Supplementary Material. Similar to 6FT-RCC3, the ^{1}H NMR spectra of 6FT-RCC1 show its good stability in a pure H_2S atmosphere (Figure S6, Supporting Information). The ^{15}N CP/MAS NMR spectra of 6FT-RCC1 powder are shown in Figure S7 (Supporting Information), the chemical shift of the main peak shifted from the high field (50.4598 ppm) to low field (47.4081 ppm) after H_2S treatment, which could be attributed to the formation of intermolecular hydrogen bond between 6FT-RCC3 and H_2S.[6,38] Previously, the Huang group reported the isomerization of Azo-bond in the solid state by ^{15}N solid-state NMR.[39] The solid-state NMR showed a relatively low chemical shift (89 ppm and 34 ppm) in the spectra of azobenzene structure. The chemical shift difference between the two types of N within the 1,3,5-triaminobenzene-based Azo-POP-4 model compound could be caused by the intramolecular hydrogen bond between amino and azo to form a six-membered ring.[40] Moreover, the main peak within the NMR spectra of as-synthesized 6FT-RCC1 is much narrower than that of H_2S-saturated, suggesting that the crystallinity of 6FT-RCC1 is decreased after adsorption of H_2S, which is consistent with the powder X-ray diffraction results (Figure S8, Supporting Information). Taking account of the results from the in situ FTIR spectroscopy, ^{13}C CP MAS NMR, and ^{15}N CP MAS NMR experiments, we believe that the non-covalent interaction between tertiary amine cage and H_2S molecules is the key to the highly efficient adsorption of H_2S.

2.3. Theoretical Calculation

To further verify our hypothesis, we performed density functional theory (DFT) calculations (see ESI for computational details). We optimized the structures of the complex between a single 6FT-RCC3 cage molecule and a single H_2S, SO_2, or H_2O guest molecule, and we then calculated the binding energy between 6FT-RCC3 and the three different molecules. Our DFT calculations indicate that among the three molecules, the binding between 6FT-RCC3 and SO_2 is the strongest (with a binding energy of −50.1 kJ mol^{-1}), followed by H_2O (with a binding energy of −46.3 kJ mol^{-1}), and H_2S (with a binding energy of −35.3 kJ mol^{-1}), i.e., the SO_2 binding energy is >40% stronger in comparison with the H_2S binding energy. This is because the O atom in the SO_2 molecule can form two hydrogen bonds with H atoms from the cage molecule. In contrast, H_2S can only form one S—H•••N hydrogen bond with the cage molecule (**Figure 4a**), which is also much weaker than the O—H•••N hydrogen bond between H_2O and the cage molecule (Figure 4b). Our DFT calculations indicate that the presence of SO_2 and H_2O will negatively affect the adsorption capacity of H_2S in POC. It is worth mentioning that we previously reported binding energies for SO_2 with the same case molecule of 68.6 kJ mol^{-1} (reference 28), which referees to the binding energy between an unbound 6FT-RCC3 moiety and SO_2, while the current work reports the binding energy between a whole 6FT-RCC3 cage molecule and SO_2. In addition, different DFT software and basis sets were used in the two sets of calculations, which may also affect the calculated binding energy numbers. In this work, we focus on the qualitative comparison between the binding energies of a 6FT-RCC3 cage molecule and a single H_2S, SO_2, or H_2O guest molecule. Thus, the H_2S binding energy that is reported here is only qualitative.

2.4. Fluorescence H_2S Sensing

In addition, the fluorescence detection properties toward H_2S of 6FT-RCC3 were investigated. Prior to the analysis, a solid-state

© 2024 Wiley-VCH GmbH

16136829, 2025, 2, Downloaded from https://onlinelibrary.wiley.com/doi/10.1002/smll.202408155 by Universidad Autonoma Metropolitana, Wiley Online Library on [30/06/2025]. See the Terms and Conditions (https://onlinelibrary.wiley.com/terms-and-conditions) on Wiley Online Library for rules of use; OA articles are governed by the applicable Creative Commons License

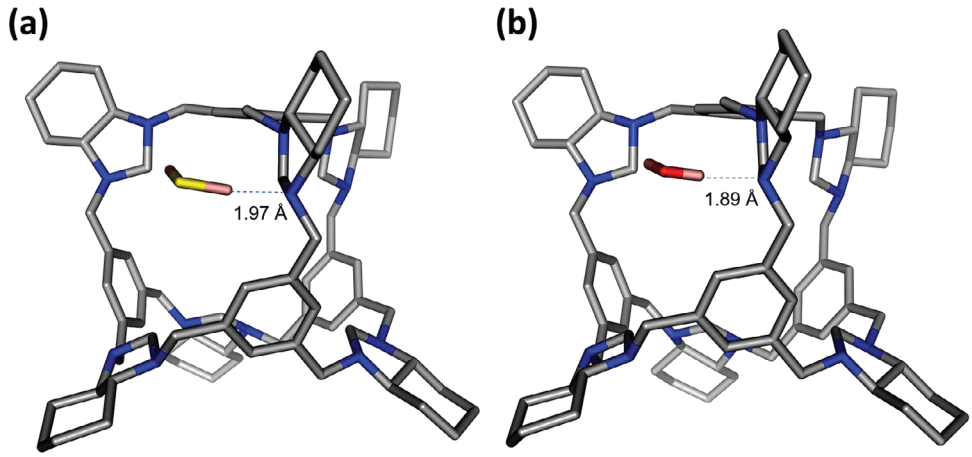


Figure 4. The visualization of tight hydrogen bonding interactions between 6FT-RCC3 and a) H_2S and b) H_2O.

UV-Vis spectra was performed (Figure S9, Supporting Information). It is observed that the material shows significant absorption in the range of 200–400 nm. Based on this, the fluorescence emission of 6FT-RCC3 was measured at different excitation wavelengths (Figure S10, Supporting Information). The higher intensity was with the excitation at 400 nm, displaying a maximum emission peak at 500 nm (Figure S11, Supporting Information). 6FT-RCC3 shows a porous organic cage structure with tertiary amine functionalization.[27] Particularly, this organic cage contains imidazolidine rings which have a bipolar structure due to the presence of two nitrogen atoms with different electronic properties: one of them acts as an electron donor and the other as an acceptor.[41] Such electronic configuration facilitates intramolecular charge transfer (ICT), which is crucial in luminescent properties, such as fluorescence.[42] Moreover, the presence of tertiary amines in their structure favors fluorescence, because this type of amines shows better fluorescent properties in comparison to their primary and secondary analoges,[43] due to the absence of nitrogen-bonded hydrogens,[44] and to the higher rigidification of the structure, favoring the emission of light.[41]

Thus, an activated 6FT-RCC3 was saturated with H_2S in a homemade saturator. Then, a change in the fluorescent intensity was detected (**Figure** 5a). A clear 160% increase in the emission intensity is observed, and this turn-on effect could be associated with the changes in the electronic structure of 6FT-RCC3. This increase in the fluorescence of the material is associated with the intermolecular hydrogen bonding interaction between the 6FT-RCC3 material and the H_2S molecule, which generates a rigidification of the organic case structure, resulting in a decrease of the non-radiative deactivation mechanism (vibrations and internal rotations), which increases the probability that the excited electrons return to the basal state by photon emission, thus increasing the fluorescence.[45]

Fluorescence analyses were performed for the three cages: 6FT-RCC3 (tertiary amine), RCC3 (secondary amine), and CC3 (primary amine). The experimental data (Figure S12, Supporting Information) demonstrate that 6FT-RCC3 exhibits a significantly higher fluorescence intensity for both the as-synthesized material and after the saturation with H_2S. Specifically, the increase in fluorescence after exposure to H_2S is considerably higher for 6FT-RCC3 (160%) in comparison to RCC3 and CC3, which incorporate secondary and primary amines, respectively (Figure S13, Supporting Information). This increase in fluorescence indicates that tertiary amines enhance the inherent optical properties of a POC material and it significantly increases its sensitivity to H_2S. The increased rigidity of tertiary amines reduces non-radiative decay processes, leading to a more efficient emission. In addition, the stronger interaction between tertiary amines and H_2S, most likely, facilitates a more pronounced response, underscoring the functional advantages of tertiary amines for these applications. Table S1 (Supporting Information) compares the H_2S sensing results of 6FT-RCC3 to other selected materials.

Therefore, an H_2S selectivity test was measured using other gases (SO_2, CO_2, and NO_2) and H_2O vapor. For CO_2 and H_2O, no apparent change is observed. However, for NO_2 and SO_2, a decrease in fluorescent emission is recorded. It can be related to the loss of crystallinity, as it was previously reported.[28] Then, time-resolved photoluminescence (TRPL) experiments were conducted using a 375 nm picosecond-pulsed laser (Figure 5b). The average fluorescence lifetime (Table S2, Supporting Information) for an activated and H_2S-saturated 6FT-RCC3 were 3.32 and 3.13 ns, respectively. These results reveal that, despite the remarkable increase in fluorescence intensity, the interaction with H_2S does not induce a significant decrease in the fluorescence decay time of the material. Moreover, to analyze the possibility of using 6FT-RCC3 as a sensor, the limit of detection (LOD) was calculated using a solution of H_2S dissolved in THF. The LOD value was calculated with the following formula: $LOD = 3\sigma\ m^{-1}$, where σ represents the standard deviation of the initial intensity of activated 6FT-RCC3 in THF and m is the slope of the linear fit from the experimental data. Different concentrations (0.05–4.00 mM) of H_2S in THF were employed (Figure S14, Supporting Information), and a linear correlation was observed in 0.27–4.00 mM, showing a LOD of 0.13 mM related to ≈4.43 ppm, as the H_2S detection limit (Figure 5c).

3. Conclusion

We demonstrated the first experimental study of a porous organic cage for capturing, detecting, and sensing H_2S. The

© 2024 Wiley-VCH GmbH

16136829, 2025, 2, Downloaded from https://onlinelibrary.wiley.com/doi/10.1002/smll.202408155 by Universidad Autonoma Metropolitana, Wiley Online Library on [30/06/2025]. See the Terms and Conditions (https://onlinelibrary.wiley.com/terms-and-conditions) on Wiley Online Library for rules of use; OA articles are governed by the applicable Creative Commons License

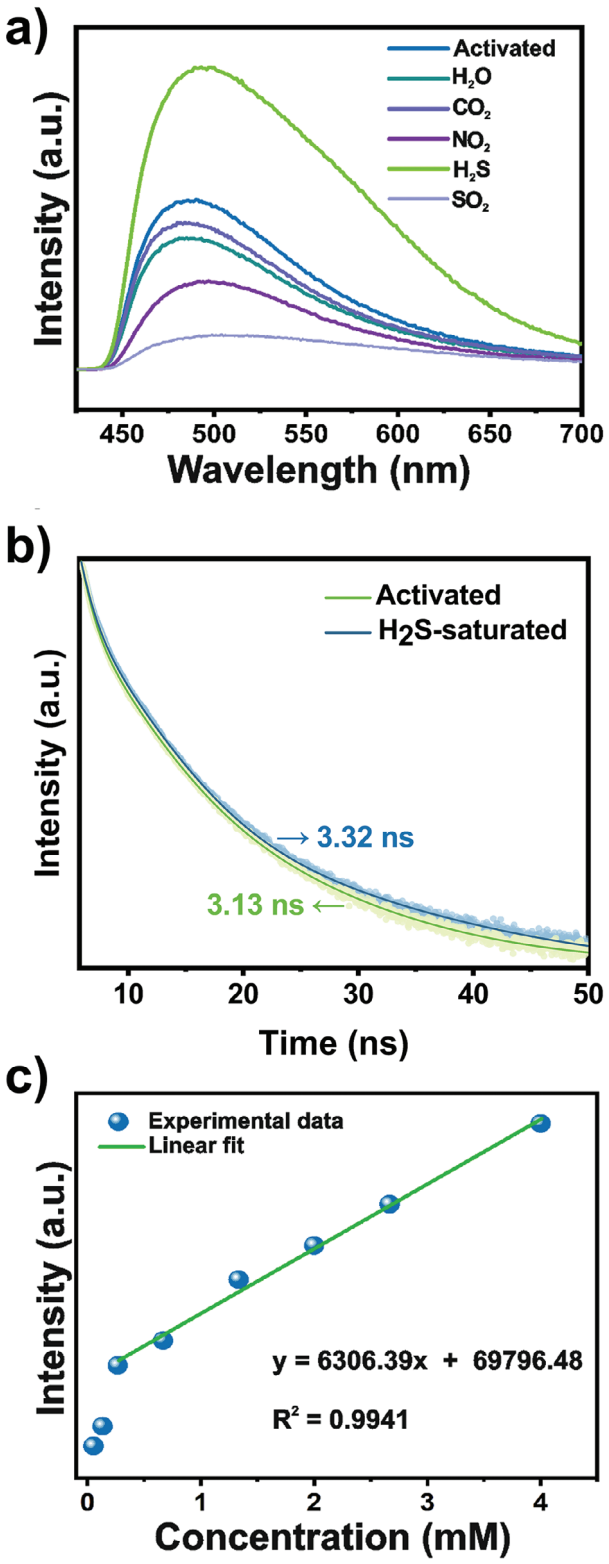


Figure 5. a) Solid-state emission spectra of 6FT-RCC3 exposed to different gases under an excitation wavelength of 400 nm b) Solid-state time-resolved photoluminesce (TRPL) spectra for H_2S-saturated and an activated 6FT-RCC3, c) calibration curve of H_2S in THF solution.

breakthrough experiments of H_2S exhibit a record high capacity of 21.7 mmol H_2S g^{-1}. The material shows high stability since the crystalline structure was retained after the H_2S adsorption. The H_2S interaction was confirmed using in situ FTIR, ^{13}C NMR, and DFT calculations, demonstrating that relatively weak interactions were established via hydrogen bonding and H_2S-H_2S interactions. Furthermore, the fluorescence performances of the cage were tested, showing a turn-on effect due to the interaction with the H_2S molecule. Remarkably, the LOD was calculated as 0.13 mM (≈4.43 ppm) of H_2S in a THF solution. Our findings thus illustrate the possibilities of 6FT-RCC3 as a strong promise for real-life H_2S capture and detection applications.

4. Experimental Section

Synthesis of CC3: CC3 was synthesized as previously reported in its homochiral form.[46] For this, a solution without stirring at room temperature was prepared. Dichloromethane (100 mL) was covered slowly onto solid triformylbenzene (5 g, 30.86 mmol). Then, trifluoroacetic acid (1 mL) was added directly to this solution as a catalyst for the imine bond formation. Finally, a solution of (R,R)-1,2-diaminocyclohexane (5 g, 44.64 mmol) in dichloromethane (100 mL) was added (without mixing). The reaction was covered and allowed to settle. After 5 days, octahedral crystals of CC3 grew on the sides of the glass reaction vessel. The crystalline product was removed by filtration and washed with 95% ethanol / 5% dichloromethane.

Synthesis of RCC3: RCC3 was synthesized and purified as previously reported.[27] By stirring, the imine cage CC3 (926 mg, 0.83 mmol) was dissolved in a $CHCl_3$/methanol mixture (1:1 v/v, 50 mL). After that, sodium borohydride (1.00 g, 26.5 mol) was added, and the reaction was stirred for 12 h at room temperature. Then, water (2 mL) was added, stirring the reaction for 12 h. The solvent was then removed under a vacuum. The resulting white solid was extracted with chloroform (2 × 50 mL), and then the combined organic phase was washed with water (2 × 100 mL). The $CHCl_3$ phase was dried using anhydrous $MgSO_4$ before being removed under vacuum. RCC3 (yield = 95.1%) was obtained as a white solid.

Synthesis of 6FT-RCC3: The 6FT-RCC3 was prepared as previously reported.[27] Paraformaldehyde (52 mg) dissolved in CH_3OH (10 mL) was stirred at 70 °C. Then, a solution of RCC3 dissolved in CH_3OH (10 mL) was added. A white precipitate appeared upon the addition of RCC3. The reaction was stirred for a further 2 h at 70 °C. The reaction was cooled to room temperature, and the precipitate was collected by filtration. 6FT-RCC3 (yield = 70%) was obtained after being washed with CH_3OH (3 × 10 mL) and dried under vacuum.

Powder X-Ray Diffraction Patterns (PXRD): The PXRD were recorded on a Rigaku Diffractometer, Ultima IV, with Cu-Kα1 radiation (λ = 1.5406 Å) using a nickel filter; the patterns were recorded in the range 2–50° 2θ with a step scan of 0.02° and a scan rate of 0.10° min^{-1}.

Nuclear Magnetic Resonance: The ^{13}C CP/MAS NMR spectra were acquired at a frequency of 75.422 MHz at a spinning rate of 6 kHz. Typical ^{13}C CP/MAS NMR conditions for ^{1}H–^{13}C polarization experiment used a $\pi/2$ pulse of 4 µs, contact time of 1 ms, delay time of 5 s, and at least 20 000 scans. Chemical shifts were referenced to a solid shift at 38.2 ppm relative to TMS. For ^{15}N CP/MAS NMR spectra. The spectra were acquired on an Avance III-HD 400 MHz NMR spectrometer at resonance frequencies of 40.56 MHz for ^{15}N, using a 3.2 mm magic-angle spinning (MAS) probe, and the ^{15}N chemical shifts were referenced to 15NH4Cl. 38.8 ppm.

N_2 Sorption Analysis: Surface areas were measured by nitrogen adsorption and desorption at 77 K using a BSD-660 M analyzer (Beishide Instrument Co, Ltd.). The sample was activated at 80 °C for 6 h under vacuum before analysis.

Solid-State UV–vis spectroscopy (UV–vis): Absorption measurements were performed from 200–800 nm using a Shimadzu spectrophotometer

© 2024 Wiley-VCH GmbH

16136829, 2025, 2, Downloaded from https://onlinelibrary.wiley.com/doi/10.1002/smll.202408155 by Universidad Autonoma Metropolitana, Wiley Online Library on [30/06/2025]. See the Terms and Conditions (https://onlinelibrary.wiley.com/terms-and-conditions) on Wiley Online Library for rules of use; OA articles are governed by the applicable Creative Commons License

UV-2600 equipped with an ISR-2600Plus integrating sphere and a BaSO4 blank.

Synchrotron Radiation X-Ray Diffraction (SR-XRD): The pristine and H_2S-treated 6FT-RCC3 powders were loaded into 0.5 mm diameter cylindrical quartz capillary tubes and sealed. The SR-XRD data were collected at BL14B1 of the Shanghai Synchrotron Radiation Facility (SSRF) using X-rays at a wavelength of 0.6887 Å. The capillary samples were heated from 30 to 110 °C at a rate of 1°C min^{-1}. To characterize the XRD patterns, the lattice parameters of 6FT-RCC3 and the Rietveld refinement were performed using jEdit and TOPAS Academic V5.

H_2S Breakthrough Experiments: H_2S experiments were made using an HP 5890 GC by continuous injections of the system exhaust; of each injection, a chromatogram was obtained. The H_2S signal from the corresponding chromatogram was integrated to obtain its quantity. Knowing the H_2S concentration from the feed, the H_2S concentration was calculated in each injection, as the saturation concentration was the original feed concentration. Dynamic breakthrough experiments were carried out in a homemade system (Scheme S1, Supporting Information).

In Situ DRIFTS of H_2S: DRIFT spectra of the 6FT-RCC3 were measured using an FTIR Nicolet 6700 spectrophotometer (DTGS detector) with a 4 cm^{-1} resolution equipped with a diffuse reflectance vacuum chamber with KBr windows. A pellet was made with the material, which was then placed in a closed system for degassing at 80 °C for 2 h under a primary vacuum. Subsequently, the system was cooled and, upon reaching room temperature (material evaluated), was saturated with a mixture of H_2S/N_2 in a composition of 15% H_2S up to a pressure of 29 bar. Then, under these conditions, DRIFT spectra were taken, and gradually, pressure was released by venting at the same time. Readings of the spectra were taken at each H_2S pressure measured until reaching 0 torr with the help of a primary vacuum.

Fluorescence Spectroscopy: It was performed on an Edinburgh Instrument FS5 fluorimeter using a continuous wave 150 W ozone-free xenon arc lamp at room temperature. It was coupled with an SC-10 solid-state sample holder for solid-state measurements and an SC-05 standard cuvette holder for dispersed samples. For the emission experiments, the solid samples were slightly ground in an agate mortar to homogenize the microcrystals. They were later packed into the quartz sample holders and positioned in the instrument. Measurements were carried out using an excitation wavelength of 400 nm, with an additional 455 nm long-pass filter on the detector side to remove any remnant light from the excitation source. The measurements were collected with a step size of 1 nm and a dwell time of 0.10 s.

Time-Resolved Photoluminescence (TRPL) Measurements: The spectra were measured in an Edinburgh Instruments FS5 Spectrofluorometer using a 375 nm EPL laser, with an excitation bandwidth of 0.01 nm and an emission bandwidth of 5.00 nm at an emission wavelength of 500 nm.

Supporting Information

Supporting Information is available from the Wiley Online Library or from the author.

Acknowledgements

J.L.O., D.H., and V.B.L.-C. contributed equally to this work. The authors thank PAPIIT-UNAM (Grant IN201123), Mexico, for financial support. The authors thank Eva Martínez-Ahumada for her support in the investigation. M.L. acknowledges the Engineering and Physical Sciences Research Council (EPSRC) (EP/N004884/1) and the Leverhulme Trust via the Leverhulme Research Centre for Functional Materials Design for funding. D. H. thanks the Overseas Study Program of Guangzhou Elite Project provided by Guangzhou City, China for financial support. M.L. thanks the National Natural Science Foundation of China (22371252), the Zhejiang Provincial Natural Science Fund (LZ23B020005), the Leading Innovation Team grant from the Department of Science and Technology of Zhejiang Province (2022R01005). The authors also thank the beamline BL14B1 & BL17U1, Shanghai SynchrotronRadiation Facility (SSRF) for providing beam time and help during the experiments. J.L.O. thanks CONAHCYT for the Ph.D. fellowships (1003953). Y.A.A.-S. acknowledges the support from the DGAPA-UNAM postdoctoral fellowship. The authors thank U. Winnberg (Euro Health) for scientific discussions and G. Ibarra-Winnberg for scientific encouragement.

Conflict of Interest

The authors declare no conflict of interest.

Data Availability Statement

The data that support the findings of this study are available on request from the corresponding author. The data are not publicly available due to privacy or ethical restrictions.

Keywords

adsorption, chemical stability, H_2S, porous organic cages, POCs

Received: September 9, 2024
Revised: October 24, 2024
Published online: November 6, 2024

[1] F. Perera, *IJERPH*. **2017**, *15*, 16.
[2] R. P. Velasco, D. Jarosińska, *Environment International*. **2022**, *170*, 107556.
[3] X. Wei, L. Duan, L. Bai, M. Tian, W. Li, B. Zhang, *Intensive Care Med*. **2012**, *38*, 1877.
[4] A. Pudi, M. Rezaei, V. Signorini, M. P. Andersson, M. G. Baschetti, S. S. Mansouri, *Sep. Purif. Technol*. **2022**, *298*, 121448.
[5] J. L. Obeso, D. R. Amaro, C. V. Flores, A. Gutiérrez-Alejandre, R. A. Peralta, C. Leyva, I. A. Ibarra, *Coord. Chem. Rev*. **2023**, *485*, 215135.
[6] M. S. Shah, M. Tsapatsis, J. I. Siepmann, *Chem. Rev*. **2017**, *117*, 9755.
[7] S. Watanabe, *Catal. Today*. **2021**, *371*, 204.
[8] M. Khabazipour, M. Anbia, *Ind. Eng. Chem. Res*. **2019**, *58*, 22133.
[9] C. Petit, B. Mendoza, T. J. Bandosz, *ChemPhysChem*. **2010**, *11*, 3678.
[10] E. Martínez-Ahumada, A. López-Olvera, V. Jancik, J. E. Sánchez-Bautista, E. González-Zamora, V. Martis, D. R. Williams, I. A. Ibarra, *Organometallics*. **2020**, *39*, 883.
[11] J. G. Flores, J. A. Zárate-Colín, E. Sánchez-González, J. R. Valenzuela, A. Gutiérrez-Alejandre, J. Ramírez, V. Jancik, J. Aguilar-Pliego, M. C. Zorrilla, H. A. Lara-García, E. González-Zamora, G. Guzmán-González, I. González, G. Maurin, I. A. Ibarra, *ACS Appl. Mater. Interfaces*. **2020**, *12*, 18885.
[12] Y. Yang, X. Liu, C. Yang, Y. Wang, H. Wang, H. Fan, *Colloids Surf. A*. **2023**, *674*, 131914.
[13] J. A. Zárate, E. Sánchez-González, T. Jurado-Vázquez, A. Gutiérrez-Alejandre, E. González-Zamora, I. Castillo, G. Maurin, I. A. Ibarra, *Chem. Commun*. **2019**, *55*, 3049.
[14] E. Sánchez-González, P. G. M. Mileo, M. Sagastuy-Breña, J. R. Álvarez, J. E. Reynolds, A. Villarreal, A. Gutiérrez-Alejandre, J. Ramírez, J. Balmaseda, E. González-Zamora, G. Maurin, S. M. Humphrey, I. A. Ibarra, *J. Mater. Chem. A*. **2018**, *6*, 16900.
[15] S. Chavan, F. Bonino, L. Valenzano, B. Civalleri, C. Lamberti, N. Acerbi, J. H. Cavka, M. Leistner, S. Bordiga, *J. Phys. Chem. C*. **2013**, *117*, 15615.
[16] L. Hamon, H. Leclerc, A. Ghoufi, L. Oliviero, A. Travert, J.-C. Lavalley, T. Devic, C. Serre, G. Férey, G. De Weireld, A. Vimont, G. Maurin, *J. Phys. Chem. C*. **2011**, *115*, 2047.

 © 2024 Wiley-VCH GmbH

16136829, 2025, 2, Downloaded from https://onlinelibrary.wiley.com/doi/10.1002/smll.202408155 by Universidad Autonoma Metropolitana, Wiley Online Library on [30/06/2025]. See the Terms and Conditions (https://onlinelibrary.wiley.com/terms-and-conditions) on Wiley Online Library for rules of use; OA articles are governed by the applicable Creative Commons License

[17] R. Freund, O. Zaremba, G. Arnauts, R. Ameloot, G. Skorupskii, M. Dincă, A. Bavykina, J. Gascon, A. Ejsmont, J. Goscianska, M. Kalmutzki, U. Lächelt, E. Ploetz, C. S. Diercks, S. Wuttke, *Angew. Chem. Int. Ed.* **2021**, *60*, 23975.
[18] J. Tian, P. K. Thallapally, S. J. Dalgarno, P. B. McGrail, J. L. Atwood, *Angew. Chem. Int. E.d* **2009**, *48*, 5492.
[19] T. Tozawa, J. T. A. Jones, S. I. Swamy, S. Jiang, D. J. Adams, S. Shakespeare, R. Clowes, D. Bradshaw, T. Hasell, S. Y. Chong, C. Tang, S. Thompson, J. Parker, A. Trewin, J. Bacsa, A. M. Z. Slawin, A. Steiner, A. I. Cooper, *Nature Mater.* **2009**, *8*, 973.
[20] M. A. Little, A. I. Cooper, *Adv Funct Materials.* **2020**, *30*, 1909842.
[21] V. Santolini, M. Miklitz, E. Berardo, K. E. Jelfs, *Nanoscale.* **2017**, *9*, 5280.
[22] M. M. Deegan, M. R. Dworzak, A. J. Gosselin, K. J. Korman, E. D. Bloch, *Chemistry A European J.* **2021**, *27*, 4531.
[23] T. Mitra, K. E. Jelfs, M. Schmidtmann, A. Ahmed, S. Y. Chong, D. J. Adams, A. I. Cooper, *Nature Chem.* **2013**, *5*, 276.
[24] J. Liang, A. Nuhnen, S. Millan, H. Breitzke, V. Gvilava, G. Buntkowsky, C. Janiak, *Angew. Chem. Int. Ed.* **2020**, *59*, 6068.
[25] K. Acharyya, P. S. Mukherjee, *Chem. Commun.* **2014**, *50*, 15788.
[26] L. Hamon, C. Serre, T. Devic, T. Loiseau, F. Millange, G. Férey, G. D. Weireld, *J. Am. Chem. Soc.* **2009**, *131*, 8775.
[27] M. Liu, M. A. Little, K. E. Jelfs, J. T. A. Jones, M. Schmidtmann, S. Y. Chong, T. Hasell, A. I. Cooper, *J. Am. Chem. Soc.* **2014**, *136*, 7583.
[28] E. Martínez-Ahumada, D. He, V. Berryman, A. López-Olvera, M. Hernandez, V. Jancik, V. Martis, M. A. Vera, E. Lima, D. J. Parker, A. I. Cooper, I. A. Ibarra, M. Liu, *Angew. Chem. Int. Ed.* **2021**, *60*, 17556.
[29] R. Zhang, D. Hu, Y. Fu, Q. Feng, C. Mu, K. Gao, H. Ma, M. Liu, M. Zhang, *Aggregate.* **2023**, e408.
[30] G. Zhu, J.-M. Y. Carrillo, A. Sujan, C. N. Okonkwo, S. Park, B. G. Sumpter, C. W. Jones, R. P. Lively, *J. Mater. Chem. A.* **2018**, *6*, 22043.
[31] M. M. Abdelnaby, K. E. Cordova, I. Abdulazeez, A. M. Alloush, B. A. Al-Maythalony, Y. Mankour, K. Alhooshani, T. A. Saleh, O. C. S. Al Hamouz, *ACS Appl. Mater. Interfaces.* **2020**, *12*, 47984.
[32] S. Fajal, S. Dutta, S. K. Ghosh, *Mater. Horiz.* **2023**, *10*, 4083.
[33] J. Gu, P. Shao, L. Luo, Y. Wang, T. Zhao, C. Yang, P. Chen, F. Liu, *Sep. Purif. Technol.* **2022**, *285*, 120377.
[34] J. Liu, Y. Wei, P. Li, Y. Zhao, R. Zou, *J. Phys. Chem. C.* **2017**, *121*, 13249.
[35] C. N. Okonkwo, J. J. Lee, A. De Vylder, Y. Chiang, J. W. Thybaut, C. W. Jones, *Chem. Eng. J.* **2020**, *379*, 122349.
[36] C. S. Pomelli, C. Chiappe, A. Vidis, G. Laurenczy, P. J. Dyson, *J. Phys. Chem. B.* **2007**, *111*, 13014.
[37] D. D. Miller, S. S. C. Chuang, *J. Phys. Chem. C.* **2016**, *120*, 1147.
[38] Z. J. Li, Y. Abramov, J. Bordner, J. Leonard, A. Medek, A. V. Trask, *J. Am. Chem. Soc.* **2006**, *128*, 8199.
[39] X.-S. Luo, H.-L. Deng, S. Chi, Y. Liu, M.-H. Huang, *J. Phys. Chem. Lett.* **2021**, *12*, 6767.
[40] M. Ya Berzina, B. Z. Eletskaya, A. L. Kayushin, E. V. Dorofeeva, O. I. Lutonina, I. V. Fateev, O. N. Zhavoronkova, A. R. Bashorin, A. O. Arnautova, O. S. Smirnova, K. V. Antonov, A. S. Paramonov, M. A. Dubinnyi, R. S. Esipov, A. I. Miroshnikov, I. D. Konstantinova, *IJMS.* **2023**, *24*, 9697.
[41] O. F. Al Sharif, L. M. Nhari, R. M. El-Shishtawy, A. M. Asiri, *Materials Today Chemistry.* **2023**, *29*, 101453.
[42] S. Kothavale, N. Sekar, *ChemistrySelect.* **2017**, *2*, 7691.
[43] Q. Ban, Y. Li, S. Wu, *VIEW.* **2022**, *3*, 20200135.
[44] L. Wang, X. Ran, H. Tang, D. Cao, *Dyes Pigm.* **2021**, *194*, 109634.
[45] X. Wang, J. Zhang, X. Mao, Y. Liu, R. Li, J. Bai, J. Zhang, C. Redshaw, X. Feng, B. Z. Tang, *J. Org. Chem.* **2022**, *87*, 8503.
[46] J. T. A. Jones, T. Hasell, X. Wu, J. Bacsa, K. E. Jelfs, M. Schmidtmann, S. Y. Chong, D. J. Adams, A. Trewin, F. Schiffman, F. Cora, B. Slater, A. Steiner, G. M. Day, A. I. Cooper, *Nature.* **2011**, *474*, 367.

© 2024 Wiley-VCH GmbH

16136829, 2025, 2, Downloaded from https://onlinelibrary.wiley.com/doi/10.1002/smll.202408155 by Universidad Autonoma Metropolitana, Wiley Online Library on [30/06/2025]. See the Terms and Conditions (https://onlinelibrary.wiley.com/terms-and-conditions) on Wiley Online Library for rules of use; OA articles are governed by the applicable Creative Commons License

Materials Today Advances 26 (2025) 100579

Contents lists available at ScienceDirect

Materials Today Advances

journal homepage: www.journals.elsevier.com/materials-today-advances/

(Hf)PCN-224(Co) as an efficient ppm-level sensor for toxic SO_2

Sergio Carrasco [a,1], Marco L. Martínez [b,c,1], Yoarhy A. Amador-Sánchez [b,1], Valeria B. López Cervantes [b], Elí Sánchez-González [b], Nora S. Portillo-Vélez [d], Ricardo A. Peralta [d], Christian A. Celaya [e], Ariel Guzmán-Vargas [c], Patricia Horcajada [a,*], Diego Solis-Ibarra [b,**], Ilich A. Ibarra [b,***]

[a] Advanced Porous Materials Unit (APMU), IMDEA Energy Institute, Avda. Ramón de la Sagra 3, E-28935, Móstoles, Madrid, Spain
[b] Laboratorio de Fisicoquímica y Reactividad de Superficies (LaFReS), Instituto de Investigaciones en Materiales, Universidad Nacional Autónoma de México, Circuito Exterior s/n, CU, Del Coyoacán, 04510, México D.F., Mexico
[c] Laboratorio de Investigación en Materiales Porosos, Catálisis Ambiental y Química Fina, Instituto Politécnico Nacional, ESIQIE-SEPI-DIQI, UPALM Edif. 7 P.B. Zacatenco, GAM, 07738, CDMX, Mexico
[d] Departamento de Química, División de Ciencias Básicas e Ingeniería, Universidad Autónoma Metropolitana-Iztapalapa, San Rafael Atlixco 186, Col. Leyes de Reforma 1ra Seccion, Iztapalapa, 09310, Ciudad de, México, Mexico
[e] Centro de Nanociencias y Nanotecnología, Universidad Nacional Autónoma de México, Km 107 Carrerera Tijuana-Ensenada, Ensenada, B.C., C.P. 22800, Mexico

ARTICLE INFO

Keywords:
SO_2 capture
Adsorption-desorption isotherm
SO_2 detection
Porphyrin
MOFs
Fluorescence
DFT

ABSTRACT

Herein, we report the first experimental investigation, supported with theoretical calculations, of a porphyrin-based metal organic framework (PMOF) to address the difficult challenge of SO_2 detection and sensing. Specifically, the highly porous hafnium cobalt-porphyrin tetracarboxylate named (Hf)PCN-224(Co) was used as probe material. (Hf)PCN-224(Co) demonstrated a moderate SO_2 sorption of 1.0 mmol g^{-1} at 0.1 bar and 298 K, and a limit of detection of 175.5 ppm, obtained by photoluminescent experiments. Furthermore, clear, different emission responses are observed for (Hf)PCN-224(Co) after the exposure to CO_2 and water vapor, compared to SO_2. Remarkably, (Hf)PCN-224(Co) shows crystalline retention after exposure to SO_2 at low concentrations (*i.e.*, 0.1 bar). The use of Hf^{4+}, as well as microwave-assisted solvothermal synthesis, lead to crystalline defects in the form of missing linkers, providing additional Hf(IV) open metal sites, able to interact with SO_2 molecules. Based on UV–Vis and X-ray photoelectron spectroscopies, we suggest ligand to metal charge transfer as primal emission mechanisms, and the coordination of SO_2 with $Hf_6(OH)_8$ coordinatively unsaturated clusters as the most plausible origin for the emission response in SO_2 detection/sensing. The tendency of this behavior is verified from the density functional theory calculations.

1. Introduction

A nominated group of chemically stable metal-organic frameworks (MOFs) with large surface areas and a high degree of functionality has been postulated as promising candidates for the capture of highly corrosive gases (*e.g.*, SO_2, NO_x, NH_3 and H_2S) [1], since the adsorption selectivity of these molecules can be accurately adjusted as a function of the topology and chemical composition of their pores [2]. Such corrosive (and highly toxic) gases can permanently dislocate the coordination bonds between the polycomplexant organic ligands and the metal centers of the MOF, triggering the collapse of its structure, as shown for MOF-177 [3]. Thus, the chemical stability of selected MOFs is then the essential prerequisite for the capture of these toxic gases, and remarkable examples have provided encouraging results, even under real working conditions (*i.e.* under moisture) [4].

Particularly, sulfur dioxide (SO_2) is categorized as one of the most corrosive and toxic chemicals, which can be easily absorbed by the respiratory system or dermal contact. Human exposure to SO_2 can cause drastic respiratory complications, principally in lung function (*i.e.*, broncho-constriction), and direct contact over 100 SO_2 ppm results

* Corresponding author.
** Corresponding author.
*** Corresponding author.
E-mail address: argel@unam.mx (I.A. Ibarra).
[1] These authors contributed equally to this work.

https://doi.org/10.1016/j.mtadv.2025.100579
Received 6 January 2025; Received in revised form 28 March 2025; Accepted 20 April 2025
Available online 2 May 2025
2590-0498/© 2025 The Authors. Published by Elsevier Ltd. This is an open access article under the CC BY license (http://creativecommons.org/licenses/by/4.0/).

deathly [5]. Although a selected group of MOFs have demonstrated outstanding SO_2 capture results [6,7], perhaps, the main disapproval of MOFs is the typical high cost of synthesis for the organic ligands and challenging scalability, which point out some of the flaws related to the economics of capturing SO_2, at the industrial level, using MOFs. In this respect, it is worth to mention that the capture of SO_2 is not the only problem related to this toxic gas. The detection and quantification (sensing) of SO_2 in closed environments (*e.g.*, laboratories, factories or industrial warehouses), results critical to protect the safety of the associated personnel to such places. For example, the concentration of SO_2 over periods of 10 min must not surpass 10 ppm, where the maximum regulated concentration limit is 0.075 ppm *per* hour [8]. Thus, specific research requires to be carefully dedicated to detecting SO_2. One of the main advantages of using MOFs for detection purposes, conversely to SO_2 capture (large amounts of MOF are necessary), is that only small amounts of a particular MOF are needed, minimizing the economic limitation and highlighting the health impact.

Among some effective strategies to detect gas molecules, optical methods such as ultraviolet (UV) absorption spectroscopy [9], multi-axis differential optical absorption spectroscopy (MAX-DOAS) [10], mass spectrometry [11], and photoluminescence spectroscopy (PL) [12] offer real-time gas monitoring. Thus, if a MOF shows photoluminescence properties, these could be modified before and after the exposure of a particular gas, such as SO_2, and used as a transduction mechanism. If there is a clear fluorescent response to SO_2 (assuming the chemical stability of the MOF) this luminescent change represents the key to pave the way towards an effective SO_2 detector.

With these perspectives in mind, can eventually MOFs be manufactured into portable and low-cost SO_2 gas sensors to closely watch the safety of workers who are exposed to SO_2 due to different industrial

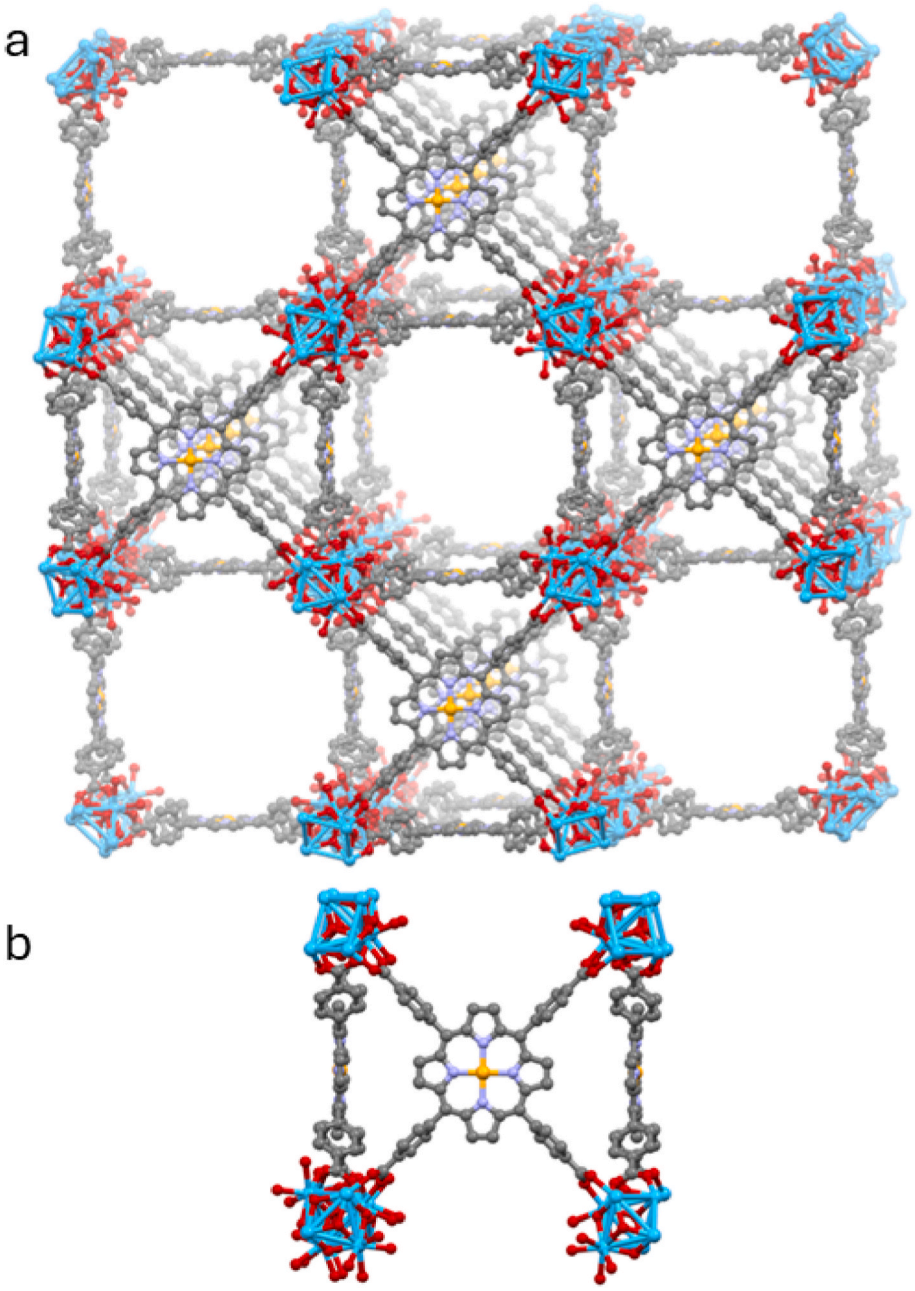


Fig. 1. a) Crystal structure of (Hf)PCN-224(Co) viewed along *a* axis. b) Close-up view of the crystal structure. It consists of TCPP(Co) coordinated *via* carboxylate groups to $Hf_6(OH)_8$ clusters. Color code: C=gray, O=red, N=purple, Co=Orange, Hf= blue. Hydrogen atoms are omitted for clarity. (For interpretation of the references to colour in this figure legend, the reader is referred to the Web version of this article).

processes? One of the first demonstrations of a MOF-based SO_2 sensor (MFM-300) was elegantly delivered by Eddaoudi et al., exhibiting a detection limit of 5 ppb with facile cyclability [13]. Later, Cao and co-workers reported a detector based on the very well-known MOF-5-NH_2, by taking the approach of the turn-on photoluminescence response of to SO_2 and demonstrating stability under measurement conditions and therefore possible reusability (up to 6 cycles in solution-sate experiments) [14].

Specifically, porphyrin-based MOFs have been widely investigated as probes in fluorescence sensing for cations, and anions, among other environmental pollutants [15,16]. However, to the best of our knowledge, there are not previous reports on porphyrin-based MOFs used as probes for SO_2 detection/sensing. Also note that some of these materials, particularly the one selected in this work, are currently being commercialized at industrial level (*e.g.*, by CD Bioparticles Ltd.). Besides, novel green synthetic pathways that facilitate the industrial take-up of porphyrins have emerged in the last years [17], highlighting the relevance of these building units as a hot topic. For instance, specialized companies (*e.g.*, PorphyChem SAS) commercialize these ligands in the large scale. We previously reported the synthesis, characterization, and catalytic properties of a microporous hafnium-based MOF entitled (Hf)PCN-224(Co) [18]. (Hf)PCN-224(Co) is built up from $Hf_6(OH)_8$ clusters linked by six square planar cobalt-metalated 5,10,15,20-tetrakis(4-carboxyphenyl) porphyrin, TCPP(Co) (Fig. 1). Herein, (Hf)PCN-224(Co) exhibited, by solid and solution-state fluorescence experiments, to be an effective detector and sensor for highly toxic SO_2 with a limit of detection (LOD) of 2.74 mM (~175 ppm) in solution-state. Thus, it is worth to mention that this is the first example where a porphyrin-based MOF is proposed as efficient SO_2 detector and sensor.

2. Methods

2.1. Reagents

Hafnium(IV) oxychloride octahydrate ($HfOCl_2{\cdot}8H_2O$, 98 %) and cobalt(II) chloride ($CoCl_2$ anhydrous, 98 %) were from Sigma-Aldrich. Benzoic acid (99 %) was acquired from Acros Organics. The organic ligand 5,10,15,20-(tetra-4-carboxyphenyl)porphyrin (TCPP, >98 %) was from PorphyChem. Trifluoromethanesulfonic acid (triflic acid, >98 %) was from TCI Chemicals. Absolute ethanol was from VWR chemicals and *N*,*N*-dimethylformamide (DMF, >99 %) from Fischer Chemicals. Reagents were used as received without further purification.

2.2. Synthesis of (Hf)PCN-224(Co)

(Hf)PCN-224(Co) was synthesized according to our previously described microwave-assisted protocol [18]. Briefly, a preliminary metalation step was performed by mixing the ligand TCPP (192.4 mg, 0.24 mmol), anhydrous $CoCl_2$ (165.4 mg, 1.27 mmol) and 6 mL DMF in a 30 mL microwave glass vial and heated under predefined conditions (175 °C, 10 min, 600 rpm, 0.7 bar, 20 W) to give solution A. The cluster solution (B) was prepared in parallel, by mixing $HfOCl_2{\cdot}8H_2O$ (523.0 mg, 1.28 mmol) and benzoic acid (5.04 g, 41.27 mmol) in 6 mL. After dissolution, the mixture was heated in the microwave reactor (140 °C, 5 min, 600 rpm, 0.5 bar, <5 W). B was poured on A under continuous stirring, and then triflic acid was added to the reactor (0.6 mL, 6.77 mmol). MOF was obtained after heating the overall pre-polymerization mixture (150 °C, 30 min, 600 rpm, 3.6 bar, 10 W). The polymer was separated from the mother liquors by centrifuging (10000 rpm, 10 min) and then washed with DMF (2×30 mL) and absolute ethanol (3×30 mL). Finally, the resulting solid was dried under vacuum (100 °C, 12 h). (Hf)PCN-224(Co) ($C_{144}H_{72}N_{12}Co_3O_{64}Hf_{12}$; ICP-OES & CHNS elem. anal.: calc. 32.5 % C; 3.2 % N; 3.3 % Co; 40.3 % Hf. Exp.: 34.5 % C; 3.4 % N; 3.3 % Co; 39.7 % Hf) 275 mg, 51 % yield.

2.3. Characterization

Further details related to instrumental techniques are presented in supplementary material.

2.4. SO_2 capture and chemical stability after SO_2 exposure

SO_2 adsorption–desorption isotherm was obtained by using a Dynamic Gravimetric Gas/Vapor Sorption Analyzer, DVS vacuum (Surface Measurement Systems Ltd), and this isotherm was performed from 0 to 1 bar at 298 K on an activated sample (453 K for 12 h under 1.4×10^{-3} torr) of (Hf)PCN-224(Co). For chemical stability, crystallinity retention was used as parameter after the exposure to SO_2

2.5. Electronic features and SO_2 detection/sensing

For detection and sensing, materials' activation was carried out by heating (Hf)PCN-224(Co) at 120 °C for 2 h under vacuum conditions. The exposure to SO_2 was carried out in our homemade *ex-situ* adsorption system (Fig. S1) for UV–Vis and solid-state photoluminescent spectroscopy.

UV–Vis absorption measurements were performed from 200 to 800 nm using a Shimadzu spectrophotometer UV-2600 equipped with an ISR-2600Plus integrating sphere and a $BaSO_4$ blank.

Fluorescence spectra were collected on a FS5 Edinburgh Instruments Spectrofluorometer using a continuous wave 150 W ozone-free xenon arc lamp at room temperature, coupled with the SC-10 Solid-state and SC-05 Standard Cuvette sample holder. The solid-state samples were packed into quartz sample holders and positioned into the instrument. For solution-state experiments 5 mg of (Hf)PCN-224(Co) were dispersed in 10 mL of THF. For LOD calculation, different titrations were made using SO_2 THF solution (0.5 M), and measured immediately after SO_2 solution addition, using quartz cuvettes. All spectra were acquired at ambient conditions (around 27 °C). Emission measurements were carried out using an excitation wavelength of 360 nm, with a LP-395 filter on the detector side to remove any remaining light from the excitation source. Emission spectra were collected with a step size of 1 nm and a dwell time of 0.1 s. The excitation bandwidth was set at 2.00 nm, and the emission bandwidth for the detector at 1.00 nm.

Time-resolved photoluminescence (TRPL) spectra were measured in an Edinburgh Instruments FS5 Spectrofluorometer using a 375 nm laser, with an excitation bandwidth of 0.01 nm and an emission bandwidth of 1 nm, at an emission wavelength of 450 nm.

2.6. Computational details

DFT calculations were performed at the B3LYP/LANL2DZ level of theory [19,20] using the Gaussian 09 software [21]. To confirm that the optimized geometries correspond to local minima, a frequency calculation was conducted to ensure the absence of imaginary frequencies. To study the stability of the interaction with the SO_2 molecule, the adsorption energies were calculated. Therefore, the contributions of the Gibbs free energies are considered in the following equation:

$$\Delta G_{ad} = G_{interaction} - [G_{SO2} + G_{cluster}] \quad (1)$$

where $G_{interaction}$ is the Gibbs free energy of the formed system, the interaction between SO_2 molecule (G_{SO2}) and cluster proposed, and the different cluster proposed ($G_{cluster}$). To investigate the electronic structure of these systems. For the lowest configuration, the natural charges and electron configurations were determined using the natural bond orbital (NBO) method [20]. To further examine the interaction between the SO_2 molecule and clusters, we analyzed the frontier molecular orbitals, including the highest occupied molecular orbital (HOMO) and the lowest unoccupied molecular orbital (LUMO) (isosurfaces of 0.02 a.u.), as well as the density of states (DOS), using the MultiWFN 3.6

computational package [22].

3. Results and discussion

3.1. Characterization

(Hf)PCN-224(Co) was synthesized *via* microwave-assisted solvothermal method, showing great advantages over other approaches such as higher efficiency, faster reaction time, and lower cost, among others [23]. Powder X-ray diffraction (PXRD) confirmed the cubic symmetry and the crystalline phase purity of (Hf)PCN-224(Co) (Fig. S2) [18,24], while the typical cubic morphology was revealed in the scanning electron micrographs (Fig. S3). Remarkably, high resolution SEM showed the truncated edges phenomenon related to the crystal growth in the presence of a large excess of modulator under microwave radiation, as previously described [25]. Later, a sample of (Hf)PCN-224(Co) was outgassed at 453 K for 12 h under vacuum (1.4×10^{-3} torr), to run a N_2 isotherm at 77 K (Fig. S4) which was used to estimate the total surface area, *i.e.*, BET (Brunauer-Emmett-Teller) surface area of 2380 ± 50 $m^2\ g^{-1}$ with a pore size of 18.0 Å (Horvath-Kawazoe method considering a spherical pore geometry) and a pore volume of 1.24 $cm^3\ g^{-1}$. Thermogravimetric analysis (TGA) and temperature-dependent PXRD for (Hf)PCN-224(Co), depicted in Fig. S5, indicate that this MOF collapsed at around 450 °C. By far, this is the highest thermal stability observed for porphyrin MOFs and comparable to that of the most stable well-known MOFs [26]. Chemical stability in aqueous media was demonstrated in a wide range of pH values (1-12) upon analyzing linker releasing by UV–Vis spectroscopy (see SI). Note that typical effluent outlets of processes involving SO_2 are released with a 30–35 % relative humidity at similar temperatures [27]. These aspects, together with the already demonstrated high affinity of cobalt towards CO_2 [18], suggested the potential use of (Hf)PCN-224(Co) as a promising candidate in SO_2 detection. Considering the large amount of defects found in (Hf)PCN-224(Co) determined by elemental analysis and TGA (see SI), typically found in materials synthesized under microwave radiation [28], it is expected an enhanced diffusion of gases throughout the MOF matrix and an increased availability of coordinatively unsaturated sites around structural metals, with a potential impact in SO_2 fixation.

3.2. SO_2 capture and chemical stability after SO_2 exposure

Fig. 2 shows the resulting isotherm obtained with a relatively fast SO_2 uptake from 0 to 0.05 bar of approximately 0.7 mmol g^{-1}. From 0.05 to 0.7 bar, the SO_2 adsorption isotherm exhibited an almost linear uptake with a total SO_2 amount of ≈3.5 mmol g^{-1}. Finally, a change on the shape of the isotherm is clearly observed, accounting for an almost plateau, leading to a total capacity (at 1 bar) of 4.0 mmol g^{-1}. The total SO_2 capture capacity of (Hf)PCN-224(Co) is considerably lower to representative chemically stable MOFs for SO_2 capture with similar BET surface areas (*e.g.* MIL-101(Cr)_4F) [7]. Thus, the structural stability following SO_2 adsorption/desorption was assessed by PXRD (see Fig. S8), showing that the crystal structure of (Hf)PCN-224(Co) was not retained.

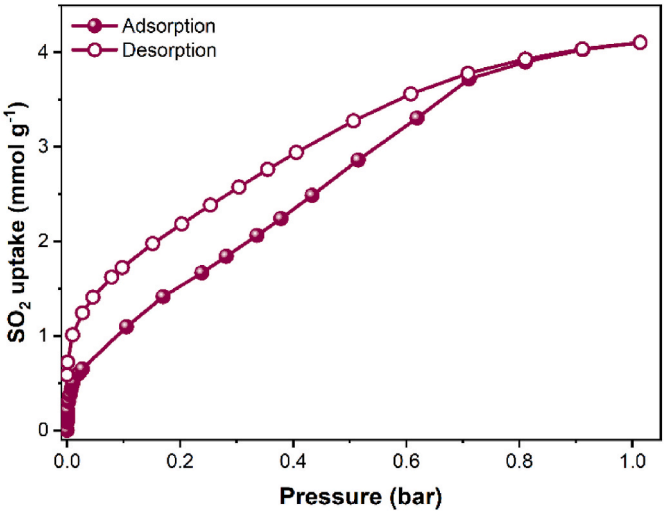


Fig. 2. SO_2 adsorption-desorption isotherm at 298 K up to 1 bar for activated (Hf)PCN-224(Co).

Although this result corroborated the structural instability of (Hf)PCN-224(Co) upon exposure to a high concentration of SO_2 (*i.e.*, 1 bar), the most meaningful property of a MOF toward SO_2 detection is a high response to SO_2 at low concentrations since the sensing of SO_2 is commonly carried out at the ppm level [29]. Thus, the total SO_2 uptake at ambient pressure (1 bar = high concentration of SO_2) turn out to be irrelevant since, for example, flue gas exhibits SO_2 typical concentrations up to 10,000 ppm [30]. Thus, with this rationalizing in mind and considering that concentration ranges for SO_2 detection are at the ppm level, such ppm levels can be inherently correlated to the SO_2 low-pressure range (*e.g.*, from 0 to 0.1 bar). We decided to test the structure stability of an activated sample of (Hf)PCN-224(Co) which was only exposed to 0.1 bar of SO_2. PXRD patterns confirmed the retention of the crystalline structure (Fig. S9) after the SO_2 sorption experiment up to 0.1 bar. Therefore, to further corroborate the crystalline retention of (Hf)PCN-224(Co) towards SO_2 at relatively low concentrations, 5 adsorption-desorption isotherms were conducted from 0 to 0.1 bar, using a fresh sample, where the total SO_2 uptake remains practically the same in the 5 cycles (around 1.2 mmol g^{-1}), see Fig. S10. Additionally, PXRD pattern reveals that (Hf)PCN-224(Co) show partial amorphization as well as small shifts to higher angles, compared to the as-synthesized material, suggesting small changes in cell parameters, see Fig. S11. Hence, since SO_2 capture is similar for all cycles and PXRD patterns are essentially retained, it is possible to establish that (Hf)PCN-224(Co) is stable towards SO_2 at low concentrations.

3.3. Electronic features and SO_2 detection/sensing

Once it was established that the SO_2 adsorption up to 0.1 bar did not affect the crystalline structure of (Hf)PCN-224(Co), we decided to evaluate its use as a fluorescent SO_2 detector. As a first approach to understand the electronic features of (Hf)PCN-224(Co), UV–Vis spectra of an activated and an exposed to SO_2 at 0.1 bar samples were acquired (Fig. 3a). According to Fig. 3a–(Hf)PCN-224(Co) shows broad absorption bands in the full UV–Vis range, as previously reported for porphyrin-based MOFs [31]. This feature is the result of the conjugated π-bonds in TCPP linker. Thus, electronic transitions might arise mainly due to π→π* transitions. In addition, two regions, from 360 to 410 and from 440 to 650 nm, are highlighted: the former is called the Soret band (or B band) ($S_0 \rightarrow S_2$ transitions) and the second region is named the Q band ($S_0 \rightarrow S_1$ transitions) [32]. According to Gouterman's four orbital model (Fig. 3b), absorption bands in free-base porphyrins appear due to transition from the highest occupied molecular orbitals (HOMO) to the lowest unoccupied molecular orbitals (LUMO) (Fig. 3c). The HOMO orbitals are a_{1u} and a_{2u}, and the LUMO orbitals are e_{gx} and e_{gy} [33]. The presence of Co^{2+} coordinated to nitrogen increases the ring symmetry, from D_{2h} in metal-free porphyrin to D_{4h} in metalated-porphyrin. Consequently, only two bands are observed for (Hf)PCN-224(Co) in the Q band region [32]. Since in solid-state spectroscopy samples are measured in high concentrations, extra precautions should be taken because additional transitions could be neglected, aspect of particular relevance in the case of (Hf)PCN-224(Co), which is a dark powdered material. Furthermore, porphyrin-based MOFs usually show other electronic phenomena, *e.g.*, ligand to metal charge transfer (LMCT) [34] or Förster resonance energy transfer (FRET) [35], which can also be neglected in the solid-state UV–Vis spectra. Fig. 3a shows that

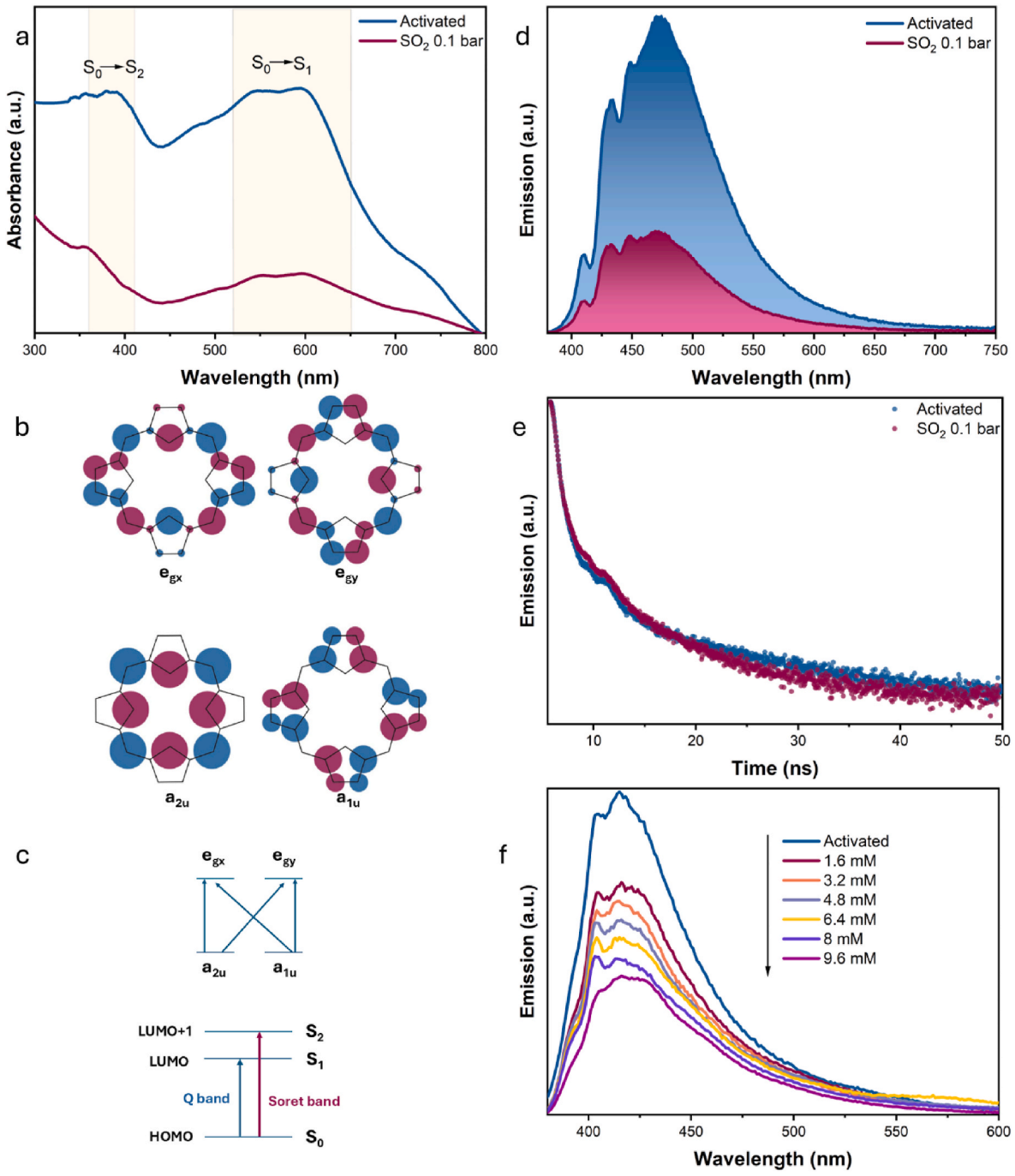


Fig. 3. a) Solid-state UV–Vis spectra of activated and exposed (Hf)PCN-224(Co) to SO_2 at 0.1 bar. Regions for transitions from ground singlet state (S_0) to first (S_1) and second singlet excited state (S_2) are highlighted. b) Gouterman's HOMO (a_{2u} and a_{1u}) and LUMO (e_{gx} and e_{gy}) frontier molecular orbitals for free-base porphyrins. c) Electronic transitions between HOMO and LUMO frontier orbitals, as well as Q and Soret bands transitions. d) Fluorescence emission spectra of activated and SO_2 exposed samples. e) Solid-state lifetime of activated and SO_2 exposed samples. f) Solution-state emission spectrum of (Hf)PCN-224(Co) titrated with SO_2 solution.

absorption intensity decreases for SO_2 exposed sample and, although this decrease is very clear, the spectrum profile practically does not get modified. This outcome indicates that SO_2 molecules interact electronically with the material, limiting the absorption process.

The excitation spectra maximum was found at 360 nm (Fig. S12). Thus, recording every emission spectrum at λ_{exc}= 360 nm gives the maximum emission intensities for all radiative relaxation-transitions. A broad emission spectrum from the activated material, from 380 to 650 nm (Fig. 3d), was obtained with a maximum emission at λ_{em}= 475 nm, which is similar to previously reported Zr-based PCN-224 MOF [34]. No emission bands around 600–800 nm (Q-bands-related emission, $S_1 \rightarrow S_0$) are observed, which can be attributed to the coordination of Co^{2+} to TCPP linker [36]. Thus, the maximum emission wavelength (475 nm) and the absence of emission from Q-bands might suggest that emission appears purely from LMCT process between oxygen from TCPP and Hf^{4+} cations, where LMCT emission for (Zr)PCN-224 has previously reported [34]. Due to the lower electronegativity of Hf(IV) in comparison to Zr (IV), an enhanced molecular orbital overlap would appear for Hf-O coordination bonds, and, as consequence, an enhancement of LMCT transition might arise [37].

For solid-state SO_2 detection purposes, another activated sample of (Hf)PCN-224(Co) was exposed to 0.1 bar of SO_2 to measure its photoluminescence properties. As it can be observed, a clear change in the fluorescent intensity was recorded (49.7 % decrease) after SO_2 exposure (Fig. 3d). This turn-off effect is associated to the changes in the electronic structure of (Hf)PCN-224(Co), in good correlation with the UV–Vis spectrum, *vide infra*.

Finally, the effect of saturation with CO_2 and water vapor on the fluorescence of (Hf)PCN-224(Co) was tested in the solid-state to compare it with the effect of SO_2 (Fig. S13). Notice that, although both molecules generate changes in fluorescence, these are different from that generated by SO_2. To begin with, the fluorescence generated by saturation with water is comparable, almost identical to the fluorescence of the material synthesized before activation. It is hypothesized that the marked difference between the intensities and shapes of the emission spectra of the material before and after activation is due to the loss of ethanol molecules, coming from the solvent used for the synthesis, coordinated to the Co(II) centers and which, subsequently, after activation ended up unsaturated. Alternatively, it would be expected that upon exposure of the activated material to water vapor, these molecules replace the coordinated ethanol molecules, to the Co(II) metal centers. The reason for the weak fluorescence emission in both cases can be related to the hydrogen bonds that may be occurring between the respective Co(II)-coordinated molecules, since it has been reported in the literature that there may be hydrogen-bond-assisted non-radiative deactivation of fluorescence [38]. On the other hand, the effect on the fluorescence generated by CO_2 is similar to that of SO_2 in terms of shape and intensity of the spectrum, which can be related to the fact that SO_2 and CO_2 do not generate hydrogen bonds with each other and also prefer to interact with Hf(IV) since this metal shows a much higher Lewis acid character than Co(II). Since clear different responses were shown after the exposure to different gases, it is expected that no important interferences would appear in real-life applications.

Lifetime measurements for the (Hf)PCN-224(Co) before and after exposition to SO_2 0.1 bar are shown in Fig. 3c. A slight decrease in lifetime was found from 1.8138 ns for the activated material to 1.3984 ns for (Hf)PCN-224(Co) exposed to SO_2 at 0.1 (Table S2), demonstrating that the fluorescence quenching is not driven by dynamic mechanisms but by static ones.

LOD was accomplished by solution-state experiments in THF (Fig. 3d). Evidently, a quenching phenomenon, as function of concentration, is observed. Interestingly, the first emission intensity decreases just at 1.6 mM (102.5 ppm) and continues up to 9.6 mM (615.0 ppm), indicating that (Hf)PCN-224(Co) can be used quantitatively for SO_2 sensing in the ppm range. Moreover, blank standard deviation is of only 2.94 %, evidencing the high reliability of the (Hf)PCN-224(Co) as sensing probe (Fig. S14). Finally, the LOD was estimated as relatively low as 175.5 ppm (Fig. S15), making (Hf)PCN-224(Co) competitive to other MOFs previously reported, see Table S3. Specifically, MOFs previously reported to be used as probes to detect SO_2, sense in ppm concentration range, as in the case of (Hf)PCN-224(Co). Additionally, some MOFs have not been analyzed to demonstrate chemical stability towards SO_2. Furthermore, some measurements are made using SO_3^{2-}, and HSO_3^-, instead of SO_2, and their selectivity tests are made again other ionic species instead of other gases that could be present in real-life situations, in contrast to (Hf)PCN-244(Co).

3.4. Interaction of (Hf)PCN-224(Co) with SO_2 and suggested sensing mechanism

To elucidate the interaction mechanism of SO_2 with (Hf)PCN-224 (Co), X-ray photoelectron spectrum (XPS) was carried out. Thus, an activated and an exposed to SO_2 at 0.1 bar samples were measured by XPS. The survey spectra (Fig. S16) shows that sulfur species are present after SO_2 exposure, which indicates the reliability of using this technique to study the electronic interactions of SO_2 with the atoms within the material framework. As previously discussed, emission phenomenon can be related to LMCT transitions between oxygen and hafnium. Additionally, SO_2 is expected to electronically interact with Co(II), and may even coordinate to it, since Co(II) coordinated to pyrrole rings of the TCPP linker displays a quasi-square planar geometry [39]. This coordination environment leaves available orbitals, allowing further ligand binding. Additionally, coordination of the guest molecules to metalated porphyrin-based MOFs is a well-known phenomenon, *e.g.*, in catalytic processes [40]. Thus, the high-resolution spectra of Hf 4f and Co 2p of both samples were fitted and compared, see Fig. 4a and b. The narrow Hf 4f spectrum of the activated sample exhibits two main peaks at 17.5 and 19.2 eV, assigned to Hf $4f_{7/2}$ and $Hf_{5/2}$ [41]. For (Hf)PCN-224(Co) exposed to SO_2, a clear binding energy shift is observed, indicating a change in the electron density around Hf(IV) [42]. This result suggests a strong interaction between SO_2 molecules and Hf(IV). For the Co 2p, the high-resolution spectrum shows significantly split spin-orbit components at 780.5 and 795.7 eV, corresponding to Co $2p_{5/2}$ and Co $2p_{3/2}$, respectively [36,43]. The presence of Co(II) is evidenced by observable satellite features around 787 and 804 eV [44], and after SO_2 exposure, (Hf)PCN-224(Co) Co 2p spectrum shifts 0.1 and 0.2 eV. Although only a small binding energy shift is observed, clear profile changes are observed in the whole spectrum. Furthermore, previous theoretical studies evidenced the interaction of SO_2 molecules with Co (II) centers in porphyrin rings [45]. Thus, both results suggest interaction of the SO_2 molecules with Hf(IV) and Co(II) metals. Regarding Hf (IV), the secondary building unit (SBU) of (Hf)PCN-224(Co) comprises $Hf_6(OH)_8$ clusters, which are coordinated to six TCPP(Co) linkers (Fig. 4c). It is known that PCN-224 materials, porphyrin-based MOFs, as well as M(IV)-based MOFs, often exhibit crystallographic defects, *i.e.*, missing linkers, which can provide open metal sites as Hf(IV) centers [46–49]. Furthermore, microwave-assisted synthesis enhances the accessibility of open metal sites in the form of missing linkers [28]. Herein, we propose that Hf(IV) open metal sites, which work as a Lewis base, are able to coordinate SO_2 molecules (Fig. 4d). Indeed, SO_2 coordination limits LMCT between oxygen and hafnium, since orbitals of Hf (IV) are more occupied after SO_2 coordination. The restricted orbitals lead to less excited species and, consequently, to less emission intensity, as seen in Fig. 3a and e.

3.5. DFT calculations

In order to evaluate the affinity of the metal center of the (Hf)PCN-224(Co) to adsorb the SO_2 molecule from the atomistic point of view, DFT-based calculations were carried out to corroborate the influence of these metallic centers (Hf and Co). Here, from the crystallographic archive [18], two characteristic molecular fragments of the MOF were identified: the first consists of an Hf cluster containing six transition metal atoms, and the second is a Co porphyrin. Based on these models, two clusters were proposed to represent the reactive site for SO_2 adsorption. The selection of structures is represented in Fig. 5a. From this structure, two molecular fragments called cluster 1 (PCN(Co)) and 2 ((Hf)PCN) are used, as shown in Fig. 5b and (c), respectively. Both structures are optimized at B3LP/LANL2DZ level of theory. For the PCN (Co) structure, it can be observed that the structural parameter between the N and Co atoms is 1.99 Å, which corroborates the signals identified from Co with the pyridine rings in the structure. In the case of (Hf)PCN, the formation of the Hf_6 cluster exhibits two distinct binding parameters: one corresponding to the O atoms of the pendant molecular benzene fragments (2.11 Å) and the other to the Hf-O bonds that form the cluster (2.05 Å) as shown in Fig. 5c. It is worth noting that the PCN(Co) and (Hf)PCN structures exhibit symmetry groups of D_4 and D_{3d}, respectively. Based on optimized geometries, the interaction of the SO_2 molecule with the metal centers (Co and Hf) was analyzed to determine the optimal adsorption site with good affinity within the MOF. Table S4 presents the adsorption energy values (ΔG_{ad}) for the SO_2/PCN(Co) and SO_2/(Hf)PCN configurations. According to the negative values ΔG_{ad} of

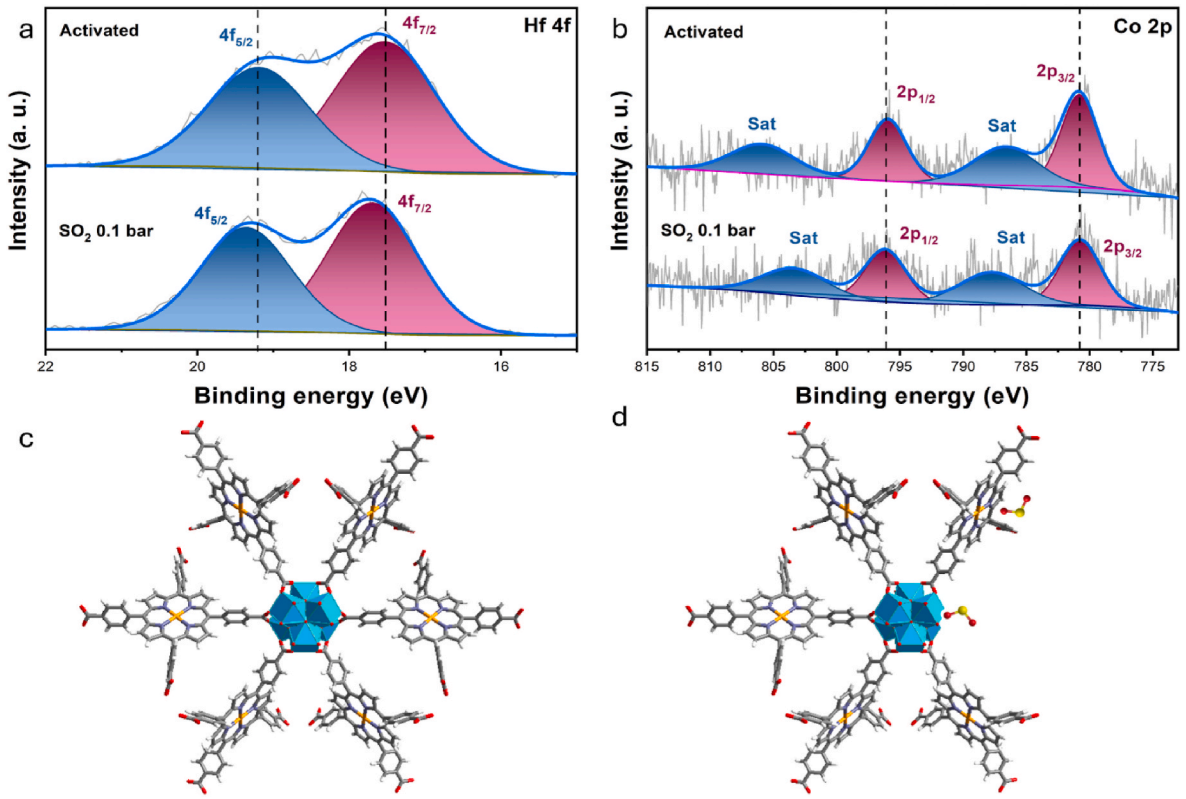


Fig. 4. a) High-resolution XPS spectra of Hf 4f. b) High-resolution XPS spectra of Co 2p. c) SBU coordinated to six TCPP(Co) linkers. d) Missing linker defect in (Hf)PCN-224(Co), as well as schematic representation of possible interaction/coordination of SO_2 with Hf(IV) and Co(II). Color code: C=gray, O=red, N=purple, Hf=blue, Co=orange, S= yellow and H=white. (For interpretation of the references to colour in this figure legend, the reader is referred to the Web version of this article).

the adsorption energies, it can be seen that the interaction of the SO_2 molecule with the MOF has an exergonic character for both cases. However, it is possible to see that the interaction on the (Hf)PCN cluster has a greater covalent attraction compared to that of the PCN(Co) system. This behavior may be due to the fact that the SO_2 molecule undergoes an elongation in the bonding length (S-O), this can be observed in Fig. 5(d–e). In addition, the interaction distance between the oxygen atom and the metal center is shorter for the O-Hf (1.88 Å) case than for the O-Co (1.91 Å) porphyrin system, hence, corroborating the XPS results.

To understand the electronic effect on the absorption of the SO_2 molecule in the study clusters, an NBO analysis was carried out on the metal centers of each interaction. Table S5 shows the natural configuration of the metallic centers before and after SO_2 adsorption. Here, a decrease in the charge population can be seen during the adsorption of SO_2, with the atomic orbitals 3*d*4*p* and 5*d*6*p* affected for Co and Hf, respectively. The charge transfer at the metal centers is relatively similar in both cases, mainly influenced by the 3*d* and 5*d* atomic orbitals, which enhance interaction with the 2*p* orbitals of the oxygen atoms. To assess the efficiency of this interaction between the SO_2 molecule and the metal centers, an electron localization function (ELF) analysis was performed on the interaction plane. Fig. 6 presents the 2D ELF maps over the metal centers and the oxygen atom of the SO_2 molecule. The ELF describes the efficiency of Pauli repulsion at a given point in real molecular space [50]. Fig. 6b, depicting the interaction of the SO_2/(Hf) PCN system, favors a greater electronic localization between the O-Hf bond (green regions), compared to the O-Co interaction where blue regions can be seen between the cluster and the SO_2 molecule (see Fig. 6a). This behavior corroborates the high adsorption energy value (−5.86 eV) reported for the SO_2/(Hf)PCN system. Finally, the contribution of the frontier molecular orbitals (FMOs) formed is analyzed from the PDOS diagrams as shown in Fig. S17. For the SO_2/PCN(Co) system, the formation of a wide energy gap between the HOMO-LUMO levels (1.95 eV) can be observed. Here, the HOMO and LUMO contribution is majority by the PCN(Co) cluster. In the case of the SO_2/(Hf)PCN system, it presents a small HOMO-LUMO energy gap (0.79 eV). It is worth noting that the HOMO contributions come from the SO_2 molecule, while the LUMO is very well localized in the (Hf)PCN cluster. This behavior suggests that the MOF ultimately exhibits a charge-accepting character during SO_2 adsorption. However, the elongation of SO_2 bonds in the SO_2/(Hf)PCN system suggests potential catalytic activity at this site within the MOF structure. As it can be seen, SO_2 interacts strongly electronically with Hf (IV), which leads to reduce the LMCT transitions between oxygen from TCPP linkers and Hf(IV), since Hf(IV) orbitals are already occupied by SO_2 molecules, thus confirming the proposed sensing mechanism in section 3.4. Additionally, since we expect the presence of open metal sites in $Hf_6(OH)_8$ clusters, SO_2 might coordinate "easier" to Hf(IV) centers, compared (Hf)PCN-224(Co) without defects, *i.e.*, without open metal sites, conducting to an even more restricted LMCT emission.

4. Conclusions

To summarize, we report the first experimental investigation on the detection and sensing of SO_2 on a porphyrin-based MOF, the microporous hafnium cobalt-porphyrin tetracarboxylate (Hf)PCN-224(Co). While the SO_2 uptake of 4.00 mmol g^{-1} (298 K and 1 bar) does not rival the other leading MOFs, and (Hf)PCN-224(Co) is structurally unstable at high pressures (1 bar), (Hf)PCN-224(Co) shows crystalline retention at low concentrations typically found for detection purposes (0.1 bar). Interestingly, using Hf^{4+} as MOF constitutive metal and the microwave-assisted solvothermal synthesis lead to Hf(IV) open metal sites in the resulting MOF, due to the intrinsic formation of defects, which is the key

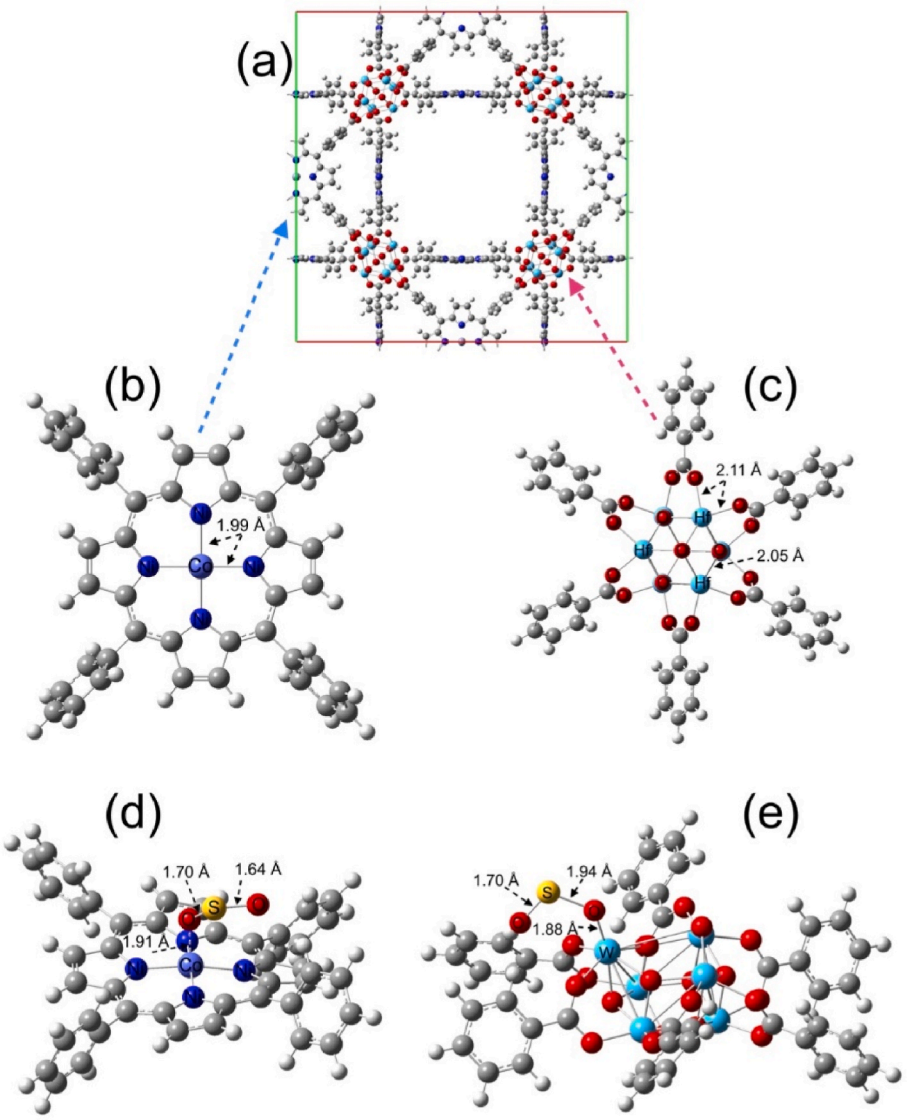


Fig. 5. Geometry optimization of molecular configurations provide the (a) (Hf)PCN-224(Co) structure (b) PCN(Co) and (c) (Hf)PCN show the molecular structure derived from the metallic centers of Hf and Co, respectively. (d) SO_2/PCN(Co), and (e) SO_2/(Hf)PCN geometry configuration of the SO_2 molecule adsorbed on the Co and Hf systems, respectively.

for the efficient detection and sensing of SO_2 at ppm-level (limit of detection = 175.5 ppm), providing a promising practical SO_2 sensor. Additionally, when compared the SO_2 emission spectra to emission spectra of CO_2 and water vapor, clear differences are observed, indicating the good selectivity of (Hf)PCN-224(Co). Furthermore, DFT calculations indicate the strong adsorption of the SO_2 molecule on the metal centers of the MOF, exhibiting a stronger affinity (ΔG_{ad}=-5.86 eV) for the Hf cluster. Finally, we believe that the implementation of porphyrin-based materials in sensor and catalytic devices due to their relevant photoelectronic features will compensate the production cost in the large scale of both starting materials and final products in the near future, as observed in the case of terephthalate-based MOFs.

CRediT authorship contribution statement

Sergio Carrasco: Writing – original draft, Investigation, Data curation. **Marco L. Martínez:** Writing – original draft, Investigation, Data curation. **Yoarhy A. Amador-Sánchez:** Writing – original draft, Methodology, Investigation, Data curation. **Valeria B. López Cervantes:** Investigation, Data curation. **Elí Sánchez-González:** Methodology, Investigation, Formal analysis, Data curation. **Nora S. Portillo-Vélez:** Validation, Data curation. **Ricardo A. Peralta:** Validation, Supervision, Investigation, Formal analysis. **Christian A. Celaya:** Data curation, Investigation, Software, Writing – review & editing. **Ariel Guzmán-Vargas:** Resources, Project administration. **Patricia Horcajada:** Writing – review & editing, Writing – original draft, Resources, Formal analysis, Conceptualization. **Diego Solis-Ibarra:** Writing – review & editing, Writing – original draft, Supervision, Conceptualization. **Ilich A. Ibarra:** Writing – review & editing, Writing – original draft, Funding acquisition, Conceptualization.

Funding sources

I.A.I. PAPIIT UNAM (IN201123), México, for financial support.

S. C. and P.H. “NAPOLION” (PID2022-139956OB-I00) and "H2-MOF" (TED2021-132092B-C21), MCIN/AEI/10.13039/501100011033, ERDF, A way of making Europe, and European Union NextGenerationEU/PRTR.

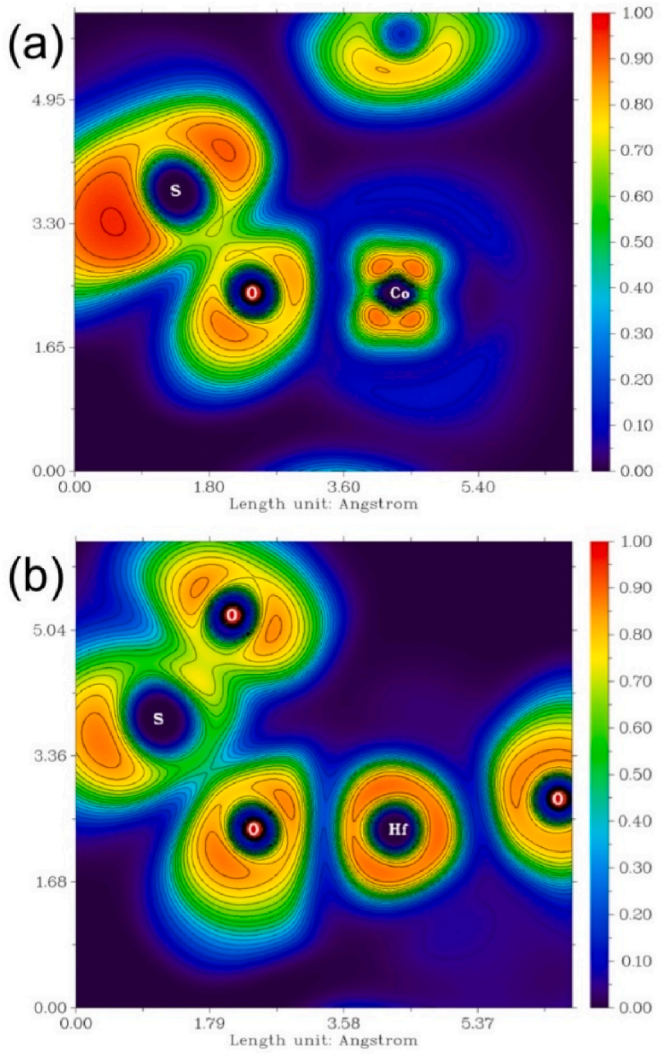


Fig. 6. Electron localization function (ELF) for the systems under study: (a) SO_2/PCN(Co) and (b) SO_2/(Hf)PCN systems. The ELF values range from 0.0 to 1.0, with 1 (red) indicating complete localization, and 0 (blue) corresponding to the absence of electron distribution. (For interpretation of the references to colour in this figure legend, the reader is referred to the Web version of this article).

Declaration of competing interest

The authors declare the following financial interests/personal relationships which may be considered as potential competing interests: Ilich A. Ibarra reports financial support was provided by UNAM. If there are other authors, they declare that they have no known competing financial interests or personal relationships that could have appeared to influence the work reported in this paper.

Acknowledgment

M.LM., and V.B.LC. thank CONAHCYT for the Ph.D. fellowships (1080048 and 1005649). M.L.M thanks M.S.L for her valuable help on artistic consultation. I.A.I. thanks PAPIIT UNAM (IN201123), México, for financial support. We thank U. Winnberg (Euro Health) for scientific discussions and G. Ibarra-Winnberg for scientific encouragement. S. C. and P.H. acknowledge "NAPOLION" (PID2022-139956OB-I00) and "H2-MOF" (TED2021-132092B-C21) projects funded by MCIN/AEI/10.13039/501100011033, ERDF, A way of making Europe, and European Union NextGenerationEU/PRTR. C.A.C. want to acknowledge SECIHTI-México for the postdoctoral fellowship.

Appendix. ASupplementary data

Supplementary data to this article can be found online at https://doi.org/10.1016/j.mtadv.2025.100579.

Data availability

Data will be made available on request.

References

[1] E. Martínez-Ahumada, M.L. Díaz-Ramírez, M. de J. Velásquez-Hernández, V. Jancik, I.A. Ibarra, Capture of toxic gases in MOFs: SO2, H2S, NH3and NOx, Chem. Sci. 12 (2021) 6772–6799, https://doi.org/10.1039/d1sc01609a.
[2] E. Martínez-Ahumada, A. López-Olvera, V. Jancik, J.E. Sánchez-Bautista, E. González-Zamora, V. Martis, D.R. Williams, I.A. Ibarra, MOF materials for the capture of highly toxic H2S and SO2, Organometallics 39 (2020) 883–915, https://doi.org/10.1021/acs.organomet.9b00735.
[3] P. Brandt, A. Nuhnen, M. Lange, J. Möllmer, O. Weingart, C. Janiak, Metal-organic frameworks with potential application for SO2 separation and flue gas desulfurization, ACS Appl. Mater. Interfaces 11 (2019) 17350–17358, https://doi.org/10.1021/acsami.9b00029.
[4] A. López-Olvera, J.A. Zárate, E. Martínez-Ahumada, D. Fan, M.L. Díaz-Ramírez, P. A. Sáenz-Cavazos, V. Martis, D.R. Williams, E. Sánchez-González, G. Maurin, I. A. Ibarra, SO2Capture by two aluminum-based MOFs: rigid-like MIL-53(Al)-TDC versus breathing MIL-53(Al)-BDC, ACS Appl. Mater. Interfaces 13 (2021) 39363–39370, https://doi.org/10.1021/acsami.1c09944.
[5] Z. Meng, Y. Liu, D. Wu, Effect of sulfur dioxide inhalation on cytokine levels in lungs and serum of mice, Inhal. Toxicol. 17 (2005) 303–307, https://doi.org/10.1080/08958370590922625.
[6] E. Martínez-Ahumada, D. won Kim, M. Wahiduzzaman, P. Carmona-Monroy, A. López-Olvera, D.R. Williams, V. Martis, H.A. Lara-García, S. López-Morales, D. Solis-Ibarra, G. Maurin, I.A. Ibarra, C.S. Hong, Capture and detection of SO2 using a chemically stable Mg(ii)-MOF, J. Mater. Chem. A Mater. 10 (2022) 18636–18643, https://doi.org/10.1039/d2ta04842f.
[7] E. Martínez-Ahumada, M.L. Díaz-Ramírez, H.A. Lara-García, D.R. Williams, V. Martis, V. Jancik, V. Jancik, E. Lima, I.A. Ibarra, High and reversible SO2capture by a chemically stable Cr(iii)-based MOF, J. Mater. Chem. A Mater. 8 (2020) 11515–11520, https://doi.org/10.1039/c9ta13524c.
[8] P. Orellano, J. Reynoso, N. Quaranta, Short-term exposure to sulphur dioxide (SO2) and all-cause and respiratory mortality: a systematic review and meta-analysis, Environ. Int. 150 (2021), https://doi.org/10.1016/j.envint.2021.106434.
[9] S. Nazari, O. Shahhoseini, A. Sohrabi-Kashani, S. Davari, R. Paydar, Z. Delavar-Moghadam, Experimental determination and analysis of CO2, SO2 and NOx emission factors in Iran's thermal power plants, Energy 35 (2010) 2992–2998, https://doi.org/10.1016/j.energy.2010.03.035.
[10] Y. Cheng, S. Wang, J. Zhu, Y. Guo, R. Zhang, Y. Liu, Y. Zhang, Q. Yu, W. Ma, B. Zhou, Surveillance of SO2 and NO2 from ship emissions by MAX-DOAS measurements and the implications regarding fuel sulfur content compliance, Atmos. Chem. Phys. 19 (2019) 13611–13626, https://doi.org/10.5194/acp-19-13611-2019.
[11] M. Speidel, R. Nau, F. Arnold, H. Schlager, A. Stohl, Sulfur dioxide measurements in the lower, middle and upper troposphere: deployment of an aircraft-based chemical ionization mass spectrometer with permanent in-flight calibration, Atmos. Environ. 41 (2007) 2427–2437, https://doi.org/10.1016/j.atmosenv.2006.07.047.
[12] H. Okabe, P.L. Splitstone, J.J. Ball, Ambient and source SO2 detector based on a fluorescence method, J. Air Pollut. Control Assoc. 23 (1973) 514–516, https://doi.org/10.1080/00022470.1973.10469797.
[13] V. Chernikova, O. Yassine, O. Shekhah, M. Eddaoudi, K.N. Salama, Highly sensitive and selective SO2 MOF sensor: the integration of MFM-300 MOF as a sensitive layer on a capacitive interdigitated electrode, J. Mater. Chem. A Mater. 6 (2018) 5550–5554, https://doi.org/10.1039/c7ta10538j.
[14] M. Wang, L. Guo, D. Cao, Amino-functionalized luminescent metal-organic framework test paper for rapid and selective sensing of SO2 gas and its derivatives by luminescence turn-on effect, Anal. Chem. 90 (2018) 3608–3614, https://doi.org/10.1021/acs.analchem.8b00146.
[15] P. Gao, S. Mukherjee, M. Zahid Hussain, S. Ye, X. Wang, W. Li, R. Cao, M. Elsner, R. A. Fischer, Porphyrin-based MOFs for sensing environmental pollutants, Chem. Eng. J. 492 (2024), https://doi.org/10.1016/j.cej.2024.152377.
[16] R. Dhir, M. Kaur, A.K. Malik, Porphyrin metal-organic framework sensors for chemical and biological sensing, J. Fluoresc. (2024), https://doi.org/10.1007/s10895-024-03674-0.
[17] S. Mondal, T. Pain, K. Sahu, S. Kar, Large-scale green synthesis of porphyrins, ACS Omega 6 (2021) 22922–22936, https://doi.org/10.1021/acsomega.1c03534.
[18] S. Carrasco, G. Orcajo, F. Martínez, I. Imaz, S. Kavak, D. Arenas-Esteban, D. Maspoch, S. Bals, G. Calleja, P. Horcajada, Hf/porphyrin-based metal-organic framework PCN-224 for CO2 cycloaddition with epoxides, Mater Today Adv 19 (2023), https://doi.org/10.1016/j.mtadv.2023.100390.

[19] P.J. Hay, W.R. Wadt, Ab initio effective core potentials for molecular calculations. Potentials for K to Au including the outermost core orbitale, J. Chem. Phys. 82 (1985) 299–310, https://doi.org/10.1063/1.448975.
[20] A.D. Becke, Density-functional thermochemistry. III. The role of exact exchange, J. Chem. Phys. 98 (1993) 5648–5652, https://doi.org/10.1063/1.464913.
[21] M.J. Frisch, G.W. Trucks, H.B. Schlegel, G.E. Scuseria, M.A. Robb, J.R. Cheeseman, G. Scalmani, V. Barone, G.A. Petersson, H. Nakatsuji, X. Li, M. Caricato, A. V Marenich, J. Bloino, B.G. Janesko, R. Gomperts, B. Mennucci, H.P. Hratchian, J. V Ortiz, A.F. Izmaylov, J.L. Sonnenberg, D. Williams-Young, F. Ding, F. Lipparini, F. Egidi, J. Goings, B. Peng, A. Petrone, T. Henderson, D. Ranasinghe, V. G. Zakrzewski, J. Gao, N. Rega, G. Zheng, W. Liang, M. Hada, M. Ehara, K. Toyota, R. Fukuda, J. Hasegawa, M. Ishida, T. Nakajima, Y. Honda, O. Kitao, H. Nakai, T. Vreven, K. Throssell, J.A. Montgomery, J.E. Peralta, F. Ogliaro, M.J. Bearpark, J. J. Heyd, E.N. Brothers, K.N. Kudin, V.N. Staroverov, T.A. Keith, R. Kobayashi, J. Normand, K. Raghavachari, A.P. Rendell, J.C. Burant, S.S. Iyengar, J. Tomasi, M. Cossi, J.M. Millam, M. Klene, C. Adamo, R. Cammi, J.W. Ochterski, R.L. Martin, K. Morokuma, O. Farkas, J.B. Foresman, Gaussian 16, Revision A.03, 2016.
[22] T. Lu, F. Chen, Multiwfn: a multifunctional wavefunction analyzer, J. Comput. Chem. 33 (2012) 580–592, https://doi.org/10.1002/jcc.22885.
[23] V. V Butova, M.A. Soldatov, A.A. Guda, K.A. Lomachenko, C. Lamberti, Metal-organic frameworks: structure, properties, methods of synthesis and characterization, Russ. Chem. Rev. 85 (2016) 280–307, https://doi.org/10.1070/rcr4554.
[24] D. Feng, W.C. Chung, Z. Wei, Z.Y. Gu, H.L. Jiang, Y.P. Chen, D.J. Darensbourg, H. C. Zhou, Construction of ultrastable porphyrin Zr metal-organic frameworks through linker elimination, J. Am. Chem. Soc. 135 (2013) 17105–17110, https://doi.org/10.1021/ja408084j.
[25] J. Łuczak, M. Kroczewska, M. Baluk, J. Sowik, P. Mazierski, A. Zaleska-Medynska, Morphology control through the synthesis of metal-organic frameworks, Adv. Colloid Interface Sci. 314 (2023), https://doi.org/10.1016/j.cis.2023.102864.
[26] C. Healy, K.M. Patil, B.H. Wilson, L. Hermanspahn, N.C. Harvey-Reid, B.I. Howard, C. Kleinjan, J. Kolien, F. Payet, S.G. Telfer, P.E. Kruger, T.D. Bennett, The thermal stability of metal-organic frameworks, Coord. Chem. Rev. 419 (2020), https://doi.org/10.1016/j.ccr.2020.213388.
[27] A.F. Chimeh, D. Kocaefe, Y. Kocaefe, Y. Robert, J. Bernier, Mathematical modelling of a semi-dry SO2 scrubber based on a Lagrangian-Eulerian approach, J. Hazard Mater. 469 (2024), https://doi.org/10.1016/j.jhazmat.2024.134065.
[28] R.M. Guerrero, I.D. Lemir, S. Carrasco, C. Fernández-Ruiz, S. Kavak, P. Pizarro, D. P. Serrano, S. Bals, P. Horcajada, Y. Pérez, Scaling-up microwave-assisted synthesis of highly defective Pd@UiO-66-NH2 catalysts for selective olefin hydrogenation under ambient conditions, ACS Appl. Mater. Interfaces 16 (2024) 24108–24121, https://doi.org/10.1021/acsami.4c03106.
[29] X. Zhang, J. Zhang, C. Li, X. Zhang, J. Yun, D. Cao, A review on nanofiber-based composites for toxic and flammable gas sensing, Adv. Compos. Hybrid Mater. 7 (2024), https://doi.org/10.1007/s42114-024-00922-6.
[30] Y. Liu, T.M. Bisson, H. Yang, Z. Xu, Recent developments in novel sorbents for flue gas clean up, Fuel Process. Technol. 91 (2010) 1175–1197, https://doi.org/10.1016/j.fuproc.2010.04.015.
[31] J. Jin, Porphyrin-based metal-organic framework catalysts for photoreduction of CO2: understanding the effect of node connectivity and linker metalation on activity, New J. Chem. 44 (2020) 15362–15368, https://doi.org/10.1039/d0nj03507f.
[32] R. Das, P. Kumar Verma, C.M. Nagaraja, Design of porphyrin-based frameworks for artificial photosynthesis and environmental remediation: recent progress and future prospects, Coord. Chem. Rev. 514 (2024), https://doi.org/10.1016/j.ccr.2024.215944.
[33] M. Gouterman, Spectra of porphyrins, J. Mol. Spectrosc. 6 (1961) 138163.
[34] E. Moradi, R. Rahimi, Y.D. Farahani, V. Safarifard, Porphyrinic zirconium-based MOF with exposed pyrrole Lewis base site as a luminescent sensor for highly selective sensing of Cd2+ and Br− ions and THF small molecule, J. Solid State Chem. 282 (2020), https://doi.org/10.1016/j.jssc.2019.121103.
[35] S.S. Rajasree, X. Li, P. Deria, Physical properties of porphyrin-based crystalline metal–organic frameworks, Commun. Chem. 4 (2021), https://doi.org/10.1038/s42004-021-00484-4.
[36] X. Lai, R. Li, B. Zhang, T. Zhang, X. Ji, L. Wang, Y. Cui, H. Xiao, D. Ning, Colorimetric strategy of Fe/Co-doped porphyrin metal-organic frameworks with enzyme-like activity for the detection of ascorbic acid, Colloids Surf. A Physicochem. Eng. Asp. 680 (2024), https://doi.org/10.1016/j.colsurfa.2023.132645.
[37] C.H. Hendon, A.J. Rieth, M.D. Korzyński, M. Dincă, Grand challenges and future opportunities for metal-organic frameworks, ACS Cent. Sci. 3 (2017) 554–563, https://doi.org/10.1021/acscentsci.7b00197.
[38] J. Maillard, K. Klehs, C. Rumble, E. Vauthey, M. Heilemann, A. Fürstenberg, Universal quenching of common fluorescent probes by water and alcohols, Chem. Sci. 12 (2021) 1352–1362, https://doi.org/10.1039/d0sc05431c.
[39] C.J. Kingsbury, M.O. Senge, The shape of porphyrins, Coord. Chem. Rev. 431 (2021), https://doi.org/10.1016/j.ccr.2020.213760.
[40] G. Ding, C. Li, L. Chen, G. Liao, Porphyrin-based metal-organic frameworks for photo(electro)catalytic CO2 reduction, Energy Environ. Sci. 17 (2024) 5311–5335, https://doi.org/10.1039/d4ee01748j.
[41] J. Hu, H.-X. Lao, X.-W. Xu, W.-K. Wang, L.-L. Wang, Q.-Q. Liu, In situ meso-tetra (4-carboxyphenyl) porphyrin ligand substitution in Hf-MOF for enhanced catalytic activity and stability in photoredox reactions, Rare Met. 43 (2024) 2682–2694, https://doi.org/10.1007/s12598.
[42] H. Zhang, Y. Fang, F. Yang, X. Liu, X. Lu, Aromatic organic molecular crystal with enhanced p-p Stacking interaction for ultrafast Zn-ion storage, Energy Environ. Sci. 13 (2020) 2515–2523, https://doi.org/10.1039/d0ee01723j.
[43] C.J. Kaminsky, S. Weng, J. Wright, Y. Surendranath, Adsorbed cobalt porphyrins act like metal surfaces in electrocatalysis, Nat. Catal. 5 (2022) 430–442, https://doi.org/10.1038/s41929-022-00791-6.
[44] Q. Peng, S. Qi, L.P. Lv, W. Sun, Y. Wang, S. Chen, A cobalt-based coordination compound with high capacity as the anode of lithium-ion battery and its stepwise reaction mechanism, J. Alloys Compd. 927 (2022), https://doi.org/10.1016/j.jallcom.2022.167064.
[45] J.V. Gajjar, D.R. Roy, Porphyrin and its Co-doped complex-based sensor devices for nitrogen and sulfur containing environmental toxic gases, IEEE Sens. J. 24 (2024) 9411–9418, https://doi.org/10.1109/JSEN.2024.3364525.
[46] A. De Vos, K. Hendrickx, P. Van Der Voort, V. Van Speybroeck, K. Lejaeghere, Missing linkers: an alternative pathway to UiO-66 electronic structure engineering, Chem. Mater. 29 (2017) 3006–3019, https://doi.org/10.1021/acs.chemmater.6b05444.
[47] Z. Wang, J. Huang, W. Wang, X. Wang, Y. Wang, B. Gao, Q. Li, Removal of norfloxacin from high salinity wastewater by Hf-porphyrin MOF with missing linker defects: insights into anion trapping and photoinduced charge transfer effects, Chem. Eng. J. 466 (2023), https://doi.org/10.1016/j.cej.2023.143194.
[48] T. Burger, M.V. Hernández, C. Carbonell, J. Rattenberger, H. Wiltsche, P. Falcaro, C. Slugovc, S.M. Borisov, Luminescent porphyrinic metal-organic frameworks for oxygen sensing: correlation of nanostructure and sensitivity, ACS Appl. Nano Mater. 6 (2023) 248–260, https://doi.org/10.1021/acsanm.2c04301.
[49] S. Yuan, J.S. Qin, L. Zou, Y.P. Chen, X. Wang, Q. Zhang, H.C. Zhou, Thermodynamically guided synthesis of mixed-linker Zr-MOFs with enhanced tunability, J. Am. Chem. Soc. 138 (2016) 6636–6642, https://doi.org/10.1021/jacs.6b03263.
[50] A.D. Becke, K.E. Edgecombe, A simple measure of electron localization in atomic and molecular systems, J. Chem. Phys. 92 (1990) 5397–5403, https://doi.org/10.1063/1.458517.

ACS APPLIED ENGINEERING MATERIALS

Open Access

This article is licensed under CC-BY 4.0

pubs.acs.org/acsaenm

Article

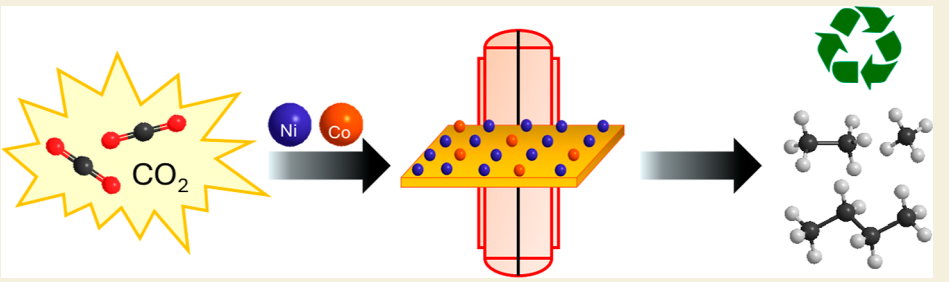
CO_2 Hydrogenation over Ni−Co/$Ce_{0.6}Zr_{0.4}O_2$ Catalysts for Light Hydrocarbons under Mild Conditions

Víctor Martínez-Jiménez, J. Gabriel Flores, Bettina Baumgartner, Juan L. Obeso, Catalina V. Flores, Bert M. Weckhuysen, J. R. Rosas-Cedillo, Pablo Marín-Rosas, Raul Perez Hernandez, Aida Gutierrez-Alejandre, Eduardo González-Zamora, Ilich A. Ibarra,* Ricardo A. Peralta,* and Jose Antonio de los Reyes*

Cite This: *ACS Appl. Eng. Mater.* 2025, 3, 957−967

Read Online

ACCESS | Metrics & More | Article Recommendations | Supporting Information



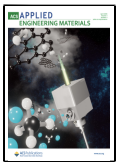
ABSTRACT: Ni and Ni−Co metal nanoparticles supported on a $Ce_{0.6}Zr_{0.4}O_2$ support (denoted as Ni/CZ-C and NiCo/CZ-C) were tested for the hydrogenation of carbon dioxide under mild conditions. The NiCo/CZ-C catalyst demonstrated remarkable performance, significantly decreasing the reaction temperature (200 °C) and achieving high selectivity toward short-chain hydrocarbons, specifically ethane and butane. In situ studies using diffuse reflectance infrared Fourier transform spectroscopy allowed for the monitoring of the evolution of methane formation and the proposal of a reaction scheme. Both catalysts produce carbonate species, which are further hydrogenated to produce CH_4. Notably, with the NiCo/CZ-C catalyst, additional hydrocarbons, such as ethane and butane, were also detected.

KEYWORDS: *heterogeneous catalysis, hydrogenation of CO_2, hydrocarbons, mechanics, bimetallic catalysts*

INTRODUCTION

The increased concentrations of greenhouse gases enhance the natural greenhouse effect, trapping more heat in the atmosphere. The primary change in greenhouse gas concentration in the atmosphere has been seen in carbon dioxide (CO_2), which has been prognosticated to continue rising over the coming years.[1] This trend is predominantly attributed to human activities, notably burning fossil fuels, deforestation, and industrial processes. Efforts to address climate change often focus on transforming CO_2 into value-added molecules, thereby reducing the extent of global warming and its associated effects.[2] Among them, hydrogenation of CO_2 to obtain hydrocarbons and oxygenated compounds has gained importance, with the main products being methanol, ethanol, formic acid, methane, ethane, and butane, among others.[3] Although being important chemical building blocks,[4] short-chain alkanes, such as ethane (C_2H_6) or butane (C_4H_{10}), can be challenging to obtain as products in hydrogenation processes due to the high tendency of catalysts to undergo further hydrogenation to form longer-chain hydrocarbons.[5,6] Light olefins are the basis for the generation of polymers such as polyethylene and polypropylene, with ethane and butane being the raw materials depending on the polymer of interest.[7] In addition to the above, butane is a compound of commercial interest with multiple uses, for example, in refrigeration systems and as an important precursor in the chemical industry.[8] The conventional source of butane is oil cracking; however, research is underway to transform CO_2 into light alkanes.[9] For instance, an Fe−K catalyst operating at 10 bar and 300 °C produced C_2−C_4 as intermediates of CO hydrogenation, along with a mixture of different products. It is worth mentioning that nonconventional separation processes must be undertaken to produce desirable pure products.[10] Thus, selective hydrogenation reactions are an excellent alternative to generate light alkanes; however, it is important

Received: January 21, 2025
Revised: April 1, 2025
Accepted: April 8, 2025
Published: April 17, 2025



Downloaded via UNIV AUTONOMA METROPOLITANA on June 30, 2025 at 22:45:07 (UTC).
See https://pubs.acs.org/sharingguidelines for options on how to legitimately share published articles.

© 2025 The Authors. Published by American Chemical Society

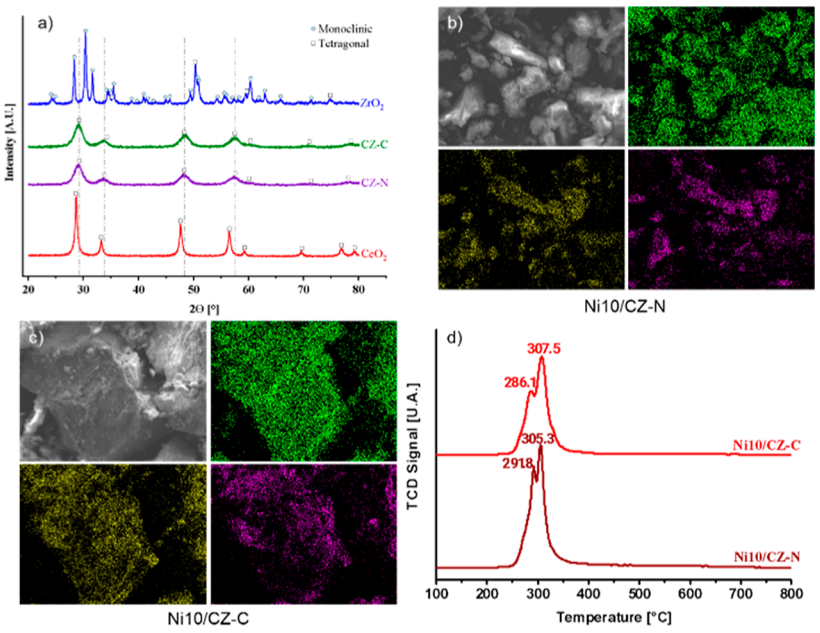


Figure 1. (a) PXRD of the materials and metal oxides: ZrO_2 (blue), CZ-C (green), CZ-N (violet), and CeO_2 (red). (b) SEM Figure of Ni10/CZ-N; EDX mapping and element analysis, including Ni (green), Zr (yellow), and Ce (violet). (c) SEM figure of Ni10/CZ-C; EDX mapping and element analysis, including Ni (green), Zr (yellow), and Ce (violet). (d) Comparison of the TPR-H_2 of catalyst at 300 °C and atmospheric pressure.

to continue exploring more systems to make this process efficient.

The CO_2 hydrogenation reaction has been characterized by diverse in situ spectroscopic techniques and DFT theoretical calculations, where depending on the catalyst, several elementary steps can affect the mechanism.[11] For example, mechanisms of hydrogenation reactions of CO_2 have been reported without the generation of molecules of CO as intermediates. The proposed sequence of these catalysts is as follows: (I) the first stage begins with the adsorption of CO_2 (CO_{2ad}) on the metal (support); (II) subsequently, the metal is reduced with H_2, which allows the CO_{2ad} to react, generating OCO_2H, which can further react to give formate (OCH_2) and H_2O molecules which are released to the medium; (III) a further hydrogenation of the formate allows the formation of methoxy species (H_3CO); (IV) in the final stage, the methoxy group formed is hydrogenated, producing methane as the majority product.[12−14] Knowing the mechanism of this reaction is key to maximizing the yield and the selectivity toward desired products. In addition to the above, understanding the mechanism allows the appropriate catalyst to be selected to generate the product of interest.

Among the transition metals used to catalyze the hydrogenation of both CO_2 and CO, Ni, Cu, and Co stand out, with Ni/Al_2O_3 being one of the most frequently used catalyst systems for obtaining methane as a reaction product. This is due to a phase that is formed at the metal−support interface that allows the metal particles to be stabilized.[13] Nevertheless, cobalt catalysts have also shown potential for this reaction by possessing high selectivity to products such as methane and CO due to a correct arrangement of the metal oxides on the surface of the alumina.[15,16] The support of the catalyst is also highly important, with Zr oxide having been widely used due to its notable catalytic characteristics. Moreover, an addition of Ce to the support enhances the stabilization of Zr and the atomic arrangements of the metals to cubic or tetragonal structures. Thus, a Ni−Ce−Zr mixed oxide catalyst has been reported to produce excellent results in CO_2 hydrogenation to obtain methane.[12] It has been shown that the Ni(II) allocated on the interface of Ce−Zr can be reduced with H_2 to generate Ni(0) atoms, while CO_2 is adsorbed on the Ce−Zr surface.[13] The reaction occurs at temperatures between 300 and 360 °C under atmospheric pressure, producing methane as the main reaction product.[17] These mild working reaction conditions have been the motivation behind continued research into this system to uncover its novel properties.

In this work, the hydrogenation of CO_2 catalyzed by Ni and Ni−Co metal nanoparticles supported on ceria-zirconia support (herein further denoted as Ni/CZ-C and NiCo/CZ-C, respectively) is presented. NiCo/CZ-C displayed outstanding performance for this reaction at a significantly lower reaction temperature (200 °C) and with high selectivity to short-chain hydrocarbons (ethane and butane). To the extent of our knowledge, this material has selectivity toward C_2−C_4 at atmospheric pressure and relatively low temperatures. Moreover, the reaction was followed in situ by diffuse reflectance infrared Fourier transform spectroscopy (DRIFTS), which allowed monitoring of stable species formed at different times during the process. Moreover, in NiCo/CZ-C catalysts, the good distribution of Ni−Co and the high concentration of methoxy groups on the surface of the material allowed the methoxy species to interact and yield the formation of products like ethane and butane. Being aware of these species is the key to rationalizing the pathway and developing design-driven materials that expand the possibilities for carbon utilization.

RESULTS AND DISCUSSION

Our first approach was to synthesize two different supports with two Zr precursor salts, $ZrO(NO_3)_2.xH_2O$ and $ZrOCl_2 \cdot 8H_2O$, with $Ce(NH_4)_2(NO_3)_6$, herein CZ-N and CZ-C respectively, the molar ratio in both samples was of Ce/Zr equal to 60/40. Also, the individual oxides CeO_2 and ZrO_2

https://doi.org/10.1021/acsaenm.5c00055
ACS Appl. Eng. Mater. 2025, 3, 957−967

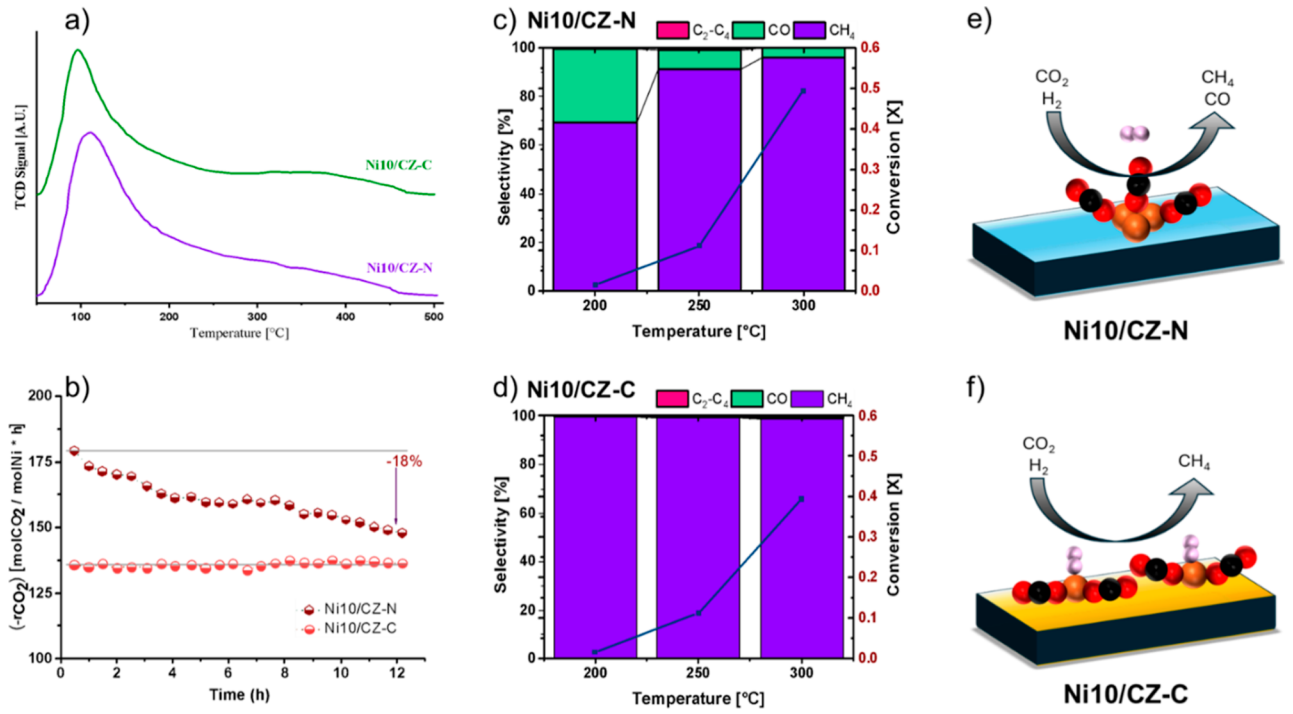


Figure 2. (a) CO_2 TPD of Ni/CZ-X catalysts by varying the Zr precursor salt in the support, Ni10CZ-N (violet), Ni10CZ-C (green). (b) Comparison of the stability of catalysts at 300 °C and atmospheric pressure. Comparison of the selectivity of (c) Ni10/CZ-N and (d) Ni10/CZ-C at atmospheric pressure and 200, 250, and 300 °C. Representation of the CO_2 interaction with (e) Ni10/-CZ-N and (f) Ni10/CZ-C.

were synthesized, and all the supports were characterized via powder X-ray diffraction (PXRD), as seen in Figure 1a. The summarized description of the synthesized catalysts is shown in Tables S1−S3. The PXRD patterns from CZ-N and CZ-C revealed four main reflections observed at approximate 2θ values of 29.1, 34.9, 48.8 and 58.3°, which represent the following families of planes of a cubic structure (c−$Ce_{0.6}Zr_{0.4}O_2$), $(111)_c$, $(200)_c$, $(220)_c$, and $(311)_c$.[18] When compared to the individual oxides, the reflections did not show a similar phase, indicating that these materials are not segregated on the CZ supports or that their crystal sizes are below the equipment sensitivity. In the PXRD patterns of the samples, a broadening of the reflections was observed, which we attribute to a decrease in the crystal size in the CZ supports compared with the individual oxides. This proves a greater resistance to sintering and may be responsible for the increase in the surface area and crystal size. Importantly, the full width at half-maximum (fwhm) of the main reflections of the CZ supports was equivalent, suggesting the isotropic growth of the crystals. Similar behavior was observed for CeO_2. Moreover, the theoretical cell parameter of the mixed oxide was calculated using Vegard's law, as shown in Table S5, which suggests that the presented materials are in a solid. This property is essential as it provides uniformity to the material and, thereby, a better distribution in the loading of the metals. Moreover, 77 K N_2 gas adsorption isotherms were performed on the supports (Figure S2). Table S6 shows the values for surface areas of 98.2 and 84.2 m^2/g were obtained for CZ-N and CZ-C, respectively; these values are in agreement with previously reported similar materials.[19] High surface area can be related to high catalytic activity since the active sites are available in the reaction.[20,21]

The different supports (CZ-N, CZ-C) were calcinated at 500 °C for 5 h; studies have shown that temperatures between 400 and 500 °C can lead to highly dispersed active species and better interaction with the support, resulting in high catalytic activity.[22,23] CZ-N and CZ-C supports were loaded with 10 wt % of Ni(II) by impregnation to obtain Ni10/CZ-N and Ni10/CZ-C, respectively. The materials were characterized by PXRD, and no significant changes were noticed, as the Ni(II) particles size on the surface was too small to be detected. Further, the material was subjected to analysis by scanning electron microscopy-energy dispersive X-ray analysis to analyze the distribution of the Ni(II) on the surface of the supports (Figures 1b,c and S4, S5). Interestingly, Ni10/CZ-N showed a more homogeneous metal distribution than Ni10/CZ-C. To analyze the surface of Ni10/CZ-N and Ni10/CZ-C, hydrogen-temperature-programmed reduction (H_2-TPR) and CO_2 temperature-programmed desorption (CO_2-TPD) were carried out. Figure 1d and Table S8 show the corresponding H_2 consumption profiles of Ni10/CZ-C and Ni10/CZ-N with variations in the Zr precursor salt. Both catalysts have two H_2 consumption regions associated with the reduction process of NiO particles on the support.[24] Ni10/CZ-C has peaks at lower temperatures, about 286 and 307 °C. On the other hand, Ni10/CZ-N has peaks at higher temperatures, located at 292 and 306 °C; this can be interpreted as a stronger interaction of the Ni with the material. It is worth noting that the consumption of H_2 on Ni10/CZ-N was 0.22 mmol H_2/g higher than in Ni10/CZ-C. This could mean higher accessibility of H_2, leading to more efficient reduction due to a better metal distribution on the surface. The CO_2-TPD analysis showed similar trends in CO_2 desorption profiles in the temperature range between 50 and 200 °C for both Ni10/CZ-N and Ni10/CZ-C (Figure 2a and Table S11). However, the Ni10/CZ-N catalyst presented an appreciably larger amount of CO_2 desorption compared to Ni10/CZ-C. The highest concentration can be found in the range between 200

https://doi.org/10.1021/acsaenm.5c00055
ACS Appl. Eng. Mater. 2025, 3, 957−967

and 500 °C, being almost double in the Ni10/CZ-N catalyst. This implies that Ni10/CZ-N possesses a higher surface area and has more available sites for CO_2 adsorption, leading to a higher amount of CO_2 desorption during the TPD experiment. This also can be corroborated by the surface area, which is higher than that of Ni10/CZ-C; see Figure S3 and Table S7 for details. Thus, H_2-TPR and CO_2-TPD techniques confirmed that Ni10/CZ-N has a better dispersion of the metal on the surface.

Ni10/CZ-N and Ni10/CZ-C were tested for hydrogenation of CO_2 in a flow reactor system at atmospheric pressure and 300 °C for 12 h; the results are summarized in Figure 2b. The nominal Turnover Frequency[25] (TOF) $\frac{(\text{mol } CO_2)}{(\text{molNi} \times \text{h})}$ of each sample was determined. Figure 2b shows that Ni10/CZ-N catalyst presented an activity almost 1.5 times greater than the Ni10/CZ-C catalyst; this is probably caused because the Ni atoms deposited on the surface of CZ-N were better dispersed as H_2-TPR, CO_2-TPD, and EDX experiments indicated above. Nevertheless, a deactivation of the Ni10/CZ-N catalyst was observed with a loss in activity of almost 18% over 12 h. Although a greater dispersion of the metallic phase can favor a higher activity, this can also result in deactivation, probably due to the sintering of Ni on the support.[26] In order to rule out the activity of the support, a blank experiment was carried out on CZ-N and CZ-C, with negligible activity in both cases. These results support the idea that Ni10/CZ-N is an inadequate catalyst for the hydrogenation of CO_2 due to deactivation over time. In comparison, the loss of catalytic activity of Ni10/CZ-C was almost negligible.

The selectivity of Ni10/CZ-N and Ni10/CZ-C was further analyzed by exploring the selective formation of CH_4, which was evaluated at reaction temperatures of 200, 250, and 300 °C after 4 h. The results in Figure 2c,d show a better selectivity for the Ni10/CZ-C catalyst compared with Ni10/CZ-N for the formation of CH_4, especially at low temperatures. The catalyst with the precursor salt $ZrOCl_2 \cdot 8H_2O$ (Ni10/CZ-C) presents selectivity close to 99% toward CH_4 in the temperature range studied; likewise, the Ni10/CZ-N catalyst has selectivity toward CH_4 at 200 °C of 69%. The results clearly show that Ni10/CZ-N has only partially reduced the CO_2 into CH_4, and thereby, subproducts such as CO are observed (Figure 2e,f). The incomplete reduction of CO_2 could be explained by the fact that less CO_2 molecules are adsorbed at temperatures between 200 and 500 °C in Ni10/CZ-N, as CO_2-TPD results showed (Table S11). This, combined with the deactivation of the material, results in a smaller interaction between H_2 and the metal catalyst. Thus, the results confirmed that Ni10/CZ-N is an inappropriate catalyst for the complete reduction of CO_2.

Effect of Metallic Ni Content on the Support CZ-C

Inspired by the results obtained with Ni10/CZ-C, we investigated the effect of the metallic Ni loading on this support was investigated. We hypothesized that the CO_2 conversion would be greatly impacted by the presence of Ni atoms until the metal segregation on the support impacts the catalytic activity. The amount of Ni loaded on the support was 1 wt % (Ni1/CZ-C), 2.5 wt % (Ni2.5/CZ-C), 5 wt % (Ni5/CZ-C), 7.5 wt % (Ni7.5/CZ-C), 10 wt % (Ni10/CZ-C), 12.5 wt % (Ni12.5/CZ-C), and 15 wt % (Ni15/CZ-C). The materials were subject to characterization by H_2-TPR (Figure S9 and Table S9) and CO_2-TPD (Figure S11 and Table S12). H_2-TPR data showed that for all of the impregnated catalysts, the formation of two reduction regions corresponding to NiO particles was observed, as mentioned above. The shifts of both Ni bands toward lower reduction temperatures were observed as the Ni content increased from 1 to 10 wt %. However, in the case of the catalyst with 15%, this effect was no longer observed, probably due to the formation of agglomerations or large NiO particles over the support. CO_2-TPD showed that between 200 and 500 °C, as the Ni loading in the material increases (from 1 to 10%), a higher concentration of CO_2 is desorbed, reaching a maximum with a content of 10%. However, for the 15% Ni catalyst, the material loses adsorption capacity, implying that bigger particles are formed, and consequently, the surface area decreases. Moreover, the individual oxides CeO_2 and ZrO_2 loaded with 10 wt % Ni were subject to study to gain further insight into the role of Ni in the reaction.

The catalysts with varied amounts of Ni loaded were evaluated for CO_2 hydrogenation. The results shown in Figure 3 showed that at 300 °C, the catalytic activity increases with

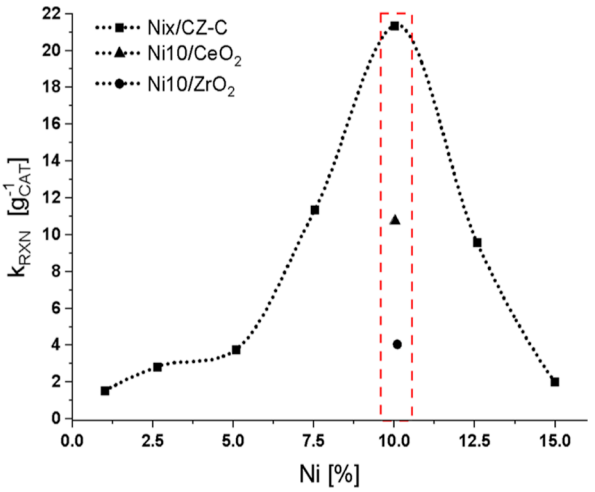


Figure 3. Catalytic activity in the reduction of CO_2 at 300 °C as a function of metal loading and type of support.

the metallic loading until it reaches 10 wt % Ni loading. However, the activity decreases sharply for loading over 10 wt %; the formation of large particles of Ni metal and deactivation by coke formation probably causes this deactivation.[26,27]

Moreover, the agglomeration effect was further investigated by a H_2-TPR analysis. Table S8 shows a relationship between the consumed hydrogen and their catalytic activity at 300 °C. The results indicate a direct correlation between the hydrogen consumed and the catalytic activity, being the highest again for Ni10/CZ-C. This suggests that for more than 10 wt %, agglomeration becomes an important phenomenon that reduces the number of active sites and leads to catalyst deactivation.[26,28,29] For a fixed metal loading of 10 wt %, the activity of the Ni10/CZ-C catalyst is approximately 2 and 5 times higher than that of the individual oxide catalyst, Ni10/CeO_2 and Ni10/ZrO_2, respectively, as shown in Figure 3, highlighting the importance of utilizing the support to achieve higher CO_2 conversions. A similar trend in the catalytic activity was observed at 250 °C, where Ni10/CZ-C was the most active compared to individual oxide catalysts, as shown in Figure S14. However, at 200 °C, the catalyst supported on CeO_2 turned out to be the most active. Nevertheless, the conversion is quite low, about 1.3% for Ni10/CeO_2 and 1.6%

https://doi.org/10.1021/acsaenm.5c00055
ACS Appl. Eng. Mater. 2025, 3, 957−967

for Ni10/CZ-C, suggesting that this reaction requires higher temperatures to proceed successfully.

In terms of selectivity, all the catalysts were between 95 and 99% selective toward the formation of CH_4 at 300 °C (Figure S15). The results suggest that the Ni loading has no influence on CH_4 selectivity; this is a good agreement with previously reported data.[12,30] Thus, the results highlight the importance of the support and temperature in achieving higher CO_2 conversion. The stability of the catalyst was evaluated after the reaction, as shown in Figure S8. The diffractograms of the prepared materials on different supports exhibit negligible differences. However, postreaction, both Ni10/CZ-C and Ni10/CZ-N catalysts show increased peaks at 44.7, 52.1, and 76.6°, characteristic of the monoclinic phase of ZrO_2.[18] This suggests the presence of phase mixtures with the possible formation of ZrO_2 particles during the process.

Effect of Co-Promotion on Bimetallic NiCo/$Ce_{0.6}Zr_{0.4}O_2$ Catalysts

Buoyed by the results obtained with Ni10/CZ-C, we investigated the influence of the catalytic activity on bimetallic-supported species. Bimetallic catalysts often exhibit synergistic effects where combining two different metals leads to properties that cannot be accessed using one species alone. This synergy can enhance catalytic activity by promoting unique reaction pathways.[31,32] On one hand, Ni has been one of the most widely used metals as catalysts for the CO_2 methanation reaction.[33] It has been reported that its good catalytic activity is related to the high adsorption of CO_2 that occurs when there is a correct dispersion of the metal.[34] The challenge for Ni catalysts is that they can present stability problems, such as metal oxidation and catalyst deactivation.[35] Furthermore, Ni has been combined with noble metals such as Rh, Ru, Pd, and Pt, inhibiting carbon deposition and particle deposition during the reaction. Nevertheless, these catalysts are limited due to their high value and unavailability.[36] It has been demonstrated that there is a synergy in bimetallic Ni-M catalysts (M = Fe, Co, Cu), improving the conversion of CO_2 in methanation.[31] The introduction of Co can be important to the type of reactions; small amounts of Co can decrease the selectivity to CO while boosting the yields of CH_4 and higher hydrocarbons.[37] Since the Ni and Co electronic structures are similar, bimetallic catalysts containing these metals have attracted attention.[36] Ni−Co catalysts showed better properties than the monometallic catalysts, Aika et al. proved that the bimetallic catalyst (Co−Ni/TiO_2) improved the stability of the material and presented resistance to oxidation.[38] Huang et al. presented a study highlighting the importance of the synergetic effect of the Co−Ni catalyst, and the material promoted low temperature catalytic activity. The addition of Co presented the apparent decrease in the activation energy of CO_2 methanation.[39]

Thus, we explored and compared the activity of mono- and bimetallic Ni and NiCo catalysts supported on CZ-C (Ni/CZ-C, Co/CZ-C and NiCo/CZ-C, respectively) as presented in Table S4. In all cases, the metal content in the materials was 10 wt %; for NiCo/CZ-C, the content is 7.5 wt % of Ni and 2.5 wt % of Co. The effect of the molecular Ni−Co ratio is important. The presence of Ni on the material aims for catalytic activity toward CO_2 hydrogenation, and a decrease could result in less hydrogenation activity and an increment in CO production. On the other hand, Co helps with the stability of the material and enhances the activity of the catalyst. Bimetallic Ni−Co catalysts have been reported, where the optimal ratio must be close to 20−30% in Co content to obtain higher yield and selectivity.[39,40] The PDRX of NiCo/CZ-C is shown in Figure S1. The maximum loading used was 10 wt % due to the results outlined above, which indicated that the metal loading was found to correlate with the catalytic activity, as presented in Figures S6 and S7. On the other hand, loading exceeding 10 wt % leads to agglomeration of the metal, thereby deactivating the active sites. The materials were characterized by H_2-TPR (Figure S10 and Table S10) and CO_2-TPD (Figure S12 and Table S13). H_2-TPR showed, for Ni/CZ-C, the appearance of two reduction regions corresponding to NiO particles. In the bimetallic catalyst, 3 reduction regions are observed in which 2 reduction peaks are most likely related to NiO and CoO particles. The amount of hydrogen consumed in reducing NiCo/CZ-C was lower than that of Ni10/CZ-C. However, the dispersion on the surface was better for NiCo/CZ-C. CO_2-TPD showed that between 200 and 500 °C, NiCo/CZ-C has a higher concentration of CO_2 desorbed, meaning a higher surface area.[41]

The catalytic activity of Ni is supported on individual oxides; Ni and NiCo supported on the CZ-C platform for the hydrogenation of CO_2 was tested. The materials were placed in a flow reactor and activated in situ with H_2 flow at 500 °C. Consequently, the samples were exposed to a gaseous reagent mixture of molar composition H_2:CO_2:N_2 equal to 5:1:4 with a total flow rate of 120 mL/min at 200, 250, and 300 °C as presented in Figure S13. CO_2 conversion is favored when the H_2/CO_2 ratio is 4:1 or higher; at least 4 times more H_2 is needed to consume CO_2 efficiently. It is worth mentioning that high pressure can be beneficial since the equilibrium can be shifted, increasing the CO_2 conversion. Nevertheless, in this work, the reaction is carried out under mild conditions, looking for a sustainable process. In addition, carbon deposition can occur when high pressure is applied to the system, which leads to deactivation of the catalyst.[42−46] The results from the CO_2 hydrogenation experiments after 4 h are shown in Figure S16. At 200 °C, the conversion of CO_2 of all the systems is quite low, and no substantial difference was noticed in their activity. At 250 °C, the activity of all of the systems increased except for Ni/ZrO_2. However, at 300 °C, the catalytic activity is substantially enhanced, implying that the catalyst requires more energy to break the bonds between the oxygen and carbon. This tendency has been observed in previous reports where, at higher temperatures, the catalyst performance is better for CO_2 reduction.[47−49] The mono- and bimetallic species supported on the CZ-C achieve higher CO_2 conversions than the individual oxides in the temperature range evaluated. Likewise, when adding Co as a cocatalyst, an improvement in activity is observed, about 81% at 300 °C. This enhancement in the catalytic activity may be due to a synergy in the material between Ni and Co. The results highlight the potential of bimetallic Ni and Co systems for the conversion of CO_2 in future efforts to prepare superior catalytic systems.

Insights into the Formation of C_2−C_4 Products

The selectivity of these materials for the formation of C_2−C_4 products (ethane and butane) was further analyzed, as seen in Figure 4. The selectivity results indicate that Ni/ZrO_2 catalyst is not selective for the formation of C_2−C_4 (0.2−0.3%). Ni/CeO_2 and Ni/CZ-C materials present very similar selectivity, the maximum being 1.0% at 200 °C. Co-/CZ-C material

https://doi.org/10.1021/acsaenm.5c00055
ACS Appl. Eng. Mater. 2025, 3, 957−967

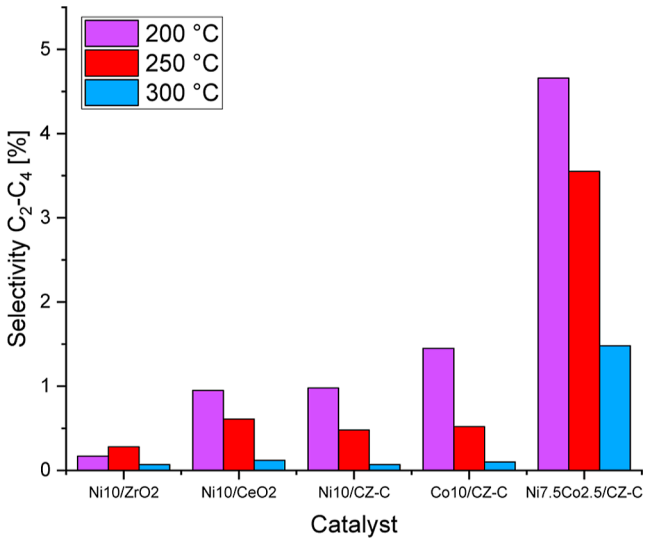


Figure 4. Selectivity 10 wt % loaded on Ni10/ZrO_2, Ni10/CeO_2, Ni10/CZ-C, Co10/CZ-C, and Ni7.5Co2.5/CZ-C in the reduction of CO_2 to C_2−C_4 species as a function of the temperature and catalyst support.

presents an improvement in the selectivity for producing light hydrocarbons under mild conditions compared with Ni materials, but the maximum selectivity is less than 2%. Thus, this suggests a synergistic effect present in bimetallic NiCo/CZ-C catalyst that promotes the formation of C_2−C_4 products, reaching a maximum selectivity of almost 4.7% at a temperature of 200 °C. Figure S17 shows the selectivity for C_2−C_4 as a function of CO_2 conversion. It can be observed that at lower CO_2 conversion, higher selectivity to C_2 and C_4 is obtained. It was found that as the temperature increases, the selectivity toward these products decreases.

The catalyst NiCo/CZ-C possesses selective activity for hydrogenation under conditions close to atmospheric pressure (Table S14). Furthermore, this catalyst showed selectivity at relatively low reaction temperatures. Our work undertakes the reaction at a pressure of 1 bar, looking for a simpler, safer, and more sustainable process. Thus, the work presented herein can be considered as a step forward in the search for new technologies that can function under mild conditions. It is worth noticing that the 0.19 and 0.82% yields obtained in our study for C_2 and C_4, respectively, are much lower than the 18.36% yields obtained at 10 bar by Garcia et al.[5] However, the conditions used in that study are harsh and cannot be directly compared to those in our work. In 2019, Corma et al. reported a comparative study under similar conditions, obtaining yields of 0.05%,[50] as shown in Table S15. Under similar conditions, Chen et al. reported negligible C_2−C_4 products,[51] highlighting the activity of the synthesized catalyst. Our material presents an improvement in yield and is important in the wider context of developing materials that can perform selective hydrogenation of CO_2 under mild reaction conditions.

To investigate the reaction pathway, in situ DRIFT spectroscopy at different temperatures (200, 250, and 300 °C; see Section S4 and Table S16 for details) and mass spectrometry (Figure S18) were performed. The IR spectra were recorded after 1, 5, 10, 15, 20, 25, and 30 min of the CO_2 hydrogenation reaction using the Ni/CZ-C catalyst. In the first minute, strong bands corresponding to CO_2 can be observed at 3370 and 2350 cm^{-1} at all temperatures. After 5 min, the bands are reduced, and no new vibrations appeared, implying the stabilization of the reaction, reiterating the excellent stability of the catalyst. The bands of CO_2 are less intense as the temperature increases and within the conversion, meaning the catalyst is more active at higher temperatures.[52,53] At 200, 250, and 300 °C, the IR bands corresponding to C−H stretching vibrations associated with CH_4 are observed at 3016 cm^{-1}. Moreover, a band at 1570 cm^{-1} is observed, corresponding to the vibrational mode of the formate species. Furthermore, new bands at 1245 and 1478 cm^{-1} became visible, which are characteristic bands of carbonates, whereas the bands at 1390 and 1303 cm^{-1} correspond to bicarbonate species.[6,52,54] The above observations suggest that during the formation of CH_4, formate, and carbonate species are present. This is reinforced by the signal at 1180 cm^{-1} (Figure S19) corresponding to C−O (H_3C−O) vibrations of alkylated species.[13,52,54,55]

When the temperature was increased to 300 °C, DRIFT analysis on the sample was carried out (Figure S20); negative bands were observed at 1415, 1317 and 1242 cm^{-1}, which may be a sign that carbonate impurities were presented on the pristine catalyst and decomposed when the temperature was raised, freeing up OH-moieties on the support. Simultaneously, bands associated with the presence of water appeared at 3500 and 1630 cm^{-1}, which suggests a strong interaction between the water molecules and the surface of the material; the effect becomes more visible as the temperature and CO_2 conversion increase.[54] It is worth mentioning the absence of M-CO bands, which are expected to appear between 2200 and 1900 cm^{-1}, suggesting a strong interaction between the metal and the support, thereby not allowing formation of this species. Furthermore, the metal could be encapsulated in the support layer and thereby inaccessible to form CO molecules.[13,53] Based on these results, for the Ni/CZ-C catalyst, the suggested reaction route involves, first, the formation of carbonate species ($HCO_3(_{ad})$), which have been detected by DIRFT, from the activation stage of the material (in traces) and subsequently with a very notable increase during the reaction, this is shown in the spectra of Figure 5a.

NiCo/CZ-C pathway of CO_2 hydrogenation was also scrutinized at different times (1, 5, 10, 15, 20, 25, and 30 min) and temperatures (200, 250, and 300 °C). The bands corresponding to CO_2 can be observed at 3370 and 2350 cm^{-1}. It is easy to observe, from the spectra, that the reaction stabilizes very quickly at the three temperatures, similar to Ni/CZ-C catalyst (after 5 min), which restates the stability of these systems.[52,53] In this case, IR bands associated with CH_4 are also observed at 3016 cm^{-1}. A band at 1570 cm^{-1} is likewise observed, corresponding to the formate species, while the bands at 1245 and 1478 cm^{-1} demonstrated the presence of carbonates. The results suggest that the formation of CH_4 requires the presence of formate and carbonate species and it is supported by the bands observed at 1180 cm^{-1}, which correspond to the vibrations of alkylated C−O (H_3C−O) bonds.[13,52,56] This alkylated band is more clearly defined at 200 °C compared to the monometallic catalyst. Following the proposed reaction scheme (Figure 5b), it is known that these species along with water molecules are essential for the formation of CH_4 and in some cases, also to produce C_2−C_4, the products could be followed by mass spectrometry to verify their presence.

Also, in the monometallic catalyst, at 300 °C, negative absorption bands were observed at 1415, 1317 and 1242 cm^{-1}, meaning again that the pristine material possessed carbonate

https://doi.org/10.1021/acsaenm.5c00055
ACS Appl. Eng. Mater. 2025, 3, 957−967

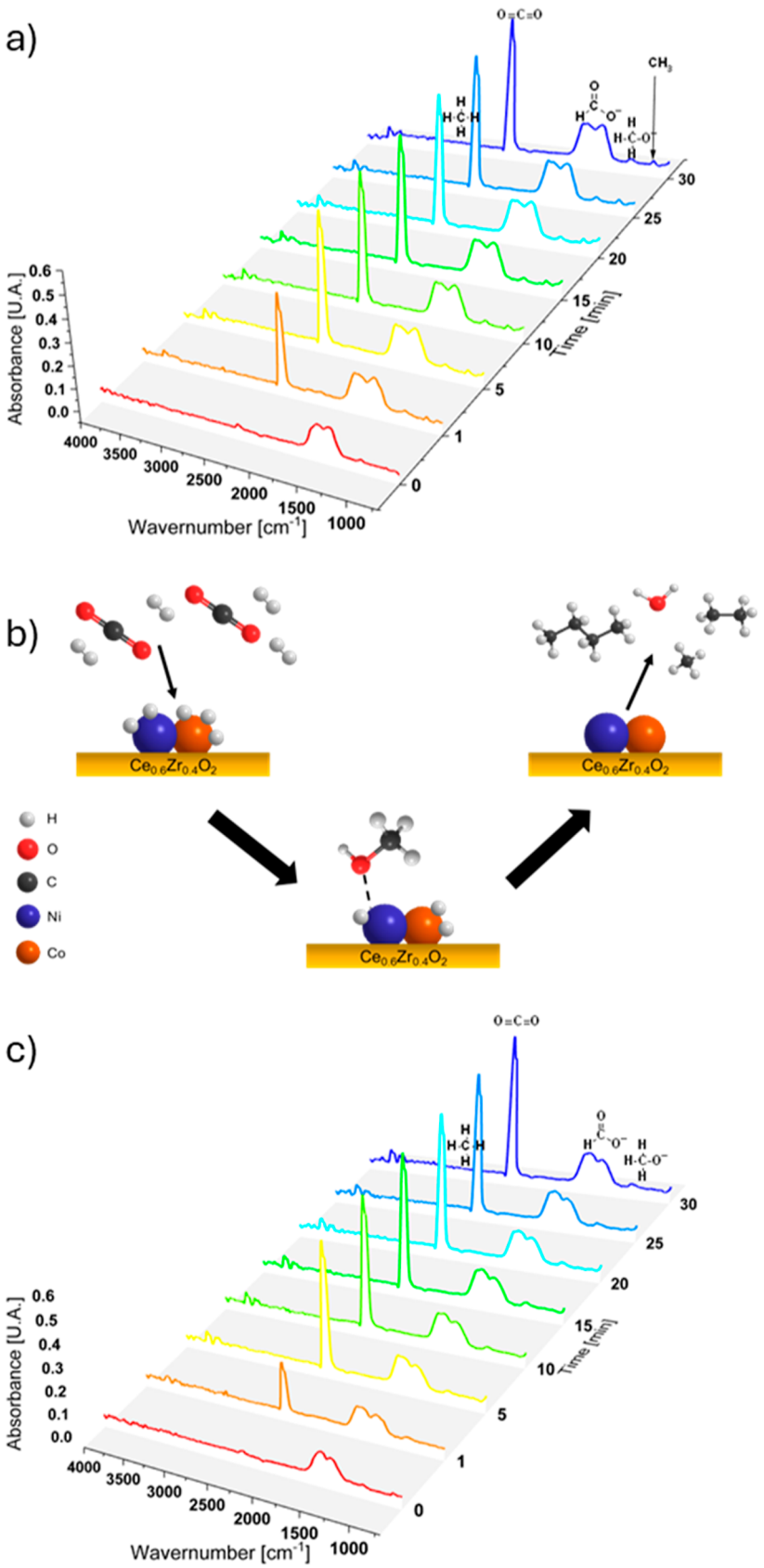


Figure 5. (a) In situ DRIFTS spectra obtained during the CO_2 hydrogenation reaction at different times and 200 °C on Ni/CZ-C. (b) Reaction scheme proposed based on DRIFT studies Ni−Co/CZ-C catalyst at 30 min and 200 °C. (c) In situ DRIFTS spectra obtained during the CO_2 hydrogenation reaction at different times and 200 °C on NiCo/CZ-C.

https://doi.org/10.1021/acsaenm.5c00055
ACS Appl. Eng. Mater. 2025, 3, 957−967

impurities, which were burned off as the temperature increased (Figure S19). At the same time, bands corresponding to water at 3500 and 1630 cm^{-1} were visible, which is probably due to a strong interaction of the water molecules produced during the reaction with the surface of the material as the temperature increases and CO_2 conversion proceeds.[54] It should be noted that these bands are less intense in the bimetallic NiCo catalyst, thus favoring a higher activity in this material since the adsorbed water species represent a source of inhibition for the activity of the catalyst. Finally, small signals were observed at 870 cm^{-1} corresponding to $-CH_3$ vibrations; the band was more noticeable at 200 and 250 °C (Figure 5c). This signal, which was not observed in the monometallic catalyst, is related to the presence of C_2 (ethane) and C_4 (butane), confirming the formation of these alkanes.[6,57]

It is worth mentioning that the yield of C_2-C_4 is close to 1%. Therefore, observing the bands for these products or intermediates in the DRIFTS analysis is unfeasible. The formation of CH_4 as the main product could be due to the particle size in the catalyst. García and co-workers have reported that decreasing the particle size increases the selectivity for CH_4 and yields byproducts such as CO and C_2-C_4 alkanes.[5] Since these products were observed via mass spectrometry, DRIFT studies, and GC we suggest that particle size has a similar effect on the reaction outcome in our study.

Based on the results obtained from the NiCo/CZ-C material, the suggested pathway produces methoxy groups, which suggests a reaction involving intermediates. Nevertheless, in order to propose a detailed reaction mechanism, other studies such as SSITKA are necessary. DRIFT studies do not allow us to propose a reaction mechanism for hydrogenation of the intermediates. This is due to the limited formation of this transient species (less than 1% in the reaction), which makes it unfeasible to detect via spectroscopy. Nevertheless, the formation of the products was corroborated through mass spectrometry and DRIFT and GC experiments. However, a hypothetical pathway for the formation of C−C bonds has been reported previously for an Fe−Co catalyst.[5,31,54,58] The formation of these intermediate species was proposed on the basis of proximal metallic centers that have a great similarity with the Ni−Co pair in our study. As shown in the proposed reaction scheme based on literature, the first step of the reaction involves the formation of CH_3OH and water. Finally, these species will evolve into different types of hydrocarbons, the majority being CH_4 with traces of C_2 and C_4 under these reaction conditions. This hypothesis can also be supported by TPD results, where a greater amount of CO_2 molecules was adsorbed (Table S13).

Regarding the existence of species such as carbonates and formates on the surface of the material after reduction, an experiment was carried out where the material/support was reduced and measured by DRIFT, and these results are shown in Figures S21 and S22. Although the experiment is qualitative, it allows us to identify the bands of the bicarbonate at 1303−1390 cm^{-1} and the formate group at approximately 1570 cm^{-1}.[54] The bicarbonate species reportedly to exist as intermediates in methanation,[59] while the formate species is primarily formed on the surface of the support and have little contribution to the reaction.[60] Although these groups are generated on the surface of the catalyst and the support, the intensity is much lower than that shown in the spectra during the reaction of NiCo/CZ-C and Ni(10)/CZ-C.

These results highlight the importance of using DRIFT studies to gain insight into the mechanism that can be used to optimize reaction conditions, such as temperature or catalyst stoichiometry. This optimization can be a step forward toward higher reaction yields, faster reaction rates, and better product selectivity.

CONCLUSIONS

Ni/CZ-C and NiCo/CZ-C catalysts were active in the hydrogenation of CO_2 under mild conditions. Particularly, NiCo/CZ-C displayed outstanding performance for this reaction by operating at a significantly lower reaction temperature (200 °C) and developing selectivity to short-chain hydrocarbons (ethane and butane). The reaction pathway was elucidated from in situ DRIFT studies, which allowed monitoring of the species formed at different times during the catalytic cycle. From the spectra, it is clear that the Ni/CZ-C catalyst has a greater affinity to water, and therefore, as the temperature increases, the water dissociation happens more rapidly, which allows the catalytic cycle to be faster than NiCo/CZ-C catalyst. Moreover, both hydrogenation catalysts produce formate species, which get further hydrogenated to produce methoxy groups. For Nico/CZ-C catalyst, the combination of the distribution of Ni−Co and the high concentration of methoxy groups on the surface of the material makes it possible to couple and form products like ethane and butane. Identifying and characterizing these species is a crucial step toward understanding the pathways through which reactants transform into products.

EXPERIMENTAL SECTION

Synthesis of Mixed Oxide Supports $Ce_{0.6}Zr_{0.4}O_2$

Solutions were appropriately prepared with molar amounts of: $Ce(NH_4)_2(NO_3)_6$ was used as the Ce precursor, and $ZrO(NO_3)_2{\cdot}XH_2O$ and $ZrOCl_2{\cdot}8H_2O$ were used as the Zr precursors. Coprecipitation was produced by adding a 1.0 M solution of NH_4OH under constant stirring until reaching pH = 9.0. The precipitate was left for 2 h under constant stirring and was subsequently filtered and washed with distilled water until a neutral pH was reached. The filtered material was left to settle overnight (∼16 h) at room temperature. After this process, the support was dried at 120 °C for 24 h. Finally, the material was calcined at 500 °C for 5 h with a temperature ramp of 3 °C/min. To avoid the presence of problems due to diffusion controls, after calcination, the supports were granulated, ground and sieved with a particle size range of 80−120 mesh.

Catalyst Synthesis

The bimetallic catalysts based on Ni and Co were prepared by the pore filling technique (incipient impregnation), and salts of $Ni(NO_3)_3{\cdot}6H_2O$ and $Co(NO_3)_3{\cdot}6H_2O$ were used as precursors. After impregnation, the catalysts were dried at 120 °C for 24 h.

ASSOCIATED CONTENT

Supporting Information

The Supporting Information is available free of charge at https://pubs.acs.org/doi/10.1021/acsaenm.5c00055.

Additional experimental details and characterization, including PDRX, BET, SEM/EDX, H_2-TPR, CO_2-TPD and DRIFTS (PDF)

https://doi.org/10.1021/acsaenm.5c00055
ACS Appl. Eng. Mater. 2025, 3, 957−967

AUTHOR INFORMATION

Corresponding Authors

Jose Antonio de los Reyes − *Departamento de Ingeniería de Procesos e Hidráulica, División de Ciencias Básicas e Ingeniería, Universidad Autónoma Metropolitana-Iztapalapa, 09340 Ciudad de México, Mexico;* orcid.org/0000-0003-1962-9848; Email: argel@unam.mx

Ricardo A. Peralta − *Departamento de Química, División de Ciencias Básicas e Ingeniería, Universidad Autónoma Metropolitana-Iztapalapa, 09340 Ciudad de México, Mexico*; Email: rperalta@izt.uam.mx

Ilich A. Ibarra − *Laboratorio de Fisicoquímica y Reactividad de Superficies (LaFReS) Instituto de Investigaciones en Materiales, Universidad Nacional Autónoma de México, Circuito Exterior s/n, CU, 04510 Ciudad de México, Mexico;* orcid.org/0000-0002-8573-8033; Email: jarh@xanum.uam.mx

Authors

Víctor Martínez-Jiménez − *Departamento de Ingeniería de Procesos e Hidráulica, División de Ciencias Básicas e Ingeniería, Universidad Autónoma Metropolitana-Iztapalapa, 09340 Ciudad de México, Mexico*

J. Gabriel Flores − *Área de Química Aplicada, Departamento de Ciencias Básicas, Universidad Autónoma Metropolitana-Azcapotzalco, 02200 Ciudad de México, Mexico*

Bettina Baumgartner − *Inorganic Chemistry and Catalysis group, Debye Institute for Nanomaterials Science, Utrecht University, 3584 CG Utrecht, The Netherlands*

Juan L. Obeso − *Laboratorio Nacional de Ciencia, Tecnología y Gestión Integrada del Agua (LNAgua), Instituto Politécnico Nacional, CICATA U. Legaria, 11500 Ciudad de México, Mexico;* orcid.org/0000-0002-8876-9484

Catalina V. Flores − *Laboratorio Nacional de Ciencia, Tecnología y Gestión Integrada del Agua (LNAgua), Instituto Politécnico Nacional, CICATA U. Legaria, 11500 Ciudad de México, Mexico*

Bert M. Weckhuysen − *Inorganic Chemistry and Catalysis group, Debye Institute for Nanomaterials Science, Utrecht University, 3584 CG Utrecht, The Netherlands;* orcid.org/0000-0001-5245-1426

J. R. Rosas-Cedillo − *Departamento de Ingeniería de Procesos e Hidráulica, División de Ciencias Básicas e Ingeniería, Universidad Autónoma Metropolitana-Iztapalapa, 09340 Ciudad de México, Mexico*

Pablo Marín-Rosas − *Departamento de Química, División de Ciencias Básicas e Ingeniería, Universidad Autónoma Metropolitana-Iztapalapa, 09340 Ciudad de México, Mexico*

Raul Perez Hernandez − *Instituto Nacional de Investigaciones Nucleares. Carretera México-Toluca S/N La Marquesa, 52750 Ocoyoacac, Mexico;* orcid.org/0000-0002-8204-9662

Aida Gutierrez-Alejandre − *UNICAT, Departamento de Ingeniería Química, Facultad de Química, Universidad Nacional Autónoma de México, 04510 Ciudad de México, Mexico*

Eduardo González-Zamora − *Departamento de Química, División de Ciencias Básicas e Ingeniería, Universidad Autónoma Metropolitana-Iztapalapa, 09340 Ciudad de México, Mexico;* orcid.org/0000-0002-3995-9126

Complete contact information is available at: https://pubs.acs.org/10.1021/acsaenm.5c00055

Notes

The authors declare no competing financial interest.

ACKNOWLEDGMENTS

Thanks are due to CONAHCYT-México for funding through project CB-A1-S-41193 and PRONACES-321073. V. Martinez-Jimenez, thanks to CONAHCYT for the doctoral position (707700). J.G.F., thanks to CONAHCYT for the postdoctoral position (687839). J. L. Obeso thanks to CONAHCYT for the doctoral position (1003953). C.V. Flores thanks to CONAHCYT for the doctoral position (1040318). P.M.-R. thanks CONAHCyT for the MSc position (1277642).

ABBREVIATIONS

DRIFTS, diffuse reflectance infrared Fourier transform spectroscopy.; SSITKA, steady-state isotopic transient kinetic analysis.

REFERENCES

(1) He, M.; Sun, Y.; Han, B. Green carbon science: scientific basis for integrating carbon resource processing, utilization, and recycling. *Angew. Chem., Int. Ed.* **2013**, *52* (37), 9620−9633.

(2) Müller, K.; Städter, M.; Rachow, F.; Hoffmannbeck, D.; Schmeißer, D. Sabatier-based CO_2-methanation by catalytic conversion. *Environ. Earth Sci.* **2013**, *70* (8), 3771−3778.

(3) Centi, G.; Perathoner, S. Opportunities and prospects in the chemical recycling of carbon dioxide to fuels. *Catal. Today* **2009**, *148* (3−4), 191−205.

(4) Heynderickx, G. J.; Schools, E. M.; Marin, G. B. Coke combustion and gasification kinetics in ethane steam crackers. *AIChE J.* **2005**, *51* (5), 1415−1428.

(5) Peng, L.; Jurca, B.; Primo, A.; Gordillo, A.; Parvulescu, V. I.; Garcia, H. High C_2-C_4 selectivity in CO_2 hydrogenation by particle size control of Co-Fe alloy nanoparticles wrapped on N-doped graphitic carbon. *iScience* **2022**, *25* (5), 104252.

(6) Wang, F.; He, S.; Chen, H.; Wang, B.; Zheng, L.; Wei, M.; Evans, D. G.; Duan, X. Active Site Dependent Reaction Mechanism over Ru/CeO_2 Catalyst toward CO_2 Methanation. *J. Am. Chem. Soc.* **2016**, *138* (19), 6298−6305.

(7) Fakhroleslam, M.; Sadrameli, S. M. Thermal/catalytic cracking of hydrocarbons for the production of olefins; a state-of-the-art review III: Process modeling and simulation. *Fuel* **2019**, *252*, 553−566.

(8) Wang, S.; Zhang, L.; Zhang, W.; Wang, P.; Qin, Z.; Yan, W.; Dong, M.; Li, J.; Wang, J.; He, L.; et al. Selective Conversion of CO_2 into Propene and Butene. *Chem.* **2020**, *6* (12), 3344−3363.

(9) Asami, K.; Zhang, Q.; Li, X.; Asaoka, S.; Fujimoto, K. Semi-indirect synthesis of LPG from syngas: Conversion of DME into LPG. *Catal. Today* **2005**, *106* (1−4), 247−251.

(10) Do, T. N.; Kim, J. Green C_2-C_4 hydrocarbon production through direct CO_2 hydrogenation with renewable hydrogen: Process development and techno-economic analysis. *Energy Convers. Manage.* **2020**, *214*, 112866.

(11) Zhang, J.; Yang, Y.; Liu, J.; Xiong, B. Mechanistic understanding of CO_2 hydrogenation to methane over Ni/CeO_2 catalyst. *Appl. Surf. Sci.* **2021**, *558*, 149866.

(12) Ashok, J.; Ang, M. L.; Kawi, S. Enhanced activity of CO_2 methanation over Ni/CeO_2-ZrO_2 catalysts: Influence of preparation methods. *Catal. Today* **2017**, *281*, 304−311.

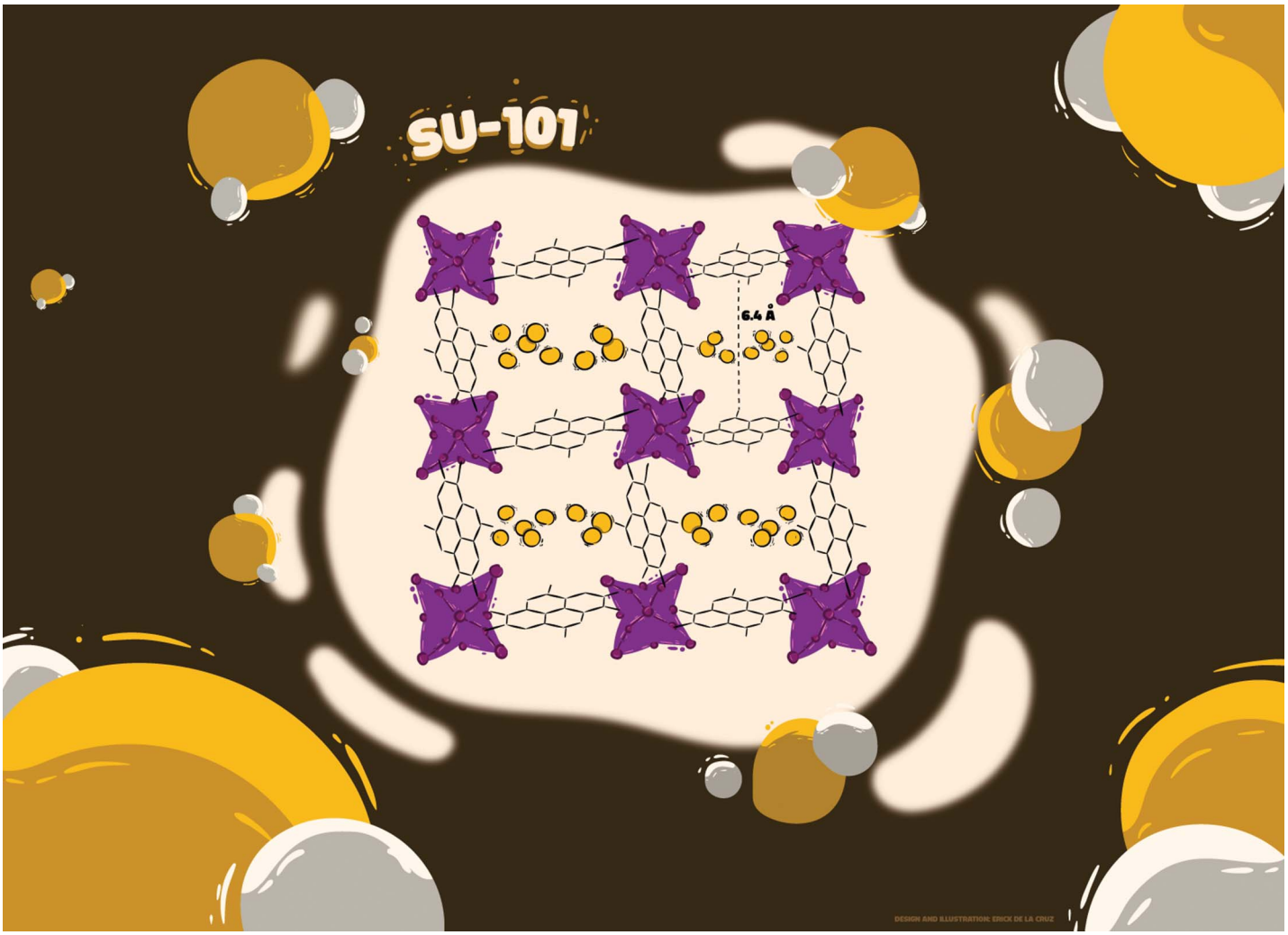
(13) Aldana, P. A. U.; Ocampo, F.; Kobl, K.; Louis, B.; Thibault-Starzyk, F.; Daturi, M.; Bazin, P.; Thomas, S.; Roger, A. C. Catalytic CO_2 valorization into CH_4 on Ni-based ceria-zirconia. Reaction mechanism by operando IR spectroscopy. *Catal. Today* **2013**, *215*, 201−207.

(14) Aziz, M. A. A.; Jalil, A. A.; Triwahyono, S.; Mukti, R. R.; Taufiq-Yap, Y. H.; Sazegar, M. R. Highly active Ni-promoted mesostructured

silica nanoparticles for CO_2 methanation. *Appl. Catal., B* **2014**, *147*, 359−368.
(15) Srisawad, N.; Chaitree, W.; Mekasuwandumrong, O.; Shotipruk, A.; Jongsomjit, B.; Panpranot, J. CO_2 hydrogenation over Co/Al_2O_3 catalysts prepared via a solid-state reaction of fine gibbsite and cobalt precursors. *React. Kinet., Mech. Catal.* **2012**, *107* (1), 179−188.
(16) Portillo-Vélez, N. S.; Velásquez-Torres, M. E.; Pérez-Hernández, R.; Ibarra, I. A.; Peralta, R. A.; Tzompantzi, F. Boosted Photocatalytic Activity of Zn/Al-Based Layered Double Hydroxides Through Cobalt Incorporation for Phenol Degradation. *ChemistrySelect* **2024**, *9* (14), No. e202304860.
(17) Aziz, M. A. A.; Jalil, A. A.; Triwahyono, S.; Ahmad, A. CO_2 methanation over heterogeneous catalysts: recent progress and future prospects. *Green Chem.* **2015**, *17* (5), 2647−2663.
(18) Ohashi, M.; Takahashi, Y.; Terakado, N.; Onoue, N.; Shinozaki, T.; Fujiwara, T. Repetitive afterglow in zirconia by pulsed near-infrared irradiation toward biological temperature sensing. *Sci. Rep.* **2022**, *12* (1), 8587.
(19) Groen, J. C.; Peffer, L. A. A.; Pérez-Ramírez, J. Pore size determination in modified micro- and mesoporous materials. Pitfalls and limitations in gas adsorption data analysis. *Microporous Mesoporous Mater.* **2003**, *60* (1−3), 1−17.
(20) Zhu, J.; Shaikhutdinov, S.; Cuenya, B. R. Structure-reactivity relationships in CO_2 hydrogenation to C_{2+} chemicals on Fe-based catalysts. *Chem. Sci.* **2025**, *16* (3), 1071−1092.
(21) Hatta, A. H.; Jalil, A. A.; Hassan, N. S.; Hamid, M. Y. S.; Haron, M. N.; Nabgan, W.; Bahari, M. B.; Asmadi, M.; Setiabudi, H. D. Ultra-high surface area fibrous silica-zirconia support for renewable energy production by CO_2 methanation. *J. Mol. Catal.* **2023**, *547*, 113311.
(22) Li, T.; Wang, S.; Gao, D.-n.; Wang, S.-d. Effect of support calcination temperature on the catalytic properties of $Ru/Ce_{0.8}Zr_{0.2}O_2$ for methanation of carbon dioxide. *J. Fuel Chem. Technol.* **2014**, *42* (12), 1440−1446.
(23) Numpilai, T.; Kidkhunthod, P.; Cheng, C. K.; Wattanakit, C.; Chareonpanich, M.; Limtrakul, J.; Witoon, T. CO_2 hydrogenation to methanol at high reaction temperatures over In_2O_3/ZrO_2 catalysts: Influence of calcination temperatures of ZrO_2 support. *Catal. Today* **2021**, *375*, 298−306.
(24) Atzori, L.; Rombi, E.; Meloni, D.; Monaci, R.; Sini, M. F.; Cutrufello, M. G. Nanostructured Ni/CeO_2-ZrO_2 Catalysts for CO_2 Conversion into Synthetic Natural Gas. *J. Nanosci. Nanotechnol.* **2019**, *19* (6), 3269−3276.
(25) Tsiotsias, A. I.; Charisiou, N. D.; Yentekakis, I. V.; Goula, M. A. Bimetallic Ni-Based Catalysts for CO_2 Methanation: A Review. *Nanomaterials* **2021**, *11* (1), 28.
(26) Riani, P.; Spennati, E.; Garcia, M. V.; Escribano, V. S.; Busca, G.; Garbarino, G. Ni/Al_2O_3 catalysts for CO_2 methanation: Effect of silica and nickel loading. *Int. J. Hydrogen Energy* **2023**, *48* (64), 24976−24995.
(27) Kesavan, J. K.; Luisetto, I.; Tuti, S.; Meneghini, C.; Iucci, G.; Battocchio, C.; Mobilio, S.; Casciardi, S.; Sisto, R. Nickel supported on YSZ: The effect of Ni particle size on the catalytic activity for CO_2 methanation. *J. CO_2 Util.* **2018**, *23*, 200−211.
(28) Miao, B.; Ma, S. S. K.; Wang, X.; Su, H.; Chan, S. H. Catalysis mechanisms of CO_2 and CO methanation. *Catal. Sci. Technol.* **2016**, *6* (12), 4048−4058.
(29) Agnelli, M.; Swaan, H. M.; Marquez-Alvarez, C.; Martin, G. A.; Mirodatos, C. CO Hydrogenation on a Nickel Catalyst: II. A Mechanistic Study by Transient Kinetics and Infrared Spectroscopy. *J. Catal.* **1998**, *175* (1), 117−128.
(30) Vrijburg, W. L.; van Helden, J. W. A.; Parastaev, A.; Groeneveld, E.; Pidko, E. A.; Hensen, E. J. M. Ceria−zirconia encapsulated Ni nanoparticles for CO_2 methanation. *Catal. Sci. Technol.* **2019**, *9* (18), 5001−5010.
(31) Ren, J.; Qin, X.; Yang, J.-Z.; Qin, Z.-F.; Guo, H.-L.; Lin, J.-Y.; Li, Z. Methanation of carbon dioxide over $Ni-M/ZrO_2$ (M = Fe, Co, Cu) catalysts: Effect of addition of a second metal. *Fuel Process. Technol.* **2015**, *137*, 204−211.
(32) Vasiliades, M. A.; Djinović, P.; Pintar, A.; Kovač, J.; Efstathiou, A. M. The effect of CeO_2−ZrO_2 structural differences on the origin and reactivity of carbon formed during methane dry reforming over $NiCo/CeO_2$−ZrO_2 catalysts studied by transient techniques. *Catal. Sci. Technol.* **2017**, *7* (22), 5422−5434.
(33) Lee, Y. H.; Ahn, J. Y.; Nguyen, D. D.; Chang, S. W.; Kim, S. S.; Lee, S. M. Role of oxide support in Ni based catalysts for CO_2 methanation. *RSC Adv.* **2021**, *11* (29), 17648−17657.
(34) Le, T. A.; Kim, M. S.; Lee, S. H.; Kim, T. W.; Park, E. D. CO and CO_2 methanation over supported Ni catalysts. *Catal. Today* **2017**, *293*−*294*, 89−96.
(35) Zhang, J.; Wang, H.; Dalai, A. K. Development of stable bimetallic catalysts for carbon dioxide reforming of methane. *J. Catal.* **2007**, *249* (2), 300−310.
(36) Wei, C.; Ding, H.; Zhang, Z.; Lin, F.; Xu, Y.; Pan, W. Research progress of bimetallic catalysts for CO_2 hydrogenation to methane. *Int. J. Hydrogen Energy* **2024**, *58*, 872−891.
(37) Wang, W.; Toshcheva, E.; Ramirez, A.; Shterk, G.; Ahmad, R.; Caglayan, M.; Cerrillo, J. L.; Dokania, A.; Clancy, G.; Shoinkhorova, T. B.; et al. Bimetallic Fe−Co catalysts for the one step selective hydrogenation of CO_2 to liquid hydrocarbons. *Catal. Sci. Technol.* **2023**, *13* (5), 1527−1540.
(38) Takanabe, K.; Nagaoka, K.; Nariai, K.; Aika, K. Titania-supported cobalt and nickel bimetallic catalysts for carbon dioxide reforming of methane. *J. Catal.* **2005**, *232* (2), 268−275.
(39) Xu, L.; Lian, X.; Chen, M.; Cui, Y.; Wang, F.; Li, W.; Huang, B. CO_2 methanation over Co Ni bimetal-doped ordered mesoporous Al_2O_3 catalysts with enhanced low-temperature activities. *Int. J. Hydrogen Energy* **2018**, *43* (36), 17172−17184.
(40) Md Ali, S. A.; Ku Hamid, K. H.; Ismail, K. N. Effect of Ni/Co Ratio on Bimetallic Oxide Supported Silica Catalyst in CO_2 Methanation. *AMM* **2015**, *802*, 431−436.
(41) Guo, M.; Lu, G. The effect of impregnation strategy on structural characters and CO_2 methanation properties over MgO modified Ni/SiO_2 catalysts. *Catal. Commun.* **2014**, *54*, 55−60.
(42) Mutz, B.; Belimov, M.; Wang, W.; Sprenger, P.; Serrer, M.-A.; Wang, D.; Pfeifer, P.; Kleist, W.; Grunwaldt, J.-D. Potential of an Alumina-Supported Ni_3Fe Catalyst in the Methanation of CO_2: Impact of Alloy Formation on Activity and Stability. *ACS Catal.* **2017**, *7* (10), 6802−6814.
(43) Gothe, M. L.; Figueredo, A. L.; Borges, L. R.; Ramos, R.; Peixoto, A. F.; Vidinha, P. High-Pressure Hydrogenation: A Path to Efficient Methane Production from CO_2. *Methane* **2024**, *3* (1), 53−64.
(44) Iloy, R. A.; Jalama, K. Effect of Operating Temperature, Pressure and Potassium Loading on the Performance of Silica-Supported Cobalt Catalyst in CO_2 Hydrogenation to Hydrocarbon Fuel. *Catalysts* **2019**, *9* (10), 807.
(45) Yarbaş, T.; Ayas, N. A detailed thermodynamic analysis of CO_2 hydrogenation to produce methane at low pressure. *Int. J. Hydrogen Energy* **2024**, *49*, 1134−1144.
(46) Gao, J.; Wang, Y.; Ping, Y.; Hu, D.; Xu, G.; Gu, F.; Su, F. A thermodynamic analysis of methanation reactions of carbon oxides for the production of synthetic natural gas. *RSC Adv.* **2012**, *2* (6), 2358.
(47) Yu, Y.; Bian, Z.; Song, F.; Wang, J.; Zhong, Q.; Kawi, S. Influence of Calcination Temperature on Activity and Selectivity of $Ni-CeO_2$ and $Ni-Ce_{0.8}Zr_{0.2}O_2$ Catalysts for CO_2 Methanation. *Top. Catal.* **2018**, *61* (15−17), 1514−1527.
(48) Bian, Z.; Chan, Y. M.; Yu, Y.; Kawi, S. Morphology dependence of catalytic properties of Ni/CeO_2 for CO_2 methanation: A kinetic and mechanism study. *Catal. Today* **2020**, *347*, 31−38.
(49) Tada, S.; Shimizu, T.; Kameyama, H.; Haneda, T.; Kikuchi, R. Ni/CeO_2 catalysts with high CO_2 methanation activity and high CH_4 selectivity at low temperatures. *Int. J. Hydrogen Energy* **2012**, *37* (7), 5527−5531.
(50) Cored, J.; Garcia-Ortiz, A.; Iborra, S.; Climent, M. J.; Liu, L.; Chuang, C. H.; Chan, T. S.; Escudero, C.; Concepcion, P.; Corma, A. Hydrothermal Synthesis of Ruthenium Nanoparticles with a Metallic Core and a Ruthenium Carbide Shell for Low-Temperature

Activation of CO_2 to Methane. *J. Am. Chem. Soc.* **2019**, *141* (49), 19304−19311.
(51) Yan, B.; Zhao, B.; Kattel, S.; Wu, Q.; Yao, S.; Su, D.; Chen, J. G. Tuning CO_2 hydrogenation selectivity via metal-oxide interfacial sites. *J. Catal.* **2019**, *374*, 60−71.
(52) Westermann, A.; Azambre, B.; Bacariza, M. C.; Graça, I.; Ribeiro, M. F.; Lopes, J. M.; Henriques, C. Insight into CO_2 methanation mechanism over NiUSY zeolites: An operando IR study. *Appl. Catal., B* **2015**, *174*−*175*, 120−125.
(53) Panagiotopoulou, P.; Kondarides, D. I.; Verykios, X. E. Mechanistic aspects of the selective methanation of CO over Ru/TiO_2 catalyst. *Catal. Today* **2012**, *181* (1), 138−147.
(54) Pan, Q.; Peng, J.; Wang, S.; Wang, S. In situ FTIR spectroscopic study of the CO_2 methanation mechanism on Ni/$Ce_{0.5}Zr_{0.5}O_2$. *Catal. Sci. Technol.* **2014**, *4* (2), 502−509.
(55) Kattel, S.; Liu, P.; Chen, J. G. Tuning Selectivity of CO_2 Hydrogenation Reactions at the Metal/Oxide Interface. *J. Am. Chem. Soc.* **2017**, *139* (29), 9739−9754.
(56) Gao, J.; Jia, C.; Liu, B. Direct and selective hydrogenation of CO_2 to ethylene and propene by bifunctional catalysts. *Catal. Sci. Technol.* **2017**, *7* (23), 5602−5607.
(57) Wang, H.; Fan, S.; Guo, S.; Wang, S.; Qin, Z.; Dong, M.; Zhu, H.; Fan, W.; Wang, J. Selective conversion of CO_2 to isobutane-enriched C_4 alkanes over $InZrO_x$-Beta composite catalyst. *Nat. Commun.* **2023**, *14* (1), 2627.
(58) Badoga, S.; Martinelli, M.; Gnanamani, M. K.; Koh, Y.; Shafer, W. D. New mechanism insight for the hydrogenation of CO/CO_2 gas mixtures to hydrocarbons over iron-based catalyst. *Catal. Commun.* **2021**, *152*, 106284.
(59) Alkhoori, A. A.; Elmutasim, O.; Dabbawala, A. A.; Vasiliades, M. A.; Petallidou, K. C.; Emwas, A.-H.; Anjum, D. H.; Singh, N.; Baker, M. A.; Charisiou, N. D.; et al. Mechanistic Features of the CeO_2-Modified Ni/Al_2O_3 Catalysts for the CO_2 Methanation Reaction: Experimental and Ab Initio Studies. *ACS Appl. Energy Mater.* **2023**, *6* (16), 8550−8571.
(60) Simons, J. F. M.; de Heer, T. J.; van de Poll, R. C. J.; Muravev, V.; Kosinov, N.; Hensen, E. J. M. Structure Sensitivity of CO_2 Hydrogenation on Ni Revisited. *J. Am. Chem. Soc.* **2023**, *145* (37), 20289−20301.

https://doi.org/10.1021/acsaenm.5c00055
ACS Appl. Eng. Mater. 2025, 3, 957−967



Showcasing research from Prof. Diego Solis-Ibarra (Director of the Institute for Materials Research), Prof. Ilich Ibarra (Laboratorio de Fisocoquímica y Reactiviadad de Superficies, LaFReS-UNAM) and Prof. Ricardo Peralta (Departamento de Química, Universidad Autónoma Metropolitana (UAM-I), Mexico City, Mexico).

Formation of polysulfides as a smart strategy to selectively detect H_2S in a Bi(III)-based MOF material

SU-101 was demonstrated to be an effective and efficient detector for H_2S, due to the facile generation of polysulfides, with a remarkable H_2S selectivity. Remarkably, the limit of H_2S detection (LOD) was calculated to be as low as approximately 22 ppm, nominating this material as a promising candidate for implementing toxic waste valorisation (i.e., capture of toxic H_2S) toward relevant applications in accurate molecular sensing.

Image reproduced by permission of Ilich A. Ibarra from *Chem. Sci.*, 2025, **16**, 5483.

As featured in:



See Diego Solis-Ibarra, Ricardo A. Peralta, Ilich A. Ibarra *et al.*, *Chem. Sci.*, 2025, **16**, 5483.

ROYAL SOCIETY OF CHEMISTRY

15 YEARS ANNIVERSARY

rsc.li/chemical-science

Registered charity number: 207890

Chemical Science

ROYAL SOCIETY OF CHEMISTRY

EDGE ARTICLE

View Article Online
View Journal | View Issue

Check for updates

Cite this: *Chem. Sci.*, 2025, **16**, 5483

All publication charges for this article have been paid for by the Royal Society of Chemistry

Open Access Article. Published on 19 February 2025. Downloaded on 6/30/2025 11:45:30 PM. This article is licensed under a Creative Commons Attribution 3.0 Unported Licence.

Formation of polysulfides as a smart strategy to selectively detect H_2S in a Bi(III)-based MOF material†

Valeria B. López-Cervantes, ‡[a] Juan L. Obeso, ‡[ab] J. Gabriel Flores,‡[cd] Aída Gutiérrez-Alejandre, [e] Raul A. Marquez, [f] José Antonio de los Reyes,[d] Catalina V. Flores, [ab] N. S. Portillo-Vélez, [g] Pablo Marín-Rosas,[g] Christian A. Celaya,[h] Eduardo González-Zamora, [g] Diego Solis-Ibarra, *[a] Ricardo A. Peralta *[g] and Ilich A. Ibarra *[ai]

SU-101 was demonstrated to be an effective and efficient detector for H_2S, due to the facile generation of polysulfides, with a remarkable H_2S selectivity. Raman and XPS analyses confirmed the formation of S_n^{2-} and S_4^{2-} polysulfide species after the H_2S adsorption (at 0.05 bar, 0.1 bar and 1 bar), without compromising the structural integrity of SU-101. The detection mechanism involves rigidification of the structure by the formation of the polysulfides and blockage of the ligand–metal charge transfer (LMCT) process, which increased the radiative emission. Additionally, theoretical simulations were carried out in order to demonstrate that the interaction of the polysulfide molecules inside the pores of SU-101 is energetically stable. Remarkably, the limit of H_2S detection (LOD) was calculated to be as low as approximately 22 ppm. Finally, SU-101 is nominated as a promising candidate for implementing toxic waste valorisation (*i.e.*, capture of toxic H_2S) toward relevant applications in accurate molecular sensing.

Received 21st October 2024
Accepted 13th February 2025

DOI: 10.1039/d4sc07144a

rsc.li/chemical-science

Introduction

Hydrogen sulphide (H_2S) is a toxic chemical in natural gas and biogas commonly emitted by different chemical industries. The desulphurization process of diverse gas streams (*e.g.*, oil refineries) is the primary source of H_2S emissions.[1] H_2S is a colourless gas that is extremely corrosive, flammable, and lethal to humans.[2] H_2S is classified as a dangerous and major air pollutant, mostly associated with acid rain and severe nervous system illnesses.[3]

Thus, the efficient detection of H_2S is desired for a cleaner environment and for human health protection. The development of methodologies for selective monitoring of H_2S is necessary. Different technologies have been reported for H_2S detection, such as colorimetry,[4] electrochemical,[5] and gas chromatography.[6] However, implementing these methodologies requires a high measurement time and high complexity devices, which leads to a decrease in the possibility of practical applications.[7] However, fluorescence techniques are much simpler alternatives for promising and potential H_2S detection since the measurement method is reliable, user-friendly, convenient, and fast.[8]

Furthermore, different materials and strategies have been implemented for fluorescence detection of H_2S. Carbon-based materials have been used to detect H_2S in aqueous conditions and live cells.[9] Silver nanoparticles were applied for H_2S sensing in water.[10] An alumina–graphene oxide nanocomposite was used for H_2S detection in lake water.[11] However, most of these materials are classified as free organic–inorganic molecules, which could exhibit fluorescence issues due to their molecular motion.[12] Also, H_2S detection is based on small molecules as fluorescent

[a]*Laboratorio de Fisicoquímica y Reactividad de Superficies (LaFReS), Instituto de Investigaciones en Materiales, Universidad Nacional Autónoma de México, Circuito Exterior s/n, CU, Coyoacán, 04510, Ciudad de México, Mexico. E-mail: argel@unam.mx*

[b]*Instituto Politécnico Nacional, CICATA U. Legaria, Laboratorio Nacional de Ciencia, Tecnología y Gestión Integrada del Agua (LNAgua), Legaria 694, Irrigación, 11500, CDMX, Mexico*

[c]*Área de Química Aplicada, Departamento de Ciencias Básicas, Universidad Autónoma Metropolitana-Azcapotzalco, 02200, Ciudad de México, Mexico*

[d]*Departamento de Ingeniería de Procesos e Hidráulica, División de Ciencias Básicas e Ingeniería, Universidad Autónoma Metropolitana-Iztapalapa, 09340, Ciudad de México, Mexico*

[e]*UNICAT, Departamento de Ingeniería Química, Facultad de Química, Universidad Nacional Autónoma de México, 04510 Ciudad de México, Mexico*

[f]*Department of Chemistry, The University of Texas at Austin, Austin, Texas 78712, USA*

[g]*Departamento de Química, División de Ciencias Básicas e Ingeniería. Universidad Autónoma Metropolitana (UAM-I), 09340, Mexico. E-mail: rperalta@izt.uam.mx*

[h]*Centro de Nanociencias y Nanotecnología, Universidad Nacional Autónoma de México, Km 107 Carretera Tijuana-Ensenada, Ensenada, B.C., C.P. 22800, Mexico*

[i]*Departamento de Química, Universidad Autónoma Metropolitana-Iztapalapa, Avenida San Rafael Atlixco 186, Leyes de Reforma 1ra Sección, Iztapalapa, Ciudad de México 09310, Mexico*

† Electronic supplementary information (ESI) available: Instrumental techniques and characterization. See DOI: https://doi.org/10.1039/d4sc07144a

‡ These authors contributed equally to this manuscript.

© 2025 The Author(s). Published by the Royal Society of Chemistry

Open Access Article. Published on 19 February 2025. Downloaded on 6/30/2025 11:45:30 PM.
This article is licensed under a Creative Commons Attribution 3.0 Unported Licence.

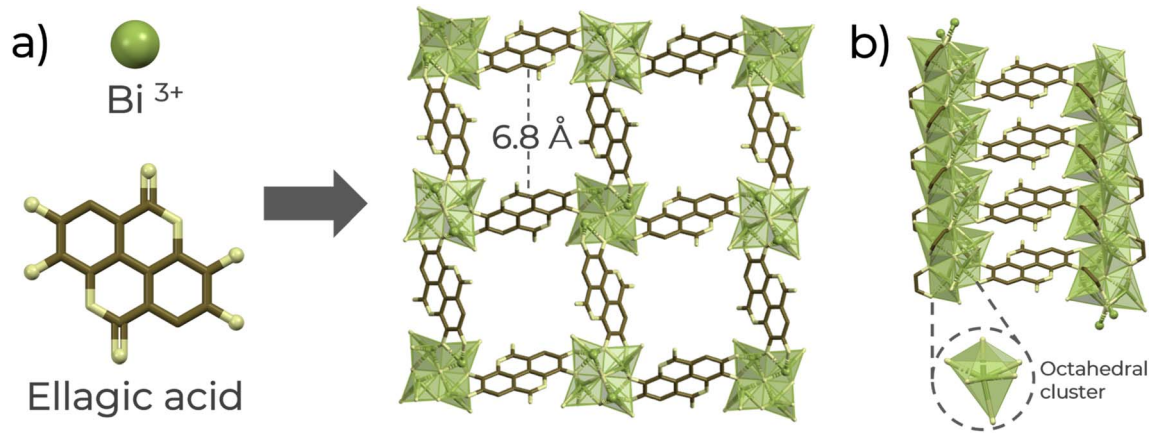


Fig. 1 (a) Schematic of the formation of the SU-101 structure along the channel *a*-axis and (b) metal cluster and linker arrangement along the *a*-axis. Atoms label: green: Bi^{3+} octahedra, brown: carbon, and yellow: oxygen.

probes, such as inorganic sulphide salts (NaHS and Na_2S). The detection is based on a chemical reaction between the material and the molecular probe *via* a nucleophilic attack, reduction, and precipitation to generate a fluorescence change.[13] The implementation of robust materials for the detection of H_2S molecules, by relatively strong interactions between H_2S and the pore walls of the materials is highly desirable.

In this context, a comparatively novel class of highly crystalline and porous materials known as metal–organic frameworks (MOFs) has been recently explored for molecule detection.[14] Based on some recent research in H_2S adsorption,[15] the high chemical stability, and the apparent advantages by only using small quantities,[16] MOF materials are promising candidates for H_2S detection. For example, fluorescence detection using MOF materials has been studied for detecting water pollutants,[17] explosives[18] and aromatic compounds.[19] Specifically, MOF materials are also applied to detect H_2S in the gas phase, for example, a Zr-MOF was used as a fluorescence turn-on detector for H_2S.[20] However, the fluoresce detection in the gas phase or the H_2S quantification is poorly studied using MOF materials.

Thus, a chemically stable Bi(III)-based MOF material denoted as SU-101 (ref. 21) (microporous bismuth ellagate framework ($Bi_2O(H_2O)_2(C_{14}H_2O_8)\cdot nH_2O$), $C_{14}H_2O_8$ = ellagate) was selected to investigate qualitative H_2S detection in the gas phase and quantitative sensing using a solution of H_2S in dry THF. SU-101 shows each Bi(III) metal centre is six coordinated, establishing three bonds with coordinating phenolates, two μ_4-oxygens, and a terminally coordinated water molecule (Fig. 1), which can be removed after an activation process.[21] Previously, SU-101 was reported for H_2S adsorption, where it was demonstrated that the H_2S adsorption generates spontaneous conversion into polysulfides.[21,22] Then, taking advantage of such specific chemical transformation, the detection of H_2S with SU-101 was investigated.

Experimental section

Synthesis of SU-101

SU-101 was synthesised following a previously reported procedure.[21] 0.015 g of ellagic acid and 0.038 g of bismuth(III) acetate were dissolved in 30 mL of a water and acetic acid mixture (6 vol% acetic acid). First, the solution was stirred vigorously at room temperature for 48 h. Later, the recovered powder was washed three times with water and ethanol. After that, the powder was dried overnight at 60 °C. Subsequently, the material was activated at 150 °C and under vacuum to evacuate any molecule trapped within the pores of SU-101.

Instruments

Detailed information on the instrumental techniques is available in Section S1.

Fluorescence experiments

Emission spectra were taken in an Edinburgh Instrument FS5 fluorimeter using a continuous wave 150 W ozone-free xenon arc lamp at room temperature, coupled with an SC-10 solid-state sample holder. Measurements were carried out using an excitation wavelength of 370 nm, with a 395 nm long-pass filter on the detector side to remove any remaining light from the excitation source. The measurements were collected with a step size of 1 nm and a dwell time of 0.2 s. The excitation bandwidth was set at 5 nm, and the emission bandwidth for the detector was set at 1 nm. Decay time spectra were measured by exciting the sample with a picosecond pulsed light emitting diode EPL-375 with an excitation wavelength of 374.2 nm and a pulse width of 52.9 ps at an emission wavelength of 460 nm. The samples were packed into quartz sample holders and positioned into the instrument for solid-state measurements. Both the activated and saturated samples were packed right after being taken out of the activation and saturation processes. A suspension of SU-101 in THF (1 mg mL^{-1}) was prepared for the solution measurements. Also, solutions of H_2S in THF at different concentrations (10–100 mM) were prepared. In this case, 2.5 mL of the SU-101 suspension and 0.5 mL of the various concentrations of H_2S were mixed and measured.

Computational methods

DFT calculations. To investigate the electronic structure properties of the SU-101 system, we performed density

© 2025 The Author(s). Published by the Royal Society of Chemistry

Open Access Article. Published on 19 February 2025. Downloaded on 6/30/2025 11:45:30 PM. This article is licensed under a Creative Commons Attribution 3.0 Unported Licence.

functional theory (DFT) calculations using SIESTA 4.1 (Spanish Initiative for Electronic Simulations with Thousands of Atoms) *ab initio* code.[23] The geometries were optimised with the generalised gradient approximation (GGA), employing the Perdew–Burke–Ernzerhof (PBE) exchange–correlation functional to describe the electronic properties.[24] Troullier–Martins pseudopotentials were applied,[25] along with a single-ζ basis set, and an energy shift of 150 meV. The calculations adhered to stringent convergence criteria: 1×10^{-4} for total energy and electron density, and Hellmann–Feynman forces were converged to less than 0.05 eV $Å^{-1}$ during structure optimization. An electronic temperature of 298 K was set for orbital occupation calculations using the Fermi–Dirac function. The Brillouin zone was sampled with a Monkhorst–Pack grid of $2 \times 2 \times 3$ *k*-point for the modelled supercell. For optical properties, the imaginary part of the dielectric function was calculated using SIESTA code, which incorporates first-order dependent perturbation theory.[26]

Results and discussion

Characterization of SU-101

Powder X-ray diffraction (PXRD) confirmed the phase purity of SU-101 (Fig. S1†). At 2θ, peaks at 6.7, 9.6, 13.4, and 26.7° can be observed, which are in good agreement with the pure crystal structure.[21] Fourier transform infrared (FT-IR) spectroscopy shows specific bands for the functional groups of SU-101 (Fig. S2†). The bands at 1703 and 1056 cm^{-1} are related to C=O stretching and O–H in-plane deformation from the organic linker.[21] The band at 1367 cm^{-1} confirms the chemical coordination between the ellagic acid and the Bi^{3+} sites. The characteristic band of phenolate stretching vibration in the ellagate anion at 3411 cm^{-1} is observed. The band at 1465 cm^{-1} is related to the aromatic ring vibrations.[21] The TGA profile of SU-101 (Fig. S3†) shows moderate thermal stability up to 280 °C and indicates that the guest solvent molecules can be removed at 150 °C after activation. SEM images (Fig. S4†) show the morphology characteristics of SU-101, displaying a homogeneous columnar crystal.

H_2S adsorption performance

Prior to the detection performance for SU-101, an activated sample was evaluated for H_2S uptake. A breakthrough H_2S experiment (4.3 vol% H_2S with 95.7 vol% of N_2) led to a gas uptake of 15.64 mmol g^{-1}, *i.e.*, 531 mg g^{-1} (Fig. S6†). This H_2S capture value is in good correlation with the previous value reported (15.95 mmol g^{-1}, *i.e.*, 542 mg g^{-1}),[21] and on a second H_2S adsorption cycle, the initial capacity was lost (0.1 mmol g^{-1}, Fig. S7†), which confirms the formation of polysulfides inside the pores of SU-101, as we previously observed.[21] The chemical stability was confirmed by PXRD (Fig. S8†); moreover, the effectiveness of SU-101 in detecting H_2S due to the chemical transformation of H_2S into polysulfides was evaluated. As a proof of concept, the conversion of H_2S (to polysulfides) as a function of time was analysed using gas chromatography (Table S1†). The conversion of H_2S was observed from 0.06 mmol g^{-1} at 120 s to 0.73 mmol g^{-1} at 670 s. It is worth mentioning that once SU-101 is exposed to H_2S, due to the chemical transformation to polysulfides, the sample cannot be re-used (re-activated).

Fluorescence H_2S detection

Furthermore, the fluorescence detection of H_2S using SU-101 was performed. First, the UV-Vis spectra of SU-101 were recorded (Fig. 3d). It was identified that at 390 nm, the material can be excited. The photoluminescence (PL) emission was measured at different excitation wavelengths (Fig. S9†). It shows a broad PL peak centred at 461 nm. The higher intensity was at the excitation wavelength of 370 nm. Subsequently, the PL emission spectra of the organic linker and SU-101 were recorded (Fig. 2a). The linker shows an emission maximum at 465 nm, whereas that of SU-101 is at 461 nm. The intense emission from the organic ligand could be related to a $\pi^* \rightarrow \pi$ electronic transition, typical in conjugated bonded systems.[27] It is observed that after the formation of SU-101, the emission from the linker is quenched, which is associated with a ligand–metal charge transfer.[28] The LMCT process occurs when, upon excitation of the system, an electron in a π^* orbital of the ligand is transferred to an empty d orbital of the metal. In the case of SU-101, Bi(III) accepts charge from the linker (ellagic acid). After coordination, the interaction between the ligand and metal orbitals can result in a slight increase in the energy difference between the excited and fundamental states,[29] which causes the emission maximum to slightly blueshift (toward 461 nm, shorter wavelengths).[30] This charge transfer also decreases the intrinsic fluorescence of the ligand at the competition between two processes: the fluorescence emission from the excited state of the ligand and the non-radiative transfer of energy to the metal.[31] As a result, the observed emission from SU-101 is not only from the ligand but is a combined phenomenon in which the charge is redistributed between the ligand and the metal.[32]

It is worth mentioning that, after the activation process, host molecules such as water, solvents or other adsorbates that may be occupying the pores of the MOF are removed. These molecules may be attenuating the fluorescence of SU-101 in its pristine state by facilitating certain non-radiative energy dissipation mechanisms, and upon removal the MOF framework is freer to emit light, resulting in higher emission efficiency. Moreover, to determine the change in the fluorescent behaviour, SU-101 was exposed to different gases (H_2S, H_2O, CO_2, and air) in an in-house designed *ex situ* adsorption system (Fig. S5†). From H_2O, CO_2, and air exposed SU-101 samples, the PL emission spectra are similar to those of the as-synthesized SU-101 (Fig. 2c), and slight minor changes are observed after exposure to these gases. However, after the exposure to H_2S, the PL emission spectra increased by 62.45% concerning the emission of activated SU-101 (and 289% concerning the as-synthesized emission), indicating the high selectivity for H_2S (Fig. 2b). This PL change in intensity could be accredited to a turn-on effect due to the electronic outcome that H_2S applies to the SU-101 framework.[33] Then, a reproducibility test was conducted (Fig. S10†). Five independent samples of SU-101 were saturated with H_2S, and consistently, the same turn-on performances were found.

Open Access Article. Published on 19 February 2025. Downloaded on 6/30/2025 11:45:30 PM.
This article is licensed under a Creative Commons Attribution 3.0 Unported Licence.

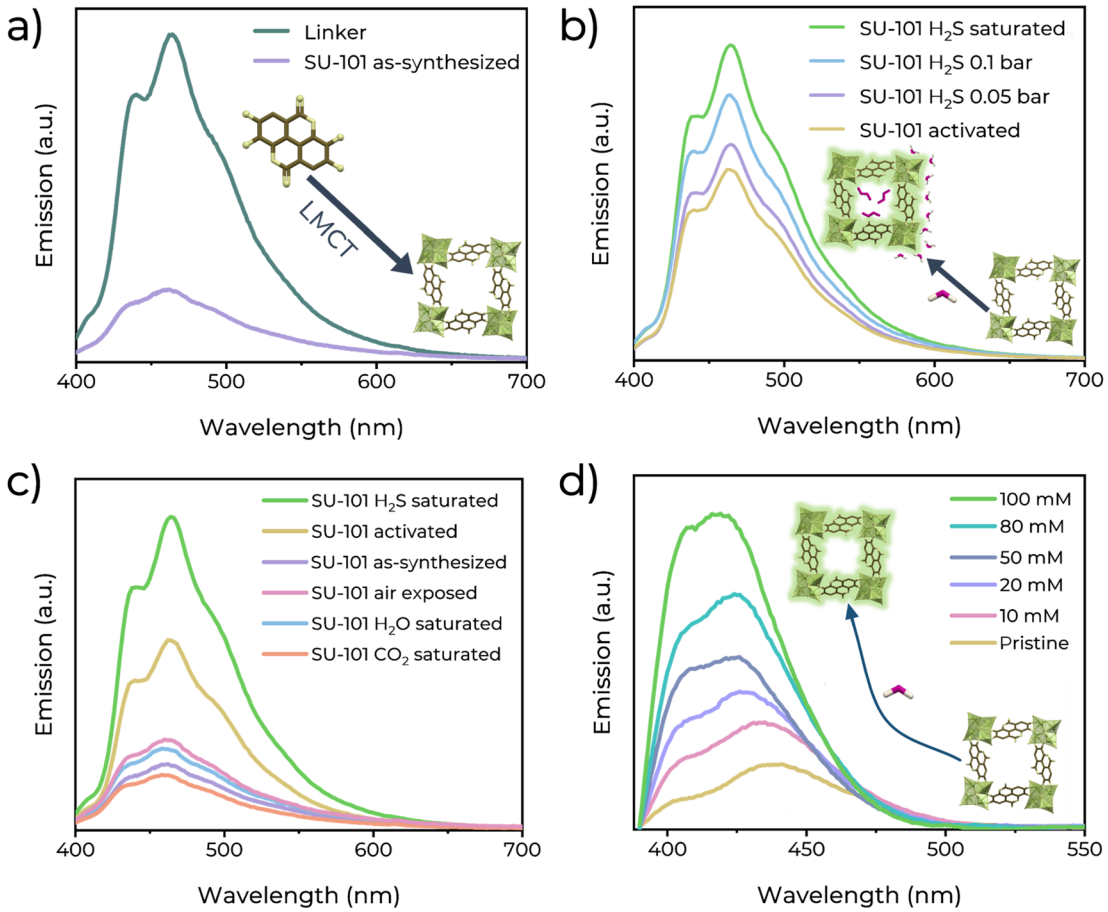


Fig. 2 (a) Solid-state emission spectra of the ellagic acid linker (brown) and as-synthesized SU-101 (yellow). (b) Comparison of the solid-state emission spectra of activated SU-101 and SU-101 exposed to different H_2S gas pressures. (c) Comparison of the solid-state emission spectra of SU-101 exposed to air, water vapour and different gases. (d) Fluorescence emission spectra of dispersed SU-101 in H_2S solutions in THF.

Then, the detection properties of SU-101 under non-saturated H_2S conditions: low H_2S pressure. H_2S pressure can be correlated with H_2S detection at low H_2S concentrations, and therefore, we needed to investigate any photoluminescence response at low H_2S pressures (0.05 and 0.1 bar, Fig. 2b). First, an activated sample of SU-101 was exposed to 0.05 bar H_2S, and the emission spectrum was measured. Interestingly, the broad photoluminescence peak remained centred at 461 nm, and an increase in emission intensity of approximately 13.74% with respect to the pristine sample (and 168.07% with respect to the as-synthesized emission) was observed. Later, an independent activated sample of SU-101 was exposed to 0.1 bar H_2S, and an increase in emission intensity of approximately 37.93% with respect to the activated sample (and 225.11% concerning the as-synthesized emission) was recorded.

Furthermore, the quantitative response (sensing) of SU-101 for H_2S was measured using a solution of H_2S in dry THF (Fig. 2d). It is observed that an enhancement in the PL emission is a function of the increased H_2S concentration (10–100 mM). The limit of detection (LOD) value was calculated with the following formula: LOD $= 3\sigma/m$ (signal-to-noise ratio, S/N = 3), where σ represents the standard deviation of the initial intensity of SU-101 in dry THF and m is the slope of the linear fit from the experimental data (Fig. S11†). The plot of fluorescence intensity *vs.* H_2S concentration exhibited an excellent linear correlation ($R^2 = 0.9628$), and the LOD was calculated to be as low as 0.65 mM (~22.16 ppm) H_2S.

Fluorescence mechanism

Finally, to investigate the plausible mechanism of H_2S detection by SU-101, X-ray photoelectron spectroscopy (XPS), Raman spectroscopy, UV-vis spectroscopy, and time-resolved photoluminescence (TRPL) experiments were conducted. XPS analysis confirmed the formation of polysulphide in SU-101; a 225 eV signal appears in the survey spectra after saturation with H_2S (Fig. 3a), which is associated with the appearance of S 2s.[34] The Bi 4f region was inspected in detail (Fig. 3b) and shows two unequal peaks at 159.3 and 164.6 eV associated with Bi $4f_{7/2}$ and $4f_{5/2}$, displaying a separation of 5.3 eV, which is in line with the Bi^{3+} oxidation state.[35] In addition, a small peak is observed at around 161.7 eV, and is assigned to terminal sulphur atoms (n-S_T^{-1}) in polysulfide compounds, indicating that a short-chain polysulfide is present after the H_2S saturation.[36] For the S 2s region it is observed that the spectrum of pristine SU-101 shows a flat signal (Fig. 3c), but in contrast, for the H_2S saturated material a signal corresponding to the different sulphur states

© 2025 The Author(s). Published by the Royal Society of Chemistry

Open Access Article. Published on 19 February 2025. Downloaded on 6/30/2025 11:45:30 PM.
This article is licensed under a Creative Commons Attribution 3.0 Unported Licence.

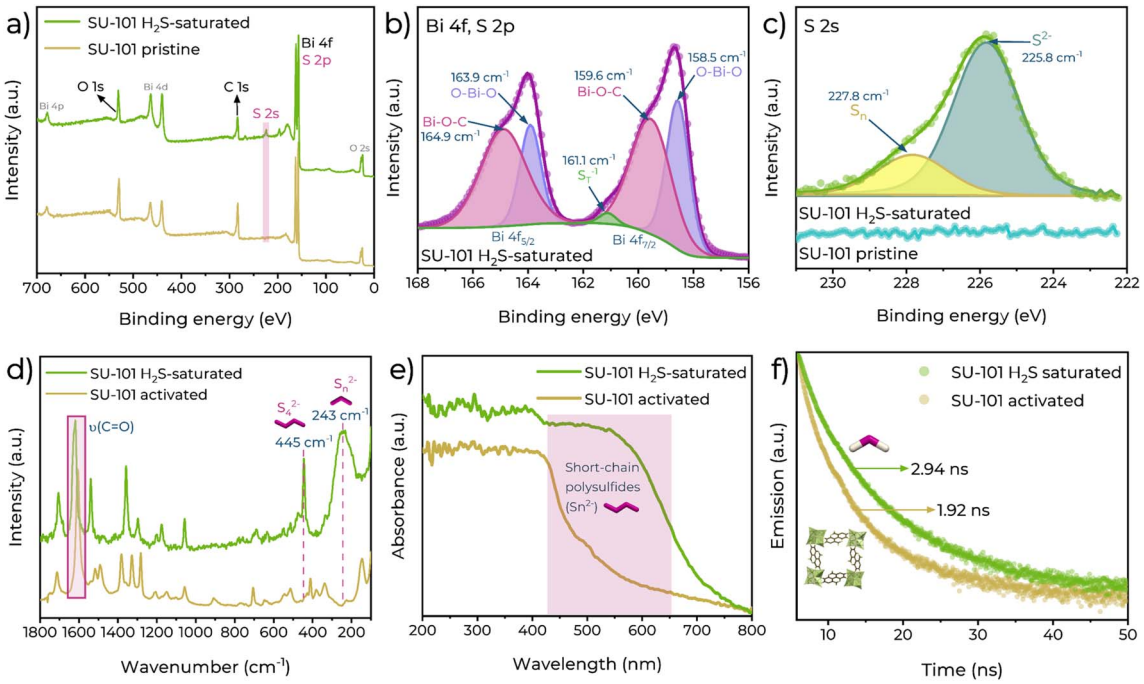


Fig. 3 (a) XPS survey spectra of activated SU-101 (yellow) and SU-101 saturated with H_2S (green). (b) Bi 4f/S 2p regions for XPS spectra of H_2S-saturated SU-101. (c) Comparison of S 2s regions for XPS spectra of SU-101 saturated with H_2S and pristine SU-101. (d) Raman spectra of activated SU-101 (yellow) and SU-101 saturated with H_2S (green). (e) UV-vis spectra of activated SU-101 (yellow) and SU-101 saturated with H_2S (green). (f) TRPL spectra of activated SU-101 (yellow) and SU-101 saturated with H_2S (green).

present in the polysulfides formed is observed. Two main contributions are obtained, one located at 225.8 eV and the other at 227.8 eV. The first signal at 225.8 eV has been assigned to the sulphide species (S^{2-}).[37,38] For the second peak, located at 227.8 eV, we propose that this corresponds to the polysulfide species (S_n) in central positions,[39] which could be slightly more oxidised. In addition, it has been reported that, in general terms, the lower energy signal is assigned to the more sulphur reduced form,[40] in good agreement with our hypothesis.

Using a saturated SU-101 sample with H_2S, a Raman spectrum (Fig. 3d) was collected. Characteristic peaks appeared at 243 cm^{-1} corresponding to different S_n^{2-} species[41] and another at 445 cm^{-1} corresponding to S_4^{2-},[42] confirming the chemical transformation of H_2S to polysulfides as we previously reported,[21] without decomposing the crystalline structure of SU-101 as confirmed by PXRD (Fig. S12†). Additionally, it is observed that the signal related to the C=O bond[43] is shifted from 1604 to 1619 cm^{-1} after the exposure to H_2S. This shift can be attributed to the change in the chemical environment of these groups after the interaction of H_2S with the metal centres of Bi^{3+}. Upon formation of the polysulfides, the structural rigidity of the system is modified, which alters the interactions between the metal and the linker and changes the electron density distribution in the C=O groups, resulting in the increase of the vibrational energy of the bonds, which translates into a shift towards higher frequencies.

Furthermore, changes due to the formation of polysulfides are also observed in the UV-vis spectra (Fig. 3e). The spectrum of activated SU-101 shows a weaker absorption that predominates in the range from 200 to 420 nm, while the spectrum of the H_2S saturated material shows a more intense and extended absorption towards longer wavelengths, up to approximately 620 nm. This extension of absorbance is related to the formation of short-chain polysulfides, and it is widely reported that S_n^{2-} species and polysulfide radicals have absorbances ranging from 270 to 610 nm.[39,44] Some examples are: $[S_4]^{2-}$ (420 nm), $[S_3]^{2-}$ (340, 270 nm), $[S_2]^{\bullet-}$ (426 nm), $[S_3]^{\bullet-}$ (617 nm), and $[S_4]^{\bullet-}$ (490 nm). This corroborates that the formation of polysulfide species directly impacts the optical properties of SU-101.

Raman and XPS results indicate that, after H_2S adsorption, polysulfides (S_n^{2-} and S_4^{2-}), more rigid structure species than H_2S, are formed within the pores of SU-101 which clearly impacts the light absorption properties and the fluorescence emission intensity of the system. Thus, the formation of polysulfides rigidifies the MOF structure, decreasing molecular motions and internal vibrations, which reduces the non-radiative energy dissipation pathways, allowing a greater proportion of the excited energy to be released in the form of fluorescence emission.[30] Likewise, the polysulfides would be blocking the LMCT process that generated the fluorescence of SU-101.[32] This process is interrupted by the interaction of the polysulfides formed, which can act as electron donors, with the Bi(III) centre, and this interaction would prevent the metal centre from accepting the charge coming from the π* orbitals of the ligand. In this way, the LMCT becomes less efficient, which favours a greater amount of excited energy being released as light instead of dissipating through the LMCT, thus resulting in the turn-on effect of fluorescence after H_2S adsorption.

Additionally, calculations of the energy gap between the HOMO–LUMO orbitals were performed using the Tauc method

Open Access Article. Published on 19 February 2025. Downloaded on 6/30/2025 11:45:30 PM.
This article is licensed under a Creative Commons Attribution 3.0 Unported Licence.

considering both direct and indirect transitions.[45] For the activated material, the energy values were 2.32 eV (direct) and 2.20 eV (indirect) (Fig. S13a and S13b†), while for the material saturated with H_2S, the values decreased to 1.83 eV (direct) and 1.73 eV (indirect) (Fig. S13c and S13d†). It is important to mention that, in molecular-type systems, the Tauc method usually underestimates or overestimates the band gap with respect to theoretical values.[46,47] However, in this work, the Tauc method is used for comparative purposes. The reduction in the HOMO–LUMO energy suggests that the interaction between SU-101 and H_2S causes an electronic restructuring of the material, in which the formation of new energy levels could be occurring.[48] Actually, it has been reported that the transition energy between the HOMO and LUMO levels is related to light absorption and the smaller the HOMO–LUMO separation, the longer the absorption wavelength,[49] which is observed in the spectrum of SU-101 exposed to H_2S. Likewise, the decrease in the energy gap observed in the H_2S-saturated material could be facilitating electronic transitions, which could explain the increase in absorption and the possible activation of new sensing mechanisms, such as the blocking of the LMCT mechanism.

It should be noted that the energy gap between the calculated HOMO–LUMO orbitals can only approximate the fundamental gap between the ground (S_0) and excited (S_1) states, as it is strongly dependent on the method used to calculate it. The separation between the S_0 and S_1 states is not only determined by the HOMO–LUMO gap, but is also influenced by the excitonic binding energy,[50] which represents the interaction between the electron and the hole after excitation. However, with the data obtained from UV-vis spectroscopy, we propose a general idea of what is happening at the molecular level. By reducing the HOMO–LUMO energy (Fig. 4a), it can be deduced that the separation between the energy levels (S_0 and S_1) of the Jablonski diagram would also be reduced (Fig. 4b), facilitating radiative transitions from the excited state (S_1) to the ground state (S_0) and reducing non-radiative losses (such as vibrations). This would increase the probability of efficient radiative emission, resulting in the observed "turn-on" effect.

On the other hand, when the material is exposed to CO_2 and H_2O there was no significant change in the fluorescence emission, in comparison to H_2S. We rationalise that this is because these molecules do not cause a significant chemical interaction within the pores of SU-101, in contrast to H_2S. In other words, these molecules do not interact with the material in a way that modifies its structure or affects the LMCT process that determines the fluorescence emission in the material. As a result, the fluorescence of the MOF remains virtually unchanged when exposed to these gases, without producing the "turn-on" or increase in fluorescence that is observed with H_2S.

Finally, TRPL experiments were carried out using a 370 nm picosecond-pulsed LED as the excitation source and performed on an activated sample of SU-101 and an H_2S-saturated sample. The PL decay spectra was measured at 461 nm (Fig. 3f), showing that the average decay lifetimes increased upon H_2S exposure (Table S3†). The average fluorescence lifetime of the activated sample was 1.92 ns, while the lifetime of the H_2S saturated

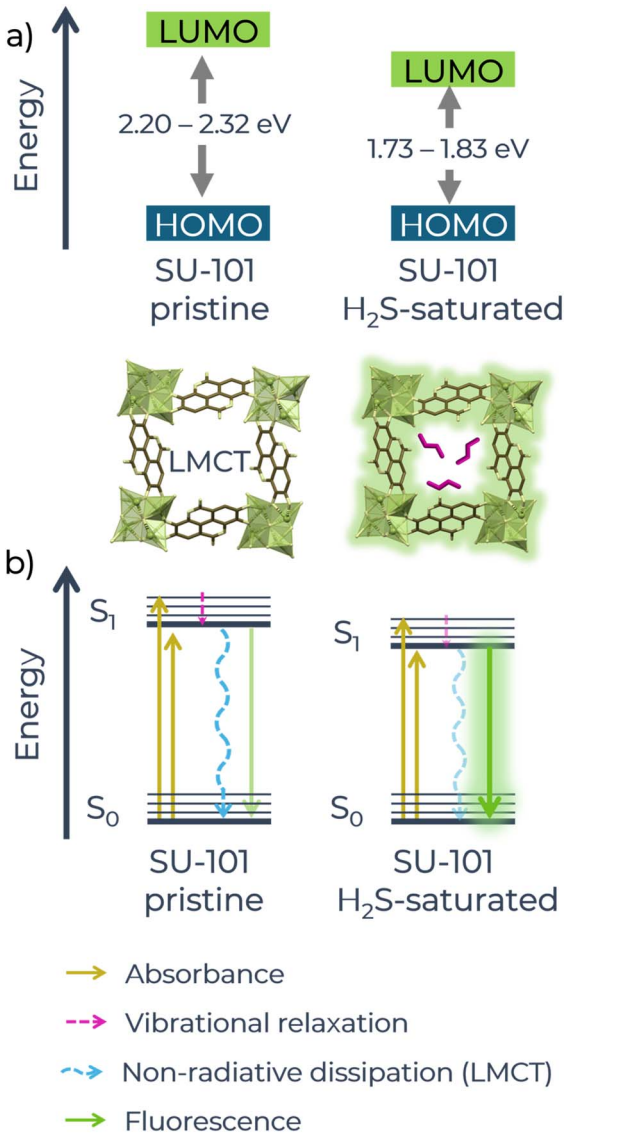


Fig. 4 (a) Schematic of the changes in the HOMO–LUMO energy of pristine and H_2S-saturated SU-101 material. (b) Schematic of the Jablonski diagram that would explain the changes in the fluorescence of the system.

sample was 2.94 ns. To provide an explanation for this increase in fluorescence time, the components (τ) and their contributions to the total fluorescence time can be examined.[51–53]

In both cases, τ_1 is the fastest component ($\tau_{1(act)} = 0.09$ ns and $\tau_{1(H2S)} = 0.06$ ns), since it has an extremely short lifetime, which suggests that it represents a fast relaxation process, probably non-radiative;[54] for the activated sample its relative contribution is $a_{1(act)} = 18.96\%$, while for the saturated sample its contribution decreases to $a_{1(H2S)} = 5.48\%$, which would be manifesting that these fast non-radiative relaxation processes decreased considerably after saturation with H_2S. On the other hand, τ_2 is a component with an intermediate lifetime ($\tau_{2(act)} = 0.87$ ns and $\tau_{2(H2S)} = 1.18$ ns), which could represent a mixture of radiative and non-radiative processes; its contribution has a slight increase after saturating the sample (from $a_{2(act)} = 34.15\%$ to $a_{2(H2S)} =$

© 2025 The Author(s). Published by the Royal Society of Chemistry

Open Access Article. Published on 19 February 2025. Downloaded on 6/30/2025 11:45:30 PM. This article is licensed under a Creative Commons Attribution 3.0 Unported Licence.

37.44%) which indicates that the intermediate decay processes have gained in efficiency, which may be due to the stiffening of the MOF framework after H_2S adsorption, which reduces the non-radiative losses. Finally, the τ_3 and τ_4 components with slow times represent different radiative mechanisms, *i.e.*, more efficient processes in light emission.[38,39] In both cases their contributions increase after saturation with H_2S, for τ_3 from $a_{3(act)} = 36.78\%$ to $a_{3(H2S)} = 41.38\%$ and for τ_4 from $a_{4(act)} = 10.11\%$ to $a_{4(H2S)} = 15.70\%$, the increase in the value of these two components is an indication that the structural stiffening induced by the formation of polysulfides and the LMCT process block generates the reduction of internal vibrations and non-radiative mechanisms, as represented in the Jablonski diagram in Fig. 4b, introducing a higher degree of stability in the system, allowing a longer and more efficient radiative emission.

Polysulfides interaction on SU-101: electronic structure calculations

In order to examine the interaction of polysulfide species formed inside the SU-101 structure from an atomistic perspective, the spatial structure of the MOF is obtained from the CIF file previously reported by Grape *et al.*[21] To start this geometry, we build a supercell of size 2 × 2 from the unit cell. The representative optimised geometry of the SU-101 is shown in Fig. S13(a).† The relaxed structure corresponds to a supercell with dimensions of $a = b = 18.62$ Å and $c = 11.09$ Å. This configuration was designed to create the characteristic micropore of SU-101, capable of stabilising small polysulfide species of varying sizes. The crystal structure is depicted in Fig. S13(b),† where the formation of octahedra around the Bi(III) metallic centres is evident. Additionally, the partial density of states (PDOS), shown in Fig. S13(c),† shows that the electronic contributions from C and O atoms are concentrated near the Fermi level, while Bi(III) atoms exhibit minimal contributions just above it. These findings suggest that charge transfer processes are primarily influenced by the ligand atoms, with the metal centres playing a comparatively minor role.

In order to investigate the stability and potential formation of polysulfide species, we examined small clusters of H_2S_x (x = 1, 2, 4, 6, 8) of different sizes. The optimised molecular structures are shown in Fig. S14,† where the average bond length between different clusters is approximately 2.09 Å (S–S). Geometry relaxed calculations were carried out for all H_2S_x clusters inside the pore of SU-101. The final configurations are illustrated in Fig. S15.† For the H_2S molecule that interacts with the surface of SU-101, it demonstrates an interaction with the metallic centre of Bi(III) at a distance of 3.12 Å, while simultaneously sharing its proton with a nearby oxygen atom (see Fig. S15(a)†). When analysing the interactions with polysulfide species, the configurations after geometry relaxation are shown in Fig. S15(b–e).† It can be observed that the $H_2S_{x=2-8}$/SU-101 molecules do not interact directly with the metallic centres of Bi(III). In these cases, the polysulfide molecules lose their initial configuration but remain confined within the pore of SU-101. In particular, the closest S–O interaction is observed in the H_2S_8/SU-101 configuration, with a distance of 2.34 Å, while the H_2S_4/SU-101 configuration exhibits the largest S–O distance of 3.56 Å. This behaviour is attributed to variations in the attraction between the molecule and the micropore surface. For H_2S_2/SU-101 and H_2S_6/SU-101, the S–O interaction distances are relatively similar, measuring 3.00 Å and 3.06 Å, respectively. These findings reveal a correlation between the size of certain polysulfides and their interaction strength with the surface of SU-101. To further understand these interactions, we performed adsorption energy calculations (E_{ads}), providing insight into the energetic stability of the studied configurations. E_{ads} is obtained from the following expression: $E_{ads} = E_{int} - (E_{SU\text{-}101} + E_{H2Sx})$, where E_{int} corresponds to the total energy of the system adsorbate/SU-101 surface; ESU-101 is the total energy of the relaxed structured MOF, and E_{H2Sx} is the total energy of the polysulfide species under study. The negative values are related to the exergonic interaction between the adsorbate and the surface of SU-101. The results of the E_{ads} values are reported in Table S4.† All E_{ads} values are exergonic, indicating a favourable interaction of the adsorbates within the pore of SU-101. Particularity, the H_2S/SU-101 configuration shows $E_{ads} = -1.30$ eV, which corroborates the formation of H_2S-saturated SU-101. It is worth mentioning that from H_2S_4

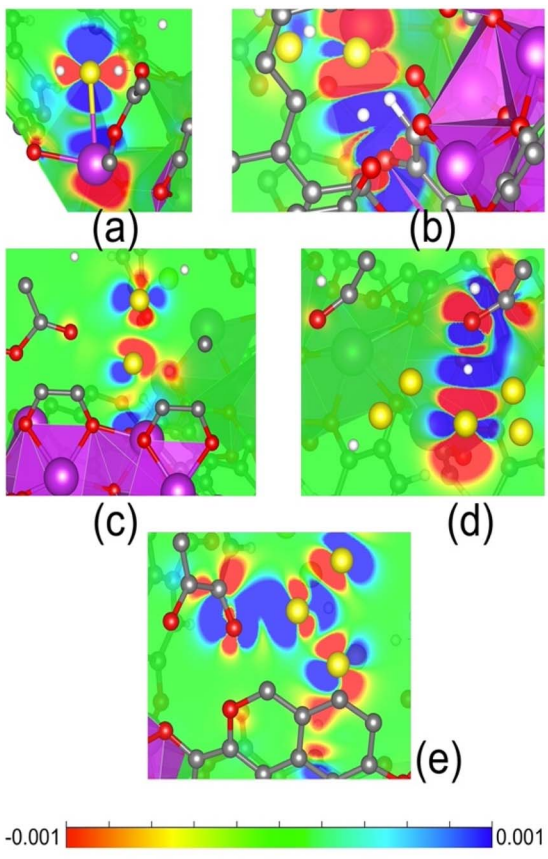


Fig. 5 2D plot of the electron density difference of (a) H_2S/SU-101, (b) H_2S_2/SU-101, (c) H_2S_4/SU-101, (d) H_2S_6/SU-101, and (e) H_2S_8/SU-101. Blue regions of 2D slices represent sites from which the electronic charge was depleted, and the red areas refer to the locations where the charge is accumulated (an isovalue of 0.001 e Å^{-3}).

Open Access Article. Published on 19 February 2025. Downloaded on 6/30/2025 11:45:30 PM. This article is licensed under a Creative Commons Attribution 3.0 Unported Licence.

(−0.87 eV), H_2S_6 (−1.01 eV), and H_2S_8 (−1.78 eV) molecules the E_{ads} values begin to increase; this behaviour corroborates the presence of polysulfide molecules of different sizes within the micropore of SU-101. To understand the charge transfer mechanism behind the interaction between the adsorbates and the SU-101 material, the density difference isosurfaces ($\Delta\rho$) were plotting according to: $\Delta\rho = \rho_{total} - \rho_{adsorbate} - \rho_{surface}$, where ρ_{total} is the electron density of the system adsorbate/SU-101 surface, $\rho_{adsorbate}$ is the electron density of the polysulfide species under study, and $\rho_{surface}$ refers to the electron density of the SU-101 structure. Fig. 5 represents the $\Delta\rho$ for each interaction under study. In the case of the H_2S/SU-101 configuration, the regions of electron density removal (Fig. 5a) between the S–Bi atoms are evident, this mechanism favours a high E_{ads} value. The same mechanism is observed for the case of the H_2S_8/SU-101 interaction between the S–O atoms (Fig. 5d). The systems H_2S_2/SU-101 and H_2S_6/SU-101 show charge accumulation (red colour) on the S atoms and charge density removal between the O–H atoms (blue colour). The H_2S_4/SU-101 interaction presents a characteristic behaviour because charge accumulations are present between the S atom and the ligand fragment. The accumulation of charge in S_{2-8} small polysulfides is evident, which can be correlated with the nature of the charge species. Thus, $\Delta\rho$ shows evidence of how the organic fragments of the MOF material are involved in the interaction process. Finally, TD-DFT calculations were performed to simulate UV-vis absorption spectra, as shown in Fig. S16.† The results reveal that the behaviour and shape of the spectra are largely influenced by the SU-101 material. In particular, the maximum absorption peak is observed when H_2S_8 interacts with SU-101. This indicates that the size of the polysulfides within the SU-101 structure significantly affects its optical response.

Conclusions

In summary, the detection properties of a structurally stable Bi(III)-based MOF material, SU-101, were investigated by fluorescence experiments. These demonstrated a significant change in the emission spectra after H_2S adsorption (chemical transformation to polysulfides), with a clear H_2S detection selectivity (over H_2O and CO_2) and a reproducible H_2S response when SU-101 was exposed to 0.05 bar H_2S, 0.1 bar H_2S and when this material was saturated with H_2S (*i.e.*, 1 bar H_2S). Remarkably, the limit of H_2S detection (LOD) was calculated to be as low as 0.65 mM (∼22.16 ppm). The fluorescence enhancement is attributed to the chemical transformation of H_2S into polysulfides within the pores of the material confirmed by Raman and XPS experiments, which induced a rigidification in the structure of the system, decreasing the molecular vibrations. In addition, the electron-donor character of the polysulfides formed generates interactions with the Bi(III) metal centre, creating a blockage in the LMCT process, which decreased certain non-radiative processes, affording a "turn-on" effect in the fluorescent emission. Analysis of the UV-vis spectra of SU-101 before and after H_2S adsorption reveals significant changes in the optical properties of the material. The reduction of the bandgap, determined by the Tauc method, shows that the polysulfide formation introduces new discrete energy levels within the original gap of the material, allowing electronic transitions at lower energies, which facilitates light absorption in a broader region of the spectrum. Time-resolved photoluminescence (TRPL) experiments provided further insight into the detection mechanism, confirming that the increased fluorescence lifetime observed after H_2S exposure is due to the reduction of non-radiative dissipation mechanisms. DFT calculations shows that the adsorption energy increases with the size of the polysulfide chain, as observed for the interaction of H_2S_4, H_2S_6, and H_2S_8 molecules within the SU-101 material. Overall, this study postulates this chemically stable Bi(III)-based MOF material, SU-101, as a promising candidate for H_2S detection.

Data availability

All data is available in the main text and in the ESI.†

Conflicts of interest

There are no conflicts to declare.

Author contributions

Valeria B. López-Cervantes: methodology, formal analysis, investigation, data curation, writing – original draft. Juan L. Obeso: methodology, formal analysis, investigation, writing – original draft. J. Gabriel Flores: methodology, formal analysis, investigation, writing – original draft. Aída Gutiérrez-Alejandre: validation, supervision, resources. Raul A. Marquez: investigation, validation, formal analysis. José Antonio de los Reyes: resources, visualization. Catalina V. Flores: investigation. N. S. Portillo-Vélez: investigation. Pablo Marín-Rosas: investigation. Christian A. Celaya: computational calculations. Eduardo González-Zamora: resources, visualization. Diego Solis-Ibarra: conceptualization, resources, project administration, supervision, visualization. Ricardo A. Peralta: conceptualization, resources, supervision, writing – review & editing, visualization. Ilich A. Ibarra: conceptualization, resources, funding acquisition, project administration, supervision, writing – review & editing, visualization.

Acknowledgements

V. B. L.-C. and J. L. O. thank CONAHCYT for the PhD fellowships (1005649 and 1003953). R. A. P. thanks the Autonomous University of Mexico-Iztapalapa, Mexico, for the financial support. V. B. L.-C. thanks Professor E. Sánchez-González for scientific discussions. We thank U. Winnberg (Euro Health) for scientific discussions and G. Ibarra-Winnberg for scientific encouragement. I. A. I. thanks PAPIIT UNAM (IN201123), México, for financial support. C. A. C. wants to acknowledge CONAHCYT-México for the postdoctoral fellowship.

© 2025 The Author(s). Published by the Royal Society of Chemistry

Open Access Article. Published on 19 February 2025. Downloaded on 6/30/2025 11:45:30 PM. This article is licensed under a Creative Commons Attribution 3.0 Unported Licence.

References

1 S. Batterman, A. Grant-Alfieri and S.-H. Seo, *Crit. Rev. Toxicol.*, 2023, **53**, 244–295.
2 D. H. Truong, M. A. Eghbal, W. Hindmarsh, S. H. Roth and P. J. O'Brien, *Drug Metab. Rev.*, 2006, **38**, 733–744.
3 R. O. Beauchamp, J. S. Bus, J. A. Popp, C. J. Boreiko, D. A. Andjelkovich and P. Leber, *CRC Crit. Rev. Toxicol.*, 1984, **13**, 25–97.
4 J. Zeng, M. Li, A. Liu, F. Feng, T. Zeng, W. Duan, M. Li, M. Gong, C. Wen and Y. Yin, *Adv. Funct. Mater.*, 2018, **28**, 1800515.
5 Z. Meng, R. M. Stolz and K. A. Mirica, *J. Am. Chem. Soc.*, 2019, **141**, 11929–11937.
6 T. Ubuka, T. Abe, R. Kajikawa and K. Morino, *J. Chromatogr. B Biomed. Sci. Appl.*, 2001, **757**, 31–37.
7 R. Ferro, G. Borzone, G. Cacciamani and R. Raggio, *Thermochim. Acta*, 2000, **347**, 103–122.
8 W. Xuan, C. Sheng, Y. Cao, W. He and W. Wang, *Angew. Chem., Int. Ed.*, 2012, **51**, 2282–2284.
9 C. Yu, X. Li, F. Zeng, F. Zheng and S. Wu, *Chem. Commun.*, 2013, **49**, 403–405.
10 A. Abbasi, S. Hanif and M. Shakir, *RSC Adv.*, 2020, **10**, 3137–3144.
11 N. A. Samak, M. S. Selim, Z. Hao and J. Xing, *Talanta*, 2020, **211**, 120655.
12 J. Liang, B. Z. Tang and B. Liu, *Chem. Soc. Rev.*, 2015, **44**, 2798–2811.
13 H. Li, Y. Fang, J. Yan, X. Ren, C. Zheng, B. Wu, S. Wang, Z. Li, H. Hua, P. Wang and D. Li, *TrAC, Trends Anal. Chem.*, 2021, **134**, 116117.
14 S. Khatua, S. Goswami, S. Biswas, K. Tomar, H. S. Jena and S. Konar, *Chem. Mater.*, 2015, **27**, 5349–5360.
15 E. Martínez-Ahumada, A. López-Olvera, V. Jancik, J. E. Sánchez-Bautista, E. González-Zamora, V. Martis, D. R. Williams and I. A. Ibarra, *Organometallics*, 2020, **39**, 883–915.
16 T. He, X.-J. Kong and J.-R. Li, *Acc. Chem. Res.*, 2021, **54**, 3083–3094.
17 E. Zhang, L. Wu, L. Jiang, K. Guo, Z. Su and P. Ju, *J. Mol. Struct.*, 2022, **1264**, 133314.
18 S. S. Nagarkar, B. Joarder, A. K. Chaudhari, S. Mukherjee and S. K. Ghosh, *Angew. Chem., Int. Ed.*, 2013, **52**, 2881–2885.
19 X. Lian and B. Yan, *RSC Adv.*, 2016, **6**, 11570–11576.
20 L. Guo, M. Wang and D. Cao, *Small*, 2018, **14**, 1703822.
21 E. S. Grape, J. G. Flores, T. Hidalgo, E. Martínez-Ahumada, A. Gutiérrez-Alejandre, A. Hautier, D. R. Williams, M. O'Keeffe, L. Öhrström, T. Willhammar, P. Horcajada, I. A. Ibarra and A. K. Inge, *J. Am. Chem. Soc.*, 2020, **142**, 16795–16804.
22 J. L. Obeso, D. R. Amaro, C. V. Flores, A. Gutiérrez-Alejandre, R. A. Peralta, C. Leyva and I. A. Ibarra, *Coord. Chem. Rev.*, 2023, **485**, 215135.
23 J. M. Soler, E. Artacho, J. D. Gale, A. García, J. Junquera, P. Ordejón and D. Sánchez-Portal, *J. Phys. Condens. Matter*, 2002, **14**, 2745–2779.
24 J. P. Perdew, K. Burke and M. Ernzerhof, *Phys. Rev. Lett.*, 1996, **77**, 3865–3868.
25 N. Troullier and J. L. Martins, *Phys. Rev. B:Condens. Matter Mater. Phys.*, 1991, **43**, 1993–2006.
26 M. Gajdoš, K. Hummer, G. Kresse, J. Furthmüller and F. Bechstedt, *Phys. Rev. B:Condens. Matter Mater. Phys.*, 2006, **73**, 045112.
27 Y. Song, Y.-Y. Chen, Q.-J. Huang, D.-L. Deng, Y.-Y. Zhao, M.-Z. Wu, S.-K. Wang and Y. Li, *Polyhedron*, 2023, **239**, 116428.
28 J. Manzur, C. Poblete, J. Morales, R. C. De Santana, L. J. Queiroz Maia, A. Vega, P. Fuentealba and E. Spodine, *Inorg. Chem.*, 2020, **59**, 5447–5455.
29 A. M. May and J. L. Dempsey, *Chem. Sci.*, 2024, **15**, 6661–6678.
30 T. K. Pal, *Mater. Chem. Front.*, 2023, **7**, 405–441.
31 F. Juliá, *ChemCatChem*, 2022, **14**, e202200916.
32 Y. Zhao, J. Wang, W. Zhu, L. Liu and R. Pei, *Nanoscale*, 2021, **13**, 4505–4511.
33 S. S. Nagarkar, T. Saha, A. V. Desai, P. Talukdar and S. K. Ghosh, *Sci. Rep.*, 2014, **4**, 7053.
34 M. Fantauzzi, B. Elsener, D. Atzei, A. Rigoldi and A. Rossi, *RSC Adv.*, 2015, **5**, 75953–75963.
35 J. Rodriguez-Pereira, S. A. Rincón-Ortiz and R. Ospina, *Surf. Sci. Spectra*, 2020, **27**, 024001.
36 R. A. Marquez, J. L. Obeso, R. R. Vaidyula, V. B. López-Cervantes, R. A. Peralta, P. Marín Rosas, J. A. De Los Reyes, C. B. Mullins and I. A. Ibarra, *J. Mater. Chem. A*, 2024, **10**, 1039.
37 V. V. Atuchin, L. I. Isaenko, V. G. Kesler and S. I. Lobanov, *J. Alloys Compd.*, 2010, **497**, 244–248.
38 T. R. N. Kutty, *Mater. Res. Bull.*, 1991, **26**, 399–406.
39 R. Steudel and T. Chivers, *Chem. Soc. Rev.*, 2019, **48**, 3279–3319.
40 E. Cato, A. Rossi, N. C. Scherrer and E. S. B. Ferreira, *J. Cult. Herit.*, 2018, **29**, 30–35.
41 O. El Jaroudi, E. Picquenard, A. Demortier, J.-P. Lelieur and J. Corset, *Inorg. Chem.*, 2000, **39**, 2593–2603.
42 H.-L. Wu, L. A. Huff and A. A. Gewirth, *ACS Appl. Mater. Interfaces*, 2015, **7**, 1709–1719.
43 K. I. Hadjiivanov, D. A. Panayotov, M. Y. Mihaylov, E. Z. Ivanova, K. K. Chakarova, S. M. Andonova and N. L. Drenchev, *Chem. Rev.*, 2021, **121**, 1286–1424.
44 N. Lau and M. D. Pluth, *Curr. Opin. Chem. Biol.*, 2019, **49**, 1–8.
45 P. H. M. Andrade, C. Volkringer, T. Loiseau, A. Tejeda, M. Hureau and A. Moissette, *Appl. Mater. Today*, 2024, **37**, 102094.
46 K. Fabrizio, K. N. Le, A. B. Andreeva, C. H. Hendon and C. K. Brozek, *ACS Mater. Lett.*, 2022, **4**, 457–463.
47 P. R. Jubu, F. K. Yam, V. M. Igba and K. P. Beh, *J. Solid State Chem.*, 2020, **290**, 121576.
48 Q. Thijssen, J. A. Carroll, F. Feist, A. Beil, H. Grützmacher, M. Wegener, S. Van Vlierberghe and C. Barner-Kowollik, *Mater. Horiz.*, 2024, **11**(24), 6184–6191.

© 2025 The Author(s). Published by the Royal Society of Chemistry

49 I. Fleming and D. Williams, in *Spectroscopic Methods in Organic Chemistry*, Springer International Publishing, Cham, 2019, pp. 55–83.
50 J.-L. Bredas, *Mater. Horiz.*, 2014, **1**, 17–19.
51 D. J. Liput, T. A. Nguyen, S. M. Augustin, J. O. Lee and S. S. Vogel, *Neuroscience*, 2020, **94**, e108.
52 T. A. Smith and K. P. Ghiggino, *Methods Appl. Fluoresc.*, 2015, **3**, 022001.
53 S. K. Panigrahi and A. K. Mishra, *J. Fluoresc.*, 2020, **30**, 1085–1094.
54 A. Sharma, D. Kim, J.-H. Park, S. Rakshit, J. Seong, G. H. Jeong, O.-H. Kwon and M. S. Lah, *Commun. Chem.*, 2019, **2**, 39.

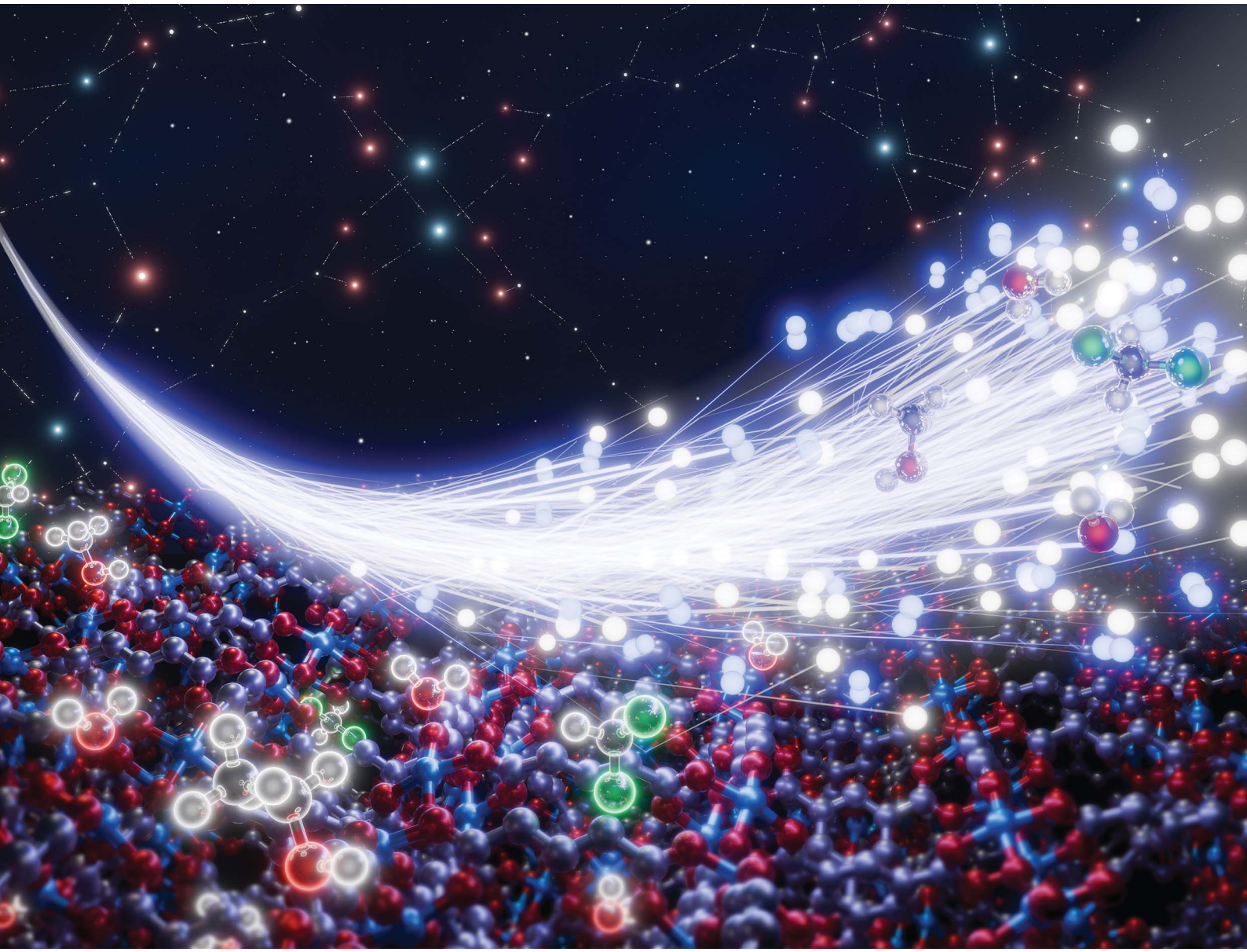
Open Access Article. Published on 19 February 2025. Downloaded on 6/30/2025 11:45:30 PM.
This article is licensed under a Creative Commons Attribution 3.0 Unported Licence.

© 2025 The Author(s). Published by the Royal Society of Chemistry

Volume 16
Number 6
14 February 2025
Pages 2467–2936

Chemical Science

rsc.li/chemical-science



ISSN 2041-6539

ROYAL SOCIETY OF CHEMISTRY

EDGE ARTICLE

Rubicelia Vargas, Jorge Garza, Nak Cheon Jeong *et al.*
Gas-flow activation of MOFs: unlocking efficient catalysis through dynamic bonding

15 YEARS ANNIVERSARY

Chemical Science

ROYAL SOCIETY OF CHEMISTRY

EDGE ARTICLE

View Article Online
View Journal | View Issue

Check for updates

Cite this: *Chem. Sci.*, 2025, **16**, 2581

All publication charges for this article have been paid for by the Royal Society of Chemistry

Gas-flow activation of MOFs: unlocking efficient catalysis through dynamic bonding†

Mariana L. Díaz-Ramírez,‡[ab] Sun Ho Park, ‡[a] Marcos Rivera-Almazo, ‡[c] Erika Medel,‡[c] Ricardo A. Peralta, [c] Ilich A. Ibarra, [d] Rubicelia Vargas, *[c] Jorge Garza*[c] and Nak Cheon Jeong *[ab]

Metal–organic frameworks (MOFs), characterized by dynamic metal–ligand coordination bonding, have pivotal roles in catalysis, gas storage, and separation processes, owing to their open metal sites (OMSs). These sites, however, are frequently occupied by Lewis-base solvent molecules, necessitating activation to expose the OMSs for practical applications. Traditional thermal activation methods involve harsh conditions, risking structural integrity. This study presents a novel 'gas-flow activation' technique using inert gases like nitrogen and argon to eliminate these coordinating solvent molecules at low temperatures, thereby maintaining the structural integrity of MOFs. We specifically explored this method with HKUST-1, demonstrating that gas-flow activation at mild temperatures is not only feasible but also superior in efficiency compared to the conventional thermal methods. This approach highlights the potential for safer, more efficient activation processes in MOF applications, making it a valuable addition to the repertoire of MOF activation techniques. This activation function of inert gas flow allows HKUST-1 as a catalyst for the hydrogenation of acetophenone even at room temperature. In addition, it is demonstrated that this 'gas-flow activation' is broadly applicable in other MOFs such as MOF-14 and UTSA-76. Furthermore, the findings reveal that dynamic coordination bonding, the repeating transient dissociation-association of solvent molecules at OMSs, are key mechanisms in facilitating this activation, pointing towards new directions for designing activation strategies that prevent structural damage.

Received 15th October 2024
Accepted 19th December 2024

DOI: 10.1039/d4sc07011a

rsc.li/chemical-science

Open Access Article. Published on 23 December 2024. Downloaded on 6/30/2025 11:45:52 PM.
This article is licensed under a Creative Commons Attribution-NonCommercial 3.0 Unported Licence.

Introduction

Metal–organic frameworks (MOFs) are crystalline porous materials composed of inorganic metal nodes connected by organic linkers. Their extensive structural diversity and the ability to finely tune physicochemical properties by modifying linkers or substituting metal nodes render MOFs promising for various applications, including catalysis,[1–4] gas storage and separation,[5–7] sensing,[8–12] energy storage,[13–16] and drug delivery.[17–19] Notably, approximately 70% of MOFs feature open metal sites (OMSs) within the first coordination sphere of the metal centers, where labile ligands can dissociate, leaving vacant sites crucial for catalytic reactions and gas adsorption.[20,21] These OMSs typically bind Lewis-basic (LB) solvent molecules in as-synthesized MOFs,[20] reducing their efficiency in such applications, thus necessitating activation to expose the OMSs for practical use. However, developing a method to remove coordinating solvent molecules under mild conditions without damaging the framework remains challenging.

The conventional activation of OMSs involves two steps: (i) solvent exchange—from a high-boiling-point solvent like water or *N*,*N*′-dimethylformamide (DMF) to a low-boiling-point solvent such as chloroform (trichloromethane, TCM), methylene chloride (dichloromethane, DCM), or methanol (MeOH); and (ii) heating the MOF typically between 120 to 200 °C under vacuum for extended periods (12 to 24 hours). Alternative methods such as freeze-drying[22] and supercritical CO_2 activation[23–25] aim to mitigate damage from surface tension and capillary forces, yet their effectiveness in removing coordinating solvents from metal centers is limited. Consequently, novel room-temperature activation methods have been developed using TCM,[26,27] DCM,[28] dimethyl ether.[29] These methods, especially so-called 'chemical activation' with such weakly coordinating solvents, effectively activate OMSs in Cu-HKUST-1 and Ni-MOF-74 by gradually replacing strongly coordinating solvents with weaker ones (see Fig. 1a).[26,27] This activation also

[a]*Department of Physics & Chemistry, DGIST, Daegu 42988, Korea. E-mail: nc@dgist.ac.kr*

[b]*Center for Basic Science, DGIST, Daegu 42988, Korea*

[c]*Departamento de Química, División de Ciencias Básicas e Ingeniería, Universidad Autónoma Metropolitana, Iztapalapa, CP 09340 CDMX, Mexico. E-mail: ruvf@xanum.uam.mx; jgo@xanum.uam.mx*

[d]*Laboratorio de Fisicoquímica y Reactividad de Superficies (LaFReS), Instituto de Investigaciones en Materiales, Universidad Nacional Autónoma de México, Circuito Exterior s/n, CU, Del. Coyoacán, 04510, Ciudad de México, Mexico*

† Electronic supplementary information (ESI) available. See DOI: https://doi.org/10.1039/d4sc07011a

‡ M. L. D.-R., S. H. P., M. R.-A., and E. M. contributed equally to this work.

© 2025 The Author(s). Published by the Royal Society of Chemistry

Open Access Article. Published on 23 December 2024. Downloaded on 6/30/2025 11:45:52 PM. This article is licensed under a Creative Commons Attribution-NonCommercial 3.0 Unported Licence.

applies to unstable MOFs like MOF-143 (DUT-34),[30] enhancing catalytic activity in processes such as the hydrogenation of acetophenone and acetone, outperforming MOFs with strongly coordinating solvents.[31,32] Nevertheless, this chemical activation method has a drawback in that large amounts of TCM, DCM, or dimethyl ether are required to replace the strongly coordinating solvents.

To overcome these MOF activation techniques, we explored 'gas-flow activation', employing inert gases like nitrogen (N_2) and argon (Ar) to remove coordinating solvents at mild temperatures, thereby maintaining MOFs' structural integrity and operational efficiency. We hypothesized that this method facilitates the dynamic coordinative bonding of LB solvent molecules, which are in a state of transient dissociation and re-association. In other words, these coordinating solvent molecules in the dynamic state instantaneously dissociate and are subsequently removed by expulsion through inert gas collisions (see Fig. 1b). We confirmed the effectiveness of this process in OMS-possessing MOFs, including HKUST-1, MOF-14, and UTSA-76. Notably, 'Ar-flow activation' has proven particularly effective for the catalytic hydrogenation of acetophenone in HKUST-1. This method highlights the potential for safer, more efficient MOF activation processes, emphasizing the dynamic coordination bonding behavior of solvent molecules as a crucial mechanism, thereby pointing towards innovative directions for designing non-destructive activation strategies.

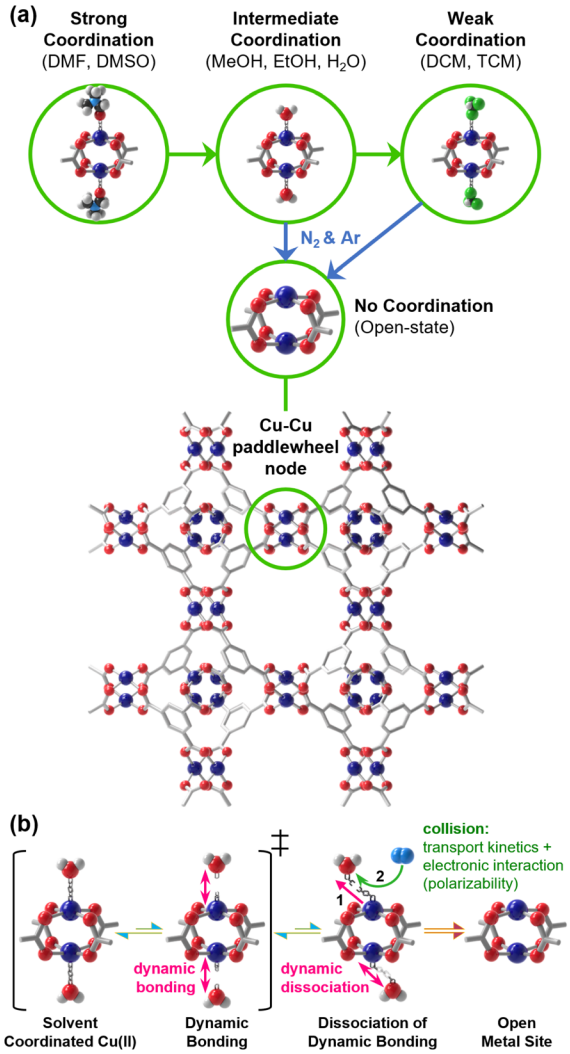


Fig. 1 (a) Schematic illustration of the coordination states of Cu(II) centers with various solvents: strong coordination (DMF, DMSO), intermediate coordination (MeOH, EtOH, H_2O), and weak coordination (DCM, TCM). The Cu–Cu paddlewheel node is depicted, showing the dynamic coordination changes. (b) Schematic representation of the dynamic dissociation processes of coordinating H_2O molecule at Cu(II) centers, highlighting the role of collision kinetics and electronic interaction with nitrogen.

Results and discussion

The dynamicity of coordinating molecules led us to investigate whether these molecules could be dissociated and subsequently removed from the OMSs using a dry inert gas flow at a temperature lower than that used in conventional thermal activation. Our initial approach was to determine whether introducing dry N_2 gas could reduce the activation temperature compared to a static atmosphere (*i.e.*, conditions without applying N_2 flow or vacuum). For this purpose, we selected HKUST-1 due to its ideal structural characteristics: its distinctive Cu–Cu paddlewheel nodes, where two oxygen atoms from each benzenetricarboxylate (btc) ligand bridge two copper centers, as depicted in Fig. 1a. Furthermore, each Cu center is linked to four oxygen atoms, each from a btc ligand. This specific coordination geometry ensures that all OMSs at Cu centers, where LB solvent molecules can bind, face the large open pore and are thus readily accessible to guest molecules. This structural arrangement results in a strong Raman scattering at the Cu–Cu node, with the band appearing approximately between 165–230 cm^{-1}, varying according to the chemical environment around the Cu centers, such as the presence or absence of coordinating LB solvent, its type, its coordination strength, and its interactions with pore-filling solvent (*i.e.*, hydrogen bonding and dipole interactions). Consequently, the Raman band distinguishes between the open (activated state) and coordinating state of OMSs.

Considering this spectroscopic feature, we prepared H_2O-loaded HKUST-1 crystals (hereafter referred to as H_2O-HK; also see the scanning electron microscope (SEM) image in Fig. S1†), following the methods outlined in Section S1 of ESI.† After verifying the phase and chemical purity of the samples by the powder X-ray diffraction (PXRD) pattern and ^1H nuclear magnetic resonance (NMR) spectrum of H_2O-HK (Fig. S2†), we measured the Raman spectrum of the H_2O-HK sample. Subsequently, we monitored changes in the Cu state (H_2O-coordination or coordination-free state) at varying temperatures, continuously supplying N_2 at a rate of 50 mL min^{-1} (Fig. S3†). Initially, the H_2O-HK exhibited a characteristic Raman band at 175 cm^{-1}, indicative of the presence of both coordinating and pore-filling H_2O molecules. After 30 minutes of N_2 flow at 25 °C, the Raman band shifted to 166 cm^{-1}, suggesting the evacuation of pore-filling H_2O molecules while leaving only the coordinating H_2O molecules. After continuing

© 2025 The Author(s). Published by the Royal Society of Chemistry

Open Access Article. Published on 23 December 2024. Downloaded on 6/30/2025 11:45:52 PM. This article is licensed under a Creative Commons Attribution-NonCommercial 3.0 Unported Licence.

the N_2 flow for 120 minutes at 25 °C, the band shifted to 230 cm^{-1}, indicating complete OMS activation. It is noteworthy that while static thermal activation without N_2 flow required 45 min at 90 °C (Fig. S4†), N_2-flow activation achieved the same result in just 5 min at a temperature of 40 °C (Fig. S3†). This result indicates that the N_2-flow method can conserve the energy with a gain of approximately 40 J g^{-1} compared to the static thermal method (Section S5†).

To demonstrate that this N_2-flow activation could be applied to other solvent coordinations, we prepared HKUST-1 crystals coordinating with TCM, DCM, MeOH, MeCN, EtOH, DMF, and DMSO (hereafter TCM-HK, DCM-HK, MeOH-HK, MeCN-HK, EtOH-HK, DMF-HK, and DMSO-HK, respectively). We then monitored the changes in the Raman band of each sample at different temperatures, applying dry N_2 flow (Fig. S5–S11†). Our findings revealed that the lowest activation temperatures for each sample correlate strongly with the coordination strength of the LB solvent, as observed in previous studies, where the Cu–Cu vibrational Raman band closely relates to the solvent's coordination strength in the order: TCM ≤ DCM < H_2O < MeOH ≈ MeCN ≤ EtOH < DMF (Fig. 2).[32,33] Thus, TCM and DCM are the most labile solvents for dissociating from Cu centers, while DMF and DMSO pose the greatest challenge (DMSO-HK were not fully activated even at 180 °C; Fig. S11†). To gain a deeper understanding of the coordination strength, we calculated the interaction energies of the solvents at Cu(II) OMS using the DFT method (Fig. 3, S12 and Tables S1–S5†). The DFT results closely agree with our experimental findings, except for MeOH, which displays an exceptionally high interaction energy due to non-conventional hydrogen bonding between the framework oxygen and methanol's C–H hydrogen. Although such hydrogen bonding does not significantly influence the actual dissociation ability, the relatively high activation temperatures of EtOH-HK and DMF-HK compared to their coordination energies can be attributed to their large molecular sizes, which impact their diffusion through the pores. To corroborate these DFT findings and further explore non-conventional hydrogen bondings, we also calculated the electron density (ρ_{BCP}) and density energy (H_{BCP}) at the bond critical point between the coordinating atom in the solvent molecule and the OMS using the theoretical package, Atoms in Molecules (AIM) (Tables S6–S13†). The AIM results generally align with the DFT results, although some calculated values appear somewhat erratic.

To test our hypothesis that another inert gas can facilitate the removal of coordinating solvents by collisional expulsion, we conducted gas-flow activation using argon (Ar, Mm = 39.948 g mol^{-1}). Like the N_2-flow experiments, we monitored the dissociation of solvent molecules under dry Ar flow using Raman analysis with samples of H_2O-HK, EtOH-HK, DMF-HK, and DMSO-HK (Fig. S13–S16†). Compared to N_2-flow activation, Ar-flow activation significantly reduced the activation temperature—from 40 to 25 °C for H_2O-HK and from 90 to 60 °C for EtOH-HK (Fig. 4)—attributable to the 42% higher kinetic energy of Ar (4.41×10^{-11} J s^{-1}) than that of N_2 (3.09×10^{-11} J s^{-1}) (Section S9†), along with their similar polarizabilities (1.6411 and 1.7403 $\times 10^{-24}$ cm^3 for Ar and N_2, respectively).[34] However, due to their high boiling points and strong

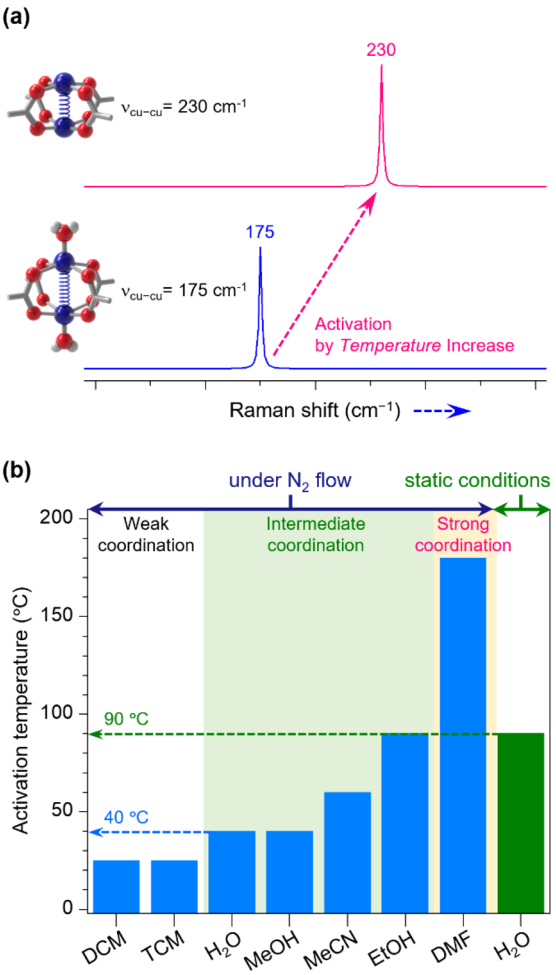


Fig. 2 (a) Schematic illustration of the Raman spectra change showing the Cu–Cu stretching vibration at 230 cm^{-1} and 175 cm^{-1} for different coordination states of Cu(II) induced by the activation. (b) Activation temperatures determined by *in situ* Raman spectroscopy under N_2 flow (blue columns) and static conditions (green column) for various solvents. The graph highlights the transition of activation temperature for H_2O-coordinating HKUST-1 from static (90 °C) to N_2 flow conditions (40 °C).

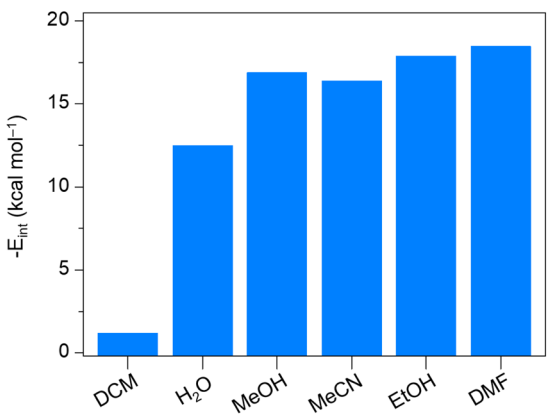


Fig. 3 DFT-calculated interaction energies for the coordination of various solvent molecules at Cu(II) OMS per unit cell of HKUST-1, indicating the coordination strength.

Open Access Article. Published on 23 December 2024. Downloaded on 6/30/2025 11:45:52 PM.
This article is licensed under a Creative Commons Attribution-NonCommercial 3.0 Unported Licence.

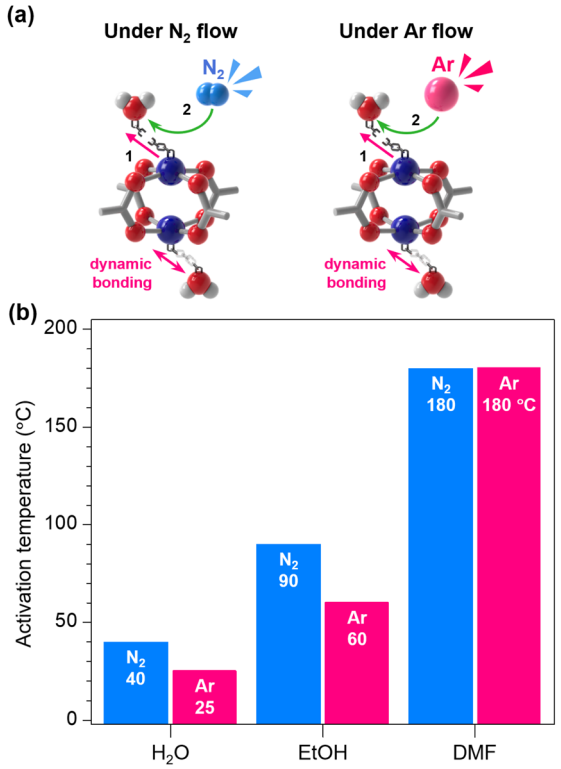


Fig. 4 (a) Schematic illustrations of the dynamic coordination bonding of H_2O molecule and its dissociation process under N_2 (left) and Ar flow (right) conditions. (b) Activation temperatures of H_2O-, EtOH-, and DMF-coordinated to HKUST-1 under N_2 (blue columns) and Ar (pink columns) flow conditions, showing the impact of different inert gases on the activation temperature.

coordination strengths, neither DMF-HK nor DMSO-HK samples were effectively activated using Ar-flow.

We also considered whether gas-flow activation might be achieved through coordination exchange, where N_2 or Ar molecules instantaneously coordinate at the OMSs after displacing pre-coordinating solvent molecules. To investigate this possibility, we conducted Raman spectroscopy with a coordination-free activated HKUST-1 sample while infusing N_2 and Ar gas into the quartz holder (Fig. S17†). We also performed control experiments under vacuum conditions (0.1 mbar) for comparison. Although we hypothesized that N_2 or Ar coordination at the OMS might cause a redshift in the Cu–Cu vibration Raman band from 230 cm^{-1}, the band remained at 230 cm^{-1} in all tests, indicating that neither N_2 nor Ar coordinates at the OMS, thus supporting the hypothesis that the transportation of transiently dissociated solvent molecules by collision is the most plausible mechanism, rather than coordination exchange.

Based on the above understanding and considering the two places where solvent molecules reside (the crystal exterior and interior), we propose two distinct mechanisms for the gas-flow activation process. The removal of non-coordinating solvent molecules on the crystal exterior occurs through direct collision with inert gas molecules, which possess high translational speed due to convection. In contrast, the removal of coordinating solvent molecules within the crystal interior proceeds in two steps: (1) dissociation of coordinating molecules by the collision with inert gas molecules and (2) diffusion of the dissociated molecules to the crystal surface, driven by a decreasing concentration gradient, after exterior drying.

Additionally, we explored the loss of coordinating solvent molecules from HKUST-1 using the thermogravimetric analysis (TGA), maintaining the sample at a stable lower temperature until weight loss stabilized, then incrementally raising the temperature to 25, 40, 50, 60, 90, 120, 150, and 180 °C. As depicted in Fig. S18,† the weight loss of DCM-HK, TCM-HK, H_2O-HK, and MeOH-HK samples reached a plateau at 90 °C, while that of MeCN-HK stabilized at 120 °C, EtOH-HK at 150 °C, DMF-HK at over 180 °C, and DMSO-HK at over 180 °C. Although this thermal analysis does not precisely distinguish between pore-filling and coordinating solvents, we calculated the stoichiometric amounts of each solvent associated with the Cu centers based on their final masses (Tables S14 and S15†). Accordingly, the temperatures at which solvents began dissociating from the OMSs—25 °C for DCM and TCM, 40 °C for H_2O, 50 °C for MeOH and MeCN, and 60 °C for EtOH—correspond closely to those observed in the Raman experiments.

While these results confirm the efficacy of gas-flow activation at the Cu centers, such experiments have thus far been conducted on single crystals or small milligram-scale samples. Therefore, we aimed to examine larger, bulk samples of more than 200 mg of HKUST-1 by employing N_2 adsorption isotherms and testing BET surface areas with EtOH-HK samples activated thermally at 180 °C and by Ar-flow at rates of 50 mL min^{-1} (Thermal-Act_EtOH-HK and Ar-Act_EtOH-HK, respectively). For the Ar-Act_EtOH-HK samples, we controlled the activation temperature at 25, 40, and 90 °C to compare the degree of activation. The results showed that Thermal-Act_EtOH-HK (180 °C) and Ar-Act_EtOH-HK (90 °C) yielded very similar BET-specific surface areas of 1992 and 1907 m^2 g^{-1}, respectively, as illustrated in Fig. 5a. However, the Ar-Act_EtOH-HK samples activated at 40 and 25 °C exhibited significantly reduced surface areas of 1350 and 948 m^2 g^{-1}, respectively, which are 29% and 50% lower, respectively, than the Ar-Act_EtOH-HK sample activated at 90 °C. In these Ar-activated samples, the total pore volume increased from 0.358 to 0.520 and up to 0.775 cm^3 g^{-1} depending on the activation temperature (25, 40, or 90 °C, respectively), as depicted in Fig. 5b. As corroborated by other studies, these lower BET surface areas and total pore volumes undoubtedly resulted from remaining EtOH molecules in the sample after Ar-flow at the lower temperatures (25 and 40 °C).[35,36] For instance, Ar-Act_EtOH-HK (25 and 40 °C) contained 1.13 and 0.93 EtOH molecules per Cu center, respectively, while Ar-Act_EtOH-HK (90 °C) contained only 0.14 EtOH molecules per Cu center, as confirmed by ^1H NMR (Fig. S19a†). Nonetheless, after N_2 sorption measurements, all samples retained their crystallinity (Fig. S19b†).

To further evaluate the effect of the kinetic energy of the gas flow on the activation of HKUST-1, we conducted bulk activation experiments using an Ar flow rate of 5 L min^{-1} at 25 and 90 °C [5L-Ar-Act_EtOH-HK (25 °C) and 5L-Ar-Act_EtOH-HK (90 °C)]. At the higher flow rate (higher kinetic energy), the BET surface area and total pore volume of 5L-Ar-Act_EtOH-HK at 25 °

© 2025 The Author(s). Published by the Royal Society of Chemistry

Open Access Article. Published on 23 December 2024. Downloaded on 6/30/2025 11:45:52 PM.
This article is licensed under a Creative Commons Attribution-NonCommercial 3.0 Unported Licence.

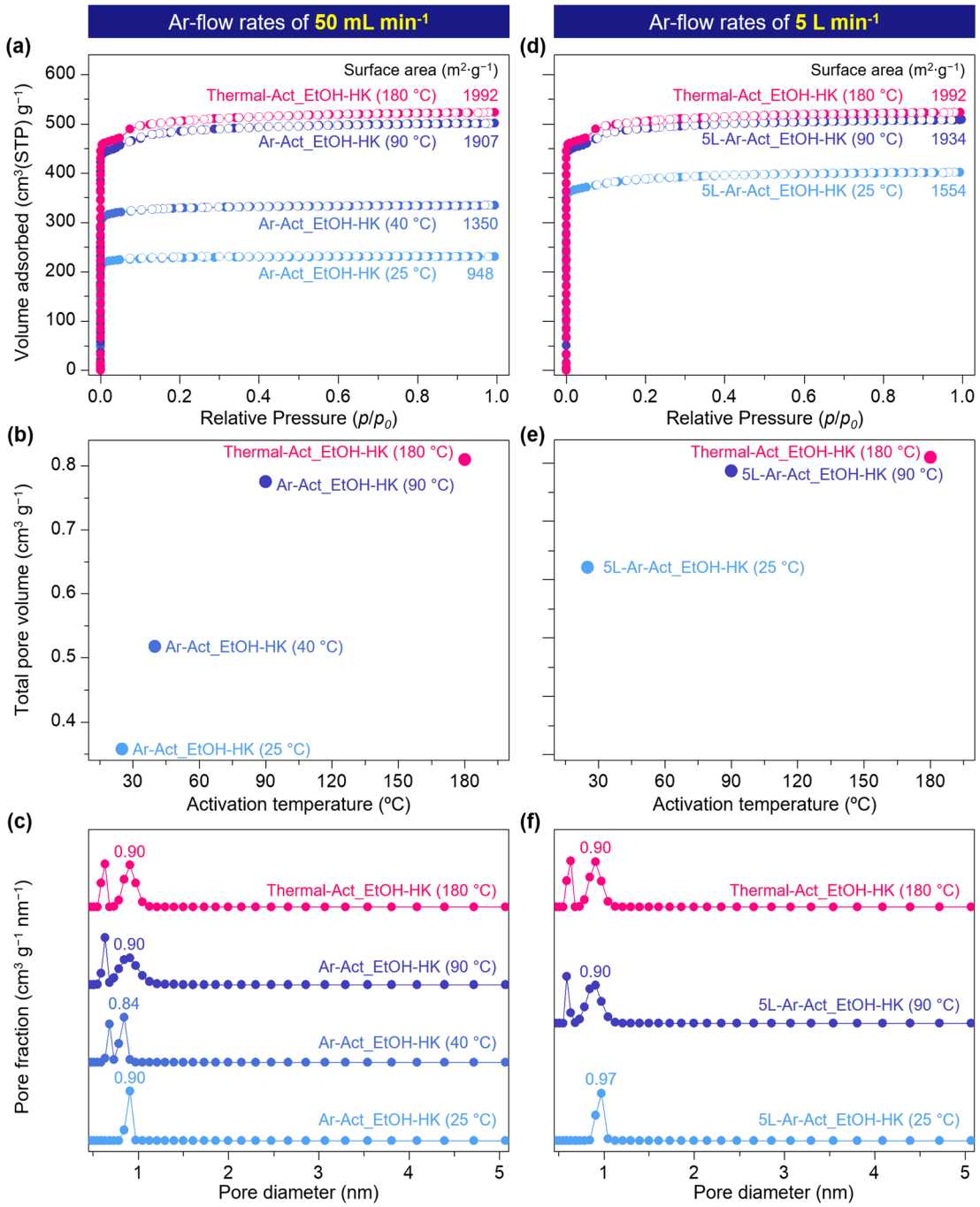


Fig. 5 (a and d) N_2 adsorption/desorption isotherms, (b and e) plot of total pore volume as a function of activation temperature, and (c and f) NLDFT calculation for the pore size distribution of EtOH-HKUST-1 under different activation conditions: thermal activation at 180 °C (pink), Ar activation at 90 °C (dark blue), Ar activation at 40 °C (blue), and Ar activation at 25 °C (light blue) after (a–c) 50 mL min^{-1} and (d–f) 5 L min^{-1} Ar-flow activation.

C increased substantially by 64% and 79%, respectively (1554 $m^2\ g^{-1}$ and 0.62 $cm^3\ g^{-1}$, as shown in Fig. 5d–f), compared to Ar-Act_EtOH-HK, which was tested under a lower flow rate. Despite these improvements, the BET surface area and total pore volume for 5L-Ar-Act_EtOH-HK (25 °C) remained significantly lower than those of Thermal-Act_EtOH-HK (180 °C), indicating that some EtOH molecules were still coordinated to Cu centers. According to ^{1}H NMR results, 0.37 EtOH molecules per Cu center remained in the sample after flowing Ar at 5 L min^{-1} for 24 hours (Fig. S20†). Moreover, 5L-Ar-Act_EtOH-HK (25 °C) exhibited only pores with a size of around 0.97 nm, with no narrower pores present (Fig. 5f), similar to the case with Ar-Act_EtOH-HK (25 °C). By contrast, 5L-Ar-Act_EtOH-HK (90 °C) showed the closest BET surface area and total pore volume values (1934 $m^2\ g^{-1}$ and 0.78 $cm^3\ g^{-1}$), along with a pore size distribution very similar to Thermal-Act_EtOH-HK (180 °C),

© 2025 The Author(s). Published by the Royal Society of Chemistry

Open Access Article. Published on 23 December 2024. Downloaded on 6/30/2025 11:45:52 PM.
This article is licensed under a Creative Commons Attribution-NonCommercial 3.0 Unported Licence.

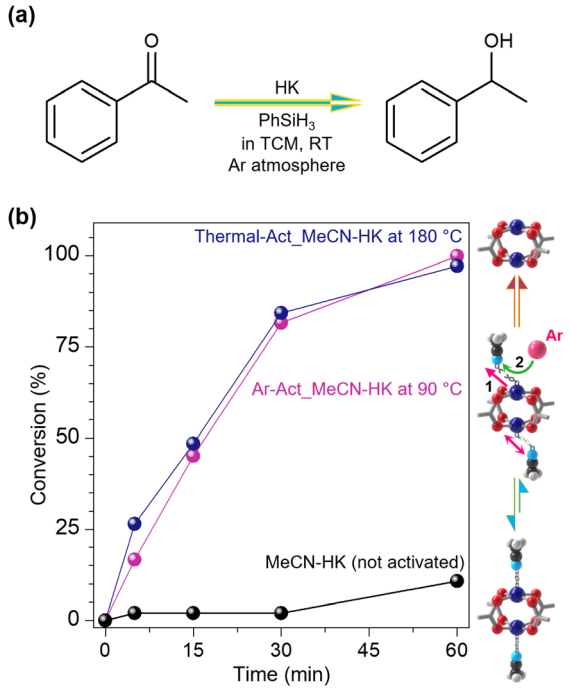


Fig. 6 (a) Schematic representation of the catalytic hydrogenation of acetophenone to 1-phenylethanol using HKUST-1. (b) Conversion rates of acetophenone to 1-phenylethanol over time for MeCN-activated HKUST-1 under different activation conditions: thermal activation at 180 °C (purple), Ar activation at 90 °C (pink), and non-activated MeCN-HKUST-1 (black). The graph demonstrates the enhanced catalytic performance of the Ar-flow-activated HKUST-1 sample.

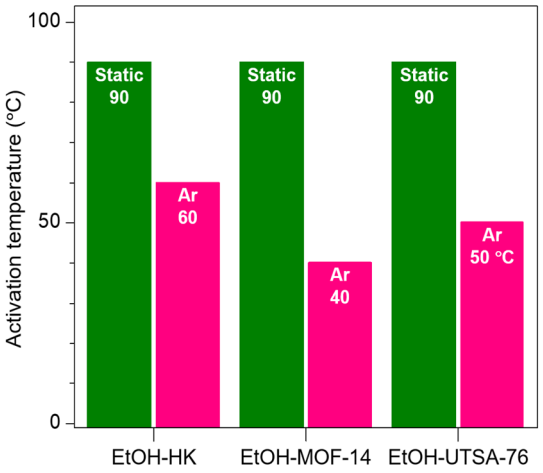


Fig. 7 Activation temperatures of EtOH-coordinated HKUST-1 (EtOH-HK), MOF-14 (EtOH-MOF-14), and UTSA-76 (EtOH-UTSA-76) under static conditions (green columns) and Ar-flow conditions (pink columns). The graph highlights the differences in activation temperatures for each MOF, indicating the efficiency of Ar flow in lowering the activation temperature compared to static conditions.

highlighting the complete removal of EtOH molecules, as confirmed by ^{1}H NMR (Fig. S20†). These results indicate that a flow of dry Ar at a moderate temperature (90 °C) effectively activates the OMSs in HKUST-1 without causing structural damage. Additionally, a comparable BET surface area to Thermal-Act_EtOH-HK (180 °C) can only be achieved with a high Ar flow rate (5 L min^{-1}) due to its greater efficacy in dissociating EtOH molecules from Cu centers as a result of its higher kinetic energy (4.91×10^{-5} J s^{-1}) compared to the lower flow rate (50 mL min^{-1}, 4.41×10^{-11} J s^{-1}).

Meanwhile, we hypothesized that Ar-Act_EtOH-HK (90 °C) would show high catalytic activity as effectively as Thermal-Act_EtOH-HK (180 °C) in the catalytic hydrogenation of acetophenone at room temperature, given that both had fully activated OMSs. As a result, Ar-Act_EtOH-HK (90 °C) exhibited high conversion efficiencies of 95% within 60 min, with a very similar profile to Thermal-Act_EtOH-HK (180 °C), whereas MeCN-HK, with Cu sites occupied by MeCN coordination, yielded a low conversion efficiency (~10%, Fig. 6). However, we observed that the framework of the HKUST-1 completely collapsed after the reaction as reported in literature,[37] indicating its limitation in recycling the catalyst (see PXRD analysis in Fig. S21†). To expand the above results, we examined additional experiments using MeCN-MOF-14 and MeCN-UTSA-76 that possess crystal sizes similar to HKUST-1 (Fig. S1 and S22†). As a result, Ar-Act_MeCN-MOF-14 exhibited higher catalytic activity compared to non-activated MeCN-MOF-14, demonstrating that Ar-flow activation enhances the catalytic performance of MOF-14 effectively. However, we found that MeCN-UTSA-76 was challenging due to its intrinsic low catalytic efficiency. These results support our hypothesis that the gas-flow activation can expose a significant number of OMSs under mild conditions; thus, it is a pretty effective activation method. These findings are promising, suggesting potential applications in an integrated experimental setup where *in situ* activation under inert gas flow followed by gas phase reactions can be conducted efficiently.

To explore whether this gas-flow activation method could broadly apply to other MOFs, we further extended our investigation to include MOF-14 and UTSA-76. In alignment with our hypotheses, when subjected to an Ar-flow activation protocol, both MOFs demonstrated complete activation at significantly lower temperatures of 40 °C, compared to the higher temperature required under static air conditions (90 °C for MOF-14 and 60 °C for UTSA-76) (Fig. 7 and S23–S27†). This experiment underscores the potential of the gas-flow activation techniques in enhancing the activation efficiency, suggesting a promising strategy for optimizing the performance of these materials in various applications.

Conclusions

This study introduces the dynamic coordinative bonding behavior of OMS-coordinating solvent molecules despite their different coordinative strength and a subsequent innovative inert gas-flow activation method for MOFs using N_2 and Ar, which significantly enhances activation efficacy under milder conditions compared to traditional methods. By employing inert gases to remove coordinating solvents at lower temperatures, this technique preserves the structural integrity of MOFs

© 2025 The Author(s). Published by the Royal Society of Chemistry

Open Access Article. Published on 23 December 2024. Downloaded on 6/30/2025 11:45:52 PM. This article is licensed under a Creative Commons Attribution-NonCommercial 3.0 Unported Licence.

and expedites activation processes without the need for high temperatures or vacuum conditions. Our findings demonstrate that this method can rapidly activate OMSs, as shown through successful applications in HKUST-1, MOF-14, and UTSA-76. The technique's effectiveness across various copper-based MOFs suggests its broad applicability for improving MOF performance in catalysis, gas storage, and separation. Future research will explore extending this method to other MOF types and assessing its industrial scalability. The potential for this gas-flow activation to revolutionize MOF preparation and utilization offers promising avenues for advanced environmental and energy applications.

Data availability

The data supporting this article have been included as part of the ESI.†

Author contributions

M. L. D.-R. and S. H. P. designed and conducted all experiments under the supervision of N. C. J., M. R.-A., E. M., R. A. P., I. A. I., R. V., and J. G. performed the theoretical study. M. L. D.-R. and S. H. P. initially drafted the manuscript, and it was subsequently revised by N. C. J. All authors approved the final version of the manuscript. M. L. D.-R., S. H. P., M. R.-A., and E. M. contributed equally to this work.

Conflicts of interest

There are no conflicts to declare.

Acknowledgements

This work was supported by the Ministry of Science and ICT (MSIT) of Korea under the auspices of the Basic Science Research Program sponsored by the National Research Foundation (NRF-2023R1A2C2004838) and by the DGIST R&D Program (25-HRHR+-01). M. L. D.-R. thanks F. B. Z. for the scientific discussions. The authors thank the facilities provided by the Laboratorio de Supercómputo y Visualización en Paralelo at the Universidad Autónoma Metropolitana-Iztapalapa. EM and M. R.-A. thanks CONAHCyT, México for PhD grants 709721 and 567379.

Notes and references

1 H. Han, X. Zheng, C. Qiao, Z. Xia, Q. Yang, L. Di, Y. Xing, G. Xie, C. Zhou, W. Wang and S. Chen, *ACS Catal.*, 2022, **12**, 10668–10679.
2 D. Mukherjee, B. Van der Bruggen and B. Mandal, *Chemosphere*, 2022, **295**, 133835.
3 T. K. Pal, D. De and P. K. Bharadwaj, *Fuel*, 2022, **320**, 123904.
4 L. Liu, S. Du, Y. Xiao, X. Guo, S. Jin, G. Shao and F. Zhang, *Appl. Catal., B*, 2023, **338**, 123094.
5 A. N. Hong, H. Yang, X. Bu and P. Feng, *EnergyChem*, 2022, **4**, 100080.
6 J. Pei, X. W. Gu, C. C. Liang, B. Chen, B. Li and G. Qian, *J. Am. Chem. Soc.*, 2022, **144**, 3200–3209.
7 K. Qu, K. Huang, J. Xu, L. Dai, Y. Wang, H. Cao, Y. Xia, Y. Wu, W. Xu, Z. Yao, X. Guo, C. Lian and Z. Xu, *Angew. Chem., Int. Ed.*, 2022, **61**, e202213333.
8 P. Qin, B. A. Day, S. Okur, C. Li, A. Chandresh, C. E. Wilmer and L. Heinke, *ACS Sens.*, 2022, **7**, 1666–1675.
9 Y. Shen, A. Tissot and C. Serre, *Chem. Sci.*, 2022, **13**, 13978–14007.
10 T. Wu, X. J. Gao, F. Ge and H. G. Zheng, *CrystEngComm*, 2022, **46**, 7881–7901.
11 S. Kamal, M. Khalid, M. S. Khan and M. Shahid, *Coord. Chem. Rev.*, 2023, **474**, 214859.
12 X. Su, Z. Zhong, X. Yan, T. Zhang, C. Wang, Y. X. Wang, G. Xu and L. Chen, *Angew. Chem., Int. Ed.*, 2023, **62**, e202302645.
13 P. E. Lokhande, S. Kulkarni, S. Chakrabarti, H. M. Pathan, M. Sindhu, D. Kumar, J. Singh, A. Kumar, Y. Kumar Mishra, D. C. Toncu, M. Syväjärvi, A. Sharma and A. Tiwari, *Coord. Chem. Rev.*, 2022, **473**, 214771.
14 F. Shahbazi Farahani, M. S. Rahmanifar, A. Noori, M. F. El-Kady, N. Hassani, M. Neek-Amal, R. B. Kaner and M. F. Mousavi, *J. Am. Chem. Soc.*, 2022, **144**, 3411–3428.
15 G. Xu, C. Zhu and G. Gao, *Small*, 2022, **18**, 2203140.
16 J. Yin, N. Li, M. Liu, Z. Li, X. Wang, M. Cheng, M. Zhong, W. Li, Y. Xu and X. H. Bu, *Adv. Funct. Mater.*, 2023, **33**, 2211950.
17 E. Linnane, S. Haddad, F. Melle, Z. Mei and D. Fairen-Jimenez, *Chem. Soc. Rev.*, 2022, **51**, 6065–6086.
18 N. Rabiee, M. Atarod, M. Tavakolizadeh, S. Asgari, M. Rezaei, O. Akhavan, A. Pourjavadi, M. Jouyandeh, E. C. Lima, A. Hamed Mashhadzadeh, A. Ehsani, S. Ahmadi and M. R. Saeb, *Microporous Mesoporous Mater.*, 2022, **335**, 111670.
19 T. Cui, Y. Zhang, G. Qin, Y. Wei, J. Yang, Y. Huang, J. Ren and X. Qu, *Nat. Commun.*, 2023, **14**, 1974.
20 J. N. Hall and P. Bollini, *React. Chem. Eng.*, 2019, **4**, 207–222.
21 U. Kökçam-Demir, A. Goldman, L. Esrafili, M. Gharib, A. Morsali, O. Weingart and C. Janiak, *Chem. Soc. Rev.*, 2020, **49**, 2751–2798.
22 L. Ma, A. Jin, Z. Xie and W. Lin, *Angew. Chem., Int. Ed.*, 2009, **48**, 9905–9908.
23 O. K. Farha, I. Eryazici, N. C. Jeong, B. G. Hauser, C. E. Wilmer, A. A. Sarjeant, R. Q. Snurr, S. T. Nguyen, A. O. Yazaydin and J. T. Hupp, *J. Am. Chem. Soc.*, 2012, **134**, 15016–15021.
24 O. K. Farha, C. E. Wilmer, I. Eryazici, B. G. Hauser, P. A. Parilla, K. O'Neill, A. A. Sarjeant, S. T. Nguyen, R. Q. Snurr and J. T. Hupp, *J. Am. Chem. Soc.*, 2012, **134**, 9860–9863.
25 T. C. Wang, W. Bury, D. A. Gomez-Gualdron, N. A. Vermeulen, J. E. Mondloch, P. Deria, K. Zhang, P. Z. Moghadam, A. A. Sarjeant, R. Q. Snurr, J. F. Stoddart, J. T. Hupp and O. K. Farha, *J. Am. Chem. Soc.*, 2015, **137**, 3585–3591.
26 J. Bae, J. S. Choi, S. Hwang, W. S. Yun, D. Song, J. Lee and N. C. Jeong, *ACS Appl. Mater. Interfaces*, 2017, **9**, 24743–24752.

© 2025 The Author(s). Published by the Royal Society of Chemistry

Open Access Article. Published on 23 December 2024. Downloaded on 6/30/2025 11:45:52 PM.
This article is licensed under a Creative Commons Attribution-NonCommercial 3.0 Unported Licence.

27 J. S. Choi, J. Bae, E. J. Lee and N. C. Jeong, *Inorg. Chem.*, 2018, **57**, 5225–5231.
28 H. K. Kim, W. S. Yun, M. B. Kim, J. Y. Kim, Y. S. Bae, J. Lee and N. C. Jeong, *J. Am. Chem. Soc.*, 2015, **137**, 10009–10015.
29 K. R. Wright, K. Nath and A. J. Matzger, *Angew. Chem., Int. Ed.*, 2022, e202213190.
30 J. Bae, C. Y. Lee and N. C. Jeong, *Bull. Kor. Chem. Soc.*, 2021, **42**, 658–666.
31 J. Bae, S. H. Park, D. Moon and N. C. Jeong, *Commun. Chem.*, 2022, **5**, 51.
32 S. H. Park, R. A. Peralta, D. Moon and N. C. Jeong, *J. Mater. Chem. A*, 2022, **10**, 23499–23508.
33 J. Bae, E. J. Lee and N. C. Jeong, *Chem. Commun.*, 2018, **54**, 6458–6471.
34 W. M. Haynes, *CRC Handbook of Chemistry and Physics*, CRC Press, Boca Raton, 2016.
35 W. Qiu, Y. Wang, C. Li, Z. Zhan, X. Zi, G. Zhang, R. Wang and H. He, *Chin. J. Catal.*, 2012, **33**, 986–992.
36 J. Bentley, G. S. Foo, M. Rungta, N. Sangar, C. Sievers, D. S. Sholl and S. Nair, *Ind. Eng. Chem. Res.*, 2016, **55**, 5043–5053.
37 A. Dhakshinamoorthy, M. Alvaro and H. Garcia, *Catal. Commun.*, 2017, **97**, 74–78.

© 2025 The Author(s). Published by the Royal Society of Chemistry

communications materials

Perspective

https://doi.org/10.1038/s43246-024-00691-1

Benefits and complexity of defects in metal-organic frameworks

Check for updates

N. S. Portillo-Vélez[1], Juan L. Obeso[2,3], José Antonio de los Reyes[4], Ricardo A. Peralta[1] ✉, Ilich A. Ibarra[2,5] ✉ & Michael T. Huxley[6] ✉

Defect engineering has developed over the last decade to become an inimitable tool with which to shape Metal-Organic Framework (MOF) chemistry; part of an evolution in the perception of MOFs from perfect, rigid matrices to dynamic materials whose chemistry is shaped as much by imperfections as it is by their molecular components. However, challenges in defect characterisation and reproducibility persist and, coupled with an as-yet opaque role for synthetic parameters in defect formation, deny chemists the full potential of reticular synthesis. Herein we map the broad implications defects have on MOF properties, highlight key challenges and explore the remarkable ways imperfection enriches MOF chemistry.

Metal-organic Frameworks (MOFs) are a burgeoning class of hybrid organic-inorganic materials composed of metal cluster nodes interconnected by multitopic organic ligands to form highly crystalline, porous and chemically mutable structures[1,2]. Such an opening line would have succinctly captured the field only a decade ago. On the surface it still largely does, yet much has changed. The classical MOF is a rigid matrix defined by the chemical properties and dimensions of its molecular components, given to being by the power of reticular synthesis. The modular, chemically mutable design allows MOFs to be tuned to suit particular applications with angstrom scale precision, at least in theory. Breaking from this crystallography-centric view, which defined its infancy, MOF chemistry has evolved in recent years to embrace the imperfect, dynamic lattice[3–6]. The underlying form remains guided by reticular synthesis, but the chemistry and physical properties are enriched by imperfections.

As with any crystalline solid, the perfect structure portrayed by crystallography belies the omnipresent lattice defects and dynamic nature of coordination bonds[3–6]. Such imperfections are a ubiquitous feature of solid-state chemistry where they influence global properties even at vanishing concentrations[7]. For instance, just 0.1% defectivity in graphene or boron arsenide causes up to 95% reduction in thermal conductivity[8,9]. In MOFs, lattice defects manifest as missing linkers (ML) and/or missing clusters (MC) and have similarly drastic physicochemical implications (Fig. 1)[10–19]. For example, the blue-green colour associated with the prototypical Cu^{II} framework HKUST-1 actually arises from ubiquitous Cu^{I} defects rather than the Cu^{II} paddlewheel motif[15]. That this was revealed only recently illustrates the challenges associated with characterising lattice imperfections and defining their role in MOF chemistry. Since the first in-depth study concerning missing linker defects in UiO-66 was published in 2011[20], an extraordinary tapestry of defectivity has been unveiled. This transformation has occurred in concert with a significant advancement in experimental characterisation techniques that allow the local environment to be probed, in some cases providing real-space visualisation of defects[19,21,22].

It is in this rapidly changing environment that defect engineering has captured the imagination of MOF chemists[23–26] and dramatically expanded the utility and richness of MOF chemistry. Defectivity has significant implications on mechanical stability[13,14,27–30], hydrophobicity[31], photophysical properties[32], thermal conductivity[33,34], catalytic activity[23,35–42], pore size[43–47] and surface area[44,48–50] which are pertinent to commercial applications[12,51,52]. Properties involving cooperative lattice phenomena, including negative thermal expansion[53,54] and negative gas adsorption[55], are also influenced by defectivity. In some cases these manifestations are desirable: for instance mass transport benefits from hierarchical porosity introduced by defect engineering[56,57]. However, in applications such as

[1]Departamento de Química, División de Ciencias Básicas e Ingeniería, Universidad Autónoma Metropolitana-Iztapalapa, San Rafael Atlixco 186, Col. Leyes de Reforma 1ra Seccion, Iztapalapa, 09310 Ciudad de México, Mexico. [2]Laboratorio de Fisicoquímica y Reactividad de Superficies (LaFReS), Instituto de Investigaciones en Materiales, Universidad Nacional Autónoma de México, Circuito Exterior s/n, CU, Coyoacán, 04510 Ciudad de México, Mexico. [3]Centro de Investigación en Ciencia Aplicada y Tecnología Avanzada, LNAgua, Instituto Politécnico Nacional, Legaria 694, Col. Irrigación, Miguel Hidalgo, 11500 Ciudad de México, Mexico. [4]Departamento de Ingeniería de Procesos e Hidráulica, División de Ciencias Básicas e Ingeniería, Universidad Autónoma Metropolitana-Iztapalapa, San Rafael Atlixco 186, Col. Leyes de Reforma 1ra Seccion, Iztapalapa, 09310 Ciudad de México, Mexico. [5]On Sabbatical as "Catedra Dr. Douglas Hugh Everett" at Departamento de Química, Universidad Autónoma Metropolitana-Iztapalapa, San Rafael Atlixco 186, Col. Leyes de Reforma 1ra Seccion, Iztapalapa, 09310 Ciudad de México, Mexico. [6]School of Physics, Chemistry and Earth Sciences, Faculty of Sciences, Engineering and Technology, The University of Adelaide, Adelaide, SA, 5005, Australia. ✉e-mail: rperalta@izt.uam.mx; argel@unam.mx; michael.huxley@adelaide.edu.au

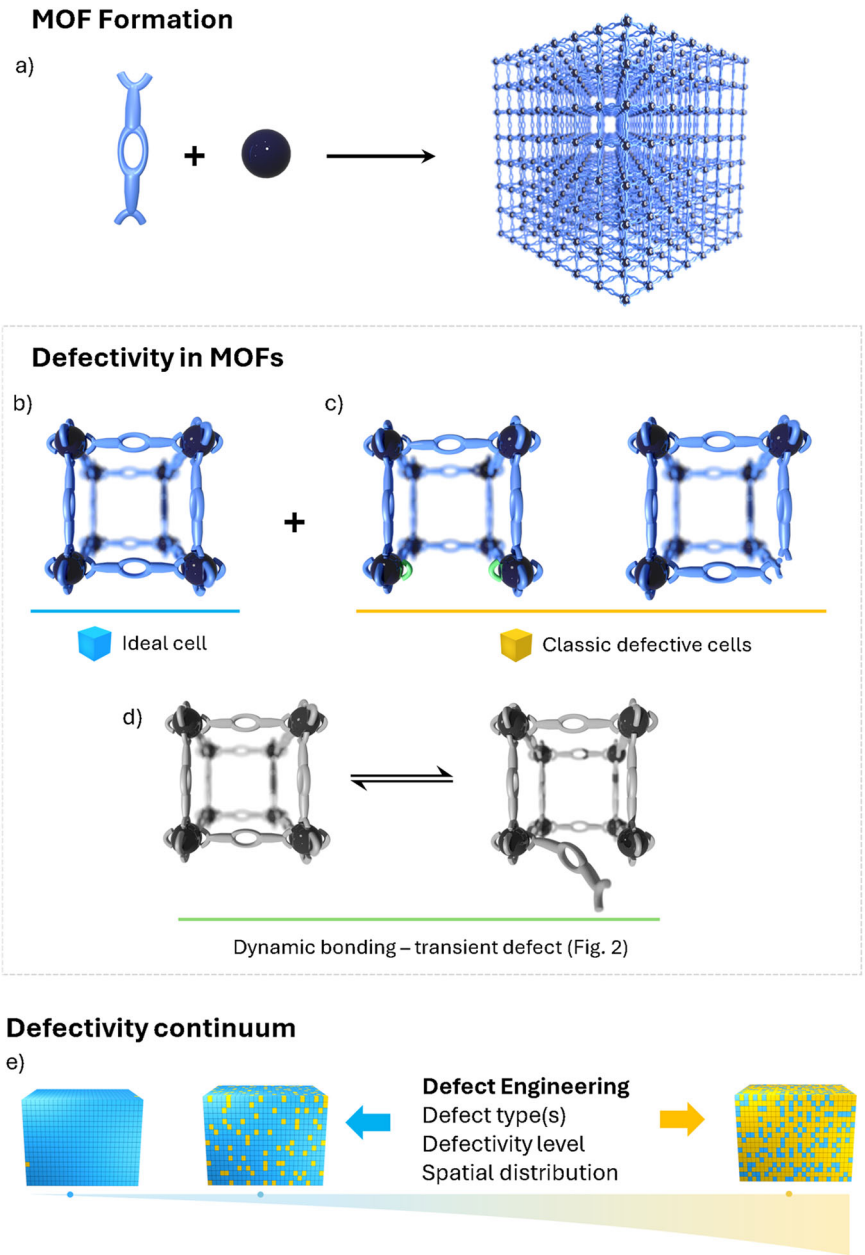


Fig. 1 | A Building block design susceptible to classical and transient defectivity. MOFs form from organic and inorganic components to produce a crystalline material (**a**) featuring a mixture of ideal cells (**b**) and a variable degree of defects, including missing linker (left) and missing cluster defects (right). Note: a green monotopic linker replaces the missing linker to complete the coordination sphere of the transition metal node (**c**). Related to classic defectivity are transient defects that arise from dynamic metal-linker bonds; this concept is explored in detail in Fig. 2. **d** The extent and type of defectivity present within a MOF sample can be modulated via both synthetic and post-synthetic methods, creating a continuum of defectivity with diverse physicochemical properties (**e**).

molecular sieving, success is dependent on angstrom scale refinement of the sieve pores, which is undermined by defectivity[58–61]. Thus, the optimum defectivity for a specific application exists somewhere along a defectivity continuum with extraordinary physicochemical diversity (Fig. 1). Harnessing this potential will require overcoming significant challenges, such as establishing the synthetic origin of defectivity, developing reliable characterisation techniques and consistent reporting, and ensuring synthesis protocols are reproducible[18,62].

This contribution posits defectivity as an intractable feature of MOF chemistry, the formation and evolution of which is intimately linked to the dynamic nature of metal-ligand coordination bonds (Fig. 2)[4,5,63,64]. The emergence of defect engineering has parallelled interest in dynamic metal-ligand bonding which persists in even the more robust Zr^{IV} frameworks[63–65]. We consider these short-lived dissociated metal-linker states as 'transient defects', distinct from the 'classical' ML or MC defects in both lifetime and in the sense that no structural components are missing. This underlying dynamic behaviour facilitates facile ligand/cation exchange[66–68], reversible guest responsive structural transformations[69–71] and the preparation of glass/liquid MOFs[4,5]. Moreover, dynamic metal-linker bonding is central to the emergence of crystallinity in MOFs, and equally so to the evolution of defectivity during crystallisation and post-synthetic handling[63]. The latter point raises an important but as yet rarely discussed question: as chemists seek to tune the extent, type and spatial distribution of defects within a fundamentally dynamic platform, how long – in terms of processing, handling and time - does it take before the engineered defects become defective? To answer this question a comprehensive understanding of dynamic processes and defectivity will be necessary. In particular, the elucidation of dynamic interactions and characterisation of disordered or defective frameworks requires new experimental and computational tools, and a departure from the classic MOF model[6,54,72–76].

Defectivity has been the focus of extensive discussion over the last decade. The benefits of defect engineering are well established[24,25,42] and are not the focus of this contribution. Rather, we explore the long-term challenges which persistently beleaguer chemists seeking to harness defect engineering. These include accurate characterisation and consistent reporting of defectivity, and the reproducible synthesis of phase pure samples with consistent defectivity. We consistently advocate that collaborative interlaboratory studies are an underutilised but effective tool for assessing reproducibility in

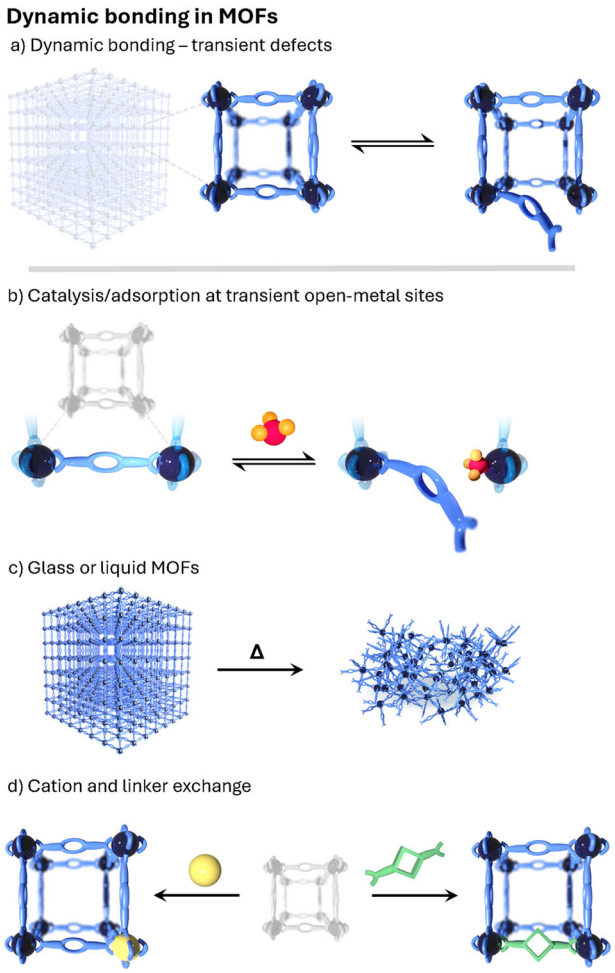


Fig. 2 | The various manifestations of dynamic metal-ligand bonding in MOFs. Related to defectivity is the presence of dynamic metal-ligand bonds (**a**) which manifest as transient open metal sites pertinent to adsorption and catalysis applications (**b**). Liquid MOFs are typically prepared by heating crystalline MOFs to form a melt state characterised by persistent dynamic coordination between molecular components, this can be quenched to form an amorphous coordination network classified as a glass (**c**). The now widely recognised tendency for MOFs to undergo facile linker or cation exchange is enabled by dynamic metal-linker interactions (**d**).

MOF synthesis and establishing the precise role of synthetic parameters in defect engineering. The value of reproducible synthesis and accurate characterisation is contingent on the stability of engineered defect landscapes. We contend that the role of dynamic bonding in defect formation and, particularly, the evolution of defect landscapes; cannot be understated (Table 1). To fully realise the promise of defect engineering, chemists must embrace the dynamic nature of coordination bonds and employ their most sophisticated experimental and computational tools to uncover the spatial, chemical and temporal diversity hiding behind the crystalline façade.

Characterisation and quantification of classical lattice defects in MOFs

Considering the pertinence of defects in all facets of MOF chemistry, their unambiguous characterisation and reproducibility are vital to harnessing the potential physicochemical diversity on offer[18,62]. To this end, a slew of characterisation techniques are regularly employed to quantify ML and MC defects, many of which were developed in the context of UiO-66 (see Box 1)[17,77]. The tools of defect analysis and their sophistication have necessarily evolved in tandem with the discovery of new defect types as well as their impact on readily measured physicochemical properties. The simplest and most widely reported defect analyses assess defectivity through its effect on MOF properties. Evoking Plato's Cave, this requires that experimentally measured metrics such as stoichiometry, surface area, diffraction pattern, thermal stability or pore-size distribution be compared to those of an ideal version of the framework. For example, Thermo-gravimetric Analysis is frequently used to quantify missing linker defects by establishing the ratio of inorganic to organic components through complete combustion of the former. By comparing the experimental value to that of the 'ideal' framework and making basic assumptions about the type of defect(s) present, an estimate of sample defectivity is obtained. The coexistence of MC and ML defects (and correlation of the former) complicates these simple assessments. Assumptions must be made. A more complete picture requires careful application of multiple complimentary techniques that can distinguish and quantify specific defect species[78].

Chemical characterisation of defect sites in-situ involves more sophisticated techniques which are less amenable to routine analysis and are more sample specific[48,79–82]. Exploiting the porosity inherent to most MOFs, various probe molecules have been employed to establish the chemical environment of defects in-situ. For example, the prototypical Cu^{II} framework HKUST-1 exhibits Cu^{I} defects which arise from impure inorganic precursors or in-situ thermally induced reduction of Cu^{II} moieties[40]. These are readily identified by monitoring CO probe molecules using IR spectroscopy because the CO stretching frequency is highly sensitive to the chemical environment of the node site to which it coordinates[79,83–85]. When supported with computational modelling, a picture emerges of the local environment at defect sites and their real-time evolution[79]. The same approach has a long history in zeolite chemistry[86–88]. Beyond CO, the catalogue of probe molecules now includes a homologous series of phosphines[80] and even fluorescent proteins[81], providing an expansive and bespoke toolbox with which to chemically and spatially distinguish defects. To observe defects in real-space however, chemists have turned to advancements in electron microscopy techniques – particularly High Resolution Transmission Electron Microscopy (HRTEM) – which enable imaging of MOF lattice defects (Fig. 3) and direct evidence for defect correlation and defective nanoregions within the crystal lattice[19,22,89]. We note that electron bombardment can also generate missing linker defects[90,91], careful consideration of these effects is essential when using HRTEM for defect analysis. It is by harnessing chemical probe experiments, computational chemistry and microscopy that chemists have revealed increasingly complex layers of defectivity in prototypical frameworks.

Even in extensively studied MOFs, new layers of previously imperceptible chemistry are being revealed using increasingly bespoke characterisation techniques[22,54,92–95]. Exemplars include defect termination and the fascinating interaction between framework nodes and guest molecules[63,96–98]. In an elegant example, Fu et al. employed in-situ ^{13}C Solid-state (SS) NMR and DFT calculations to identify the coordination geometry and location of formate defects in MOF-74[48]. Perhaps because the formate in question arises from in-situ decomposition of DMF during solvothermal synthesis rather than intentional addition of formic acid modulator, the defects had previously escaped notice. Yet they significantly impact on adsorptive properties: the surface area of Mg-MOF-74 decreases from 1900 m^2g^{-1} in the ideal framework to 700 m^2g^{-1} in defective frameworks, accompanied by concomitant reduction in CO_2 adsorption. This study underscores two key points that lie at the core of this contribution: (1) undetected and physicochemically significant defectivity persists even in prototypical frameworks due to challenges in identifying such species and (2) sophisticated computational and experimental techniques are becoming essential for elucidating more obscure MOF chemistry which is not perceptible via classic diffraction techniques[63,65,92,96,98,99]. The latter is true in the emerging field of amorphous MOFs[74,75,95,100] and is becoming so more generally as materials scientists seek to unravel the local chemical environment within crystalline frameworks and its effect on global properties[4,5,99].

The devil is in the details

While the subtle physicochemical implications have long been appreciated in solid-state chemistry, the overt outcomes of defectivity such as hierarchical

https://doi.org/10.1038/s43246-024-00691-1

Table 1 | Selected seminal works on defect engineering in MOFs

Notes on methodology	Defect type and implications[a]	MOF(s)	Year	Ref.
UiO Series				
Solvothermal synthesis (intrinsic defectivity)	Missing linker	UiO-66	2011	20
Solvothermal, modulator and reaction time varied	Missing linker defects tuned by varying modulator/reaction time	UiO-66	2013	45
Solvothermal, modulated synthesis	Correlated missing cluster defects	UiO-66(Hf)	2014	21
High linker/SBU ratio and high synthesis temperature	Minimal defectivity	UiO-66	2014	111
Acid modulation in solvothermal synthesis	Missing linker in each Zr_6 node	UiO-67	2015	146
Solvothermal, modulated synthesis	Predominantly missing cluster defects	UiO-66	2016	147
Post-synthetic thermal decomposition of doped thermolabile linker	Missing linker defects	UiO-66 mixed linker	2017	127
Modulated synthesis with trifluoroacetic acid followed by heat treatment	Trifluoracetic acid coordinated at missing linker defects can be removed by heating at 320 °C under vacuum to enhance mesopore size, or retained if heated at 200 °C.	UiO-66	2017	148
Synthesis at temperatures from 25–130 °C	Increasing synthesis temperature results in reduced defectivity	UiO-66-X (X = NH_2, OH, NO_2)	2017	149
Solvothermal synthesis using formic, acetic and benzoic acid modulators	Formic acid observed to form pore blockage defects, benzoic acid generates cluster defects/microporosity and acetic acid was associated with missing linker defects	UiO-AZB	2017	150
Solvothermal synthesis using excess modulator and sub-stoichiometric linker.	Hierarchical porosity produced by missing linkers/clusters	UiO-66, MOF-808, MIL-53, DUT-5	2017	151
Post-synthetic healing of missing linker defects	Missing linker defects healed by post-synthetic treatment with solution containing excess linker. Improved sieving capacity observed.	UiO-66-$(OH)_2$	2017	152
Solvothermal synthesis using acid modulator	Missing linker defects, detrimental towards butane isomer separation	MOF-801	2018	60
Solvothermal synthesis, post-synthetic heat treatment	IR spectroscopy used to monitor highly sensitive CO probe molecules in UiO-66, revealing missing linker defects (coordinatively unsaturated Zr^{IV} sites) and evolution of defect landscape during post-synthetic heat treatment of MOF.	UIO-66	2018	79
Solvothermal synthesis using acid modulator	Defects found to be detrimental towards C3 hydrocarbon sieving properties.	MOF-801	2019	59
Acid modulation in solvothermal synthesis	Ordered missing linker and missing cluster defects	UiO-66	2019	19
Post-synthetic defect healing	Missing linker defects healed by post-synthetic reaction with solution containing excess linker. Samples with reduced defectivity exhibit enhanced Kr/Xe selectivity.	NU-403	2020	61
Modulator free solvothermal synthesis, water conc. controlled	Predominantly missing cluster defects	UiO-66	2020	153
Solvothermal synthesis using 4-sulfonatobenzoate as both modulator to generate defects and hemilabile structural linker. H_2SO_4 post-synthetic treatment increases missing linker defectivity.	Up to six missing linkers per cluster. Increased thermal stability observed in defective structure due to hemilabile linker.	UiO-66	2020	154
Acid modulated solvothermal synthesis, varied linker/SBU ratio	Direct imaging of correlated defects with scanning electron diffraction	UiO-66(Hf)	2020	89
Targeted removal of Zn clusters via acid wash, Zr-oxo clusters intact	Missing cluster defects	UiO-66(Zn,Zr)	2021	155
Solvothermal synthesis temperature used to tune defectivity	Tuning hydrophobicity via defectivity	UiO-66	2022	31
Solvothermal synthesis using mixed linker approach which includes the thermolabile adipic acid linker.	Missing linker defects generated during thermolysis of adipic acid linkers at 300 °C.	UiO-66	2022	156
Solvothermal, modulators (*p*-nitrobenzoic acid or *p*-hydroxybenzoic acid) act as defective linkers.	Missing linker defects arising from incorporation of modulators in structure.	UiO-66	2022	157
Solvothermal, 80 °C, 15-fold ligand/SBU ratio	Minimal defectivity	UiO-66	2023	58
Structural evolution under electron beam	Missing linker defects	UiO-66	2023	90
Solvothermal synthesis, varied linker and modulator concentration	Controlled correlated missing linker and cluster defects	UiO-66	2023	158
Acid modulated solvothermal synthesis	Missing linker defects promote longer lifetime excited states for catalysis	UiO type framework	2024	159
Cluster-cluster co-nucleation (CCCN) strategy	Well-defined cluster defects	UiO-66	2024	160

Table 1 (continued) | Selected seminal works on defect engineering in MOFs

Notes on methodology	Defect type and implications[a]	MOF(s)	Year	Ref.
Reaction-diffusion process at room temperature	Missing linkers	UiO-66(OH)$_2$	2024	161
Acetic acid modulated reaction diluted using ethanol to promote ultrasmall nanocrystals (4–6 nm)	Highly defective nanocrystals, up to 45% missing linkers	UiO- and MOF-801 frameworks	2024	162
HKUST Series				
Solvothermal synthesis (intrinsic defectivity)	Low defectivity, missing linkers	HKUST-1 (SURMOF)	2012	108
Incorporation of defective linkers	Defective linkers create partial 'missing linker' defects.	HKUST-1(Ru)	2014	37
Incorporation of defective linkers	Defective linkers create partial 'missing linker' defects.	HKUST-1	2014	83
Reversible linker dissociation	Reversible linker dissociation implicated in catalysis	HKUST-1	2014	118
Linker fragmentation	Incorporating defects to modulate gas uptake properties	NU-125, HKUST-1	2014	50
Doping structure with defective linkers	Mixture of missing cluster defects as well as partial missing linker defects and reduced Ru centres.	HKUST-1(Ru)	2016	163
Defective linker and variation of synthesis parameters	Defective Cu^{II}-Cu^{I} nodes, missing cluster defects	HKUST-1	2017	164
Layer by layer thin film growth incorporating sonication	Minimal defectivity	HKUST-1	2017	15
Water modulated, synthesis of MOF thin films	Reduced defectivity	HKUST-1 (SURMOF)	2018	165
Post-synthetic acid etching strategy	The disassembly of a cluster and linkers	HKUST-1	2019	166
Defective linker introduced by 'mixing' or 'alternating' method during thing film synthesis to tune defect formation	Defective Cu^{II}-Cu^{I} nodes	HKUST-1 (SURMOF)	2020	167
Thermal treatment	Coordinatively unsaturated sites, reduced Ru/Rh centres	Ru/Rh HKUST-1	2020	84
Liquid/Salt assisted grinding, treatment with alcohols	Cu^{I} defects, dissociated carboxylate sites	HKUST-1	2020	168
Defective linker strategy	Defect type and distribution characterised using Raman micro-spectroscopy.	HKUST-1	2020	169
Defective linker strategy	Defect type and distribution characterised by full-field tomographic X-ray adsorption spectroscopy.	HKUST-1	2021	170
Thermally induced decarboxylation, reversible under CO_2 treatment	Defective Cu^{II}-Cu^{I} nodes, predominantly at surface	HKUST-1	2021	92
MIL series				
Microwave-assisted solvothermal synthesis with urea modulator	Ligand replacement	MIL-53(Al)	2018	43
Structural evolution under electron beam	Structural rearrangement, deformation of crystal	MIL-101(Cr)	2020	91
Photothermal treatment of MIL-125(Ti)-NH2 in presence of Triethanolamine reduces Ti^{IV} to Ti^{III}, weakening coordination bonds and thereby facilitating missing linker defect formation.	Missing linker defects	MIL-101(Ti)-NH2	2020	171
Microwave synthesis at low temperature	Missing linkers	MIL-125	2022	172
Reversible photo-induced metal-linker dissociation	Reversible linker dissociation	MIL-101(Fe)	2023	129
MgMOF-74				
Graphene oxide modulator	Missing cluster defects	Mg-MOF-74	2023	44
Solvothermal synthesis, in-situ formation of formate	Missing linker (formate substitution)	Mg-MOF-74	2023	48
Solvothermal synthesis, defective linker strategy	Unsaturated metal centres formed by insufficient donors on defective linker (1,4-benzenedicarboxylate)	Mg-MOF-74	2023	173
MUV series				
Synthesis in sub-stoichiometric linker conditions	Missing cluster vacancies	MUV-10	2021	174
Solvothermal, systematic investigation into effect of modulator	Up to 40% missing linker defects	MUV-10	2021	175

Table 1 (continued) | Selected seminal works on defect engineering in MOFs

Notes on methodology	Defect type and implications[a]	MOF(s)	Year	Ref.
Solvothermal, systematic investigation using variety of chemically functionalised modulators	Missing linker/cluster defects	MUV-10	2022	176
Solvothermal, hydroxy- or fluoro-isophthalic acid modulators	Defect extent tuned by modulator choice. Effect of defects on photocatalytic activity.	MUV-10	2022	177
NOTT-100				
Thermal treatment or defective linker strategy	Coordinatively unsaturated sites, defective Cu^{II}-Cu^{I} nodes	NOTT-100	2020	85
Incorporation of defective linkers	Coordinatively unsaturated sites, defective Cu^{II}-Cu^{I} nodes	NOTT-100	2020	178
ZIF series				
NA	Density Functional Theory based study of defect propagation in ZIFs.	ZIF-8	2019	179
^{60}Co gamma radiation employed to generate defects under ambient conditions	Extensive missing linker defects	ZIF-7	2023	180
ZIF-8 thin films and powders	Missing linker and cluster defects identified via vibrational spectra, molecular dynamics simulations	ZIF-8	2024	181
MOF-808				
Solvothermal, linker/SBU ratio 1:3, 2 days (compared to 1:1 and 7 days for pristine sample)	Missing linker defects	MOF-808	2021	182
Solvent free synthesis. Precursors are ground in mortar and pestle, then crystallised in autoclave at temperatures between 90–130 °C.	Missing linker/cluster defects.	MOF-808	2023	183
Defective linker strategy	Defective Zr-oxo cluster nodes due to incorporation of bi- rather than tri-carboxylate linkers.	MOF-808	2024	184
Defective linker strategy	Defective Zr-oxo cluster nodes due to incorporation of bi- rather than tri-carboxylate linkers.	MOF-808	2024	185
Miscellaneous frameworks				
Thermal treatment induces defect formation in surface mounted MOF	Cu^{I}-Cu^{II} node defects with missing linkers	UHM-3	2015	186
Competitive coordination strategy using Lauric acid.	Hierarchical porosity arising from missing linkers/clusters	MOF-5	2016	187
Solvothermal synthesis, using L-lac or propanoic acid as modulator to generate missing linker defects.	Missing linker defects impact chiral separation capacity of homochiral framework.	$[Zn_2(bdc)(L\text{-lac})(dmf)]$[b]	2017	188
Multistep post-synthetic partial linker exchange	Ditopic linker partially exchanged for monotopic pyridine-carboxylate (missing linker defects) which form a trans-pyridine binding site for metalation.	PCN-160	2018	189
Solvothermal synthesis, systematic variation of reaction conditions to promote phase purity and modulate defectivity	Sterically demanding modulators found to favour missing cluster defects. Smaller and moderately acidic modulators predominantly generated missing linker defects.	PCN-222, PCN-223, MOF-525	2019	78
Solvothermal synthesis	Missing linker defects featuring bridging or mono-dentate methoxide (depending on the activation temperature).	COK-47	2019	190
Solvothermal synthesis (intrinsic defectivity)	Missing linkers	PCN-221	2021	110
Synthesis with linker mixture	Formation of Cu^{I}-Cu^{II} coordinatively unsaturated sites	Cu-BDC	2022	191
Reversible defect formation upon guest sorption	Reversible linker dissociation	$Cu_2(BDC)_2DABCO$[b]	2022	119
Incorporation of defective linkers	Coordinatively unsaturated sites, defective Cu^{II}-Cu^{I} nodes	$[Cu_2(Me\text{-}trz\text{-}ia)_2]$[b]	2024	192

[a]Studies published prior to 2014 were prepared before missing cluster defects first observed in UiO-66.

[b]Me-trz-ia = 3-methyl-triazolyl isophthalate, BDC = 1,4-benzenedicarboxylate, DABCO = 1,4-diazabicyclo[2.2.2]octane, dmf = dimethylformamide, *L*-lac = *L*-lactic acid.

Where possible, entries are presented in date order and grouped according to MOF type.

Box 1 | UiO-66: the preeminent platform for studying defectivity

The central protagonist in the story of MOF defectivity is UiO-66, a robust framework composed of $[M_6(OH)_4(O)_4]^{12+}$ (M = Zr^{IV} or Hf^{IV}) nodes interconnected by 12 benzene-1,4-dicarboxylate (BDC) linkers in the ideal structure (Fig. 3)[77,193]. The intense interest in defect engineering UiO-66 arises from its capacity to tolerate loss of up to 6 ligands per cluster[154], providing scope to explore defect-enhanced catalytic[35] and adsorptive properties[25,147]. Missing linker (ML) defects were first identified in UiO-66 in 2011 by Valenzano et al. [20]. Later, in 2014, Cliffe and co-workers confirmed the presence of missing cluster (MC) defects in UiO-66(Hf) which form correlated defect nanoregions with reo network topology (the ideal framework features fcu topology)[21]. Interestingly, diffuse scattering arising from short-range order of correlated defects was originally attributed to disordered solvent[194], highlighting how our understanding of defectivity has continued to evolve as earlier assumptions about MOF chemistry are re-assessed. In 2019, missing cluster defects concurrent with missing linkers were observed to form localised scu topology in UiO-66[19]. Calculations indicate that defects with local reo, scu and bcu topologies (encompassing the MC/ML defects described above) all attract a similar energy penalty relative to the ideal fcu topology, suggesting that they are all accessible under MOF synthesis conditions and can coexist within a sample (Fig. 3)[19]. The presence of missing linker and cluster defects within the UiO-66 lattice, including the correlation of MC defects to form defect nanoregions is now well established[21], along with synthetic tools with which to tune the extent and type of defectivity expressed within a sample[147,153,158]. It is likely that further research will unveil novel defect types as the UiO family is scrutinised with new experimental and computational techniques. Success in the UiO space has motivated defect engineering studies involving other prototypical frameworks such as HKUST-1[14], MUV-10[174,175] and MOF-74 (see Table 1 for seminal defect engineering studies)[44,48]. Yet, although synthetic parameters play a major role in modulating defectivity in as-synthesised MOFs[150,153,175], the precise role of specific parameters is not fully understood even in the intensively studied UiO family[18,150].

porosity or catalytic activity have garnered more attention from MOF chemists. But defectivity is increasingly understood to impact MOF bulk modulus, mechanical stability and thermal conductivity[13,14,27–30,33,34,101,102]. Such subtle implications are not always prioritised (or evident) in the laboratory, but can become pronounced at scale and as MOFs are increasingly integrated into hybrid materials[51]. For example, to avoid cracking and delamination in devices, the thermal expansion properties of a MOF must be compatible with those of materials with which it is interfaced[51]. Similarly, thermal conductivity becomes more influential at scale due to the need to efficiently dissipate the heat released during processes such as adsorption[103–105]. Yet thermal expansion and thermal conductivity remain poorly represented in MOF literature and the effects of defectivity are less understood than for other physicochemical properties.

Extraordinary surface areas and chemical mutability has placed MOFs at the forefront of future gas adsorption applications. Adsorption is however an exothermic process and since MOFs exhibit poor thermal conductivity, heat dissipation therefore becomes a concern. Low density and high porosity restrict thermal transport in MOFs which explains why ZIF glasses exhibit higher thermal conductivity than their crystalline (and more porous) counterparts[106]. Porosity is not the only culprit though. In solid-state materials, phonons play an integral role in thermal conductivity[8,9] and it is increasingly evident that lattice defects in MOFs (and adsorbate molecules[105]) induce phonon scattering that reduces thermal conductivity further than intrinsic porosity would demand[33,34]. Intriguingly, correlated MC defects are associated with an increase in thermal conductivity compared to randomly distributed MC or ML defects[33]. This behaviour is attributed to reduced phonon scattering in the direction of thermal transport and hints at a complex interplay between defectivity, phonon scattering and thermal transport that may concern other processes in which phonons are implicated[107]. Thus the effects of defectivity on MOF chemistry concern as much the infinitesimal details of lattice vibrational modes as they do the palpable outcomes of defect engineering. While much anticipation accompanies the latter, the devil is in the details and commercial emphasis on benchmark physicochemical properties will refocus attention accordingly. At present though, studies concerning the thermal transport properties of MOFs typically assume a 'defect-free' material or do not consider defects at all[33,34]. In this conceptual simplification a vital opportunity to define fundamental physicochemical attributes in the context of defectivity is overlooked.

Reproducible MOF synthesis

While challenges remain in distinguishing, quantifying and spatially elucidating defectivity; advancements in characterisation will only benefit the field if defectivity in a given framework can be reliably reproduced across time and place. Indeed, variable phase purity or defectiveness is incompatible with commercial applications[62]. Discussion of MOF defectivity naturally intersects with this broader debate around reproducibility of MOF synthesis outcomes. For example, Kieslich and colleagues attribute the significant variability in experimental bulk moduli to poor defect reproducibility across samples of the same MOF analysed by different laboratories[28]. Part of this issue arises from phase impurities[62] (including amorphous impurities) and/or variable and inadequately characterised defectivity. Even different samples of the same MOF can exhibit varying defectivity between for instance, powder and epitaxial forms, which reflects differences in synthesis conditions[108]. One strategy for eliminating variable sample defectivity is to prepare one large batch of MOF on which all analysis is performed[109]. While this sidesteps the core issue, the paucity of studies on defect reproducibility, coupled with genuine characterisation challenges, currently leaves little alternative.

The question of reproducible phase purity and defectivity in MOFs was underscored in an insightful interlaboratory study by Boström et al.[62]. The focus was a family Zr^{IV} Porphyrinic Coordination Network (PCN) MOFs which can form multiple phases under the same synthesis conditions[62,110] and are highly susceptible to defects[78]. Strikingly, under the interlaboratory study only 1 in 10 syntheses targeting PCN-222 yielded phase pure product despite implementing an identical literature procedure across the participating laboratories. Synthesis of phase pure ligand ordered PCN-224 failed in all cases. Factors including reaction vessel dimensions, hydration of the inorganic precursor and ambient humidity are likely contributors to the erratic reproducibility. This rouses an unavoidable question: if subtle parameters so profoundly impact MOF morphology, why should defectivity be any less susceptible to variation? Considering the potent implications on physicochemistry, defect reproducibility remains conspicuously underexplored. We note that the interlaboratory study cited above did report – albeit cautiously, considering the erratic phase purity of the samples - variable defectivity across PCN samples. This work simultaneously highlights the challenge facing reproducible MOF synthesis and outlines an effective roadmap for much needed interlaboratory studies concerning defect reproducibility and characterisation.

Defect-free MOFs?

Having established defectivity as an easily obfuscated but central determinant of MOF physicochemistry, we turn now to its minimisation and the temporal stability of defect landscapes. The popular term 'defect-free' is a misnomer: defects cannot be entirely eliminated, but can be minimised

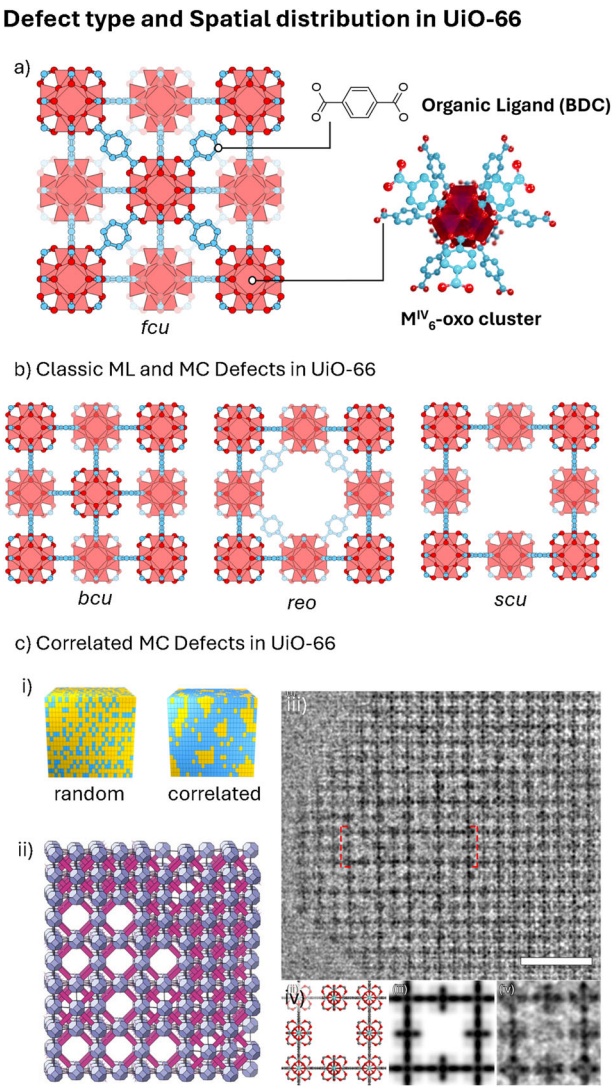


Fig. 3 | Defect type and spatial distribution in UiO-66. The MOF UiO-66 is composed of BDC linkers interconnected by 12 connected M^{IV}-oxo clusters (M = Zr, Hf) to form a robust and highly porous network. A representation of the ideal structure with fcu net, including the ideal 12-connected cluster, is presented (**a**). The material is highly susceptible to defects including ML (bcu net) and MC (reo or scu net) (**b**). MC defects are known to form correlated defect nanoregions in some UiO samples, leading to aggregation of defects which is represented schematically in i) and ii). HRTEM image showing significant correlation of missing cluster defects adopting the scu net (scale bar represents 5 nm) iii. The scu structural model, simulated potential map and actual averaged HRTEM image representing one unit cell (left to right, iv). Image components c(ii) adapted with permission from ref. 21. Copyright 2014 Springer Nature and c(iii)-c(iv) adapted with permission from ref. 19. Copyright 2019 Springer Nature.

using synthetic[58,111] and post-synthetic strategies[19,112]. Samples with minimal defectivity show improved stability, are better model materials and find virtue in applications such as molecular sieving and sensing[15,58,111]. Thus, two motivations for defect minimisation can be distinguished: the preparation of model materials for fundamental studies and the optimisation of materials for applications such as molecular sieving or sensing. Embodying the former scenario, a recent study explored the epitaxial growth of optically pure, defect-free HKUST-1 thin films which are of interest in fundamental chemistry and sensing applications (Fig. 4)[15]. Rather than exhibiting the blue hue synonymous with HKUST-1, the films are colourless owing to the effective elimination of strongly absorbing Cu^{I}/Cu^{II} defects. Recent work by Liu et al. epitomises the latter category: a series of ultra-low defectivity UiO membranes with precisely tuned pore apertures were prepared and demonstrated exceptional H_2/CO_2 selectivity an order of magnitude greater than defective analogues (Fig. 4)[58]. The examples above demonstrate that defectivity can be minimised to obtain materials that closely approximate their ideal counterparts. The question that is particularly apparent in this context, but is just as relevant in classic defect engineering scenarios, is how effectively can specific defect landscapes be maintained under operating conditions given the persistence of dynamic metal-ligand bonding in extended frameworks?[4,5].

While appreciation of dynamic metal-ligand bonding continues to grow in the MOF community, the chemistry is not new. For instance, the facile displacement of labile ligands is central to transition metal catalysis[113,114]. In MOFs, dynamic metal-ligand bonding is implicated in the mechanism of hydrothermal decomposition which can be considered as an accumulation of defects that culminates in loss of crystallinity[56,115–117]. Facile linker and cation exchange as well as the emergence of glass and liquid MOFs is predicated on dynamic bonding. Reversible dissociation of metal-linker bonds has been invoked in catalytic and adsorptive applications that exploit the resulting transitory open metal sites (Fig. 2)[70,118–124]. Thus, one could make the case that reversible metal-linker dissociation events create a transient defect which is separate from classic ML defects only in as far as life-time is concerned. Spectroscopy experiments have confirmed that such species (or at least the soft-mode precursory states) are ubiquitous in carboxylate MOFs[64,65,107,125] and that temperature[65], particle size[125,126] and guest molecules[64] modulate the relative populations of 'tight' and 'loose' states. However, we posit that MOF defects as we define them here constitute a departure from ideal stoichiometry – that is, components are missing rather than momentarily detached. In this sense dynamic bonding is an explanation for evolving defectivity within a crystal such as occurs during activation, crystal growth or post-synthetic modification; but is itself distinct from classic ML or MC defectivity. We define 'transient defects' to capture this distinction. The fact that post-synthetic defect engineering is frequently affected by design[40,111,127] but also unintentionally during processes such as activation, sorption and solvent exchange attests that designer defect profiles are liable to change under forcing conditions[79]. Even during crystallisation, the relative abundance of MC and ML defects in UiO-66 evolves due to Ostwald Ripening processes that produce larger crystals with less MC defects[19]. Washing UiO-66 has been observed to increase defectivity, most likely due to exchange of hydrolysed linkers with solvent[111]. The underlying dynamic nature of MOFs must be reconciled with the long-term stability of engineered defect landscapes, particularly when intended operating conditions are likely to expedite structural evolution.

Chemists have already revised the classical MOF to include myriad defects in the crystal lattice. Perhaps this revision does not go far enough. If one considers the continuous rotation of linker functional groups, dynamic coordination chemistry, phonon modes, guest responsive behaviour (such as breathing, gate opening etc.) as well as the motion of guests colliding and interacting with the framework themselves, the lattice is not only imperfect but an evolving, heaving kaleidoscope of molecular activity. Routine characterisation techniques are blind to such local dynamics and their influence on defectivity. Indeed time was recently posited as a fourth dimension in which MOF chemistry can be intentionally engineered[128]. This necessitates that framework materials be probed with techniques that can provide a time-resolved understanding of dynamic molecular processes[63,76,94,129,130]. Steps have already been taken in this direction. Ultra-fast spectroscopy experiments coupled with molecular dynamics simulations have, for instance, uncovered the surprising picosecond rearrangement of hydrogen bonding networks involving MOF-pore confined water molecules[131]. Solid-state ultrafast magic-angle spinning ^{19}F NMR has determined the metal-linker exchange rates in Zn(II) coordination polymers to be on the order of $3 \times 10^4\ s^{-1}$ at room temperature[73]. The metal-ligand dynamics responsible for liquid MOF formation, are known to occur on the order of picoseconds on the basis of molecular simulations[75]. Evidently, characterisation and simulation tools required to elucidate the dynamics underpinning defect propagation exist but their application is limited by the bespoke sample-

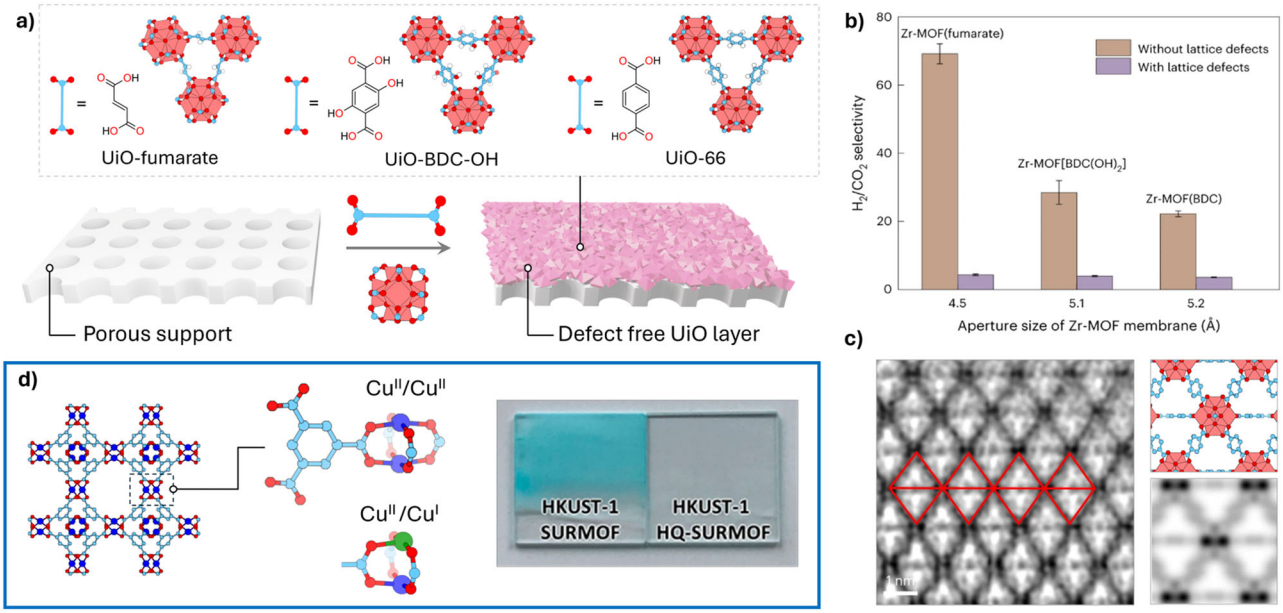


Fig. 4 | Defect-free MOFs. a Defect-free UiO membranes are synthesised from fumaric acid, BDC or BDC-OH linkers to form a family of supported membranes with precisely regulated pore sizes. **b** The H_2/CO_2 selectivity UiO membranes is dependent on the pore size determined by linker choice and strongly degraded by increased defectivity. **c** HRTEM image of UiO-fumarate membrane provides evidence for a near ideal lattice. Figure elements adapted with permission from ref. 58. Copyright 2023 Springer Nature. **d** The structure of HKUST-1 is composed of Cu^{II} paddlewheel nodes bridged by BTC linkers. A known defect involves reduction of one Cu^{II} centre and loss of a single carboxylate linker. Defective HKUST-1 SURMOF samples exhibit a blue colour while high quality thin films are colourless. Figure elements adapted with permission from ref. 15. Copyright 2017 American Chemical Society.

specific experiments, specialist instrumentation and data analysis required. Our understanding of defectivity (among many other aspects of MOF chemistry) will remain incomplete until the underlying local dynamics are resolved. The application of experimental and computational expertise to this end must therefore be prioritised.

Our intention in raising these points is not to dissuade efforts to minimise defectivity or indeed, engineer it. Rather, we argue that these efforts are central to maximising the utility of MOFs in wide-ranging applications. Yet the transformative potential and ubiquity of dynamic bonding demands that more scrutiny be placed on the long-term stability of defect landscapes. Perhaps what is needed most is an interlaboratory study that assesses both defect reproducibility and stability in MOFs, focusing on the effects of routine processing on defect extent, type and distribution.

Future directions and concluding remarks

The preceding decade has seen defect engineering claim in MOF chemistry a similar eminence to what it has long enjoyed in semiconductor science. While MOFs spanning the full spectrum of defectivity, from amorphous to 'defect-free', find merit in specific applications, it is only by learning to reproducibly tune and characterise defectivity that chemists can fully realise the precision promised by reticular chemistry. A wealth of defect engineering research has proven beyond doubt that defect extent, type and spatial distribution to be tuned by judicious choice of synthetic parameters. Yet the exact role of temperature, stoichiometry and modulator remains unclear and often conflicting[18]. It is evident from existing work concerning the reproducibility of PCN frameworks that subtle factors wield significant influence over sample morphology and this conclusion likely extends to defectivity[62]. Delineating these relationships is a challenging task well suited to large-scale interlaboratory studies.

Attached to the question of reproducibility is the difficulty in characterising and consistently reporting defectivity. Despite the historical significance of crystallography, defect characterisation requires that chemists look beyond diffraction and towards methodologies that probe local chemistry. MOF characterisation is therefore guided ever more by materials science fields that never enjoyed the luxury of crystallinity[73,75,100,132]. In this sense defect characterisation shares challenges with glass, liquid and heterometallic/multicomponent MOFs wherein the relationship between the spatial distribution of disordered molecular components and emerging properties is only revealed by sophisticated analysis[72,133]. The value of computational chemistry in this process - linking structural and physicochemical properties in framework materials – cannot be understated, especially where disorder is present. This role will grow as machine learning is increasingly adopted[52,99,134–137]. This evolution in computational and experimental techniques is well underway and will undoubtedly reveal new defect types and correlations in the future. All of this is not to diminish the extraordinary role crystallinity plays in the archetypal properties and conceptual elegance of extended framework materials, nor the insight crystallography provides MOF chemists[76,138,139]. Nonetheless, a crystal structure cannot capture the whole picture, which is textured with a vastly richer chemistry than the classical MOF lattice can convey.

That MOFs undergo facile linker/cation exchange[68,140,141] and post-synthetic structural transitions to new crystalline[142,143] or amorphous glass phases[74] confirms that coordination bonds do not relinquish their dynamic nature when incorporated in extended framework materials. Yet the role of labile coordination bonds in propelling the evolution of defectivity in MOFs, including during crystallization, activation and solvent exchange remains underexplored[63]. While defectivity is routinely analysed in as-synthesised samples, the stability of defect landscapes under operating conditions must be established to confirm that properties imbued by defect engineering are retained. Considering the significant – often beneficial - impact defects have on physicochemical properties, the unintended effects of post-synthetic processing in shaping the defect landscape over time would seem just as important as synthetic parameters are in shaping the initial defectivity.

We emphasise again that by underscoring challenges surrounding defect characterisation, reproducibility, and stability our intention is to inspire rather than discourage further work in this vital field. Indeed, defectivity and dynamic bonding are part of an expansive and ongoing reimagination of MOFs. Inspiration can be found in the revolution underway in the field of structural biology where advanced Electron Cryomicroscopy enables time-resolved atomic-resolution snapshots to be obtained which capture the

extraordinary dynamic properties from which biological function is derived[144,145]. Insight garnered from this transformative technology far exceeds traditional crystallographic or NMR based techniques, confirming that even within well-established fields opportunity remains to avail deeper understanding from emerging technologies. We posit that while the underlying dynamic processes in MOFs are challenging experimental subjects today, their effects should not evade our imagination. Based on the evidence available already, the role of dynamic metal-linker interactions cannot be overestimated in any attempt to conceptualise or engineer defectivity.

Much has been reaped from the fertile chemical landscape that MOFs present. Increasingly, advancement has stemmed from embracing - and exploiting - the imperfections and dynamic properties of the crystalline lattice. The ascendency of glass MOFs is the ultimate manifestation of this transformation[74,75,100]. While the popular description of MOFs emphasises crystalline order and reticular synthesis; it is increasingly evident that imperfections grant access to new layers of chemical complexity and extraordinary opportunity.

Received: 23 April 2024; Accepted: 29 October 2024;
Published online: 08 November 2024

References

1. Furukawa, H., Cordova, K. E., O'Keeffe, M. & Yaghi, O. M. The chemistry and applications of metal-organic frameworks. *Science* **341**, 974–985 (2013).
2. Yaghi, O. M. et al. Reticular synthesis and the design of new materials. *Nature* **423**, 705–714 (2003).
3. Morris, R. E. & Brammer, L. Coordination change, lability and hemilability in metal-organic frameworks. *Chem. Soc. Rev.* **46**, 5444–5462 (2017).
4. Obeso, J. L. et al. The role of dynamic metal-ligand bonds in metal-organic framework chemistry. *Coord. Chem. Rev.* **496**, 215403 (2023).
5. Svensson Grape, E., Davenport, A. M. & Brozek, C. K. Dynamic metal-linker bonds in metal–organic frameworks. *Dalt. Trans.* **53**, 1935–1941 (2024).
6. Allendorf, M. D., Stavila, V., Witman, M., Brozek, C. K. & Hendon, C. H. What Lies beneath a Metal–Organic Framework Crystal Structure? New Design Principles from Unexpected Behaviors. *J. Am. Chem. Soc.* **143**, 6705–6723 (2021).
7. Queisser, H. J. & Haller, E. E. Defects in Semiconductors: Some Fatal, Some Vital. *Science* **281**, 945–950 (1998).
8. Bouzerar, G., Thébaud, S., Pecorario, S. & Adessi, C. Drastic effects of vacancies on phonon lifetime and thermal conductivity in graphene. *J. Phys. Condens. Matter* **32**, 295702 (2020).
9. Protik, N. H., Carrete, J., Katcho, N. A., Mingo, N. & Broido, D. Ab initio study of the effect of vacancies on the thermal conductivity of boron arsenide. *Phys. Rev. B* **94**, 045207 (2016).
10. Liu, J. et al. Photoinduced Charge-Carrier Generation in Epitaxial MOF Thin Films: High Efficiency as a Result of an Indirect Electronic Band Gap? *Angew. Chem. Int. Ed.* **54**, 7441–7445 (2015).
11. Thornton, A. W., Babarao, R., Jain, A., Trousselet, F. & Coudert, F. X. Defects in metal–organic frameworks: a compromise between adsorption and stability? *Dalt. Trans.* **45**, 4352–4359 (2016).
12. Burtch, N. C., Heinen, J., Bennett, T. D., Dubbeldam, D. & Allendorf, M. D. Mechanical Properties in Metal–Organic Frameworks: Emerging Opportunities and Challenges for Device Functionality and Technological Applications. *Adv. Mater.* **30**, 1704124 (2018).
13. Rogge, S. M. J. et al. Thermodynamic Insight in the High-Pressure Behavior of UiO-66: Effect of Linker Defects and Linker Expansion. *Chem. Mat.* **28**, 5721–5732 (2016).
14. Wang, B., Ying, P. & Zhang, J. Effects of Missing Linker Defects on the Elastic Properties and Mechanical Stability of the Metal–Organic Framework HKUST-1. *J. Phys. Chem. C.* **127**, 2533–2543 (2023).
15. Müller, K. et al. Defects as Color Centers: The Apparent Color of Metal–Organic Frameworks Containing Cu2+-Based Paddle-Wheel Units. *ACS Appl. Mater. Interfaces* **9**, 37463–37467 (2017). **This work showed that the blue colour associated with the prototytpical framework HKUST-1 arrises not from the Cu-paddlewheel motif upon which its structure is based, but instead from defects**.
16. Siddiqui, S. A., Prado-Roller, A. & Shiozawa, H. Room temperature synthesis of a luminescent crystalline Cu–BTC coordination polymer and metal–organic framework. *Mater. Adv.* **3**, 224–231 (2022).
17. Sannes, D. K., Øien-Ødegaard, S., Aunan, E., Nova, A. & Olsbye, U. Quantification of Linker Defects in UiO-Type Metal–Organic Frameworks. *Chem. Mat.* **35**, 3793–3800 (2023).
18. Cox, C. S., Slavich, E., Macreadie, L. K., McKemmish, L. K. & Lessio, M. Understanding the Role of Synthetic Parameters in the Defect Engineering of UiO-66: A Review and Meta-analysis. *Chem. Mat.* **35**, 3057–3072 (2023). **This work analyses the role of synthetic parameters in UiO-66 defect engineering, highlighting the often conflicting role of synthetic parameters in determininng defectivity**.
19. Liu, L. et al. Imaging defects and their evolution in a metal–organic framework at sub-unit-cell resolution. *Nat. Chem.* **11**, 622–628 (2019).
20. Valenzano, L. et al. Disclosing the Complex Structure of UiO-66 Metal Organic Framework: A Synergic Combination of Experiment and Theory. *Chem. Mat.* **23**, 1700–1718 (2011). **This study was the first to explore the presence of missing linker defects in UiO-66**.
21. Cliffe, M. J. et al. Correlated defect nanoregions in a metal–organic framework. *Nat. Commun.* **5**, 4176 (2014). **This study was the first to reveal the presence of missing cluster defects in UiO-66**.
22. Liu, L., Zhang, D., Zhu, Y. & Han, Y. Bulk and local structures of metal–organic frameworks unravelled by high-resolution electron microscopy. *Commun. Chem.* **3**, 99 (2020).
23. Moore, S. C., Smith, M. R., Trettin, J. L., Yang, R. A. & Sarazen, M. L. Kinetic Impacts of Defect Sites in Metal–Organic Framework Catalysts under Varied Driving Forces. *ACS Energy Lett.* **8**, 1397–1407 (2023).
24. Fang, Z., Bueken, B., De Vos, D. E. & Fischer, R. A. Defect-Engineered Metal–Organic Frameworks. *Angew. Chem. Int. Ed.* **54**, 7234–7254 (2015).
25. Feng, Y., Chen, Q., Jiang, M. & Yao, J. Tailoring the Properties of UiO-66 through Defect Engineering: A Review. *Ind. Eng. Chem. Res.* **58**, 17646–17659 (2019).
26. Jrad, A. et al. Critical Role of Defects in UiO-66 Nanocrystals for Catalysis and Water Remediation. *ACS Appl. Nano Mater.* **6**, 18698–18720 (2023).
27. Wu, H., Yildirim, T. & Zhou, W. Exceptional Mechanical Stability of Highly Porous Zirconium Metal–Organic Framework UiO-66 and Its Important Implications. *J. Phys. Chem. Lett.* **4**, 925–930 (2013).
28. Vervoorts, P., Stebani, J., Méndez, A. S. J. & Kieslich, G. Structural Chemistry of Metal–Organic Frameworks under Hydrostatic Pressures. *ACS Mater. Lett.* **3**, 1635–1651 (2021).
29. Hobday, C. L. et al. A Computational and Experimental Approach Linking Disorder, High-Pressure Behavior, and Mechanical Properties in UiO Frameworks. *Angew. Chem. Int. Ed.* **55**, 2401–2405 (2016).
30. Rogge, S. M. J. et al. Charting the Metal-Dependent High-Pressure Stability of Bimetallic UiO-66 Materials. *ACS Mater. Lett.* **2**, 438–445 (2020).
31. Jajko, G. et al. Defect-induced tuning of polarity-dependent adsorption in hydrophobic–hydrophilic UiO-66. *Commun. Chem.* **5**, 120 (2022).
32. Halder, A. et al. Enhancing Dynamic Spectral Diffusion in Metal–Organic Frameworks through Defect Engineering. *J. Am. Chem. Soc.* **145**, 1072–1082 (2023).

33. Islamov, M., Boone, P., Babaei, H., McGaughey, A. J. H. & Wilmer, C. E. Correlated missing linker defects increase thermal conductivity in metal–organic framework UiO-66. *Chem. Sci.* **14**, 6592–6600 (2023).
34. Islamov, M., Babaei, H. & Wilmer, C. E. Influence of Missing Linker Defects on the Thermal Conductivity of Metal–Organic Framework HKUST-1. *ACS Appl. Mater. Interfaces* **12**, 56172–56177 (2020). **This study employed molecular dynamics simualtions to reveal the substantiall reduction in thermal conductivity associated with increased defectivity**.
35. Lázaro, I. A., Popescu, C. & Cirujano, F. G. Controlling the molecular diffusion in MOFs with the acidity of monocarboxylate modulators. *Dalt. Trans.* **50**, 11291–11299 (2021).
36. Mautschke, H. H., Drache, F., Senkovska, I., Kaskel, S. & Llabrés i Xamena, F. X. Catalytic properties of pristine and defect-engineered Zr-MOF-808 metal organic frameworks. *Catal. Sci. Technol.* **8**, 3610–3616 (2018).
37. Kozachuk, O. et al. Multifunctional, Defect-Engineered Metal–Organic Frameworks with Ruthenium Centers: Sorption and Catalytic Properties. *Angew. Chem. Int. Ed.* **53**, 7058–7062 (2014).
38. Korzyński, M. D., Consoli, D. F., Zhang, S., Román-Leshkov, Y. & Dincă, M. Activation of Methyltrioxorhenium for Olefin Metathesis in a Zirconium-Based Metal–Organic Framework. *J. Am. Chem. Soc.* **140**, 6956–6960 (2018).
39. Vermoortele, F. et al. Synthesis Modulation as a Tool To Increase the Catalytic Activity of Metal–Organic Frameworks: The Unique Case of UiO-66(Zr). *J. Am. Chem. Soc.* **135**, 11465–11468 (2013).
40. Wang, W. et al. Interplay of Electronic and Steric Effects to Yield Low-Temperature CO Oxidation at Metal Single Sites in Defect-Engineered HKUST-1. *Angew. Chem. Int. Ed.* **59**, 10514–10518 (2020).
41. Xue, Z. et al. Missing-linker metal-organic frameworks for oxygen evolution reaction. *Nat. Commun.* **10**, 5048 (2019).
42. Feng, X. et al. Generating Catalytic Sites in UiO-66 through Defect Engineering. *ACS Appl. Mater. Interfaces* **13**, 60715–60735 (2021).
43. Liang, W. et al. Linking defects, hierarchical porosity generation and desalination performance in metal–organic frameworks. *Chem. Sci.* **9**, 3508–3516 (2018).
44. Niu, J. et al. Defect Engineering of Low-Coordinated Metal–Organic Frameworks (MOFs) for Improved CO2 Access and Capture. *ACS Appl. Mater. Interfaces* **15**, 31664–31674 (2023).
45. Wu, H. et al. Unusual and Highly Tunable Missing-Linker Defects in Zirconium Metal–Organic Framework UiO-66 and Their Important Effects on Gas Adsorption. *J. Am. Chem. Soc.* **135**, 10525–10532 (2013).
46. Abánades Lázaro, I., Wells, C. J. R. & Forgan, R. S. Multivariate Modulation of the Zr MOF UiO-66 for Defect-Controlled Combination Anticancer Drug Delivery. *Angew. Chem. Int. Ed.* **59**, 5211–5217 (2020).
47. Forse, A. C. et al. Unexpected Diffusion Anisotropy of Carbon Dioxide in the Metal–Organic Framework Zn2(dobpdc). *J. Am. Chem. Soc.* **140**, 1663–1673 (2018).
48. Fu, Y. et al. Solvent-derived defects suppress adsorption in MOF-74. *Nat. Commun.* **14**, 2386 (2023).
49. Choi, J., Lin, L.-C. & Grossman, J. C. Role of Structural Defects in the Water Adsorption Properties of MOF-801. *J. Phys. Chem. C.* **122**, 5545–5552 (2018).
50. Barin, G. et al. Defect Creation by Linker Fragmentation in Metal–Organic Frameworks and Its Effects on Gas Uptake Properties. *Inorg. Chem.* **53**, 6914–6919 (2014).
51. Burtch, N. C. et al. Negative Thermal Expansion Design Strategies in a Diverse Series of Metal–Organic Frameworks. *Adv. Funct. Mater.* **29**, 1904669 (2019).
52. Wu, Y., Duan, H. & Xi, H. Machine Learning-Driven Insights into Defects of Zirconium Metal–Organic Frameworks for Enhanced Ethane–Ethylene Separation. *Chem. Mat.* **32**, 2986–2997 (2020).
53. Cliffe, M. J., Hill, J. A., Murray, C. A., Coudert, F.-X. & Goodwin, A. L. Defect-dependent colossal negative thermal expansion in UiO-66(Hf) metal–organic framework. *Phys. Chem. Chem. Phys.* **17**, 11586–11592 (2015).
54. Chen, Z. et al. Node Distortion as a Tunable Mechanism for Negative Thermal Expansion in Metal–Organic Frameworks. *J. Am. Chem. Soc.* **145**, 268–276 (2023).
55. Krause, S. et al. Impact of Defects and Crystal Size on Negative Gas Adsorption in DUT-49 Analyzed by In Situ 129Xe NMR Spectroscopy. *Chem. Mat.* **32**, 4641–4650 (2020).
56. Feng, L., Wang, K.-Y., Day, G. S., Ryder, M. R. & Zhou, H.-C. Destruction of Metal–Organic Frameworks: Positive and Negative Aspects of Stability and Lability. *Chem. Rev.* **120**, 13087–13133 (2020).
57. Kim, Y. et al. Hydrolytic Transformation of Microporous Metal–Organic Frameworks to Hierarchical Micro- and Mesoporous MOFs. *Angew. Chem. Int. Ed.* **54**, 13273–13278 (2015).
58. Liu, G. et al. Eliminating lattice defects in metal–organic framework molecular-sieving membranes. *Nat. Mater.* **22**, 769–776 (2023).
59. Iacomi, P. et al. Role of Structural Defects in the Adsorption and Separation of C3 Hydrocarbons in Zr-Fumarate-MOF (MOF-801). *Chem. Mat.* **31**, 8413–8423 (2019).
60. Chen, Z. et al. Enhanced Separation of Butane Isomers via Defect Control in a Fumarate/Zirconium-Based Metal Organic Framework. *Langmuir* **34**, 14546–14551 (2018).
61. Idrees, K. B. et al. Tailoring Pore Aperture and Structural Defects in Zirconium-Based Metal–Organic Frameworks for Krypton/Xenon Separation. *Chem. Mat.* **32**, 3776–3782 (2020).
62. Boström, H. L. B. et al. How reproducible is the synthesis of Zr–porphyrin metal–organic frameworks? An interlaboratory study. *Adv. Mater.* **36**, 2304832 (2023).
63. Hajek, J. et al. On the intrinsic dynamic nature of the rigid UiO-66 metal–organic framework. *Chem. Sci.* **9**, 2723–2732 (2018).
64. Fabrizio, K., Andreeva, A. B., Kadota, K., Morris, A. J. & Brozek, C. K. Guest-dependent bond flexibility in UiO-66, a “stable” MOF. *Chem. Commun.* **59**, 1309–1312 (2023).
65. Andreeva, A. B. et al. Soft Mode Metal-Linker Dynamics in Carboxylate MOFs Evidenced by Variable-Temperature Infrared Spectroscopy. *J. Am. Chem. Soc.* **142**, 19291–19299 (2020).
66. Wang, J.-H. et al. Solvent-Assisted Metal Metathesis: A Highly Efficient and Versatile Route towards Synthetically Demanding Chromium Metal–Organic Frameworks. *Angew. Chem. Int. Ed.* **56**, 6478–6482 (2017).
67. Burnett, B. J., Barron, P. M., Hu, C. & Choe, W. Stepwise Synthesis of Metal–Organic Frameworks: Replacement of Structural Organic Linkers. *J. Am. Chem. Soc.* **133**, 9984–9987 (2011).
68. Fei, H., Cahill, J. F., Prather, K. A. & Cohen, S. M. Tandem Postsynthetic Metal Ion and Ligand Exchange in Zeolitic Imidazolate Frameworks. *Inorg. Chem.* **52**, 4011–4016 (2013).
69. Tian, Y. et al. Synthesis and structural characterization of a single-crystal to single-crystal transformable coordination polymer. *Dalt. Trans.* **43**, 1519–1523 (2014).
70. Sato, H. et al. Self-Accelerating CO Sorption in a Soft Nanoporous Crystal. *Science* **343**, 167–170 (2014).
71. Sen, S. et al. Cooperative Bond Scission in a Soft Porous Crystal Enables Discriminatory Gate Opening for Ethylene over Ethane. *J. Am. Chem. Soc.* **139**, 18313–18321 (2017).
72. Sikma, R. E., Butler, K. S., Vogel, D. J., Harvey, J. A. & Sava Gallis, D. F. Quest for Multifunctionality: Current Progress in the Characterization of Heterometallic Metal–Organic Frameworks. *J. Am. Chem. Soc.* **146**, 5715–5734 (2024).
73. Kurihara, T. et al. Three-Dimensional Metal–Organic Network Glasses from Bridging MF62– Anions and Their Dynamic Insights by Solid-State NMR. *Inorg. Chem.* **61**, 16103–16109 (2022).

74. Bennett, T. D. & Horike, S. Liquid, glass and amorphous solid states of coordination polymers and metal–organic frameworks. *Nat. Rev. Mater.* **3**, 431–440 (2018).
75. Gaillac, R. et al. Liquid metal–organic frameworks. *Nat. Mater.* **16**, 1149–1154 (2017).
76. Kang, J. et al. Dynamic three-dimensional structures of a metal–organic framework captured with femtosecond serial crystallography. *Nat. Chem.* **16**, 693–699 (2024).
77. Winarta, J. et al. A Decade of UiO-66 Research: A Historic Review of Dynamic Structure, Synthesis Mechanisms, and Characterization Techniques of an Archetypal Metal–Organic Framework. *Cryst. Growth Des.* **20**, 1347–1362 (2020).
78. Shaikh, S. M. et al. Synthesis and Defect Characterization of Phase-Pure Zr-MOFs Based on Meso-tetracarboxyphenylporphyrin. *Inorg. Chem.* **58**, 5145–5153 (2019).
79. Driscoll, D. M. et al. Characterization of Undercoordinated Zr Defect Sites in UiO-66 with Vibrational Spectroscopy of Adsorbed CO. *J. Phys. Chem. C.* **122**, 14582–14589 (2018).
80. Yin, J. et al. Molecular identification and quantification of defect sites in metal-organic frameworks with NMR probe molecules. *Nat. Commun.* **13**, 5112 (2022).
81. Sha, F. et al. Probing Structural Imperfections: Protein-Aided Defect Characterization in Metal–Organic Frameworks. *ACS Mater. Lett.*, 1396–1403, https://doi.org/10.1021/acsmaterialslett.4c00199 (2024).
82. Klet, R. C., Liu, Y., Wang, T. C., Hupp, J. T. & Farha, O. K. Evaluation of Brønsted acidity and proton topology in Zr- and Hf-based metal–organic frameworks using potentiometric acid–base titration. *J. Mater. Chem. A* **4**, 1479–1485 (2016).
83. Fang, Z. et al. Structural Complexity in Metal–Organic Frameworks: Simultaneous Modification of Open Metal Sites and Hierarchical Porosity by Systematic Doping with Defective Linkers. *J. Am. Chem. Soc.* **136**, 9627–9636 (2014).
84. Heinz, W. R. et al. Thermal Defect Engineering of Precious Group Metal–Organic Frameworks: A Case Study on Ru/Rh-HKUST-1 Analogues. *ACS Appl. Mater. Interfaces* **12**, 40635–40647 (2020).
85. Wang, J. et al. Defect-Engineered Metal–Organic Frameworks: A Thorough Characterization of Active Sites Using CO as a Probe Molecule. *J. Phys. Chem. C.* **125**, 593–601 (2021).
86. Liang, A. J. et al. A Site-Isolated Rhodium−Diethylene Complex Supported on Highly Dealuminated Y Zeolite: Synthesis and Characterization. *J. Phys. Chem. B* **109**, 24236–24243 (2005).
87. Perez-Aguilar, J. E., Chen, C.-Y., Hughes, J. T., Fang, C.-Y. & Gates, B. C. Isostructural Atomically Dispersed Rhodium Catalysts Supported on SAPO-37 and on HY Zeolite. *J. Am. Chem. Soc.* **142**, 11474–11485 (2020).
88. Sánchez, F., Iglesias, M., Corma, A. & del Pino, C. New rhodium complexes anchored on silica and modified Y-zeolite as efficient catalysts for hydrogenation of olefins. *J. Mol. Cat.* **70**, 369–379 (1991).
89. Johnstone, D. N. et al. Direct Imaging of Correlated Defect Nanodomains in a Metal–Organic Framework. *J. Am. Chem. Soc.* **142**, 13081–13089 (2020).
90. Wang, L. et al. Real-Space Imaging of the Molecular Changes in Metal–Organic Frameworks under Electron Irradiation. *ACS Nano* **17**, 4740–4747 (2023).
91. Zhou, Y. et al. Local Structure Evolvement in MOF Single Crystals Unveiled by Scanning Transmission Electron Microscopy. *Chem. Mat.* **32**, 4966–4972 (2020).
92. Braglia, L. et al. Catching the Reversible Formation and Reactivity of Surface Defective Sites in Metal–Organic Frameworks: An Operando Ambient Pressure-NEXAFS Investigation. *j. Phys. Chem. Lett.* **12**, 9182–9187 (2021).
93. Romero-Muñiz, I. et al. Revisiting Vibrational Spectroscopy to Tackle the Chemistry of Zr6O8 Metal-Organic Framework Nodes. *ACS Appl. Mater. Interfaces* **14**, 27040–27047 (2022).
94. Cerasale, D. J., Ward, D. C. & Easun, T. L. MOFs in the time domain. *Nat. Rev. Chem.* **6**, 9–30 (2022).
95. Sapnik, A. F. et al. Mapping nanocrystalline disorder within an amorphous metal–organic framework. *Commun. Chem.* **6**, 92 (2023).
96. Tan, K. et al. Defect Termination in the UiO-66 Family of Metal–Organic Frameworks: The Role of Water and Modulator. *J. Am. Chem. Soc.* **143**, 6328–6332 (2021).
97. McDonnell, R. P. et al. Anomalous Infrared Intensity Behavior of Acetonitrile Diffused into UiO-67. *Chem. Mat.* **35**, 8827–8839 (2023).
98. Yang, D. & Gates, B. C. Elucidating and Tuning Catalytic Sites on Zirconium- and Aluminum-Containing Nodes of Stable Metal–Organic Frameworks. *Acc. Chem. Res.* **54**, 1982–1991 (2021).
99. Formalik, F., Shi, K., Joodaki, F., Wang, X. & Snurr, R. Q. Exploring the Structural, Dynamic, and Functional Properties of Metal-Organic Frameworks through Molecular Modeling. *Adv. Funct. Mater.* 2308130, https://doi.org/10.1002/adfm.202308130 (2023).
100. Hou, J. et al. Halogenated Metal–Organic Framework Glasses and Liquids. *J. Am. Chem. Soc.* **142**, 3880–3890 (2020).
101. Yang, L.-M., Ganz, E., Svelle, S. & Tilset, M. Computational exploration of newly synthesized zirconium metal–organic frameworks UiO-66, -67, -68 and analogues. *J. Mater. Chem. C.* **2**, 7111–7125 (2014).
102. Dissegna, S. et al. Tuning the Mechanical Response of Metal–Organic Frameworks by Defect Engineering. *J. Am. Chem. Soc.* **140**, 11581–11584 (2018).
103. Lamaire, A., Wieme, J., Hoffman, A. E. J. & Van Speybroeck, V. Atomistic insight in the flexibility and heat transport properties of the stimuli-responsive metal–organic framework MIL-53(Al) for water-adsorption applications using molecular simulations. *Faraday Discuss.* **225**, 301–323 (2021).
104. Wieme, J. et al. Thermal Engineering of Metal–Organic Frameworks for Adsorption Applications: A Molecular Simulation Perspective. *ACS Appl. Mater. Interfaces* **11**, 38697–38707 (2019).
105. Babaei, H. et al. Observation of reduced thermal conductivity in a metal-organic framework due to the presence of adsorbates. *Nat. Commun.* **11**, 4010 (2020).
106. Sørensen, S. S. et al. Metal–Organic Framework Glasses Possess Higher Thermal Conductivity than Their Crystalline Counterparts. *ACS Appl. Mater. Interfaces* **12**, 18893–18903 (2020).
107. Andreeva, A. B. et al. Cooperativity and Metal–Linker Dynamics in Spin Crossover Framework Fe(1,2,3-triazolate)2. *Chem. Mat.* **33**, 8534–8545 (2021).
108. St. Petkov, P. et al. Defects in MOFs: A Thorough Characterization. *ChemPhysChem* **13**, 2025–2029 (2012).
109. Krause, S. et al. The role of temperature and adsorbate on negative gas adsorption transitions of the mesoporous metal–organic framework DUT-49. *Faraday Discuss.* **225**, 168–183 (2021).
110. Koschnick, C. et al. Understanding disorder and linker deficiency in porphyrinic zirconium-based metal–organic frameworks by resolving the Zr8O6 cluster conundrum in PCN-221. *Nat. Commun.* **12**, 3099 (2021).
111. Shearer, G. C. et al. Tuned to Perfection: Ironing Out the Defects in Metal–Organic Framework UiO-66. *Chem. Mat.* **26**, 4068–4071 (2014).
112. Lee, S. J. et al. Multicomponent Metal–Organic Frameworks as Defect-Tolerant Materials. *Chem. Mat.* **28**, 368–375 (2016).
113. Xiong, S. et al. Impact of Labile Ligands on Catalyst Initiation and Chain Propagation in Ni-Catalyzed Ethylene/Acrylate Copolymerization. *ACS Catal.* **13**, 5000–5006 (2023).
114. Huang, Y. et al. Ligand coordination- and dissociation-induced divergent allylic alkylations using alkynes. *Chem* **7**, 812–826 (2021).
115. Yuan, S. et al. Stable Metal–Organic Frameworks: Design, Synthesis, and Applications. *Adv. Mater.* **30**, 1704303 (2018).

116. McHugh, L. N. et al. Hydrolytic stability in hemilabile metal–organic frameworks. *Nat. Chem.* **10**, 1096–1102 (2018).
117. Haigis, V., Coudert, F.-X., Vuilleumier, R., Boutin, A. & Fuchs, A. H. Hydrothermal Breakdown of Flexible Metal–Organic Frameworks: A Study by First-Principles Molecular Dynamics. *J. Phys. Chem. Lett.* **6**, 4365–4370 (2015).
118. Položij, M., Rubeš, M., Čejka, J. & Nachtigall, P. Catalysis by Dynamically Formed Defects in a Metal–Organic Framework Structure: Knoevenagel Reaction Catalyzed by Copper Benzene-1,3,5-tricarboxylate. *ChemCatChem* **6**, 2821–2824 (2014).
119. Baumgartner, B., Mashita, R., Fukatsu, A., Okada, K. & Takahashi, M. Guest Alignment and Defect Formation during Pore Filling in Metal–Organic Framework Films. *Angew. Chem. Int. Ed.* **61**, e202201725 (2022).
120. Peralta, R. A. et al. Engineering Catalysis within a Saturated In(III)-Based MOF Possessing Dynamic Ligand–Metal Bonding. *ACS Appl. Mater. Interfaces* **15**, 1410–1417 (2023).
121. Obeso, J. L. et al. Gas-phase organometallic catalysis in MFM-300(Sc) provided by switchable dynamic metal sites. *Chem. Commun.* **59**, 3273–3276 (2023).
122. Lyu, P. et al. Ammonia Capture via an Unconventional Reversible Guest-Induced Metal-Linker Bond Dynamics in a Highly Stable Metal–Organic Framework. *Chem. Mat.* **33**, 6186–6192 (2021).
123. Peralta, R. A. et al. Switchable Metal Sites in Metal–Organic Framework MFM-300(Sc): Lewis Acid Catalysis Driven by Metal–Hemilabile Linker Bond Dynamics. *Angew. Chem. Int. Ed.* **61**, e202210857 (2022).
124. Rayder, T. M. et al. Unveiling Unexpected Modulator-CO2 Dynamics within a Zirconium Metal–Organic Framework. *J. Am. Chem. Soc.* **145**, 11195–11205 (2023).
125. Fabrizio, K. & Brozek, C. K. Size-Dependent Thermal Shifts to MOF Nanocrystal Optical Gaps Induced by Dynamic Bonding. *Nano Lett.* **23**, 925–930 (2023).
126. Davenport, A. M. et al. Size-Dependent Spin Crossover and Bond Flexibility in Metal–Organic Framework Nanoparticles. *J. Am. Chem. Soc.* **146**, 23692–23698 (2024).
127. Bueken, B. et al. Tackling the Defect Conundrum in UiO-66: A Mixed-Linker Approach to Engineering Missing Linker Defects. *Chem. Mat.* **29**, 10478–10486 (2017).
128. Evans, J. D., Bon, V., Senkovska, I., Lee, H. C. & Kaskel, S. Four-dimensional metal-organic frameworks. *Nat. Commun.* **11**, 2690 (2020).
129. Ye, Q. et al. Photoinduced Dynamic Ligation in Metal–Organic Frameworks. *J. Am. Chem. Soc.* **146**, 101–105 (2024).
130. Nishida, J. et al. Structural dynamics inside a functionalized metal–organic framework probed by ultrafast 2D IR spectroscopy. *Proc. Nat. Acad. Sci.* **111**, 18442–18447 (2014).
131. Valentine, M. L., Yin, G., Oppenheim, J. J., Dincă, M. & Xiong, W. Ultrafast Water H-Bond Rearrangement in a Metal–Organic Framework Probed by Femtosecond Time-Resolved Infrared Spectroscopy. *J. Am. Chem. Soc.* **145**, 11482–11487 (2023).
132. Hadjiivanov, K. I. et al. Power of Infrared and Raman Spectroscopies to Characterize Metal-Organic Frameworks and Investigate Their Interaction with Guest Molecules. *Chem. Rev.* **121**, 1286–1424 (2021).
133. Lee, G. & Hwang, J. Direct Synthesis of Mixed-Metal Paddle-Wheel Metal–Organic Frameworks with Controlled Metal Ratios under Ambient Conditions. *Inorg. Chem.* **62**, 19457–19465 (2023).
134. Vandenhaute, S., Cools-Ceuppens, M., DeKeyser, S., Verstraelen, T. & Van Speybroeck, V. Machine learning potentials for metal-organic frameworks using an incremental learning approach. *npj Comput. Mater.* **9**, 19 (2023).
135. Tang, H., Duan, L. & Jiang, J. Leveraging Machine Learning for Metal–Organic Frameworks: A Perspective. *Langmuir* **39**, 15849–15863 (2023).
136. Larionov, K. P. & Evtushok, V. Y. From Synthesis Conditions to UiO-66 Properties: Machine Learning Approach. *Chem. Mat.* **36**, 4291–4302 (2024).
137. Allegretto, J. A., Onna, D., Bilmes, S. A., Azzaroni, O. & Rafti, M. Unified Roadmap for ZIF-8 Nucleation and Growth: Machine Learning Analysis of Synthetic Variables and Their Impact on Particle Size and Morphology. *Chem. Mat.* **36**, 5814–5825 (2024).
138. Gonzalez, M. I. et al. Structural characterization of framework-gas interactions in the metal-organic framework Co_2(dobdc) by in situ single-crystal X-ray diffraction. *Chem. Sci.* **8**, 4387–4398 (2017).
139. Bloch, W. M., Champness, N. R. & Doonan, C. J. X-ray Crystallography in Open-Framework Materials. *Angew. Chem., Int. Ed.* **54**, 12860–12867 (2015).
140. Karagiaridi, O., Bury, W., Mondloch, J. E., Hupp, J. T. & Farha, O. K. Solvent-Assisted Linker Exchange: An Alternative to the De Novo Synthesis of Unattainable Metal–Organic Frameworks. *Angew. Chem. Int. Ed.* **53**, 4530–4540 (2014).
141. Brozek, C. K. & Dincă, M. Cation exchange at the secondary building units of metal–organic frameworks. *Chem. Soc. Rev.* **43**, 5456–5467 (2014).
142. Kitaura, R. et al. Rational Design and Crystal Structure Determination of a 3-D Metal−Organic Jungle-Gym-like Open Framework. *Inorg. Chem.* **43**, 6522–6524 (2004).
143. Lin, W. et al. Snapshots of Postsynthetic Modification in a Layered Metal–Organic Framework: Isometric Linker Exchange and Adaptive Linker Installation. *Inorg. Chem.* **60**, 11756–11763 (2021).
144. Papasergi-Scott, M. M. et al. Time-resolved cryo-EM of G-protein activation by a GPCR. *Nature* **629**, 1182–1191 (2024).
145. Mazhab-Jafari, M. T. & Rubinstein, J. L. Cryo-EM studies of the structure and dynamics of vacuolar-type ATPases. *Sci. Adv.* **2**, e1600725 (2016).
146. Gutov, O. V., Hevia, M. G., Escudero-Adán, E. C. & Shafir, A. Metal–Organic Framework (MOF) Defects under Control: Insights into the Missing Linker Sites and Their Implication in the Reactivity of Zirconium-Based Frameworks. *Inorg. Chem.* **54**, 8396–8400 (2015).
147. Shearer, G. C. et al. Defect Engineering: Tuning the Porosity and Composition of the Metal–Organic Framework UiO-66 via Modulated Synthesis. *Chem. Mat.* **28**, 3749–3761 (2016).
148. Jiao, Y. et al. Heat-Treatment of Defective UiO-66 from Modulated Synthesis: Adsorption and Stability Studies. *J. Phys. Chem. C.* **121**, 23471–23479 (2017).
149. DeStefano, M. R., Islamoglu, T., Garibay, S. J., Hupp, J. T. & Farha, O. K. Room-Temperature Synthesis of UiO-66 and Thermal Modulation of Densities of Defect Sites. *Chem. Mat.* **29**, 1357–1361 (2017).
150. Epley, C. C., Love, M. D. & Morris, A. J. Characterizing Defects in a UiO-AZB Metal–Organic Framework. *Inorg. Chem.* **56**, 13777–13784 (2017).
151. Cai, G. & Jiang, H.-L. A Modulator-Induced Defect-Formation Strategy to Hierarchically Porous Metal–Organic Frameworks with High Stability. *Angew. Chem. Int. Ed.* **56**, 563–567 (2017).
152. Wang, X. et al. Improving Water-Treatment Performance of Zirconium Metal-Organic Framework Membranes by Postsynthetic Defect Healing. *ACS Appl. Mater. Interfaces* **9**, 37848–37855 (2017).
153. Chammingkwan, P. et al. Modulator-free approach towards missing-cluster defect formation in Zr-based UiO-66. *RSC Adv.* **10**, 28180–28185 (2020).
154. Feng, X. et al. Engineering a Highly Defective Stable UiO-66 with Tunable Lewis- Brønsted Acidity: The Role of the Hemilabile Linker. *J. Am. Chem. Soc.* **142**, 3174–3183 (2020).
155. Feng, X. et al. Creation of Exclusive Artificial Cluster Defects by Selective Metal Removal in the (Zn, Zr) Mixed-Metal UiO-66. *J. Am. Chem. Soc.* **143**, 21511–21518 (2021).
156. Tan, T. T. Y. et al. UiO-66 metal organic frameworks with high contents of flexible adipic acid co-linkers. *Chem. Commun.* **58**, 11402–11405 (2022).

157. Fu, G. et al. Enhanced Water Adsorption Performance of UiO-66 Modulated with p-Nitrobenzoic or p-Hydroxybenzoic Acid: Introduced Defects and Functional Groups. *Inorg. Chem.* **61**, 17943–17950 (2022).
158. Tatay, S. et al. Synthetic control of correlated disorder in UiO-66 frameworks. *Nat. Commun.* **14**, 6962 (2023).
159. Guo, Z., Liu, X., Che, Y. & Xing, H. Crystal-Defect-Induced Longer Lifetime of Excited States in a Metal–Organic Framework Photocatalyst to Enhance Visible-Light-Mediated CO2 Reduction. *Inorg. Chem.* **63**, 13005–13013 (2024).
160. Xing, S. et al. Cluster–Cluster Co-Nucleation Induced Defective Polyoxometalate-Based Metal–Organic Frameworks for Efficient Tandem Catalysis. *Small*, 2400410, https://doi.org/10.1002/smll.202400410.
161. Damacet, P., Hannouche, K., Gouda, A. & Hmadeh, M. Controlled Growth of Highly Defected Zirconium–Metal–Organic Frameworks via a Reaction–Diffusion System for Water Remediation. *ACS Appl. Mater. Interfaces*. https://doi.org/10.1021/acsami.3c16327 (2024).
162. Dai, S. et al. Highly defective ultra-small tetravalent MOF nanocrystals. *Nat. Commun.* **15**, 3434 (2024).
163. Zhang, W. et al. Ruthenium Metal–Organic Frameworks with Different Defect Types: Influence on Porosity, Sorption, and Catalytic Properties. *Chem. Eur. J.* **22**, 14297–14307 (2016).
164. Zhang, W. et al. Impact of Synthesis Parameters on the Formation of Defects in HKUST-1. *Eur. J. Inorg. Chem.* **2017**, 925–931 (2017).
165. Müller, K. et al. Water as a modulator in the synthesis of surface-mounted metal–organic framework films of type HKUST-1. *Dalt. Trans.* **47**, 16474–16479 (2018).
166. Doan, H. V., Sartbaeva, A., Eloi, J.-C., A. Davis, S. & Ting, V. P. Defective hierarchical porous copper-based metal-organic frameworks synthesised via facile acid etching strategy. *Sci. Rep.* **9**, 10887 (2019).
167. Wang, Z. et al. Defect Creation in Surface-Mounted Metal–Organic Framework Thin Films. *ACS Appl. Mater. Interfaces* **12**, 2655–2661 (2020).
168. Steenhaut, T., Grégoire, N., Barozzino-Consiglio, G., Filinchuk, Y. & Hermans, S. Mechanochemical defect engineering of HKUST-1 and impact of the resulting defects on carbon dioxide sorption and catalytic cyclopropanation. *RSC Adv.* **10**, 19822–19831 (2020).
169. Rivera-Torrente, M., Filez, M., Meirer, F. & Weckhuysen, B. M. Multi-Spectroscopic Interrogation of the Spatial Linker Distribution in Defect-Engineered Metal–Organic Framework Crystals: The [Cu3(btc)2−(cydc)] Showcase. *Chem. Eur. J.* **26**, 3614–3625 (2020).
170. Ferreira Sanchez, D. et al. Spatio-Chemical Heterogeneity of Defect-Engineered Metal–Organic Framework Crystals Revealed by Full-Field Tomographic X-ray Absorption Spectroscopy. *Angew. Chem. Int. Ed.* **60**, 10032–10039 (2021).
171. Horiuchi, Y. et al. Linker defect engineering for effective reactive site formation in metal–organic framework photocatalysts with a MIL-125(Ti) architecture. *J. Catal.* **392**, 119–125 (2020).
172. Wang, C. et al. Titanium-Oxo Cluster Assisted Fabrication of a Defect-Rich Ti-MOF Membrane Showing Versatile Gas-Separation Performance. *Angew. Chem. Int. Ed.* **61**, e202203663 (2022).
173. Shim, C. H., Oh, S., Lee, S., Lee, G. & Oh, M. Construction of defected MOF-74 with preserved crystallinity for efficient catalytic cyanosilylation of benzaldehyde. *RSC Adv.* **13**, 8220–8226 (2023).
174. Lázaro, I. A., Almora-Barrios, N., Tatay, S., Popescu, C. & Martí-Gastaldo, C. Linker depletion for missing cluster defects in non-UiO metal–organic frameworks. *Chem. Sci.* **12**, 11839–11844 (2021).
175. Lázaro, I. A., Almora-Barrios, N., Tatay, S. & Martí-Gastaldo, C. Effect of modulator connectivity on promoting defectivity in titanium–organic frameworks. *Chem. Sci.* **12**, 2586–2593 (2021).
176. Lázaro, I. A. Rationalising the multivariate modulation of MUV-10 for the defect-introduction of multiple functionalised modulators. *J. Mater. Chem. A* **10**, 10466–10473 (2022).
177. Lázaro, I. A. et al. Tuning the Photocatalytic Activity of Ti-Based Metal–Organic Frameworks through Modulator Defect-Engineered Functionalization. *ACS Appl. Mater. Interfaces* **14**, 21007–21017 (2022).
178. Fan, Z. et al. Defect Engineering of Copper Paddlewheel-Based Metal–Organic Frameworks of Type NOTT-100: Implementing Truncated Linkers and Its Effect on Catalytic Properties. *ACS Appl. Mater. Interfaces* **12**, 37993–38002 (2020).
179. Han, R., Tymińska, N., Schmidt, J. R. & Sholl, D. S. Propagation of Degradation-Induced Defects in Zeolitic Imidazolate Frameworks. *J. Phys. Chem. C.* **123**, 6655–6666 (2019).
180. Chen, J. et al. Radiation-Induced De Novo Defects in Metal–Organic Frameworks Boost CO2 Sorption. *J. Am. Chem. Soc.* **145**, 23651–23658 (2023).
181. Ahmad, M. et al. ZIF-8 Vibrational Spectra: Peak Assignments and Defect Signals. *ACS Appl. Mater. Interfaces* **16**, 27887–27897 (2024).
182. Hardian, R. et al. Tuning the Properties of MOF-808 via Defect Engineering and Metal Nanoparticle Encapsulation. *Chem. Eur. J.* **27**, 6804–6814 (2021).
183. Ye, G. et al. Boosting Catalytic Performance of MOF-808(Zr) by Direct Generation of Rich Defective Zr Nodes via a Solvent-Free Approach. *Inorg. Chem.* **62**, 4248–4259 (2023).
184. Xu, C. et al. Direct visualisation of metal–defect cooperative catalysis in Ru-doped defective MOF-808. *J. Mater. Chem. A* **12**, 19018–19028 (2024).
185. Le, H. V. et al. A sulfonate ligand-defected Zr-based metal–organic framework for the enhanced selective removal of anionic dyes. *RSC Adv.* **14**, 16389–16399 (2024).
186. Wang, Z. et al. Tunable coordinative defects in UHM-3 surface-mounted MOFs for gas adsorption and separation: A combined experimental and theoretical study. *Micropor. Mesopor. Mat.* **207**, 53–60 (2015).
187. He, S. et al. Competitive coordination strategy for the synthesis of hierarchical-pore metal–organic framework nanostructures. *Chem. Sci.* **7**, 7101–7105 (2016).
188. Slater, B., Wang, Z., Jiang, S., Hill, M. R. & Ladewig, B. P. Missing Linker Defects in a Homochiral Metal–Organic Framework: Tuning the Chiral Separation Capacity. *J. Am. Chem. Soc.* **139**, 18322–18327 (2017).
189. Yuan, S. et al. Exposed Equatorial Positions of Metal Centers via Sequential Ligand Elimination and Installation in MOFs. *J. Am. Chem. Soc.* **140**, 10814–10819 (2018).
190. Smolders, S. et al. A Titanium(IV)-Based Metal–Organic Framework Featuring Defect-Rich Ti-O Sheets as an Oxidative Desulfurization Catalyst. *Angew. Chem. Int. Ed.* **58**, 9160–9165 (2019).
191. Guo, C. et al. Precise regulation of defect concentration in MOF and its influence on photocatalytic overall water splitting. *Nanoscale* **14**, 15316–15326 (2022).
192. Chetry, S. et al. Exploring Defect-Engineered Metal–Organic Frameworks with 1,2,4-Triazolyl Isophthalate and Benzoate Linkers. *Inorg. Chem.* **63**, 10843–10853 (2024).
193. Cavka, J. H. et al. A New Zirconium Inorganic Building Brick Forming Metal Organic Frameworks with Exceptional Stability. *J. Am. Chem. Soc.* **130**, 13850–13851 (2008).
194. Jakobsen, S. et al. Structural determination of a highly stable metal-organic framework with possible application to interim radioactive waste scavenging: Hf-UiO-66. *Phys. Rev. B* **86**, 125429 (2012).

Acknowledgements

J.L.O. thanks CONAHCYT for the Ph.D. fellowship (1003953). R.A.P. thanks the Autonomous Metropolitan University-Iztapalapa, Mexico, for the financial support. We thank U. Winnberg (Euro Health) for scientific discussions and G. Ibarra-Winnberg for scientific encouragement.

Author contributions

N.S.P.V., J.L.O. and J.A.R. writing and conceptualization. R.A.P. writing, conceptualization, and organization. M.T.H. writing, conceptualization, and organization I.A.I. validated the discussion, and revised the paper. All authors contributed to reviewing and enhancing the manuscript.

Competing interests

The authors declare no competing interests.

Additional information

Supplementary information The online version contains supplementary material available at https://doi.org/10.1038/s43246-024-00691-1.

Correspondence and requests for materials should be addressed to Ricardo A. Peralta, Ilich A. Ibarra or Michael T. Huxley.

Peer review information *Communications materials* thanks Martina Lessio, Jin Zhang and the other, anonymous, reviewer(s) for their contribution to the peer review of this work. Primary Handling Editors: Jet-Sing Lee and John Plummer. A peer review file is available.

Reprints and permissions information is available at http://www.nature.com/reprints

Publisher's note Springer Nature remains neutral with regard to jurisdictional claims in published maps and institutional affiliations.

Open Access This article is licensed under a Creative Commons Attribution-NonCommercial-NoDerivatives 4.0 International License, which permits any non-commercial use, sharing, distribution and reproduction in any medium or format, as long as you give appropriate credit to the original author(s) and the source, provide a link to the Creative Commons licence, and indicate if you modified the licensed material. You do not have permission under this licence to share adapted material derived from this article or parts of it. The images or other third party material in this article are included in the article's Creative Commons licence, unless indicated otherwise in a credit line to the material. If material is not included in the article's Creative Commons licence and your intended use is not permitted by statutory regulation or exceeds the permitted use, you will need to obtain permission directly from the copyright holder. To view a copy of this licence, visit http://creativecommons.org/licenses/by-nc-nd/4.0/.

© The Author(s) 2024

Dalton Transactions

ROYAL SOCIETY OF CHEMISTRY

PAPER

View Article Online
View Journal | View Issue

Published on 04 December 2024. Downloaded by Universidad Autonoma Metropolitana-Iztapalapa on 6/30/2025 11:46:41 PM.

Check for updates

Cite this: *Dalton Trans.*, 2025, **54**, 1646

UTSA-16(Zn) for SO_2 detection: elucidating the fluorescence mechanism†

Valeria B. López-Cervantes,‡[a] Marco L. Martínez,‡[a,b] Juan L. Obeso,[a,c,d] Celene García-Carvajal,[a,e] Nora S. Portillo-Vélez,[f] Ariel Guzmán-Vargas,[b] Ricardo A. Peralta,[f] Eduardo González-Zamora,[f] Ilich A. Ibarra,[a] Diego Solis-Ibarra,*[a] John Luke Woodliffe*[g] and Yoarhy A. Amador-Sánchez*[a,f]

Received 11th October 2024,
Accepted 27th November 2024

DOI: 10.1039/d4dt02852j

rsc.li/dalton

In this study, the potential of the metal–organic framework UTSA-16(Zn) as a fluorescence detector for SO_2 is explored. The material was synthesized and characterized by powder X-ray diffraction (PXRD), infrared spectroscopy (FTIR) and thermogravimetric analysis (TGA), and its fluorescence behavior was analyzed before and after SO_2 exposure. A significant decrease in fluorescence intensity was observed and a LOD of 1.79 mM (~114.6 ppm) was obtained. With the help of time-resolved photoluminescence (TRPL) experiments and X-ray photoelectron (XPS) and ultraviolet-visible (UV-vis) spectroscopy, a static quenching mechanism due to the formation of a non-fluorescent complex in the ground state (GSC) was elucidated.

Introduction

Global warming is a paramount issue for humankind. Global warming arises, particularly, due to the emission of gases from fossil fuel combustions. Specifically, CO_2 is one of the most important gases that generate the greenhouse effect.[1] Moreover, gases emitted from fossil fuels can contain traces of sulfur dioxide (SO_2) and hydrogen sulfide (H_2S), which may also be dangerous to human health.[2,3] For instance, when humans are exposed to sulfur dioxide, SO_2 can cause pulmonary symptoms, even at short-term exposure and extremely low concentrations. Orellano *et al.* reported that, for an exposure of 10 minutes, the concentration of SO_2 must not be beyond 10 ppm.[4]

For this reason, in addition to reducing, capturing and/or reusing the emissions of pollutant gases, being able to detect and monitor them effectively is also an important objective to achieve. Several strategies have been developed to optimize the capture and reuse of these gases, for example, the catalytic reutilization of CO_2 and H_2S,[5,6] the use of energy storage devices to reduce fossil fuel consumption,[7] and the utilization of porous solids to capture the gases.[8] However, there is still a huge opportunity to explore detection methods for these pollutants.

In this context, a new class of materials known as metal organic frameworks (MOFs) have been extensively investigated to evaluate their gas capture properties.[9–11] MOFs are self-assembled crystalline porous coordination materials. These materials have the capability of high tunability in their crystalline structure due to their molecular nature.[12] For this reason, MOFs are capable of adsorbing considerable quantities of emitted gases from fossil fuel combustion.[13] Additionally, these materials are easily functionalized to have functional groups that can be used to bind more gaseous species (*e.g.* OH and halogen groups).

Recently, MOFs have emerged as highly versatile materials in the study of luminescence properties due to their porous structure, functionalization capacity and the presence of active

[a]*Laboratorio de Fisicoquímica y Reactividad de Superficies (LaFReS), Instituto de Investigaciones en Materiales, Universidad Nacional Autónoma de México, Circuito Exterior s/n, CU, Coyoacán, 04510 Ciudad de México, Mexico. E-mail: diego.solis@unam.mx, yoarhy@xanum.uam.mx*

[b]*ESIQIE – Instituto Politécnico Nacional, Avenida IPN UPALM Edificio 7, Zacatenco, 07738 México D.F, Mexico*

[c]*Instituto Politécnico Nacional, CICATA U. Legaria, Laboratorio Nacional de Ciencia, Tecnología y Gestión Integrada del Agua (LNAgua), Legaria 694, Irrigación, 11500 Miguel Hidalgo, CDMX, Mexico*

[d]*División de Ingeniería en Sistemas Automotrices, Tecnológico de Estudios Superiores del Oriente del Estado de México, Tecnológico Nacional de México, Estado de México 56400, Mexico*

[e]*Laboratorio de Sólidos Porosos (LabSoP) – INFAP-CONICET, Universidad Nacional de San Luis, San Luis, Argentina*

[f]*Departamento de Química, Universidad Autónoma Metropolitana-Iztapalapa, Av. Ferrocarril San Rafael Atlixco 186, Col. Leyes de Reforma 1A Sección, Iztapalapa, 09310 Ciudad de México, Mexico*

[g]*Advanced Materials Research Group, Faculty of Engineering, University of Nottingham, Nottingham NG7 2RD, UK. E-mail: luke.woodliffe1@nottingham.ac.uk*

†Electronic supplementary information (ESI) available: Instrumental techniques and characterization. See DOI: https://doi.org/10.1039/d4dt02852j

‡These authors contributed equally to this manuscript.

This journal is © The Royal Society of Chemistry 2025

Published on 04 December 2024. Downloaded by Universidad Autonoma Metropolitana-Iztapalapa on 6/30/2025 11:46:41 PM.

metal sites that allow MOFs to present modulable fluorescence emissions. This makes MOFs ideal candidates for applications in the molecular detection of gases, pollutants or biomolecules, which upon interaction with them alter their electronic properties, allowing the selective and sensitive detection of diverse species.[14] The design of MOFs generates multiple mechanisms for their fluorescence behavior and therefore for the detection of these molecules, where changes in the intensity and wavelength of emission are observed, correlated with the nature of the host–material interaction.[15,16]

A family of MOF materials named UTSA-16 have shown excellent CO_2 capture performance with high selectivity over N_2.[17] Originally, UTSA-16 was synthesized using cobalt atoms and citric acid as the metal center and linker, respectively, resulting in a material with an anatase-type structure made up by tetrahedral Co(II) atoms linked to tetranuclear cobalt citrate clusters in an octahedral geometry. UTSA-16 also contains four potassium ions (K^+) inside the pores, each one coordinated to two structural water molecules.[18,19] This material has been extensively investigated for CO_2 capture, and several studies conclude that this can be attributed to the interactions of the gas with K^+ and the organic linker, which function as adsorption sites. Specifically, it has been found that CO_2 associates with the material due to the formation of $K^+\cdots O{=}C{=}O$ supramolecular interactions.[20]

In 2020 Gaikwad and coworkers reported UTSA-16(Zn), which replaces Co(II) atoms with Zn(II), conserving the same crystal structure (Fig. 1). UTSA-16(Zn), whose empirical formula is $K(H_2O)_2Zn_3(cit)(Hcit)$ (cit = fully dehydroxylated citrate anion (4-) and Hcit = citrate anion (3-)), exhibits enhanced CO_2 capture performance and enhanced selectivity over N_2. Furthermore, this material showed superior stability to acid gases (*i.e.* SO_2 and NO_2) compared to UTSA-16(Co).[21] Thus, UTSA-16(Zn) can be considered a very promising adsorbent for CO_2 capture applications because of its excellent capture performance and low material cost, since both citric acid and Zn have a low price.[22,23]

Taking advantage of the superior CO_2 capture performance and stability of UTSA-16(Zn) towards SO_2 we decided to analyze this material's luminescence performance. In this way, UTSA-16(Zn) could act as an adsorbent while also being applied as a sensor for SO_2. To the best of our knowledge, this is the first report on the luminescence properties and possible application of the UTSA-16 family of materials for SO_2 sensing.

Results and discussion

Synthesis and characterization of UTSA-16(Zn)

The UTSA-16(Zn) material was synthesized as previously described in the literature by mixing zinc acetate dihydrate ($Zn(O_2CCH_3)_2(H_2O)_2$), citric acid monohydrate ($C_6H_8O_7{\cdot}H_2O$) and potassium hydroxide (KOH) in water, adding an antisolvent (ethanol) and heating using microwaves.[24] A white polycrystalline powder was obtained, which was washed with methanol and dried overnight in an oven. The crystalline structure was corroborated by powder X-ray diffraction (PXRD), obtaining a diffractogram coincident with the simulated pattern (CCDC database identifier: RAZXIA01) (Fig. S4†). The Fourier transform infrared (FTIR) spectrum (Fig. S5†) showed two signals at 1575 and 1398 cm^{-1} characteristic of the symmetric and asymmetric vibrational modes of the stretching of the carboxylic groups of UTSA-16(Zn) ($-COO^-$),[25] as well as a pronounced signal at 3427 cm^{-1} corresponding to the stretching vibration of the O–H bonds of the structural water molecules of the material and adsorbed from the environment.[26]

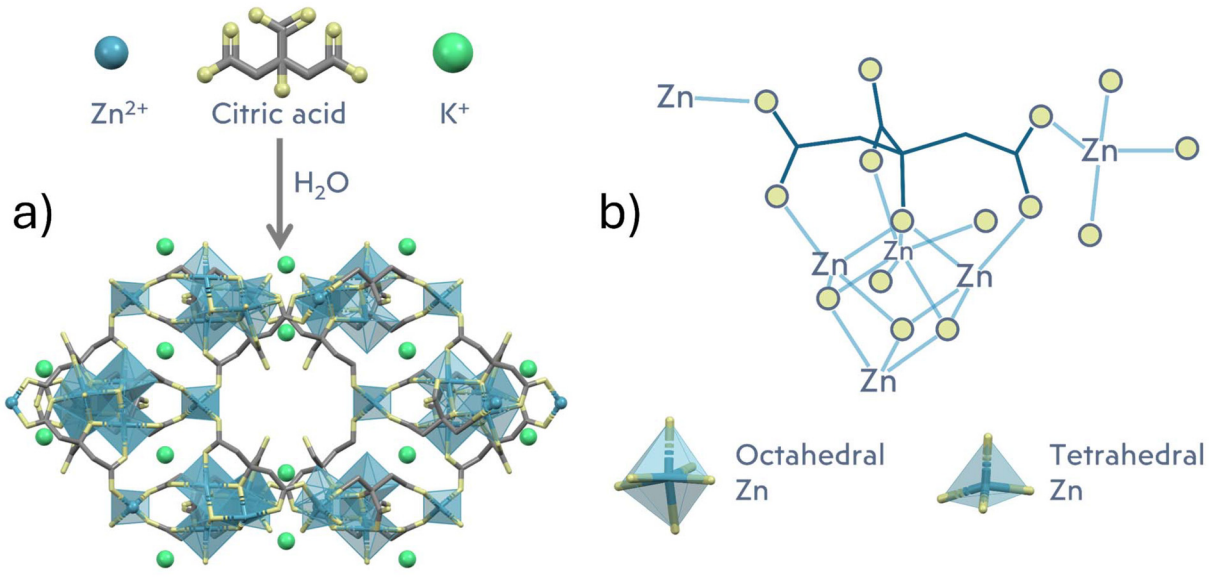


Fig. 1 (a) Schematic of the formation of the UTSA-16 material, with the pore seen through the *b*-axis. (b) Schematic of the coordination of the linker with the Zn(II) atoms. Colour code: carbon (grey), oxygen (yellow), cobalt (blue), and potassium (green). Hydrogens are omitted for clarity.

Published on 04 December 2024. Downloaded by Universidad Autonoma Metropolitana-Iztapalapa on 6/30/2025 11:46:41 PM.

In addition, thermogravimetric analysis (Fig. S7†) shows that the material is thermally stable above 300 °C, as previously reported.[18] In the thermogram, a loss of 14.7 w% is observed in the range of 25 to 130 °C corresponding to the evaporation of water molecules adsorbed in the structure,[21] impurities of the sample and structural water molecules interacting with the K^+ ion, indicating a low interaction energy of water inside the material. Subsequently, an abrupt loss of mass is observed, caused by the decomposition of the material following the decoordination of citric acid,[27] due to its decarboxylation (release of CO_2) starting at 350 °C.[28] Finally in the region of 350 to 600 °C the formation of a ZnO residue is expected, possibly in the form of hexagonal nanosheets,[29] as well as the release of gases such as CO_2 and CO.[27]

UTSA-16(Zn) fluorescence behaviour

Once the material was well characterized, solid-state emission spectra of UTSA-16(Zn) were obtained at different excitation wavelengths in order to determine which would be the optimal. The best emission was obtained at 360 nm; thus this excitation wavelength was chosen to perform all fluorescence experiments. First, the emission spectra of an activated UTSA-16(Zn) sample and its linker citric acid were obtained to explain the origin of the fluorescence behavior of the material (Fig. 2a). The first thing that can be observed is that citric acid ($C_6H_8O_7$) alone has a relatively weaker fluorescence compared to that of the UTSA-16(Zn) framework.

Citric acid, like other small organic molecules, has a weak fluorescence because its molecular structure does not favor the efficient delocalization of electrons;[30] in contrast, these tend to be located in their respective bonds and functional groups. As for its electronic transitions, citric acid presents n → π* transitions where the non-bonding electrons (n) of the oxygen atoms in the carboxyl and hydroxyl groups are promoted to π* antibonding orbitals,[31–33] as well as π → π* transitions in the carboxyl groups that typically occur in systems with conjugated double bonds, as in the carboxyl groups.[34] These transitions can be observed in the UV-Vis absorption spectra (Fig. S9†), as the n → π* transitions usually appear at longer wavelengths (around 425 nm), while the π → π* transitions occur at shorter wavelengths (around 200–300 nm).[34,35] The n → π* transitions are usually not efficient in light emission, as the excited electrons are more likely to relax through non-radiative processes,[36] such as energy dissipation in the form of vibration or heat. On the other hand, the π → π* transitions of the ligand are limited and less efficient in generating fluorescence due to the lack of conjugation between the π bonds in the molecule. Therefore, the combination of unfavorable electronic tran-

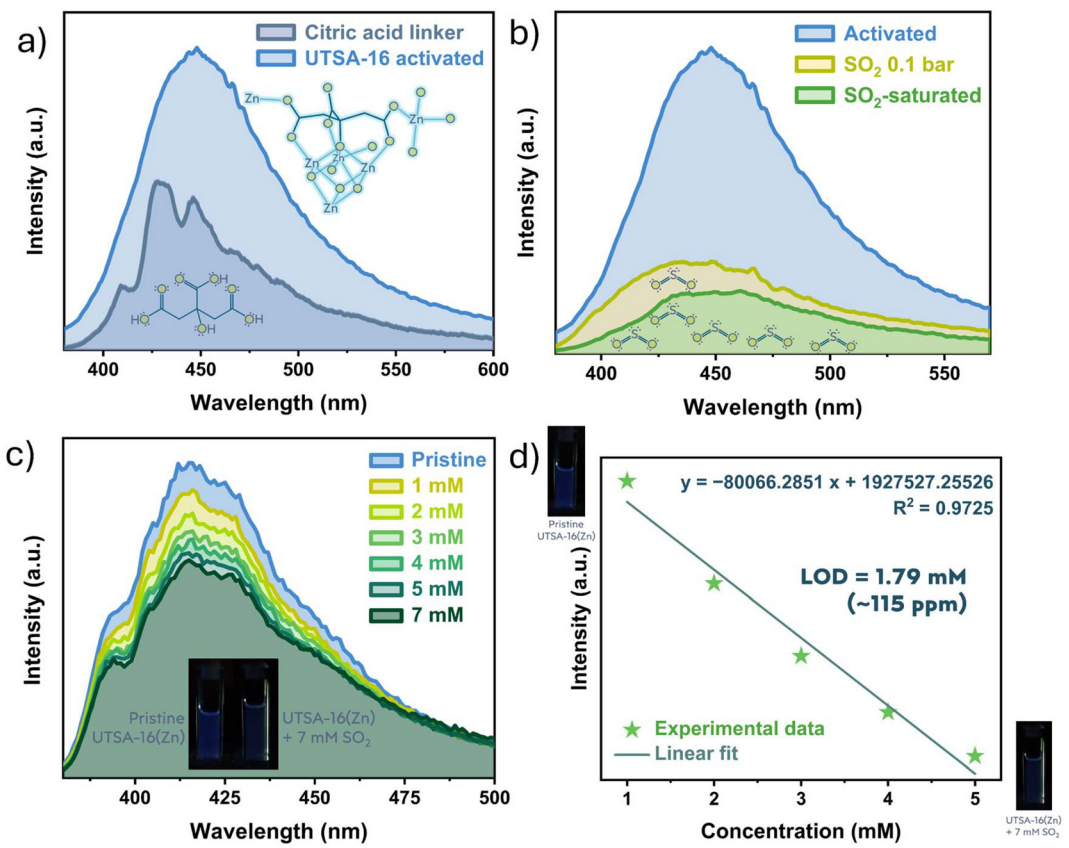


Fig. 2 (a) Comparison of emission spectra of the citric acid linker and UTSA-16(Zn). (b) Comparison of emission spectra of activated UTSA-16(Zn) samples, exposed to 0.1 bar SO_2 and saturated with SO_2. (c) Emission spectra of UTSA-16(Zn) suspensions in THF exposed to SO_2. (d) Linear fit to obtain the LOD of 1.79 mM.

This journal is © The Royal Society of Chemistry 2025

Published on 04 December 2024. Downloaded by Universidad Autonoma Metropolitana-Iztapalapa on 6/30/2025 11:46:41 PM.

sitions and the high probability of nonradiative relaxation explains the low fluorescence observed in citric acid. Additionally, the quantum yield (QY) of the ligand was estimated by the absolute method using an integrating sphere, which captures all the light emitted by the sample and compares it with the absorbed light, obtaining a value of 3.48%.

Nevertheless, it can be observed that after the formation of UTSA-16(Zn), the fluorescence is enhanced. This enhancement occurs because the coordination of citric acid with Zn(II) generates a rigidification of the ligand structure, decreasing the internal movements of citric acid and reducing the possible conformations that it could adopt, allowing a greater amount of excited energy to relax in a radiative way. This rigidification increases the fluorescence efficiency,[37] which is corroborated by obtaining a QY of 7.25% for the MOF. Additionally, the coordination of the carboxyl groups of citric acid with Zn(II) ions stabilizes the non-bonding electrons (n), affecting the electronic distribution of the linker, preventing the excited electrons from losing energy nonradiatively. Another aspect worth highlighting is the d^{10} configuration of the Zn(II) center. Having all of its d orbitals completely filled avoids d–d transitions,[38] as well as linker-to-metal charge transfer (LMCT), both non-radiative mechanisms, avoiding fluorescence quenching processes.[39,40]

Solid-state time-resolved photoluminescence (TRPL) spectra were obtained for both the linker and UTSA-16(Zn) (Fig. S14†), determining fluorescence times of 0.52 ns and 2.09 ns for the linker and MOF, respectively. In both cases, four components (τ_n) were required to fit the exponential model (Table S2†). It can be observed that in both cases, the first component τ_1 is quite fast, which may be related to non-radiative mechanisms,[41,42] such as molecular vibrations, which are quite fast (10^{-12} to 10^{-10} s).[43] The contribution of that component decreases from 72.88% to 31.63% after the formation of UTSA-16(Zn), which confirms the decrease of these non-radiative dissipations due to the stiffening of the structure caused by the coordination with Zn(II). On the other hand, the τ_3 and τ_4 components, which show longer times, can be related to radiative mechanisms on the order of 10^{-9} s (nanoseconds).[44] It can be observed that the contributions of both components increase significantly (from 7.00% to 23.62% for τ_3 and from 1.13% to 12.84% for τ_4) after framework formation, explaining and corroborating the fluorescence enhancement.

Considering the UV-vis spectrum of the MOF (Fig. S9†), absorption is significantly attenuated after coordination with Zn(II) and the signals observed above 250 nm disappear, suggesting that the $n \rightarrow \pi^*$ transitions are restricted. This is because when citric acid coordinates with the Zn(II) ion, the non-bonding electron pairs (n) found on the oxygen atoms of the carboxyl and most of the hydroxyl groups interact with the metal, thus limiting their mobility. The decrease in absorption in the region below 250 nm would also indicate that the $\pi \rightarrow \pi^*$ transitions of the linker are affected by the coordination and stiffening of the material structure. Additionally, HOMO–LUMO energy gap values were estimated for citric acid and UTSA-16(Zn) using the Tauc method (Fig. S13†), considering both direct and indirect transitions (Table S1†). In both cases, an increase in the HOMO–LUMO energy difference was observed, which corroborates that there are changes in the absorption properties of the system, suggesting that more energy is required to excite an electron in the MOF compared to its linker. If related to the increase in fluorescence emission, the change in HOMO–LUMO energy would generate an efficient separation between the two orbitals,[45,46] making it more difficult for the electrons to relax their energy through non-radiative mechanisms. It should be noted that, for molecular-type systems, the Tauc method usually underestimates the band gap from theoretical values.[47,48] However, the Tauc method is employed here for comparative purposes.

Thus it can be concluded that the fluorescence behavior of UTSA-16(Zn) is linker-centered, while Zn(II) provides structural rigidity and a favorable environment for the linker electrons to excite and emit light more efficiently, due to its fully filled d^{10} configuration.

SO_2 detection measurements

Once the fluorescence behaviour of UTSA-16(Zn) was understood, its capability as a SO_2 detector was evaluated by saturating an activated sample in a custom-built *ex situ* gas generator system (Fig. S1†) and measuring its solid-state fluorescence spectrum immediately after removal from the system. It can be seen that there was a quenching of the fluorescence, decreasing by 77.92% with respect to the activated sample (Fig. 2b). Subsequently, its sensitivity was tested when exposed to only 0.1 bar of SO_2 (Fig. 2b), observing a quenching of fluorescence similar to that of the saturated sample, decreasing its intensity by 64.66% with respect to the activated sample. This decrease in fluorescence can be attributed to the change in the electronic structure generated by the intermolecular interactions between SO_2 and UTSA-16(Zn). The QYs are 5.03% and 4.89% for the samples exposed to 0.1 bar and saturated with SO_2, respectively, corroborating the decrease in fluorescence efficiency after gas incorporation.

Once the fluorescence tests were performed, characterisation of the samples exposed to 0.1 bar SO_2 and saturated with SO_2 was carried out. In the PXRD experiments (Fig. S4†), it was observed that the sample exposed to 0.1 bar SO_2 maintains its crystallinity, showing that the intensity of the main peaks does not change. However, when the material is saturated with SO_2, the crystallographic reflections become less intense and defined, which indicates that structural disorganization occur due to the adsorption of SO_2 on the material. It is theorized that this could be due to SO_2 molecules displacing the structural water molecules interacting with the K^+ ions, with SO_2 taking their place by interacting electrostatically *via* its highly electronegative O-atom with the K^+ cations. From FTIR spectroscopy (Fig. S5†), it is generally observed that the SO_2 adsorption does not alter the vibrations of the bonds of the material. However, a tiny band appears at 1335 cm^{-1} (Fig. S6†), attributed to the asymmetric stretching vibration of the S=O bond of the SO_2 molecule,[49,50] which corroborates the presence of the

Published on 04 December 2024. Downloaded by Universidad Autonoma Metropolitana-Iztapalapa on 6/30/2025 11:46:41 PM.

gas inside UTSA-16(Zn). In addition, it can be noticed that the signals at 3427 cm^{-1}, attributed to the O–H bond of the water, widen and decrease slightly, supporting the idea that the adsorbed SO_2 molecules displace the structural water. Finally, using TGA analysis (Fig. S7†) it can be deduced that SO_2 adsorption does not alter the thermal stability of the material by obtaining thermal behaviours similar to those of the as-synthesized material. However, some changes are observed at low temperatures (30 to 150 °C), where the samples exposed to SO_2 lose less weight in this range, which could also suggest that some SO_2 molecules replace structural coordinated water in the framework.

To add further evidence of the stability of UTSA-16(Zn) against SO_2, we performed a SO_2 adsorption experiment at 25 °C and 0 to 1 bar on a pristine sample, previously activated with vacuum and at 120 °C, obtaining a total capture value of 4.27 mmol g^{-1}. Subsequently, after reactivation of the sample, we obtained another isotherm with the same conditions, obtaining a total capture value of 3.81 mmol g^{-1}. A minimal decrease in total capture of less than 0.5 mmol g^{-1} may suggest that exposure to 1 bar SO_2 causes a minimal perturbation of the structure that fails to significantly decrease the adsorption behaviour of the material. Additionally, five SO_2 adsorption–desorption cycles at 0.1 bar were performed on a sample of UTSA-16(Zn), showing a minimal variation in the average SO_2 uptake value (3.63 $mmol^{-1}$), which supports the idea that the structural and functional stability of the material is maintained even after repeated SO_2 exposure at low pressures.

On the other hand, to test the recyclability of the material, the fluorescence of the SO_2-saturated sample was measured four more times after being exposed to SO_2 activation and saturation cycles (Fig. S15†), showing that, at least five times, the material can recover its original fluorescence.

Subsequently, in order to test the selectivity of UTSA-16(Zn) towards SO_2, it was exposed to different gases such as CO_2, H_2S and water vapour (Fig. S16†). It was observed that water does not generate a significant change, and although CO_2 and H_2S do induce a decrease in fluorescence, these are lower compared to that obtained with SO_2. This can be explained by looking at the polarity of each molecule and the interactions it can form with UTSA-16(Zn). CO_2 is a molecule with a linear molecular geometry which makes it non-polar, while the dipole moments of H_2O, H_2S and SO_2 are 1.85, 0.98 and 1.63 D,[51,52] respectively. Another important aspect is the kinetic diameter, which roughly describes the collision probability of the molecules in the hard sphere model; the values reported for CO_2, H_2O, H_2S and SO_2 are 3.3, 2.65, 3.6 and 4.1 Å,[53] respectively. Thus SO_2 having one of the highest polarities, combined with its higher kinetic diameter, can generate better interactions with UTSA-16(Zn) that alter its electronic structure.

Finally, to determine the limit of detection (LOD) of UTSA-16(Zn) (see S2.4. section†), a homogeneous suspension of UTSA-16(Zn) in THF (12 mg in 25 mL) was made. Then, 0.5 mL of THF solutions with known concentrations of SO_2 were added to 2.5 mL aliquots of the UTSA-16(Zn) suspension. The fluorescence of the suspensions of UTSA-16(Zn) exposed to 1–8 mM SO_2 was measured (Fig. 2c). The LOD value was calculated according to the formula: $LOD = -3\sigma/m$,[54] where σ represents the standard deviation of the initial intensity of pristine UTSA-16(Zn) in THF and m is the slope of the linear fit from the experimental data. The LOD value was then calculated as 1.79 mM (~114.6 ppm) (Fig. 2d). In fact, it is possible to observe a slight quenching of fluorescence with the naked eye when the suspensions are exposed to ultraviolet light.

To assess the effect of THF on the framework of UTSA-16(Zn) and the possible leaching of the linker, a sample of UTSA-16(Zn) was immersed in THF for 12 hours, and then the THF solution was filtered to remove all the solid to obtain a UV-vis spectrum (Fig. S12†). It was observed that no significant traces of the linker were found in the THF solution. Such results suggest that the material could be stable against THF immersion, supporting the idea that the structure does not suffer significant degradation under the conditions evaluated.

Proposed fluorescence mechanism

To further investigate the possible quenching phenomena, XPS data of both activated UTSA-16(Zn) and UTSA-16(Zn) saturated with SO_2 at 1 bar were acquired. The high-resolution K 2p and C 1s spectra of the activated material exhibit two peaks at 293.2 and 296.0 eV assigned as K $2p_{1/2}$ and K $2p_{3/2}$, respectively (Fig. 3a). Additionally, the peaks at 284.8 and 286.5 and 288.6 eV are attributed to the C═C, C–OH and C═O bonds.[55,56] On the other hand, for the SO_2 saturated material, evident changes are visualized (Fig. 3c). First, the K 2p core-level binding energies shifted 0.2 eV, highlighting a change in electron density in K^+ cations after saturation with SO_2. This can be explained knowing that some water molecules de-coordinate from the potassium cations during the activation process. Then, when the material is saturated with SO_2, it interacts with K^+ *via* supramolecular interactions. It is theorized that the interaction would occur between the O-atom of the SO_2 molecule, which is electronegative, and the K^+ cation. Furthermore, the C═O binding energy in the SO_2 saturated material also shifts from 288.6 to 288.4 eV, indicating a change in electron density around the C═O bond as well. This can also be explained by supramolecular interactions of sulfur dioxide with the citric acid linker. Both phenomena are well-known for CO_2 interactions with UTSA-16-type materials.[20]

In order to confirm these statements, the O 1s spectra for the SO_2 saturated and activated materials were studied. The activated MOF O 1s spectra (Fig. 3b) can be fitted into three peaks at 530.8, 531.9 and 532.9 eV, corresponding to O–Zn, O–H and O═C bonds, respectively.[57] For the SO_2 saturated spectra (Fig. 3d) a small new peak around 534.1 eV appears, which can be correlated with an O–S bond.[58] In addition, the O═C binding energy shifts from 532.9 eV in the pristine material to 532.8 eV when SO_2 saturated. This shift might also be ascribed to a change in the electronic density arising from SO_2–linker interactions through the S-atom, which has a positive polarity within the SO_2 molecule due to the higher electro-

 This journal is © The Royal Society of Chemistry 2025

Published on 04 December 2024. Downloaded by Universidad Autonoma Metropolitana-Iztapalapa on 6/30/2025 11:46:41 PM.

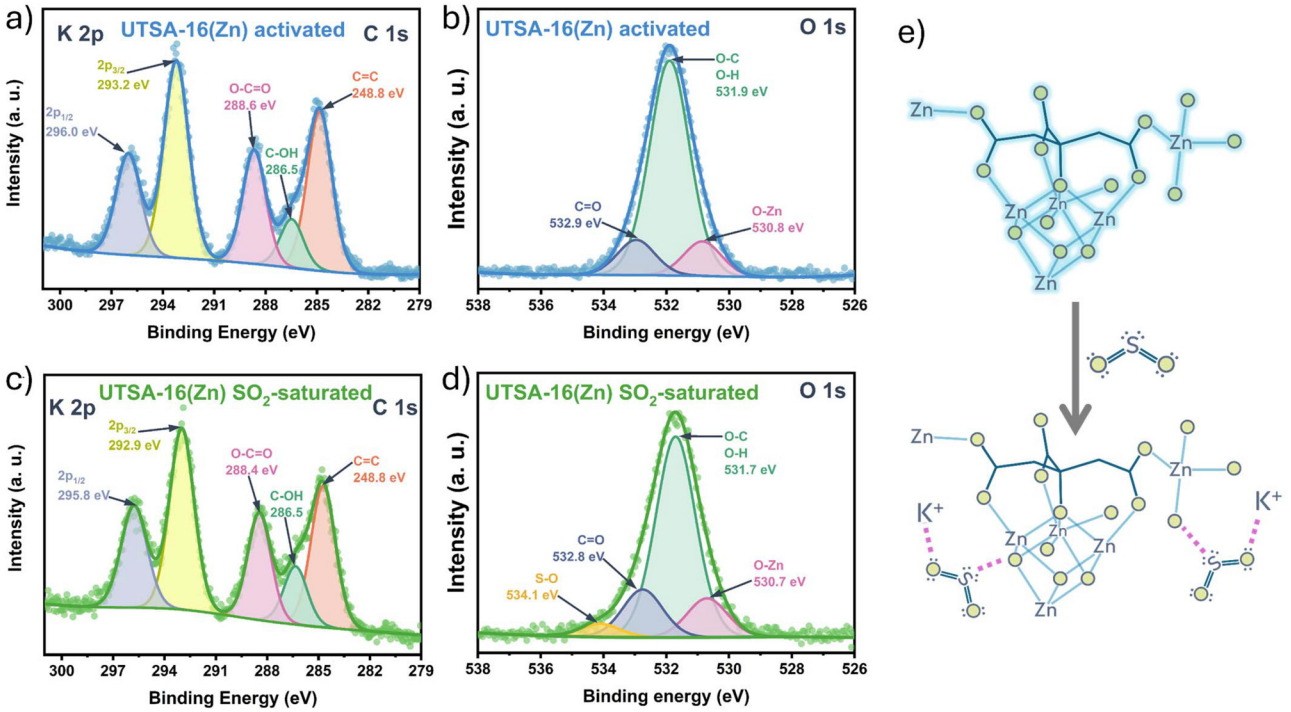


Fig. 3 XPS characterization of UTSA-16(Zn) before and after SO_2 exposure: (a) K 2p and C 1s regions for the activated sample, (b) O 1s region for the activated sample, (c) K 2p and C 1s regions after SO_2 saturation, and (d) O 1s region for the saturated sample. (e) Schematic of the possible intermolecular interactions between SO_2 and UTSA-16(Zn).

negativity of the O-atoms to which it is bonded (Pauling electronegativity values of 2.82 and 3.78 for S and O,[59] respectively), with the O atoms of the O═C (Fig. 3e).

In addition to the above, in a previous study by Masala *et al.*[20] it was determined by *in situ* IR and ^{13}C SSRMN spectroscopy that the main binding site between CO_2 and UTSA-15 is between the K^+ cation and the O-atom of the material and that, subsequently, CO_2 also interacts with the organic bonds of the material, although with lower adsorption energy.

Additionally, with the data from the high-resolution XPS spectra, the atomic percentages of the activated and SO_2-saturated samples were determined, and the results are shown in Table 1.

Solid-state TRPL experiments were performed for the SO_2-exposed samples (Fig. 4) and a slight decrease in fluorescence lifetime was observed from 2.09 ns (activated sample) to 1.65 ns and 1.43 ns for the 0.1 bar SO_2 and SO_2-saturated samples, respectively, indicating that the quenching in fluorescence is not driven by a dynamic mechanism, but rather a static one.

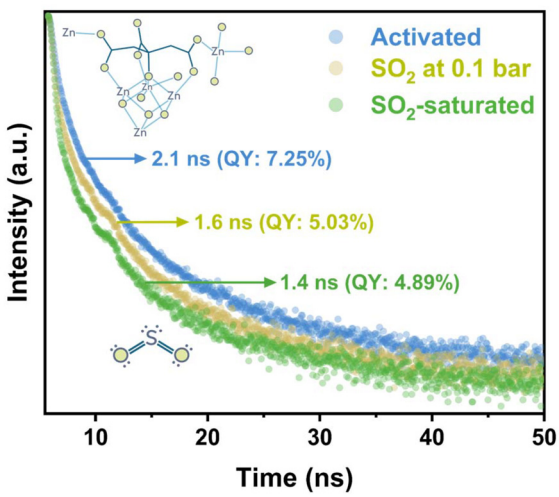


Fig. 4 Comparison of TRPL spectra for activated, 0.1 bar SO_2-exposed, and SO_2-saturated UTSA-16(Zn) samples.

Table 1 Atomic composition of UTSA-16(Zn)

Element	Activated	SO_2-saturated
O 1s	40.3%	40.9%
C 1s	34.1%	34.0%
K 2p	6.6%	6.7%
Zn $2p^3$	19.0%	17.7%
S 2p	—	0.7%

Although the overall decrease is minimal, changes can be observed in the contributions of the different components to the fluorescence lifetimes (Table S2†). For example, in the case of the sample exposed to 0.1 bar SO_2, an increase of almost 20% is observed for the fast component τ_1, which represents the non-radiative mechanism. However, for the slow components τ_3 and τ_4, which are associated with radiative dissipations, decreases in their contributions are observed. In the

Published on 04 December 2024. Downloaded by Universidad Autonoma Metropolitana-Iztapalapa on 6/30/2025 11:46:41 PM.

case of the SO_2 saturated sample, τ_1 increases by 31%, while τ_3 and τ_4 decrease by 10% and 6%, respectively. Thus, it can be confirmed that SO_2 adsorption on UTSA-16(Zn) favours the non-radiative mechanisms in a static quenching mechanism.

Having identified the interactions occurring between UTSA-16(Zn) and SO_2 and the changes occurring in the component contributions to the fluorescence times, it is proposed that the fluorescence quenching mechanism occurs *via* a static quenching mechanism by the formation of a non-fluorescent complex in the ground state (GSC) between the MOF and SO_2.[54] Once the interactions are formed the electron density distribution is altered, stabilising the complex, which favours the dissipation of the excited energy by non-radiative pathways as observed in the fluorescence time contributions. It is reported in the literature that the formation of these non-fluorescence GSCs are accompanied by changes in the UV-vis spectra, as observed in Fig. S10.† There is a significant increase in absorption in the 200–300 nm region upon exposure of UTSA-16(Zn) to SO_2 (at 0.1 bar and saturated), suggesting that SO_2 interacts with the functional groups of the linker, probably affecting the $\pi \rightarrow \pi^*$ transitions and perhaps introducing new electronic transitions due to the interaction between the gas orbitals and the MOF. In addition, slight but important modifications are observed in the region between 300 and 400 nm, related to the $n \rightarrow \pi^*$ transitions that could be due to the non-shared electron pairs present in the SO_2 molecule. In fact, similar changes can be observed in the UV-vis spectra measured for two UTSA-16(Zn) samples dispersed in pristine THF and in 7 mM SO_2 in THF (Fig. S11†).

In addition, the emission spectrum of pristine UTSA-16(Zn) dispersed in THF and the absorption spectrum of a SO_2 solution were compared and they showed no spectral overlap (Fig. S17†). This lack of overlap between the emission and absorption bands rules out the possibility of dynamic quenching, which typically requires significant spectral overlap to enable energy transfer between the fluorophore and quencher.[60]

With the obtained solid-state UV-vis spectra, the energy between the HOMO–LUMO of the system after SO_2 adsorption was determined by direct and indirect methods (Fig. S13 and Table S1†). It was found that for both the sample exposed to 0.1 bar SO_2 and the SO_2 saturated sample, decreases in the energy between the HOMO–LUMO occurred in both direct and indirect methods,[61] which corroborates the perturbation that SO_2 generates in the electronic structure of the material, decreasing the energy required for the electronic transitions. The fact that this is accompanied by a decrease in fluorescence emission indicates that the separation between the two orbitals is less efficient than in the pristine system,[45] favouring non-radiative dissipations. Tauc plot analysis is not inherently an independent characterization of absorption properties; however, it does provide a comparative means to demonstrate the electronic effect of SO_2 on UTSA-16(Zn). Such results were consistent with the postulation of a static quenching model, *i.e.*, SO_2 forms a ground state complex (GSC) with UTSA-16(Zn) to produce a non-fluorescent species and perturbed electronic environment for facilitating non-radiative pathways. Theoretical methods should also validate these effects with calculations of the respective HOMO–LUMO gap but are outside the scope of this study.

Conclusions

In conclusion, this study demonstrates the strong potential of the metal–organic framework UTSA-16(Zn) as a fluorescence sensor for detecting sulfur dioxide (SO_2). Synthesis and comprehensive characterization by PXRD, FTIR, and TGA confirmed the material's structural integrity and stability, while fluorescence spectroscopy revealed a pronounced quenching effect in response to SO_2, with an impressive detection limit of 1.79 mM (~114.6 ppm). Time-resolved photoluminescence (TRPL) studies, XPS, and UV-vis spectroscopy pointed to a static quenching mechanism, likely due to the formation of a non-fluorescent ground-state complex (GSC) between SO_2 and UTSA-16(Zn). This interaction is facilitated by the coordination between K^+ ions in the framework and oxygen atoms in SO_2, as well as between the carbonyl groups on the organic linkers and sulfur atoms of SO_2. XPS analysis further revealed electron density shifts around K^+ and C═O groups upon SO_2 exposure, emphasizing the role of supramolecular interactions in modulating the MOF's electronic structure. Additionally, UV-vis spectroscopy indicated a decrease in the HOMO–LUMO energy gap following SO_2 adsorption, providing deeper insight into the sensing mechanism. Overall, UTSA-16(Zn) exhibits exceptional sensitivity toward SO_2, making it a promising candidate for applications in environmental monitoring and quality control.

Author contributions

Valeria B. López-Cervantes: Methodology, formal analysis, investigation, data curation, and writing – original draft. Marco L. Martínez: Methodology, formal analysis, investigation, and writing – original draft. Juan L. Obeso: Methodology and formal analysis. Celene García-Carvajal: Methodology and formal analysis. Nora S. Portillo-Vélez: Formal analysis. Ariel Guzmán-Vargas: Supervision. Ricardo A. Peralta: Resources and investigation. Eduardo González-Zamora: Resources, investigation, and project administration. Ilich A. Ibarra: Conceptualization, resources, investigation, project administration, funding acquisition, and writing – review & editing. Diego Solis-Ibarra: Conceptualization, resources, investigation, project administration, and writing – review & editing. John Luke Woodliffe: Conceptualization, resources, investigation, project administration, and writing – review & editing. Yoarhy A. Amador-Sánchez: Conceptualization, validation, resources, investigation, project administration, and writing – review & editing.

Data availability

The data supporting this article have been included in the ESI.†

This journal is © The Royal Society of Chemistry 2025

Published on 04 December 2024. Downloaded by Universidad Autonoma Metropolitana-Iztapalapa on 6/30/2025 11:46:41 PM.

Conflicts of interest

There are no conflicts to declare.

Acknowledgements

V. B. L.-C. and M. L. M. thank CONACYT for the Ph.D. fellowships (1005649 and 1080048). I. A. I. thanks PAPIIT UNAM (IN201123), México, for financial support. J. L. W. thanks the EPSRC for a Doctoral Prize Fellowship (EP/W524402/1). The authors thank Professor L. Huerta for the XPS measurements and for the determination of the elemental composition of the material. V. B. L.-C. thanks Professor E. Sánchez-González and D. Zugasti for scientific discussions. The authors also thank U. Winnberg (Euro Health) for scientific discussions and G. Ibarra-Winnberg for scientific encouragement.

References

1 C. Pénard-Morand and I. Annesi-Maesano, *Breathe*, 2004, **1**, 108–119.
2 M. Szyszkowicz, E. Porada, N. Tremblay and E. Grafstein, *Stroke Res. Treat.*, 2012, **2012**, 1–7.
3 J. Q. Koenig, in *Health Effects of Ambient Air Pollution*, Springer, Boston, MA, 2000, pp. 99–114.
4 P. Orellano, J. Reynoso and N. Quaranta, *Environ. Int.*, 2021, **150**, 106434.
5 R. A. Marquez, J. L. Obeso, R. R. Vaidyula, V. B. López-Cervantes, R. A. Peralta, P. Marín Rosas, J. A. de los Reyes, C. B. Mullins and I. A. Ibarra, *J. Mater. Chem. A*, 2024, **12**, 32735–32744.
6 J. L. Obeso, J. G. Flores, C. V. Flores, V. B. López-Cervantes, V. Martínez-Jiménez, J. A. de los Reyes, E. Lima, D. Solis-Ibarra, I. A. Ibarra, C. Leyva and R. A. Peralta, *Dalton Trans.*, 2023, **52**, 12490–12495.
7 J. Vazquez-Samperio, P. Acevedo-Peña, M. M. González, M. Oliver-Tolentino, I. Padilla-Martínez, A. Guzmán-Vargas and E. Reguera, *Electrochim. Acta*, 2020, **346**, 136253.
8 E. Martínez-Ahumada, M. L. Díaz-Ramírez, M. D. J. Velásquez-Hernández, V. Jancik and I. A. Ibarra, *Chem. Sci.*, 2021, **12**, 6772–6799.
9 E. Martínez-Ahumada, A. López-Olvera, V. Jancik, J. E. Sánchez-Bautista, E. González-Zamora, V. Martis, D. R. Williams and I. A. Ibarra, *Organometallics*, 2020, **39**, 883–915.
10 K. Tan, S. Zuluaga, Q. Gong, Y. Gao, N. Nijem, J. Li, T. Thonhauser and Y. J. Chabal, *Chem. Mater.*, 2015, **27**, 2203–2217.
11 K. Sumida, D. L. Rogow, J. A. Mason, T. M. McDonald, E. D. Bloch, Z. R. Herm, T. H. Bae and J. R. Long, *Chem. Rev.*, 2012, **112**, 724–781.
12 J. L. C. Rowsell and O. M. Yaghi, *Microporous Mesoporous Mater.*, 2004, **73**, 3–14.
13 A. Ö. Yazaydın, R. Q. Snurr, T.-H. Park, K. Koh, J. Liu, M. D. LeVan, A. I. Benin, P. Jakubczak, M. Lanuza, D. B. Galloway, J. J. Low and R. R. Willis, *J. Am. Chem. Soc.*, 2009, **131**, 18198–18199.
14 T. Wu, X.-jing Gao, F. Ge and He.-gen Zheng, *CrystEngComm*, 2022, **24**, 7881–7901.
15 J. X. Wang, J. Yin, O. Shekhah, O. M. Bakr, M. Eddaoudi and O. F. Mohammed, *ACS Appl. Mater. Interfaces*, 2022, **14**, 9970–9986.
16 T. K. Pal, *Mater. Chem. Front.*, 2023, **7**, 405–441.
17 S. Xiang, X. Wu, J. Zhang, R. Fu, S. Hu and X. Zhang, *J. Am. Chem. Soc.*, 2005, **127**, 16352–16353.
18 A. Masala, J. G. Vitillo, F. Bonino, M. Manzoli, C. A. Grande and S. Bordiga, *Phys. Chem. Chem. Phys.*, 2016, **18**, 220–227.
19 S. Xiang, Y. He, Z. Zhang, H. Wu, W. Zhou, R. Krishna and B. Chen, *Nat. Commun.*, 2012, **3**, 954.
20 A. Masala, F. Grifasi, C. Atzori, J. G. Vitillo, L. Mino, F. Bonino, M. R. Chierotti and S. Bordiga, *J. Phys. Chem. C*, 2016, **120**, 12068–12074.
21 S. Gaikwad, S.-J. Kim and S. Han, *J. Ind. Eng. Chem.*, 2020, **87**, 250–263.
22 R. Gaikwad, S. Gaikwad and S. Han, *J. Ind. Eng. Chem.*, 2023, **126**, 444–453.
23 J. L. Woodliffe, J. Molinar-Díaz, R. Clowes, O. H. Hussein, E. Lester, R. Ferrari, I. Ahmed and A. Laybourn, *J. Environ. Chem. Eng.*, 2024, **12**, 114167.
24 J. L. Woodliffe, A.-L. Johnston, M. Fay, R. Ferrari, R. L. Gomes, E. Lester, I. Ahmed and A. Laybourn, *Mater. Adv.*, 2023, **4**, 5838–5849.
25 Q. Xie, F. Li, H. Guo, L. Wang, Y. Chen, G. Yue and D.-L. Peng, *ACS Appl. Mater. Interfaces*, 2013, **5**, 5508–5517.
26 R. Gaikwad, S. Gaikwad and S. Han, *J. Ind. Eng. Chem.*, 2022, **111**, 346–355.
27 C. Healy, K. M. Patil, B. H. Wilson, L. Hermanspahn, N. C. Harvey-Reid, B. I. Howard, C. Kleinjan, J. Kolien, F. Payet, S. G. Telfer, P. E. Kruger and T. D. Bennett, *Coord. Chem. Rev.*, 2020, **419**, 213388.
28 L. Zhang and Y. H. Hu, *J. Phys. Chem. C*, 2010, **114**, 2566–2572.
29 S. Gadipelli and Z. Guo, *Chem. Mater.*, 2014, **26**, 6333–6338.
30 J. Ren, L. Malfatti and P. Innocenzi, *C*, 2020, **7**, 2.
31 R. W. Newberry and R. T. Raines, *Acc. Chem. Res.*, 2017, **50**, 1838–1846.
32 B. Sahariah and B. K. Sarma, *J. Phys. Chem. C*, 2020, **22**, 26669–26681.
33 S. K. Singh and A. Das, *J. Phys. Chem. C*, 2015, **17**, 9596–9612.
34 P. Li, S. Xue, L. Sun, X. Zong, L. An, D. Qu, X. Wang and Z. Sun, *Light: Sci. Appl.*, 2022, **11**, 298.
35 Q. Zhang, R. Wang, B. Feng, X. Zhong and K. Ostrikov, *Nat. Commun.*, 2021, **12**, 6856.
36 Y. Huang, J. J. Ferrie, X. Chen, Y. Zhang, D. M. Szantai-Kis, D. M. Chenoweth and E. J. Petersson, *Chem. Commun.*, 2016, **52**, 7798–7801.
37 Z. Wei, Z.-Y. Gu, R. K. Arvapally, Y.-P. Chen, R. N. McDougald, J. F. Ivy, A. A. Yakovenko, D. Feng,

Published on 04 December 2024. Downloaded by Universidad Autonoma Metropolitana-Iztapalapa on 6/30/2025 11:46:41 PM.

M. A. Omary and H.-C. Zhou, *J. Am. Chem. Soc.*, 2014, **136**, 8269–8276.
38 M. D. Allendorf, C. A. Bauer, R. K. Bhakta and R. J. T. Houk, *Chem. Soc. Rev.*, 2009, **38**, 1330.
39 W. Xie, J. Wu, X. Hang, H. Zhang, K. Shen and Z. Wang, *Front. Chem.*, 2021, **9**, 708314.
40 G. Liu, S. Han, Y. Gao, N. Xu, X. Wang and B. Chen, *CrystEngComm*, 2020, **22**, 7952–7961.
41 S. K. Panigrahi and A. K. Mishra, *J. Fluoresc.*, 2020, **30**, 1085–1094.
42 S. De Camillis, J. Miles, G. Alexander, O. Ghafur, I. D. Williams, D. Townsend and J. B. Greenwood, *J. Phys. Chem. C*, 2015, **17**, 23643–23650.
43 B. Valeur and M. N. Berberan-Santos, *Molecular Fluorescence*, Wiley, 2012.
44 U. Noomnarm and R. M. Clegg, *Photosynth. Res.*, 2009, **101**, 181–194.
45 J.-L. Bredas, *Mater. Horiz.*, 2014, **1**, 17–19.
46 M. Chen, Y. Chen, Y. Li, Y. Lin and Y. Wu, *RSC Adv.*, 2024, **14**, 6494–6500.
47 K. Fabrizio, K. N. Le, A. B. Andreeva, C. H. Hendon and C. K. Brozek, *ACS Mater. Lett.*, 2022, **4**, 457–463.
48 P. R. Jubu, F. K. Yam, V. M. Igba and K. P. Beh, *J. Solid State Chem.*, 2020, **290**, 121576.
49 M. Savage, Y. Cheng, T. L. Easun, J. E. Eyley, S. P. Argent, M. R. Warren, W. Lewis, C. Murray, C. C. Tang, M. D. Frogley, G. Cinque, J. Sun, S. Rudić, R. T. Murden, M. J. Benham, A. N. Fitch, A. J. Blake, A. J. Ramirez-Cuesta, S. Yang and M. Schröder, *Adv. Mater.*, 2016, **28**, 8705–8711.
50 S. Xing, J. Liang, P. Brandt, F. Schäfer, A. Nuhnen, T. Heinen, I. Boldog, J. Möllmer, M. Lange, O. Weingart and C. Janiak, *Angew. Chem., Int. Ed.*, 2021, **60**, 17998–18005.
51 A. A. A. Azzam, L. Lodi, S. N. Yurchenko and J. Tennyson, *J. Quant. Spectrosc. Radiat. Transfer*, 2015, **161**, 41–49.
52 S. L. Shostak, W. L. Ebenstein and J. S. Muenter, *J. Chem. Phys.*, 1991, **94**, 5875–5882.
53 S. Kentish, C. Scholes and G. Stevens, *Recent Pat. Chem. Eng.*, 2008, **1**, 52–66.
54 A. Sharma, D. Kim, J. H. Park, S. Rakshit, J. Seong, G. H. Jeong, O. H. Kwon and M. S. Lah, *Commun. Chem.*, 2019, **2**, 1–8.
55 J. Jiang, L. Huang, X. Liu and L. Ai, *ACS Appl. Mater. Interfaces*, 2017, **9**, 7193–7201.
56 L. Zheng, M. Zhou, Z. Huang, Y. Chen, J. Gao, Z. Ma, J. Chen and X. Tang, *Environ. Sci. Technol.*, 2016, **50**, 11951–11956.
57 Y. Liu, S. Dong, L. Wang, G. Chen, Y. Hou, Z. Cao and Y. Zhang, *J. Solid State Electrochem.*, 2022, **26**, 2301–2313.
58 G. Zhou, L.-C. Yin, D.-W. Wang, L. Li, S. Pei, I. R. Gentle, F. Li and H.-M. Cheng, *ACS Nano*, 2013, **7**, 5367–5375.
59 C. Tantardini and A. R. Oganov, *Nat. Commun.*, 2021, **12**, 2087.
60 S. Rajendran, V. UshaVipinachandran, K. H. Badagoppam Haroon, I. Ashokan and S. K. Bhunia, *Anal. Methods*, 2022, **14**, 4263–4291.
61 P. H. M. Andrade, C. Volkringer, T. Loiseau, A. Tejeda, M. Hureau and A. Moissette, *Appl. Mater. Today*, 2024, **37**, 102094.

This journal is © The Royal Society of Chemistry 2025

RSC Advances

PAPER

View Article Online
View Journal | View Issue

Check for updates

Cite this: *RSC Adv.*, 2024, **14**, 35090

Effective BPA degradation in water: the integration of bimetallic UiO-66 Ce–Zr†

Leidy Marcela Gallo,[a] Juan L. Obeso,[ab] Nora S. Portillo-Vélez,[c] Carlos E. Garduño-Albino,[c] Catalina V. Flores,[a] Leonardo Herrera-Zuñiga,[c] Alejandro Islas-Jácome,[c] Ricardo A. Peralta *[c] and Carolina Leyva *[a]

Received 7th September 2024
Accepted 21st October 2024

DOI: 10.1039/d4ra06460g

rsc.li/rsc-advances

In this work, a bimetallic MOF UiO-66 Ce–Zr to degrade bisphenol A (BPA) in water was synthesised. The material exhibited a remarkable degradation efficiency of 84.3% under UV irradiation for 240 minutes. Combining cerium (Ce) and zirconium (Zr) in the MOF structure enhanced the catalytic activity and reinforced its structural stability. Comprehensive characterisation was performed using PXRD, FT-IR, SEM-EDS, XPS, and N_2 adsorption–desorption isotherms. Scavenger tests confirmed that hydroxyl ($^{\bullet}OH$) and superoxide ($^{\bullet}O_2^-$) radicals played a crucial role in the photocatalysis. The material demonstrated excellent reusability, maintaining high performance over three cycles with minimal structural changes. Furthermore, a toxicological evaluation of the degradation by-products was conducted using UPLC-MS, reaffirming the potential of the material as an efficient water treatment system. This study underscores the potential of UiO-66 Ce–Zr as a stable and effective photocatalyst for water treatment applications, particularly in removing emerging pollutants such as BPA.

Open Access Article. Published on 04 November 2024. Downloaded on 6/30/2025 11:47:13 PM.
This article is licensed under a Creative Commons Attribution-NonCommercial 3.0 Unported Licence.

Introduction

Water, the lifeblood of our planet, is gravely under siege. Despite its indispensable role, our water bodies are increasingly and alarmingly contaminated, which is a crisis fueled mainly by human activities, such as agriculture, industry, and urban development.[1] Among the culprits are emerging contaminants (ECs) and unregulated organic compounds like pesticides, pharmaceuticals, and endocrine disruptors (EDCs).[2] Classic EDCs include pesticides, herbicides, phthalates, and bisphenols. Bisphenol A (BPA) is a synthetic chemical agent recognised for its alarming ability to disrupt the endocrine system. Its uses include manufacturing essential consumer products, such as water bottles, baby bottles, canned goods, and various plastics.[3] BPA has been associated with a myriad of diseases, such as cancer, polycystic ovary syndrome, depression, obesity, insulin resistance, reproductive disorders, and cardiovascular problems.

Different techniques have been explored to remove contaminants from water sources, including adsorption, coagulation, filtration, and sedimentation.[4] Although these techniques remove contaminants from water, they do not chemically degrade or destroy them, which can result in waste that requires further treatment. On the other hand, heterogeneous photocatalysis has proven to be an environmentally friendly, cost-effective, and efficient tool for degrading contaminants in water.[5] This technique relies on semiconductor photocatalysis, which generates reactive oxygen species, such as superoxide radicals ($^{\bullet}O_2^-$) and hydroxyl radicals ($^{\bullet}OH$), which are essential for degradation.[6] Additionally, materials such as zeolites, graphene oxide, and carbon nanomaterials have been evaluated and widely used for degradation.[7,8] However, in some cases, these materials exhibit instability, low efficiency, lack of reusability, and recombination; these materials need further research to overcome these limitations.

A novel alternative to tackle this problem is using metal–organic frameworks (MOFs), which contain metal nodes coordinated to organic ligands, forming a bi- or tri-dimensional structure.[9] MOFs are notable for their large surface area, design flexibility, high porosity, and elevated volume.[10] These characteristics make them highly versatile in energy storage, catalysis, and contaminant degradation applications.[11,12] In water remediation, MOFs have been employed to degrade BPA. For example, Liu *et al.*[13] employed enzyme encapsulation within the MOF (HRP-ZIF-8), achieving a high efficacy of 94.7% in BPA degradation. Despite these promising results, the high cost of

[a]*Instituto Politécnico Nacional, Centro de Investigación en Ciencia Aplicada y Tecnología Avanzada, Laboratorio Nacional de Ciencia, Tecnología y Gestión Integrada del Agua, Legaria 694, Col. Irrigación, Miguel Hidalgo, 11500, CDMX, Mexico. E-mail: zleyva@ipn.mx*

[b]*División de Ingeniería en Sistemas Automotrices, Tecnológico de Estudios Superiores del Oriente del Estado de México (TESOEM), Tecnológico Nacional de México, Estado de México 56400, Mexico*

[c]*Departamento de Química, División de Ciencias Básicas e Ingeniería, Universidad Autónoma Metropolitana (UAM-I), 09340, Mexico. E-mail: rperalta@izt.uam.mx*

† Electronic supplementary information (ESI) available: Instrumental techniques and characterization. See DOI: https://doi.org/10.1039/d4ra06460g

© 2024 The Author(s). Published by the Royal Society of Chemistry

Open Access Article. Published on 04 November 2024. Downloaded on 6/30/2025 11:47:13 PM.
This article is licensed under a Creative Commons Attribution-NonCommercial 3.0 Unported Licence.

synthesis is a significant challenge for its commercial application. Conversely, Guan *et al.*[14] conducted a modification that involved doping with iron in the MOF UiO-66 Zr. Cerium (Ce) and zirconium (Zr) are two metals that stand out in materials science and environmental chemistry. Ce is notable in various applications as it was the first lanthanide to be discovered and can switch between oxidation states +3 and +4, making it an ideal component in catalytic processes. This property highlights its importance in oxidation and reduction reactions, making it a key element in degrading organic pollutants like phenol and bisphenol A.[15,16] The choice of cerium in this work optimises the catalytic reactivity and provides cost and efficiency benefits, helping to address pollution challenges.[17,18] Conversely, Zr is known for its exceptional corrosion resistance and thermal stability. For instance, zirconium dioxide (ZrO_2) has established itself as a catalytic support in the oxidation of organic compounds such as phenol, contributing to the remediation of industrial wastewater. Additionally, zirconium is part of nanostructures that enhance catalytic processes due to its ability to withstand extreme conditions without losing efficiency.[16,19,20]

Based on this, incorporating this metal mixture could enhance the degradation performance. Hence, this study introduces a bimetallic MOF UiO-66 Ce–Zr as a potential game-changer in the effective degradation of BPA in water solutions. The MOF material was subjected to rigorous characterisation using powder X-ray diffraction (PXRD), Fourier-transform infrared spectroscopy (FT-IR), scanning electron microscopy with energy-dispersive X-ray spectroscopy (SEM-EDX), X-ray photoelectron spectroscopy (XPS), and N_2 adsorption. Moreover, the results show a degradation efficiency of 84.3%, achieved at a BPA concentration of 50 ppm after just 4 hours. This could indicate the potential of the bimetallic MOF UiO-66 Ce–Zr in the water treatment field.

Experimental section

Materials

Detailed information on the materials is available in Section S1.†

Synthesis of the MOFs

Synthesis of the MOF UiO-66 Zr. The MOF UiO-66 Zr was synthesized using the solvothermal method. During the synthesis, 2.5 mmol of terephthalic acid was dissolved in 20 mL of DMF, and the mixture was stirred for approximately 10 minutes. Next, 2.38 mmol of $ZrOCl_2 \cdot 8H_2O$ was added and stirred in the mixture for 10 minutes. The solution was transferred to a 100 mL Teflon vessel and heated to 150 °C for 24 hours. After cooling, the solid was washed three times with DMF and three times with acetone. Finally, we dried the solid at 70 °C.

Synthesis of the MOF UiO-66 Ce. The method described by N. Stock *et al.*[21] was followed to synthesize the MOF UiO-66 Ce. A 1.25 mmol quantity of terephthalic acid was dissolved in 7.5 mL of DMF and stirred for 10 minutes. Similarly, 1.5 mmol of Ce $(NH_4)_2(NO_3)_6$ was stirred in 2.5 mL of water for about 10 minutes. The two solutions were mixed and transferred to a 50 mL Teflon vessel and subsequently heated to 100 °C for 15 minutes. After the product had cooled, it was washed with DMF and methanol three times.

Synthesis of the MOF UiO-66 Ce–Zr. The synthesis was carried out using the solvothermal method described by Sharma *et al.*[22] Initially, two mmol of terephthalic acid was dissolved in 10 mL of a DMF–water mixture in a 1 : 2 ratio, and the mixture was stirred for approximately 10 minutes. Then, two mmol of $ZrOCl_2 \cdot 8H_2O$ and one mmol of $Ce(NH_4)_2(NO_3)_6$ were added to the mixture and stirred for 5 minutes. The solution was transferred to a 150 mL Teflon vessel and heated to 150 °C for 72 hours. After cooling, the product was washed three times with DMF and acetone. Finally, the obtained solid was dried at 150 °C for 24 hours.

Analytical instruments

Detailed information on the instrumental techniques is available in Section S1.†

Electrochemical characterisation

Electrochemical impedance spectroscopy (EIS) studies were conducted in a three-electrode cell to evaluate the semiconductors electrochemically. Electrodes of fluorine-doped tin oxide (FTO) glass with a specific area of 0.7×0.7 cm^2 were used. These electrodes underwent cleaning cycles by sonication in Milli-Q water and ethanol, each for 30 minutes, followed by drying at 75 °C for an hour Rangel-Váquez *et al.*[23] previously explained how to make a suspension of UiO-66 Ce, UiO-66 Zr, and UiO-66 Ce–Zr, which are artificial MOFs. It was simple to use the drop-casting method to evenly spread 8 mg of the MOF, 1.5 mL of ethanol, and 150 μL of Nafion on the FTO glass's active surface. A 0.5 M aqueous sodium sulfate solution was used as the supporting electrolyte, with a platinum counter electrode and an Ag/AgCl reference electrode. The semiconducting properties of the photocatalyst films were determined by analysing Mott–Schottky plots at various potentials.

Photocatalytic tests for bisphenol A degradation

The photocatalytic activity of the derived MOFs UiO-66 was evaluated for the degradation of BPA (Fig. S1†). This evaluation was carried out in a cylindrical double-walled photoreactor with a capacity of 250 mL, maintaining room temperature with constant stirring and air bubbling in each experiment. A mercury lamp (a PenRay lamp with primary energy at 254 nm) was used as the UV irradiation source. The photocatalytic tests were conducted by adding 50 mg of MOFs (UiO-66) to 50 mL of a BPA solution (50 ppm). Before initiating the photocatalytic reaction, the solution containing the photocatalyst was left to stand for 30 minutes without turning on the lamp to achieve adsorption–desorption equilibrium on the catalyst surface. After the equilibrium period, the lamp was turned on to begin the contaminant degradation. The BPA degradation was then monitored every hour for 4 hours. A Waters ACQUITY UPLC H-Class Series ultra-high-performance liquid chromatography system was used to quantify the BPA concentration. A quadrupole mass detector (ACQUITY QDa) with electrospray ionization

Open Access Article. Published on 04 November 2024. Downloaded on 6/30/2025 11:47:13 PM. This article is licensed under a Creative Commons Attribution-NonCommercial 3.0 Unported Licence.

(ESI) was used to determine the by-products in the UPLC system.

The following equation was used to determine the efficiency of photodegradation:

$$\text{Photodegradation efficiency } (\%) = \left(1 - \frac{C}{C_0}\right) \times 100 \quad (1)$$

Scavenger tests

Whole and radical trapping tests were conducted to thoroughly investigate the reactive oxygen species (ROS) responsible for BPA degradation. Different scavenging agents were used (Fig. S2†), such as salicylic acid (SA) to study the hydroxyl radicals ($^{\bullet}OH$). For example, it was demonstrated that the reaction of salicylic acid with $^{\bullet}OH$ produces hydroxylated derivatives such as 2,3-dihydroxybenzoic acid, which can be quantified by UV-Vis spectrophotometry, allowing the estimation of $^{\bullet}OH$ concentration,[24] citric acid (CA) to identify photogenerated holes (h^+), *p*-benzoquinone (PBQ) to determine the effect of superoxide radicals ($^{\bullet}O_2^-$), and DMSO to examine the role of electrons (e^-) in the process. The concentration of these agents in the photocatalytic reaction system was set at 1 mM, surpassing the concentration of BPA. Each agent was added independently, adhering to the previously described degradation process in Section S1.† The variation in the photocatalytic efficiency of bisphenol A (BPA) with the addition of each agent was subsequently evaluated, thereby determining their specific contributions to the degradation process.[25]

Computational analysis methodology

To achieve optimal performance at the PBE/cc-pVTZ level, a water solvent model must be added based on the density of charge (SMD). The BPA ligand was tuned using the Gaussian 09 quantum chemistry software. The GGA Perdew–Burke–Ernzerhof (PBE) approach has been used in a significant number of first-principles (DFT) material research studies, which led to the selection of this particular computational level. The foundation set was selected due to attempts to balance cost and accuracy.[26] Several different sources, such as the Cambridge Structural Database (CSD) (**https://www.ccdc.cam.ac.uk/**), were used to acquire the structures of the MOFs that are the focus of this investigation. Immediately after the docking procedure, the same degree of theory was used to compute the energetic interactions that took place between the MOF and the BPA. In the MOF-BPA docking process, AutoDock Vina 1.1.2 was employed to estimate the binding score between BPA and the MOF. One hundred iterations of the Lamarckian evolutionary algorithm were carried out, resulting in one hundred optimum conformations that were suitable for BPA screening grid maps. We used Chimera to depict all BPA-MOF complexes.[27] The volumes of MOF and ligand were calculated with the MoloVol software.[28] The conformation that possessed the lowest score was selected. We used the SwissADME and ProTox-3.0 software to carry out the analysis of the pharmacokinetic and toxic characteristics (ADMETox) of the degradation products to estimate their toxicity and ecotoxicity.

Results and discussion

Characterisation of MOFs UiO-66

The materials were synthesised using the solvothermal method. The XRD patterns (Fig. S3†) corroborate the pure phase of UiO-66 Ce and UiO-66 Zr. Moreover, MOF UiO-66 Ce–Zr showed index patterns in the pristine UiO-Ce and UiO-Zr.[22] The FT-IR spectra of the three synthesised MOFs (Fig. S4†) show the characteristic bands for the UiO-66 materials. The Ce–O bond stretching vibrations are seen at 545 cm^{-1}. Between 750 and 680 cm^{-1}, the symmetric bands correspond to the Zr–O bond vibrations. The peaks at 1590 and 1400 cm^{-1} were associated with the antisymmetric and symmetric vibrations of the carboxylate groups.[29] Furthermore, using the SEM technique, a well-defined rod-like morphology of the MOF UiO-66 Ce–Zr was observed (Fig. S7†), which yields similar results to those reported by Sharma *et al.*[22] Elemental composition was performed to corroborate the presence of carbon (C), oxygen (O), cerium (Ce), and zirconium (Zr), corroborating the effectiveness of the synthesis. Elemental mapping EDS analysis confirmed the Ce : Zr ratio 1 : 2. Based on the N_2 adsorption–desorption isotherm (Fig. S8†) for the MOF UiO-66 Ce–Zr, the BET surface area and pore volume were calculated, displaying 328 $m^2\ g^{-1}$ and 0.32 $cm^3\ g^{-1}$, respectively.

The electrochemical characterisation was carried out to calculate the flat-band potential (EFB) and corroborate the type of semiconductor (Fig. S9†) presented by Mott–Schottky (M–S). In each case, a positive slope in the M–S curve is observed. This is characteristic of an n-type semiconductor, indicating the presence of an excess of electrons in the material. The results suggest that the materials are suitable photocatalytic materials because they make more charge carriers (electron–hole pairs) available, which are necessary to break down contaminants.[30] For the UiO-66 Ce MOF, the energy level of the conduction band (CB) is more negative than the standard redox potential of superoxide ($E(O_2/^{\bullet}O_2^-) = -0.33$ V *vs.* NHE). This allows superoxide radicals ($^{\bullet}O_2^-$) to degrade BPA more efficiently. In contrast, the valence band (VB) has a less positive potential than the redox potential of hydroxyl radicals ($E(H_2O/^{\bullet}OH) = 2.40$ V *vs.* NHE), which prevents the generation of hydroxyl radicals ($^{\bullet}OH$). Although the MOF UiO-66 Zr can generate superoxide radicals, its high VB energy reduces hydroxyl radical generation. Conversely, combining the properties of Ce and Zr metals in the bimetallic MOF UiO-66 Ce–Zr improves the photocatalytic properties. It shows a band gap of 3.2 eV, suggesting that UiO-66 Ce–Zr exhibits excellent stability under ultraviolet irradiation, similar to its components. Also, UiO-66 Ce–Zr CB at −0.211 V *vs.* NHE is enough to break down molecular oxygen and create superoxide radicals. At the same time, the VB, which is at +2.99 V *vs.* NHE, allows water oxidation to produce hydroxyl radicals following the scavenger test.[31]

Photocatalytic activity

Considering this analysis, our first approach to perform photocatalytic experiments was to use Uio-66 Ce. This material has been previously reported as possessing excellent photocatalytic

© 2024 The Author(s). Published by the Royal Society of Chemistry

Open Access Article. Published on 04 November 2024. Downloaded on 6/30/2025 11:47:13 PM.
This article is licensed under a Creative Commons Attribution-NonCommercial 3.0 Unported Licence.

properties because of the abundant Ce^{4+} ions, which can change oxidation states from Ce^{4+} to Ce^{3+}.[21] The material was effectively synthesised and employed for BPA degradation in the presence of UV light over 4 hours. The degradation kinetics were monitored hourly, commencing with a half-hour stage of adsorption in the absence of light, followed by hourly measurements until the completion of the four hours. The results were remarkable, with a degradation efficiency of 94%, which is notable considering the quick and straightforward synthesis of the material. Nevertheless, PXRD confirmed that the material structure lacks crystallinity (Fig. S12†), making its reuse unfeasible. These findings indicate that, although the Ce^{4+} MOF has potential in photocatalysis, the lack of stability is an important consideration to be addressed for its potential use for the degradation of contaminants.[32]

MOF UiO-66 Zr stands out due to the presence of Zr^{4+} species, which gives it greater resilience. This robustness helps to overcome the structural stability issues found in UiO-66 Ce. The UiO-66 framework possesses a characteristic connection of zirconium clusters. Each Zr_6 cluster is linked to 12 BDC linkers, forming a three-dimensional cubic network that provides the material with remarkable thermal and chemical stability and well-defined porosity.[33] This MOF was successfully synthesised and then subjected to the same conditions for BPA degradation (Fig. 1a and b), achieving a remarkable degradation efficiency of 74%. While the percentage is smaller than the cerium MOF, PXRD structural testing (Fig. S13†) demonstrated that the material maintains its crystalline structure without any alterations, making it easier to reuse.[34]

Inspired by this robustness of the UiO-66 Zr material, a bimetallic MOF UiO-66 Ce–Zr was synthesised to merge the catalytic benefits of cerium MOF with the structural durability of zirconium MOF. This strategy aims to exploit the outstanding photocatalytic properties of Ce^{4+} in combination with the durability of Zr^{4+}, resulting in a material that is not only highly effective in breaking down pollutants like BPA but also maintains its crystalline structure (Fig. 1c), enabling its reuse in long-term applications. The material also maintained the rod-like morphology after the degradation process (Fig. S11†). The N_2 adsorption–desorption isotherm (Fig. S15†) indicates preserving the BET surface area (286.19 $m^2\ g^{-1}$). Moreover, studies conducted by Y. Wang *et al.*[35] highlight the potential of bimetallic MOFs, particularly when incorporating Zr, as this imparts superior stability and efficiency to the material in degradation processes. By synthesising and evaluating the bimetallic MOF UiO-66 Ce–Zr, we discovered that it achieved an efficiency of 84.3% in the photodegradation of BPA, which outperformed different materials (Table S3†). This efficiency surpassed that of Zr MOF (74%) but fell short of the efficiency of MOF Ce (94%).

This performance demonstrates the ideal equilibrium between the stability of Zr and the catalytic reactivity of Ce. Additionally, a study was conducted to examine the reusability of MOF UiO-66 Ce–Zr, which demonstrated its chemical stability and exceptional effectiveness in removing BPA. The recovered catalyst was subjected to three more reaction cycles to evaluate its potential for reuse (Fig. 1d). The results

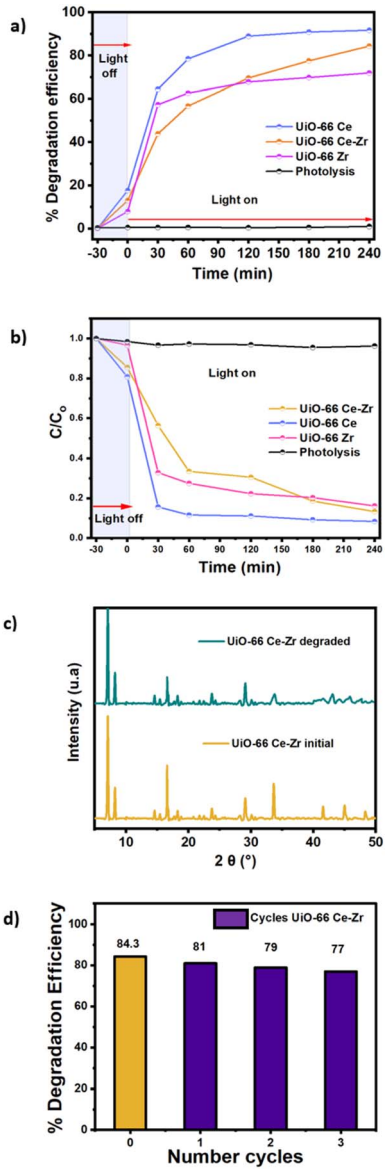


Fig. 1 (a and b) Photodegradation efficiency of the MOFs UiO-66 in kinetic studies without and with a lamp. (c) PXRD patterns of the initial MOF UiO-66 Ce–Zr and degraded MOF UiO-66 Ce–Zr. (d) Recyclability of the MOF UiO-66 Ce–Zr for three cycles.

demonstrated that MOF UiO-66 Ce–Zr exhibited BPA conversion rates of 82%, 79%, and 77% for the first, second, and third cycles, respectively. This suggests a gradual decline in the catalytic efficiency of the MOF with each successive cycle. The minor drop in efficiency may be attributed to alterations in the crystallinity of the material (Fig. S14†).

Pseudo-first-order and pseudo-second-order kinetics models were used to describe the degradation of BPA using UiO-66 Ce–Zr. The material shows a superior overall fit, particularly in the pseudo-second-order model (Fig. S10†), with an R^2 value of 0.96 (Table S2†). This implies that the degradation process of BPA pollutants followed the pseudo-second-order kinetics model, suggesting that the degradation of BPA is driven by rapid adsorption.[36] This is in line with the high degradation efficiency achieved at 240 min. The presence of both Ce and Zr in the MOF

© 2024 The Author(s). Published by the Royal Society of Chemistry

Open Access Article. Published on 04 November 2024. Downloaded on 6/30/2025 11:47:13 PM.
This article is licensed under a Creative Commons Attribution-NonCommercial 3.0 Unported Licence.

enhances its stability and degradation efficiency. The degradation process involves the initial adsorption of BPA, followed by interaction with radicals formed on the catalyst's surface. Thus, UiO-66 Ce–Zr exhibits great potential for use in pollutant treatment.

Scavenger test

Scavenging tests were performed to identify the reactive oxygen species (ROS) responsible for the photocatalytic degradation activities, such as superoxide ($^{\bullet}O_2^-$) radicals, positively charged holes (h^+), hydroxyl radicals ($^{\bullet}OH$) and (e^-). The $^{\bullet}O_2^-$, h^+, $^{\bullet}OH$, and e^- scavengers used for the study were *p*-benzoquinone (PBQ), citric acid (CA), salicylic acid (SA), and dimethyl sulfoxide (DMSO), respectively. Fig. 2 illustrates the effect of chemical scavengers on the photocatalytic activity of MOF UiO-66 Ce–Zr.

The photodegradation efficiency of BPA was inhibited when SA was added, suggesting that $^{\bullet}OH$ played an essential role in the photodegradation of BPA. With the addition of PBQ, the photodegradation rate of BPA also decreased, suggesting that $^{\bullet}O_2^-$ also plays a crucial role in photocatalytic degradation. CA causes a minor effect in decreasing photoactivity, and h^+ has a lower participation. However, no significant decrease is seen in the photocatalytic degradation rate of BPA in the presence of DMSO, suggesting that the contribution of e^- is minimal. Thus, it can be inferred that the $^{\bullet}OH$, $^{\bullet}O_2^-$ and h^+ radicals took part in the photodegradation of BPA with MOF UiO-66 Ce–Zr under UV light irradiation, with significant contributions from $^{\bullet}OH$ and $^{\bullet}O_2^-$ as supported by other studies,[37,38] rather than h^+.

XPS characterisation was performed to confirm the stability of UiO-66 Ce–Zr MOF. The survey analysis (Fig. S16†) shows no significant changes after BPA photodegradation. The high-resolution XPS spectra of C 1 s (Fig. 3a) exhibit peaks at 284.7, 286.1, 288.4, and 289.9 eV related to C=C in the aromatic rings, C–OH, –C=O and π–π*. After the photoreaction, the peaks shift to 284.6, 285.6, 288.6, and 289.6 eV, respectively. The most evident change (0.5 eV) in the binding energy to lower energies was for the peak associated with C–OH. For the O 1 s region (Fig. 3b), the displayed peaks at 530.1, 531.5, and 533.3 eV are related to M-O, C–H/C=O, and C=O, respectively. After BPA photodegradation, only the peaks of C–H/C=O and C=O shifted to lower energies by 0.2 eV and 0.6 eV, respectively, which is associated with increased electron density due to organic subproducts. The high-resolution XPS spectra of Zr 3d (Fig. 3c) show two peaks at around 182.6 and 184.9 eV ($\Delta = 2.3$ eV), which can be assigned to Zr $3d_{5/2}$ and Zr $3d_{3/2}$, respectively.[39] After the photoreaction, a slight shift of 0.1 eV to higher binding energies was observed.

The high-resolution XPS spectra of Ce 3d (Fig. 3d) display a significant spin–orbit separation between the $3d_{5/2}$ and $3d_{3/2}$ emission features ($\Delta = 18.6$ eV). The presence of Ce^{3+} can be identified by two peaks associated with each spin-orbital (v^0/v^1 and u^0/u^1). These two characteristic peaks present binding energies of 883.9 eV and 902.5 eV. The "v" peaks are associated with the $3d_{5/2}$ spin–orbit peaks and the "u" peaks with the $3d_{3/2}$ peaks. The peak shift in the Ce spectra was 0.3 eV to lower binding energies.[40] These shifts in the binding energies for Zr and Ce 3d to lower values can be related to a change in the chemical environment of the metal centres in UiO-66.

Computational analysis methodology

Based on these results, density functional theory (DFT) and docking simulations were used to examine the interaction between BPA and the octahedral and tetrahedral pores of the

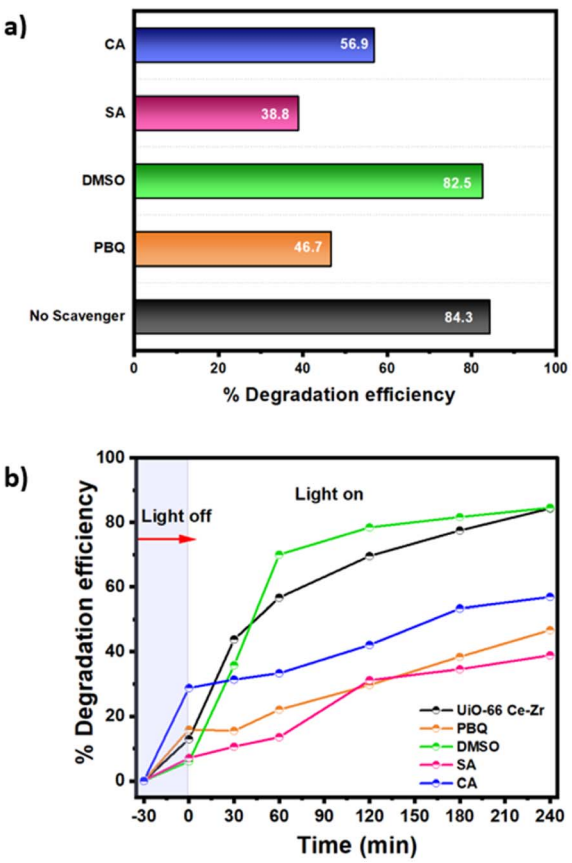


Fig. 2 (a) Scavenger test of the MOF UiO-66 Ce–Zr. (b) Photodegradation efficiency of the MOFs UiO-66 Ce–Zr in kinetic studies without and with a lamp using the scavenger test.

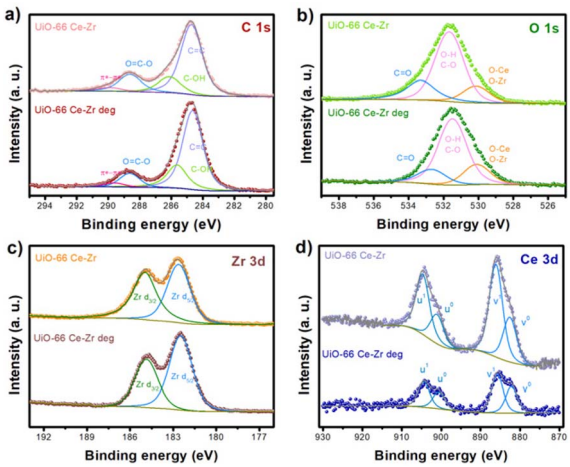


Fig. 3 High-resolution XPS spectra before and after BPA photodegradation of (a) C 1 s, (b) O 1 s, (c) Zr 3d, and (d) Ce 3d.

© 2024 The Author(s). Published by the Royal Society of Chemistry

Open Access Article. Published on 04 November 2024. Downloaded on 6/30/2025 11:47:13 PM.
This article is licensed under a Creative Commons Attribution-NonCommercial 3.0 Unported Licence.

UiO-66 framework. The calculated aggregate volumes and surface areas of the UiO-66 pores and the amount of BPA provide a valuable understanding of the observed variations in binding behaviour. More precisely, the octahedral volume of 3428.016 Å^3 and the surface area of 69.34754 Å^2 provided a better spatial fit for BPA, which in turn had a volume of 324.6 Å^3 (Table S9†). The significant volume-to-surface-area ratio of this material promotes efficient interactions, which is shown by the negative binding energy and emphasises its compatibility with BPA. Also, docking investigations were carried out (Fig. S17†) to achieve an accurate geometric recognition between BPA and the octahedral pores of the framework, yielding favourable interaction energy. Conversely, the tetrahedral conformation shows a less satisfactory alignment within the pore, consistent with the positive binding energy obtained from the DFT calculations (Table S10†).

In an effort to understand the photocatalytic by-products generated during the degradation of BPA, an analysis of the degraded samples was conducted using UPLC-MS (Ultra-performance liquid chromatography-mass spectrometry). The reaction pathway for the photocatalytic degradation of bisphenol A with UiO-66 Ce–Zr illuminated with UV light is illustrated in Fig. S18.† The most abundant by-products were successfully identified, such as (2*Z*)-but-2-enedioic acid; 5-[2-(4-hydroxyphenyl) propan-2-yl] benzene-1,2,3-triol; and phenol (see Table S13† for the complete by-products after degradation). Furthermore, a toxicology *in silico* study of the degradation products was carried out, with but-2-enedioic acid and 5-[2-(4-hydroxyphenyl) propan-2-yl] benzene-1,2,3-triol being less harmful than BPA. Conversely, phenol has a high degree of intestinal permeability, has increased toxicity (LD_{50}: 270 mg kg^{-1}), and poses the risks of neurotoxicity and ecotoxicity (see ESI† for details). These results highlight the importance of analysing the products formed after the degradation of BPA, as we can produce by-products that could be not only less toxic but also more lethal, such as phenol, than the original compound.

Conclusions

In summary, this study highlights the effective degradation of BPA from water solution. Incorporating a bimetallic MOF material UiO-66 Ce–Zr boosted the chemical stability of the degradation processes, displaying a remarkable degradation efficiency of 84.3% under UV irradiation for 240 minutes. The strength and efficacy of the MOF Ce–Zr UiO-66 catalyst have been successfully demonstrated, as it retains its catalytic activity over three cycles. The degradation by-products analysis was conducted using UPLC-MS, and a toxicological evaluation confirmed the potential of the material for safe and efficient water treatment. This makes it a promising alternative for degradation contaminants like BPA in aqueous environments, highlighting its potential for water treatment applications.

Data availability

The data supporting this article have been included as part of the ESI.†

Conflicts of interest

There are no conflicts to declare.

Acknowledgements

L. M. G. and J. L. O. thank CONACYT for PhD fellowships (1272650 and 1003953). C. E. G. A. thanks CONACYT for the Master fellowship (1331235). R. A. P., C. E. G. A. and L. D. H. Z. thank the Laboratorio de Supercómputo y Visualización en Paralelo (Yoltla) for providing the computational resources to prepare this work. C. L. thanks the IPN projects (20242829, 20241189, 20231282 and 20232785).

References

1 M. J. Currell and D. Han, *Environment: Science and Policy for Sustainable Development*, 2017, **59**, 16–29.
2 V. Geissen, H. Mol, E. Klumpp, G. Umlauf, M. Nadal, M. Van Der Ploeg, S. E. A. T. M. Van De Zee and C. J. Ritsema, *Int. Soil Water Conserv. Res.*, 2015, **3**, 57–65.
3 H. Gao, B.-J. Yang, N. Li, L.-M. Feng, X.-Y. Shi, W.-H. Zhao and S.-J. Liu, *Medicine*, 2015, **94**, e211.
4 S. Zhang, J. Wang, Y. Zhang, J. Ma, L. Huang, S. Yu, L. Chen, G. Song, M. Qiu and X. Wang, *Environ. Pollut.*, 2021, **291**, 118076.
5 S. Garcia-Segura and E. Brillas, *J. Photochem. Photobiol., C*, 2017, **31**, 1–35.
6 C. Belver, J. Bedia, A. Gómez-Avilés, M. Peñas-Garzón and J. J. Rodriguez, in *Nanoscale Materials in Water Purification*, Elsevier, 2019, pp. 581–651.
7 N. Munir, A. Javaid, Z. Abideen, B. Duarte, H. Jarar, A. El-Keblawy and M. S. Sheteiwy, *Environ. Sci. Pollut. Res.*, 2023, **31**, 1695–1718.
8 O. O. Oluwasina and A. A. Adelodun, *Nanotechnol. Environ. Eng.*, 2024, **9**, 389–409.
9 C. Pettinari and A. Tombesi, *Inorganics*, 2023, **11**, 65.
10 M.-A. Gatou, I.-A. Vagena, N. Lagopati, N. Pippa, M. Gazouli and E. A. Pavlatou, *Nanomaterials*, 2023, **13**, 2224.
11 J. L. Obeso, V. B. López Cervantes, C. V. Flores, C. García-Carvajal, C. E. Garduño-Albino, R. A. Peralta, V. M. Trejos, L. Huerta Arcos, I. A. Ibarra, D. Solis-Ibarra, S. Cordero-Sánchez, N. S. Portillo-Vélez and J. M. Esparza-Schulz, *Dalton Trans.*, 2024, **53**, 12208–12214.
12 A. López-Olvera, J. A. Zárate, J. L. Obeso, E. Sánchez-González, J. A. De Los Reyes, R. A. Peralta, E. González-Zamora and I. A. Ibarra, *Inorg. Chem.*, 2023, **62**, 20901–20905.
13 Y. Liu, Y. Liu, L. Gu, J. Han, W. Zhi, Y. Wang and L. Wang, *Colloids Surf., B*, 2021, **208**, 112099.
14 Z. Guan, S. Zhu, S. Ding, D. Xia and D. Li, *Chemosphere*, 2022, **299**, 134481.
15 J.-T. Lu, H. Huang, H. Wu, S.-P. Wen, K.-Y. Gao, X.-L. Wu and Z.-R. Nie, *Rare Met.*, 2023, **42**, 672–679.
16 D. Yong, J. Tian, R. Yang, Q. Wu and X. Zhang, *Chin. J. Chem.*, 2024, **44**, 1343.
17 S. Sangeetha and G. Krishnamurthy, *Bull. Mater. Sci.*, 2020, **43**, 269.

© 2024 The Author(s). Published by the Royal Society of Chemistry

Open Access Article. Published on 04 November 2024. Downloaded on 6/30/2025 11:47:13 PM.
This article is licensed under a Creative Commons Attribution-NonCommercial 3.0 Unported Licence.

18 Z. Li, D. Jia, W. Zhang, Y. Li, M. Wang and D. Zhang, *Front. Chem. Sci. Eng.*, 2024, **18**, 31.
19 P. Wang, X. Bian and Y. Li, *Chin. Sci. Bull.*, 2012, **57**, 33–40.
20 J.-X. Cui, Q. Luo, Z.-G. Zhang, J.-T. Zhu and B.-L. Shen, *Rare Met.*, 2023, **42**, 3430–3442.
21 M. Lammert, M. T. Wharmby, S. Smolders, B. Bueken, A. Lieb, K. A. Lomachenko, D. D. Vos and N. Stock, *Chem. Commun.*, 2015, **51**, 12578–12581.
22 A. Sharma, S. Bedi, K. Verma, B. Lal, V. John, R. Kumar, S. Kaushal and R. Badru, *Polyhedron*, 2023, **242**, 116517.
23 I. Rangel-Vázquez, G. Del Angel, E. Ramos-Ramírez, P. Acevedo-Peña, C. Martínez Gómez, F. Tzompantzi, N. Gutiérrez Ortega and J. G. Torres-Torres, *RSC Adv.*, 2023, **13**, 19832–19845.
24 E. Peralta, G. Roa, J. A. Hernandez-Servin, R. Romero, P. Balderas and R. Natividad, *Electrochim. Acta*, 2014, **129**, 137–141.
25 J. Li, Y. Fan, R. Zhang, D. Ban, Z. Duan, X. Liu and L. Liu, *Mater. Chem. Front.*, 2024, **8**, 3509–3527.
26 F. Keshavarz, V. Kavun, M. A. Van Der Veen, E. Repo and B. Barbiellini, *Chem. Eng. J.*, 2022, **440**, 135905.
27 E. F. Pettersen, T. D. Goddard, C. C. Huang, G. S. Couch, D. M. Greenblatt, E. C. Meng and T. E. Ferrin, *J. Comput. Chem.*, 2004, **25**, 1605–1612.
28 J. B. Maglic and R. Lavendomme, *J. Appl. Crystallogr.*, 2022, **55**, 1033–1044.
29 K. Chakarova, I. Strauss, M. Mihaylov, N. Drenchev and K. Hadjiivanov, *Microporous Mesoporous Mater.*, 2019, **281**, 110–122.
30 S. Bargozideh, M. Tasviri, S. Shekarabi and H. Daneshgar, *New J. Chem.*, 2020, **44**, 13083–13092.
31 Y. L. Wang, S. Zhang, Y. F. Zhao, J. Bedia, J. J. Rodriguez and C. Belver, *J. Environ. Chem. Eng.*, 2021, **9**, 106087.
32 A. Loosen, C. Simms, S. Smolders, D. E. De Vos and T. N. Parac-Vogt, *ACS Appl. Nano Mater.*, 2021, **4**, 5748–5757.
33 C. S. Cox, E. Slavich, L. K. Macreadie, L. K. McKemmish and M. Lessio, *Chem. Mater.*, 2023, **35**, 3057–3072.
34 K. Nikoofar and Z. Khademi, *Res. Chem. Intermed.*, 2016, **42**, 3929–3977.
35 Y. Wang, N. Zhang, R. Wang, Y. He, H. Zhou, X. Li, G. Gao, H. Sun and X. Liu, *Dalton Trans.*, 2023, **52**, 10079–10088.
36 B. Guo, T. Xu, L. Zhang and S. Li, *J. Environ. Manage.*, 2020, **272**, 111047.
37 H. Chen, C. Liu, W. Guo, Z. Wang, Y. Shi, Y. Yu and L. Wu, *Catal. Sci. Technol.*, 2022, **12**, 1812–1823.
38 K. Zhou, Y. Zhang, M. Liu, Z. Zhao, X. Liu, Z. Bao, Q. Yang, Q. Ren and Z. Zhang, *Catal. Sci. Technol.*, 2024, **14**, 1605–1612.
39 D. Chen, H. Sun, Y. Wang, H. Quan, Z. Ruan, Z. Ren and X. Luo, *Appl. Surf. Sci.*, 2020, **507**, 145054.
40 E. E. Ghadim, M. Walker and R. I. Walton, *Dalton Trans.*, 2023, **52**, 11143–11157.

© 2024 The Author(s). Published by the Royal Society of Chemistry

ORGANIC CHEMISTRY FRONTIERS

RESEARCH ARTICLE

View Article Online
View Journal | View Issue

Check for updates

Cite this: *Org. Chem. Front.*, 2025, **12**, 2607

Dual-state emission of pyrazolyl-pyrrolo[3,4-*b*]pyridin-5-ones *via* excited-state intramolecular proton transfer (ESIPT): multicomponent synthesis and optical characterization†

Julio C. Flores-Reyes,‡[a] Yoarhy A. Amador-Sánchez, ‡[a] Alejandro Valderrama-Celestino,[a] Bertha D. Barrios-Campos,[a] Ricardo A. Peralta, [a] Michael T. Huxley,[b] Ilich A. Ibarra, [c] Alejandro Islas-Jácome, [a] Diego Solis-Ibarra *[c] and Eduardo González-Zamora *[a]

Received 2nd December 2024,
Accepted 17th February 2025

DOI: 10.1039/d4qo02256d

rsc.li/frontiers-organic

The dual-state emission (DSE) phenomenon has become crucial for developing dual-state emission luminogens (DSEgens) that exhibit efficient luminescence in both solution and solid states, addressing the limitations of conventional, phase-restricted fluorophores. Compounds exhibiting excited-state intramolecular proton transfer (ESIPT) mechanisms are especially valuable for enhancing emission stability across these states, offering significant potential in optoelectronics, bioimaging, and sensing applications. In this study, we report the synthesis of six new pyrazolyl-pyrrolo[3,4-*b*]pyridin-5-ones through an Ugi-Zhu-3CR coupled to an aza-Diels–Alder/*N*-acylation/decarboxylation/dehydration cascade sequence. An X-ray ORTEP confirms unequivocally the structure of one of the synthesized compounds. These ones demonstrate intriguing photophysical properties such as large Stokes shifts (>11 900 cm^{-1}) in solution and robust solid-state emission *via* ESIPT mechanism. Complementary DFT and TD-DFT calculations confirm weak but allowed transitions involving both pyrazole and pyrrolo[3,4-*b*]pyridin-5-one moieties, in agreement with experimental observations. This work represents the first application of an isocyanide-based multicomponent reaction for DSEgen synthesis, paving the way for innovative advances in the design of organic luminescent materials.

Open Access Article. Published on 17 February 2025. Downloaded on 6/30/2025 11:47:36 PM.
This article is licensed under a Creative Commons Attribution-NonCommercial 3.0 Unported Licence.

Introduction

The DSE phenomenon has garnered significant attention within the scientific community due to its potential to enable DSEgens that emit effectively in both solution and solid states.[1] Such materials bridge a critical gap left by traditional fluorophores, which are often restricted to single-phase emission. Achieving efficient DSE requires strategic incorporation of functional groups to sustain emission across varying states. Notably, the integration of triphenylamine (TPA)[2] and tetraphenylethylene (TPE)[3] units has proven effective for their strong emission properties and ability to minimize aggregation-caused quenching (ACQ)[4] by reducing detrimental π–π stacking-type interactions in conjugated aromatic systems.[5] Further, modifications with long-chain C–C organic species create "isolated" solid-state environments, enhancing emission with improved quantum yields. Incorporating aliphatic chains also enhances compound solubility, facilitating solution-processability for device applications and supporting robust DSE behavior.[6] Compounds with ESIPT capabilities are also under active investigation, as this mechanism improves emission stability and intensity in both solution and solid phases. These advancements in DSE design show substantial promise for optoelectronics, bioimaging, and sensing technologies, where stable and versatile emission characteristics are essential.[7]

Alongside, pyrazole-based heteroaromatic compounds have gained significant interest due to their presence in various biologically and industrially important molecules, including

[a]*Departamento de Química, Universidad Autónoma Metropolitana-Iztapalapa, Av. Ferrocarril San Rafael Atlixco 186, Col. Leyes de Reforma 1A Sección, Iztapalapa, 09310 Ciudad de México, Mexico. E-mail: egz@xanum.uam.mx*
[b]*School of Physics, Chemistry and Earth Sciences, Faculty of Sciences, Engineering and Technology, The University of Adelaide, Adelaide, SA, 5005, Australia*
[c]*Laboratorio de Fisicoquímica y Reactividad de Superficies, (LaFReS), Instituto de Investigaciones en Materiales, Universidad Nacional Autónoma de México, Circuito Exterior S/N, CU, Coyoacán, Ciudad de México, Mexico.*
E-mail: diego.solis@unam.mx

†Electronic supplementary information (ESI) available. CCDC 2402623. For ESI and crystallographic data in CIF or other electronic format see DOI: https://doi.org/10.1039/d4qo02256d

‡These authors contributed equally to this work.

Open Access Article. Published on 17 February 2025. Downloaded on 6/30/2025 11:47:36 PM.
This article is licensed under a Creative Commons Attribution-NonCommercial 3.0 Unported Licence.

natural products,[8] antimicrobial agents,[9] and emissive chromophores.[10] These aromatic systems serve as essential building blocks for the rapid development of optoelectronic devices, such as organic light-emitting diodes (OLEDs).[11] To this end, synthetic strategies that provide high yields and excellent atom economy are highly desirable, enabling the efficient generation of diverse molecular architectures. Among these approaches, multicomponent reactions (MCRs) stand out for their ability to produce key emissive motifs with valuable biological[12] and optical properties[13] while circumventing the limitations of multi-step procedures, such as low yields and labor-intensive purification steps.[14] Moreover, pyrazole-based compounds are particularly appealing for designing luminescent materials due to their neighboring nitrogen atoms, which can act as hydrogen bond acceptors, facilitating highly desirable emissive phenomena like the ESIPT effect.[15] This process begins with the photoexcitation of the material, resulting in the formation of two tautomers (enol and keto forms) with distinct electronic structures. In the ground state these molecules adopt an enol (E) configuration since they are stabilized by an intramolecular hydrogen bond. Upon light absorption, the enol tautomer enters an excited state (E*), during which the electronic charge is redistributed resulting in an increased acidity of the H-donor and an increased basicity of the H-acceptor, causing a proton transfer to occur, generating a new excited keto tautomer (K*). As the system relaxes to its ground state, a recombination mechanism takes place, resulting in light emission (K) distinct than from absorbed in the first step of the ESIPT process. The K form tautomerizes back to the E form by a reverse proton transfer, completing a four-level photochemical cycle (Fig. 1).

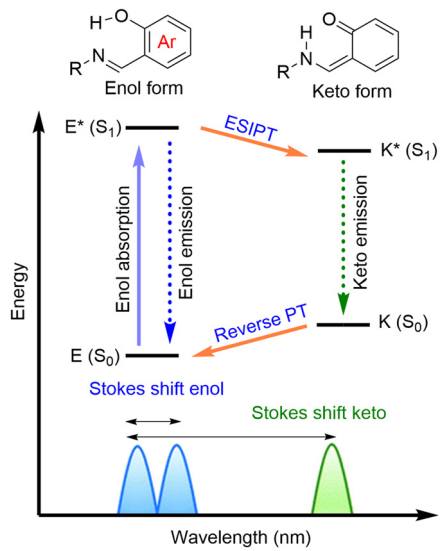


Fig. 1 Representation of the ESIPT mechanism in emissive compounds.

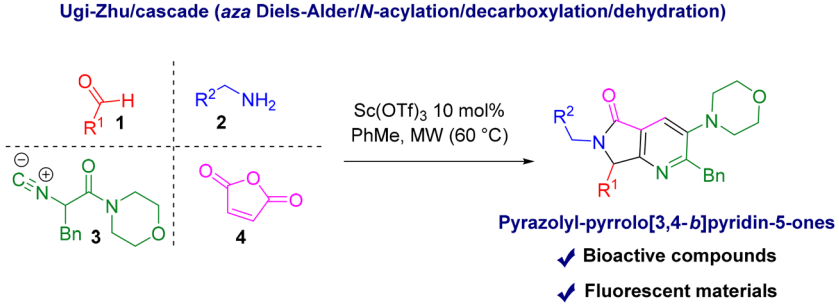
Our research group has previously developed novel methodologies based on the Ugi-Zhu reaction (UZ-3CR), utilizing various amines, aldehydes, and key α-isocyanoacetamides to assemble 5-aminooxazoles.[16] These latter are subsequently subjected to a cascade sequence (intermolecular aza Diels–Alder cycloaddition/*N*-acylation/decarboxylation/dehydration) with maleic anhydride, yielding a series of pyrrolo[3,4-*b*]pyridin-5-ones with promising biological[17] and optical[18] properties (Scheme 1).

As part of our ongoing efforts to synthesize novel and complex polyheterocyclic compounds, we have developed several methodologies that utilize the Ugi-Zhu three-component reaction as a key synthetic tool. This strategy has proven effective for preparing various pyrrolo[3,4-*b*]pyridin-5-one series, either fused, bound, or linked to heterocyclic frameworks of interest for their optical and medicinal properties. In this study, we successfully synthesized a series of pyrazole-derived pyrrolo[3,4-*b*]pyridin-5-one dual-state emitters through an Ugi-Zhu/cascade (aza Diels–Alder/*N*-acylation/decarboxylation/dehydration) sequence with emission in both solution and solid states. To the best of our knowledge, this is the first report in which an isocyanide-based multicomponent reaction has been employed for the creation of DSEgens. Additionally, optical characterization revealed intriguing fluorescence properties, underscoring the potential applications of these compounds in the field of photonics and as bioactive agents.

Results and discussion

Organic synthesis

To access the target pyrazolyl-pyrrolo[3,4-*b*]pyridin-5-one scaffold, we synthesized the corresponding *O*-protected pyra-



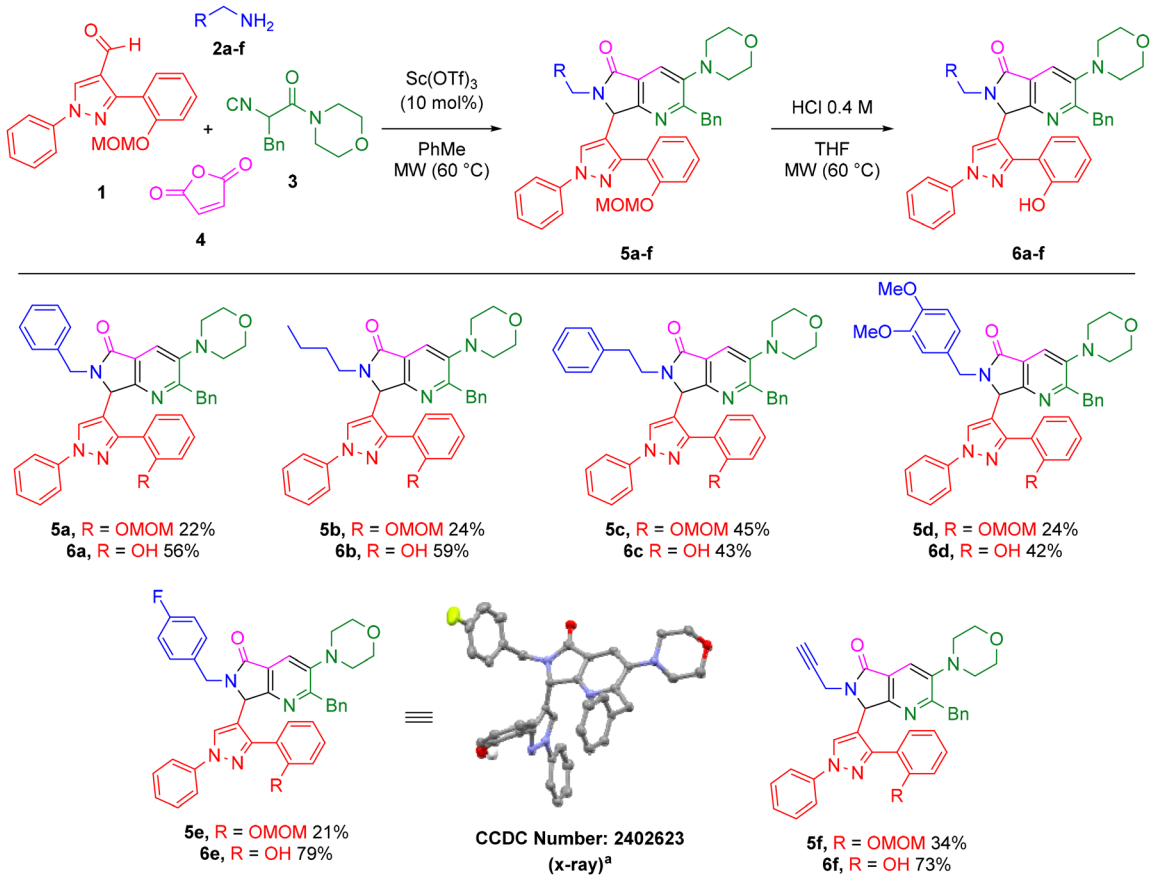
Scheme 1 Ugi-Zhu/aza Diels–Alder sequence for the multicomponent assembly of pyrrolo[3,4-*b*]pyridin-5-ones.

 This journal is © the Partner Organisations 2025

Open Access Article. Published on 17 February 2025. Downloaded on 6/30/2025 11:47:36 PM.
This article is licensed under a Creative Commons Attribution-NonCommercial 3.0 Unported Licence.

zole-derived aldehyde, which is crucial for the Ugi-Zhu reaction. First, a condensation was performed between phenylhydrazine and 2′-hydroxyacetophenone, followed by the incorporation of the aldehyde moiety using the classic Vilsmeier–Haack protocol, yielding the desired pyrazole **1′** with an isolated yield of 38% in a two-step process. After this, the hydroxy group was protected by introducing the methoxymethyl (MOM) protecting group by reacting the aldehyde with methoxymethyl chloride in the presence of sodium hydride. The MOM-protected aldehyde **1** was obtained in 64% yield (see ESI S1 and S2†).[19] The protection of the hydroxyl group is essential to obtaining the desired compounds, as the reaction does not proceed when using the unprotected aldehyde. We attributed this to an increased resonance stabilization upon the loss of the acidic proton, rendering the aldehyde unreactive toward nucleophilic attack by the amine. With compound **1** in hand, the α-isocyanoacetamide **3** was synthesized following a slightly modified protocol established by Zhu and Bienaymé (see ESI S3†).[16] It is noteworthy that the previously obtained synthetic modules are pivotal for the expedited access to the desired pyrazolyl-pyrrolo[3,4-*b*]pyridin-5-one scaffolds using the Ugi-Zhu/cascade (aza Diels–Alder/*N*-acylation/decarboxylation/dehydration) sequence. As shown in Scheme 2, the multicomponent methodology proceeded efficiently by incorporating the corresponding *O*-protected pyrazole-carbaldehyde **1**, the α-isocyanoacetamide **3**, various aliphatic amines (**2a–f**), and maleic anhydride (**4**) in dry toluene. The reaction was catalyzed by 10 mol% of $Sc(OTf)_3$ under microwave heating (60 °C, 100 W) for 1.5 hours. After purification and isolation, the desired MOM-protected heterocycles **5a–f** were obtained in 22% to 45% yields. At this stage, the MOM deprotection was necessary to obtain the desired ESIPT scaffolds. The MOM deprotection protocol was conducted under mild conditions (0.4 M HCl in THF), yielding the expected **6a–f** products with yields ranging from 42% to 79% (see Scheme 2). Considering factors such as atom economy (up to 84.82%), structural complexity, and the number of steps composing the overall one-pot process, the isolated yields are deemed satisfactory. It is worth noting that all compounds were characterized by ^{1}H, ^{13}C, and ^{19}F NMR, as well as high-resolution mass spectrometry (HRMS). Fortunately, high-quality crystals of compound **6e** were successfully obtained for X-ray diffraction analysis, which unequivocally confirmed its polycyclic structure (see the ESI Table S1† for complete X-ray analysis).

The process begins with a condensation between aldehyde **1** and the primary amines **2a–f**, resulting in the formation of



Scheme 2 Pyrazolyl-pyrrolo[3,4-*b*]pyridin-5-ones and their respective deprotections synthetized by an Ugi-Zhu/cascade (aza Diels–Alder/*N*-acylation/decarboxylation/dehydration) sequence. (a) Thermal ellipsoids are drawn at 50% probability, with all hydrogen atoms omitted for clarity, except for the hydrogen atom of the pyrazole moiety (key for the ESIPT photochemical cycle).

Open Access Article. Published on 17 February 2025. Downloaded on 6/30/2025 11:47:36 PM. This article is licensed under a Creative Commons Attribution-NonCommercial 3.0 Unported Licence.

imines **7**, which are activated by Sc[III]. This activation promotes α-addition by the isocyanide **3**, leading to the formation of nitrilium ion intermediates **8**. These crucial intermediates are then intramolecularly captured by the amide oxygen through a 5-*endo*-dig cyclization, forming 5-aminooxazoles **10**.[16] The 5-aminooxazoles **10** react with maleic anhydride (**4**) in a cascade sequence of reactions, beginning with an intermolecular aza Diels–Alder cycloaddition producing the oxa-bridged intermediates **11**. These ones undergo an *N*-acylation followed by a decarboxylation, and a final dehydration process, ultimately yielding the target pyrazolyl-pyrrolo[3,4-*b*]pyridin-5-ones **5** (Scheme S5†).

Photophysical properties

To determine the optical properties of compounds **6a–f**, we first measured the absorption spectra of the deprotected pyrazole aldehyde **1** at a concentration of 10^{-5} M. The molar absorptivity coefficients were found to be 1256 M^{-1} cm^{-1} in chloroform ($CHCl_3$), 11 637 M^{-1} cm^{-1} in acetonitrile (MeCN), and 13 342 M^{-1} cm^{-1} in dimethyl sulfoxide (DMSO). Based on these results, we recorded the full absorption and emission spectra in these three solvents. The deprotected compound showed absorption maxima at 254 nm, 275 nm, and 288 nm in $CHCl_3$, MeCN, and DMSO, respectively, indicating a bathochromic shift with increasing solvent polarity. The emission maxima of deprotected **1**, corresponding to its keto form, were observed at 350 nm, 348 nm, and 354 nm, with Stokes shifts of 10 799 cm^{-1}, 7628 cm^{-1}, and 6474 cm^{-1} in $CHCl_3$, MeCN, and DMSO, respectively. Conversely, an additional emission maximum at 308 nm was observed, corresponding to enol emission in both MeCN and DMSO. Fig. 2 presents the normalized absorption and emission spectra in these solvents, while Table 1 summarizes the optical characterization data.

With these data, we proceeded to measure the normalized absorption and emission spectra of compounds **6a–f** in $CHCl_3$ at a concentration of 10^{-5} M (Fig. 3A and B) to compare their optical properties with those of the starting material **1**. A prominent absorption peak at 278 nm, corresponding to the pyrrolo[3,4-*b*]pyridin-5-one core, was observed, along with a secondary, weaker absorption band between 297 and 303 nm, likely due to the pyrazole moiety. The polarity of the solvents had a minor effect on the absorption band positions. In MeCN and DMSO, the bands appeared at nearly identical wavelengths, while $CHCl_3$ exhibited a slight bathochromic shift of 2 to 6 nm relative to MeCN and 4 to 5 nm compared to DMSO (Table 2). The emission spectra of compounds **6a–f** in $CHCl_3$ are shown in Fig. 3B.

Table 1 Summary of photophysical properties of the pyrazole aldehyde **1**

Solvent	Absorption λ_{max} [nm] (ε) [M^{-1} cm^{-1}]	Emission λ_{max} [nm]	Stokes shifts $\Delta\tilde{\nu}$ [cm^{-1}]
$CHCl_3$	254 (12 568)	350	10 799
MeCN	275 (11 637)	348	7628
DMSO	288 (13 342)	354	6313

As shown in Table 2, excitation of compounds **6a–f** at 265 nm revealed that **6b** and **6c** exhibited the highest fluorescence intensity with emission maxima at 422 nm, while compound **6a** displayed the lowest intensity at 419 nm. Notably, compound **6f** demonstrated a bathochromic shift of approximately 11 nm. In general, these compounds exhibited bathochromic shifts with increasing solvent polarity. Compared to their emission in $CHCl_3$, the respective emissions of compounds **6a–f** in MeCN and DMSO occurred at significantly longer wavelengths, suggesting a higher dipole moment in the excited state.[20] When a fluorophore is in the excited state, solvent molecules can relax around the excited dipole by reorienting themselves *via* electrostatic solute-solvent interactions. Higher solvent polarity and an increased excited state dipole moment of the fluorophore will enhance these interactions. This stabilizes and lowers the energy of the excited fluorophore, resulting in a red-shifted emission spectrum. Various excitation wavelengths were tested to acquire these spectra; however, the emission profiles consistently revealed a single emission band, indicating the predominance of one tautomer across the compounds. It is important to note that the Stokes shifts for compounds **6a–f** exceeded

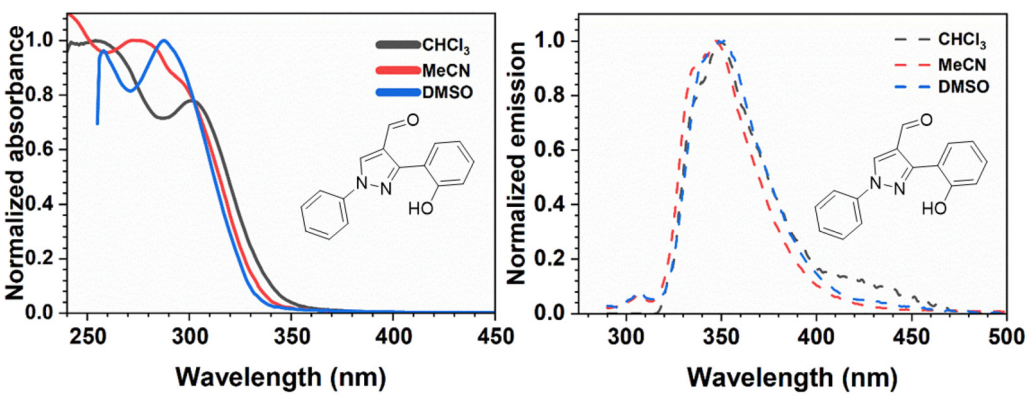


Fig. 2 Absorption (left) and emission (right) spectra of the pyrazole aldehyde **1**, measured at 254 nm, 275 nm, and 288 nm in $CHCl_3$, MeCN, and DMSO, respectively.

 This journal is © the Partner Organisations 2025

Open Access Article. Published on 17 February 2025. Downloaded on 6/30/2025 11:47:36 PM.
This article is licensed under a Creative Commons Attribution-NonCommercial 3.0 Unported Licence.

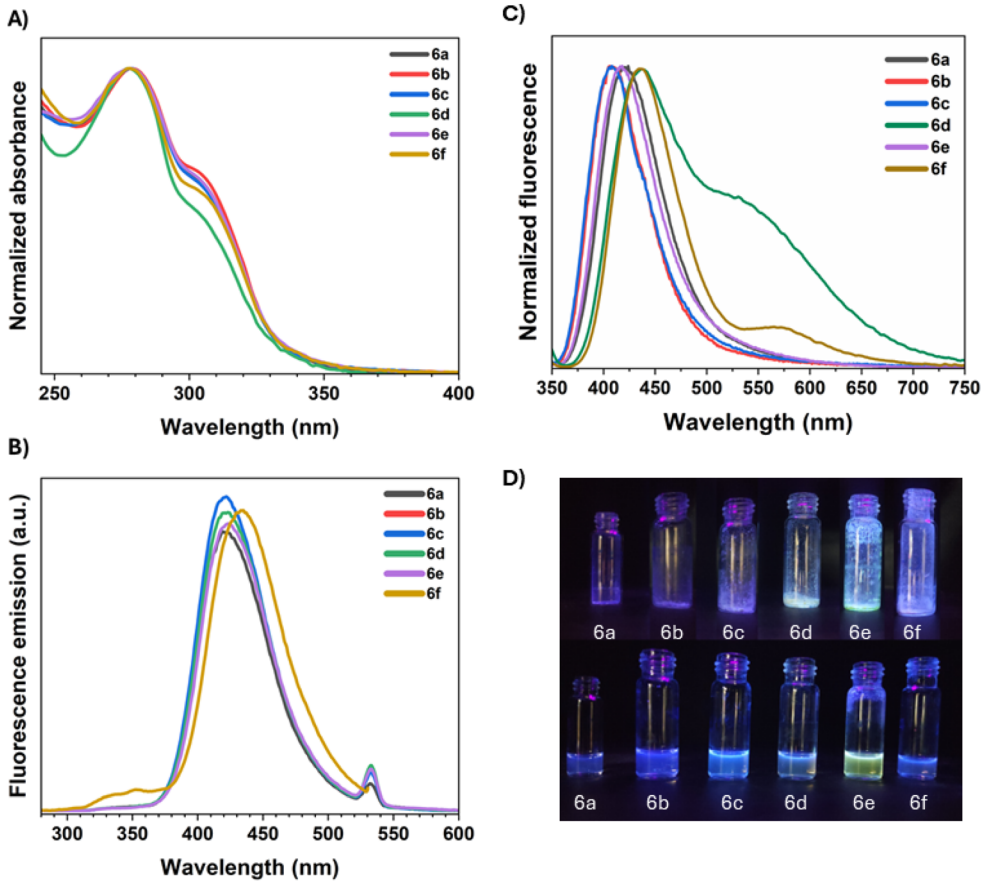


Fig. 3 (A) Absorption, (B) emission espectra of pyrrolo[3,4-*b*]pyridin-5-ones **6a–f** at 10^{-5} M in $CHCl_3$, (C) solid-state emission of compounds **6a–f** λ_{ex} = 343 nm, (D) naked-eye-visible emission of compounds **6a–f** under UV illumination λ_{ex} = 365 nm, observed in the solid-state (top) and in solution (bottom).

11 900 cm^{-1} in all three solvents, particularly in MeCN and DMSO. This observation suggests the potential for an ESIPT, as compounds exhibiting ESIPT typically show large Stokes shifts due to structural differences between the emissive enol and keto forms.[21] However, the presence of a single emission band for both the aldehyde and the products, combined with the large Stokes shifts observed in polar solvents, makes ESIPT unlikely in solution. Proton transfer is expected to be inhibited in such environments, particularly in DMSO. Instead, the observed Stokes shifts are more likely related to the integration of the fluorophore within the pyrrolo[3,4-*b*]pyridin-5-one framework, a phenomenon previously reported in similar systems.[18]

Additionally, the photoluminescence quantum yields (PLQYs) of compounds **6a–f** in chloroform were measured as 1.5%, 2.4%, 2.4%, 1.5%, 1.4%, and 1.6%, respectively. It is noteworthy that all PLQYs were relatively low (<2.5%), indicating a strong preference for non-radiative relaxation pathways (Table 2).[22] In the solid state, however, ESIPT can be modulated by molecular aggregation and restricted vibrational motion, potentially enhancing emission by minimizing non-radiative losses.[23] This phenomenon is exemplified by aggregation-induced emission (AIE) materials, which are typically weakly emissive or non-emissive in solution but become strongly emissive in the solid state due to restricted molecular motion.[5]

For compounds **6b**, **6c**, and **6e**, solid-state emissions were observed at λ_{em} = 407, 407, and 417 nm, respectively, showing blue shifts of 15 nm for **6b** and **6c** and 7 nm for **6e** compared to their emissions in $CHCl_3$ solution. Compound **6a**, however, exhibited nearly identical fluorescence emission maxima in both solution and solid states. Notably, compounds **6d** and **6f** showed a prominent solid-state ESIPT effect, with dual emission bands at 437 and 532 nm for **6d**, and at 435 and 572 nm for **6f**, corresponding to the enol and keto tautomers, respectively, when excited at λ_{ex} = 343 nm and 374 nm. Additionally, solid-state excitation at λ_{ex} = 500 nm enhanced the longer-wavelength maxima, 532 nm for **6d** and 572 nm for **6f** (Fig. 4), supporting the presence of ESIPT and its role in solid-state emission.

In the solid state, compounds **6a–f** exhibited PLQYs of 21.5%, 14.2%, 13.2%, 7.1%, 17.9%, and 11.1%, respectively, demonstrating a substantial enhancement of fluorescence compared to $CHCl_3$ solutions, with increases ranging from 5-fold for **6d** to 14-fold for **6a**. The fluorescence enhancement observed in the solid state among **6a–f** can be attributed to the

Open Access Article. Published on 17 February 2025. Downloaded on 6/30/2025 11:47:36 PM.
This article is licensed under a Creative Commons Attribution-NonCommercial 3.0 Unported Licence.

Table 2 Optical properties of compounds **6a–f** in both solution and in the solid-state

Compound	Solvent	Absorbance λ_{max} [nm] (ε) [M^{-1} cm^{-1}]	Emission λ_{max} [nm]	Stokes Shifts[a] $\Delta\tilde{\nu}$ [cm^{-1}]	Φ(%)
6a	MeCN	275 (24 525)	444	13 841.1	—
	$CHCl_3$	279 (23 827)	419	11 976.0	1.5
	DMSO	274 (23 712)	447	14 125.0	—
	Solid	—	420	—	21.5
6b	MeCN	275 (25 943)	441	13 687.9	—
	$CHCl_3$	278 (24 153)	422	12 274.5	2.4
	DMSO	274 (24 034)	445	14 024.4	—
	Solid	—	407	—	14.2
6c	MeCN	275 (23 032)	441	13 687.9	—
	$CHCl_3$	278 (22 497)	422	12 274.5	2.4
	DMSO	273 (24 823)	444	14 107.5	—
	Solid	—	407	—	13.2
6d	MeCN	278 (20 892)	442	13 346.8	—
	$CHCl_3$	278 (22 494)	423	12 330.6	1.5
	DMSO	278 (33 064)	448	13 649.8	—
	Solid	—	437, 532	—	7.1
6e	MeCN	272 (22 453)	441	14 089.0	—
	$CHCl_3$	278 (23 072)	424	12 386.3	1.4
	DMSO	278 (23 537)	447	13 599.9	—
	Solid	—	417	—	17.9
6f	MeCN	276 (21 309)	450	14 009.7	—
	$CHCl_3$	278 (18 859)	435	12 982.7	1.6
	DMSO	275 (17 533)	451	14 190.7	—
	Solid	—	435, 572	—	11.1

[a] The Stokes shifts were calculated as $\Delta\tilde{\nu} = 1/\lambda_{max(abs)} - 1/\lambda_{max(em)}$.

restriction of molecular motions and the effective prevention of detrimental π–π stacking, which inhibits non-radiative decay pathways. In the crystal structure of compound **6e**, the pyrazole moiety and the pyrrolo[3,4-*b*]pyridin-5-one core participate in π–π stacking interactions, with centroid-to-centroid distances of approximately 6.897 Å and 4.332 Å, respectively (see the ESI, Fig. S42–S44†). These distances are significantly larger than the typical detrimental π–π stacking distance (~3.35–3.50 Å), supporting the conclusion that the solid-state emission is enhanced due to the absence of strong π–π interactions that would otherwise quench fluorescence.[1,24] Also, similar results have been observed in squaraine-type ESIPT fluorophores reported by Xia and Wang, where solid-state conformations assisted for a ESIPT mechanism suppress π-stacking, leading to low emission in solution but strong fluorescence in the solid state.[25]

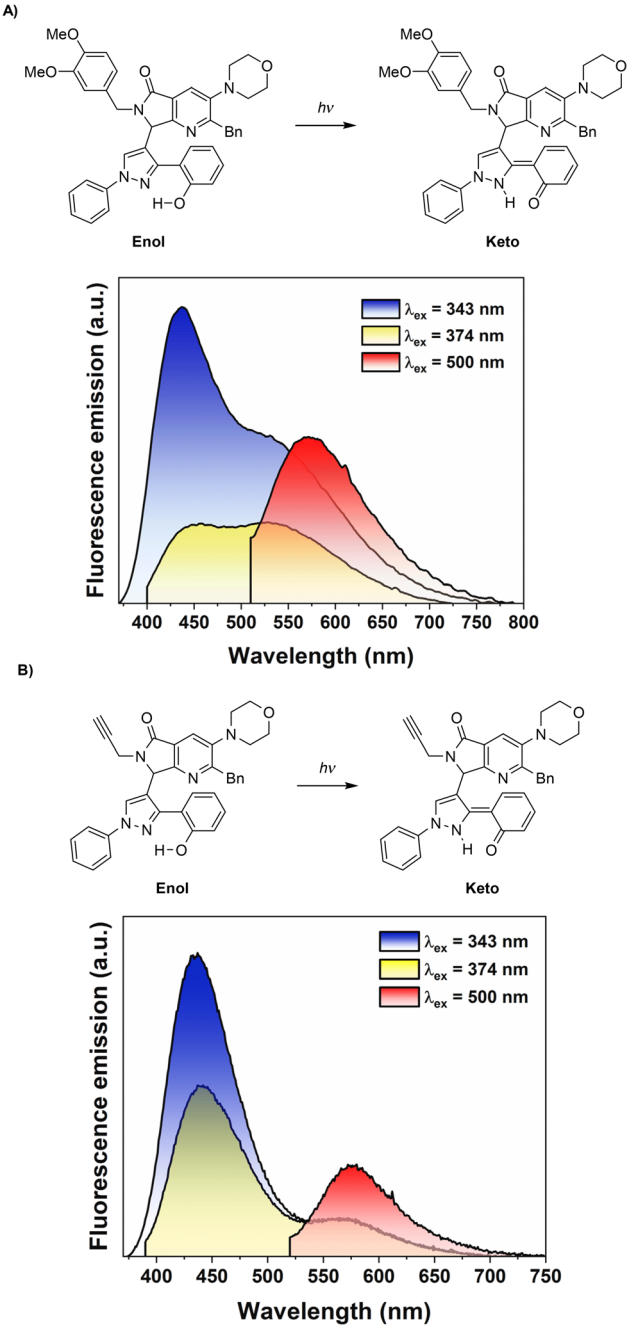


Fig. 4 Solid-state emission spectra at λ_{ex} = 343 nm, 374 nm and 500 nm of compound **6d** (A) and compound **6f** (B).

Electronic structure

The geometries of the ground-state structures of the molecules were optimized through DFT calculations using the Gaussian 09 program,[26] employing the B3LYP functional[27] and the 6-311G(d,p) basis set.[28] The solvation model based on density (SMD) using $CHCl_3$ as solvent was applied to allow comparison with the experimental results. A frequency analysis was performed to ensure that all structures were at an energy minimum and not in a transition state. The theoretical absorption spectra reproduced the experimental results with good accuracy, although all absorption maxima for the pyrrolo[3,4-*b*]pyridin-5-one showed a hypsochromic shift between 3 and 5 nm, while for the pyrazole, there was a bathochromic shift between 6 and 10 nm. The computed oscillator strength values are generally lower compared to those of previous series, indicating that the transitions are weak but allowed. In general, all absorptions are composed of electronic transitions between various orbitals, and notably, in no case is the HOMO → LUMO transition the most significant, unlike other reports of similar systems.[29] The absorption of the pyrazole fragment is

This journal is © the Partner Organisations 2025

Open Access Article. Published on 17 February 2025. Downloaded on 6/30/2025 11:47:36 PM.
This article is licensed under a Creative Commons Attribution-NonCommercial 3.0 Unported Licence.

Table 3 Experimental and TD-DFT data on the absorption maxima of compounds **6a–f**. $\lambda_{max,abs}$ (nm)

Compound	Experimental	Calculated	Oscillator strength *f*	Main contributions
6a	279	274	0.192	HOMO−4 → LUMO (21%) HOMO−3 → LUMO (31%) HOMO−2 → LUMO+1 (27%)
	302	310	0.363	HOMO → LUMO+1 (94%)
6b	278	273	0.247	HOMO−3 → LUMO (46%) HOMO−2 → LUMO+1 (34%) HOMO → LUMO3 (10%)
	301	308	0.344	HOMO → LUMO+1 (89%)
6c	278	275	0.260	HOMO−8 → LUMO (16%) HOMO−3 → LUMO (49%) HOMO−2 → LUMO+1 (13%)
	303	309	0.361	HOMO → LUMO+1 (92%)
6d	278	274	0.193	HOMO−8 → LUMO (8%) HOMO−4 → LUMO (49%) HOMO−3 → LUMO+1 (20%)
	303	309	0.323	HOMO−1 → LUMO (10%) HOMO−1 → LUMO+1 (10%) HOMO → LUMO+1 (78%)
6e	278	275	0.186	HOMO−4 → LUMO (24%) HOMO−3 → LUMO (52%) HOMO−2 → LUMO+1 (18%)
	303	310	0.347	HOMO → LUMO+1 (91%)
6f	278	276	0.119	HOMO−2 → LUMO+1 (53%) HOMO → LUMO+2 (38%)
	302	312	0.380	HOMO → LUMO+1 (100%)

predominantly composed of a HOMO → LUMO+1 transition in all cases, while the absorption of the pyrrolo[3,4-*b*]pyridin-5-one is predominantly composed of a HOMO−3 → LUMO transition in compounds **6a**, **6b**, **6c**, and **6e**. For compound **6d**, the predominant transition is HOMO−4 → LUMO, and for compound **6f**, it is HOMO−2 → LUMO+1. These data are summarized in Table 3.

In compounds **6a–c** and **6e**, the HOMO−3 orbital (HOMO−4 for compound **6d**) is distributed over the pyrrolo[3,4-*b*]pyridin-5-one fragment with its substituents, including the benzyl group and the pyrrole substituent, while the LUMO is localized solely on the pyrrolo[3,4-*b*]pyridin-5-one structure with a node at the methine group. For compound **6f**, the most intense absorption consists of two main contributions: one

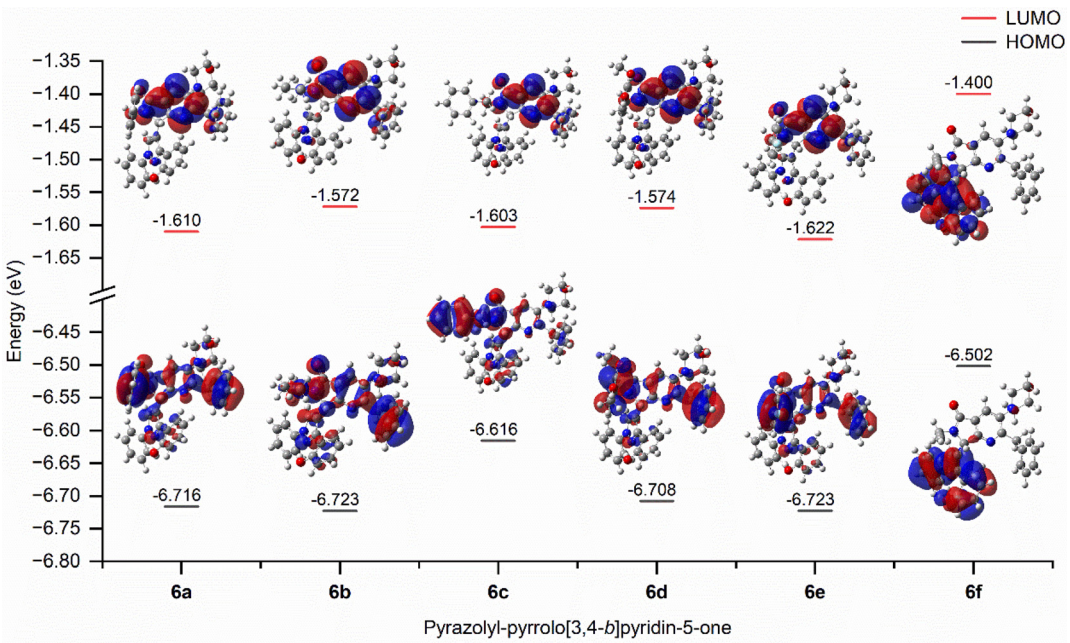


Fig. 5 Representation of the frontier molecular orbitals involved in the strongest absorption band for compounds **6a–f**. For **6a–c** and **6e** HOMO−3 → LUMO is shown. For **6d** HOMO−4 → LUMO is shown. For **6f** HOMO−2 → LUMO+1 is shown.

Open Access Article. Published on 17 February 2025. Downloaded on 6/30/2025 11:47:36 PM.
This article is licensed under a Creative Commons Attribution-NonCommercial 3.0 Unported Licence.

from the HOMO−2 → LUMO+1 orbital (53%), which is distributed over the pyrazole and its substituents, and the other contribution from the HOMO → LUMO+2 orbital (38%), where the HOMO is localized on the pyrazole and the two rings attached to it, while the LUMO+2 is located on the pyrrolo[3,4-*b*]pyridin-5-one, though in this case, the node is located on the nitrogen of the pyrrole. Fig. 5 shows the distribution of the HOMO and LUMO orbitals involved in the strongest absorption band in the synthesized compounds.

The HOMO distribution is primarily localized within the pyrazole ring, while the LUMO is situated in the pyrrolo[3,4-*b*] pyridin-5-one moiety, indicating that the pyrazole fragment is more electron-rich. Generally, the substituents have little effect on the HOMO energy; however, a greater impact is observed on the LUMO energy. For example, the LUMO of compounds **6b** and **6d** is destabilized by 0.038 eV and 0.036 eV, respectively, relative to compound **6a**. Conversely, the LUMO of compound **6f** is stabilized by 0.014 eV compared to **6a**. These results suggest that no clear relationship can be established between the nature of the substituents and their influence on the LUMO, as no consistent trend is apparent (Fig. S51†).

Conclusions

In closing, in this study six new pyrazolyl-pyrrolo[3,4-*b*]pyridin-5-ones were successfully synthesized in a one-pot fashion coupling a multicomponent Ugi-Zhu reaction to a cascade sequence (aza Diels–Alder/*N*-acylation/decarboxylation/dehydration), achieving isolated yields between 42% and 79%, which are acceptable considering the structural complexity of synthesized polyheterocycles, and that only a couple of molecules of water and one carbon dioxide were released in all synthetic procedure. These compounds exhibited DSE properties. Comprehensive photophysical analysis revealed impressive fluorescence features, including large Stokes shifts in solution and intense solid-state emissions, attributed to restricted intramolecular motions. Notably, the PLQYs were significantly higher in the solid state than in solution, highlighting the beneficial role of molecular conformation in reducing π–π stacking interactions to enhance fluorescence emission. Additionally, some compounds demonstrated a prominent ESIPT, a valuable property for applications requiring stable dual-state emissions. Complementary TD-DFT calculations accurately predicted the absorption maxima, with minor deviations in certain transitions. Electronic structure analysis indicated that the HOMO is predominantly localized on the pyrazole fragment, while the LUMO is centered on the pyrrolo[3,4-*b*]pyridin-5-one scaffold. Substituent modifications had a minimal impact on HOMO energy but significantly influenced LUMO energy. These findings underscore the effectiveness of multicomponent reactions in constructing complex heterocyclic frameworks with tunable optical properties, emphasizing their potential in photonic and bioimaging applications. In summary, the synthetic efficiency, structural diversity, and unique photophysical properties of these pyrazole-derived pyrrolo[3,4-*b*]pyridin-5-ones position them as promising candidates for further investigation in optoelectronic applications, particularly in the development of luminescent materials.

Data availability

The data supporting this article have been included in the ESI.†

Conflicts of interest

There are no conflicts to declare.

Acknowledgements

Authors thank Mónica A. Rincón-Guevara (HRMS), and Atilano Gutierrez-Carrillo (NMR) for spectra. A. I.-J. acknowledges "Proyecto Apoyado por el Fondo Sectorial de Investigación *para* la Educación CONAHCyT-SEP CB-2017-2018 (A1-S-32582)" for financial support. E. G. Z acknowledges DCBI-UAM-I/PEAPDI 2024 for financial support. J. C. F.-R. thanks CONAHCYT for his PhD scholarship (886026). Single-crystal X-ray diffraction data were collected using a Rigaku XtaLAB Synergy-s diffractometer equipped with a HyPix-6000HE detector funded by the Australian Research Council (ARC LE210100163). We are grateful to Prof. A. Paulina Gómora-Figueroa for providing access to the FT-IR instrument.

References

1 J. L. Belmonte-Vázquez, Y. A. Amador-Sánchez, L. A. Rodríguez-Cortés and B. Rodríguez-Molina, Dual-State Emission (DSE) in Organic Fluorophores: Design and Applications, *Chem. Mater.*, 2021, **33**(18), 7160–7184.
2 F. Yu, H. Zhao, Y. Li, G. Xia and H. Wang, D–A-Type fluorophores with efficient dual-state emission for imaging at ultralow concentration, *Mater. Chem. Front.*, 2022, **6**(2), 155–162.
3 Z. Huang, A. Ding, J. Yang, C. Wang and F. Tang, Conjugating Coumarin with Tetraphenylethylene to Achieve Dual–State Emission for Reversible Mechanofluorochromism and Live Cell Imaging, *Chem. – Eur. J.*, 2023, **29**, e202203628.
4 Ein Konzentrationsumschlag der Fluoreszenz, *Z. Phys. Chem.*, 1954, **1**(56), 275–277.
5 J. Mei, N. L. C. Leung, R. T. K. Kwok, J. W. Y. Lam and B. Z. Tang, Aggregation-Induced Emission: Together We Shine, United We Soar!, *Chem. Rev.*, 2015, **115**(21), 11718–11940.
6 L. A. Rodríguez-Cortés, A. Navarro-Huerta and B. Rodríguez-Molina, One molecule to light it all: The era of dual-state emission, *Matter*, 2021, **4**(8), 2622–2624.

 This journal is © the Partner Organisations 2025

Open Access Article. Published on 17 February 2025. Downloaded on 6/30/2025 11:47:36 PM. This article is licensed under a Creative Commons Attribution-NonCommercial 3.0 Unported Licence.

7 (*a*) G. Xia, Q. Shao, K. Liang, Y. Wang, L. Jiang and H. Wang, A phenyl-removal strategy for accessing an efficient dual-state emitter in the red/NIR region guided by TDDFT calculations, *J. Mater. Chem. C*, 2020, **8**(39), 13621–13626; (*b*) M. Durko-Maciag, G. Ulrich, D. Jacquemin, J. Mysliwiec and J. Massue, Solid-state emitters presenting a modular excited-state proton transfer (ESIPT) process: recent advances in dual-state emission and lasing applications, *Phys. Chem. Chem. Phys.*, 2023, **25**(22), 15085–15098.

8 V. Kumar, K. Kaur, G. K. Gupta and A. K. Sharma, Pyrazole containing natural products: Synthetic preview and biological significance, *Eur. J. Med. Chem.*, 2013, **69**, 735–753.

9 A. Burke, M. di Filippo, S. Spiccio, A. M. Schito, D. Caviglia, C. Brullo and M. Baumann, Antimicrobial Evaluation of New Pyrazoles, Indazoles and Pyrazolines Prepared in Continuous Flow Mode, *Int. J. Mol. Sci.*, 2023, **24**(6), 5319.

10 A. Tigreros and J. Portilla, Recent progress in chemosensors based on pyrazole derivatives, *RSC Adv.*, 2020, **10**(33), 19693–19712.

11 (*a*) I. v. Taydakov, A. A. Akkuzina, R. I. Avetisov, A. v. Khomyakov, R. R. Saifutyarov and I. Ch, Avetissov, Effective electroluminescent materials for OLED applications based on lanthanide 1.3-diketonates bearing pyrazole moiety, *J. Lumin.*, 2016, **177**, 31–39; (*b*) M. Jin, Y. Chen, W. Song, H. Lian, H. Guo, Q. Dong, J. Huang and J. Su, Synthesis, characterization, and electroluminescent properties of indazole, pyrazole, and triazole/triphenylamine-based compounds, *Dyes Pigm.*, 2020, **173**, 106912.

12 A. Dömling, W. Wang and K. Wang, Chemistry and Biology of Multicomponent Reactions, *Chem. Rev.*, 2012, **112**(6), 3083–3135.

13 L. Levi and T. J. J. Müller, Multicomponent syntheses of functional chromophores, *Chem. Soc. Rev.*, 2016, **45**(10), 2825–2846.

14 (*a*) I. A. Ibarra, A. Islas-Jácome and E. González-Zamora, Synthesis of polyheterocycles *via* multicomponent reactions, *Org. Biomol. Chem.*, 2018, **16**(9), 1402–1418; (*b*) J. C. Flores-Reyes, V. d. C. Cotlame-Salinas, I. A. Ibarra, E. González-Zamora and A. Islas-Jácome, Pseudo-multicomponent reactions, *RSC Adv.*, 2023, **13**(24), 16091–16125; (*c*) J. C. Flores-Reyes, A. Islas-Jácome and E. González-Zamora, The Ugi three-component reaction and its variants, *Org. Chem. Front.*, 2021, **8**(19), 5460–5515.

15 D. Udhayakumari, P. Jerome, N. Vijay and T. H. Oh, ESIPT: An approach and future perspective for the detection of biologically important analytes, *J. Lumin.*, 2024, **267**, 120350.

16 X. Sun, P. Janvier, G. Zhao, H. Bienaymé and J. Zhu, A Novel Multicomponent Synthesis of Polysubstituted 5-Aminooxazole and Its New Scaffold-Generating Reaction to Pyrrolo[3,4-*b*]pyridine, *Org. Lett.*, 2001, **3**(6), 877–880.

17 (*a*) I. Morales-Salazar, F. P. Montes-Enríquez, C. E. Garduño-Albino, M. A. García-Sánchez, I. A. Ibarra, Y. Rojas-Aguirre, M. E. García-Hernández, R. E. Sarmiento-Silva, S. L. Alcaraz-Estrada, E. Díaz-Cervantes, E. González-Zamora and A. Islas-Jácome, Synthesis of bis-furyl-pyrrolo[3,4-*b*]pyridin-5-ones *via* Ugi–Zhu reaction and *in vitro* activity assays against human SARS-CoV-2 and *in silico* studies on its main proteins, *RSC Med. Chem.*, 2023, **14**(1), 154–165; (*b*) I. Morales-Salazar, C. E. Garduño-Albino, F. P. Montes-Enríquez, D. A. Nava-Tapia, N. Navarro-Tito, L. D. Herrera-Zúñiga, E. González-Zamora and A. Islas-Jácome, Synthesis of Pyrrolo[3,4-*b*]pyridin-5-ones via Ugi–Zhu Reaction and In Vitro–In Silico Studies against Breast Carcinoma, *Pharmaceuticals*, 2023, **16**(11), 1562; (*c*) I. Morales-Salazar, C. E. Garduño-Albino, F. P. Montes-Enríquez, A. Gutiérrez-Carrillo, Y. Rojas-Aguirre, N. V. Estrada-Toledo, J. Sandoval-Basilio, S. L. Alcaraz-Estrada, E. Díaz-Cervantes, E. González-Zamora and A. Islas-Jácome, In Vitro and In Silico Studies of Bis-furyl-pyrrolo[3,4-*b*]pyridin-5-ones on Dengue Virus, *J. Mex. Chem. Soc.*, 2024, **68**(1), 170–183.

18 (*a*) J. C. Flores-Reyes, S. M. Rojas-Montoya, L. Blancarte-Carrazco, E. Xochitiotzi-Flores, C. A. Guarin, N. Farfán, A. Galano, A. Islas-Jácome and E. González-Zamora, Multicomponent synthesis and photophysical properties of meso-thienyl BODIPY-pyrrolo[3,4-*b*]pyridin-5-ones. An experimental and theoretical study, *J. Lumin.*, 2024, **273**, 120698; (*b*) J. C. Flores-Reyes, A. Galano, S. M. Rojas-Montoya, L. Blancarte-Carrazco, E. Xochitiotzi-Flores, H. García-Ortega, N. Farfán, A. Islas-Jácome and E. González-Zamora, Synthesis of BODIPY-pyrrolo[3,4-*b*]pyridin-5-ones via Ugi-Zhu/cascade reactions and studies of fluorescence response toward viscosity, *Front. Chem.*, 2024, **12**, 1488933.

19 I. Ali, A. Haque, K. Saleem and M. F. Hsieh, Curcumin-I Knoevenagel's condensates and their Schiff's bases as anticancer agents: Synthesis, pharmacological and simulation studies, *Bioorg. Med. Chem.*, 2013, **21**(13), 3808–3820.

20 A. Kawski, On the Estimation of Excited-State Dipole Moments from Solvatochromic Shifts of Absorption and Fluorescence Spectra, *Z. Naturforsch., A: Phys. Sci.*, 2002, **57**(5), 255–262.

21 A. C. Sedgwick, L. Wu, H.-H. Han, S. D. Bull, X.-P. He, T. D. James, J. L. Sessler, B. Z. Tang, H. Tian and J. Yoon, Excited-state intramolecular proton-transfer (ESIPT) based fluorescence sensors and imaging agents, *Chem. Soc. Rev.*, 2018, **47**(23), 8842–8880.

22 K.-L. Wong, J.-C. G. Bünzli and P. A. Tanner, Quantum yield and brightness, *J. Lumin.*, 2020, **224**, 117256.

23 V. S. Padalkar and S. Seki, Excited-state intramolecular proton-transfer (ESIPT)-inspired solid state emitters, *Chem. Soc. Rev.*, 2016, **45**(1), 169–202.

24 (*a*) J. Shi, L. E. Aguilar Suarez, S. J. Yoon, S. Varghese, C. Serpa, S. Y. Park, L. Lüer, D. Roca-Sanjuán, B. Milián-Medina and J. Gierschner, Solid State Luminescence Enhancement in π-Conjugated Materials: Unraveling the Mechanism beyond the Framework of AIE/AIEE, *J. Phys. Chem. C*, 2017, **121**(41), 23166–23183; (*b*) K. Shirai, M. Matsuoka and K. Fukunishi, Fluorescence quenching by intermolecular π–π interactions of 2,5-bis(*N,N*-dialkyla-

Open Access Article. Published on 17 February 2025. Downloaded on 6/30/2025 11:47:36 PM.
This article is licensed under a Creative Commons Attribution-NonCommercial 3.0 Unported Licence.

mino)-3,6-dicyanopyrazines, *Dyes Pigm.*, 1999, **42**(1), 95–101.

25 Q. Shao, K. Liang, H. Ling, Y. Wang, Z. Yan, G. Xia and H. Wang, Tetraphenylethylene-incorporated squaraine dyes: structural and theoretical insights into the diverse emission behaviors in solution and solid state, *J. Mater. Chem. C*, 2020, **8**(13), 4549–4556.

26 M. J. Frisch, *et al.*, *Gaussian 09, Revision B.01*, Gaussian, Inc., Wallingford CT, 2010.

27 (*a*) A. D. Becke, Density–functional thermochemistry. III. The role of exact exchange, *J. Chem. Phys.*, 1993, **98**, 5648–5652; (*b*) C. Lee, W. Yang and R. Parr, Development of the Colle-Salvetti correlation-energy formula into a functional of the electron density, *Phys. Rev. B: Condens. Matter Mater. Phys.*, 1988, **37**, 785.

28 R. Krishnan, J. S. Binkley, R. Seeger and J. People, Self–consistent molecular orbital methods. XX. A basis set for correlated wave functions, *J. Chem. Phys.*, 1980, **72**, 650–654.

29 (*a*) H. Zhuang, W. Shi, G. Zhao and Y. Li, Regulating and controlling the stepwise ESDPT channel of $BP(OH)_2DCEt_2$ using the strategy of solvent polarity and external electric field, *Phys. Chem. Chem. Phys.*, 2024, **26**, 12016–12026; (*b*) X. Xin, W. Shi, G. Zhao and Y. Li, Effectively regulation of the ESIPT process via ring-annelation modification for schiff base derivatives: A theoretical study, *Dyes Pigm.*, 2024, **224**, 112020.

 This journal is © the Partner Organisations 2025

Check for updates

Received: 26 October 2024 | Revised: 7 February 2025 | Accepted: 10 February 2025

DOI: 10.1002/bkcs.70005

REVIEW

BKCS BULLETIN OF THE KOREAN CHEMICAL SOCIETY

Low-toxicity metal–organic frameworks: Sustainable solutions for versatile applications

Juan L. Obeso[1,2,3] | **Catalina V. Flores**[1,2] | **Aldo G. Gutiérrez**[1] | **Carolina Leyva**[1] | **Juan Carlos Valdivia-Corona**[3] | **Leonardo D. Herrera-Zúñiga**[4,5] | **José Antonio de los Reyes**[6] | **Ricardo A. Peralta**[7] | **Ilich A. Ibarra**[2]

[1]Instituto Politécnico Nacional, CICATA U. Legaria, Laboratorio Nacional de Ciencia, Tecnología y Gestión Integrada del Agua (LNAgua), Miguel Hidalgo, Mexico

[2]Laboratorio de Fisicoquímica y Reactividad de Superficies (LaFReS), Instituto de Investigaciones en Materiales, Universidad Nacional Autónoma de México, Circuito Exterior s/n, CU, Ciudad de México, Mexico

[3]División de Ingeniería en Sistemas Automotrices, Tecnológico Nacional de México, Tecnológico de Estudios Superiores del Oriente del Estado de México, Estado de México, Mexico

[4]Departamento de Química, Area de biofisicoquímica, Universidad Autónoma Metropolitana-Iztapalapa, Ciudad de México, Mexico

[5]Departamento de Ciencias Naturales, Universidad Autonoma Metropolitana Unidad Cuajimalpa, Ciudad de México, Mexico

[6]Departamento de Ingeniería de Procesos e Hidráulica, División de Ciencias Básicas e Ingeniería, Universidad Autónoma Metropolitana-Iztapalapa, Mexico City, Mexico

[7]Departamento de Química, División de Ciencias Básicas e Ingeniería, Universidad Autónoma Metropolitana, Mexico City, Mexico

Correspondence
Ricardo A. Peralta, Departamento de Química, División de Ciencias Básicas e Ingeniería, Universidad Autónoma Metropolitana, Mexico City, Mexico.
Email: rperalta@izt.uam.mx

Ilich A. Ibarra, Laboratorio de Fisicoquímica y Reactividad de Superficies (LaFReS), Instituto de Investigaciones en Materiales, Universidad Nacional Autónoma de México, Circuito Exterior s/n, CU, Ciudad de México, Mexico.
Email: argel@unam.mx

Abstract

The conventional synthesis of metal-organic framework (MOF) materials generates high amounts of waste solvents, which are directly associated with human and environmental issues. Developing green and affordable MOF materials is necessary since this strategy is based on methods that prioritize sustainability and minimize environmental impact. In this scenario, less toxic metals such as Zn, Zr, Al, and Fe can be applied in addition to linkers from renewable sources. This review discusses eco-friendly synthesis pathways, such as hydrothermal, mechanochemical, at room temperature, ionic liquid, and renewable resources. The current methodologies from specific low-toxicity MOF materials are highlighted. Applications include water treatment, sensing, drug delivery, catalysis, and gas storage, which are mentioned and examined. Interestingly, developing low-impact MOF materials as eco-friendly platforms for diverse applications can be a remarkable opportunity to achieve a sustainable future in the quality of the planet.

KEYWORDS
ecofriendly materials, green synthesis, low-toxicity MOFs, mild synthesis, MOFs, non-toxic metals, versatile application MOFs

INTRODUCTION

The development of new compounds is a rising target for chemists; consequently, the synthesis of widely different compounds has been reported to this day, particularly in the field of inorganic chemistry, where the reticular chemistry field has continuously increased.[1] Understanding the formation of compounds to generate a crystalline compound has impacted the synthesis of new valuable materials.[2] Based on this idea, metal–organic frameworks (MOFs) have emerged as a non-stop crystalline material. MOFs are organic–inorganic materials constructed using

This is an open access article under the terms of the Creative Commons Attribution License, which permits use, distribution and reproduction in any medium, provided the original work is properly cited.
© 2025 The Author(s). *Bulletin of the Korean Chemical Society* published by Korean Chemical Society and Wiley-VCH GmbH.

metal ions and organic ligands.[3] The coordination environment of many MOFs has been studied mainly due to their extensibility assets and unique molecular coordination chemistry,[4] showing high surface area, thermal and chemical stability.[5]

Based on their outstanding properties, the design has focused on developing particular MOF materials related to a specific application since, in most cases, the synthesis routes impact the MOF crystallization, which can be associated with the MOF properties.[6–8] Since its intrinsic porosity and well-porous distribution, the adsorption process is the most useful application for this material.[9] Since reducing CO_2 emissions is still challenging for our modern society, CO_2 capture and separation (over N_2 and O_2) have been efficiently applied using MOF.[10] MOF materials have shown high adsorption capacities for highly toxic and corrosive gases such as SO_2,[11] H_2S,[12] NH_3,[13] and volatile organic compounds.[14] The applications can also be extended to catalysis,[15] water harvesting,[16] drug carrier/delivery,[17] water pollutants adsorption,[18] detection/sensing,[19] and bio-applications.[20] Interestingly, studying this material in different fields has generated the possibility of using it on an industrial scale.[21]

The base of these applications is related to MOF stability in different environments, where screening suitable MOFs with potential is necessary. The use of reticular synthesis has achieved the successful preparation of different MOF materials for these purposes.[22] Various synthetic routes have been published for specific metal ions and organic ligands.[23] Generally, the synthesis methodology involves hydrothermal and solvothermal reactions, reflux, microwave, and mechanochemical approaches.[24] These methodologies are conducted under different conditions by varying the temperature, stoichiometric amounts, pressure, solvents, modulator, and time. These factors alter the yield, purity, and crystallinity.[25] Although the most common synthesis routes show high efficiency for MOF preparation, the negative impact on the environment is crucial. The use of harmful solvents that can be toxic and flammable, the high waste generation, and the energy consumption are highlighted. For this, the development of green synthesis pathways is necessary.[26] The main idea is to prevent pollution at the molecular level, which, in MOF synthesis, is related to green raw materials (avoiding organic solvents), decreasing energy demand, and avoiding the formation of by-products that can be more dangerous to the environment.[27]

Employing toxic solvents or metal ions has been common in MOF synthesis. Different strategies have been reported to replace carcinogenic solvents for an eco-friendly environment.[28] However, it is difficult since most MOF syntheses use *N,N*-dimethylformamide (DMF). In some cases, different approaches have been conducted to employ sodium hydroxide (NaOH) to avoid organic solvents. The employment of low-toxicity metal ions is also an alternative. For this, clusters based on Zn^{2+}, Zr^{4+}, Al^{3+}, and Fe^{3+} are applied to develop green MOF chemistry.[29] Also, selected organic linkers have been postulated for their eco-friendly nature. Ellagic acid is a common natural antioxidant that can synthesize bismuth ellagate MOF materials, displaying biocompatibility and colloidal stability.[30]

Thus, this review aims to establish the different green synthesis methodologies and their highlighting applications by drawing on the principal contributions. The primary intent is to survey and categorize environmentally friendly MOF production methods. The discussion about the relevance of employing eco-friendly metal-linker nodes is mentioned. The review will emphasize the most significant advancements and discoveries within the MOF field.

METAL–ORGANIC FRAMEWORKS: ECO-FRIENDLY METAL-LINKER NODES

MOFs have attracted interest in producing materials with improved characteristics, such as surface area, porosity, and stability. However, researchers are particularly interested in green MOFs. This characteristic derives from avoiding organic and toxic solvents in the synthesis by employing friendly organic linkers and low-toxicity metal centers.[31] An overview of different metal clusters with low toxicity and the utilization of eco-friendly linkers in MOFs is necessary to analyze.

Metal clusters in MOF

The main components of a MOF material are the metal center, which can be called Secondary Building Units (SBUs), and the organic ligand, which is connected via coordination metal–oxygen bonds.[2–4] A high amount of MOF can be constructed due to the different SBU units and ligands. Employing low-toxicity metal centers can generate eco-friendly building blocks for the green development of MOF materials. The design of green building blocks can enhance future applications due to the high homogeneous distribution of the active metal in the crystal lattice since the geometry and coordination environment can be different.

Focused on Zn^{2+} ions, the SBUs can form di-, tri-, tetra-, and pentanuclear Zn clusters, which may be modified by the synthesis method. For example, Zn-HKUST-1 (HKUST = Hong Kong University of Science and Technology and BTC = 1,3,5-benzenetricarboxylate), which is an isostructural analogue of Cu-HKUST-1,[32] displays a zinc paddle-wheel cluster based on the dimeric metal tetracarboxylate units.[33] The framework is electrically neutral with 12 carboxylate oxygens from the two BTC ligands coordinated to three metal ions of the formula unit. The material shows a 3D connected network of pores, with an arrangement of large hexagonal-shaped windows. Then, MOF-5

12259949, 2025, 3, Downloaded from https://onlinelibrary.wiley.com/doi/10.1002/bkcs.70005 by Universidad Autonoma Metropolitana, Wiley Online Library on [30/06/2025]. See the Terms and Conditions (https://onlinelibrary.wiley.com/terms-and-conditions) on Wiley Online Library for rules of use; OA articles are governed by the applicable Creative Commons License

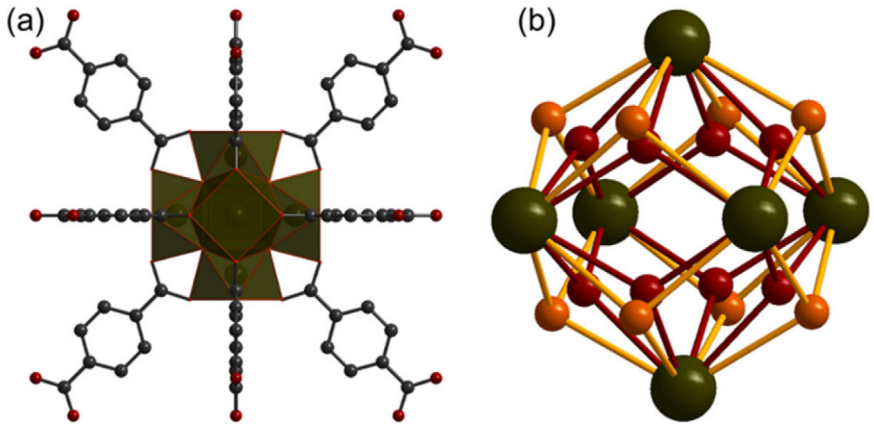


FIGURE 1 Schematic representation of the UiO-66 structure according to crystallographic data COD ID 4512072. (a) Dark green polyhedral represents the Zr-O cluster; gray spheres represent carbon atoms, and dark red represents oxygen. (b) Schematic representation of $Zr_6O_4(OH)_4$ SBU. Both oxygen positions are provided: μ_3-O (dark red) and μ_3-OH (orange). (Reprinted with permission from ref. 39 Copyright 2022 MDPI under the terms and conditions of the CC BY License).

(BDC = 1,4-benzodicarboxylate) exhibits octahedral Zn-O clusters in a cubic framework. The MOF-5 structure is formed by ZnO_4 tetrahedra, which coordinate with dicarboxylate units from the linker.[34] Different isoreticular MOFs (IRMOF) were designed from this material. The SBU is constructed from six carboxylates bridging a ZnO_4 cluster to form an octahedron-shaped geometry with a 3D cubic structure. Diverse organic linkers were used to exhibit this geometry. IRMOF-2 to IRMOF-7 are built using a functionalized BDC linker with bromo, amino, n-propoxy, n-pentoxy, cyclobutyl, and fused benzene, displaying a decorated pore with the groups pointing into the voids. A linker expansion is also possible from IRMOF, employing an enlarged linker, such as NDC (IRMOF-8, 2,6-naphthalenedicarboxylate), BPDC (IRMOF-9, biphenyl-4,4-dicarboxylate), HPDC (IRMOF-11, 4,5,9,10-tetrahydro-2,7-pyrenedicarboxylate), PDC (IRMOF-13, 2,7-pyrenedicarboxylate), and TPDC (IRMOF-15, p-terphenyl-4,4″-dicarboxylate).[35]

Zr-based MOFs show high stability due to the strong Zr-O bonds in their structure. The material UiO-66 (UiO = University of Oslo, BDC) presents an inner six-centered octahedral zirconium oxide unit forming $Zr_6O_4(OH)_4(CO_2)_{12}$ with a 12-coordinated number (Figure 1).[36] The crystal is a face-centered cubic structure containing an fm−3 m symmetry with a lattice parameter of 20.7 Å. According to the Reticular Chemistry Structure Resource (RCSR),[37] UiO-66 shows a fcu topology. For the NU-1000 material (NU = Northwestern University and TBAPy = 1,3,6,8-tetrakis(p-benzoate)pyrene), the structure is composed of $Zr_6(\mu_3\text{-}OH)_4(\mu_3\text{-}O)_4(OH)_4(OH_2)_4$ nodes. The Zr_6 clusters are coordinated with 12 linkers, displaying a csq topology.[38] This arrangement displays a high-size channel of 31 and 12 Å, forming a window connection of 10 × 8 Å. In the case of NU-901 (TBAPy), the change in synthesis conditions can form different connectivity. The structure comprises eight connected nodes with a scu topology, displaying diamond-shaped channels with a pore size of 29 Å.

Generally, in Al-based MOF, the Al^{3+} center exhibits an octahedral geometry, forming –Al–OH– chains via bridging hydroxyl groups (μ_2-OH) since the coordination number for Al^{3+} is 4 and 6, showing six-coordinate AlO_6 clusters.[40] For example, DUT-4 (DUT = Dresden University of Technology, NDC) shows a 3D framework with rectangular tunnels of 8.5 × 8.5 Å in dimensions.[41] Each Al^{3+} ion is coordinated with four NDC linkers and two hydroxyl groups. The same structure can be obtained using a BPDC linker to form DUT-5 with slightly larger pores (11.1 × 11.1 Å). MIL-53(Al) (MIL = Matériaux Institut Lavoisier, BDC) displays an octahedrally coordinated structure by six oxygen atoms, forming Al-OH chains. The trans chains of corner-sharing $AlO_4(OH)_2$ octahedra clusters are connected with the BDC linker to create 1D rhombic-shaped tunnels, forming a 3D network.[42] MOF-303 (PZDC = 1-H-pyrazole-3,5-dicarboxylate) displayed an alternating cis-trans corner-shared AlO_6 octahedra.[43] The Al^{3+} center is coordinated with four carboxyl groups and two μ_2-OH groups, showing an xhh topology. MFM-300 (MFM = Manchester Framework Material and BPTC = biphenyl-3,3′,5,5′-tetracarboxylate) crystallizes in the chiral tetragonal space group $I4_122$.[44] The structure exhibits chains of $AlO_4(OH)_2$ octahedra clusters, where the Al^{3+} center is coordinated to six oxygen atoms, four from carboxylates, and two from bridging cis hydroxyl groups μ_2-OH.

On the other hand, Fe-based MOF displays [$Fe_3(\mu_3\text{-}O)(COO_6)$] clusters but also Fe-OH chains in its structures (Figure 2). MIL-100(Fe) (BTC) displays an octahedral cluster built by trimers of iron octahedra and BTC ligand sharing a common vertex μ_3-O, displaying a pore size of 29.40 Å.[45] MIL-53(Fe) (BDC) shows the inorganic Fe-OH chains, forming the trans-FeO_6 octahedral core clusters. These chains are coordinated with BDC linkers to create a

12295949, 2025, 3, Downloaded from https://onlinelibrary.wiley.com/doi/10.1002/bkcs.70005 by Universidad Autonoma Metropolitana, Wiley Online Library on [30/06/2025]. See the Terms and Conditions (https://onlinelibrary.wiley.com/terms-and-conditions) on Wiley Online Library for rules of use; OA articles are governed by the applicable Creative Commons License

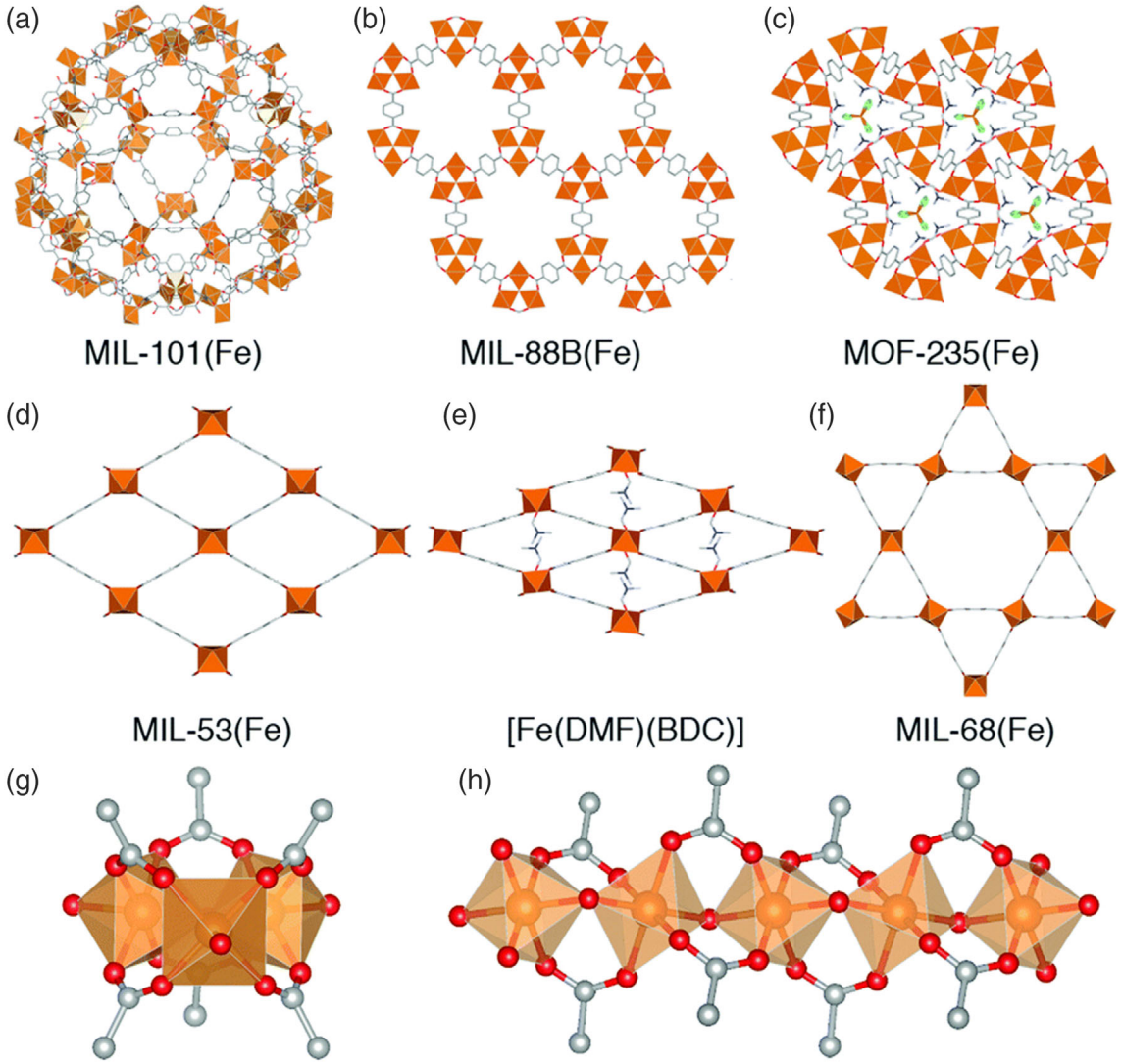


FIGURE 2 Known Fe-terephthalate phases are classified according to inorganic SBU. The top row shows MOFs connected by the trimeric Fe_3O SBU: (a) MIL-101(Fe), (b) MIL-88B(Fe), and (c) MOF-235(Fe). The middle row shows MOFs connected by one-dimensional chain SBUs: (d) MIL-53(Fe), (e) [Fe(DMF)(BDC)], and (f) MIL-68(Fe). The bottom row shows the two SBUs: (g) $[Fe_3O(RCO_2)_6(OH_2)_2X]$, where X is a monoanion such as Cl, F, or OH, and (h) $[Fe(\mu_2\text{-}OH)(RCO_2)_2]n$. Note that in [Fe(DMF)(BDC)], the μ_2-OH is replaced by an O-donor μ_2-DMF ligand. H atoms were removed for clarity. (Reprinted with permission from ref. 48 Copyright 2021 Royal Society of Chemistry under Creative Commons Attribution 3.0 Unported License).

3D structure, generating rhombohedral channels and I2/a space group.[46]

Distinctive linkers in MOF

Environmentally friendly MOFs are investigated using eco-friendly linkers. The ecologically friendly organic linkers enhance the bio-properties that characterize the green MOF. Aimed to incorporate renewable source organic linkers and easy synthesis methods, Chen et al.[47] employed an adenine-based MOF, namely, bio-MOF-11, for air remediation, removing several volatile organic compounds (VOCs), such as methanol, acetone, benzene, and toluene.

Employing a facile solvothermal synthesis, they obtained an effective VOC adsorbent in ethanol as a solvent. Adenine in MOF, as one of the nitrogen bases in deoxyribonucleic acid (DNA) and ribonucleic acid (RNA),[49] derived multiple available nitrogen atoms and amino groups for VOC adsorption, reaching adsorption capacities of 0.73–3.57 mmol g^{-1}, in order: toluene < benzene < acetone < methanol and founding an inversely proportional adsorption capacity to the molecular size. The bio-MOF-11, a multi-pollutant adsorbent, exhibits high thermal stability around 277°C, 580 cm^2 g^{-1} of BET surface area, and a pore size of 0.53 nm. However, an exothermic process derived from VOC properties was observed. Thus, a decrease in adsorption was observed with a rise in temperature.

12259949, 2025, 3, Downloaded from https://onlinelibrary.wiley.com/doi/10.1002/bkcs.70005 by Universidad Autonoma Metropolitana, Wiley Online Library on [30/06/2025]. See the Terms and Conditions (https://onlinelibrary.wiley.com/terms-and-conditions) on Wiley Online Library for rules of use; OA articles are governed by the applicable Creative Commons License

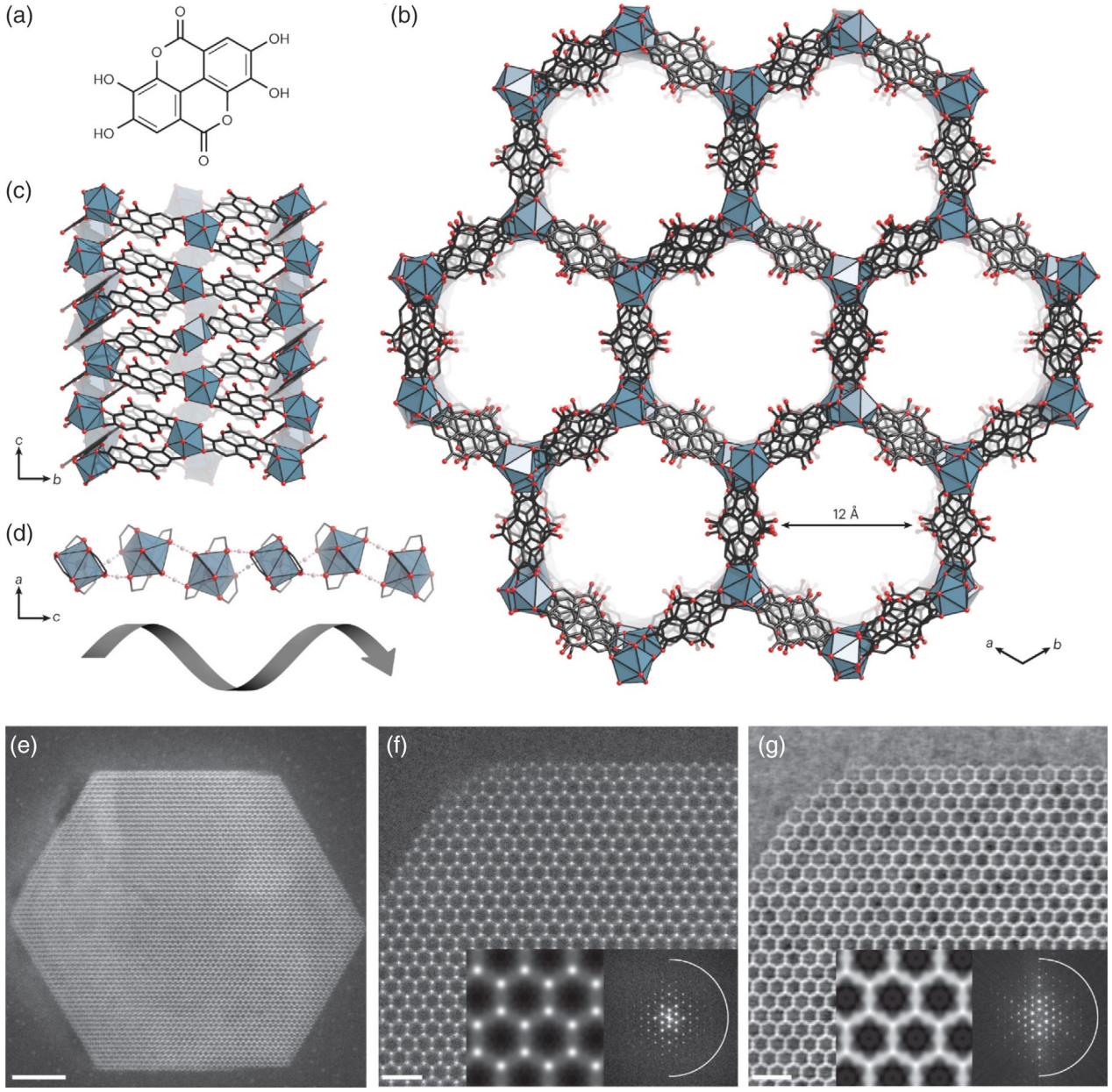


FIGURE 3 Structure of the Zr-ellagate SU-102 (a) molecular structure of ellagic acid. (b) The crystal structure of SU-102 is viewed down the one-dimensional channels that extend along the c axis. Hydrogen atoms and charge-balancing guest species have been omitted for clarity. ZrO8 units are shown as blue polyhedra. (c) Side view of a channel wall, as viewed along the a axis. (d) ZrO8 units stacked along the c axis and bridged by pairs of strong hydrogen bonds between phenol and phenolate groups to form helices. O–H bonds are drawn as dashed lines, and only phenolate-bonded carbons are shown. (e) ADF STEM image of a crystal of SU-102 (scale bar, 20 nm). (f, g) STEM images of SU-102 using ADF (f) and iDPC (g) signals (scale bars, 5 nm). Insets in f and g show each image's lattice-averaged maps with p6mm symmetry imposed (left) and Fourier transforms (right). The half circles indicate a resolution of 2.5 Å. (Reprinted with permission from ref. 52 Copyright 2023 Springer Nature Limited under Creative Commons Attribution 4.0 International License).

Plant-derived organics exhibit promising biological properties.[50] Controlled drug delivery through the bio-MOFs is also a newly explored area. In medicine, part of the fight against cancer is to develop appropriate delivery mechanisms for pharmaceutical administration. The release of curcumin (Cur) and doxorubicin hydrochloride (DOX-HCl), with the polydopamine coating to prevent accelerated degradation, was usefully performed through the bio-MOF synthesized by Yang et al.[51] Zinc acetate dihydrate and Cur as base plant, a polyphenolic compound found in *Curcuma longa*,[50] organic linkers constituted the bio-MOF employed for the biodegradable multifunctional photothermal drug delivery nanoparticles (MPH NPs). In an acid environment, 5 pH demonstrates the release of 19.15 μg mL^{-1} Cur from the degradation of 1 mg of bio-MOF. The Cur penetrates the cancer cell via electron interaction through selective

12259949, 2025, 3, Downloaded from https://onlinelibrary.wiley.com/doi/10.1002/bkcs.70005 by Universidad Autonoma Metropolitana, Wiley Online Library on [30/06/2025]. See the Terms and Conditions (https://onlinelibrary.wiley.com/terms-and-conditions) on Wiley Online Library for rules of use; OA articles are governed by the applicable Creative Commons License

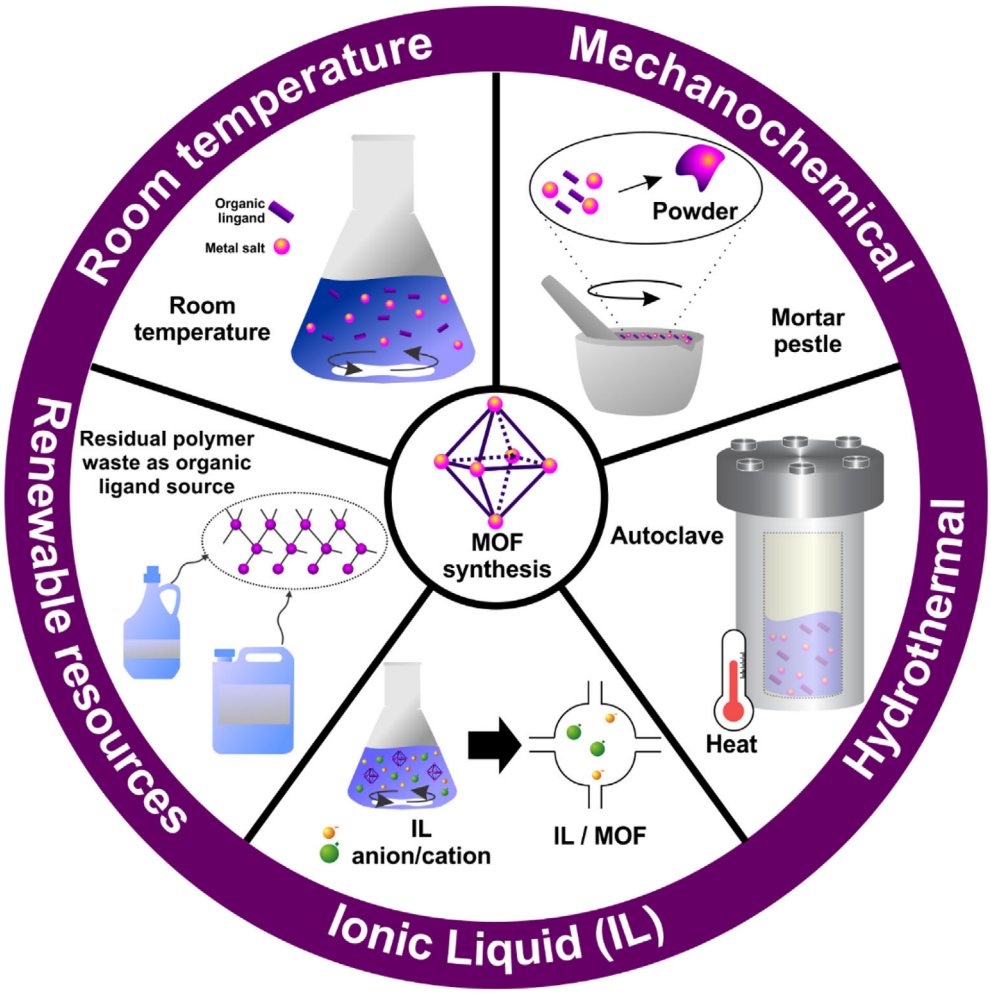


FIGURE 4 Schematic representation of the different methods for green synthesis of metal-organic framework (MOF) materials.

targeting of the CD44 receptors on cancer cells by the MPH NPs.

A directly plant-based metal–organic framework called SU-102 was reported (Figure 3). The material is constructed of nontoxic and sustainably sourced building blocks. The organic linker is ellagic acid, and the metal center is Zr^{4+} cations. Ellagic acid is an abundant phytochemical that can be extracted from plant material such as tree bark and fruit peels. The materials can be synthesized under solvothermal conditions, displaying a rhombohedral structure with an R3-c space group with channels of 12 Å. The Zr^{4+} metal clusters form ZrO_8 units binding with ellagate anions, showing a 3D framework with a pts topology.

SUSTAINABLE SYNTHESIS APPROACHES TO MOF PRODUCTION

The sustainability approach to materials synthesis focuses on minimizing environmental impact and maximizing resource efficiency throughout a material's lifecycle. In this case, a green synthesis attempt has been established since it is described as the designing and manufacturing of chemical products that reduce or eliminate the use of hazardous substances.[53] Based on this, different green synthesis methodologies have been reported for MOF materials production. Applying eco-friendly metal-linker nodes has impacted the production of diverse MOF materials by using low-toxicity salts as metal ions (Zn, Zr, Al, and Fe) and environmental linkers.[54] In this context, MOF design has been impacted by different green synthesis pathways (Figure 4), such as (i) hydrothermal, (ii) mechanochemical, (iii) at room temperature, (iv) ionic liquid, and (v) renewable resources.

For example, (i) hydrothermal synthesis, the method uses water as the primary solvent, reducing waste with high energy efficiency; (ii) mechanochemical synthesis, the method relies on the complete elimination of solvent and increases the yield by using most of the raw materials; (iii) at room temperature synthesis, the method highlights low energy consumption for the synthesis, contributing to a smaller carbon footprint; (iv) ionic liquid synthesis, the method improves safety by reducing the risk of fires and explosions associated with volatile organic solvents; and

12259549, 2025, 3, Downloaded from https://onlinelibrary.wiley.com/doi/10.1002/bkcs.70005 by Universidad Autonoma Metropolitana, Wiley Online Library on [30/06/2025]. See the Terms and Conditions (https://onlinelibrary.wiley.com/terms-and-conditions) on Wiley Online Library for rules of use; OA articles are governed by the applicable Creative Commons License

TABLE 1 A summarizing of the advantages and disadvantages of the green synthesis methods.

Synthesis method	Advantages	Disadvantages
Hydrothermal synthesis	High crystallinity products, low waste, and energy efficiency.	High cost, corrosive environments, and byproduct formation.
Mechanochemical synthesis	Free solvent and high yield.	Low crystallinity products and limited control over morphology and crystal size.
Room temperature synthesis	Low cost, low energy consumption, and low carbon footprint.	Slow synthesis rates, potential high defects, and impurities.
Ionic liquid synthesis	High-stability products and safety.	High toxicity, high cost, and low solubility.
Renewable resources	Low-cost and environmentally friendly sources.	High manufacturing costs and limited availability and variability.

(v) renewable resources, the method employs sustainable feedstocks, minimizing their environmental impact at the end of their lifecycle. The main advantages and disadvantages of these methodologies are listed in Table 1.

Hydrothermal synthesis

It is a method for crystallizing MOF materials in underwater solutions by applying high temperature and vapor pressure. The hydrothermal methodology follows the same principle as the solvothermal synthesis. However, in this case, the primary solvent is water. A stainless-steel autoclave is usually used as a sealed container, where a Teflon liner is placed with the reaction solutions. The reaction conditions are different for each material, using high temperatures (130–250°C) and high vapor pressure (0.3–4 MPa).[55]

The synthesis of Zn-BTC material was reported using a hydrothermal method.[56] Zinc acetate salt (1.5 mmol) and BTC ligand (1.0 mmol) were employed. Both chemicals were dissolved using water (10 mL) as a solvent at room temperature. Then, the solution was transferred into a 25-mL autoclave and heated at 120°C for 48 h. After this, the powder was washed with distilled water and hot ethanol. This green synthesis path improves the electrochemical pseudocapacitance performance of P-type conductive polymer. Usually, Zn-BTC is synthesized using DMF as a solvent. Park et al.[57] reported the hydrothermal synthesis of three Zn-BDC (BDC, 1,4-benzenedicarboxylic acid) with 1,2,4-triazole-based MOF materials. Triethylamine (TEA) and butanol (BuOH) were used as modulators in the reaction with water. Nikmehr et al.[58] reported a Zn-MOF using cyanoguanidine as a ligand. A zinc sulfate and cyanoguanidine solution in water (1–3 M) was employed. The reaction was conducted at 80°C for 20 h. Zn-MOF powder was filtered and washed with DMF, water, and ethanol several times.

Yaghi et al.[59] reported an Al(III)-MOF called MOF-303 via hydrothermal synthesis, which is highly stable in water conditions.[60] Different green synthesis approaches have been reported in order to increase the MOF yield. In a typical synthesis, 375 mg of 3,5-pyrazole carboxylic acid (PZDC) linker and 520 mg of $AlCl_3{\cdot}6H_2O$ were stirred with 36 mL of water under vigorous shaking for 1 h. After that, a 1.5 mL solution with 130 mg of NaOH was added drop by drop to the solution under agitation until completely dissolved. Finally, the solution was transferred to a 75-mL autoclave and placed in an oven at 100°C for 24 h. However, this synthesis route shows a low yield (35%). A reflux synthesis of MOF-303 was performed to increase the yield ratio. Approximately 1.74 g of PZDC and 1.2 g of NaOH were dissolved in a flask using 50 mL of deionized water. Separately, a solution of 2.41 g of $AlCl_3{\cdot}6H_2O$ in 50 mL of deionized water was prepared. After that, the metal solution was added to the linker solution under constant stirring dropwise at 1 mL min^{-1}. Then, the reaction mixture was heated to 120°C using an oil bath under reflux for 2 h, displaying a 94% yield. A vessel synthesis was conducted for large-scale MOF-303 production. In a 200-L reaction vessel, 45 L of deionized water was added, and 2.4 kg of NaOH was incorporated into the reactor slowly. After that, 3.48 kg of PZDC was mixed for 30 min until the solution dissolved. Separately, 4.82 kg of $AlCl_3{\cdot}6H_2O$ was dissolved in 15 L of deionized water and added slowly to the linker solution at a rate of 1 mL min^{-1}. The reaction mixture was heated to 120°C with a reflux for 6 h, showing a 91% yield. In addition, the microwave synthesis was performed for MOF-303. The linker, the inorganic base, and water were dissolved in a 20-mL scintillation vial. Separately, $AlCl_3{\cdot}6H_2O$ was dissolved and added to the first solution. The solution was transferred into a Pyrex pressure reaction vessel and heated at 120°C at 300 W while stirring in a microwave reactor for 5 min. Thus, MOF-303 was washed with water and methanol several times. These green methodologies decrease the time for synthesis to only 5 min (microwave synthesis), improving the applicability to the industrial sector due to the use of water harvesting.

Furthermore, MIL-100(Fe) was synthesized via the hydrothermal method under acid conditions, employing the BTC ligand.[61] In this case, a molar ratio Fe:BTC: HNO_3: H_2O of 1: 0.67:0.6:166 was used for the synthesis. The reagents were mixed and transferred to a Teflon autoclave, which was placed in an oven and heated at 150 °C for 12 h. Then, MIL-100(Fe) powder was purified by soaking it in water at 80°C for 1 h and in ethanol at 60°C for 3 h. The material was applied as a drug delivery platform for isoniazid, displaying adequate biocompatibility and reasonable and controlled drug release kinetics. Peh et al.[62] reported

12295949, 2025, 3, Downloaded from https://onlinelibrary.wiley.com/doi/10.1002/bkcs.70005 by Universidad Autonoma Metropolitana, Wiley Online Library on [30/06/2025]. See the Terms and Conditions (https://onlinelibrary.wiley.com/terms-and-conditions) on Wiley Online Library for rules of use; OA articles are governed by the applicable Creative Commons License

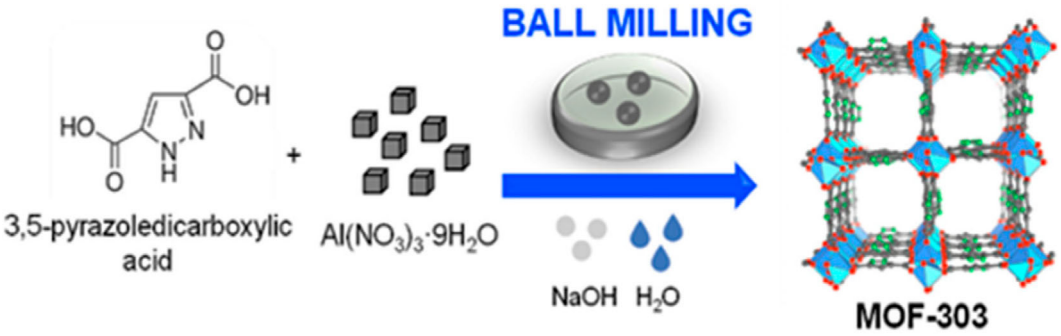


FIGURE 5 Scheme illustrating the mechanochemical synthesis of MOF-303. C—gray, N—green, O—red, Al—blue polyhedra. (Reprinted with permission from ref. 68 Copyright 2024 MDPI Creative Commons Attribution-NonCommercial License 4.0 (CC BY-NC).

the hydrothermal synthesis of Zr-MOF with BDC and functional X-BDC, where X = H, NH_2, NO_2, Br, and F_4. In the synthesis, 0.3 mmol of $ZrOCl_2{\cdot}8H_2O$ was dissolved in 2 mL of water. Then, the solid ligand was introduced into Teflon liners. For H, NH_2, NO_2, Br, and F_4, 0.3, 0.6, 0.5, 0.5, and 0.6 mmol of the linker and 175, 90 120, 120, and 175 equivalents of acetic acid were used, respectively. In all cases, sealed autoclaves were kept in a preheated isothermal oven at 120°C for 24 h for NH_2-BDC and at 150°C for 20 h for the other MOFs. After that, the powders were washed with water and methanol.

Mechanochemical synthesis

The synthesis uses a mechanochemical reaction performed in mortar grinders and mills: planetary (ball), mixer (shaker), cryo-mill, drum, and extruder. The reaction synthesis is conducted via chemical transformations caused by mechanical stress, compression, or friction, avoiding the use of high amounts of solvents.[63]

Julien et al.[64] reported the synthesis of Zn-MOF-74 from metal oxide and without bulk solvent, employing a mechanochemical milling approach. In the synthesis, 220 mg (1.1 mmol) of 2,5-dihydroxyterephthalic acid and 180.7 mg of ZnO (2.2 mmol) were placed in separate halves of the PMMA milling vessel. Also, water (250 μL) and DMF (250 μL) were used as grinding liquids. The reaction mixture was milled for 45 minutes. This route enables the achievement of a fast and efficient gram-scale mechanosynthesis of Zn-MOF-74. The implementation of in situ synchrotron X-ray diffraction suggests that following the mechanochemistry approach, the reaction is driven by two new phases and an unusual stepwise process in which a close-packed intermediate reacts to form the open framework.

Fidelli et al.[65] reported the mechanochemical synthesis of NU- and UiO-type MOFs. NU-901 and UiO-67 were synthesized using a conventional extranuclear zirconium methacrylate precursor.[66] First, an oxo zirconium methacrylate cluster was prepared following the method previously reported. A 1 mL solution of Zr (IV) propoxide (% 70 wt. % 1-propanol solution) (0.73 g) was added to 1 mL methacrylic acid (11.8 mmol), and crystals were grown overnight by evaporation. After that, for NU-901, 0.042 g of H_4TBAPY (4,4′,4″,4‴-(Pyrene-1,3,6,8-tetrayl)tetrabenzoic acid) was added to one half of PTFE milling vessel, followed by 100 μL of DMF and 2 stainless-steel balls (7 mm diameter). Then, the as-prepared Zr cluster was added to the powder mixture and placed in the MM400 mixer mill, with a reaction time of 1 h at a 30-Hz oscillation rate. For Ui-67, the metal cluster (170 mg) and 4,4'-H_2BPA (biphenyl-4,4′-dicarboxylic acid) (145 mg) were placed in a milling jar and gently mixed in a 1:6 molar ratio. Then, 600 μL of DMF was added to the powder mixture in two portions, each 90 min for a total of 180 min. Both Zr-MOFs were washed with DMF at the end. Samal et al.[67] reported a kitchen grinder synthesis approach for MIL-101(Fe). In this synthesis, a mixture of BTC linker (2.63 g) and $Fe(NO_3)2.9H_2O$ (5.08 g) was mixed in a stainless-steel kitchen grinder jar with 5 mL of 0.4 M NaOH. The speed was set at 500 RPM for 1 h. The powder was washed with hot ethanol, hot water, and acetone.

Głowniak et al.[68] reported the mechanochemical synthesis of MOF-303 (Figure 5). A mixture of 3,5-pyrazole carboxylic acid, NaOH, and only 2 mL of water was milled for 10 min. After that, the metal source, in this case, $Al(NO_3)_3{\cdot}9H_2O$, was added and milling for 30 min. A paste was obtained, washed with methanol several times, and dried in air. The material shows an excellent CO_2 adsorption capacity of 9.5 mmol g^{-1} at 0°C and under 1 bar.

Room temperature synthesis

At room temperature, MOF is synthesized by stirring the precursory salt under a solvent mixture. This technique is suitable for rapid synthesis and easy scale-up for large-scale production.[69] The room temperature synthesis was reported for MOF-5 and MOF-74.[70] For MOF-5, the terephthalic acid solution was dissolved in DMF and TEA. After that, the zinc acetate was added to the solution and stirred at room temperature. The reaction was conducted

12295949, 2025, 3, Downloaded from https://onlinelibrary.wiley.com/doi/10.1002/bkcs.70005 by Universidad Autonoma Metropolitana, Wiley Online Library on [30/06/2025]. See the Terms and Conditions (https://onlinelibrary.wiley.com/terms-and-conditions) on Wiley Online Library for rules of use; OA articles are governed by the applicable Creative Commons License

for 2.5 h until a white precipitate formed. In this particular case, the formation of MOF-5 can also be performed without TEA since it was found that the MOF-5 formed after 45 min. Similarly, MOF-74 was synthesized using a zinc acetate salt only by stirring with DMF overnight. The employment of acetate salts led to the formation of basic solutions, where the acetate anion could deprotonate the carboxylic acid of the linkers.

Pakamorė et al.[71] conducted a study for synthesizing at room temperature of NH_2-UiO-66(Zr) underwater solution. Basically, 0.322 g of $ZrOCl_2{\cdot}8H_2O$ was dissolved in 3 mL of water with a determinate amount of acetic acid. Then, a disodium amino terephthalate solution was added to form a yellow mixture. Next, the solution was gently stirred at ambient temperature at different times. In this study, the acetic acid concentration varied from 0.25 to 4 mL, and the reaction synthesis was from 1 to 168 h. The primary pathway reaction was the inorganic building blocks in aqueous media by employing sodium salts instead of protonated acids, which increased the linker concentration and the solubility. Finally, NH_2-UiO-66(Zr) was washed with water and ethanol several times. In a similar approach, Huelsenbeck et al.[72] reported a high-speed room temperature UiO-66(Zr) synthesis by varying the pH value. A metal ion and linker solution were prepared separately. A 10 mL of linker solution was placed in a 50-mL conical centrifuge tube, and the pH value was adjusted with 20 M NaOH or 37 wt.% HCl, employing water to achieve a total volume of 13.5 mL. Then, a metal solution (10 mL) was mixed and stirred in a centrifuge at 12000 rpm for 5 min. The precipitate was placed in an oven at 70°C for a minimum of 8 h and washed with a 0.01 M HCl solution, 0.001 M NaOH solution, DMSO, and methanol to remove unreacted and soluble precipitate components. Interestingly, the rapid synthesis enables cotton coating with up to 20 wt % UiO-66-NH_2 using a sequential dip-coating (SQD) technique, showing a particulate matter (PM_{1-4}) filtration of up to 85%.

Huang et al.[73] reported the room temperature synthesis of NH_2-MIL-101(Fe). A first solution was prepared by dissolving various molar ratios (0:1, 1:1, 1:2, 1:3, and 1:0) of BDC and NH_2-BDC (3.95 mmol) in 8.32 g of 1 M aqueous NaOH and stirred for 5 min. Then, 2.135 g of $FeCl_3{\cdot}4H_2O$ was dissolved in 48.6 mL of water. The solutions were mixed and stirred vigorously at room temperature for 24 h. The powder was washed several times with double distilled water and ethanol. The material shows an improvement in the reduction reaction and Fe(III)/Fe(II) cycle, which increased the degradation of bisphenol A in water. Furthermore, MIL-53 (Al) was synthesized using a salt linker precursor at room temperature to increase the solubility of the linker.[74] A solution of 8.4 g of disodium terephthalate (Na_2BDC) in 57.6 mL of water was mixed with a metal solution composed of 30 g of $Al(NO_3)_3{\cdot}9H_2O$ in 57.6 mL of water, and it was stirred at room temperature for 7 days. The powder was washed with water several times.

Ionic liquid method

Ionic liquids are a technique for MOF synthesis. It uses salts that melt below 100°C, polar and non-polar components that contribute to the formation of microemulsions, and a surfactant that decreases the surface tension.[75]

Ye et al.[76] reported Zn-BTC synthesis using ionic liquid microemulsions stabilized by the surfactant TX-100 under room temperature. First, an ionic liquid was synthesized, where 1-butyl-3-methylimidazolinium chloride (30.14 g, 0.172 mol) and an excess of KPF_6 (37.98 g, 0.206 mmol) were stirred underwater (150 mL) at room temperature for 12 h. Then, a microemulsion was formed using the surfactant TX-100. After that, $Zn(NO_3)_2{\cdot}6H_2O$ (1.0 mmol), NaOH (1.0 mmol), and BTC (1.0 mmol) and the microemulsion were mixed and stirred at room temperature for 24 h. Dang et al.[77] reported a template strategy via room temperature synthesis of Zn-BDC. The route was followed by stirring two separate solutions. First, 7.2 mmol ZnO powder was dispersed in 36 mL of DMF and 16 mL of water under sonication for 30 min. Then, 14.4 mmol of zinc nitrate hexahydrate was dissolved in 36 mL water. Both solutions were mixed. After that, the surfactant (7.2 mmol of cetyltrimethylammonium bromide (CTAB)) and the organic linker (10.8 mmol of BDC) were dissolved in 32 mL ethanol. Finally, the metal and organic solutions were mixed under fast magnetic stirring for 1 minute and then allowed to stand for 5 min. This technique enables the synthetization of MOF materials in a short period.

Sang et al.[78] reported the ionic liquid synthesis of UiO-66(Zr) in 1-octyl-3-methylimidazolium chloride ([Omim]Cl), where $ZrOCl_2{\cdot}8H_2O$ (0.4 mmol) and BDC (0.4 mmol) were added into 10 mL [Omim]Cl, followed by the addition of acetic acid (3 mL), and stirring at room temperature for 1 h. The ionic liquid accelerates the crystallization of the material, displaying a small particle size with missing linker defects and a large surface area, which can be applied as heterogeneous catalysts for the Meerwein–Ponndorf–Verley reaction. Seoane et al.[79] reported an Al-MOF synthesis in the presence of surfactants. Generally, 0.844 g of $Al(NO_3)_3{\cdot}9H_2O$ was dissolved in 15 mL of distilled water. In another solution, 0.331 g of BTC and CTAB (cetyltrimethylammonium bromide) were dissolved in 15 mL of ethanol. Then, both solutions were mixed and stirred for 30 min; after that, the solution was transferred to a lined stainless-steel autoclave and heated at 120°C for 12 h under static conditions. The powder was washed with fresh ethanol. Under this condition, the Al-MOF could only be synthesized at pH 2.1. Liu et al.[80] reported that Fe-MOF synthesis uses PVP as a surfactant. For this, $FeCl_3$ (300 mg), NH_2-BDC (1100 mg), and 0–16 g of PVP (0, 2, 4, 8, and 16 g) in a solution (73 mL) of DMF and water were dissolved. A Teflon autoclave was used at 115°C for 3 h. The powder was washed with anhydrous ethanol and DMF several times. The change in water concentrations in the solvent and the amount of the PVP surfactant enables the controlling of the size of the MOF crystals over 344–5.14 μm, while the aspect ratio of the crystals can be varied widely over 1.0–7.1.

12259549, 2025, 3, Downloaded from https://onlinelibrary.wiley.com/doi/10.1002/bkcs.70005 by Universidad Autonoma Metropolitana, Wiley Online Library on [30/06/2025]. See the Terms and Conditions (https://onlinelibrary.wiley.com/terms-and-conditions) on Wiley Online Library for rules of use; OA articles are governed by the applicable Creative Commons License

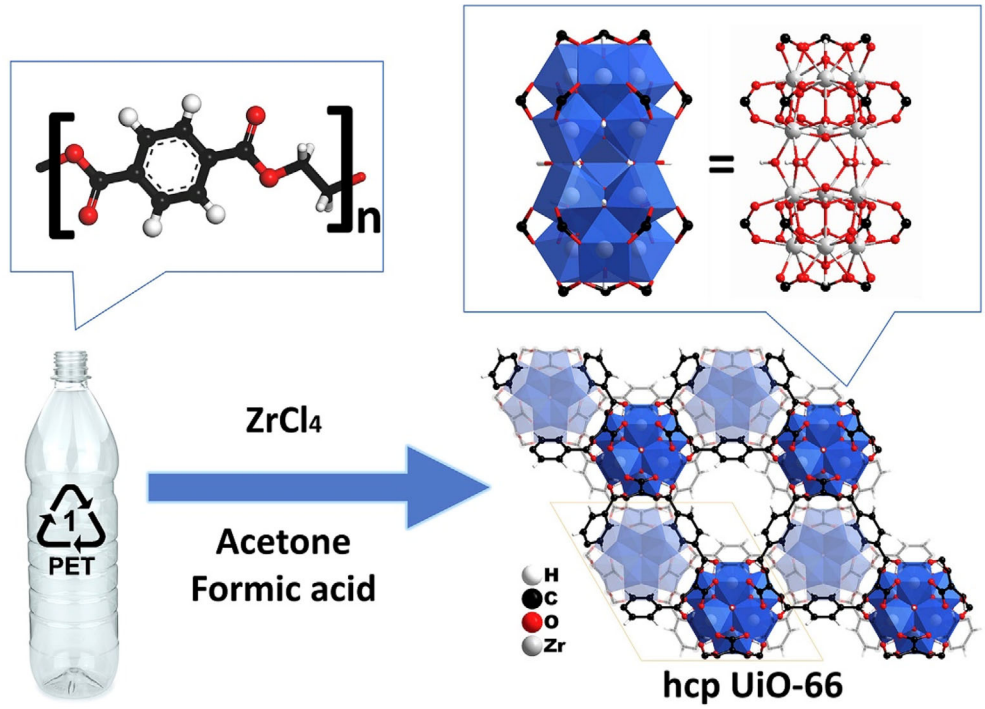


FIGURE 6 Schematic representation of the strategic employment of waste PET bottles for the green direct synthesis of Zr_{12} cluster-based hcp UiO-66 (Reprinted from ref. 83 Copyright 2019 with permission from Elsevier.).

Renewable resource synthesis

The renewable resource synthesis of MOF materials is based on using specific renewable resources as the starting reagent for the organic linker synthesis. In this sense, the waste material generation can be avoided.[81]

Dreischarf et al.[82] reported the synthesis of a Zr-CAU-28 using 2,5-furandicarboxylic acid (FDC) as the organic linker. Interestingly, this linker is categorized as a bio-renewable organic building unit. Generally, the linker can be synthesized from sugars, which are facilely available from biomass. Glucose and fructose can be dehydrated to 5-hydroxylmethylfurfural and then oxidized to FDC. In this case, 45 mg (0.28 mmol) of FDC, 60 mg (0.19 mmol) of $ZrOCl_2{\cdot}8H_2O$, 700 μL of acetic acid, and 800 μL of water were mixed. The reaction occurs in a microwave oven at 80°C for 1 h. Similarly, UiO-66(Zr) was synthesized using poly(ethylene terephthalate) waste as a linker (Figure 6).[83] Exactly, 105 mg of $ZrCl_4$, 75 mg of bottle chips from a PET package of "Evian natural spring water" without further purification, 3 mL of formic acid, and 3 mL of acetone were mixed and placed in a 25-mL Teflon-lined steel autoclave. The reaction was heated in an oven at 160°C for different times (12, 18, 24, 30, and 36 h, respectively) to monitor their progress. The powder was washed with DMF and methanol. By breakthrough experiments, the material shows good performances for separating benzene/cyclohexane due to a competitive adsorption process.

Deleu et al.[84] reported the synthesis of MOF using waste PET bottles as a raw material for the BDC linker. PET contains up to 85 wt% of BDC linker in its composition. PET material was hydrolyzed in a Milestone Ethos Microsynth microwave oven for this. PET chips (1.5 × 1.5 cm) were cut out of PET bottles, and the surface was exposed to 7 M nitric acid under reflux conditions for 1 h. Then, MIL-53(Al) was synthesized in a Schott bottle containing $AlCl_3{\cdot}(H_2O)_6$, H_2O, NaOH, and BDC. The mixture was heated in an oven at 100°C for a week. In a similar approach, MOF-5 was synthesized using PET waste.[85] First, the alkalosis of PET (6 × 6 mm, 2 g) was performed with 5 mL of ethylene glycol in a domestic microwave oven for 5 min. The linker was precipitated in two steps using 2 M H_2SO_4 and 0.1 M NaOH. This linker was used to prepare MOF-5.

MOF APPLICATIONS FOR DRIVING SUSTAINABILITY

MOF materials have been applied in a wide range of applications (Figure 7), such as (*i*) water treatment, (*ii*) sensing, (*iii*) drug delivery, (*iv*) catalysis, and (*v*) gas storage.

Water treatment

Water treatment has gained interest all over the world. Since water pollution has developed proportionally with the industry, several anthropogenic activities contributed significantly to water pollution overall.[86] Water pollutants

12259949, 2025, 3, Downloaded from https://onlinelibrary.wiley.com/doi/10.1002/bkcs.70005 by Universidad Autonoma Metropolitana, Wiley Online Library on [30/06/2025]. See the Terms and Conditions (https://onlinelibrary.wiley.com/terms-and-conditions) on Wiley Online Library for rules of use; OA articles are governed by the applicable Creative Commons License

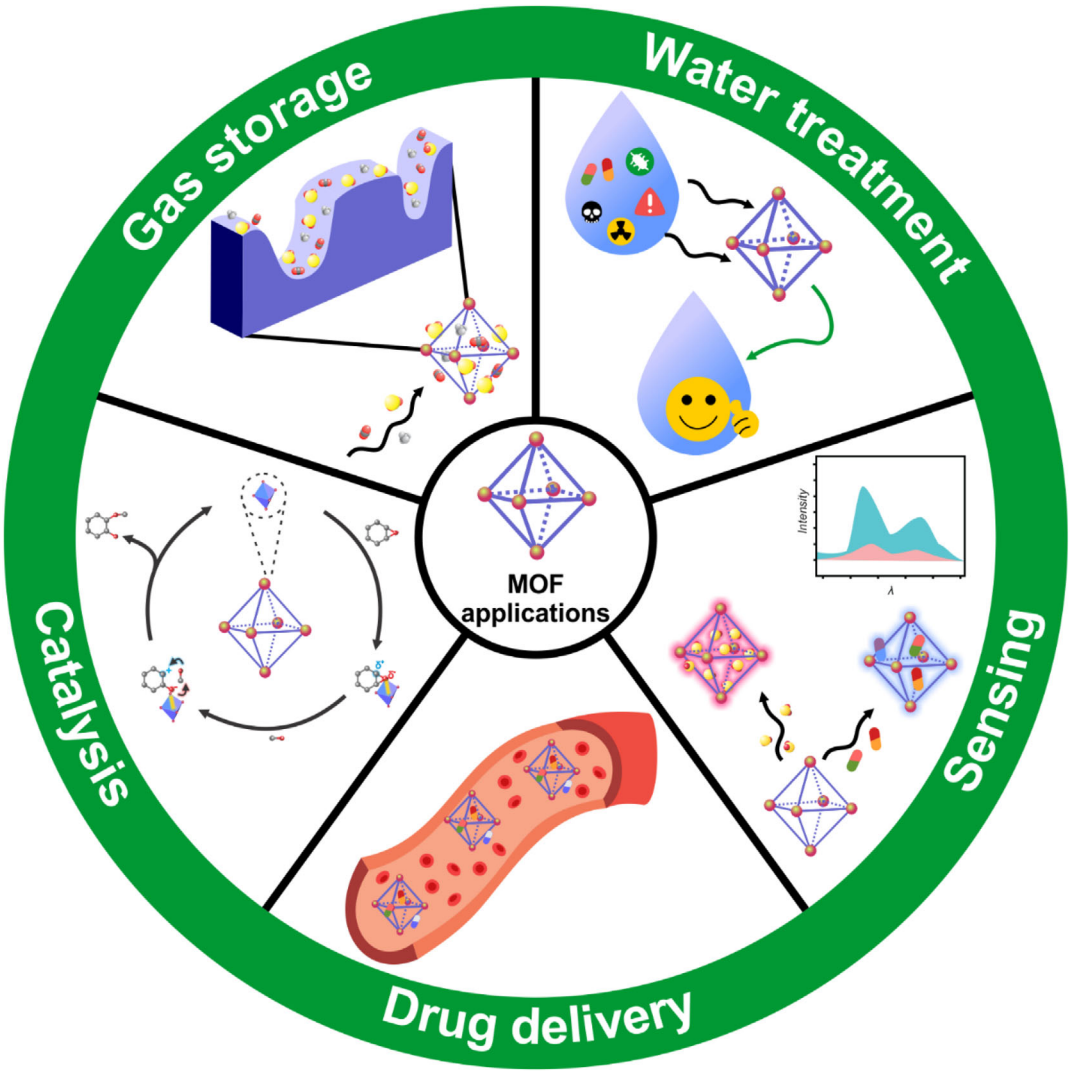


FIGURE 7 Schematic representation of the outstanding applications for low-toxicity metal-organic framework (MOF) materials.

can be classified into two groups: conventional pollutants, which are regulated and monitored by governments (heavy metals, nutrients, and organisms, among others), and emerging pollutants (EPs), which are in contrast to the conventional, are not controlled, and their effects are not fully understood (pharmaceuticals, personal care products, perfluorinated compounds, and hormones).[87] These contaminants are introduced into the wastewater by releasing organic matter from domestic use, that is, through the discharge of gray water. Thus, different methods have been employed to remove several pollutants from water. The green synthesis MOFs provide free hazardous organic solvent materials for removing diverse water pollutants.

Occasionally, the same MOF can handle more than one pollutant species. This can be observed in MIL-88(Fe) for the effective and fast photocatalytic degradation of tetracycline in 90 min, with high reusability; additionally, it possesses high adsorption capacity rates for the direct red 80 dye removal.[88] Another example of this is the low-cost UiO-66(Zr), which, through adsorption, removes methylene blue, Pb^{2+}, and Cd^{2+} from water, obtaining Langmuir adsorption capacities of 37, 169, and 100 mg g^{-1}, respectively.[89] Green synthesis MOF-based hybrid materials can also be employed, reaching high adsorption capacity and efficient adsorption time. The DE-Al-MOF reaches a removal efficiency of 98.13% within 15 min of adsorption, obtaining a maximum adsorption capacity of 181.82 mg g^{-1}.[90] In adsorption, the functionalized surface improves the interactions between ionic pollutants, such as several dyes. The electrostatic interactions are promoted between the negatively charged surface of the microporous cubic CZM(Zn) MOF and the cationic malachite green dye, reaching a maximum adsorption capacity of 953.14 mg g^{-1}.[91] Microfiltration is also employed with excellent removal performance. The result of the modified membrane of polytetrafluoroethylene (PTFE) and ZIF-8(Zn) shows a 40% increment in the removal of progesterone, in contrast to the unmodified one. Similar to the adsorbents, the PTFE-ZIF-8 membrane possesses excellent reusability, maintaining a 95% removal efficiency after three generation cycles.[92]

12259949, 2025, 3, Downloaded from https://onlinelibrary.wiley.com/doi/10.1002/bkcs.70005 by Universidad Autonoma Metropolitana, Wiley Online Library on [30/06/2025]. See the Terms and Conditions (https://onlinelibrary.wiley.com/terms-and-conditions) on Wiley Online Library for rules of use; OA articles are governed by the applicable Creative Commons License

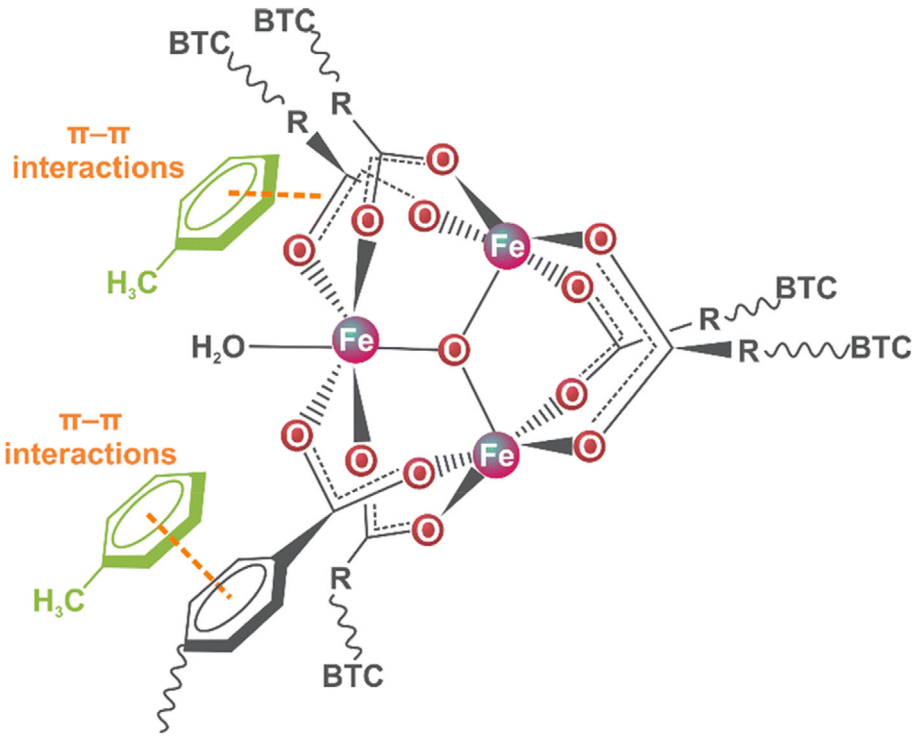


FIGURE 8 Possible adsorption mechanism for toluene adsorption using MIL-100(Fe). (Reprinted with permission from ref. 100 Copyright 2024 Royal Society of Chemistry under a Creative Commons Attribution 3.0 Unported License).

Flores et al.[93] reported a bimetallic ZnCu-MOF-74, which was synthesized at room temperature and applied in the tetracycline removal from water. Tetracycline is a widely used antibiotic pharmaceutical because it has been found in high concentrations in various sources of water. ZnCu-MOF-74 has a maximum adsorption capacity of 775 mg g^{-1}. The material shows high thermal stability, over 200°C, and chemical stability, with a 4–8 pH solution stability.

Another EP that has raised concerns about its pollution is microplastics (MPs). MPs are derived from larger plastics due to fragmentation through diverse mechanisms, such as UV, mechanical, and microbial.[94] Problems generated by MPs are not limited to environmental effects but are also related to public health. Numerous investigations identified the presence of MPs in human organs and body fluids, organs such as the liver, blood, heart, placenta, breast milk, semen, and urine.[95] Due to multiple characteristics, such as high surface area, porosity, and functionalization, MOFs are feasible for compound implementation that eases their application in pollutant removal from water. An example is the development of magnetic metal–organic frameworks, such as Fe_3O_4@MIL-53(Al), employed for the multiple pollutant remediation, bisphenol a, tetracycline, congo red, and methylene blue.[96] Fe_3O_4@MIL-53(Al) exhibits outstanding Langmuir maximum adsorption of 205 mg g^{-1} for bisphenol A; in addition, 78.9, 148.8, and 179.5 mg g^{-1} for tetracycline, methylene blue, and congo red, respectively. After adsorption, following the addition of Fe_3O_4 magnetic particles, they were quickly separated by an external magnetic field.

Furthermore, pollutants with complex and stable structures need facile and standardized methods for detection and quantification from aqueous media. Volatile organic compounds are chemical compounds that quickly evaporate at room temperature and atmospheric pressure and possess poor solubility in water.[97] As a result, highly toxic compounds such as aromatic hydrocarbons, benzene, toluene, and xylenes have been detected in natural water sources worldwide.[98] Thus, researchers investigate methods for removing VOCs from water and suitable methods for quantifying VOCs. Among the MOFs extensively employed in water treatment are the Materials of Institute Lavoisier (MIL) family due to their high stability in water.[99] MILs have numerous MOFs containing low-toxicity metal centers, such as Fe, Al, and Ni, and low-cost organic ligands, such as terephthalic and trimesic acid. Therefore, MIL-100(Fe) and gas chromatography combined with liquid–liquid extraction successfully adsorbed and determined toluene from water.[100] Besides achieving a Langmuir maximum adsorption of 318 mg g^{-1}, they found that MIL-100(Fe) can be repeatedly used with negligible loss in adsorption capacity. The adsorption interaction was proposed using FTIR and XPS analysis (Figure 8). The toluene molecule could enter the MIL-100(Fe) pore and interrelate via π–π interaction with the organic linkers. The toluene quantification was through small-volume liquid–liquid extraction and conventional gas chromatography coupled with a flame ionization detector.

12295949, 2025, 3, Downloaded from https://onlinelibrary.wiley.com/doi/10.1002/bkcs.70005 by Universidad Autonoma Metropolitana, Wiley Online Library on [30/06/2025]. See the Terms and Conditions (https://onlinelibrary.wiley.com/terms-and-conditions) on Wiley Online Library for rules of use; OA articles are governed by the applicable Creative Commons License

Furthermore, MOF materials and advanced detection methods are promising techniques for improving the removal of traditional pollutants and developing methods for EPs.

Sensing

Sensing applications using MOF materials are highly interesting due to their properties. In the environment, pollutant detection has increased due to the continuous discharge of contaminants. Due to this, the modulated selectivity adsorption of MOFs is advantageous in developing pollutant detectors in water and air.[101] Selectivity results from the diverse controlled pore sizes that limit the adsorption of specific molecules, in addition to the ligand's functionalization. This modification introduces specifics-controlled interaction sites. Various MOFs, including green synthesis MOF, are employed in a broad range of detection sensors. Detecting environmental contaminants improves people's quality of life and preserves the environment. Through early and accurate detection, it is possible to implement remediation measures to protect the environment.[102] An appropriate detection method is characterized by high and precise sensitivity, practicality, simplicity, low cost, and efficiency. Among the detection methods for pollutants that can be found are luminescence, mass change, and electrochemical methods. The luminescence method uses fluorescent materials, including MOFs. The MOF luminescence is due to the metal centers; however, in other cases, it is due to the nature of the organic ligands. The detection of heavy metals, As^{5+} and Cr^{6+}, by luminescence has been possible through Al-MOF1.[103] The limit of detection (LOD) achieved is below 50 ppb of these metals in water. Besides showing a high adsorption capacity of As (71.9 mg g^{-1}) and a fast equilibrium time (1 min), it has a unique stability in the range of 2–12 pH, far above other MOFs such as MIL-53(Al) and high selectivity in the presence of different anions. Moreover, for Cr^{6+}, at neutral pH, it has a high adsorption capacity of 124.5 mg g^{-1}. Due to its low surface area and small pore size, electrostatic interactions occur between the positively charged external surface and the oxo anions.

A wide variety of contaminants are found in water. Some are particularly dangerous, such as picric acid (PA), a high-explosive contaminant. Zn-MOF, by fluorescence, showed selective sensing in water. In the presence of other compounds, such as nitro-compounds (p-NP, m-NA, o-NP, and 2,4-DNPH), metal ions (Na^{+}, K^{+}, Zn^{2+}, Cd^{2+}, Co^{2+}, Ni^{2+}, Mg^{2+}, Pb^{2+}, Ag^{+}, Sr^{2+}), $KMnO_4$, $K_2Cr_2O_7$, and paraquat, the fluorescence shift intensity is less than 0.1, displaying a high detection sensitivity of 340 nM.[104] For nitrobenzene detection, a comparison of stilbene ligand-based metal–organic frameworks was conducted. $Zn_3(SDC)_3(bpy)$ and Zn(SDC)(bpy)·2DMF were reported, displaying a quenching efficiency with a low detection limit of 14.28 and 25.42 μM, respectively.[105]

In addition to conventional pollutants, highly harmful and toxic agricultural products used in agriculture are also found in the water. Glyphosate, a widely applied herbicide, is the most commonly used herbicide in the world. Zr-MOF shows a high affinity with the phosphate groups of glyphosate due to the contained Zr-OH group, resulting in high selectivity and adsorption. It shows easy separation due to the integration of Fe_3O_4 in its structure. A low LOD of 0.093 mg L^{-1} was achieved by fluorescence.[106] Robust sensors are required to detect toxic gases in the environment. Therefore, electrical detection is suitable since its simplicity and high compatibility with ordinary electrical devices allow it to be used in various applications. Iodine, a gas from sea spray, has been detected through resistance change in the MFM-300 family of MOFs by impedance spectroscopy. The MFM-300 (Al) demonstrated a higher resistance. Moreover, the MFM-300(Fe) showed high adsorption stability and resistance change over five cycles.[107]

Drug delivery

Drug delivery is associated with drug species' controlled loading and release to treat diseases. Simple and low-cost MOFs can be employed for drug delivery. Horcajada et al.[108] reported MIL-53(Fe) loaded with ibuprofen by impregnation. Chemical analysis, by UV–vis spectroscopy, TGA, and X-ray fluorescence (XRF) analysis, indicated adsorption of 20 wt% of ibuprofen. DFT simulation made it possible to determine the location of ibuprofen molecules in the MIL-53(Fe) structure, resulting in one molecule per pore. HPLC determined the release time of ibuprofen in a simulated body fluid. It was found to have a slow release, reaching complete release after 3 weeks. Due to the flexibility of the material and pore size, zero-order drug release kinetics were obtained.

Abanades et al.[109] employed the biocompatible UiO-66(Zr) modulated for the loading and release of four different drugs, dichloroacetic acid (DCA), 5-fluorouracil, alendronate (5-FU), α-cyano-4-hydroxycinnamic acid (α-CHC), distributed in the MOF through coordination with the metal center. The loading of the drugs was achieved by one-pot syntheses in a process called MTV modulation. The percentage of loading achieved for each drug was 11.0% (DCA), 1.6% (5-FU), 2.0% (α-CHC), and 27.5% (AL) (w/w). Aghazadeh et al.[110] fabricated Al-MOF/GO composites, achieving 78.4% and 65.7% loading of 5-Fu and doxorubicin (DOX). For drug delivery, Al-MOF/GO was encapsulated in chitosan (CS) due to its high biocompatibility, biodegradability, and high content of amino groups, which are attributed to a pH dependence observed in the drug delivery. After 30 days, a 71.2% biodegradation of the drug-loaded capsule was achieved. El-Bindary et al.[111] evaluated ZIF-8(Zn) for loading and distribution of DOX on the viability of human breast and liver cancer cell lines. Similar to Al-MOF/GO, DOX release

12259849, 2025, 3, Downloaded from https://onlinelibrary.wiley.com/doi/10.1002/bkcs.70005 by Universidad Autonoma Metropolitana, Wiley Online Library on [30/06/2025]. See the Terms and Conditions (https://onlinelibrary.wiley.com/terms-and-conditions) on Wiley Online Library for rules of use; OA articles are governed by the applicable Creative Commons License

was influenced by pH, releasing a higher percentage, 65%, at 12 days than at higher pH. By UV–vis, it was possible to determine the amount of DOX released. In addition, the antibacterial activity was analyzed by the agar well diffusion method. The results showed that the DOX-loaded ZIF-8 has effective antibacterial activity.

Catalysis

Catalyst in MOF chemistry is widely employed because MOF materials possess catalytic sites required during a catalysis process. An example of this is MOF-184(Zn) for CO_2 cycloaddition. Tran et al.[112] reported that through interaction with acetonitrile vapor via ATR-FTIR, it was possible to determine the strongest Lewis acidity derived from Zn cations. This strong acidity is related to the high catalytic activity upon the cycloaddition of CO_2 with the highest catalytic performance in the formation of styrene carbonate with highly epoxide conversion (96%), selectivity (85%), and yield (82%) in a solvent-free environment at 80°C for 6 h. Then, Fe-BTC was employed to reduce oxygen and evolve reactions.[113] Using an alkaline electrolyte, the biocatalytic activity was evaluated by cyclic voltammetry and rotating disk electrode voltammetry. Fe-BTC performed well due to its high surface area, numerous unsaturated metal centers, and high microporosity. Fe-BTC offers a practical, low-cost, environmentally friendly catalyst for the rechargeable lithium–air battery. Mautschke et al.[114] performed Meerwein–Ponndorf–Verley (MPV) reduction of carbonyl compounds using MOF-808(Zr), synthesized from a mixture of tricarboxylate ligands with dicarboxylate ligands. This replacement improved the catalytic activity of MOF-808 because of less hindered Zr open metal sites, which favor the formation of the 6-membered cyclic transition state. Compared to the UiO-66, the synthesized MOF-808 showed better performance. This is because the MOF-808 exhibits more Zr^{4+} sites available for interaction. Also, MIL-53(Al) was applied for Friedel–Crafts alkylation of benzene with ethanol in a gas phase reaction.[115]

Gas storage

Gas storage is one of the most critical aspects of energy chemistry and materials. The design of MOFs for gas storage is through the modulation of hydrophilicity, pore architecture, functionalization, and pore size. MOFs are employed as an alternative for storing and separating methane, acetylene, hydrogen, and carbon dioxide in the chemical industry.[116] MOFs can be modulated in several methods (including exposure of open metal sites, functional group modification, tunable pores, construction of flexible structures, and framework interpenetration) to improve thermal equilibrium, kinetic effects, and molecular sieving—factors that regulate gas storage and separation. The gas adsorption applications focus on N_2, CO_2, H_2, and CH_4.[117]

CONCLUSION AND PERSPECTIVE

MOFs are multidisciplinary emergent materials that possess a large surface area, combined with the robustness of these materials aimed at different applications, such as gas storage, water treatment, catalysis, drug delivery, and sensing. Nevertheless, while these characteristics are important for their potential use, ensuring minimum environmental impact is another key factor to consider. Thus, the low-toxicity MOF development and production has recently attracted a growing interest. Various MOFs synthesized through more friendly methods, such as hydrothermal, mechanochemical, room temperature, ionic liquid, and renewable sources, exhibit enhanced characteristics that lead to efficient use of these MOFs in different areas. Renewable resource synthesis offers low-cost sources and the opportunity to use environmental waste, such as PET bottles and other polymer sources, to produce high-quality MOFs. In the present review, we present, besides synthesis methods, low-toxicity metallic centers, such as Zn, Zr, Al, and Fe. Overall, low-toxicity MOF materials can be postulated as candidates for environmental remediation in general and can be used in an industrial way to solve problems of everyday life.

ACKNOWLEDGMENTS

J.L.O. and C.V.F. thank CONACYT for the Ph.D. fellowship (1003953, 1040318). C.L. thanks IPN projects (20242829, 20241189, 20231282, and 20232785) and the Laboratorio Nacional de Ciencia, Tecnología y Gestión Integrada del Agua (LNAgua). Open access funding provided by UNAM. Publication cost of this paper was supported by the Korean Chemical Society. [Correction added on 14 March 2025, after first online publication: The Acknowledgment section has been updated in this version.]

ORCID

Juan L. Obeso https://orcid.org/0000-0002-8876-9484
Catalina V. Flores https://orcid.org/0000-0002-4291-9272
Aldo G. Gutiérrez https://orcid.org/0009-0007-2679-7715
Carolina Leyva https://orcid.org/0000-0003-4327-9569
Ricardo A. Peralta https://orcid.org/0000-0001-7573-2968
Ilich A. Ibarra https://orcid.org/0000-0002-8573-8033

REFERENCES

[1] H. Jiang, D. Alezi, M. Eddaoudi, *Nat. Rev. Mater.* **2021**, *6*, 466.
[2] O. M. Yaghi, *J. Am. Chem. Soc.* **2016**, *138*, 15507.
[3] H.-C. ". J.". Zhou, S. Kitagawa, *Chem. Soc. Rev.* **2014**, *43*, 5415.
[4] S. L. James, *Chem. Soc. Rev.* **2003**, *32*, 276.
[5] H.-C. Zhou, J. R. Long, O. M. Yaghi, *Chem. Rev.* **2012**, *112*, 673.
[6] M. Choe, H. Lee, H. C. Choi, *Bull. Korean Chem. Soc.* **2024**, *45*, 584.
[7] G. Lee, S. Oh, M. Oh, *Bull. Korean Chem. Soc.* **2024**, *45*, 67.
[8] K. A. Jannath, M. M. Karim, H. A. Saputra, K. Seo, K. B. Kim, Y. Shim, *Bull. Korean Chem. Soc.* **2023**, *44*, 407.
[9] T. Düren, Y.-S. Bae, R. Q. Snurr, *Chem. Soc. Rev.* **2009**, *38*, 1237.
[10] Y. Lin, C. Kong, Q. Zhang, L. Chen, *Adv. Energy Mater.* **2017**, *7*, 1601296.

12295949, 2025, 3, Downloaded from https://onlinelibrary.wiley.com/doi/10.1002/bkcs.70005 by Universidad Autonoma Metropolitana, Wiley Online Library on [30/06/2025]. See the Terms and Conditions (https://onlinelibrary.wiley.com/terms-and-conditions) on Wiley Online Library for rules of use; OA articles are governed by the applicable Creative Commons License

[11] J. L. Obeso, E. Martínez-Ahumada, A. López-Olvera, J. Ortiz-Landeros, H. A. Lara-García, J. Balmaseda, S. López-Morales, E. Sánchez-González, D. Solis-Ibarra, C. Leyva, I. A. Ibarra, *ACS Appl. Energy Mater.* **2023**, *6*, 9084.
[12] J. L. Obeso, D. R. Amaro, C. V. Flores, A. Gutiérrez-Alejandre, R. A. Peralta, C. Leyva, I. A. Ibarra, *Coord. Chem. Rev.* **2023**, *485*, 215135.
[13] L. Guo, J. Hurd, M. He, W. Lu, J. Li, D. Crawshaw, M. Fan, S. Sapchenko, Y. Chen, X. Zeng, M. Kippax-Jones, W. Huang, Z. Zhu, P. Manuel, M. D. Frogley, D. Lee, M. Schröder, S. Yang, *Commun. Chem.* **2023**, *6*, 55.
[14] K. Yang, F. Xue, Q. Sun, R. Yue, D. Lin, *J. Environ. Chem. Eng.* **2013**, *1*, 713.
[15] J. L. Obeso, J. G. Flores, C. V. Flores, M. T. Huxley, J. A. De Los Reyes, R. A. Peralta, I. A. Ibarra, C. Leyva, *Chem. Commun.* **2023**, *59*, 10226.
[16] H. Kim, S. Yang, S. R. Rao, S. Narayanan, E. A. Kapustin, H. Furukawa, A. S. Umans, O. M. Yaghi, E. N. Wang, *Science* **2017**, *356*, 430.
[17] P. Horcajada, T. Chalati, C. Serre, B. Gillet, C. Sebrie, T. Baati, J. F. Eubank, D. Heurtaux, P. Clayette, C. Kreuz, J.-S. Chang, Y. K. Hwang, V. Marsaud, P.-N. Bories, L. Cynober, S. Gil, G. Férey, P. Couvreur, R. Gref, *Nature Mater.* **2010**, *9*, 172.
[18] J. L. Obeso, A. López-Olvera, C. V. Flores, E. Martínez-Ahumada, R. Paz, H. Viltres, A. Islas-Jácome, E. González-Zamora, J. Balmaseda, S. López-Morales, M. A. Vera, E. Lima, I. A. Ibarra, C. Leyva, *J. Mol. Liq.* **2022**, *368*, 120758.
[19] P. Kumar, A. Deep, K.-H. Kim, *TrAC, Trends Anal. Chem.* **2015**, *73*, 39.
[20] J. Aguila-Rosas, B. A. García-Martínez, C. Ríos, A. Diaz-Ruiz, J. L. Obeso, C. T. Quirino-Barreda, I. A. Ibarra, A. Guzmán-Vargas, E. Lima, *RSC Adv.* **2024**, *14*, 855.
[21] A. U. Czaja, N. Trukhan, U. Müller, *Chem. Soc. Rev.* **2009**, *38*, 1284.
[22] H. Furukawa, K. E. Cordova, M. O'Keeffe, O. M. Yaghi, *Science* **2013**, *341*, 1230444.
[23] M. Safaei, M. M. Foroughi, N. Ebrahimpoor, S. Jahani, A. Omidi, M. Khatami, *TrAC Trends Anal. Chem.* **2019**, *118*, 401.
[24] C. P. Raptopoulou, Materials. **2021**, *14*, 310.
[25] X. Cai, Z. Xie, D. Li, M. Kassymova, S.-Q. Zang, H.-L. Jiang, *Coord. Chem. Rev.* **2020**, *417*, 213366.
[26] S. Kumar, S. Jain, M. Nehra, N. Dilbaghi, G. Marrazza, K.-H. Kim, *Coord. Chem. Rev.* **2020**, *420*, 213407.
[27] J. Fu, Y. Wu, *Chem. – Eur. J.* **2021**, *27*, 9967.
[28] D. Morelli Venturi, F. Campana, F. Marmottini, F. Costantino, L. Vaccaro, *ACS Sustainable Chem. Eng.* **2020**, *8*, 17154.
[29] H. Reinsch, *Eur. J. Inorg. Chem.* **2016**, *2016*, 4290.
[30] E. S. Grape, J. G. Flores, T. Hidalgo, E. Martínez-Ahumada, A. Gutiérrez-Alejandre, A. Hautier, D. R. Williams, M. O'Keeffe, L. Öhrström, T. Willhammar, P. Horcajada, I. A. Ibarra, A. K. Inge, *J. Am. Chem. Soc.* **2020**, *142*, 16795.
[31] T. Friščić, P. A. Julien, C. Mottillo, in *ACS Symposium Series* (Eds: S. O. Obare, R. Luque), American Chemical Society, Washington, DC **2014**, p. 161.
[32] S. S.-Y. Chui, S. M.-F. Lo, J. P. H. Charmant, A. G. Orpen, I. D. Williams, *Science* **1999**, *283*, 1148.
[33] M. K. Bhunia, J. T. Hughes, J. C. Fettinger, A. Navrotsky, *Langmuir* **2013**, *29*, 8140.
[34] N. L. Rosi, J. Eckert, M. Eddaoudi, D. T. Vodak, J. Kim, M. O'Keeffe, O. M. Yaghi, *Science* **2003**, *300*, 1127.
[35] M. Eddaoudi, J. Kim, N. Rosi, D. Vodak, J. Wachter, M. O'Keeffe, O. M. Yaghi, *Science* **2002**, *295*, 469.
[36] J. Winarta, B. Shan, S. M. Mcintyre, L. Ye, C. Wang, J. Liu, B. Mu, *Cryst. Growth Des.* **2020**, *20*, 1347.
[37] M. O'Keeffe, M. A. Peskov, S. J. Ramsden, O. M. Yaghi, *Acc. Chem. Res.* **2008**, *41*, 1782.
[38] T. Islamoglu, K. Otake, P. Li, C. T. Buru, A. W. Peters, I. Akpinar, S. J. Garibay, O. K. Farha, *CrystEngComm* **2018**, *20*, 5913.
[39] V. V. Butova, O. A. Burachevskaya, V. A. Podshibyakin, E. N. Shepelenko, A. A. Tereshchenko, S. O. Shapovalova, O. I. Il'in, V. A. Bren', A. V. Soldatov, *Polymer* **2021**, *13*, 4052.
[40] W. Fan, K.-Y. Wang, C. Welton, L. Feng, X. Wang, X. Liu, Y. Li, Z. Kang, H.-C. Zhou, R. Wang, D. Sun, *Coord. Chem. Rev.* **2023**, *489*, 215175.
[41] I. Senkovska, F. Hoffmann, M. Fröba, J. Getzschmann, W. Böhlmann, S. Kaskel, *Microporous Mesoporous Mater.* **2009**, *122*, 93.
[42] T. Loiseau, C. Serre, C. Huguenard, G. Fink, F. Taulelle, M. Henry, T. Bataille, G. Férey, *Chem. – Eur. J.* **2004**, *10*, 1373.
[43] N. Hanikel, X. Pei, S. Chheda, H. Lyu, W. Jeong, J. Sauer, L. Gagliardi, O. M. Yaghi, *Science* **2021**, *374*, 454.
[44] S. Yang, J. Sun, A. J. Ramirez-Cuesta, S. K. Callear, W. I. F. David, D. P. Anderson, R. Newby, A. J. Blake, J. E. Parker, C. C. Tang, M. Schröder, *Nature Chem.* **2012**, *4*, 887.
[45] Y. Fang, Z. Yang, H. Li, X. Liu, *Environ. Sci. Pollut. Res.* **2020**, *27*, 4703.
[46] F. Millange, N. Guillou, M. E. Medina, G. Férey, A. Carlin-Sinclair, K. M. Golden, R. I. Walton, *Chem. Mater.* **2010**, *22*, 4237.
[47] R. Chen, Z. Yao, N. Han, X. Ma, L. Li, S. Liu, H. Sun, S. Wang, *ACS Omega* **2020**, *5*, 15402.
[48] D. Bara, E. G. Meekel, I. Pakamorė, C. Wilson, S. Ling, R. S. Forgan, *Mater. Horiz.* **2021**, *8*, 3377.
[49] Y. Li, J. Liu, *Analyst* **2020**, *145*, 6753.
[50] M. Kharat, D. J. McClements, *J. Colloid Interface Sci.* **2019**, *557*, 506.
[51] S. Yang, Z. Zhao, Y. Xie, J. Lin, B. Zhang, J. Fan, *Int. J. Pharm.* **2022**, *623*, 121912.
[52] E. Svensson Grape, A. J. Chacón-García, S. Rojas, Y. Pérez, A. Jaworski, M. Nero, M. Åhlén, E. Martínez-Ahumada, A. E. Galetsa Feindt, M. Pepillo, M. Narongin-Fujikawa, I. A. Ibarra, O. Cheung, C. Baresel, T. Willhammar, P. Horcajada, A. K. Inge, *Nat. Water* **2023**, *1*, 433.
[53] M. Huston, M. DeBella, M. DiBella, A. Gupta, *Nanomaterials* **2021**, *11*, 2130.
[54] X.-J. Kong, J.-R. Li, *Engineering* **2021**, *7*, 1115.
[55] W. Chen, L. Du, C. Wu, *Metal-Organic Frameworks for Biomedical Applications* (Ed: M. Mozafari), Woodhead Publishing, Sawston, Cambridge **2020**, p. 141.
[56] H. Mostaanzadeh, M. Shahmohammadi, A. Ehsani, M. Moharramnejad, E. Honarmand, *J. Mater. Sci.: Mater. Electron.* **2021**, *32*, 26539.
[57] H. Park, D. M. Moureau, J. B. Parise, *Chem. Mater.* **2006**, *18*, 525.
[58] S. Nikmehr, M. Kazemzad, M. M. Sabzehmeidani, L. Nikzad, T. Ebadzadeh, M. Mousaei, *Results Chem.* **2023**, *5*, 100973.
[59] Z. Zheng, H. L. Nguyen, N. Hanikel, K. K.-Y. Li, Z. Zhou, T. Ma, O. M. Yaghi, *Nat. Protoc.* **2023**, *18*, 136.
[60] F. Fathieh, M. J. Kalmutzki, E. A. Kapustin, P. J. Waller, J. Yang, O. M. Yaghi, *Sci. Adv.* **2018**, *4*, eaat3198.
[61] M. A. Simon, E. Anggraeni, F. E. Soetaredjo, S. P. Santoso, W. Irawaty, T. C. Thanh, S. B. Hartono, M. Yuliana, S. Ismadji, *Sci. Rep.* **2019**, *9*, 16907.
[62] S. B. Peh, Y. Cheng, J. Zhang, Y. Wang, G. H. Chan, J. Wang, D. Zhao, *Dalton Trans.* **2019**, *48*, 7069.
[63] B. Szczęśniak, S. Borysiuk, J. Choma, M. Jaroniec, *Mater. Horiz.* **2020**, *7*, 1457.
[64] P. A. Julien, K. Užarević, A. D. Katsenis, S. A. J. Kimber, T. Wang, O. K. Farha, Y. Zhang, J. Casaban, L. S. Germann, M. Etter, R. E. Dinnebier, S. L. James, I. Halasz, T. Friščić, *J. Am. Chem. Soc.* **2016**, *138*, 2929.
[65] A. M. Fidelli, B. Karadeniz, A. J. Howarth, I. Huskić, L. S. Germann, I. Halasz, M. Etter, S.-Y. Moon, R. E. Dinnebier, V. Stilinović, O. K. Farha, T. Friščić, K. Užarević, *Chem. Commun.* **2018**, *54*, 6999.
[66] G. Kickelbick, U. Schubert, *Chem. Ber.* **1997**, *130*, 473.
[67] M. Samal, J. Panda, B. P. Biswal, R. Sahu, *CrystEngComm* **2018**, *20*, 2486.
[68] S. Głowniak, B. Szczęśniak, J. Choma, M. Jaroniec, *Molecules* **2024**, *29*, 2698.
[69] N. Stock, S. Biswas, *Chem. Rev.* **2012**, *112*, 933.
[70] D. J. Tranchemontagne, J. R. Hunt, O. M. Yaghi, *Tetrahedron* **2008**, *64*, 8553.
[71] I. Pakamorė, J. Rousseau, C. Rousseau, E. Monflier, P. Á. Szilágyi, *Green Chem.* **2018**, *20*, 5292.

12295949, 2025, 3, Downloaded from https://onlinelibrary.wiley.com/doi/10.1002/bkcs.70005 by Universidad Autonoma Metropolitana, Wiley Online Library on [30/06/2025]. See the Terms and Conditions (https://onlinelibrary.wiley.com/terms-and-conditions) on Wiley Online Library for rules of use; OA articles are governed by the applicable Creative Commons License

[72] L. Huelsenbeck, H. Luo, P. Verma, J. Dane, R. Ho, E. Beyer, H. Hall, G. M. Geise, G. Giri, *Cryst. Growth Des.* **2020**, *20*, 6787.
[73] P. Huang, L. Yao, Q. Chang, Y. Sha, G. Jiang, S. Zhang, Z. Li, *Chemosphere* **2022**, *291*, 133026.
[74] M. Sánchez-Sánchez, N. Getachew, K. Díaz, M. Díaz-García, Y. Chebude, I. Díaz, *Green Chem.* **2015**, *17*, 1500.
[75] M. Hejazifar, O. Lanaridi, K. Bica-Schröder, *J. Mol. Liq.* **2020**, *303*, 112264.
[76] R. Ye, M. Ni, Y. Xu, H. Chen, S. Li, *RSC Adv.* **2018**, *8*, 26237.
[77] Y. T. Dang, M.-H. D. Dang, N. X. D. Mai, L. H. T. Nguyen, T. B. Phan, H. V. Le, T. L. H. Doan, *J. Sci.: Adv. Mater. Dev.* **2020**, *5*, 560.
[78] X. Sang, J. Zhang, J. Xiang, J. Cui, L. Zheng, J. Zhang, Z. Wu, Z. Li, G. Mo, Y. Xu, J. Song, C. Liu, X. Tan, T. Luo, B. Zhang, B. Han, *Nat. Commun.* **2017**, *8*, 175.
[79] B. Seoane, A. Dikhtiarenko, A. Mayoral, C. Tellez, J. Coronas, F. Kapteijn, J. Gascon, *CrystEngComm* **2015**, *17*, 1693.
[80] J. Liu, J. Yang, S. An, M. Wen, X. Wang, R. Gong, Y. Nie, *J. Mater. Sci.: Mater. Electron.* **2022**, *33*, 14228.
[81] L. Halasz, G. Povoden, M. Narodoslawsky, *Resour. Conserv. Recycl.* **2005**, *44*, 293.
[82] A. C. Dreischarf, M. Lammert, N. Stock, H. Reinsch, *Inorg. Chem.* **2017**, *56*, 2270.
[83] L. Zhou, S. Wang, Y. Chen, C. Serre, *Microporous Mesoporous Mater.* **2019**, *290*, 109674.
[84] W. P. R. Deleu, I. Stassen, D. Jonckheere, R. Ameloot, D. E. De Vos, *J. Mater. Chem. A* **2016**, *4*, 9519.
[85] P. Manju, A. Kumar Roy, C. Ramanan, Rajagopal, *Mater. Lett.* **2013**, *106*, 390.
[86] A. Deletic, H. Wang, Engineering. **2019**, *5*, 839.
[87] A. Ahamad, S. Madhav, A. K. Singh, A. Kumar, P. Singh, in *Sensors in Water Pollutants Monitoring: Role of Material* (Eds: D. Pooja, P. Kumar, P. Singh, S. Patil), Springer Singapore, Singapore **2020**, p. 21.
[88] B. Rabeie, N. M. Mahmoodi, *J. Colloid Interface Sci.* **2024**, *654*, 495.
[89] M. N. Nimbalkar, B. R. Bhat, *J. Environ. Chem. Eng.* **2021**, *9*, 106216.
[90] V. Hegde, U. T. Uthappa, O. R. Arvind Swami, S. S. Han, H.-Y. Jung, T. Altalhi, M. D. Kurkuri, *Mater. Today Commun.* **2022**, *32*, 103887.
[91] I. M. El-Sewify, A. Radwan, A. Shahat, M. F. El-Shahat, M. M. H. Khalil, *Microporous Mesoporous Mater.* **2022**, *329*, 111506.
[92] D. Ragab, H. G. Gomaa, R. Sabouni, M. Salem, M. Ren, J. Zhu, *Chem. Eng. J.* **2016**, *300*, 273.
[93] C. V. Flores, A. Machín-Garriga, J. L. Obeso, J. G. Flores, I. A. Ibarra, N. S. Portillo-Vélez, C. Leyva, R. A. Peralta, *Dalton Trans.* **2024**, *53*, 18917.
[94] M. N. Issac, B. Kandasubramanian, *Environ. Sci. Pollut. Res.* **2021**, *28*, 19544.
[95] C. E. Enyoh, A. Devi, H. Kadono, Q. Wang, M. H. Rabin, *Environments* **2023**, *10*, 194.
[96] G. Zhang, R. Wo, Z. Sun, G. Hao, G. Liu, Y. Zhang, H. Guo, W. Jiang, *Nanomaterials* **2021**, *11*, 1917.
[97] Y. Peng, X. Wei, Y. Wang, W. Li, S. Zhang, J. Jin, *ACS Nano* **2022**, *16*, 8329.
[98] R. Lei, Y. Sun, S. Zhu, T. Jia, Y. He, J. Deng, W. Liu, *Molecules* **2021**, *26*, 5988.
[99] S. Qiu, Y. Wang, J. Wan, J. Han, Y. Ma, S. Wang, *Appl. Surf. Sci.* **2020**, *525*, 146511.
[100] C. V. Flores, J. L. Obeso, H. Viltres, R. A. Peralta, I. A. Ibarra, C. Leyva, *Environ. Sci.: Water Res. Technol.* **2024**, *10*, 2142.
[101] M. Daniel, G. Mathew, M. Anpo, B. Neppolian, *Coord. Chem. Rev.* **2022**, *468*, 214627.
[102] Y. Zhang, Y. Zhu, Z. Zeng, G. Zeng, R. Xiao, Y. Wang, Y. Hu, L. Tang, C. Feng, *Coord. Chem. Rev.* **2021**, *431*, 213681.
[103] X.-Y. Yin, Y.-Q. Zhang, Y.-Y. Ma, J.-Y. He, H. Song, Z.-G. Han, *Inorg. Chem.* **2022**, *61*, 13174.
[104] E. Zhang, L. Wu, L. Jiang, K. Guo, Z. Su, P. Ju, *J. Mol. Struct.* **2022**, *1264*, 133314.
[105] J. Kim, C. Na, Y. Son, M. Prabu, M. Yoon, *Bull. Korean Chem. Soc.* **2023**, *44*, 507.
[106] Q. Yang, J. Wang, X. Chen, W. Yang, H. Pei, N. Hu, Z. Li, Y. Suo, T. Li, J. Wang, *J. Mater. Chem. A* **2018**, *6*, 2184.
[107] L. J. Small, R. C. Hill, J. L. Krumhansl, M. E. Schindelholz, Z. Chen, K. W. Chapman, X. Zhang, S. Yang, M. Schröder, T. M. Nenoff, *ACS Appl. Mater. Interfaces* **2019**, *11*, 27982.
[108] P. Horcajada, C. Serre, G. Maurin, N. A. Ramsahye, F. Balas, M. Vallet-Regí, M. Sebban, F. Taulelle, G. Férey, *J. Am. Chem. Soc.* **2008**, *130*, 6774.
[109] I. Abánades Lázaro, C. J. R. Wells, R. S. Forgan, *Am. Ethnol.* **2020**, *132*, 5249.
[110] E. Aghazadeh Asl, M. Pooresmaeil, H. Namazi, *Mater. Chem. Phys.* **2023**, *293*, 126933.
[111] A. A. El-Bindary, E. A. Toson, K. R. Shoueir, H. A. Aljohani, M. M. Abo-Ser, *Applied Organom Chemis* **2020**, *34*, e5905.
[112] Y. B. N. Tran, P. T. K. Nguyen, Q. T. Luong, K. D. Nguyen, *Inorg. Chem.* **2020**, *59*, 16747.
[113] G. Song, Z. Wang, L. Wang, G. Li, M. Huang, F. Yin, *Chin. J. Catal.* **2014**, *35*, 185.
[114] H.-H. Mautschke, F. Drache, I. Senkovska, S. Kaskel, F. X. Llabrés I Xamena, *Catal. Sci. Technol.* **2018**, *8*, 3610.
[115] E. Rahmani, M. Rahmani, *Ind. Eng. Chem. Res.* **2018**, *57*, 169.
[116] H. Li, L. Li, R.-B. Lin, W. Zhou, Z. Zhang, S. Xiang, B. Chen, *EnergyChem.* **2019**, *1*, 100006.
[117] I. Choi, J. Gu, H. Kim, Y. Kim, S. Huh, *Bull. Korean Chem. Soc.* **2023**, *44*, 780.

How to cite this article: J. L. Obeso, C. V. Flores, A. G. Gutiérrez, C. Leyva, J. C. Valdivia-Corona, L. D. Herrera-Zúñiga, J. A. de los Reyes, R. A. Peralta, I. A. Ibarra, *Bull. Korean Chem. Soc.* **2025**, *46*(3), 265. https://doi.org/10.1002/bkcs.70005

12259949, 2025, 3, Downloaded from https://onlinelibrary.wiley.com/doi/10.1002/bkcs.70005 by Universidad Autonoma Metropolitana, Wiley Online Library on [30/06/2025]. See the Terms and Conditions (https://onlinelibrary.wiley.com/terms-and-conditions) on Wiley Online Library for rules of use; OA articles are governed by the applicable Creative Commons License

3. Divulgación

EL INSTITUTO POLITÉCNICO NACIONAL

CICATA LEG

a través del **Centro de Investigación en Ciencia Aplicada y Tecnología Avanzada** otorga la presente

Constancia de participación en el:

XLIII Simposio en Tecnología Avanzada

a:

Dr. Ricardo Atahualpa Peralta Ávila

con el tema:

"Heterogenización de complejos catalíticamente activos soportados en sólidos con alta área superficial"

Que se llevó a cabo del **17 al 21 de junio del 2024.**

"La Técnica al Servicio de la Patria"

[redacted]

DRA. ROCÍO GUADALUPE CASAÑAS PIMENTEL
COORDINADORA DEL POSGRADO EN TECNOLOGÍA AVANZADA

INSTITUTO POLITÉCNICO NACIONAL
ESTADOS UNIDOS MEXICANOS
SEP
CENTRO DE INVESTIGACIÓN EN CIENCIA APLICADA Y TECNOLOGÍA AVANZADA
CICATA SECRETARÍA

[redacted]

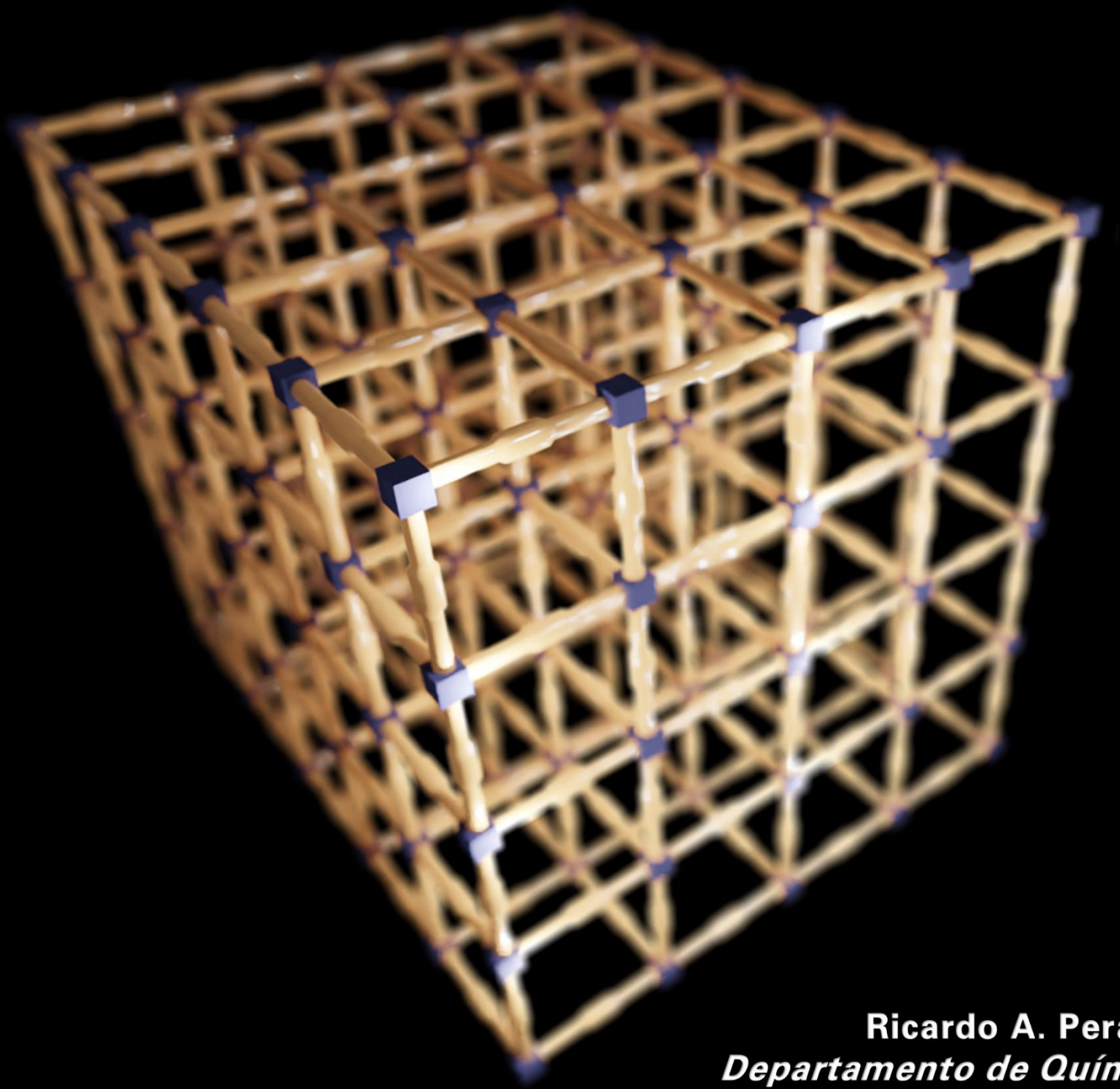
DRA. DELIA QUINTANA ZAVALA
SUBDIRECTORA ACADÉMICA

[redacted]

DR. ISAIAS MIRANDA VIRAMONTES
DIRECTOR DE LA UNIDAD

Scanned with CamScanner

Heterogenización de complejos catalíticamente activos soportados en sólidos con alta área superficial



Ricardo A. Peralta
Departamento de Química
Universidad Autónoma Metropolitana - Iztapalapa

Heterogenización de complejos catalíticamente activos soportados en sólidos con alta área superficial

Resumen:

Los materiales híbridos metal-orgánicos-MOFs (Metal Organic Frameworks; por sus siglas en inglés). Son una relativa nueva clase de materiales sólidos cristalinos porosos que en los últimos años han experimentado una apreciable evolución en comparación del primer material reportado. Esto ha sido posible debido a las numerosas investigaciones que se han llevado a cabo en dicho campo y que continúa incrementándose cada año. Los materiales poseen estructuras bien definidas debido a los fuertes enlaces de coordinación entre metal-ligando. Las posibles combinaciones de elementos orgánicos (ligante) e inorgánicos (metal) ofrecen un número infinito de variantes estructurales, que dan como resultado redes únicas con diferente porosidad y grupos funcionales. Esta extraordinaria diversidad es una característica importante que la diferencia de otros materiales porosos convencionales, por ejemplo, las zeolitas y el carbón activado. Debido a estas únicas propiedades se pueden utilizar en una amplia gama de aplicaciones en diferentes campos como, por ejemplo, catálisis heterogénea.

XLIII SIMPOSIO EN TECNOLOGÍA AVANZADA
PROGRAMA GENERAL

Fecha y hora	Lunes 17 de junio	Martes 18 de junio	Miércoles 19 de junio	Jueves 20 de junio	Viernes 21 de junio
8:00-8:30	Inauguración **Dr. Isaías Miranda Viramontes**	Hernández Guerrero Benito Alexis	Gutiérrez Leal Stephany	Vilches Cabrera Lázaro Damián	Morales Ricárdez Eduardo
8:30-9:00	Vázquez Flores Norma	Jiménez Jiménez Florencio	Gutiérrez Salinas Daniel	García Hurtado Alisson de la Caridad	Salazar Flores Samuel Alexis
9:00-9:30	Bernando Lino Janneth	Jurado Flores Javier	Chávez Camacho Enrique Alejandro	Quintanilla Serrano Edgar Arturo	Borges Segundo Alejandro
9:30-10:00	Flores Camacho Bertha Lizbeth	Vega Urrutia Ana Laura	Tenopala Peralta Jorge Eduardo	Reséndiz Hernández Omar	Lizárraga Medina Erika
10:00-10:15	RECESO				
10:15-10:45	Martínez González Ángel Alejandro	Escalera Martínez Nestor Alain	Chávez Rodríguez Luis Mariano	Gallo Guerrero Leidy Marcela	Martínez González María Fernanda
10:45-11:15	Salvatierra Bazán Natalia	Cruz González Leira	Ramírez Guerrero Nancy Cecilia	Díaz Ascencio Mónica Alejandra	Arellanes Ovando Ivete Berenice
11:15-11:45	Ortiz Vazquez Luis Fernando	Nolasco Altamirano Daniel	González Rodríguez Omar Alejandro	Sánchez Obeso Juan Luis	Aguilar Ramírez Arturo
11:45-12:00	RECESO				
12:00-13:00	**Dra. Goahua Sun** Computación cuántica **Centro de Investigación en Cómputo IPN**	**Dr. Ciro Falcony Guajardo** Luminiscencia **CINVESTAV Zacatenco**	**M. en C. Agustín Carrillo García** Casos de éxito en la vinculación Academia – Industria: Lecciones aprendidas en el ámbito de los Dispositivos Médicos **Novoinjertos S.C.**	**Dr. Ricardo Peralta** Heterogenización de complejos catalíticamente activos soportados en sólidos con alta área superficial **UAM-Iztapalapa**	**Dr. Tupak García Fernández** Plática de fotofísica **UACM**
13:00-13:15	RECESO				
13:15-13:45	González Amezcua Andrea Vanessa	García Zúñiga Roberto Carlos	Almeida Montes Rey Daniel	Rodríguez Ortega Azucena Georgina	García Valdés Ehekatzin
13:45-14:15	Ramírez Pérez Lizbeth Alejandra	Colin Vidal Adrian Alberto	Barrera Hernéndez Daniel	Guzmán Silva Raúl Erick	Gallegos Hernández Verónica Edith
14:15-14:45	Medina Ramos Luis Alberto	Vega Zuleta Lucio Rodrigo	López López José Luis	Raymundo Silva Karla Scanda	Moreno Bazan Erika
14:45-16:00	Sesión de pósters				Dr. José Manuel Domínguez Esquivel **Instituto Mexicano del Petróleo** Clausura **Dr. Isaías Miranda Viramontes**

Pósters

Lunes	Martes	Miércoles	Jueves
1er semestre doctorado	3er y 5o semestre de doctorado	7o y 8o semestre de doctorado	4o semestre de maestría

Reconocimiento mejores presentaciones por día
Comisión
Reconocimiento 1, 2 y 3 lugar en pósters
Comisión

Ricardo Peralta realizó su licenciatura en Ingeniería química en la Facultad de Química de la UNAM y la maestría en el Instituto de Investigaciones de Materiales bajo la supervisión del profesor Ilich Argel Ibarra Alvarado. Gracias a los resultados obtenidos en la maestría, realizó el doctorado en Australia, con una beca financiada por la Universidad de Adelaide. En esa misma universidad realizó una pequeña estancia postdoctoral, para posteriormente continuar su travesía en Corea. En Corea, realizó un posdoctorado de 1 año y medio con un "fellowship" llamado "Brain-pool program", para después regresar a México en la UAM-Iztapalapa como profesor visitante en el área de catálisis. Actualmente es nivel 1 del Sistema Nacional de Investigadores (SNII 1) del CONACYT. HA publicado 31 artículos en revistas internacionales de alto impacto, incluyendo una entrevista por la editorial RSC destacando la investigación que realiza dentro de la UAM. Además, cuenta con 1 libro publicado por la Editorial CBI de la UAM-Iztapalapa y es el editor en jefe del Podcast del Departamento de Química UAM-Iztapalapa.



4. Difusión de la ciencia

COLEGIO DE BACHILLERES

DIPLOMA

DE PARTICIPACIÓN A:

Dr. Ricardo A. Peralta Ávila

Por haber impartido la conferencia "*Materiales Porosos ¿Son útiles?*" el día 19 de noviembre de 2024 en el Colegio de Bachilleres Plantel 17 Huayamilpas-Pedregal, en el evento de divulgación COLBACH - UAMI 2024 "Jóvenes hacia las ciencias y las ingenierías".

[redacted]

Lic. Haydee Margarita Barrueta Guerrero
Directora

Plantel 17
Huayamilpas-Pedregal

CamScanner

CONSTANCIA
DE PARTICIPACIÓN

COLEGIO DE BACHILLERES

Plantel 9 Aragón

OTORGADA A:

Dr. Ricardo A. Peralta Ávila

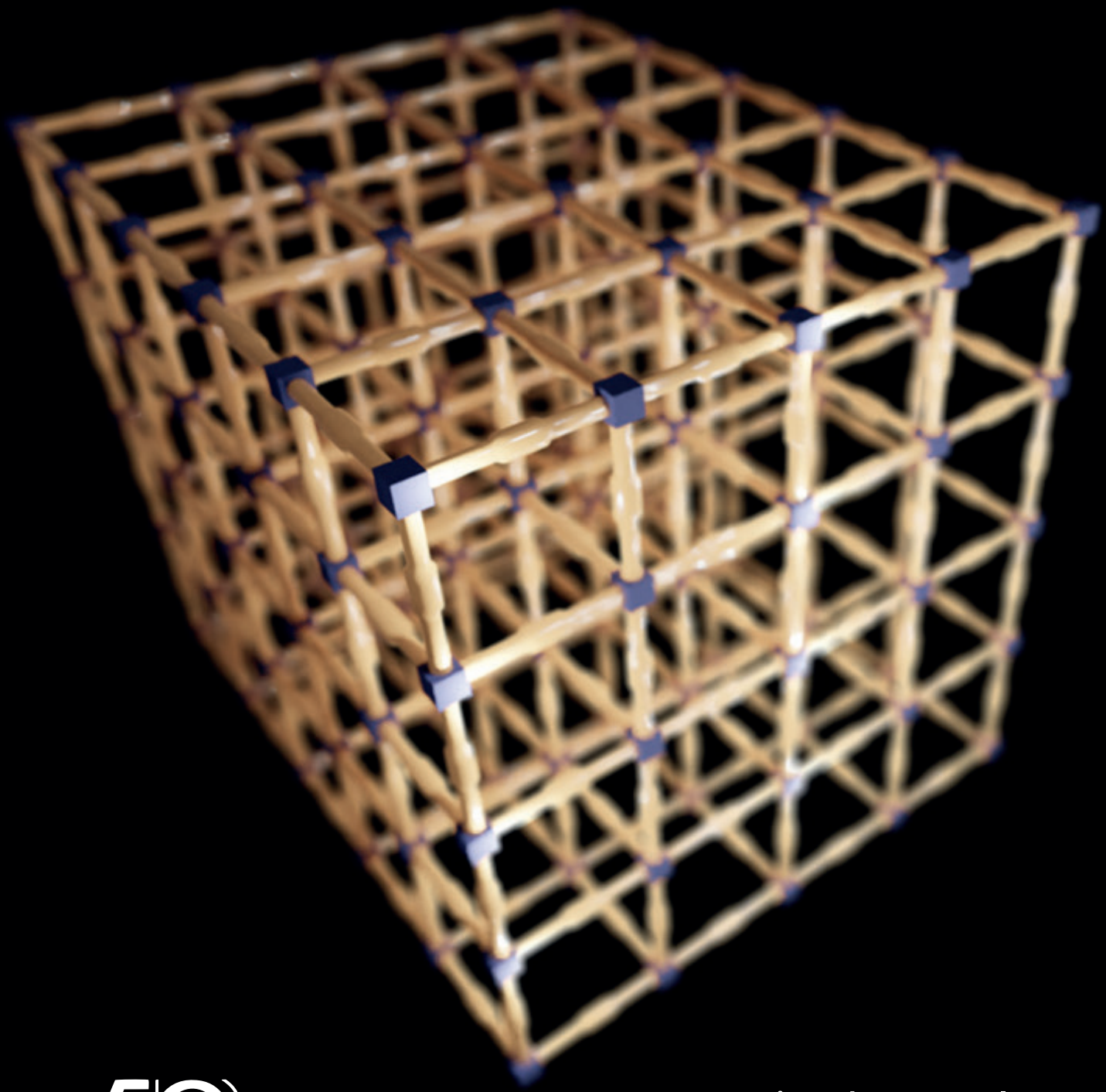
Por haber participando en la organización del evento de divulgación COLBACH - UAMI 2025 "Jóvenes hacia las ciencias y las ingenierías" en el Colegio de Bachilleres Plantel 9 Aragón los días 2-3 de abril de 2025.

[redacted]

Dra. Norma Ivette Montoya Arriola
Directora del Plantel

CamScanner

La quimica detrás de los MOFs: sus grandes aplicaciones



Casa abierta al tiempo

Ricardo A. Peralta
Departamento de Química,
Universidad Autónoma Metropolitana-Iztapalapa

Foto proporcionada por el autor

Resumen
El desarrollo de nuevos y mejores materiales es una necesidad inherente del ser humano para desplegar un mejor avance científico en diversas áreas como el medio ambiente y la tecnología industríal. Para ello, es importante entender el funcionamiento y diversas aplicaciones que un material pueda tener. Como una nueva alternativa en el estudio de materiales en estado sólido, nacen las redes metal-orgánicas, las cuales tienen como fundamento la química reticular con base en la química inorgánica. Este tipo de materiales han mostrado una amplia versatilidad en términos de diseño, síntesis y aplicaciones. Algunas de las aplicaciones que mi grupo de investigación se encuentra desarrollando son én adsorción de gases y contaminantes en agua, detección, sensores, dosificación de fármacos y catálisis. Estos problemas en un futuro no muy lejano serán de gran importancia y las maneras en que mi grupo de investigación las está abordando puede ser una herramienta útil para solucionarlas.

Palabras clave
Redes metal-orgánicas, adsorción, catálisis, contaminación

Abstract
Developing new and better materials is an inherent human need to deploy better scientific advancement. For this, it is important to understand the performance and various applications that a material may have. As a new alternative in the study of solid-state materials, metal-organic networks have emerged based on lattice chemistry based on inorganic chemistry. This material class has shown wide versatility in design, synthesis and applications. My research group is developing applications in the adsorption of gases and contaminants in water, detection, sensors, drug dosing and catalysis. These problems in the not-too-distant future will be of great importance, and how my research group addresses them can be a useful tool to solve them.

Keywords
Metal-organic framework, adsorption, catalysis, contamination

Introducción

La química del estado sólido analiza diversos materiales basados en compuestos moleculares, metálicos, cristalinos y cerámicos. El principal estudio es la síntesis, es decir la estructura y sus propiedades fisicoquímicas. Diversos materiales sólidos han sido estudiados a lo largo de los años, entre ellos, los que más destacan son los óxidos metálicos y las zeolitas. Estos materiales generaron un gran impacto en la sociedad debido a su basta aplicación en diferentes áreas. Los óxidos metálicos han sido ampliamente usados para la conversión de energía. Por otra parte, las zeolitas son aluminosilicatos de origen natural o sintético con canales y cavidades en su estructura; las cuales han sido aplicadas como catalizadores en la industria. Aun así, este tipo de materiales tienen desventajas muy puntuales con una baja porosidad y área superficial, así como una rápida desactivación después de procesos cataliticos. Por ello, el diseño de nuevos materiales sólidos ha ido en aumento en los últimos años.

Las Redes metal-orgánicas (MOFs por sus siglas en inglés Metal-Organic Framework) son compuestos descubiertos recientemente que surgen como una alternativa para emplearlos en diversas aplicaciones. Estos

emanan a partir de la química reticular con base en la química inorgánica. Estableciendo la idea de la química reticular, los materiales tipo MOF han surgido como compuestos cristalinos ininterrumpidos. (James, 2003) En general, un MOF es un material orgánico-inorgánico, el cual es construido usando iones metálicos y ligandos. El ambiente químico de un MOF es a base de enlaces de coordinación, lo que permite tener materiales altamente estables con únicas propiedades.

Este tipo de materiales permite diferentes diseños que pueden ser utilizados para una determinada aplicación debido a que puede cambiar el centro metálico, el ligante orgánico, o también, su funcionalización. Para ello, hay un número abundante de este tipo de materiales MOFs y una vasta línea de investigación. En otras palabras, el estudio de los materiales tipo MOFs es una progresión de posibilidades en diseño y aplicaciones, incluso en el área industrial.

La naturaleza química de los materiales tipo MOF

Los principales componentes de un material MOF son el centro metálico, que puede denominarse unidad secundaria de construcción (SBU), y las moléculas orgánicas multidentadas (ligandos orgánicos), que se conectan mediante enlaces de coordinación para formar estruturas bien definidas. La fuerza de los enlaces de coordinación le confiere la estabilidad en estos materiales. Por lo tanto, los MOFs con alta estabilidad suelen tener fuertes enlaces de coordinación (estabilidad termodinámica) o un impedimento estérico significativo (estabilidad dinámica) para evitar que moléculas dentro del poro, como solvente o reactivo, rompan los enlaces de coordinación dentro de la estructura. (Sun et al., 2021).

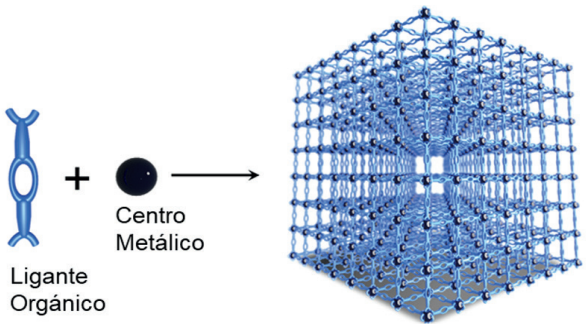


Figura 1. Estructura general de los materiales tipo MOF.

El arreglo ordenado de la parte metálica y orgánica en estos materiales hace que en su mayoría sean materiales altamente porosos y con una gran área superficial. Estos pueden formar redes 2D y 3D con poros bien definidos y una distribución homogénea de los sitios metálicos. Gracias a estas incomparables propiedades, diferentes materiales tipo MOFs han sido reportados. Las redes metal-orgánicas han sido bautizados con las siglas de los nombres de las universidades donde se realizaron los descubrimientos. Por ejemplo, HKUST-1 fue nombrado así por la Universidad de Ciencia y Tecnología de Hong Kong y los materiales DUT nombrados por la Universidad Técnica de Dresden, ambos acrónimos son escritos de esta manera por sus siglas en inglés.

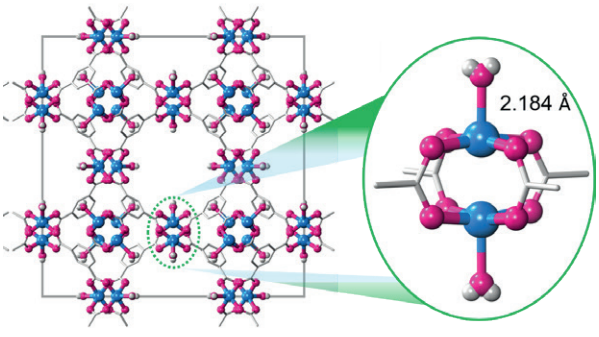


Figura 2. Estructura tridimensional del HKUST-1 obtenida por medio de difracción de Rayos-X.

Debido a su alta cristalinidad es posible estudiar su arreglo en el estado sólido por medio de Difracción de Rayos X. Por ejemplo, uno de los primeros MOFs sintetizados fue el HKUST-1 y con ayuda de esta técnica pudo ser posible saber su estructura cristalina. Este material está formado por iones cobre (Cu(II)) y un ligante orgánico (1,3,5-bencenotricarboxilato). La estructura es neutra, mostrando 12 átomos de oxígeno enlazados con 3 átomos de cobre para dar origen a una estructura en 3D con grandes poros hexagonales interconectados entre si, las que son consideradas como cavidades con diámetros uniformes y homogéneos, **Figura 2**. (Park et al., 2022) El poder explorar su arquitectura con tan precisa exactitud, nos da la oportunidad de estudiar sus propiedades y aplicaciones en diferentes ramas como las que planeo desarrollar en mi equipo de investigación en la Universidad Autónoma Metropolitana – Iztapalpa, como lo son: adsorción de gases y contaminantes en agua, detección, sensores, biocatálsis, baterías, catálisis, entre otras. (**Figura 3**).

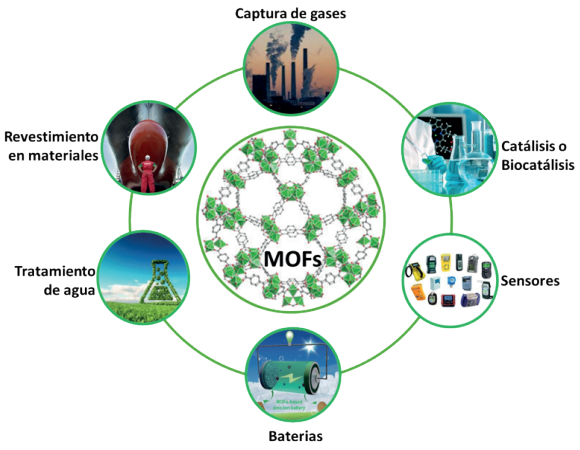


Figura 3. Algunas aplicaciones de los MOFs

Aplicaciones de MOF: Adsorción y sensores de gases contaminantes

El principal objetivo del diseño de materiales tipo MOF ha sido su evaluación en la captura de diversos gases. Principalmente en la captura selectiva de CO_2. La finalidad es aplicar estos materiales que contienen un alta área superficial y numerosos sitios de adsorción disponibles. Además, el estudio para la captura de gases tóxicos como SO_2, NH_3, NO, NO_2 y H_2S ha sido ampliamente investigado. Esta aplicación surge de la necesidad mundial para mitigar la contaminación ambiental.

En la búsqueda de materiales altamente competitivos para esta aplicación se ha explorado que estos tengan un área superficial mayor a 1000 $m^2\ g^{-1}$. Además, debido a la gran variedad de estos materiales, se han estudiado la síntesis de diferentes MOFs con mayores sitios de interacción entre la molécula que se desea capturar y estos sistemas porosos. En general los sitios coordinados insaturados y las funcionalizaciones de los ligantes son los más explorados para incrementar la captura de estos contaminantes gaseosos. (Martínez-Ahumada et al., 2021) De esta manera es como mi grupo de investigación ha tratado de erradicar por ejemplo gases tan corrosivos con el SO_2. La investigación sigue en curso en colaboración con un grupo de investigación de la UNAM, ya que este es un tema que requiere extensa investigación y los MOFs han demostrados ser altamente competitivos en la captura de dicho gas y seguiremos en la búsqueda de erradicarlo de la atmósfera. (Obeso, Amaro, et al., 2023; Obeso, López-Cervantes, et al., 2024).

Aplicaciones de MOF: Remediación del agua

Una de las aplicaciones en ascenso para los materiales tipo MOF es la remoción o eliminación de contaminantes en al agua. Debido a su alta porosidad y robustes de

estos sistemas que es conferido por el fuerte enlace de coordinación metal-oxigeno. La estabilidad en el agua ha sido reportada para enlances del tipo Al-O, Zr-O, Fe-O, Cu-O, Ho-O entre otros. Por ello, se han podido aplicar la remediación de metales pesados, colorantes, e incluso medicamentos disueltos en el agua.

En general, los MOFs con cluster Zr-O muestran gran potencial para remover arsénico debido a que se puede obtener capacidades de adsorción mayores a los 100 mg g^{-1} con estabilidad a un rango alto de pH. Además, los MOFs con centros metálicos de Fe han mostrado buena capacidad de adsorción para colorantes orgánicos, especialmente para azul de metileno, un colorante altamente usado en la industria textil. Asimismo, MOFs con base de cluster Al-O, han mostrado alta capacidad de remover medicamentos disueltos en el agua. En su mayoría diclofenaco, paracetamol, tetraciclina entre otros. Estos últimos son de suma importancia que se remuevan del agua debido a los problema de salud pública que podría generar, ya que podrían ayudar a formar una mayor resistencia bacteriana. Por lo tanto, los medicamentos perderían su eficacia para tratar enfermedades.

En resumen, la remoción de todos estos tipos de contaminantes orgánicos e inorgánicos es de suma importancia debido a que diversos estudios muestran una alta contaminación de las aguas en la Republica Mexicana. Por ello, mi investigación se plantea el uso de materiales MOFs para una alternativa a mitigar o disminuir las concentraciones de contamiantes en diversos cuerpos de agua. (Obeso, Viltres, et al., 2024)

Aplicaciones de MOF: Catálisis

Los MOFs pueden ser utilizado como soporte de un compuesto o como el catalizador propio, se pueden realizar modificaciones en el ligante orgánico para unir otros grupos activos como centros ácidos de Brønsted (ácido sulfónico), centros básicos (amino), entre otros. También se pueden utilizar los poros del material para encapsular partículas activas como polímeros, biomoléculas, por mencionar algunas. Esto se hace con la intención de enriquecer los sitios activos y promover reacciones específicas para que se lleven a cabo. (Peralta et al., 2020)

Finalmente, algunos MOFs también cuentan con sitios de coordinación libres, los cuales son conocidos como metales insaturados (OMS por sus siglas en inglés Open Metal Sites). Estos tienen al menos un ligante relativamente lábil o moléculas de disolvente, que mediante desplazamiento o eliminación por elevación de temperatura puede generar un centro insaturado activo manteniendo su integridad estructural. A menudo, los catalizadores MOF intentan utilizar sus OMS como centros catalíticamente activos. Después de su formación, el OMS actuará como un ácido de Lewis y estará disponible para aceptar densidad electrónica de cualquier molécula donante que pueda estar presente, donde se lleva a cabo la reacción química.

Hemos reportado varios estudios que han utilizado el uso de los clústeres o nodos metálicos como sistemas catalíticamente activos. (Flores et al., 2023; Obeso, Flores, et al., 2023) Recientemente, descubrimos que MOFs con metales saturados en los nodos de los MOFs también pueden exhibir actividad catalítica. Este es un descu-

brimiento fundamental y posible debido a que muestra una interacción dinámica entre el metal-ligante en estructura, lo que permite tener una red con metales semi abiertos que pueden ser utilizados como sitios catalíticamente activos. Esta característica sigue siendo investigada por mi grupo y esperamos explotarla en un futuro próximo para catálisis selectiva.

Aplicaciones de MOF: Biocatálisis

La inmovilización de enzimas mediante el uso de materiales amigables permite conservar y, en algunos casos, potenciar sus propiedades de estabilidad en condiciones adversas. Esta inmovilización facilita la separación y recuperación de las enzimas, convirtiéndolas en materiales reutilizables. Entre los materiales más destacados para este propósito se encuentran los MOFs. La unión de metal y ligando mediante enlaces de coordinación confiere una estabilidad significativa a las enzimas.

Principalmente, existen tres estrategias básicas para la inmovilización de proteínas: bioconjugación, infiltración y encapsulación. La estrategia de bioconjugación implica la inmovilización de biomacromoléculas en la superficie exterior de los MOF, ya sea mediante una unión covalente o mediante la adsorción inducida por las interacciones electrostáticas. La infiltración se refiere a la inmovilización de biomacromoléculas dentro de la red de poros del material mediante procesos de difusión. Las estrategias de encapsulación implican el crecimiento de una capa de MOF alrededor de una bioentidad objetivo y esta metodología es el foco de la revisión actual. Una variedad de bioentidades que abarcan una amplia gama de tamaños, desde pequeñas proteínas hasta células y virus más grandes, han sido encapsuladas con éxito mediante una cubierta de MOFs. Esto se debe a que el método de encapsulación no está limitado por el tamaño de los poros del MOF, ya que el MOF crece alrededor de la bioentidad. La integración de biomacromoléculas dentro de una capa de MOF se puede lograr mediante métodos de creación de plantillas o mediante la síntesis “one-pot” MOF en presencia de la biomolécula. Esta última estrategia es la que mi grupo se encuentra explorando debido a todas las propiedades mencionadas. Además, es una de las más prometedoras en el encapsulamiento de biomacreomoléculas como, por ejemplo la enzima que deseamos encapsular en nuestro sistema es la lacasa. Esta enzima la prentendemos encapsular para medios de remediación del agua y mi grupo de investigación la esta explorando.

Conclusiones

En conclusión, los temas de investigación tocados en este artículo han sido o se plantean desarrrolar en la UAM-I. Los logros obtenidos y proyectados son avances en cuanto a las aplicaciones que se les puedan dar, pero es posible que apenas hayamos visto la punta del iceberg con respecto al potencial uso de estos sistemas. Estas aplicaciones nos pueden a ayudar a solucionar muchos de los problemas que la sociedad enfrenta actualmente y que en un futuro (no muy lejano) se pueden volver caóticos. Además, nuevas aplicaciones surgirán a medida que sigamos investigando y más grupos de investigación continúen estudiando. Es por esto, que el futuro de este campo luce prometedor y ciertamente muy brillante.

Agradecimientos

El autor le agradece al Departamento de Química de la UAM-I por proporcionarme

un espacio para poder desarrollar los temas de investigación antes mencionados.

Referencias

Flores, J. G., Obeso, J. L., Martínez-Jiménez, V., Martín-Guaregua, N., Islas-Jácome, A., González-Zamora, E., Serrano-Espejel, H., Mondragón-Rodríguez, B., Leyva, C., Solís-Casados, D. A., Ibarra, I. A., Peralta, R. A., Aguilar-Pliego, J., & Antonio de los Reyes, J. (2023). Evaluation of the catalytic activity of Zn-MOF-74 for the alcoholysis of cyclohexene oxide [10.1039/D3RA03122E]. *RSC Advances*, 13(39), 27174-27179. https://doi.org/10.1039/D3RA03122E

James, S. L. (2003). Metal-organic frameworks [10.1039/B200393G]. *Chemical Society Reviews*, 32(5), 276-288. https://doi.org/10.1039/B200393G

Martínez-Ahumada, E., Díaz-Ramírez, M. L., Velásquez-Hernández, M. d. J., Jancik, V., & Ibarra, I. A. (2021). Capture of toxic gases in MOFs: SO2, H2S, NH3 and NOx [10.1039/D1SC01609A]. *Chemical Science*, 12(20), 6772-6799. https://doi.org/10.1039/D1SC01609A

Obeso, J. L., Amaro, D. R., Flores, C. V., Gutiérrez-Alejandre, A., Peralta, R. A., Leyva, C., & Ibarra, I. A. (2023). Chemical transformations of highly toxic H2S to promising clean energy in MOFs. *Coordination Chemistry Reviews*, 485, 215135. https://doi.org/https://doi.org/10.1016/j.ccr.2023.215135

Obeso, J. L., Flores, J. G., Flores, C. V., López-Cervantes, V. B., Martínez-Jiménez, V., de los Reyes, J. A., Lima, E., Solis-Ibarra, D., Ibarra, I. A., Leyva, C., & Peralta, R. A. (2023). SU-101: a Bi(iii)-based metal–organic framework as an efficient heterogeneous catalyst for the CO2 cycloaddition reaction [10.1039/D3DT01743E]. *Dalton Transactions*, 52(35), 12490-12495. https://doi.org/10.1039/D3DT01743E

Obeso, J. L., López-Cervantes, V. B., Flores, C. V., Martínez, A., Amador-Sánchez, Y. A., Portillo-Velez, N. S., Lara-García, H. A., Leyva, C., Solis-Ibarra, D., & Peralta, R. A. (2024). CYCU-3: an Al(iii)-based MOF for SO2 capture and detection [10.1039/D3DT04073A]. *Dalton Transactions*, 53(10), 4790-4796. https://doi.org/10.1039/D3DT04073A

Obeso, J. L., Viltres, H., Flores, C. V., López-Cervantes, V. B., Serrano-Fuentes, C., Rajabzadeh, A. R., Srinivasan, S., Peralta, R. A., Ibarra, I. A., & Leyva, C. (2024). Al(iii)-based MOF for the selective adsorption of phosphate and arsenate from aqueous solutions [10.1039/D3LF00061C]. *RSC Applied Interfaces*, 1(1), 147-154. https://doi.org/10.1039/D3LF00061C

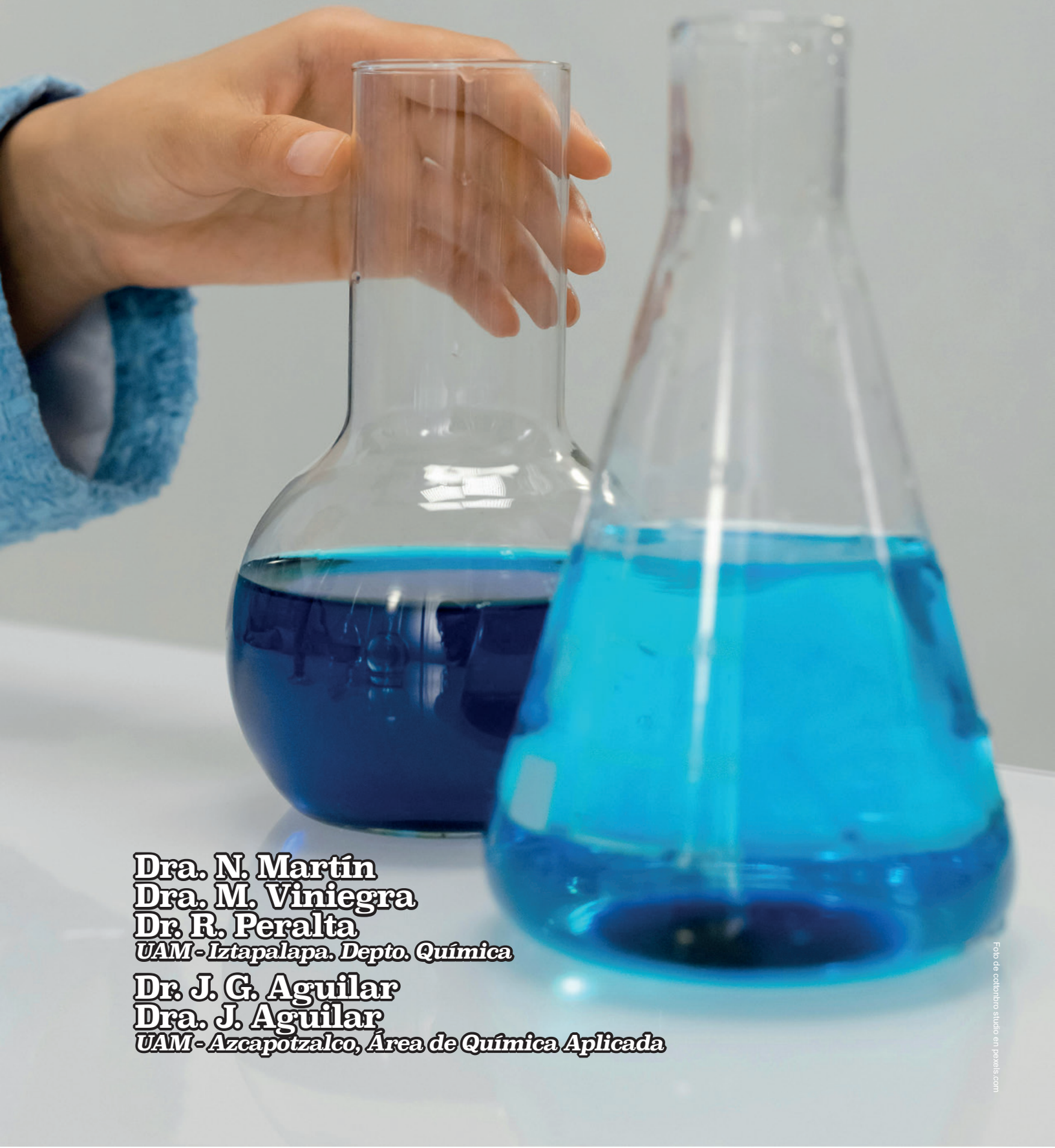
Park, S. H., Peralta, R. A., Moon, D., & Jeong, N. C. (2022). Dynamic weak coordination bonding of chlorocarbons enhances the catalytic performance of a metal–organic framework material [10.1039/D2TA06208A]. *Journal of Materials Chemistry A*, 10(44), 23499-23508. https://doi.org/10.1039/D2TA06208A

Peralta, R. A., Huxley, M. T., Evans, J. D., Fallon, T., Cao, H., He, M., Zhao, X. S., Agnoli, S., Sumby, C. J., & Doonan, C. J. (2020). Highly Active Gas Phase Organometallic Catalysis Supported Within Metal–Organic Framework Pores. *Journal of the American Chemical Society*, 142(31),

13533-13543. https://doi.org/10.1021/jacs.0c05286

Sun, D.-W., Huang, L., Pu, H., & Ma, J. (2021). Introducing reticular chemistry into agrochemistry [10.1039/C9CS00829B]. *Chemical Society Reviews*, 50(2), 1070-1110. https://doi.org/10.1039/C9CS00829B

Nanopartículas metálicas soportadas como catalizadores



Dra. N. Martín
Dra. M. Viniegra
Dr. R. Peralta
UAM - Iztapalapa. Depto. Química

Dr. J. G. Aguilar
Dra. J. Aguilar
UAM - Azcapotzalco, Área de Química Aplicada

Foto de cottonbro studio en pexels.com

Resumen
Desde su creación en 1987, el grupo "*catálisis heterogénea*", de la UAM-Iztapalapa, ha desarrollado investigación centrada en la síntesis, desarrollo y evaluación de catalizadores sólidos a base de metales y óxidos de metales en reacciones diversas como son, la reformación de naftas, oxidación de alcoholes, transformación de glicerol, hidrodecloración de dicloroetileno, entre otras. Se presenta una cronología histórica de las líneas de investigación realizadas.

Palabras Clave: Catálisis heterogénea, Nanopartículas metálicas; MOFs; Catalizadores metálicos; Metales soportados.

Abstract
Since its creation in 1987, the "heterogeneous catalysis" group, at the UAM-Iztapalapa, has developed research focused on the synthesis, development and evaluation of solid catalysts based on metals and metal oxides in diverse reactions such as the reforming of naphtha, oxidation of alcohols, transformation of glycerol, hydrodechlorination of dichloroethylene, among others. A historical chronology of the lines of research carried out is presented.

Keywords: Heterogeneous catalysis; Metallic nanoparticles; MOFs; Metallic catalysts; supported metals.

Introducción

Presentamos una revisión de las líneas de investigación que el grupo *catálisis heterogénea* de la UAM-Iztapalapa ha trabajado durante 4 décadas. Entre ellas, se incluye el trabajo con colaboraciones realizadas con el Depto. de Ingeniería Química y de Procesos e Hidráulica de la misma UAM-I y con el área de Química Aplicada de la UAM-Azcapotzalco.

La UAM se crea en el año 1974 y es en 1978 que se crea el área de catálisis dentro del departamento de química de la UAM-Iztapalapa, con el tema, principalmente, de catálisis heterogénea. En 1984 se inició el posgrado en ciencias (química) en la institución. Posteriormente, en 1987 el área se dividió y se tuvo la formación de nuestro grupo de investigación con el nombre temporal de "*La Perestroika*", llamado así por los acontecimientos históricos de la época (década de los 80), integrado por profesoras y profesores que en aquel momento estaban como candidatos a doctor (de la UAM-I): el Dr. Gilberto Córdoba, el Maestro Alejandro López-Gaona, la Dra. Nancy C. Martín, la Dra. Patricia Villamil y la Dra. Margarita Viniegra.

El grupo que luego se llamó *catálisis heterogénea*, inició con investigación propia en 1990 y, en forma general, se enfocó en las dos líneas de investigación siguientes: el uso de nanopartículas de metales u óxidos metálicos soportados como catalizadores en reacciones de oxidación e hidrogenación de hidrocarburos y posteriormente, se incorporó la del desarrollo y estudio teórico de materiales con aplicaciones tecnológicas.

Antes de presentar la primera línea de investigación, se hará una breve introducción sobre qué son las nanopartículas metálicas soportadas y luego, se abordarán los trabajos realizados por el grupo en cada período desde 1990.

Nanopartículas metálicas soportadas

La catálisis heterogénea, llamada también catálisis en la interfase, se caracteriza por tener a los reactivos y los catalizadores en diferentes fases. En la mayoría de los procesos el catalizador es un sólido y los reactivos son gases o líquidos. Para un

catalizador sólido los componentes activos como los metales u óxidos de metales, usualmente en baja concentración, se fijan en un estado disperso sobre un soporte.

Desde hace muchas décadas las nanopartículas (NPs) metálicas, llamadas así por su tamaño, el cual se encuentra entre 1 y 100 nm, son la base de diversos procesos químicos catalíticos. La catálisis por metales de transición es una rama muy atractiva y con aplicaciones varias en procesos de reacciones de oxidación y de hidrogenación bajo condiciones moderadas de presión y de temperatura (Thomas y Thomas, 1997).

El fenómeno de la catálisis es parte de nuestra vida cotidiana y también de los seres vivos, puesto que todos los procesos del cuerpo dependen de catalizadores biológicos, llamados enzimas, que generalmente son proteínas. Por su parte, los catalizadores que se utilizan en los procesos químicos y en el control ambiental son primordialmente compuestos de naturaleza inorgánica que pueden clasificarse en metales, óxidos, sulfuros y ácidos sólidos, aunque en la práctica los catalizadores casi siempre contienen compuestos de al menos dos de estas categorías. En particular los metales deben utilizarse en forma de nanopartículas para maximizar el área accesible a los reactivos, pero dado que son inestables en ese estado, es necesario unirlos a la superficie de un soporte, de tal manera que las NPs no puedan estar en contacto unas con otras; este tipo de catalizadores son llamados catalizadores metálicos soportados (Zanella *y col.* 2014). Las NPs inorgánicas resultan interesante debido a sus propiedades ópticas, electrónicas, magnéticas y catalíticas, únicas (Grieve *et al.*, 2000; Lu *y col.*, 2007; Medintz *y col.*, 2005; Shipway *y col.*, 2000), muchas de las cuales pueden ser diseñadas con sólo cambiar su tamaño, forma, o la funcionalización de la superficie de la nanopartícula, sin cambiar la composición del material.

Cuando los átomos se aglomeran en grupos de tres o cuatro átomos sobre un soporte se dice que tenemos átomos superficiales en forma aglomerada (*clusters*). Pueden rodearse de vecinos y crecer a lo largo de una superficie. Con frecuencia se describe a la partícula metálica de un tamaño finito por su dispersión metálica, que se define como la relación de los átomos que están en la superficie y el número total de átomos. (Figura 1) y se correlaciona con el número de partículas.

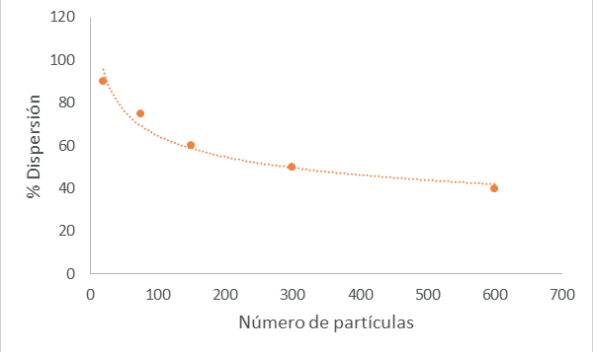


Figura 1. *Porcentaje de dispersión metálica en función del número de partículas*

La disminución del tamaño de partícula conduce a que una gran cantidad de átomos estén disponibles como sitios activos en la superficie de las partículas, lo que generará catalizadores altamente reactivos, pues la actividad química en muchas reacciones es proporcional al número de especies activas accesibles a los reactivos (Thomas y Thomas, 1997). Así, la llamada nanocatálisis tiene como fin controlar las reacciones catalíticas por medio de la optimización del tamaño, dimensionalidad,

composición química y morfología de las nanopartículas que constituyen la fase activa del catalizador (Wachs, 2001).

El efecto de las NPs metálicas sobre diversos soportes tienen muchas ventajas. El soporte de un catalizador puede ser inerte o activo en las reacciones y puede actuar como estabilizador para evitar la aglomeración de NPs metálicas. Los soportes pueden cooperar con éstas para promover reacciones simultáneas. Por tanto, la elección del soporte adecuado es un tema relevante.

La importancia del tamaño y forma de las nanopartículas de metal u óxido soportados correlacionadas con su estructura electrónica se estudia mediante técnicas térmicas y fotoinducidas. Se ha reportado, en catalizadores metálicos soportados, que las propiedades fisicoquímicas difieren al comparar partículas del orden de 0.1 nm (un solo átomo, *single atom*), con partículas de 1 nm (aglomerados, *clusters*), o de 5 nm (nanopartículas) y debido a estas diferencias en tamaño se observan cambios en las interacciones con el soporte y su evolución durante la reacción, lo cual afecta la actividad y la selectividad catalítica. Por tanto, es importante analizar los efectos geométrico y electrónico del catalizador según cada una de estas especies: un solo átomo, aglomerados o nanopartículas (Liu y Corma, 2018).

Se considera que los grupos pequeños (<1–2 nm) pierden sus propiedades electrónicas, esto es, cuando desaparecen las características asociadas al enlace metálico (3-50 nm) y las partículas se describen mejor con la teoría de orbitales moleculares o atómicos; se puede inferir que las partículas metálicas cambian sus propiedades electrónicas fuertemente cuando están por debajo de tamaños subnanométricos (~ 1 nm) (Figura 2). Se podría esperar que los metales cuando se agrupan en tamaños subnano interactuarán de manera diferente con los reactivos, mostrando reactividad distinta en comparación con las nanopartículas grandes. La estructura electrónica dependiente del tamaño es más significativa cuando las nanopartículas metálicas constan de menos de 40 átomos (Liu y Corma, 2018).

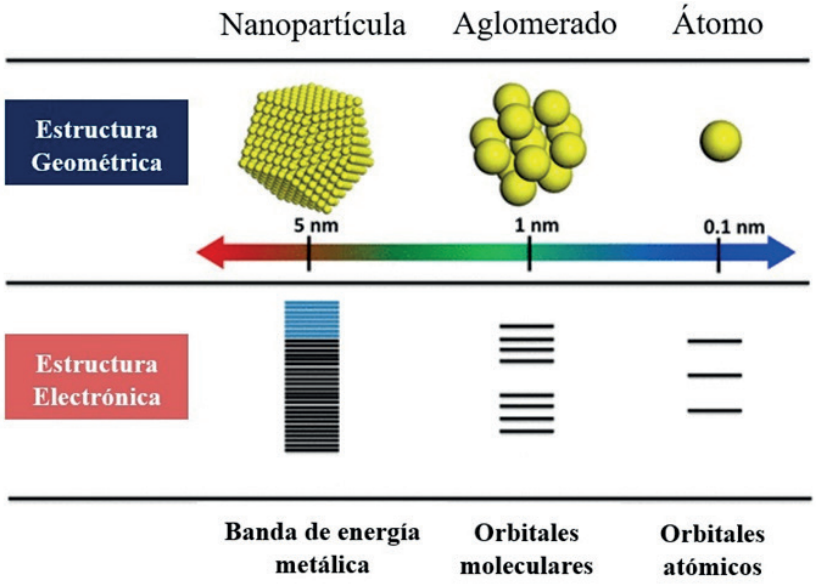


***Figura 2**. Diferencias entre nanopartículas, aglomerados y un átomo. (Editado de Liu y Corma 2018)*

Período 1990-1999
(Hidrogenación y metales)

Después de la segunda guerra mundial, las arcillas tratadas con ácidos fueron muy usadas para el craqueo catalítico por su estabilidad en un largo tiempo de reacción. Posteriormente, fueron sustituidas por catalizadores sintéticos de silica-alúmina que resultaron más estables y con una mejor selectividad a una gran distribución de productos. Para 1960, se reportan a las zeolitas sintéticas como catalizadores activos y selectivos para reacciones de isomerización de hidrocarburos. En 1974, se introduce a la zeolita sintética ZSM-5 para nuevos procesos industriales, en particular para el proceso MTG para convertir metanol a gasolinas, en el cual resultó tener propiedades excelentes como la selectividad de forma, el carácter ácido, la resistencia a la desactivación por coque, entre otras. En la década de los 70, para el reformado catalítico, como el reformado de naftas, se reporta como catalizador el de platino finamente disperso en una γ-Al_2O_3, el cual, por su carácter dual, de la fase metálica y el carácter ácido del soporte, le confieren propiedades hidrogenantes y deshidrogenantes necesarias en el proceso. Para hacer más eficiente la hidrogenólisis (ruptura de los enlaces C-C) y disminuir el envenenamiento por coque de los catalizadores de Pt se introduce el uso de catalizadores bimetálicos (Pt-Ir) (Thomas y Thomas, 1997).

En la década de los 90, sigue en auge la investigación de catalizadores para los diversos procesos de la industria petrolera, en particular, para los procesos de reformación de naftas e hidrocraqueo de hidrocarburos. El soporte estrella de la época, y lo sigue siendo actualmente, por sus múltiples propiedades y muy usado en catálisis, es la gamma alúmina (γ-Al_2O_3). NPs de Pt soportadas en alúmina han mostrado ser muy activas en muchas reacciones (Thomas y Thomas, 1997).

Uno de los estudios realizados en este período de los 90 fue el de la hidrogenación de o-xileno sobre catalizadores de paladio soportados sobre sílice, alúmina y sílice-alúmina (M. Viniegra *y col.* 1990)]. El objetivo de este trabajo fue establecer como la dispersión del metal o el soporte jugaban un papel importante en la determinación de la estereoselectividad del paladio. Se observó que la producción del producto trans-hidrogenado, aumentaba con la acidez del soporte (SiO_2 < Al_20_3 < SiO_2 - Al_20_3) y disminuía en presencia de moléculas donadoras de electrones como la piridina. Estos resultados se explicaron en términos del carácter electrofílico del paladio cuando está soportado sobre soportes ácidos, como la γ-alúmina y la sílice-alúmina (Figueras F. *y col.*, 1973), y considerando que el o-xileno actúa como una base de Lewis hacia la superficie del metal (Stairs P., 1982). Esto es, que la fuerza del enlace entre los reactivos y la superficie determinan la estereoselectividad del paladio e influye en la composición de los productos termodinámicamente favorecidos (Viniegra M. *y col.*, 1991).

Para continuar con estos estudios y ver si este modelo era aplicable a otros metales, se realizó la hidrogenación de o-xileno sobre catalizadores de Ru con diferente dispersión soportados sobre sílice y sílice-alúmina. Los resultados aquí reportados llevaron a las siguientes conclusiones: i) La selectividad del Ru se ve alterada por la dispersión del metal, la acidez del soporte y la presencia de residuos carbonosos. 2) El modelo de reacción de “reinversión”

se puede aplicar a la hidrogenación de o-xileno sobre Ru para explicar la formación del producto trans-hidrogenado. 3) El Ru debería adsorber o-xileno y especies intermedias más débilmente que el Pd para producir más producto cinéticamente preferido (cis-DMCH). 4) La diferencia entre Ru y Pd, en cuanto al efecto de la dispersión sobre la actividad catalítica y el proceso de desactivación, puede deberse a una falta de hidrógeno activado en la superficie del Ru (Viniegra M. *y col.*, 1992). En catalizadores bimetálicos Ru-Pd/SiO_2 se observó un pequeño máximo de actividad a temperaturas en las que el paladio está inactivo. La estereoselectividad de los catalizadores bimetálicos difería notablemente de la del rutenio monometálico. Se sugiere que un efecto ligando entre los átomos de Ru y Pd de la superficie es el responsable del comportamiento catalítico de los catalizadores bimetálicos (Viniegra M. *y col.*, 1995).

Periodo 2000-2010
(Desactivación por coque
e hidrodeclorinación)

En un proyecto de colaboración con el Instituto Mexicano del Petróleo (IMP), se realizaron estudios de desactivación por coque de catalizadores de reformación. Se investigaron la cantidad y naturaleza de los depósitos de carbono en catalizadores de platino soportados sobre una mezcla de alúmina-β-zeolita, no neutralizada y neutralizada con cesio, y se compararon con los de un catalizador comercial (Pt/Al_2O_3). Los catalizadores se desactivaron en la reacción modelo de metilciclopentano. La caracterización del coque se realizó mediante análisis elemental, oxidación a temperatura programada (TPO), transformada de Fourier infrarroja (FTIR) y RMN de 13C (CP/MAS). La diferencia significativa entre Pt/Al2O3 y Pt soportado sobre una mezcla de γ-alúmina y β-zeolita es la naturaleza de los depósitos de carbón. El análisis elemental, TPO, FTIR y RMN de ^{13}C (CP/MAS) señalaron diferentes características de los depósitos. El catalizador zeolítico neutralizado por Cs presentó cantidades similares de residuos de carbono, pero fue el más desactivado. Los resultados señalan sitios ácidos con diferentes respuestas a los residuos carbonosos (Martin N. y col, 2004).

En otro estudio, se analizaron los depósitos de carbono en catalizadores industriales de Pt-Sn/γ-Al_2O_3 se caracterizaron mediante una combinación de diferentes técnicas, incluido el análisis elemental, AFM, TPO y espectroscopía de RMN ^{13}C-CP/MAS. Además de la evaluación cualitativa y cuantitativa detallada, que mostró la misma cantidad de carbono en todas las muestras, se encontró que el coque en los catalizadores industriales era de tipo aromático, independiente del número de ciclos de uso. El análisis de TPO señaló una diferencia entre los catalizadores industriales y el catalizador tratado en el laboratorio como un sistema modelo, mostrando claramente que existen dos tipos de coque o dos tipos de sitios (interfase sustrato versus metal-sustrato) en la formación de coque. El análisis AFM reveló características de dos tipos de morfología del coque, descritas como fases de coque laminada (estructura en forma de disco elíptico) y granular (esférica). Se observaron grandes agregados de coque en defectos superficiales, como bordes de grano. En general, nuestros resultados mostraron que la naturaleza del coque depende del proceso de desactivación, y que el coque en el catalizador industrial podría describirse y definirse con éxito (Martin N. *y col.*, 2005).

También se estudió el efecto del óxido de lantano sobre la resistencia al coque de un catalizador Pt/Al_2O_3. Se evaluó la actividad y selectividad en la reacción modelo de hidrogenólisis de metil-ciclopentano, obteniendo el siguiente orden de actividad: Pt/Al_2O_3 >> Pt/Al_2O_3-La_2O_3 > Pt/La_2O_3. En cuanto a selectividad, fueron similares en todas las muestras, característica de los catalizadores bifuncionales, esto es, productos de apertura de anillo (2-metilpentano, 3-metilpentano, n-hexano) y productos ligeros, así como también de alargamiento de cadena (c-hexano y benceno) y formación de alquenos (metil-penteno y hexeno). El benceno fue el producto mayoritario, el cual se produce por la combinación de la función metálica y la función ácida del soporte. En relación con la formación de coque, fue similar en los soportados en alúmina y alúmina-lantana y mayor que en el soportado en lantana (Martin N *y col.*, 2007).

En un giro de la investigación y en colaboración con un proyecto del área de ingeniería química, se estudió a la reacción de hidrodecloración (HDCl) en fase líquida, la cual es una vía efectiva para el tratamiento de compuestos orgánicos clorados, que son contaminantes del suelo y agua. Se estudiaron catalizadores de Pt y Pd soportados en MCM-41 y SiO_2 en la hidrodecloración de 1,2-dicloroetano, donde fueron activos en el siguiente orden: Pd/MCM > Pd/SiO_2 > Pt/MCM > Pt/SiO_2. Además, se encontró una alta selectividad hacia el etileno en todos los catalizadores. Las diferencias en actividad estuvieron relacionadas con las estructuras entre ambos soportes obteniendo una mayor dispersión metálica en los soportes mesoporosos (Martin N. *et al.* 2008). De igual forma se evaluó la actividad en la HDCl de 1,2-dicloroetano (DCE) de catalizadores de Pt soportados en una sílice mesoporosa (HMS) sintetizada en el laboratorio. Se obtuvo una mayor actividad en el catalizador mesoporoso en relación con el soportado en sílice, lo cual estuvo relacionado con el tamaño más pequeño de las partículas de platino en el primero (Martin N. *y col.*, 2011). También se evaluó la actividad en la reacción de hidrogenación de benceno e hidrogenólisis de metil-ciclopentano obteniendo una mayor actividad en los soportados en el HMS (Martin N. *y col.*, 2010). El efecto de TiO_2 en catalizadores de Pt, Pd y Rh soportados en Al_2O_3 (Pt/At; Pd/AT; Rh/AT) fue estudiado en la HDCl de 1,2-dicloroetano obteniendo mayor actividad y mejor selectividad a los compuestos no clorados en los catalizadores con mayor proporción de titania y en el bimetálico PtPd (Tabla 1) (Martín N. *y col.* 2012).

Por otro lado, es sabido que los metales IB muestran distintas propiedades en catálisis heterogénea. Los catalizadores de Cu se utilizan industrialmente a baja temperatura en la reacción de desplazamiento de gas-agua (WGS) y la síntesis de metanol a partir de gas de síntesis. Los catalizadores de Ag son aptos exclusivamente para la epoxidación de eteno.

Catalizador	Pt/HMS	Pt/AT	Rh/AT	Pd/AT	PtPd/AT
$vx10^{-3}$ ($mol.g^{-1}.min^{-1}$)	3.36	0.20	0.80	2.40	3.10
% S (No clorados)	82	80	95	72	85

Tabla 1*. Velocidad (v) de HDCl de DCE a 523 K, presión atmosférica y 60 min de reacción.*

Los catalizadores de Au con partículas metálicas de menos de 5 nm son altamente activos para la oxidación de CO y la reacción de WGS a baja temperatura en estudios de laboratorio (Tsubota *y col.*, 1998, Zhu Y. *y col.*, 2018).

Algunos estudios han relacionado no sólo el tamaño de las NPs, sino también su forma con la actividad catalítica, así, por ejemplo, se sabe que las nanopartículas de Au soportadas en óxidos son muy activas en la reacción de oxidación de monóxido de carbono con oxígeno molecular, ($CO + ½\ O_2 \rightarrow CO_2$). A pesar de que el oro es el más noble de todos los metales de transición, cuando se logra obtener en forma de nanopartículas de menos de 5 nm, soportado en la superficie de varios óxidos, por ejemplo, TiO_2, muestra actividades excepcionalmente altas hacia la reacción de oxidación de CO a temperaturas por debajo de la temperatura ambiente (Zanella R., 2014). Estos estudios demostraron el denominado efecto carga entre las nanopartículas metálicas y el soporte, el cual consiste en la transferencia de carga del soporte a las nanoestructuras, si éstas se localizan en sitios con vacancias de oxígeno, entonces el soporte podría donar carga a las nanopartículas y hacerlas altamente activas en la reacción de oxidación de monóxido de carbono (Figura 5), ya que la reacción transcurre, según la teoría de orbitales moleculares, mediante una transferencia de electrones de los orbitales de más alta energía de las nanopartículas al orbital de más baja energía del CO, esto ocasiona la disociación del sustrato y la subsecuente reacción. Por el contrario, si las partículas están soportadas en sitios donde el óxido no presenta defectos estructurales la reacción no ocurre.

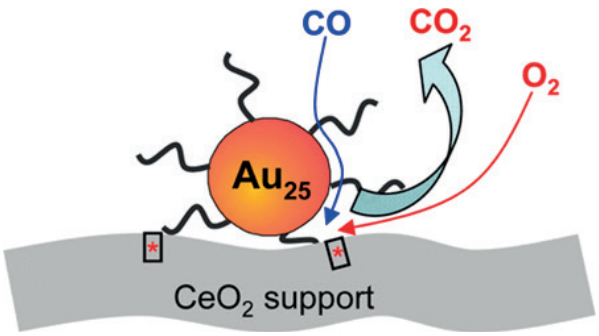


***Figura 3**. Nanopartículas de oro soportadas en CeO_2 en la reacción de oxidación de CO. ACS Nano 2012, 6, 7, 6014–6022, https://doi.org/10.1021/nn301019f*

Por tanto, para lograr un catalizador eficiente para la oxidación catalítica se requiere alta movilidad del oxígeno en la red y buena conductividad electrónica. En general, para una reacción selectiva el requerimiento de oxígeno es menos demandante que para las reacciones no selectivas.

En el grupo se evaluó la actividad catalítica de catalizadores de CuO/ZrO_2 preparados por impregnación y por el método sol-gel in situ, en la oxidación de CO; los primeros mostraron una mayor actividad catalítica. Esta observación se explicó por la presencia de pequeñas partículas de CuO sobre el catalizador preparado por impregnación (mayor dispersión), lo cual no ocurre en los catalizadores obtenidos por el método sol-gel in situ donde una cantidad importante de iones Cu^{2+} fueron incorporados a la red del sólido, que se consideran catalíticamente inactivos (Viniegra M. *y col.*, 2010).

Período 2011-2020
(Transformación de glicerol)

Para 2014, se tuvo un proyecto con la UAM-A sobre la transformación catalítica de glicerol en fase gas, el cual resulta ser un producto secundario en la producción de biodiesel. La reacción de transformación

de glicerol tiene un esquema bastante amplio, con la obtención de productos de alto valor agregado según la ruta que se pueda seguir (Figura 4).

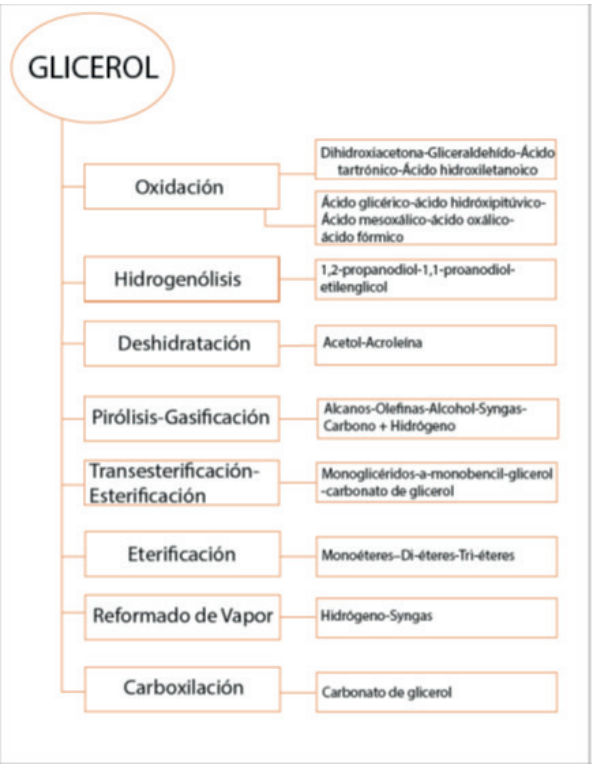


Figura 4*. Posibles rutas de transformación del glicerol (BSQM, 26, 2018).*

En un estudio con catalizadores a base de Pt soportados en ceria y alúmina en la deshidratación de glicerol, ambos catalizadores resultaron activos; bajo nuestras condiciones de reacción los productos principales identificados fueron la acroleína (AC), el alcohol alílico (AA), la hidroxiacetona o acetol (HA) y otros compuestos líquidos y gaseosos no identificados, siendo la selectividad hacia acroleína, la mayor en el Pt/Al_2O_3 en tanto que el Pt/CeO_2 presentó mayor selectividad hacia el acetol. Esto fue explicado por las propiedades óxido reductoras del segundo soporte (Martin N. *y col.*, 2018). De igual forma, para esta reacción se estudiaron catalizadores másicos de hierro sintetizados por el método de micelas invertidas, los cuales mostraron alta actividad, estabilidad y una alta selectividad hacia la acroleína, indicativo de que la estructura afecta el mecanismo de la reacción. Posteriormente, se evaluaron catalizadores mono- y bi-metálicos a base de óxidos de hierro y níquel soportados en una alúmina comercial. El orden de actividad fue el siguiente: $Ni/Al_2O_3 > Fe/Al_2O_3 \approx Fe\text{-}Ni/Al_2O_3$. Se encontró que todos los catalizadores tenían actividades similares con diferencias notables en su selectividad. Estas diferencias se explican por la interacción entre los óxidos metálicos de los catalizadores bimetálicos, lo que produce cambios en la relación Fe^{+3}/Fe^{+2}. La producción de alcohol alílico a partir de óxidos bimetálicos puede explicarse por las propiedades redox de estos catalizadores. Una disminución de la relación Fe^{+3}/Fe^{+2} favorece la formación de alcohol alílico (Martin N. *y col.*, 2020).

Período 2020-2023 (Materiales a base de redes metal-orgánicas)

Con el fin de probar nuevos materiales como catalizadores se inició un proyecto con la UAM-A con el uso de las estructuras metal-orgánicas (MOF), donde no se tienen nanopartículas, pero sí metales; estos materiales son relativamente nuevos con creciente relevancia en procesos de adsorción de contaminantes y catálisis heterogénea (Aguilar J. *y col.*, 2022). Estas aplicaciones son posibles debido a propiedades como alta porosidad, fácil síntesis y versatilidad de estructuras, permitiendo el diseño personalizado, según la aplicación de interés. En catálisis los MOF se usan comúnmente como sitios ácidos de Lewis debido a que algunos de estos materiales poseen moléculas de solvente lábiles que pueden ser

eliminadas mediante activación térmica o química para formar sitios abiertos de metal (OMS) (Zhou Y. y col, 2018).

En el grupo se reportó (Aguilar J. *y col.*, 2022) sobre las propiedades inherentes de los MOF que pueden permitir ser excelentes catalizadores. La buena dispersión de los sitios activos y las diversas morfologías de MOF son deseables para una interacción mejorada de los reactivos con el material (Figura 5). Una adecuada disposición de la estructura permite una alta dispersión de los sitios activos, reduciendo así el riesgo de envenenamiento de estos. Además, la fuerza de unión entre el metal y el ligando es suficiente para generar estructuras estables (porosidad y arquitectura), lo cual es ideal para aplicaciones catalíticas (Aguilar J. y col, 2023). Esta extraordinaria diversidad estructural es una característica importante que diferencia los MOFs de otros materiales porosos convencionales como las zeolitas o el carbón activado.

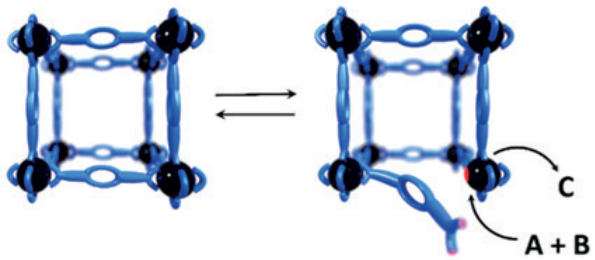


***Figura 5**. Representación de sitios metálicos semiabiertos en los MOFs generados por enlaces metal-ligando móviles que pueden ser empleados en catálisis (Cortesía de Peralta R. y col. 2023).*

En un estudio realizado en el grupo, se sintetizó un material de Zn-MOF-74, a temperatura ambiente, que resultó ser un catalizador heterogéneo eficiente para la alcohólisis de apertura de anillo del óxido de ciclohexeno catalizada por ácido. Esta reacción se rige por la termodinámica, siendo 50 °C la temperatura óptima, donde se obtiene la mayor conversión. Este efecto puede deberse a que el catalizador se regenera más rápido y los reactivos acceden a los sitios insaturados de Zn (II) dentro del material. Bajo las condiciones usadas, se obtuvo una conversión mayor al 73% en las primeras 21 horas y alrededor de 94% en menos de dos días de reacción. De igual forma, el catalizador no mostró degradación, lixiviación, ni disminución de su actividad catalítica en 3 ciclos de reacción (Aguilar J. *y col.*, 2023).

Conclusiones

Los resultados obtenidos durante cuatro décadas a partir de los proyectos de investigación realizados han contribuido al desarrollo de nuestro grupo de catálisis, con énfasis en la síntesis, caracterización y evaluación de materiales a base de metales y óxidos de metales, en procesos catalíticos. Muchos de los sólidos sintetizados han tenido un excelente desempeño en reacciones tales como reformación de naftas, oxidación de glicerol y de CO, deshidratación de alcoholes, hidrodecloración de 1,2-dicloroetileno, entre otras.

El laboratorio desde su creación ha disminuido su personal, pero están por ingresar tres profesores jóvenes, que podrán seguir trabajando y promoviendo el quehacer científico con el fin de aportar soluciones a muchas de las necesidades actuales. De igual forma, es importante seguir en la búsqueda de financiamiento externo para continuar con los proyectos de investigación en curso.

Referencias

1. Flores J. G., Aguilar-Pliego, J., Mar-

tín-Guaregua N., Ibarra I. A. y Sánchez-Sánchez M. Catal. Today, 394-396, 295 (2022); I*dem Royal Society Chemistry Adv.*, 13, 27174 (2023); *Idem Coord. Chem. Rev.*, 496, 215403 (2023).

2. Figueras R., Gómez R. y Primet M., *Adv. Chem., Set.*, I_22, 480 (1973).

3. Grieve, K., Mulvaney, P. y Grieser, F. Synthesis and electronic properties of semiconductor nanoparticles/quantum dots. *Current Opinion in Colloid and Interface Science*, 5: 168-172 (2000). DOI: 10.1016/S1359-0294(00)00050-9

4. Lu, A. H., Salabas, E. L. y Schuth, F. Magnetic nanoparticles: Synthesis, protection, functionalization, and applications. *Angew. Chem. Int. Ed.*, 46: 1222-1244 (2007). https://doi.org/10.1002/anie.200602866

5. López-Gaona A., De los Reyes José A., Aguilar J. y Martín N. *React. Kinet. Mech. & Catal.*, 99 (1), 177 (2010); *Idem React. Kinet. Mech & Catal.*, 101. 491 (2010); Idem, RMIQ, 11(3), 463 (2012).

6. Liu L. y Corma A. Metal catalysts for heterogeneous catalysis: from single atoms to nanoclusters and nanoparticles. *Chem Rev* 118:4981–5079 (2018). https :// doi.org/10.1021/acs.chemr ev.7b007.

7. Martínez-Rico M., Aguilar-Pliego J., Gutiérrez-Arzaluz M., Viniegra-Ramírez M., Martín-Guaregua N. y Garcia-Ruiz M. *RMIQ*, 17 (2), 523 (2018); *Idem JAR&T*, 16, 511 (2018); *Idem* JMCS, 64 (4), 327 (2020).

8. Medintz, I. L., Uyeda, H. T., Goldman, E. R. y Mattoussi, H. Quantum dot bioconjugates for imaging, labelling and sensing. *Nature Mat.*, 4: 435-446 (2005).

9. Martin N., Córdoba G., López-Gaona A. y Viniegra M. *React. Kinet. & Catal. Lett.*, 44 381 (1991); *Idem J. Mol. Catalysis*, 58, 107 (1990); *Idem React. Kinet. & Catal. Lett.*, 49 (2), 353 (1993); *Idem, J. Molec. Catalysis*, 96 (2), 155 (1995). https://doi.org/10.1016/1381-1169(94)00041-7.

10. Martín N., Viniegra M., Lima E. y Espinosa G. *Ind. Eng. Chem. Res.*, 43, 1206 (2004); *Idem*, *Catal Today*, 107-108 (2005), 719-725; *Idem, Ind. Eng. Chem. Res.*, 46, 4335 (2007); *Idem, Materials Research Innovations*, 14(2). 183-188 (2010).

11. Sapi András, Rajkumar T., Kiss Janos, Kukovecz Ákos, Kónya Zoltán y Somorjai Gabor A., Metallic Nanoparticles in Heterogeneous Catalysis, *Catalysis Letters* 151:2153–2175 (2021). https://doi.org/10.1007/s10562-020-03477-5

12. Shipway, A. N., Katz, E. y Willner, I. Nanoparticle arrays on surfaces for electronic, optical, and sensor application. *Chem. Phys. Chem.*, 1: 18-52 (2000). https://doi.org/10.1002/1439-7641(20000804)1:1<18::AID-CPHC18>3.0.CO;2-L

13. Stair P. C. The concept of Lewis acids and bases applied to surfaces. *J. Am. Chem. Soc.*, 104, 4044 (1982). https://doi.org/10.1021/ja00379a002

14. Thomas J. M. y Thomas W. J. *Principles and practice of heterogeneous catalysis*. VCH Alemania (1997).

15. Tsubota, S., Nakamura, T., Tanaka, K. y Haruta, M. (1998) Effect of calcination temperature on the catalytic activity of

Au colloids mechanically mixed with TiO2 powder for CO oxidation. *Catal*. *Lett.*, 56: 131-135. Zanella Rodolfo. Aplicación de los nanomateriales a la catálisis. *Mundo Nano*, 7 (12), 66 (2014).

16. Zhou Y., Yin Ch, Li Y. y Shen W. Dynamic behavior of metal nanoparticles for catalysis. *Nanotoday*, 20, 101-120 (2018). https://doi.org/10.1016/j.nantod.2018.04.005.

UNIVERSIDAD AUTÓNOMA METROPOLITANA
Casa abierta al tiempo
Unidad Iztapalapa

2025 Instituto Carlos Graef 14 años guiando jóvenes hacia la ciencia y la ingeniería

Los Departamentos de Física, Matemáticas, Ingeniería Eléctrica, Ingeniería de Procesos e Hidráulica y Química de la División de Ciencias Básicas e Ingeniería

Otorgan la presente

CONSTANCIA

a

Dr. Ricardo A. Peralta Ávila

Por su participación como miembro del comité organizador de las actividades del Instituto Carlos Graef, Jóvenes hacia la Ciencia y la Ingeniería, celebrado los sábados 08, 15, 22 y 29 de marzo, así como el 05 de abril de 2025. Ciudad de México.

[redacted]

Dr. Román Linares Romero
Director de División CBI



UNIVERSIDAD AUTÓNOMA METROPOLITANA
UNIDAD IZTAPALAPA
DEPARTAMENTO DE QUÍMICA

DQ.0335.2024

Diciembre 02, 2024

A quien corresponda
P r e s e n t e.

Por este medio me permito informarle que el Dr. Ricardo Atahualpa Peralta Ávila es parte del Comité Editorial del Podcast del Departamento de Química, Q-UAM-I. Esta asignación comenzó el 06 de julio de 2023 y continúa hasta la fecha. Es importante mencionar que Q-UAM-I se realiza a través de las cápsulas informativas que aporta nuestra comunidad científica y que son publicadas a través de una revisión por pares, en ese sentido el Comité Editorial de Q-UAM-I es similar a un comité editorial de revistas científicas. Sin duda, la participación universitaria del Dr. Peralta es crucial para la difusión y divulgación de nuestro quehacer científico.

Se hace constancia de lo anterior para los fines que necesite realizar o tramitar el Dr. Peralta Ávila.

A t e n t a m e n t e
Casa abierta al tiempo

[redacted]

Dr. Jorge Garza Olguín
Jefe del Departamento de Química

UNIDAD IZTAPALAPA
División de Ciencias Básicas e Ingeniería
Departamento de Química
Ave. Ferrocarril San Rafael Atlixco 186. Col. Leyes de Reforma 1A Sección. Iztapalapa C.P. 09310. CdMx, México.
Apartado Postal 55-534.

CamScanner

5. Gestión de recursos financieros

Casa abierta al tiempo
UNIVERSIDAD AUTÓNOMA METROPOLITANA

CDMX a 9 Enero del 2025

Comisión Dictaminadora de Área de CBI
P R E S E N TE

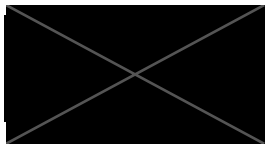
El proyecto “Bio-MOFs: Hacia la erradicación selectiva de contaminantes emergentes en aguas” ha sido seleccionado en la convocatoria de la UAM y cuenta con la valiosa participación del Dr. Ricardo A. Peralta Ávila, profesor visitante del Departamento de Química de la Unidad Iztapalapa.

Gracias a su experticia en [área de especialización], el Dr. Peralta Ávila ha sido fundamental en el diseño experimental y la obtención de resultados preliminares prometedores. El objetivo principal de este proyecto es desarrollar materiales innovadores basados en Bio-MOFs para eliminar de manera selectiva contaminantes emergentes presentes en el agua, contribuyendo así a la protección del medio ambiente.

Este proyecto representa un avance significativo en la búsqueda de soluciones sostenibles para la contaminación del agua y posiciona a la UAM como líder en esta área de investigación. Invitamos a la comunidad universitaria a conocer más sobre este proyecto y a participar en futuras colaboraciones."

Sin más por el momento, quedo de ustedes para cualquier comentario.

Atentamente,



Julia Aguilar Pliego
Departamento de Ciencias Básicas
Área de Química Aplicada
UAM-Azcapotzalco

Casa abierta al tiempo
UNIVERSIDAD AUTÓNOMA METROPOLITANA
Unidad Iztapalapa

Departamento de Química
División de Ciencias Básicas e Ingeniería

CDMX a 25 Noviembre del 2024

ASUNTO
Justificación de “rol” en proyectos financiados
A quien corresponda
P R E S E N TE

Por este medio comunico que el que suscribe, Dr. Ricardo Atahualpa Peralta Ávila, que actualmente me desempeño como profesor visitante del Departamento de Química, no he podido participar como titular en el proyecto financiado adjunto. Esto ha sido debido a que, para la presente convocatoria se ha solicitado que el responsable fuera de personal de tiempo indeterminado dentro de la institución. Debido a que me encuentro actualmente como profesor de tiempo determinado dentro de la institución, me ha imposibilitado postularme como titular del presente proyecto. Sin embargo, es importante resaltar que he participado activamente durante todo en el proceso para poder obtener la presente financiación.

Sin más por el momento, quedando de ustedes para cualquier comentario.
Reciban un Cordial Saludo



Ricardo Atahualpa Peralta Avila
División de Ciencias Básicas e Ingeniería
UAM - Iztapalapa

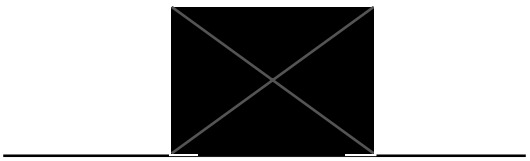
DAI/09/10

La Rectoría General de la Universidad Autónoma Metropolitana, a través de la Dirección de Apoyo a la Investigación (DAI), extiende la siguiente

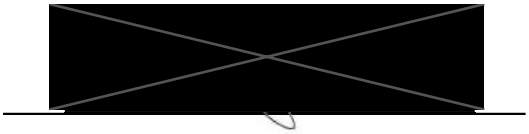
CONSTANCIA

a la Doctora **Julia Aguilar Pliego**, profesora investigadora adscrita a la Unidad Azcapotzalco de la Universidad Autónoma Metropolitana como responsable del proyecto **Bio-MOFs: Hacia la erradicación selectiva de contaminantes emergentes en aguas.** Proyecto que fue seleccionado por el Comité Evaluador en el marco de la Convocatoria para Postulación de Proyectos de Investigación relacionados con desafíos actuales.

Se extiende la presente en la Ciudad de México a los 7 días del mes de mayo del 2024.



Dr. José Antonio De los Reyes Heredia
Rector General



Dr. Rafael Bojalil Parra
Director de Apoyo a la Investigación

PARTICIPANTES DE LA UAM-AZCAPOTZALCO

- Dra. Julia Aguilar Pliego, (UAM-A), Número Económico: 12475
  Actividades:
  - Dirigir y supervisar las actividades relacionadas con la síntesis y caracterización del material nanoestructurado.
  - Contribuir en la elaboración de informes técnicos y científicos, así como en la redacción de artículos para publicación.

PARTICIPANTES DE LA UAM-IZTAPALAPA

- Dr. Ricardo Atahualpa Peralta Ávila, (UAM-I), Número Económico: 45029
  Actividades:
  - Sintetizar el SU-101 (MOF de bismuto) utilizando su experiencia en la síntesis de MOFs.
  - Caracterizar fisicoquímicamente el SU-101 mediante técnicas como DRX, Isotermas de N2, RMN, TGA, SEM, UV-Visible y FT-IR.

  Contribución:
  - Aportar conocimientos especializados en MOFs y catalización química para el desarrollo y caracterización del material nanoestructurado.
- Dra. Nancy Coromoto Martín Guaregua, (UAM-I), Número Económico: 10356
  Actividades:
  - Contribuir en la optimización de las condiciones experimentales para la degradación de contaminantes emergentes.
  - Investigar sobre oxidación de los contaminantes emergente mediante el uso de Bio-Mof.

  Contribución:
  - Investigar sobre materiales avanzados con aplicaciones tecnológicas que puedan complementar el desarrollo del proyecto
- Dr. Juan Marco Esparza Schulz, (UAM-I), Número Económico: 14365
  Actividades:
  - Realizar simulaciones de procesos de sorción de los contaminantes para estudiar la estructura y propiedades del bio-MOF.

  Contribución:
  - Aportar conocimientos en síntesis y caracterización de sólidos mesoporosos y en simulación de procesos de sorción para el estudio del material nanoestructurado.
- Dra. Nora Soyuki Portillo Vélez, (UAM-I), Número Económico: 32739
  Actividades:
  - Inmovilizar la enzima lacasa en el SU-101 utilizando su experiencia en nanomateriales y fotodegradación.
  - Caracterizar biofisicoquímicamente el bio-MOF obtenido (lacasa/SU-101).

  Contribución:
  - Aplicar sus conocimientos en nanomateriales y catalizadores para la síntesis y caracterización del bio-MOF.
- Dra. Leonardo David Herrera Zúñiga, (UAM-I), Número Económico: 29400
  Actividades:
  - Contribuir en la caracterización biológica de la enzima lacasa en estado libre e inmovilizada.

Dirección de Apoyo a la Investigación

Vinculación uam

Convocatoria para la postulación de Proyectos de Investigación relacionados con Desafíos Actuales

Resultados de la Convocatoria

La Rectoría General de la Universidad Autónoma Metropolitana, a través de la Dirección de Apoyo a la Investigación (DAI), se complace en anunciar los resultados de la convocatoria para Proyectos de Investigación relacionados con Desafíos Actuales.

Después de un proceso de revisión, el comité evaluador concluyó que los siguientes proyectos presentados en su versión final, cumplen con los estándares de calidad necesarios para recibir el apoyo.

Próximamente se enviará un correo electrónico que proporcionará detalles sobre los pasos necesarios para formalizar el respaldo de los proyectos. Este mensaje incluirá instrucciones detalladas sobre los procedimientos administrativos y los documentos necesarios.

• Valorización del sustrato residual en la producción de conidios fúngicos contra plagas agrícolas: tendencia a cero residuos y mejora de cultivos.

• Deterioro cognitivo y obesidad en mujeres adultas mayores: en búsqueda de una solución integral para un problema de salud pública.

• Transición de las plantas de tratamiento de aguas residuales hacia la economía circular y la sostenibilidad mediante el uso de microalgas.

• Estudio del potencial probiótico de bacterias aisladas de individuos sanos mexicanos con efectos benéficos sobre la enfermedad de hígado graso no alcohólico.

• Alimentación sostenible: diseño de agroecosistemas, medio ambiente y política pública para la Ciudad de México.

• Estrategias biotecnológicas para la producción de verbascósido y de otros compuestos fenólicos, moléculas activadoras de AMPK, una enzima clave para mantener "metabólicamente saludable" al organismo.

• Desarrollo de un sistema de fotobiorreactores para los procesos acoplados de mitigación de CO2 y producción de carotenoides por microalgas, con aplicación acuícola sustentable.

• Proyecto Agua Viva: aportes desde la UAM para lograr el acceso al agua en la comunidad rural de Jamiltepec, Oaxaca, México.

• Bio-MOFs: Hacia la erradicación selectiva de contaminantes emergentes en aguas.

• Estrategias para gestionar la Escasez de Agua en la

Ciudad de México (CDMX).

Rectoría Azcapotzalco Cuajimalpa

Iztapalapa Lerma Xochimilco

Universidad Autónoma Metropolitana, 2024

Contacto

PROYECTOS DE INVESTIGACIÓN EN TORNO A UN DESAFÍO ACTUAL

Título de la propuesta

" Bio-MOFs: Hacia la erradicación selectiva de contaminantes emergentes en aguas"

Responsable del proyecto:

Dra. Julia Aguilar Pliego

Universidad Autónoma Metropolitana - Azcapotzalco

CBI, Área de Química Aplicada

Ciudad de México, 03/Marzo/2024

PARTICIPANTES DE LA UAM-AZCAPOTZALCO

- Dra. Julia Aguilar Pliego, (UAM-A), Número Económico: 12475
  Actividades:
  - Dirigir y supervisar las actividades relacionadas con la síntesis y caracterización del material nanoestructurado.
  - Contribuir en la elaboración de informes técnicos y científicos, así como en la redacción de artículos para publicación.

PARTICIPANTES DE LA UAM-IZTAPALAPA

- Dr. Ricardo Atahualpa Peralta Ávila, (UAM-I), Número Económico: 45029
  Actividades:
  - Sintetizar el SU-101 (MOF de bismuto) utilizando su experiencia en la síntesis de MOFs.
  - Caracterizar fisicoquímicamente el SU-101 mediante técnicas como DRX, Isotermas de N2, RMN, TGA, SEM, UV-Visible y FT-IR.

  Contribución:
  - Aportar conocimientos especializados en MOFs y catalización química para el desarrollo y caracterización del material nanoestructurado.
- Dra. Nancy Coromoto Martín Guaregua, (UAM-I), Número Económico: 10356
  Actividades:
  - Contribuir en la optimización de las condiciones experimentales para la degradación de contaminantes emergentes.
  - Investigar sobre oxidación de los contaminantes emergente mediante el uso de Bio-Mof.

  Contribución:
  - Investigar sobre materiales avanzados con aplicaciones tecnológicas que puedan complementar el desarrollo del proyecto
- Dr. Juan Marco Esparza Schulz, (UAM-I), Número Económico: 14365
  Actividades:
  - Realizar simulaciones de procesos de sorción de los contaminantes para estudiar la estructura y propiedades del bio-MOF.

  Contribución:
  - Aportar conocimientos en síntesis y caracterización de sólidos mesoporosos y en simulación de procesos de sorción para el estudio del material nanoestructurado.
- Dra. Nora Soyuki Portillo Vélez, (UAM-I), Número Económico: 32739
  Actividades:
  - Inmovilizar la enzima lacasa en el SU-101 utilizando su experiencia en nanomateriales y fotodegradación.
  - Caracterizar biofisicoquímicamente el bio-MOF obtenido (lacasa/SU-101).

  Contribución:
  - Aplicar sus conocimientos en nanomateriales y catalizadores para la síntesis y caracterización del bio-MOF.
- Dra. Leonardo David Herrera Zúñiga, (UAM-I), Número Económico: 29400
  Actividades:
  - Contribuir en la caracterización biológica de la enzima lacasa en estado libre e inmovilizada.

- Participar en la determinación de la actividad catalítica óptima del bio-MOF para la degradación de contaminantes emergentes en agua.

Contribución:

- Aportar sus conocimientos en bioquímica catalítica y estructura de proteínas para el análisis de la actividad enzimática.

Av. San Pablo Xalpa 180, San Martin Xochinahuac, Azcapotzalco, 02128 Ciudad de México, CDMX

Tel/Fax 55 5318 9000

E-mail: apj@azc.uam.mx

Desafío por abordar:

La reutilización de aguas residuales es un aspecto crucial en la gestión sostenible del agua. Esto implica tratar las aguas residuales para eliminar contaminantes y luego utilizarlas para diversos fines en lugar de simplemente desecharlas como aguas negras. En este sentido, la eliminación de contaminantes emergentes presentes en aguas es esencial ya que, pueden ocasionar daños ambientales y de salud en el ser humano, aunado a que se carece de una regulación que determine y establezca los límites permitidos de dichos compuestos.

Justificación, relevancia y pertinencia:

La problemática de los contaminantes emergentes ha surgido recientemente y experimentado un crecimiento exponencial en los últimos años (Case Studies in Chemical and Environmental Engineering, 6 (2022), 100219). Dichos contaminantes son compuestos recién identificados que pueden ocasionar daños ambientales y de salud, caracterizándose por su aumento en el entorno y su capacidad de bioacumulación. La monitorización de estos elementos resulta problemática, y su regulación aún se encuentra en una fase incipiente. A pesar de ello, a medida que se descubren los efectos tóxicos y ecotóxicos asociados, se revela su importancia. Su origen comprende diversas fuentes, como procesos industriales, actividades agrícolas, productos farmacéuticos, y otros derivados de la actividad humana, como medicamentos, hormonas y compuestos químicos liberados en el medio ambiente a través de desechos líquidos. La necesidad de abordar la eliminación de estos contaminantes acuáticos resulta crucial, y aunque existen diversos sistemas y tecnologías como procesos avanzados de oxidación, métodos electroquímicos, adsorción por polímeros, carbón activado, fotocatálisis y procesos biológicos, algunos no han logrado el éxito deseado. En ocasiones, los productos generados por estos procesos resultan más contaminantes que los compuestos originales, perpetuando la contaminación en la cadena alimentaria terrestre y marina, con efectos potencialmente desconocidos. Dada esta problemática, se requiere una investigación extensa para desarrollar tecnologías más efectivas y sostenibles para mitigar la presencia de estos contaminantes en el agua. La creación de materiales biocompatibles y eficientes, para la eliminación de contaminantes emergentes en aguas, se presenta como una solución viable, económica y ecológica en el marco de una química verde, crucial para el desarrollo sostenible de nuestro país y región.

OBJETIVO GENERAL Y OBJETIVOS PARTICULARES

Objetivo General:

- Desarrollar un material nanoestructurado (bio-MOFs) mediante la combinación de un Marco Orgánico-Metálico (MOF) y una proteína, con el fin de posibilitar la eliminación de contaminantes emergentes presentes en cuerpos de agua.

Objetivos Particulares:

- Sintetizar el SU-101 (MOF de bismuto) a partir de ácido elágico comercial.
- Caracterizar fisicoquímicamente el SU-101 mediante DRX, Isotermas de N_2, RMN TGA, Microscopia electrónica de barrido (SEM), Espectroscopías UV-Visible y Espectroscopia FT-IR.
- Inmovilizar la enzima lacasa en el SU-101, mediante el método de encapsulación.
- Caracterizar biofisicoquimica del bio-MOF obtenido (lacasa/SU-101).
- Determinar la actividad catalítica optima del bio-MOF para la degradación de contaminantes emergente en agua, paracetamol y metformina.

METAS Y ESTRATEGIAS DETALLADAS

Metas:

- Establecer una metodología para la obtención del bio-MOF: lacasa/SU-101.
- Optimizar los parámetros para la degradación de los contaminantes emergentes paracetamol y metformina en el agua.
- Coadyuvar al fortalecimiento y crecimiento de los grupos y áreas de investigación en las instituciones participantes.
- Apoyar en la formación de recursos humanos a nivel licenciatura y posgrado mediante la dirección y/o co-dirección de al menos un par de tesis o proyectos terminales.
- Publicación de al menos dos artículos originales en revistas científicas indizadas.
- Continuar con la búsqueda de financiamiento que permita la continuación del presente proyecto.

Estrategia integral para abordarlo:

En la actualidad, se ha encontrado que algunos sistemas biológicos son considerablemente más eficientes que los métodos convencionales en la absorción y degradación de compuestos orgánicos. Las enzimas desempeñan un papel fundamental en los procesos de biodegradación, catalizando la descomposición de diversos contaminantes en sustancias menos nocivas o no tóxicas. La degradación enzimática surge como un enfoque ecológico y sostenible para eliminar los contaminantes emergentes del agua. Sin embargo, el uso de enzimas en estado libre presenta desafíos, ya que muchas de ellas pierden su actividad catalítica en condiciones extremas, como

bajos o altos niveles de pH. Una de las rutas para proveer mayor estabilidad y mejorar su rendimiento es la inmovilización, la cual ha tenido excelentes resultados a nivel industrial y de investigación.

La lacasa, una enzima altamente valiosa y versátil, encuentra su origen en diversas fuentes, tales como hongos, bacterias, arqueas y plantas, desempeñando roles cruciales en los mecanismos metabólicos. Estas fuentes heterogéneas proporcionan una amplia variedad de propiedades y aplicaciones para la lacasa, abarcando desde procesos industriales hasta la remediación ambiental. La lacasa opera a través de un mecanismo bi-funcional que abarca actividades anabólicas y catabólicas. Cataliza oxidaciones directas e indirectas, limitadas por el potencial de ionización del sustrato. La enzima se especializa en la oxidación de las subunidades fenólicas de la lignina, induciendo la oxidación de C(alfa), la ruptura del enlace C(alfa)-C(beta) y el arilo-alquilo. Este proceso catalítico implica la reducción del Cu tipo 1 por el sustrato reductor, seguida de la transferencia interna de electrones a un clúster trinuclear para la reducción de oxígeno al agua. La función del clúster trinuclear en la unión y reducción del oxígeno diatómico culmina en la liberación de agua. En consecuencia, comprender los mecanismos moleculares de la lacasa mejora significativamente sus aplicaciones biotecnológicas, facilitando la replicación de sus actividades para diversos propósitos (Chemical Physics 517 (2019) 253–26).

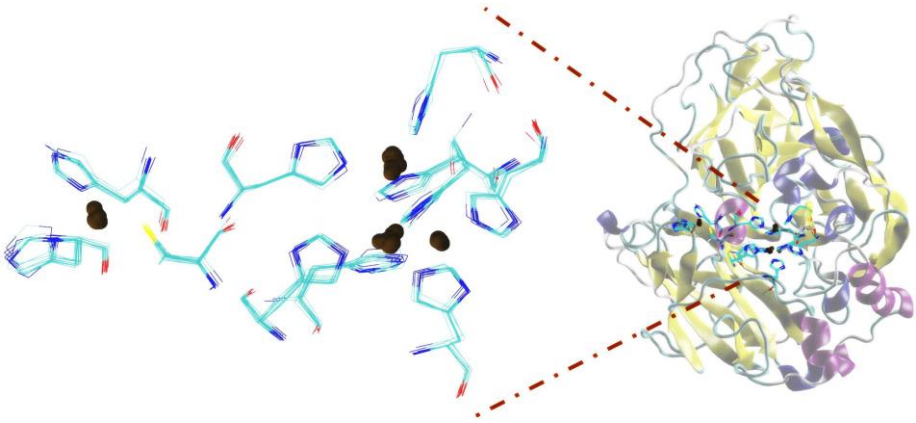


Figura 1. Estructura y sitio catalítico de la enzima Lacasa

Investigaciones recientes se centran en abordar la contaminación ambiental mediante enfoques innovadores que exploran microorganismos y enzimas para la biodegradación. En particular, nuestra investigación se orienta hacia la optimización de las características de oxido-reducción de la lacasa, dirigida a sustratos ambientalmente adversos, y la aplicación de técnicas de inmovilización económicamente viables para el tratamiento de aguas residuales. Estos métodos innovadores buscan mejorar la reutilización de la lacasa en condiciones extremas de pH y concentración de sal. Las tecnologías de inmovilización "green" fomentan el uso de biomateriales rentables, prometiendo contribuir significativamente a la reducción de la contaminación (Microbial Cell Factories 18(1), 2019, 18:200). Se espera que la creciente demanda de lacasas inmovilizadas (materiales porosos) y eficientes impulse los procesos comerciales de oxidación, ofreciendo así una valiosa contribución a la sostenibilidad ambiental.

La inmovilización de enzimas mediante el uso de materiales amigables permite conservar y, en algunos casos, potenciar sus propiedades de estabilidad en condiciones adversas. La inmovilización facilita la separación y recuperación de las enzimas, convirtiéndolas en materiales reutilizables. Entre los materiales más destacados para este propósito se encuentran los Materiales Híbridos Metal-Orgánicos (MOFs, por sus siglas en ingles), una categoría de materiales cristalinos sólidos porosos que ha experimentado un notable avance en los últimos años (Coordination Chemistry Reviews, 496 (2023), 215403). Estos sistemas se componen de clústeres o nodos metálicos conectados por moléculas orgánicas, generando estructuras unidimensionales, bidimensionales o tridimensionales. La unión de metal y ligando mediante enlaces de coordinación confiere una estabilidad significativa a las enzimas. La diversidad estructural única de los MOFs, derivada de las combinaciones de elementos orgánicos e inorgánicos, los distingue de otros materiales porosos convencionales, como las zeolitas o el carbón activado. Esto permite que la inmovilización en las enzimas sea de maneras diversas y con diferentes perspectivas. Principalmente, existen tres estrategias básicas para la inmovilización de proteínas: bioconjugación, infiltración y encapsulación. (Coordination Chemistry Reviews, 429 (2021), 213651). La estrategia de bioconjugación implica la inmovilización de biomacromoléculas en la superficie exterior de los MOF, ya sea mediante una unión covalente o mediante la adsorción inducida por las interacciones electrostáticas. La infiltración se refiere a la inmovilización de biomacromoléculas dentro de la red de poros del material mediante procesos de difusión. Las estrategias de encapsulación implican el crecimiento de una capa de MOF alrededor de una bioentidad objetivo y esta metodología es el foco de la revisión actual. Una variedad de bioentidades que abarcan una amplia gama de tamaños, desde pequeñas proteínas hasta células y virus más grandes, han sido encapsuladas con éxito mediante una cubierta de MOF. Esto se debe a que el método de encapsulación no está limitado por el tamaño de los poros del MOF, ya que el MOF crece alrededor de la bioentidad. La integración de biomacromoléculas dentro de una capa de MOF se puede lograr mediante métodos de creación de plantillas o mediante la síntesis “one-pot” MOF en presencia de la biomolécula. Esta última estrategia ha sido ampliamente explorada debido a todas las propiedades mencionadas y es una de las más prometedoras en el encapsulamiento de biomacreomoléculas como, por ejemplo, la lacasa.

La creación de materiales biocompatibles y eficientes, para la eliminación de contaminantes emergentes en aguas, se presenta como una solución viable, económica y ecológica en el marco de una química verde, crucial para el desarrollo sostenible de nuestro país y región. Uno de los contaminantes emergentes de las últimas décadas es el bisfenol A (BPA), el cual es comúnmente utilizado para la producción de algunos plásticos y resinas epóxicas. Debido a la alta demanda de plástico en las últimas décadas la cantidad de BPA es cada vez más abundante y, por lo tanto, la migración a alimentos y aguas se produce más fácilmente. Ingerir este compuesto ha atraído múltiples preocupaciones, ya que se sabe que el BPA tiene efectos estrogénicos, lo que significa que puede imitar la hormona estrógeno en el cuerpo (Nat Rev Endocrinol, 9 (2013), 9-10). Esto ha generado preocupación sobre su potencial para alterar el sistema endocrino, particularmente durante etapas sensibles del desarrollo. Debido a las complicaciones que este y demás contaminantes emergentes puedan generar, se ha investigado utilizar materiales porosos capaces de soportar enzimas para su la degradación. Un ejemplo de

este enfoque se observa en la investigación llevada a cabo por Yang *et al.* (International Journal of Biological Macromolecules, 233 (2023), 123410), donde se realizó la encapsulación de la lacasa en un MOF bimetálico Cu/Zn con el propósito de mejorar su estabilidad y facilitar su reutilización en la decolorización de aguas residuales contaminadas con tintes orgánicos. En este contexto, el MOF bimetálico exhibió una efectiva protección y una notable estabilidad operativa, revelando el potencial de estos materiales en la remediación del agua. Otro ejemplo es la investigación dirigida por Emre Birhanlı *et al.* (Chemosphere, 292 (2022), 133382) que diseñó un MOF de cobalto (Co) y cobre (Cu) capaz de soportar la lacasa, para la eliminación de colorantes textiles. En este contexto, Emre demostró la viabilidad de la reutilización de la enzima encapsulada, ofreciendo una perspectiva prometedora para aplicaciones futuras en la eliminación eficiente de colorantes textiles en aguas residuales industriales. Debido a estas propiedades, el presente proyecto ha enfocado su atención en degradar BPA por medio de lacasa que se encontrará encapsulada en un sólido poroso generado por una síntesis amigable con el medio ambiente.

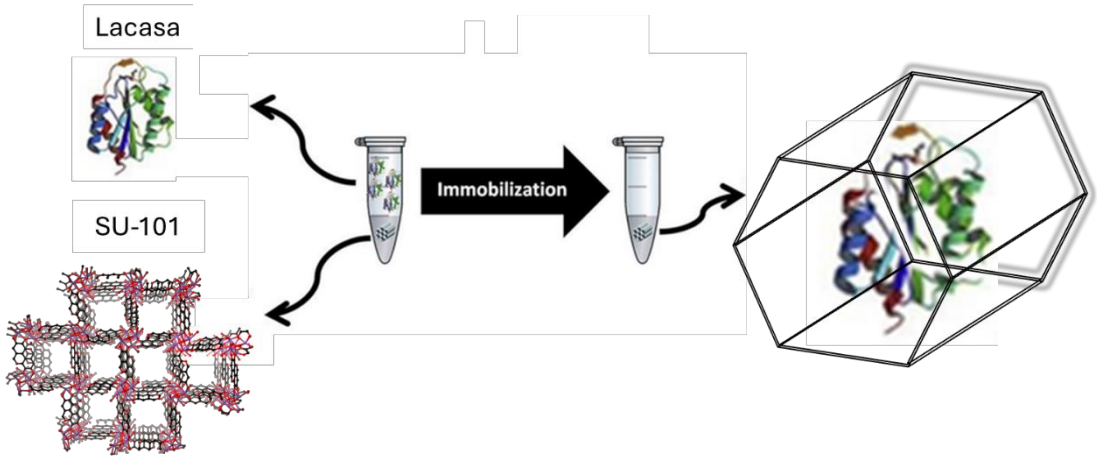


Figura 2. Inmovilización de enzimas en Red metal-orgánicas (MOFs; por sus siglas en ingles).

Inspirados por la estabilidad potencial de los MOF a base de fenolato, junto con la creciente demanda global de ampliar el uso de recursos renovables, hemos recurrido a los taninos para la síntesis de MOF “verdes”, específicamente, galotaninos y elagitaninos, que contienen ácido gálico o ácido elágico, como subunidades, respectivamente. Si bien el ácido gálico, que consta de grupos funcionales de ácido carboxílico y fenol, se ha utilizado como conector para la síntesis de un puñado de MOF, sorprendentemente el ácido elágico se ha utilizado solamente una ocasión para la síntesis de MOF. El ácido elágico se encuentran en alimentos como fresas, frambuesas, uvas, nueces y granadas, así como en bebidas como el vino, el whisky y otras bebidas espirituosas. Por lo tanto, el ligante utilizado en la síntesis del material es totalmente no tóxico, por otro lado, el bismuto que forma parte de la parte inorgánica se encuentra en medicamentos antidiarreicos, aportando de igual manera una síntesis totalmente verde.

PLAN DE TRABAJO Y CRONOGRAMA DE ACTIVIDADES DETALLADO

Plan de trabajo y metodología

El SU-101 (MOF de bismuto) se preparará a partir de una suspensión acuosa de acetato de bismuto y ácido elágico (inicialmente, se plantea comprar el ácido elágico a Sigma, posteriormente se plantea corroborar si se puede sintetizar con suplementos alimenticios que contienen ácido elágico) agitada en condiciones ambientales (es decir, temperatura ambiente y presión atmosférica en aire) durante 48 h. La pureza de la fase y la reproducibilidad de la síntesis se mejoran mediante la introducción de ácido acético como modulador (6 % en volumen, ya sea de ácido acético glacial o de una solución madre de vinagre blanco destilado, pH ≈ 2,3). Esta concentración de ácido acético está dentro del rango de lo que se encuentra en el vinagre doméstico común (5-12 % en volumen de ácido acético en vinagre blanco destilado). Es importante mencionar que, se puede hablar de una síntesis amigable con el medio ambiente por los reactivos utilizados durante la síntesis. El producto se separará para poder lavarlo con agua, etanol, acetona y secarlo posteriormente. El material será caracterizado por medio de difracción de rayos X en polvo (PXRD), Isotermas de N_2, Resonancia Magnética Nuclear en el estado sólido (SRMN), análisis termogravimétrico (TGA), Microscopia electrónica de barrido (SEM), Espectroscopía UV-Visible y Espectroscopia FT-IR. Es importante recalcar que, la isoterma de N_2 es indispensable para saber si la enzima se encuentra encapsulada dentro del material, ya que, se espera que haya un cambio en el tipo de isoterma de un tipo I a tipo II. Con esto, aseguraremos que dentro del material haya un cambio de microambiente en el material, de un microporoso a mesoporoso, y con esto confirmando que la enzima confinada dentro del material modificó la porosidad del material.

Caracterización Biológica

Para caracterizar la parte biológica, se procederá a cuantificar las proteínas en ambas condiciones (libre e inmovilizada) utilizando el método bicinconínico. Para ello, se prepararán estándares de proteína en concentraciones conocidas y se añadirá el reactivo bicinconínico a las muestras, midiendo la absorbancia a la longitud de onda apropiada para determinar las concentraciones de proteínas. Posteriormente, se evaluará la capacidad catalítica de la enzima lacasa en estado libre y en su forma inmovilizada. En el caso de la enzima libre, se realizarán ensayos con ABTS a diferentes pH y temperaturas, midiendo la absorbancia a 420 nm a intervalos regulares para registrar la cinética de la reacción. Se construirán curvas de Michaelis-Menten mediante experimentos a diferentes concentraciones de enzima y sustrato. Para la enzima inmovilizada con bismuto y ácido elágico, se seguirá un procedimiento similar, comparando las cinéticas de reacción con la enzima libre con el fin de evaluar posibles mejoras en la estabilidad y actividad catalítica provocada por la inmovilización. Luego, se llevará a cabo un estudio de la estructura de la enzima mediante colorismo circular (CD). Las muestras de enzima en ambos estados se diluirán a una concentración adecuada en un tampón compatible con el análisis de CD. Se realizarán medidas en un espectrofotómetro de CD en el rango de longitud de onda apropiado para evaluar la estructura secundaria de la enzima. Los resultados se analizarán para identificar posibles cambios en la estructura secundaria entre la enzima libre y la inmovilizada. Finalmente, se compararán y analizarán los resultados obtenidos, evaluando la influencia de diferentes pH y temperaturas en la actividad catalítica, así como la

estabilidad estructural de la enzima. Las conclusiones derivadas de este protocolo proporcionarán una comprensión más completa de las características cinéticas y estructurales de la lacasa en sus formas libre e inmovilizada con bismuto y ácido elágico.

Determinación de la degradación enzimática

Para llevar a cabo el seguimiento de la actividad biológica relacionada con la adsorción y degradación de contaminantes emergentes, como paracetamol, metformina e ibuprofeno, mediante la enzima lacasa en sus formas libre e inmovilizada, se propone un protocolo integrado. En primer lugar, se prepararán soluciones de los contaminantes emergentes en concentraciones conocidas en un medio acuoso adecuado para la actividad enzimática. Posteriormente, se llevarán a cabo ensayos con la enzima lacasa en su forma libre, incubando cada sustrato en condiciones óptimas de pH y temperatura. Durante estos ensayos, se realizará un seguimiento cinético midiendo la absorbancia característica a intervalos regulares para registrar la cinética de la reacción de degradación de cada contaminante. Se construirán curvas de degradación y se determinarán las velocidades iniciales de la reacción. Luego, se repetirán los ensayos utilizando la enzima lacasa inmovilizada con bismuto y ácido elágico. La actividad de degradación de la enzima inmovilizada se comparará con la de la enzima libre para evaluar la eficiencia de la inmovilización. Además, se optimizarán las condiciones experimentales, variando parámetros como pH, temperatura y concentraciones de sustrato para maximizar la actividad de degradación en ambas formas enzimáticas. Para identificar y cuantificar los productos de degradación, se emplearán técnicas cromatográficas, como la cromatografía líquida de alta resolución (HPLC). La eficiencia de degradación se comparará entre la enzima lacasa libre e inmovilizada para cada contaminante emergente. Se evaluará la estabilidad de la enzima inmovilizada a lo largo del tiempo y se observarán posibles cambios en la eficiencia de degradación. El análisis de los resultados permitirá extraer conclusiones sobre la idoneidad de la enzima lacasa inmovilizada para la degradación de contaminantes emergentes, considerando aspectos de eficiencia y estabilidad. Este enfoque integral proporcionará información valiosa para aplicaciones ambientales y de tratamiento de aguas residuales, destacando las posibles ventajas de la biocatálisis en remediación de aguas y en búsquedas de la eliminación de contaminantes emergentes que puedan dañar nuestra salud.

CRONOGRAMA DE ACTIVIDADES

Actividad	Meses											
	1-2	3-4	5-6	7-8	9-10	11-12	13-14	15-16	17-18	19-20	21-22	23-24
A1	■	■	■									
A2		■	■	■	■							
A3				■	■	■						
A4							■	■	■	■		
A5									■	■	■	
A6										■	■	■	■									
A7										■	■	■	■	■								
A8												■	■	■	■							
A9													■	■	■	■						
A10													■	■	■	■	■	■	■			
A11																	■	■	■	■	■	
A12																						■

Nomenclatura:

A1:

- Preparación del SU-101 a partir de ácido elágico comercial.
- Caracterización fisicoquímica del SU-101 mediante DRX, Isotermas de N2, RMN, TGA, SEM, Espectroscopía UV-Visible y FT-IR.

A2:

- Inicio de la formación de recursos humanos a nivel licenciatura y posgrado.
- Inmovilización de la Enzima Lacasa en el SU-101
- Desarrollo del método de encapsulación de la enzima lacasa en el SU-101.
- Caracterización biofisicoquímica del bio-MOF obtenido (lacasa/SU-101).

A3:

- Evaluación y ajuste de las condiciones de inmovilización para maximizar la actividad catalítica de lacasa/SU-101.

A4:

- Cuantificación de las proteínas en ambas condiciones (libre e inmovilizada) mediante método bicinconínico.
- Evaluación de la actividad catalítica óptima de lacasa/SU-101.

A5:

- Continuación de la formación de recursos humanos a nivel licenciatura y posgrado.
- Redacción y envío del primer artículo original para su publicación en revistas científicas indizadas.

A7:

- Caracterización de los contaminantes emergentes mediante técnicas analíticas.

A8:

- Conclusión de la formación de recursos humanos a nivel licenciatura y posgrado.
- Evaluación de Degradación Enzimática
- Realización de ensayos de degradación de los contaminantes emergentes utilizando lacasa libre e inmovilizada.
- Seguimiento cinético de la reacción de degradación.
- Optimización de condiciones experimentales para maximizar la actividad de degradación.

A9:

- Empleo de técnicas cromatográficas (HPLC) para identificar y cuantificar los productos de degradación.
- Comparación de la eficiencia de degradación entre lacasa libre e inmovilizada.
- Evaluación de la estabilidad de la enzima inmovilizada a lo largo del tiempo.

A10:.

- Extracción de conclusiones sobre la idoneidad de lacasa inmovilizada para la degradación de contaminantes emergentes.

A11:

- Redacción y envío del segundo artículo original para su publicación en revistas científicas indizadas.

A12:

- Escritura de Informe Final

RESULTADOS ESPERADOS DETALLADOS (APORTES, RELEVANCIA, IMPLICACIONES CIENTÍFICAS, TECNOLÓGICAS O SOCIALES)

Resultados esperados:

Resultados a Corto Plazo:

1. Establecimiento de Metodologías:
   - Desarrollo y optimización de las metodologías para la obtención de bio-MOFs.
   - Establecimiento de condiciones de síntesis y caracterización para asegurar la reproducibilidad y eficacia del proceso.
2. Caracterización y Evaluación de Bio-MOFs:
   - Caracterización de los bio-MOFs obtenidos mediante técnicas fisicoquímicas avanzadas.
   - Evaluación de la capacidad de los bio-MOFs para la eliminación de contaminantes emergentes presentes en el agua.
3. Publicación en Revista Indizada:
   - Redacción y envío de un artículo original a una revista científica indizada.
   - Divulgación de los resultados obtenidos en el proceso de investigación a la comunidad científica internacional.
4. Formación de Recursos Humanos:
   - Orientación y formación de estudiantes a nivel de posgrado y licenciatura en el marco del proyecto.
   - Transferencia de conocimientos y habilidades para impulsar el desarrollo de futuros investigadores en el campo.

Resultados a Largo Plazo:

1. Obtención de Recursos mediante Proyectos:
   - Consolidación del proyecto como plataforma para la obtención de financiamiento adicional mediante la presentación de nuevos proyectos.
   - Ampliación de recursos para continuar la investigación y desarrollo en el área de los biomateriales y su aplicación en la remediación ambiental.
2. Publicaciones Científicas y Divulgativas:
   - Publicación de al menos un segundo artículo en revista científica indizada, destacando los avances y descubrimientos obtenidos.
   - Contribución con un artículos de divulgación para compartir los resultados con un público más amplio y promover el conocimiento en el área.
3. Continuación de Formación de Recursos Humanos:
   - Continuación y fortalecimiento de la formación de recursos humanos a nivel de posgrado y licenciatura.
   - Impulso al crecimiento académico y profesional de estudiantes, fomentando su participación en la investigación científica y tecnológica.
4. Retribución y Apropiación Social de la Ciencia:
   - Realización de actividades de divulgación científica dirigidas a la comunidad local y regional, con el fin de sensibilizar sobre la importancia de la investigación en la resolución de problemas ambientales.

- Establecimiento de colaboraciones con instituciones gubernamentales, organizaciones no gubernamentales y empresas para la aplicación práctica de los resultados obtenidos, contribuyendo así a la solución de problemas reales en la sociedad.

Av. San Pablo Xalpa 180, San Martin Xochinahuac, Azcapotzalco, 02128 Ciudad de México, CDMX

Tel/Fax 55 5318 9000

E-mail: apj@azc.uam.mx

PRESUPUESTO DETALLADO

Propuesta general del presupuesto:

Los proponentes del presente proyecto, contamos con la infraestructura especializada necesaria para la ejecución de la experimentación, no obstante, nos encontramos limitados en los insumos, así como por la insuficiencia de materiales menores. El desglose financiero a continuación presentado sobre las actividades aborda aspectos generales del proceso, a continuación, se presenta el presupuesto para la realización de cada uno de los siguientes puntos:

- Cuantificación de la actividad de lacasa libre e inmovilizada: $100,000.00
  Adquisición de reactivos y sustratos esenciales para evaluar la actividad enzimática en ambas formas.
- Cuantificación de proteína libre, inmovilizada y de lavados: $40,000.00
  Aplicación del método bicinconínico para la cuantificación precisa de las concentraciones proteicas en las muestras.
- Ultrafiltración y diálisis: $50,000.00
  Compra de ultrafiltro, membranas y nitrógeno destinados a realizar la ultrafiltración y diálisis de las muestras pertinentes.
- Purificación de la lacasa por cromatografía de intercambio iónico: $100,000.00
  Adquisición de columnas para FPLC y reactivos especializados necesarios para la efectiva purificación de la enzima mediante cromatografía.
- Caracterización bioquímica y estructural (kcat, pH y Temperatura) de la lacasa libre e inmovilizada: $60,000.00
  Empleo de técnicas bioquímicas para estudiar detalladamente las propiedades de la lacasa mediante técnicas de UV-Vis y Dicroismo Circular.
- Inmovilización de la actividad de la enzima lacasa con bismuto y ácido elágico: $80,000.00
  Compra de bismuto, ácido elágico y otros insumos esenciales para llevar a cabo el proceso de inmovilización de la enzima.
- Pruebas de eficiencia enzimática y Caracterización de contaminantes emergentes: $70,000.00
  Realización de ensayos de cinética enzimática para evaluar con precisión la eficiencia de la enzima en el proceso de degradación de contaminantes emergentes. Además, análisis con espectroscopia de masas y HPLC permiten identificar y cuantificar productos de degradación, evaluando la eficacia del proceso enzimático y formación de productos secundarios.

Adicionalmente, se destaca que, aunque el alcance inicial del proyecto se centra en la degradación de uno o dos contaminantes emergentes, el respaldo financiero permitirá realizar investigaciones exhaustivas con aplicabilidad extensiva a diversos contaminantes, incluyendo fármacos disponibles en el laboratorio o mediante colaboraciones externas. Este proyecto contribuirá sustancialmente a la formación de recursos humanos, colaboración de varias divisiones, promoción de la investigación y desarrollo de biomateriales completamente sustentables en consonancia con los principios de la química verde.

ESTRATEGIAS PARA OBTENER RECURSOS ADICIONALES

Para obtener recursos adicionales para nuestro proyecto de investigación, podemos implementar diversas estrategias y aprovechar las oportunidades que ofrecen distintas instituciones y entidades tanto a nivel nacional como internacional. Algunas estrategias específicas que podríamos considerar:

CONACHyT (Consejo Nacional de Ciencia, Humanidades y Tecnología):

- Aplicar a los distintos programas de financiamiento que ofrece el CONACHyT para proyectos de investigación en diversas áreas del conocimiento.
- Participar en convocatorias específicas del CONACHyT para obtener becas, fondos de investigación y apoyo para la formación de recursos humanos en ciencia y tecnología.

CECTEI (Comisión de Ciencia, Tecnología e Innovación):

- Presentar nuestra propuesta de investigación en conjunto con otra institución que nos permita obtener la asignación de recursos para proyectos de investigación.

Fondos Sectoriales:

- Identificar los fondos sectoriales relacionados con nuestras áreas de investigación y participar en convocatorias para obtener financiamiento específico para proyectos alineados con las prioridades de cada sector.
- Establecer alianzas con instituciones y organismos vinculados a los distintos sectores para acceder a oportunidades de financiamiento y colaboración.

Empresas e Industrias:

- Explorar oportunidades de colaboración con empresas e industrias que puedan beneficiarse de los resultados de nuestros proyectos de investigación.
- Ofrecer servicios de consultoría, desarrollo tecnológico o innovación a empresas interesadas en financiar proyectos de investigación en áreas específicas.

Fondos Internacionales:

- Buscar convocatorias de financiamiento de organismos internacionales, como la Unión Europea, el Banco Mundial o la UNESCO, que apoyen proyectos de investigación en países en desarrollo.
- Participar en redes de colaboración internacional y programas de cooperación que faciliten el acceso a recursos financieros y oportunidades de investigación a nivel global.

Centros de Investigación y Laboratorios Nacionales:

- Establecer alianzas estratégicas con centros de investigación y laboratorios nacionales para compartir recursos, infraestructura y conocimientos en proyectos colaborativos.
- Participar en programas de financiamiento y convocatorias específicas de los centros de investigación y laboratorios nacionales para obtener apoyo adicional para nuestros proyectos.

SOLICITUD DE UTILIZACIÓN DE EQUIPOS PROPIEDAD DE LA UAM, EN SU CASO

No Aplica

Av. San Pablo Xalpa 180, San Martin Xochinahuac, Azcapotzalco, 02128 Ciudad de México, CDMX

Tel/Fax 55 5318 9000

E-mail: apj@azc.uam.mx

MANIFESTACIÓN DE APEGO Y CUMPLIMIENTO DEL CÓDIGO DE ÉTICA DE LA UNIVERSIDAD AUTÓNOMA METROPOLITANA

Yo, **Dra. Julia Aguilar Pliego**, en mi calidad de miembro de la comunidad universitaria de la Universidad Autónoma Metropolitana (UAM), manifiesto mi firme compromiso con los principios y valores establecidos en el Código de Ética de nuestra institución.

Reconozco la importancia de cultivar un ambiente de respeto, integridad, honestidad y responsabilidad en todas mis acciones y decisiones dentro y fuera de la universidad. Asimismo, entiendo que como parte de la comunidad universitaria tengo la responsabilidad de promover el bienestar común, la equidad y la diversidad, así como de contribuir al desarrollo integral de la sociedad.

Me comprometo a:

1. Respetar los derechos y la dignidad de todas las personas, sin importar su origen étnico, género, orientación sexual, religión, edad o cualquier otra característica.
2. Actuar con integridad y honestidad en todas mis actividades académicas, de investigación y administrativas, evitando cualquier forma de plagio, fraude o comportamiento deshonesto.
3. Cumplir con todas las normativas y políticas institucionales establecidas por la Universidad Autónoma Metropolitana, así como con las leyes y regulaciones aplicables en el ámbito académico y social.
4. Fomentar un ambiente de diálogo, tolerancia y respeto mutuo, promoviendo el intercambio de ideas y el debate constructivo en el marco del respeto a la diversidad de opiniones.
5. Contribuir activamente a la preservación del medio ambiente y al desarrollo sostenible, adoptando prácticas responsables en el uso de los recursos naturales y en la gestión de residuos.
6. Denunciar cualquier forma de discriminación, acoso, abuso o corrupción que pueda afectar la integridad y el bienestar de la comunidad universitaria.

En virtud de lo anterior, manifiesto mi compromiso de cumplir con los principios y valores establecidos en el Código de Ética de la Universidad Autónoma Metropolitana, contribuyendo así a fortalecer la integridad y la excelencia académica de nuestra institución.

Julia Aguilar Pliego
Profesor-Investigador Titular C
Departamento de Ciencias Básicas
Área de Química Aplicada
Universidad Autónoma Metropolitana-Azcapotzalco

Casa abierta al tiempo
UNIVERSIDAD AUTÓNOMA METROPOLITANA

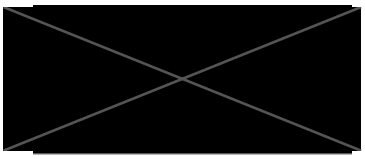
CDMX a 9 Enero del 2025

ASUNTO
Notificación de participación del Dr. Ricardo A. Peralta Avila
A quien corresponda
P R E S E N TE

Por este medio le comunico que el Dr. Ricardo A. Peralta Avila, el cual se desempeña como profesor visitante del Departamento de Química, colabora como participante en el proyecto “Objetos Digitales de Aprendizaje para la enseñanza de la química experimental en el bachillerato de la CDMX”. Dicha propuesta fue favorecida en la convocatoria 2024 para presentar proyectos científicos, de desarrollo tecnológico e innovación y divulgación para la atención de problemas específicos de la Ciudad de México, la cual fue ganadora el 22 de julio del 2024. El Dr. Ricardo fue clave para poder ganar el proyecto y participa activamente en el proyecto para que sea desarrollado exitosamente.

Se expide esta constancia para los fines que más convenga al interesado.

Reciban un Cordial Saludo



Jorge Garza Olguín
Responsable Técnico
Jefe de Departamento de Química
División de Ciencias Básicas e Ingeniería
UAM

Gmail proyecto sectei

Redactar

Mail

Recibidos

Chat Destacados

Pospuestos

Meet Enviados

Borradores 6

Más

Etiquetas

Proyecto aprobado ante la SECTEI

Usuarios externos Recibidos ×

JORGE GARZA OLGUIN
para mí, LEONARDO, nsoyuk, RUBICELIA, MARGARITA, NANCY, JOSE

Estimadas colegas y estimados colegas,

el año pasado participamos (tod@s nosotr@s) en una convocatoria de la SECTEI con el proyecto

Objetos Digitales de Aprendizaje para la enseñanza de la química experimental en el bachillerato de la CDMX

Dicho proyecto no fue aprobado.

Este año sometimos el mismo proyecto con la participación de colegas de la Prepa Nacional (UNAM) y de la CDMX. P
solicitado fue de $1,577,366.20 MN del cual fueron aprobados $930,646.06 MN (reducción del 41%). Considero que si
cumplir con lo que deseamos del proyecto.

En la primera fase se realizarán los videos (Ricardo, Nora, Leo y yo) y luego invitaremos a tod@s para participar en la
actividad. L@s mantendremos al tanto.

Les puedo decir que estoy muy contento porque con este proyecto podremos incidir directamente con la educación me
comenzaremos con la CDMX).

Un fuerte abrazo y que tengan un buen fin de semana.

Jorge Garza

P.D. Ricardo, Nora y Leo, les enviaré un mensaje donde les comentaré sobre los rubros que tenemos atender para la f

- Contribuir en el diseño del programa y la logística del evento, incluyendo la coordinación de fechas, espacios y la promoción del coloquio y seminario.

- Revisión del informe final del proyecto:
  - Evaluar y revisar el informe final del proyecto, verificando la coherencia entre los objetivos, los resultados obtenidos, los impactos esperados y las metas alcanzadas en relación con el proyecto.
  - Proporcionar comentarios y sugerencias para mejorar la redacción, la estructura y el contenido del informe final, asegurando su rigurosidad científica y su claridad.

Estas actividades permitirán a la ***Dra. Martín*** contribuir de manera significativa al desarrollo y éxito del proyecto, aportando su experiencia en catálisis para la elaboración y revisión de guías didácticas, el diseño de objetos de aprendizaje, la organización de eventos académicos centrados en la catálisis y la revisión final del informe.

Dr. Ricardo A. Peralta Ávila, Profesor Visitante adscrito al Departamento de Química UAM-I, especialista en Materiales y adscrito al área de Catálisis:

- Realización de los objetos digitales de aprendizaje en el laboratorio:
  - Investigar y recopilar información relevante sobre la química de mezclas, separaciones, catálisis, analítica y su aplicación en el laboratorio de química experimental
  - Contribuir en la elaboración de objetos digitales de aprendizaje que integren experimentos y prácticas relacionadas con la química general, catálisis, mezclas, química analítica entre otros utilizando recursos multimedia como videos, animaciones y simulaciones
  - Trabajar en colaboración con el equipo de desarrollo multimedia para asegurar la calidad y precisión científica de los objetos digitales de aprendizaje.

- Formación de los recursos humanos mediante la dirección del proyecto terminal:
  - Supervisar y dirigir a estudiantes que estén realizando proyectos terminales relacionados con la enseñanza de química experimental en el laboratorio
  - Brindar orientación y asesoramiento a los estudiantes en la planificación, diseño y ejecución de los proyectos terminales, asegurando su relevancia y coherencia con los objetivos del proyecto
  - Evaluar y proporcionar retroalimentación a los estudiantes en el desarrollo de sus proyectos terminales, fomentando el aprendizaje y la adquisición de habilidades en el campo de la catálisis.

- Elaboración del material audiovisual, así como la edición de este:

- Participar en la elaboración y producción de material audiovisual relacionado con la enseñanza de la química experimental, que pueda ser utilizado en los objetos digitales de aprendizaje
- Realizar la grabación de experimentos y prácticas en el laboratorio, asegurando la captura de imágenes y vídeos de alta calidad
- Llevar a cabo la edición y postproducción de los materiales audiovisuales, asegurando su coherencia, claridad y adecuación a los objetivos de aprendizaje.

- Desarrollo del seminario y coloquio del proyecto:
  - Participar en la planificación y organización de un seminario y coloquio centrado en la química experimental y su aplicación en el contexto de química cotidiana.
  - Contribuir en el diseño del programa, la logística y la promoción del seminario y coloquio, buscando la participación activa de estudiantes, profesores e investigadores interesados en el tema.

- Redacción del informe final del proyecto:
  - Recopilar y analizar los resultados obtenidos a lo largo del proyecto, considerando los objetivos, la problemática abordada y los impactos esperados.
  - Redactar el informe final del proyecto, en el cual se documenten de manera clara y precisa las actividades realizadas, los resultados alcanzados y las conclusiones obtenidas.
  - Revisar y asegurar la calidad y rigurosidad científica del informe final, incluyendo referencias bibliográficas pertinentes y recomendaciones para futuras investigaciones.

Estas actividades permitirán al ***Dr. Peralta*** contribuir de manera significativa al desarrollo del proyecto, aplicando sus conocimientos y experiencia en catálisis para la realización de objetos digitales de

Dr. Leonardo David Herrera Zuñiga, Profesor Curricular adscrito al Departamento de Química UAM-I, Especialista en Biofisicoquímica:

- Realización de los objetos digitales de aprendizaje en el laboratorio:
  - Investigar y recopilar información relevante sobre biofisicoquímica, procesos industriales, química teórica y su aplicación en el laboratorio de química experimental.
  - Contribuir en la elaboración de objetos digitales de aprendizaje que integren experimentos y prácticas relacionadas con la biofisicoquímica, procesos industriales y química teórica, utilizando recursos multimedia como videos, animaciones y simulaciones.
  - Trabajar en colaboración con el equipo de desarrollo multimedia para asegurar la calidad y precisión científica de los objetos digitales de aprendizaje.

Registro finalizado correctamente

Registro finalizado correctamente el Martes 21 de Mayo de 2024, 19:46 horas

Registro

Responsable técnico	Folio	Título del proyecto
Jorge Garza Olguín	3732c24	Objetos Digitales de Aprendizaje para la enseñanza de la química experimental en el bachillerato de la CDMX

Ciudad de México, a 22 de julio de 2024

Resultados
"Convocatoria 2024 para presentar proyectos científicos, de desarrollo tecnológico e innovación y divulgación para la atención de problemas específicos de la Ciudad de México"

Con fundamento en lo preceptuado por los artículos 2 párrafo primero, 11 fracción I, 13 párrafo primero, 14, 16 fracción VII, 18, 20 fracciones III y IX parte primera, y 32 Inciso A) fracción I, inciso B) fracciones I, III, VII, VIII, XVIII, XX, XXV, XXVI, XXVIII, XXXIX y XLVII de la Ley Orgánica del Poder Ejecutivo y de la Administración Pública de la Ciudad de México; 33 fracción XX del Reglamento Interior del Poder Ejecutivo y de la Administración Pública de la Ciudad de México; y una vez concluido el proceso de revisión, evaluación y selección se tiene a bien emitir los siguientes **resultados de carácter inapelable**.

#	Folio
1	4231c24*
2	3738c24
3	3683c24*
4	3331c24
5	3817c24
6	3692c24
7	3591c24
8	3801c24
9	3637c24*
10	3390c24*
11	3936c24
12	3653c24*
13	3952c24
14	3592c24
15	3699c24
16	4250c24
17	3524c24

#	Folio
18	3788c24*
19	3785c24*
20	3998c24
21	3602c24
22	3965c24*
23	3928c24
24	3703c24*
25	4033c24
26	3684c24
27	4009c24*
28	3256c24
29	3581c24
30	4166c24*
31	4175c24
32	3425c24*
33	3932c24*
34	4061c24

#	Folio
35	3512c24*
36	4085c24
37	4048c24*
38	3732c24*
39	3865c24
40	3631c24*
41	3719c24*
42	3863c24
43	3234c24*
44	3799c24*
45	3923c24*
46	3617c24
47	3635c24*
48	3476c24*
49	3442c24
50	3650c24*
51	3522c24*

Nota: Los folios marcados con * están sujetos a cambios derivado de reajustes sugeridos por la Comisión de Evaluación y a la suficiencia presupuestal.

Para mayores informes comunicarse al teléfono 5555121012 ext. 2012 y 2022.

CONVOCATORIA 2024

Para Presentar Proyectos Científicos, De Desarrollo Tecnológico E Innovación Y Divulgación Para La Atención De Problemas Específicos De La Ciudad De México

Proyecto

Objetos Digitales de Aprendizaje para la enseñanza de la química experimental en el bachillerato de la CDMX

(ODAQ-UAMI)

1. ANTECEDENTES

La educación a través del aprendizaje con apoyo de herramientas digitales ha experimentado un crecimiento significativo en los últimos años. Los avances en la tecnología han permitido la creación de entornos virtuales de aprendizaje (EVA) que ofrecen una amplia gama de recursos y herramientas interactivas que apoyan las clases presenciales y la divulgación de ciencia mediante EVA. Estos entornos en línea brindan a los estudiantes la flexibilidad de acceder al contenido del curso y participar en las actividades de aprendizaje en cualquier momento y lugar, lo que permite una difusión de la ciencia.

Los EVA tienen la ventaja que los jóvenes pueden acceder a la información, participar, divulgar y difundir el aprendizaje de manera asíncrona, lo que les brinda la libertad de adaptar su horario de estudio a sus necesidades individuales. Esto es especialmente beneficioso para aquellos que no pueden asistir con constancia a programas educativos en persona debido a restricciones geográficas, responsabilidades laborales o personales.

La tendencia hacia el uso de herramientas digitales se fortaleció aún más con la pandemia de COVID-19. La **Figura 1 (ver documento anexo)** muestra los datos nacionales sobre matrículas, a todos los niveles, en México, revelando un mayor acceso de recursos tecnológicos en la población escolar.

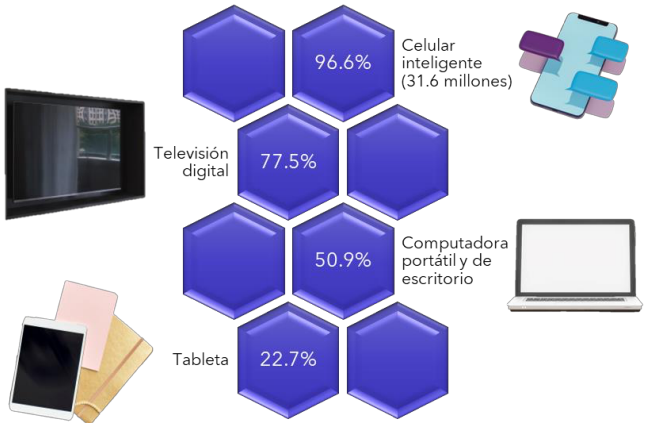


Figura 1. *Población de 3 a 29 años inscrita en el ciclo escolar 2021-2022 según herramientas tecnológicas en la vivienda. Fuente: INEGI. Encuesta Nacional sobre Acceso y Permanencia en la Educación (ENAPE) 2021.*

En el nivel de educación media superior, también se observa una tendencia hacia la adopción de herramientas y recursos digitales en el proceso educativo y de divulgación. La **Figura 2 (ver documento anexo)** muestra la modalidad de asistencia de los estudiantes en el nivel de educación media superior en México durante el ciclo escolar 2021-2022. Se puede apreciar que una proporción significativa de estudiantes combinó clases presenciales y de forma híbrida (59.2%).

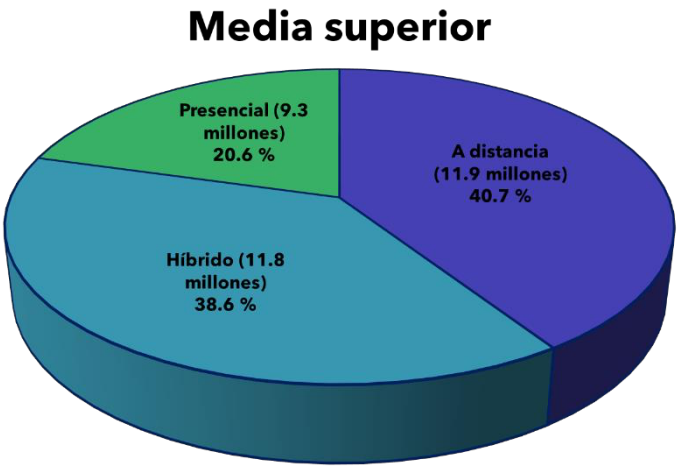


Figura 2. *Población de 3 a 29 años inscrita en el ciclo escolar 2021-2022 según su modalidad de asistencia en el nivel media superior. Fuente: INEGI. Encuesta Nacional sobre Acceso y Permanencia en la Educación (ENAPE) 2021.*

Además, el uso de herramientas didácticas y de divulgación mediadas por la tecnología se ha vuelto común entre los estudiantes de educación media superior en México. La **Figura 3 (ver documento anexo)** muestra el uso de herramientas para la difusión de las clases, mientras que la **Figura 4 (ver documento anexo)** muestra el uso de herramientas digitales para realizar tareas. Estos datos indican que los estudiantes están adoptando activamente recursos digitales y tecnológicos para apoyar su aprendizaje, difundir y divulgar conocimientos, mejorando de esta manera su experiencia educativa.



Figura 3. *Población de 3 a 29 años inscrita en el ciclo escolar 2021-2022 en el nivel media superior, según uso de herramientas didácticas para las clases. Fuente: INEGI. Encuesta Nacional sobre Acceso y Permanencia en la Educación (ENAPE) 2021.*

Estos antecedentes demuestran que la difusión, y divulgación del aprendizaje apoyado por las herramientas digitales y virtuales son tendencias en crecimiento en el campo educativo. El acceso a recursos educativos digitales y la adopción de herramientas tecnológicas están transformando la forma en que los estudiantes aprenden y participan en el proceso educativo. En este contexto, es importante divulgar y fortalecer el desarrollo de habilidades científicas y tecnológicas en los estudiantes para prepararlos para los desafíos del siglo XXI y aprovechar al máximo las oportunidades que ofrece la educación mediada por la tecnología.

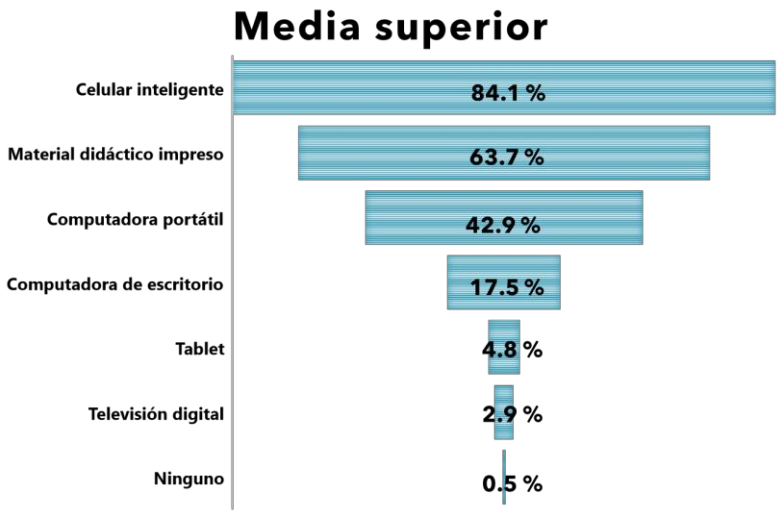


Figura 4. *Población de 3 a 29 años inscrita en el ciclo escolar 2021-2022 en el nivel media superior, según su uso de herramientas virtuales para realizar tareas. Fuente: INEGI. Encuesta Nacional sobre Acceso y Permanencia en la Educación (ENAPE) 2021.*

En este contexto se destaca la posibilidad de difundir el acceso a herramientas digitales que apoyen el aprendizaje presencial del laboratorio en química. La divulgación adecuada del aprendizaje en el laboratorio de química es igual de relevante que la acción en el aula, tanto con el uso o no de las herramientas tecnológicas.

Es común encontrar manuales de prácticas de laboratorio (*in-situ*) que simplemente plantean el experimento sin proporcionar una guía de enseñanza-aprendizaje o su divulgación, lo que resulta en una actividad que no cumple con su propósito de ser una experiencia de aprendizaje significativa. Por lo tanto, siempre es necesario desarrollar un documento que guíe el proceso de aprendizaje en el laboratorio, estableciendo objetivos claros y siguiendo el proceso cognitivo de los estudiantes.

Una forma de organizar y estructurar las actividades de aprendizaje de un tema en el laboratorio es mediante el uso de secuencias didácticas. Estas secuencias son una organización de las actividades de aprendizaje diseñadas para crear situaciones que fomenten un aprendizaje significativo (Díaz-Barriga, 2013). Al basarse en el conocimiento pedagógico del contenido (Garritz y Trinidad-Velasco, 2004) y la experiencia docente en la disciplina, las secuencias didácticas se convierten en herramientas útiles para guiar el proceso de enseñanza-aprendizaje.

Una secuencia didáctica debe establecer objetivos de aprendizaje claros y alcanzables que servirán de base para planificar las actividades. Por lo general, las secuencias didácticas se estructuran en tres tipos de actividades: apertura, desarrollo y cierre (Díaz-Barriga, 2013). Además, se deben considerar tanto la evaluación formativa como la sumativa en diferentes momentos del proceso de aprendizaje, ya que la evaluación no se limita a una única instancia, sino que se integra de manera continua a lo largo del proceso.

Una forma de materializar una secuencia didáctica es a través de objetos de aprendizaje (Callejas-Cuervo et. al, 2011). Estos objetos son recursos autocontenidos que se crean con el propósito de lograr objetivos de aprendizaje específicos y pueden ser utilizados en diferentes temas o cursos. Al utilizar objetos de aprendizaje, se facilita la planificación y adaptación de las actividades en el laboratorio de química.

El grupo de trabajo que presenta este proyecto cuenta con la experiencia necesaria en la docencia, el desarrollo difusión y divulgación de materiales didácticos en química; ha elaborado secuencias didácticas para el nivel medio y superior, así como libros y manuales de prácticas construidos sobre estas secuencias. Este proyecto se propone desde el Departamento de Química de la UAM-Iztapalapa con la colaboración del personal académico de distintas áreas académicas (Biofisicoquímica, Catálisis, Fisicoquímica teórica y Química analítica), así mismo con la participación personal académico de las instituciones: Instituto de Educación Media Superior de la Ciudad de México (IEMS) y la Universidad Nacional Autónoma de México (Escuela Nacional Preparatoria).

En resumen, el proyecto propuesto es de gran relevancia para la educación media superior en el campo de ciencia, tecnología, ingeniería y matemáticas (STEM), ya que se enfoca en destacar la importancia del aprendizaje experimental de la química. A través de la difusión y divulgación científica de una planificación cuidadosa, el uso de secuencias didácticas y objetos de aprendizaje, se busca proporcionar una experiencia de aprendizaje significativa y efectiva en el laboratorio de química, el contexto de la educación presencial, híbrida o a distancia.

2. JUSTIFICACIÓN

La educación mediada por la tecnología ha experimentado un aumento significativo a raíz de la pandemia mundial, lo que ha llevado a la necesidad de explorar nuevas formas de difundir y divulgar la enseñanza y aprendizaje de las ciencias. A medida que el aprendizaje electrónico se ha vuelto más accesible y aceptado, surge la oportunidad de utilizarlo como complemento de la apropiación de la ciencia ante la educación presencial tradicional. Los recursos educativos digitales que apoyan la enseñanza presencial permiten a los estudiantes acceder a material adicional y obtener una experiencia de aprendizaje más integral. En este contexto, la tecnología de la información ha permitido que las universidades y otras instituciones educativas amplíen su alcance más allá de las limitaciones geográficas, brindando oportunidades de aprendizaje a un número cada vez mayor de estudiantes, divulgando su ciencia mediante el aprendizaje.

La enseñanza de la química experimental es un tema apasionante pero también costoso. Los laboratorios de química modernos se conciben como espacios de aprendizaje integrales, donde los estudiantes pueden poner a prueba sus ideas previas, adquirir habilidades de investigación científica y tecnológica, y trabajar de manera individual y colectiva. En este sentido el concepto del laboratorio de química se ha modernizado y ahora es un espacio divulgativo del aprendizaje en toda su extensión y no sólo un lugar en dónde se comprueban leyes y conceptos revisados en el salón de clase (Olubu, 2015; Nakhleh et al, 2002). El Instituto de Educación Media Superior de la Ciudad de México (IEMS) ha considerado este nuevo concepto al establecer en su plan de estudios lo siguiente:

"…El aula-laboratorio es el espacio ideal para someter a prueba sus ideas previas y donde el estudiante va a adquirir individual y colectivamente una metodología propia del trabajo de investigación científica y tecnológica, por ello es de primordial importancia usar cotidianamente este espacio de manera racional y responsable".

Sin embargo, en la Ciudad de México, existe una problemática significativa relacionada con la falta de infraestructura y consumibles necesarios para la formación experimental en química. Ante esta problemática, el presente proyecto propone el desarrollo de objetos digitales de aprendizaje para la enseñanza de la química experimental a nivel bachillerato, mismos que pretenden funcionar como medio de divulgación de la ciencia Química para estudiantes de educación media superior. Estos objetos de aprendizaje serán auto contenidos y digitales, e incluirán vídeos detallados de los procedimientos experimentales y científicos. El objetivo principal es fortalecer la calidad de la educación media superior y superior, brindando a los estudiantes una alternativa accesible y de calidad para adquirir conocimientos y habilidades en el campo de la química experimental.

El diseño de secuencias didácticas adecuadas es fundamental para lograr los objetivos de aprendizaje en este proyecto. Se definirán y organizarán los objetivos de aprendizaje de cada unidad didáctica de acuerdo con el programa de estudios de Química del IEMS. Además, se elaborarán las secuencias didácticas necesarias para alcanzar dichos objetivos. Estas secuencias didácticas de aprendizaje y divulgación servirán como guías instruccionales que permitirán a los estudiantes desarrollar habilidades prácticas y comprender los conceptos

fundamentales de la química experimental y brindarán a los maestros herramientas poderosas para facilitar el aprendizaje de sus estudiantes.

La implementación de objetos de aprendizaje digitales en la enseñanza de la química experimental ofrece numerosos beneficios. En primer lugar, permite superar la limitación de la infraestructura y los consumibles necesarios para llevar a cabo experimentos en un laboratorio físico. Esto garantiza que todos los estudiantes tengan acceso a una experiencia de aprendizaje práctica y significativa, sin importar las limitaciones de recursos. Además, los objetos digitales de aprendizaje ofrecen flexibilidad en el desarrollo de los planes de estudio, ya que se pueden adaptar y actualizar fácilmente para abordar los avances y cambios en el campo de la química experimental, siendo una herramienta de divulgación científica adecuada para los procesos de enseñanza aprendizaje.

El Plan de estudios de la ENP describe a esta institución como un centro educativo que imparte el nivel bachillerato en una modalidad escolarizada a través de cuatro ejes de formación: Matemáticas, Histórico-Social, Lenguaje-Comunicación-Cultura y Ciencias Naturales. Esta última área del conocimiento tiene como objetivo superar la enseñanza demostrativa de la ciencia pretendiendo así, fomentar en el estudiantado una cultura científica básica y ambiental. Para lograrlo, contempla asignaturas tales como la Química (Plan de estudios ENP, 1996).

A este respecto; el propósito de la química es que los educandos utilicen los principios químicos necesarios para analizar problemáticas relacionadas con el ambiente, salud y tecnología. Lo anterior encaminado a la construcción de conocimientos, desarrollo de habilidades y actitudes para tomar decisiones fundadas en una alfabetización científica. Esto a partir de la investigación documental y el acercamiento a la experimentación escolar (Programa Química III, 2017).

Derivado de la transición hacia una docencia no presencial, por la pandemia de SARS-Cov-2, la implementación de trabajos prácticos, como estrategia didáctica, se vio afectada en cierta medida por la desarticulación de la teoría con la experimentación, amalgama indispensable en el aprendizaje de la Química. Lo anterior por falta de acceso a los espacios físicos escolares y de experiencia en algunos profesores por impartir asignaturas teórico-prácticas en un sistema escolar mediado por tecnologías.

En sus inicios este proceso costó trabajo y en la actualidad que regresamos a la presencialidad es imperante que como docentes recuperemos lo aprendido durante la pandemia y se amalgame con nuestra forma de abordar la parte experimental de forma presencial.

¿Por qué centrarse en la experimentación? Debido a que el aprendizaje basado en el laboratorio es un componente esencial en el proceso de construcción de saberes en asignaturas del área de Ciencias Naturales ya que el estudiantado puede hacer conexiones significativas entre la teoría con los fenómenos que nos rodean, tienen la oportunidad de desarrollar el pensamiento científico y el manejo tanto de reactivos como de materiales. Lo anterior se logra siempre y cuando el laboratorio escolar se utilice con un objetivo didáctico y pueda ser una oportunidad de divulgación de la ciencia (Enneking, K. M. et al. 2019).

¿Qué pasa cuando no se tiene acceso a materiales, reactivos o laboratorio aun estando en la modalidad presencial? Se busca la implementación de un “Laboratorio Híbrido”. Es decir, conjuntar el tipo “cara a cara”, casero y virtual; lo cual dé a los estudiantes una oportunidad para integrar sus habilidades cognitivas, afectivas y psicomotoras; requisito necesario para

un aprendizaje significativo (Enneking, K. M. et al. 2019). Por lo anterior, es necesario enfatizar que su uso debe tener un objetivo didáctico, lo cual permita (Wang y Ren, 2020):

- Usar métodos físicos o analíticos para analizar teorías o leyes discutidas en clase.
- Promover y desarrollar el pensamiento científico (generación de preguntas, hipótesis, procedimientos, análisis de resultados, modelos o argumentos).
- Preparar a los estudiantes con las habilidades básicas de laboratorio necesarias para cursos posteriores.
- Estimular el interés por la ciencia del siglo XXI en los laboratorios de química.

El "Laboratorio Híbrido" se caracteriza por su flexibilidad teniéndose así, cuatro posibilidades, las cuales se pueden usar dependiendo el tópico, los recursos y los aprendizajes esperados. Considera lo siguiente:

- Realismo: se refiere a qué tan cercana está la experiencia del trabajo en el laboratorio escolar en sí.
- Alterar la realidad indica si se puede simplificar, intencionadamente, la realidad o incluso, modificarla. Esto con el fin de facilitar la comprensión de determinados conceptos.
- Costos hace referencia a cuán costoso tiende a ser cada variante en función del tiempo.
- Función adicional hace alusión al hecho de que algunas variantes admiten funciones de software adicionales para mejorar o ampliar la experiencia de aprendizaje. Por ejemplo, superponer una realidad física con lo no visible a partir de animaciones o interactivos para una mejor comprensión.
- Dependencia de TIC indica si las variantes necesitan medios digitales como animaciones, videos o sonido.



	Laboratorio escolar	Experimento casero	Laboratorio mediante videos	Experimentos con simuladores
Realismo	Muy alto	Alto	Mediano	Bajo
Alterar realidad	No	No	No	Sí
Costoso	Alto	Bajo	Mediano	Bajo
Función adicional	No	No	Sí	Sí
Depende de TIC	No	Mediano	Sí	Sí

Figura 5. *Tipos de experimentos a desarrollar en el modelo híbrido Fuente: Adaptado de Rodriguez-Gil, Garcia-Zubia, Orduña y López-de-Ipina (2017).*

El sistema híbrido es una oportunidad para que el profesorado presente a los educandos varios formatos de trabajos experimentales, e incluso mediante un sistema rotativo, fomentando así, los diversos estilos de aprendizaje, saberes conceptuales, procedimentales y actitudinales. Esto, a partir de amalgamar la presencialidad con la virtualidad, además de contemplar la didáctica, disciplina, las TIC y el contexto busca generar una reflexión para entornos específicos con el fin de promover soluciones factibles y no genéricas.

Lo anterior concuerda con el Plan de Desarrollo de la UNAM 2023-2027, esto en su línea tres "Fortalecimiento y renovación de la docencia" y cuatro "Consolidar y apoyo a la investigación", ya que este proyecto busca fortalecer el bachillerato universitario, buscar e implementar programas de apoyo a la docencia, fomentar la interacción entre entidades académicas en proyectos de investigación, fortalecimiento de la infraestructura experimental, divulgar la ciencia, por mencionar algunas.

Lo descrito en el párrafo de arriba concuerda con los objetivos del Plan de Desarrollo de la ENP, en específico en el Programa 1.1 Formación Académica, Cultural y Artística.

En resumen, este proyecto busca abordar la problemática de la infraestructura -generalmente insuficiente- y consumibles requeridos para la formación experimental en química en la Ciudad de México, mediante el desarrollo y divulgación de objetos digitales de aprendizaje. Estos objetos permitirán a los estudiantes de bachillerato acceder a recursos educativos de alta calidad, auto contenidos y digitales, que incluirán vídeos detallados de procedimientos experimentales. Al fortalecer la calidad de la educación media superior y superior en el campo de la química experimental, se promoverá el aprendizaje integral y el desarrollo de habilidades científicas y tecnológicas en los estudiantes.

Problemática por atender en la Ciudad de México:

La infraestructura insuficiente o limitada, así como los recursos consumibles necesarios para llevar a cabo la formación experimental en química en las instituciones educativas de nivel medio superior en la Ciudad de México pueden limitar la capacidad de las instituciones educativas de nivel medio superior para brindar a los estudiantes una formación experimental adecuada. En este contexto, surge la necesidad de desarrollar, difundir y divulgar objetos de aprendizaje digitales que permitan a los estudiantes acceder a experiencias de aprendizaje significativo en química experimental, incluso en ausencia de laboratorios físicos completos. Este proyecto busca brindar a los estudiantes de bachillerato en la Ciudad de México la oportunidad de acceder a experiencias de aprendizaje en química experimental, utilizando recursos digitales innovadores. De esta manera, se busca superar las limitaciones físicas y facilitar el desarrollo de habilidades, adquisición de conocimientos y formación de actitudes en química, contribuyendo así a una formación integral de los estudiantes en el campo STEM.

3. ACRÓNIMO

ODAQ-UAMI

4. OBJETIVO

Generar y divulgar objetos de aprendizaje y digitales autocontenidos, que incluyen videos, para la formación de estudiantes de bachillerato en química experimental. Estos objetos de aprendizaje están diseñados para proporcionar a los estudiantes una experiencia interactiva y práctica, que les permita desarrollar habilidades y conocimientos en química experimental.

Objetivos Particulares:

- Definir y organizar los objetivos de aprendizaje de cada unidad didáctica de acuerdo con el programa de estudios de Química del IEMS. Esto implica identificar los conceptos y habilidades clave que se deben abordar en cada unidad, estableciendo metas claras y alcanzables para el aprendizaje de los estudiantes.
- Diseñar y elaborar las secuencias didácticas necesarias para lograr los objetivos de aprendizaje establecidos. Estas secuencias didácticas serán cuidadosamente estructuradas y planificadas, considerando la secuencia lógica de las actividades y promoviendo el aprendizaje significativo de los estudiantes.
- Construir objetos digitales de aprendizaje que estén alineados con las secuencias didácticas propuestas y que permitan el desarrollo de habilidades y conocimientos en química experimental. Estos objetos de aprendizaje serán recursos interactivos y autocontenidos, que incluirán videos explicativos cortos, ejercicios prácticos, así como evaluaciones formativas y sumativas.
- Implementar una estrategia de divulgación integral mediante un portal plataforma interactiva donde se alojarán y compartirán recursos educativos. Se establecerán canales de comunicación en redes sociales y boletines informativos para llegar a una audiencia diversa, incluyendo docentes, estudiantes y otros interesados en la enseñanza y aprendizaje de la química.

5. META

La meta del proyecto es desarrollar, crear y divulgar Objetos Digitales de Aprendizaje que proporcionen una guía efectiva para los estudiantes de nivel bachillerato en el proceso de enseñanza-aprendizaje de la química experimental. Estos objetos estarán diseñados con base en secuencias didácticas y contendrán recursos interactivos, videos explicativos y actividades prácticas, con el objetivo de promover el desarrollo de habilidades y conocimientos en química experimental, a pesar de las limitaciones de infraestructura y recursos consumibles existentes en las instituciones educativas de la Ciudad de México.

6. CRONOGRAMA DE ACTIVIDADES

Actividades	Mes																	
	1	2	3	4	5	6	7	8	9	10	11	12	13	14	15	16	17	18
Materiales Audiovisuales																		
Objeto digital de aprendizaje 1																		
Programas de Socialización de la Ciencia																		
Objeto digital de aprendizaje 2																		
Programas de Socialización de la Ciencia																		
Objeto digital de aprendizaje 3																		
Programas de Socialización de la Ciencia																		
Objeto digital de aprendizaje 4																		
Programas de Socialización de la Ciencia																		
Objeto digital de aprendizaje 5																		
Programas de Socialización de la Ciencia																		
Objeto digital de aprendizaje 6																		
Programas de Socialización de la Ciencia																		
Objeto digital de aprendizaje 7																		
Programas de Socialización de la Ciencia																		
Objeto digital de aprendizaje 8																		
Programas de Socialización de la Ciencia																		
Objeto digital de aprendizaje 9																		

Programas de Socialización de la Ciencia																			
Objeto digital de aprendizaje 10																			
Programas de Socialización de la Ciencia																			

1.

Actividades	Mes																	
	1	2	3	4	5	6	7	8	9	10	11	12	13	14	15	16	17	18
Formación de recursos humanos																		
Licenciatura																		
Proyecto terminal																		
Programa de socialización de la ciencia																		
Seminario																		
Coloquio																		
Programa de socialización de la ciencia																		
Material impreso																		
Objeto digital de aprendizaje																		
Programa de socialización de la ciencia																		
Seminario																		
Presentación de seminario institucional/departamental																		
Publicaciones																		
Artículo en revista no indexada																		
Artículo De Divulgación																		
Otro																		
Plan de trabajo de proyecto terminal - Plan de trabajo de proyecto																		
Informe final																		
Auditoría																		

7. ENTREGABLES CLAROS, VISIBLES Y CUANTIFICABLES

Mes 1 / Otro / Plan de trabajo de proyecto

Descripción:

Se elaborará el plan de acción o proyecto rector, que servirá como guía para la ejecución exitosa de todas las actividades. Además, se confeccionará el plan de trabajo para los estudiantes que colaborarán en la construcción de los objetos digitales de aprendizaje (ODA), guías didácticas y otros entregables del proyecto, contribuyendo así a su formación académica.

Actividades:

1. Establecer objetivos específicos del proyecto ejecutivo y definir metas y resultados esperados.
2. Elaborar un plan de trabajo detallado que incluya todas las etapas y tareas del proyecto, estableciendo plazos y un cronograma para su ejecución y seguimiento.
3. Organizar los recursos necesarios y al equipo de trabajo para llevar a buen fin el proyecto. Involucrar a estudiantes interesados en participar y contribuir a su formación académica.
4. Realizar una convocatoria para la selección de estudiantes interesados en formar parte del proyecto, estableciendo criterios de selección y elegir a los candidatos más aptos.
5. Elaborar un plan de acción detallado que describa las actividades específicas a realizar en cada etapa del proyecto, asignando responsables y asignando recursos necesarios.
6. Realizar una revisión exhaustiva del plan de trabajo, identificando posibles mejoras o ajustes necesarios. Realizar los cambios pertinentes para asegurar su viabilidad y eficacia.
7. Presentar el plan de trabajo entre colaboradores y partes interesadas.

El objetivo principal del plan de trabajo de proyecto ejecutivo es proporcionar una estructura organizada para el desarrollo del trabajo individual y para la coordinación de actividades, con responsabilidades claras para asegurar el logro de los objetivos. Así mismo, la participación de estudiantes contribuirá a su formación académica y al desarrollo pleno de cada una de las actividades del proyecto rector.

Mes 2 / Programas de Socialización de la Ciencia / Materiales Audiovisuales / Objeto digital de aprendizaje 1 (ODA-1)

Descripción:

Se trabajará en la creación del primer objeto digital de aprendizaje, titulado "Conoce tu laboratorio: Medidas de seguridad y cálculos para preparación de soluciones". Este objeto de aprendizaje tiene como objetivo principal proporcionar a los estudiantes los conocimientos necesarios para manejar de forma segura los reactivos químicos y realizar cálculos para la preparación de soluciones. Se abordará el enfoque de la química verde, donde se prioriza el uso responsable y sostenible de los recursos. Manejar con seguridad los reactivos químicos, conociendo, previo a la experimentación, sus propiedades físicas, químicas y toxicológicas. Además, dará a conocer los métodos de estudio y fundamentos que rigen los procesos experimentales, así como la posibilidad de comprender el método científico para realizar los experimentos de química propuestos. Mostrará cómo realizar adecuadamente manipulaciones y procedimientos de laboratorio que involucren instrumentación para la síntesis y análisis de sistemas químicos. Empleará soluciones acuosas y permitirá identificar a los componentes de estas.

Actividades:

1. Planeación de la logística necesaria: Se llevará a cabo la planificación de la logística requerida para la realización del objeto de aprendizaje. Esto incluye la identificación y adquisición de los reactivos y materiales necesarios, así como la asignación de espacios y tiempos para las prácticas.

2. Filmación didáctica de las prácticas: Se realizará la filmación del objeto de aprendizaje de manera didáctica, enfocándose en los aspectos relevantes para el aprendizaje de los estudiantes. Se utilizarán recursos audiovisuales, como explicaciones detalladas, imágenes y gráficas, para facilitar la comprensión de los conceptos y procedimientos.

3. Edición de los videos: Se realizará la edición de los videos grabados durante la realización del objeto de aprendizaje. Se optimizará la calidad del material audiovisual, se agregarán elementos gráficos y se organizará de manera coherente para su mejor comprensión.

4. Redacción de la guía didáctica: Se redactará la guía didáctica que acompañará al objeto de aprendizaje. Esta guía proporciona instrucciones detalladas sobre los procedimientos del proceso enseñanza-aprendizaje, estrategias metodológicas, información teórica relevante, y ejemplos prácticos entre otros.

El objetivo final es crear un objeto digital de aprendizaje completo y accesible, que combine los videos interactivos y la guía didáctica, y que pueda ser utilizado por los estudiantes/profesores como una herramienta efectiva para adquirir/distribuir los conocimientos y habilidades necesarios en el ámbito de la química fundamental.

Mes 3 / Programas de Socialización de la Ciencia / Materiales Audiovisuales / Objeto digital de aprendizaje 2 (ODA-2)
Descripción:

Se trabajará en la creación del segundo ODA, titulado "¿Hundirse o flotar?; Preparación de disoluciones y determinación de su densidad". El objetivo principal de este objeto de aprendizaje es proporcionar a los estudiantes los conocimientos necesarios para comprender el concepto de densidad, practicar con las diferentes unidades de concentración y habilitarse en la preparación de disoluciones a diferentes concentraciones. Además, se abordará el tema de la medición precisa de la densidad de las soluciones y se analizarán las posibles fuentes de error en estas mediciones.

Actividades:

1. Planeación de la logística necesaria: Se llevará a cabo la planificación de la logística requerida para la realización del objeto de aprendizaje. Esto implica identificar y adquirir los reactivos y materiales necesarios, así como asignar espacios y tiempos para las prácticas.
2. Filmación didáctica de las prácticas: Se realizará la filmación del objeto de aprendizaje de manera didáctica, enfocándose en los aspectos relevantes para el aprendizaje de los estudiantes. Se utilizarán recursos audiovisuales, explicaciones detalladas, imágenes y gráficas para facilitar la comprensión de los conceptos y procedimientos.
3. Edición de los videos: Se llevará a cabo la edición de los videos grabados durante la realización del ODA. Se optimizará la calidad del material audiovisual, se agregarán elementos gráficos y se organizará de manera coherente para mejorar la comprensión.
4. Redacción de la guía didáctica: Se redactará la guía didáctica que acompañará al objeto de aprendizaje. Esta guía proporciona instrucciones detalladas sobre los procedimientos del proceso de enseñanza-aprendizaje, estrategias metodológicas, información teórica relevante y ejemplos prácticos, entre otros.

El objetivo final es crear un objeto de aprendizaje completo y accesible que combine los videos interactivos y la guía didáctica, y que pueda ser utilizado por los estudiantes y profesores como una herramienta efectiva para adquirir y distribuir los conocimientos y habilidades necesarios en el ámbito de la química de soluciones y el uso de las densidades.

Mes 4 / Programas de Socialización de la Ciencia / Materiales Audiovisuales / Objeto digital de aprendizaje 3 (ODA-3)

Descripción:

Se trabajará en la creación del tercer ODA titulado "Formas de expresar concentraciones y valoración de las soluciones". El objetivo principal de este objeto de aprendizaje es proporcionar a los estudiantes habilidades y reforzar los conocimientos fundamentales adquiridos con los anteriores ODA en la química de las soluciones, así como en la preparación y cálculo de concentraciones de soluciones. Esto les permitirá aplicar estos conceptos en su futuro trabajo en el laboratorio.

Actividades:

1. Planeación de la logística necesaria: Se llevará a cabo la planificación de la logística requerida para la realización del objeto de aprendizaje. Esto incluye la identificación y adquisición de los reactivos y materiales necesarios, así como la asignación de espacios y tiempos para las prácticas.
2. Filmación didáctica de las prácticas: Se realizará la filmación del objeto de aprendizaje de manera didáctica, enfocándose en los aspectos relevantes para el aprendizaje de los estudiantes. Se utilizarán recursos audiovisuales, explicaciones detalladas, imágenes y gráficas para facilitar la comprensión de los conceptos y procedimientos.
3. Edición de los videos: Se llevará a cabo la edición de los videos grabados durante la realización del objeto de aprendizaje. Se optimizará la calidad del material audiovisual, se agregarán elementos gráficos y se organizará de manera coherente para mejorar la comprensión.
4. Redacción de la guía didáctica: Se redactará la guía didáctica que acompañará al objeto de aprendizaje. Esta guía proporciona instrucciones detalladas sobre los procedimientos del proceso de enseñanza-aprendizaje, estrategias metodológicas, información teórica relevante y ejemplos prácticos, entre otros.

El objetivo final es crear un objeto de aprendizaje completo y accesible que combine los videos interactivos y la guía didáctica, y que pueda ser utilizado por los estudiantes y profesores como una herramienta efectiva para adquirir y distribuir los conocimientos y habilidades necesarios en el ámbito introductorio de la química analítica.

Mes 5 / Programas de Socialización de la Ciencia / Materiales Audiovisuales / Objeto digital de aprendizaje 4 (ODA-4)

Descripción:

Se enfocará en la creación del cuarto objeto digital de aprendizaje, titulado "¿Cuánto alcohol tiene la caguamita?". El objetivo principal de este ODA es proporcionar a los estudiantes una comprensión de los principios fisicoquímicos de la destilación simple y su aplicación en la separación de una bebida alcohólica comercial.

Actividades:

1. Planeación de la logística necesaria: Se realizará la planificación de la logística requerida para llevar a cabo el objeto de aprendizaje. Esto implica identificar y adquirir los reactivos y materiales necesarios, así como asignar espacios y tiempos para las prácticas de destilación.
2. Filmación didáctica de las prácticas: Se realizará la filmación del objeto de aprendizaje de manera didáctica, enfocándose en los aspectos relevantes para el aprendizaje de los estudiantes. Se utilizarán recursos audiovisuales, explicaciones detalladas, imágenes y gráficas para facilitar la comprensión de los conceptos y procedimientos relacionados con la destilación simple.
3. Edición de los videos: Se llevará a cabo la edición de los videos grabados durante la realización del objeto de aprendizaje. Se optimizará la calidad del material audiovisual, se agregarán elementos gráficos y se organizará de manera coherente para mejorar la comprensión.
4. Redacción de la guía didáctica: Se redactará la guía didáctica que acompañará al objeto de aprendizaje. Esta guía proporcionará instrucciones detalladas sobre los procedimientos del proceso de enseñanza-aprendizaje, estrategias metodológicas, información teórica relevante y ejemplos prácticos relacionados con la destilación y la determinación de la concentración de alcohol en una bebida destilada.

El objetivo final es crear un objeto de aprendizaje completo y accesible que combine los videos interactivos y la guía didáctica. Este recurso será utilizado por los estudiantes y profesores como una herramienta efectiva para adquirir y distribuir los conocimientos y habilidades necesarios en el ámbito introductorio de la química de los procesos de separación de soluciones simples mediante destilación.

Mes 6 / Programas de Socialización de la Ciencia / Materiales Audiovisuales / Objeto digital de aprendizaje 5 (ODA-5)

Descripción:

En este periodo, se trabajará en la creación del quinto objeto de aprendizaje, titulado "¿Inesperado, momentáneo y fugaz?: aromas -Separación de aceites esenciales por destilación por arrastre de vapor". El objetivo principal de este ODA es proporcionar a los estudiantes una comprensión de los principios fisicoquímicos involucrados en la separación de aceites esenciales utilizando la técnica de destilación por arrastre de vapor.

Actividades:

1. Planeación de la logística necesaria: Se llevará a cabo la planificación de la logística requerida para la realización del objeto de aprendizaje. Esto incluye la identificación y adquisición de los reactivos y materiales necesarios, así como la asignación de espacios y tiempos para las prácticas de destilación por arrastre de vapor.
2. Filmación didáctica de las prácticas: Se realizará la filmación del objeto de aprendizaje de manera didáctica, centrándose en los aspectos relevantes para el aprendizaje de los estudiantes. Se utilizarán recursos audiovisuales, explicaciones detalladas, imágenes y gráficos para facilitar la comprensión de los conceptos y procedimientos relacionados con la destilación por arrastre de vapor.
3. Edición de los videos: Se llevará a cabo la edición de los videos grabados durante la realización del objeto de aprendizaje. Se optimizará la calidad del material audiovisual, se agregarán elementos gráficos y se organizará de manera coherente para mejorar la comprensión.
4. Redacción de la guía didáctica: Se redactará la guía didáctica que acompañará al objeto de aprendizaje. Esta guía proporcionará instrucciones detalladas sobre los procedimientos del proceso de enseñanza-aprendizaje, estrategias metodológicas, información teórica relevante y ejemplos prácticos relacionados con la destilación por arrastre de vapor y la separación de aceites esenciales.

El objetivo final es crear un objeto de aprendizaje completo y accesible que combine los videos interactivos y la guía didáctica. Este recurso será utilizado por los estudiantes y profesores como una herramienta efectiva para adquirir y distribuir los conocimientos y habilidades necesarios en el ámbito de la química para los procesos de separación de mezclas complejas mediante destilación por arrastre de vapor, especialmente enfocado en la separación de aceites esenciales, e introducir el concepto de fases miscibles e inmiscibles.

Mes 7 / Programas de Socialización de la Ciencia / Materiales Audiovisuales / Objeto digital de aprendizaje 6 (ODA-6)

Descripción:

En este periodo, se trabajará en la creación del sexto ODA, titulado "Extracción de cafeína en bebidas: refresco de cola, café y bebida energética". El objetivo principal de este objeto de aprendizaje es proporcionar a los estudiantes una comprensión profunda de los principios y técnicas de extracción utilizados para separar la cafeína de diferentes bebidas. Los estudiantes podrán identificar la extracción como un método de separación de mezclas y explorar sus características, así como comprender los factores que intervienen en el proceso y cómo afectan la eficiencia de la extracción.

Actividades:

1. Planeación de la logística necesaria: Se llevará a cabo la planificación de la logística requerida para la realización del objeto de aprendizaje. Esto incluye la identificación y adquisición de los reactivos y materiales necesarios, así como la asignación de espacios y tiempos para las prácticas de extracción.
2. Filmación didáctica de las prácticas: Se realizará la filmación del objeto de aprendizaje de manera didáctica, centrándose en los aspectos relevantes para el aprendizaje de los estudiantes. Se utilizarán recursos audiovisuales, explicaciones detalladas, imágenes y gráficas para facilitar la comprensión de los conceptos y procedimientos relacionados con la extracción de cafeína.
3. Edición de los videos: Se llevará a cabo la edición de los videos grabados durante la realización del objeto de aprendizaje. Se optimizará la calidad del material audiovisual, se agregarán elementos gráficos y se organizará de manera coherente para mejorar la comprensión.
4. Redacción de la guía didáctica: Se redactará la guía didáctica que acompañará al objeto de aprendizaje. Esta guía proporcionará instrucciones detalladas sobre los procedimientos del proceso de enseñanza-aprendizaje, estrategias metodológicas, información teórica relevante y ejemplos prácticos relacionados con la extracción de cafeína y su aplicación en el control de calidad de la industria alimentaria y la protección al consumidor.

El objetivo final es crear un objeto de aprendizaje completo y accesible que combine los videos interactivos y la guía didáctica. Este recurso será utilizado por los estudiantes y profesores como una herramienta efectiva para adquirir y distribuir los conocimientos y habilidades necesarios en el ámbito de la química de las extracciones y su aplicación en el análisis de bebidas y el control de calidad. Los estudiantes podrán comprender la importancia de la extracción de cafeína, tanto desde el punto de vista científico como en relación a su impacto en la salud y la regulación de la industria alimentaria.

Mes 9 / Programas de Socialización de la Ciencia / Materiales Audiovisuales / Objeto digital de aprendizaje 7 (ODA-7)

Descripción:

En este periodo, se trabajará en la creación del séptimo ODA, "A desintoxicar y depurar el organismo: Extracción de ácido cítrico de frutas cítricas". El objetivo principal de este objeto de aprendizaje es proporcionar a los estudiantes una comprensión de los principios fisicoquímicos involucrados en el proceso de extracción de ácido cítrico a partir de frutas cítricas, resaltando sus propiedades alimenticias, cosméticas y benéficas para la salud.

Actividades:

1. Planeación de la logística necesaria: Se llevará a cabo la planificación de la logística requerida para la realización del objeto de aprendizaje. Esto incluye la identificación y adquisición de los reactivos y materiales necesarios, así como la asignación de espacios y tiempos para las prácticas de extracción.
2. Filmación didáctica de las prácticas: Se realizará la filmación del objeto de aprendizaje de manera didáctica, centrándose en los aspectos relevantes para el aprendizaje de los estudiantes. Se utilizarán recursos audiovisuales, explicaciones detalladas, imágenes y gráficas para facilitar la comprensión de los conceptos y procedimientos relacionados con la extracción de ácido cítrico.
3. Edición de los videos: Se llevará a cabo la edición de los videos grabados durante la realización del objeto de aprendizaje. Se optimizará la calidad del material audiovisual, se agregarán elementos gráficos y se organizará de manera coherente para mejorar la comprensión.
4. Redacción de la guía didáctica: Se redactará la guía didáctica que acompañará al objeto de aprendizaje. Esta guía proporcionará instrucciones detalladas sobre los procedimientos del proceso de enseñanza-aprendizaje, estrategias metodológicas, información teórica relevante y ejemplos prácticos relacionados con la extracción de ácido cítrico y sus aplicaciones industriales y de otro tipo.

El objetivo final es crear un objeto de aprendizaje completo y accesible que combine los videos interactivos y la guía didáctica. Este recurso será utilizado por los estudiantes y profesores como una herramienta efectiva para adquirir y distribuir los conocimientos y habilidades necesarios en el ámbito de la química para los procesos de extracción de sustancias con un alto valor industrial y de múltiples aplicaciones, centrándose específicamente en la extracción de ácido cítrico de frutas apropiadas.

Mes 11 / Programas de Socialización de la Ciencia / Materiales Audiovisuales / Objeto digital de aprendizaje 8 (ODA-8)

Descripción:

En este periodo, se trabajará en la creación del octavo objeto digital de aprendizaje, titulado "¡Pinta tu sonrisa de colores!: Identificación y separación de compuestos vegetales por cromatografía en capa fina". El objetivo principal de este ODA es describir a los estudiantes la cromatografía en capa fina como una técnica útil para separar y analizar sustancias presentes en un extracto vegetal. Los estudiantes podrán comprender los principios fundamentales de esta técnica, así como la relación entre la polaridad de las sustancias y la selección adecuada de los eluyentes para lograr una separación efectiva.

Actividades:

1. Planeación de la logística necesaria: Se llevará a cabo la planificación de la logística requerida para la realización del objeto de aprendizaje. Esto incluye la identificación y adquisición de los reactivos y materiales necesarios, así como la asignación de espacios y tiempos para las prácticas de extracción.
2. Filmación didáctica de las prácticas: Se realizará la filmación del objeto de aprendizaje de manera didáctica, centrándose en los aspectos relevantes para el aprendizaje de los estudiantes. Se utilizarán recursos audiovisuales, explicaciones detalladas, imágenes y gráficas para facilitar la comprensión de los conceptos y procedimientos relacionados con la extracción de ácido cítrico.
3. Edición de los videos: Se llevará a cabo la edición de los videos grabados durante la realización del objeto de aprendizaje. Se optimizará la calidad del material audiovisual, se agregarán elementos gráficos y se organizará de manera coherente para mejorar la comprensión.
4. Redacción de la guía didáctica: Se redactará la guía didáctica que acompañará al ODA. Esta guía proporcionará instrucciones detalladas sobre los procedimientos del proceso de enseñanza-aprendizaje, estrategias metodológicas, información teórica relevante y ejemplos prácticos relacionados con la extracción de compuestos vegetales y sus aplicaciones ancestrales e industriales.

El objetivo final es crear un ODA completo y accesible que combine los videos interactivos y la guía didáctica. Este recurso será utilizado por los estudiantes y profesores como una herramienta efectiva para adquirir y distribuir los conocimientos y habilidades necesarios en el ámbito de la química como una ciencia ancestral sobre todo en la separación de pigmentos de un extracto vegetal.

Mes 13 / Programas de Socialización de la Ciencia / Materiales Audiovisuales / Objeto digital de aprendizaje 9 (ODA-9)

Descripción:

En este periodo, se trabajará en la creación del noveno objeto de aprendizaje, titulado "Ser como Popeye: Aislamiento de clorofila y pigmentos carotenoides de espinacas por cromatografía en columna". El objetivo principal de este ODA es describir a los estudiantes la cromatografía en columna como una técnica utilizada para separar mezclas complejas de compuestos, en este caso, los pigmentos vegetales presentes en las hojas de espinaca. Los estudiantes podrán adquirir habilidades prácticas en técnicas de laboratorio y comprender la teoría detrás de esta técnica, que es ampliamente utilizada en la industria química y farmacéutica para purificar productos y separar mezclas.

Actividades:

1. Planeación de la logística necesaria: Se llevará a cabo la planificación de la logística requerida para la realización del ODA. Esto incluye la identificación y adquisición de los reactivos y materiales necesarios, así como la asignación de espacios y tiempos para las prácticas de cromatografía en columna.
2. Filmación didáctica de las prácticas: Se realizará la filmación del objeto de aprendizaje de manera didáctica, centrándose en los aspectos relevantes para el aprendizaje de los estudiantes. Se utilizarán recursos audiovisuales, explicaciones detalladas, imágenes y gráficas para facilitar la comprensión de los conceptos y procedimientos relacionados con la cromatografía en columna.
3. Edición de los videos: Se llevará a cabo la edición de los videos grabados durante la realización del objeto de aprendizaje. Se optimizará la calidad del material audiovisual, se agregarán elementos gráficos y se organizará de manera coherente para mejorar la comprensión.
4. Redacción de la guía didáctica: Se redactará la guía didáctica que acompañará al objeto de aprendizaje. Esta guía proporcionará instrucciones detalladas sobre los procedimientos del proceso de enseñanza-aprendizaje, estrategias metodológicas, información teórica relevante y ejemplos prácticos relacionados con la cromatografía en columna y sus aplicaciones en la industria farmacéutica y bioquímica.

El objetivo final es crear un ODA completo y accesible que combine los videos interactivos y la guía didáctica. Este recurso será utilizado por los estudiantes y profesores como una herramienta efectiva para adquirir y distribuir los conocimientos y habilidades necesarios en el ámbito de la química, especialmente en la industria farmacéutica y bioquímica, para separar compuestos naturales de alto valor contenidos en mezclas complejas.

Mes 15 / Programas de Socialización de la Ciencia / Materiales Audiovisuales / Objeto digital de aprendizaje 10 (ODA-10)

Descripción:

En este periodo, se trabajará en la creación del décimo ODA, titulado "Dejar de hablar y empezar a hacer. Proyecto integrador". El objetivo principal de este objeto de aprendizaje es aplicar los conceptos teóricos y prácticos adquiridos por los estudiantes durante su formación en química para generar productos artesanales que puedan ser vendidos, fomentando así la cultura emprendedora y el desarrollo de habilidades en para la aplicación de los conceptos fisicoquímicos mostrados con anterioridad.

Actividades:

1. Planeación de la logística necesaria: Se llevará a cabo la planificación de la logística requerida para la realización del proyecto integrador. Esto incluye la identificación y adquisición de los reactivos y materiales necesarios, así como la asignación de espacios y tiempos para la producción y venta de los productos.
2. Filmación didáctica de las prácticas: Se realizará la filmación del proceso de desarrollo de los productos de manera didáctica, centrándose en los aspectos relevantes para el aprendizaje de los estudiantes. Se utilizarán recursos audiovisuales, explicaciones detalladas, imágenes y gráficas para facilitar la comprensión de los conceptos y procedimientos relacionados con la formulación y fabricación de los productos.
3. Edición de los videos: Se llevará a cabo la edición de los videos grabados durante el proyecto integrador. Se optimizará la calidad del material audiovisual, se agregarán elementos gráficos y se organizará de manera coherente para mejorar la comprensión.
4. Redacción de la guía didáctica: Se redactará la guía didáctica que acompañará al objeto de aprendizaje. Esta guía proporcionará instrucciones detalladas sobre los procedimientos del proceso de enseñanza-aprendizaje, estrategias metodológicas, información teórica relevante y ejemplos prácticos relacionados con el desarrollo y comercialización de productos químicos artesanales.

El objetivo final es crear un ODA completo y accesible que combine los videos interactivos y la guía didáctica. Este recurso será utilizado por los estudiantes y profesores como una herramienta efectiva para adquirir y distribuir los conocimientos y habilidades necesarios en el ámbito de la química, en el contexto de un proyecto real de emprendimiento y producción de productos químicos artesanales para el consumo personal o venta local.

Mes 10, 11, 17, 18 / Formación de Recursos Humanos / Licenciatura / Proyecto Terminal

Descripción:

Se llevará a cabo la formación de estudiantes de nivel licenciatura mediante la realización de un proyecto terminal para la obtención del grado académico. El proyecto terminal (trabajo de investigación de los Planes de estudio UAM) permitirá a los estudiantes participar activamente en la creación de los ODA, involucrándose en la realización de experiencias en el laboratorio, la grabación de videos, tareas de edición, entre otros aspectos.

Actividades:

1. Redacción del protocolo del proyecto terminal: En esta etapa se definirá la metodología que se seguirá para el desarrollo del Proyecto Terminal, estableciendo los pasos y procedimientos necesarios.
2. Revisión de la literatura: Se realizará una exhaustiva revisión de la literatura relacionada con la temática de los ODA, con el fin de obtener una base sólida actualizada de conocimiento y fundamentos teóricos.
3. Propuesta y redacción de la metodología de los objetos de aprendizaje: Se elaborará una propuesta detallada y precisa de la metodología que se emplea para la creación de los objetos de aprendizaje. Esta metodología deberá contemplar aspectos como el diseño de las prácticas de laboratorio, la estructura de los videos, y los recursos pedagógicos a utilizar.
4. Preparación y filmación del ODA: se llevará prepararán y se realizarán las prácticas de laboratorio necesarias para la creación del ODA. Se filmarán las diferentes etapas de las prácticas con el objetivo de capturar de manera precisa y detallada las actividades realizadas.
5. Edición del material audiovisual: Se realizará la edición del material audiovisual obtenido durante la filmación de las prácticas de laboratorio. Se realizarán ajustes, se agregarán elementos gráficos y se optimizará la presentación del video para su posterior utilización en el objeto de aprendizaje.
6. Elaboración del objeto de aprendizaje: Con base en el material audiovisual editado y en los recursos pedagógicos previamente definidos, se procederá a la elaboración del ODA. Este consistirá en un video de prácticas de laboratorio en materia de química fundamental, acompañado de una guía didáctica que permita su adecuada utilización por parte de los estudiantes.
7. Creación del material compilado: Finalmente, se compilará y organizará el material creado, incluyendo el video y la guía didáctica, en un formato accesible y amigable para su difusión y distribución.

Mes 16 / Programas De Socialización De La Ciencia / Seminario /Coloquio

Descripción:

El coloquio "Divulgación y apropiación de los saberes educativos de la química en México: Avances y perspectivas" es un evento de divulgación científica que se realizará con el objetivo de dar a conocer las diferentes actividades realizadas durante el proyecto a la comunidad académica y a la sociedad en general. Este coloquio busca obtener retroalimentación para el proyecto y establecer colaboraciones interinstitucionales para futuras actividades similares. Durante el coloquio se contará con la participación de panelistas especiales de la Secretaría de Educación, Ciencia, Tecnología e Innovación (SECTEI) de la Ciudad de México, quienes compartirán su experiencia y conocimientos en el campo de la educación y la divulgación científica. Su participación en el evento enriquecerá las discusiones y ofrecerá una perspectiva institucional relevante.

Actividades:

1. Creación del comité organizador: Se conformará un comité encargado de la logística y planificación del coloquio. Este comité será responsable de coordinar las diferentes actividades y asegurar el cumplimiento de los objetivos del evento.
2. Programación de pláticas: Se establecerá un programa de conferencias para el coloquio, el cual constará de un día completo de actividades. Se buscará la participación de profesionales de universidades hermanas, quienes impartirán tres conferencias relacionadas con el tema del proyecto. Estas conferencias ofrecerán una visión amplia y actualizada de los avances en el campo de la química y su relevancia educativa.
3. Presentación de resultados del proyecto: Se dedicará una plática especial para presentar los resultados obtenidos durante el desarrollo del proyecto. En esta presentación se recopilarán los objetivos alcanzados, las guías de aprendizaje elaboradas y los principales logros del proyecto.
4. Certificados para los ponentes: Se otorgarán certificados a los ponentes que participen en el coloquio. Estos certificados reconocerán su contribución al evento y podrán ser utilizados por los ponentes en su currículum académico y profesional.

El objetivo principal del coloquio es promover la divulgación y apropiación de los saberes de la enseñanza de la química en México, brindando un espacio de intercambio de conocimientos y experiencias. Asimismo, se busca establecer vínculos de colaboración entre instituciones para futuros proyectos que contribuyan al desarrollo de la educación química en el país.

Mes 16 / Programas De Socialización De La Ciencia / Material Impreso / Compendio de guías didácticas de los Objetos digitales de aprendizaje

Descripción:

Se escribirá un libro de divulgación de la enseñanza de la química experimental con base en los objetos de aprendizaje desarrollados anteriormente. Este libro tiene como objetivo principal proporcionar una guía detallada, precisa y flexible para la realización de prácticas de laboratorio en las Unidades de Enseñanza-Aprendizaje de las instituciones de educación media superior en la Ciudad de México. El texto será sometido a un riguroso proceso de evaluación por pares expertos en pedagogía y química, para garantizar su calidad y pertinencia.

Actividades:

1. Obtención de la evaluación por pares: El libro será enviado a expertos en pedagogía y química, quienes realizarán una revisión exhaustiva del contenido. Estos evaluadores analizarán la precisión de las instrucciones, la coherencia de los procedimientos y la adecuación de los conceptos teóricos presentados. Sus comentarios y sugerencias se utilizarán para mejorar y enriquecer el contenido del manual.
2. Revisión y corrección del texto: Con base en las evaluaciones de los pares, se realizarán las correcciones y ajustes necesarios en el manual. Se prestará especial atención a la claridad y concisión de las instrucciones, la inclusión de medidas de seguridad adecuadas y la coherencia entre la teoría y la práctica. También se garantizará que el manual cumpla con los estándares pedagógicos y científicos establecidos.
3. Impresión y publicación del libro para el laboratorio: Una vez finalizada la revisión y corrección, se procederá a su impresión en un formato de alta calidad. Se seleccionará cuidadosamente el diseño y la presentación para facilitar su uso durante las actividades prácticas en el laboratorio. Posteriormente, se publicará y se pondrá a disposición de los estudiantes en las Unidades de Enseñanza-Aprendizaje correspondientes de las instituciones educativas.

El objetivo final del libro para el laboratorio es proporcionar a los estudiantes una herramienta completa y confiable que les guíe en la realización de las actividades experimentales. Incluirá instrucciones detalladas sobre los procedimientos de laboratorio, el manejo seguro de reactivos y equipos, así como explicaciones teóricas pertinentes y actividades para la autoevaluación. Además, se presentarán ejemplos prácticos y se fomentará la comprensión de los conceptos químicos involucrados en cada actividad experimental.

Mes 17 / Programas De Socialización De La Ciencia / Presentación de seminario institucional/departamental

Descripción:

Se presentarán los resultados, actividades realizadas y logros educativos del proyecto en los seminarios del departamento de química de la UAMI. El objetivo principal es compartir y difundir las experiencias y contribuciones adquiridas, mediante los trabajos realizados para el proyecto, con la comunidad académica, tanto especializada como no especializada. La presentación se realizará en un formato de seminario y se transmitirá vía streaming para llegar a una audiencia amplia y diversa. Se busca generar retroalimentación sobre el proyecto y fomentar la colaboración interinstitucional para futuros proyectos similares.

Actividades:

1. Preparación de la presentación: Se recopilarán los resultados más relevantes y significativos del proyecto, así como las lecciones aprendidas y las conclusiones obtenidas. Se organizará la información de manera clara y coherente, resaltando los aspectos más importantes del proyecto y su impacto en la enseñanza de la química. Además, se preparará diapositivas y material visual complementario para respaldar la presentación.
2. Desarrollo del seminario: Durante la presentación, se expondrán los objetivos del proyecto, las actividades realizadas, los recursos y las herramientas utilizadas, así como los resultados obtenidos. Se destacarán aquellos aspectos que puedan resultar más relevantes e interesantes para la audiencia, como los avances en la enseñanza de la química y la promoción de la divulgación científica. Se fomentará la participación activa de la audiencia, invitándole a realizar preguntas y comentarios.
3. Retroalimentación y colaboración: Al concluir la presentación, se abrirá un espacio para la discusión y la retroalimentación por parte de la audiencia. Se invitará a los asistentes a compartir sus opiniones, sugerencias y experiencias relacionadas con el proyecto. Además, se explorarán posibles oportunidades de colaboración intrainstitucional para futuros proyectos similares, con el objetivo de fortalecer la enseñanza de la química y la divulgación científica.

El objetivo principal de la presentación del seminario es compartir los resultados y las experiencias del proyecto, así como fomentar el intercambio de ideas y la colaboración entre colegas. Se busca crear un espacio de reflexión y discusión sobre las prácticas educativas en la enseñanza de la química, con la finalidad de mejorar la calidad de la educación y promover el desarrollo de futuros proyectos innovadores en este campo.

Mes 17 / Publicaciones / Artículo En Revista No Indexada / Artículo De Divulgación

Descripción:

Se redactará un artículo de divulgación con el propósito de dar a conocer las diferentes actividades realizadas durante este proyecto. El objetivo principal es difundir el proyecto y contribuir al enriquecimiento intelectual en la enseñanza de la química experimental. El artículo estará dirigido a un público amplio y buscará resaltar los resultados más relevantes que puedan facilitar la implementación de programas similares en el futuro.

Actividades:

1. Escritura del artículo: Se redactará el artículo acerca del proyecto realizado, centrándose en los aspectos más importantes y destacados. Se describirán las actividades, los objetivos perseguidos y los resultados obtenidos. Se utilizará un lenguaje claro y accesible para que el artículo sea comprensible para el público general. Además, se incluirán ejemplos prácticos y se resaltarán las implicaciones educativas y científicas del proyecto.
2. Revisión y edición del artículo: Una vez redactado, se procederá a la revisión y edición del artículo. Se verificará la precisión de la información, se corregirán posibles errores gramaticales o de estilo, y se asegurará la coherencia y cohesión del texto. Se prestará especial atención a la claridad y la fluidez de la exposición, así como a la correcta estructura del artículo.
3. Formato y presentación del artículo: Se adecuará el formato del artículo según las pautas establecidas por la revista (no indexada) en la que se planea publicar. Se organizarán las secciones del artículo de acuerdo con las normas de la revista y se preparará una presentación visual atractiva que complemente el contenido escrito.
4. Envío y seguimiento de la publicación: Una vez finalizada la revisión y edición, se enviará el artículo a la revista no indexada para su consideración y posible publicación. Se realizará un seguimiento del proceso de revisión por parte de los editores y se atenderán las sugerencias o modificaciones que sean requeridas.

El objetivo principal del artículo de divulgación es dar a conocer las actividades realizadas durante el proyecto, compartir los resultados obtenidos y promover la replicación de programas similares en el futuro. También se pretende difundir el proyecto y contribuir al enriquecimiento intelectual en la enseñanza de la química experimental, tanto en el ámbito educativo como científico, y fomentar la divulgación del conocimiento en la comunidad académica y general.

Mes 18 / Otro / Informe final

Descripción:

Se llevará a cabo la elaboración del informe final. Esta actividad es fundamental para evaluar lo desarrollado y documentar de manera exhaustiva las acciones y los resultados del proyecto. El informe final servirá como un registro detallado de todas las etapas y los logros del proyecto.

Actividades:

1. Recopilación de información: se recopilará toda la información relevante relacionada con el proyecto, incluyendo los objetivos iniciales, las actividades realizadas, los recursos utilizados, los resultados obtenidos y las lecciones aprendidas. Se revisarán los documentos, registros y datos recopilados a lo largo del proyecto para asegurar una visión completa de su desarrollo.
2. Elaboración del informe final: con base en la información recopilada, se redactará el informe final del proyecto. Este informe deberá incluir una introducción que describa el contexto y los objetivos del proyecto, así como una descripción detallada de las actividades realizadas y los resultados alcanzados. Se destacarán los logros más significativos y se presentarán recomendaciones para futuras acciones.
3. Presentación del informe y resultados de la auditoría: una vez finalizado el informe y concluida la auditoría, se presentarán los resultados ante los responsables del proyecto, los colaboradores y las partes interesadas.
4. Archivo y difusión del informe final: el informe final será archivado y puesto a disposición de la SECTEI. Se asegurará su accesibilidad para consultas futuras y se considerará su difusión, en caso de ser pertinente, para compartir los conocimientos adquiridos y las mejores prácticas desarrolladas durante el proyecto.

El objetivo principal del informe final es realizar una evaluación exhaustiva del proyecto, documentar los resultados y las lecciones aprendidas, y proporcionar una base sólida para futuras iniciativas similares.

Mes 18 / Otro / Auditoría

Descripción:

Se realizará una auditoría del proyecto. Estas actividades son fundamentales para evaluar y documentar, verificar y validar la gestión y el cumplimiento de los objetivos establecidos.

Actividades:

1. Realización de la auditoría (externa): se llevará a cabo una auditoría exhaustiva del proyecto para evaluar su gestión, eficiencia y cumplimiento de los objetivos establecidos. Se revisarán los procesos, los recursos utilizados, la calidad de los resultados y el cumplimiento de los plazos establecidos. La auditoría también permitirá identificar posibles áreas de mejora y asegurar la transparencia y la integridad de todo el proceso.
2. Se realizará una exposición clara y detallada de los hallazgos, conclusiones y recomendaciones derivadas del informe y la auditoría. Además, se brindará la oportunidad de discutir y resolver posibles dudas o inquietudes.

La auditoría nos permitirá realizar una evaluación exhaustiva del proyecto, documentar los resultados y las lecciones aprendidas, y proporcionar una base sólida para futuras iniciativas similares. Estas actividades contribuirán a la transparencia, la rendición de cuentas y la mejora continua en la gestión de proyectos científicos y educativos.

8. IMPACTOS ESPERADOS

- Mejora en la calidad de la educación: se espera que la implementación de los Objetos Digitales de Aprendizaje en la enseñanza de la química experimental a nivel bachillerato conduzca a una mejora significativa en la calidad de la enseñanza de la química experimental. Esto se reflejará en un aumento en el nivel de comprensión y dominio de los conceptos y habilidades relacionados con esta ciencia por parte de los estudiantes. Además, se espera que los materiales didácticos desarrollados promuevan un aprendizaje más activo, participativo y significativo, fomentando el pensamiento crítico y la resolución de problemas.
- Acceso equitativo a la educación: al proporcionar recursos educativos digitales accesibles y autocontenidos, el proyecto tiene como objetivo incidir en la infraestructura y recursos consumibles para la enseñanza experimental en las disciplinas STEM en las instituciones educativas de la Ciudad de México. Esto permitirá que un mayor número de estudiantes tengan acceso a una educación integral en química experimental. Asimismo, se espera que los materiales digitales faciliten la aplicación de modelos híbridos de enseñanza-aprendizaje y el aprendizaje autónomo, lo que contribuirá a una mayor equidad en el acceso a la educación.
- Incremento en el interés y la participación de los estudiantes: se espera que la implementación de los Objetos Digitales de Aprendizaje genere un mayor interés y entusiasmo en los estudiantes por la química experimental. Mediante el uso de recursos visuales interactivos y prácticos, se busca despertar la curiosidad científica y promover una actitud positiva hacia el aprendizaje de esta disciplina. Asimismo, se espera que los materiales didácticos fomenten la participación activa de los estudiantes en el proceso de enseñanza-aprendizaje, a través de la realización de experimentos virtuales y la resolución de problemas desafiantes.
- Innovación educativa y desarrollo profesional docente: El proyecto también busca promover la innovación educativa y el desarrollo profesional docente en el campo de la química experimental. Al diseñar y elaborar secuencias didácticas y objetos de aprendizaje de alta calidad, se pretende impulsar la adopción de enfoques pedagógicos más efectivos y actualizados. Esto contribuirá al fortalecimiento de las habilidades y conocimientos de los docentes en la enseñanza de la química experimental, así como a la generación de nuevas prácticas educativas basadas en evidencia.
- Transferencia de conocimiento y escalabilidad: Se espera que los resultados y los recursos desarrollados en este proyecto puedan ser transferidos y adaptados a otras instituciones educativas tanto a nivel local como nacional. Al ser objetos digitales de aprendizaje autocontenidos, existe la posibilidad de escalar su implementación y compartir las buenas prácticas y lecciones aprendidas con otras comunidades educativas. De esta manera, se busca generar un impacto más amplio en el ámbito de la educación en química experimental, impulsando la mejora continua y el avance de la enseñanza y el aprendizaje de esta disciplina.

9. DESGLOSE FINANCIERO ESTRUCTURADO DEL PROYECTO DE ACUERDO CON LOS RUBROS ELEGIBLES POR ETAPA, JUSTIFICANDO CADA RUBRO.

- **GASTOS DE AUDITORÍA DEL INFORME FINANCIERO FINAL**

Con la finalidad de llevar un control, comprobación y evidencia de los gastos realizados se contempla una auditoría de estos, así como un informe final financiero y de actividades para reportar en tiempo y forma la conclusión del proyecto.

Monto: $22,000.00

- **APOYO A ESTUDIANTES ASOCIADOS CON EL PROYECTO**

Debido a que en el proyecto se planea que estudiantes de los últimos trimestres de las carreras afines, puedan realizar su proyecto terminal, llevando a cabo diversas actividades de investigación y desarrollo de los objetos digitales de aprendizaje (ODA), se contempla el otorgamiento de un apoyo económico para cada estudiante en forma de una beca.

$3,500.00 al mes, $30.800 por 8 meses

Monto: $123,200.00 para 4 estudiantes

- **BIENES INFORMÁTICOS Y MOBILIARIO Y EQUIPO EDUCACIONAL**

Para la realización de los objetos digitales de aprendizaje (ODA), se requiere de equipo y bienes informáticos como software de edición de videos, computadoras portátiles, cámara de video, entre otros.

EQUIPO	Marca	Importe ($)
Computadoras portátiles	2 MacBook Pro 16" MNW93E/A Chip M2 Pro CPU12 GPU19 16GB 1TB Gris Espacial	$132,000.00
	2 ThinkPad X1 Yoga 8va Gen Procesador Intel® Core™ i5-1345U vPro® de 13ª Generación 512 GB SSD M.2 2280	$68,000.00
Cámara de video	PANASONIC LUMIX FZ1000 II - Cámara digital de 20.1 MP, lente LEICA DC de 16 x 25-400 mm, video 4K, estabilizador óptico de imagen y pantalla de 3 pulgadas, cámara de apuntar y disparar - DC-FZ1000 II (negro)	$19,800.00
Micrófonos	ALVOXCON Sistema de Micrófono Inalámbrico Lavalier UHF Doble Wireless Mic de Solapa/Diadema para iPhone, Cámara DSLR, Smartphone, Altavoz PA, Recargable, Audio Superior ideal para Video Youtube, Grabación Vocal, Podcast, Vlog, Conferencia, Presentación, Enseñanza	$2,420.00
Cortina verde	Aimosen 2.14 X 3.05M Fondo de Pantalla Verde para Fotografía, Fondo de Pantalla Verde Puro Chromakey, Cortina de Tela de Poliéster con 4 Abrazaderas para Zoom Reunión Youtube Video Streaming Gaming	$660.00
Lámparas	Neewer Kit de 2 Unidades Bi-color 480 LED Video Luz Regulable con Soporte de Luz Incluye: 3200-5600K CRI 96+ LED Panel con U Bracket, 19	$4,180.00

	Centímetros Tripié de Luz para YouTube Estudio Video Shooting	
Software para edición de video	Camtasia	$6,050.00
Pizarrón inteligente	BenQ 65"	$77,000

Monto: $310,110.00

- **EQUIPO DE LABORATORIO**

Para una adecuada elaboración de los objetos digitales de aprendizaje (ODA), se requiere de algunos equipos de laboratorio que resultan imprescindibles.

MATERIAL de vidrio, metal o porcelana	***Capacidad***	***Importe ($)***
Agitador de vidrio	N. A.	$330.00
Agitadores magnéticos	15 mm y 30 mm	$660.00
Anillo metálico	8 cm	$220.00
Buretas	50 ml y 100 ml	$1,430.00
Embudos de vidrio	90 mm y 65 mm	$1,320.00
Embudos de Buchner	30, 60 y 120 mm	$2,200.00
Matraces Erlenmeyer	50, 125, 250, 500 y 1000 ml	$4,972.00
Matraz Kitasato	250 y 500 ml	$1,210.00
Perillas de succión	N. A.	$220.00
Pinzas de tres dedos	N. A.	$264.00
Pinzas para bureta	N. A.	$550.00
Pinzas para capsula de porcelana	N. A.	$286.00
Pinzas para tubos de ensaye	N. A.	$165.00
Pipeta graduada	1, 2, 5 y 10 ml	$1,716.00
Pipeta volumétrica	1 y 10 ml	$473.00
Probeta	10, 100 y 250 ml	$682.00
Soporte universal	N. A.	$550.00
Tubo de ensaye	16 ml	$1,430.00
Vaso de precipitados	10, 50, 100, 250, 500 y 1000 ml	$451.00
Vidrio de reloj	60 y 79 mm	$440.00
Picnómetro	10 ml	$462.00
Nuez	N. A.	$605.00
Pinzas de 3 dedos	N. A.	$264.00
Perlas o cuerpos de ebullición	N. A.	$220.00
piseta de alcohol	250 ml	$308.00
piseta de agua	250 ml	$275.00
Manguera de látex	6.3 mm	$2,750.00
Espátula de metal	15 – 20 cm	$275.00
Micro espátula	N. A.	$187.00
Cristalizador de vidrio	100 x 50 mm	$1,375.00
Mortero con pistilo	50, 100 y 250 ml	$2,156.00
Gradillas para tubos de ensaye de 16 ml	N. A.	$737.00

Monto: $29,183.00

EQUIPOS	***Características***	***Importe ($)***
Balanza analítica	0.0001 gramos	$100,000.00
Baño maría	N. A.	$2,200.00
Densímetro digital portátil		$55,000.00
Sonicador		$6,600.00
Potenciómetro de mesa		$8,800.00
Termómetro	–10 a 150 °C	$1,870.00
Parrilla de agitación y calentamiento		$25,000.00
Equipo Quickfit		$10,000.00
Mantillas de calentamiento	250 ml	$1,540.00
Reóstato		$440.00
Recirculador		$8,250.00
Rotaevaporador, baño, vidrieria tipo b, bomba vacio, baño recirculador		$290,000.00
Bomba de vacío	1/2 HP	$5,500.00
Desecador al vacío	30 cm	$5,000.00
Celdas de cuarzo	1 cm	$11,000.00
UV-vis	200 – 1100 nm	$400,000.00
Exprimidor de jugos		$1,210.00
Placas cromatográficas de sílica	2,5 x 7,5 cm	$3,388.00
Lámpara de luz UV	25 cm	$10,000.00
Pipeta Pasteur	caja	$1,100.00
Microcentrífuga de enfriamiento con rotor	24 x 1.5/2. 0ml	$80,000.00
Micropipetas	20 a 100 ml	$5,000.00
	100 a 200 ml	$5,000.00
	100 a 1000 ml	$5,000.00
Multímetro		$1,650.00
Puntas para micropipetas	200 ml	$2,640.00
Puntas para micropipetas	1000 ml	$2,640.00
Tubos eppendorf	2mL	$1000.00

Monto: $1,049,828.00

REACTIVOS	***Marca***	***Importe ($)***
Papel ph 0-14	Merck	$792.00
Ácido sulfúrico (95-98%) A.C.S. 4 L	Meyer	$1,452.00
Ácido clorhídrico 36.5-38% ACS 4 L	Meyer	$1,331.00
Ácido cítrico anhidro ACS 500 gr	Meyer	$506.00
Sodio hidróxido escamas reactivo 500 gr	Meyer	$209.00
Fenolftaleína polvo indicador A.C.S. 500 gr	Meyer	$1,496.00
Buffer de referencia a pH 4.00 +/- 0.01	Meyer	$313.50
Buffer de referencia a pH 7.00 +/- 0.01	Meyer	$418.00
Buffer de referencia a pH 10.00 +/- 0.02	Meyer	$522.50
Cloroformo A.C.S. 4 L	Meyer	$3,680.60
Magnesio sulfato anhidro polvo reactivo 500 g	Meyer	$563.20
Calcio cloruro anhidro granulado A.C.S. 2.5 kg	Meyer	$3,624.50
Etilo acetato A.C.S. 4 L	Meyer	$2,552.00
Acetona ACS (2-propanona) 4 L	Meyer	$1,848.00
Alcohol etílico absoluto A.C.S. 4 L	Meyer	$2,735.70
Potasio permanganato cristal A.C.S. 500 gr	Meyer	$7,612.00
Metileno cloruro A.C.S. 4 L	Meyer	$2,673.00
Hexano A.C.S. 4 L	Meyer	$2,450.80
Sodio sulfato anhidro A.C.S. 500 g	Meyer	$459.80
Glicerina A.C.S. 1 L	Meyer	$3,080.00
Aceite de coco 1 kg	Meyer	$4,070.00
Potasio hidróxido escamas reactivo 500 g	Meyer	$655.60

Monto: $43,045.20

RUBRO	**MONTOS**
Gastos de auditoría del informe financiero final	$22,000.00
Apoyo a estudiantes asociados con el proyecto	$123,200.00
Bienes informáticos y mobiliario y equipo educacional	$310,110.00
Equipo de laboratorio (material de vidrio)	$29,183.00
Equipo de laboratorio (equipos)	$1,049,828.00
Equipo de laboratorio (reactivos)	$43,045.20
SUBTOTAL	**$1,577,366.20**
IVA	**$252,378.59**
TOTAL	**$1,829,744.79**

RELACIÓN DEL GRUPO DE TRABAJO, EL CUAL INCLUYA NOMBRES, ESPECIALIDAD, ACTIVIDADES A DESARROLLAR EN EL PROYECTO.

El grupo de trabajo que desarrollará el presente proyecto forma parte del Departamento de Química de la Universidad Autónoma Metropolitana Unidad Iztapalapa, en conjunto con el Instituto de Educación Media Superior de la Ciudad de México (IEMS) y la Universidad Nacional Autónoma de México (Escuela Nacional Preparatoria)..

A continuación, se mencionan a los Docentes-Investigadores que participarán en el proyecto, así como su especialidad y las actividades que desarrollarán:

Dr. Jorge Garza Olguín, jefe del Departamento de Química UAM-I, especialista en Fisicoquímica Teórica:

- Liderazgo y coordinación del proyecto:
  - Establecer la visión y los objetivos del proyecto en consulta con el equipo de trabajo.
  - Asignar roles y responsabilidades a los miembros del equipo de proyecto.
  - Coordinar y supervisar la realización adecuada de las etapas del proyecto.
  - Facilitar la comunicación y colaboración entre los miembros del equipo.

- Control de calidad:
  - Implementar un plan de control de calidad para garantizar la excelencia en la ejecución del proyecto.
  - Establecer criterios de evaluación y estándares de calidad para cada etapa del proyecto.
  - Realizar revisiones y seguimiento periódico del progreso del proyecto para asegurar el cumplimiento de los estándares establecidos.
  - Identificar y abordar posibles desviaciones o problemas que puedan surgir durante la ejecución del proyecto.

- Generación del proyecto rector:
  - Elaborar el documento del proyecto rector que incluya los antecedentes, justificación, objetivos, problemática, impactos esperados y metas del proyecto.
  - Integrar de manera coherente y estructurada la información recopilada en cada una de las secciones del proyecto rector.
  - Asegurar que el proyecto rector refleje de manera clara y precisa la propuesta del proyecto de desarrollo de Objetos Digitales de Aprendizaje para la enseñanza de la química experimental a nivel bachillerato.

- Gestión del tiempo:
    - Establecer un cronograma detallado que defina las fechas límite y las actividades clave para cada sección del proyecto.
    - Monitorear el avance del proyecto en relación con el cronograma establecido.
    - Identificar posibles desviaciones en el cumplimiento de los plazos y tomar las acciones correctivas necesarias para mantener el proyecto en tiempo y forma.
    - Realizar reuniones periódicas con el equipo de trabajo para revisar el estado del proyecto y garantizar el cumplimiento de los tiempos establecidos.

Estas actividades permitirán al ***Dr. Garza*** liderar y supervisar de manera efectiva el desarrollo del proyecto, asegurando la calidad, la coherencia y el cumplimiento de los plazos.

Mtro. en D. Alan Javier Pérez Vázquez, jefe del Departamento de del Colegio de Química, Escuela Nacional Preparatoria - UNAM:

- Promoción, difusión y divulgación:
    - Participar en la promoción del material audiovisual relacionado con la enseñanza de la química experimental, para que pueda ser utilizado en los objetos digitales de aprendizaje en las Escuelas Nacionales Preparatorias - UNAM:
    - Llevar a cabo la difusión de los materiales audiovisuales, asegurando su coherencia, claridad y adecuación a los objetivos de aprendizaje en las Escuelas Nacionales Preparatorias - UNAM:
    - Participar en la promoción, difusión y divulgación del seminario y coloquio centrado en la química experimental y su aplicación en el contexto de química cotidiana.
    - Contribuir en el diseño del programa, la logística y la promoción del seminario y coloquio, buscando la participación de estudiantes, profesores e investigadores interesados en el tema.

Lic. Rufino Trinidad Velasco, Docente Investigador del el Instituto de Educación Media Superior de la Ciudad de México (IEMS):

- Promoción, difusión y divulgación:
    - Participar en la promoción del material audiovisual relacionado con la enseñanza de la química experimental, para que pueda ser utilizado en los objetos digitales de aprendizaje Instituto de Educación Media Superior de la Ciudad de México (IEMS)

- Llevar a cabo la difusión de los materiales audiovisuales, asegurando su coherencia, claridad y adecuación a los objetivos de aprendizaje en las Escuelas Nacionales Preparatorias - UNAM:
- Participar en la promoción, difusión y divulgación del seminario y coloquio centrado en la química experimental y su aplicación en el contexto de química cotidiana.
- Contribuir en el diseño del programa, la logística y la promoción del seminario y coloquio, buscando la participación de estudiantes, profesores e investigadores interesados en el tema.

Dra. Rubicelia Vargas Fosada, Profesora Titular C adscrita al Departamento de Química UAM-I, con 35 años de experiencia docente, especialista en Fisicoquímica Teórica.

- Elaboración y revisión de guías didácticas:
  - Investigar y recopilar información relevante para la elaboración de guías didácticas destinadas a la enseñanza de química experimental en el nivel bachillerato.
  - Diseñar un formato estructurado y claro para las guías didácticas, asegurando que estén alineadas con los objetivos y contenidos del programa de estudios de Química de las IEMS.
  - Desarrollar actividades y ejercicios prácticos que promuevan un aprendizaje significativo y experimental.
  - Revisar y mejorar las guías didácticas existentes, incorporando sugerencias y retroalimentación del equipo de proyecto.

- Realización del guión de los objetos de aprendizaje:
  - Definir la estructura y el contenido de los objetos de aprendizaje, considerando los objetivos de aprendizaje y las secuencias didácticas propuestas.
  - Elaborar el guión detallado que incluya los elementos multimedia, como videos, animaciones o simulaciones, que serán utilizados en los objetos de aprendizaje.
  - Colaborar con el equipo de desarrollo multimedia para garantizar la coherencia entre el guión y la implementación final de los objetos de aprendizaje.

- Diseño y logística del coloquio y seminario del proyecto:
  - Planificar y organizar un coloquio y seminario relacionado con el proyecto, donde se presenten los avances y resultados obtenidos.
  - Coordinar la participación de expertos en el área de química experimental y educación en STEM para enriquecer los debates y discusiones.
  - Establecer la logística del coloquio, incluyendo la selección de fechas, el diseño de programas, la gestión de ponentes y la difusión del evento.

- Revisión del informe final del proyecto:

- Evaluar y revisar el informe final del proyecto, asegurándose de que cumpla con los estándares de calidad y los requisitos establecidos.
- Verificar la coherencia entre los objetivos, resultados, impactos esperados y metas alcanzadas descritas en el informe.
- Realizar correcciones y mejoras necesarias en la redacción, estructura y contenido del informe final.

Estas actividades permitirán a la ***Dra. Vargas*** contribuir de manera significativa al desarrollo y éxito del proyecto, aportando su experiencia en docencia para la elaboración de guías didácticas, la creación de objetos de aprendizaje, la organización de eventos académicos y la revisión final del informe.

Dr. José Luis Córdova, Profesor Titular C adscrito al Departamento de Química UAM-I, del área de Química analítica, con doctorado en matemática educativa y 45 años de experiencia en la docencia en química:

- Elaboración y revisión de guías didácticas:
  - Investigar y recopilar información relevante para la elaboración de guías didácticas destinadas a la enseñanza de química experimental en el nivel bachillerato.
  - Analizar y evaluar las guías didácticas existentes, identificando áreas de mejora y asegurando su alineación con los objetivos de aprendizaje y el programa de estudios de Química de las IEMS.
  - Contribuir en la elaboración de actividades y ejercicios prácticos que fomenten un aprendizaje experimental y significativo.
  - Revisar y proporcionar retroalimentación para mejorar las guías didácticas desarrolladas por el equipo.

- Realización del guión de los objetos de aprendizaje:
  - Colaborar en la definición de la estructura y el contenido de los objetos de aprendizaje, considerando los objetivos de aprendizaje y las secuencias didácticas propuestas.
  - Elaborar el guión detallado que incluya los elementos multimedia, como videos, animaciones o simulaciones, que serán utilizados en los objetos de aprendizaje.
  - Trabajar en conjunto con el equipo de desarrollo multimedia para asegurar la coherencia entre el guión y la implementación final de los objetos de aprendizaje.

- Diseño y logística del coloquio y seminario del proyecto:
  - Participar en la planificación y organización de un coloquio y seminario relacionado con el proyecto, que permita presentar los avances y resultados obtenidos.
  - Contribuir en la selección de fechas, el diseño del programa y la gestión de ponentes y conferencistas expertos en química experimental y educación en STEM.

- Apoyar en la logística del coloquio, incluyendo la coordinación de espacios, la difusión del evento y la interacción con los participantes.

- Revisión del informe final del proyecto:
  - Proporcionar comentarios y sugerencias para mejorar la redacción, la estructura y el contenido del informe final.
  - Colaborar en la revisión de la documentación complementaria, como anexos y referencias bibliográficas, para garantizar su precisión y relevancia.

Estas actividades permitirán al ***Dr. Córdova*** contribuir de manera significativa al desarrollo y éxito del proyecto, aportando su experiencia en la enseñanza-aprendizaje de la química, para la elaboración y revisión de guías didácticas, el diseño de objetos de aprendizaje, la organización de eventos académicos y la revisión final del informe.

Dra. Margarita Viniegra Ramírez, Profesora Titular C adscrita al Departamento de Química UAM-I, especialista en Catálisis:

- Elaboración y revisión de guías didácticas:
  - Investigar y recopilar información relevante sobre catálisis y su aplicación en química experimental, enfocándose en el nivel bachillerato.
  - Coadyuvar en la elaboración de guías didácticas que integren los conceptos fundamentales de la química experimental, así como de sus aplicaciones.
  - Revisar y proporcionar retroalimentación para mejorar las guías didácticas desarrolladas por el equipo, asegurando su claridad, coherencia y pertinencia.

- Realización del guión de los objetos de aprendizaje:
  - Colaborar en la definición de la estructura y el contenido de los objetos de aprendizaje, considerando los objetivos de aprendizaje y las secuencias didácticas propuestas.
  - Elaborar el guión detallado que incluya los elementos multimedia, como videos, animaciones o simulaciones, para transmitir los conceptos y experimentos relacionados con la catálisis.
  - Trabajar en conjunto con el equipo de desarrollo multimedia para asegurar la precisión científica y didáctica de los objetos de aprendizaje.

- Diseño y logística del coloquio y seminario del proyecto:
  - Participar en la planificación y organización de un coloquio y seminario centrado en la enseñanza de la química experimental.
  - Colaborar en la selección de ponentes y expertos en la educación de la química, especialistas STEM y miembros de las IEMS para enriquecer el contenido del coloquio.

- Contribuir en el diseño del programa y la logística del evento, incluyendo la coordinación de fechas, espacios y la promoción del coloquio y seminario.

- Revisión del informe final del proyecto:
  - Evaluar y revisar el informe final del proyecto, verificando la coherencia entre los objetivos, los resultados obtenidos, los impactos esperados y las metas alcanzadas en relación con el proyecto.
  - Proporcionar comentarios y sugerencias para mejorar la redacción, la estructura y el contenido del informe final, asegurando su rigurosidad científica y su claridad.

Estas actividades permitirán a la ***Dra. Viniegra*** contribuir de manera significativa al desarrollo y éxito del proyecto, aportando su experiencia en docencia y catálisis, para la elaboración y revisión de guías didácticas, el diseño de objetos de aprendizaje, la organización de eventos académicos centrados en la catálisis y la revisión final del informe.

Dra. Nancy Coromoto Martín Guaregua, Profesora Titular C adscrita al Departamento de Química UAM-I, especialista en Catálisis:

- Elaboración y revisión de guías didácticas:
  - Investigar y recopilar información relevante en química experimental y sus aplicaciones, enfocándose en el nivel bachillerato.
  - Aportar en la elaboración de guías didácticas que integren los conceptos fundamentales de la catálisis y su relación con la química experimental.
  - Revisar y proporcionar retroalimentación para mejorar las guías didácticas desarrolladas por el equipo, asegurando su claridad, coherencia y pertinencia.

- Realización del guión de los objetos de aprendizaje:
  - Colaborar en la definición de la estructura y el contenido de los objetos de aprendizaje, considerando los objetivos de aprendizaje y las secuencias didácticas propuestas.
  - Elaborar un guión detallado que incluya los elementos multimedia, como videos, animaciones o simulaciones, para transmitir los conceptos y experimentos relacionados con la catálisis.
  - Trabajar en conjunto con el equipo de desarrollo multimedia para asegurar la precisión científica y didáctica de los objetos de aprendizaje.

- Diseño y logística del coloquio y seminario del proyecto:
  - Participar en la planificación y organización de un coloquio y seminario centrado en la enseñanza de la química experimental.
  - Colaborar en la selección de ponentes y expertos en la enseñanza de la química para enriquecer el contenido del coloquio.

- Contribuir en el diseño del programa y la logística del evento, incluyendo la coordinación de fechas, espacios y la promoción del coloquio y seminario.

- Revisión del informe final del proyecto:
  - Evaluar y revisar el informe final del proyecto, verificando la coherencia entre los objetivos, los resultados obtenidos, los impactos esperados y las metas alcanzadas en relación con el proyecto.
  - Proporcionar comentarios y sugerencias para mejorar la redacción, la estructura y el contenido del informe final, asegurando su rigurosidad científica y su claridad.

Estas actividades permitirán a la ***Dra. Martín*** contribuir de manera significativa al desarrollo y éxito del proyecto, aportando su experiencia en catálisis para la elaboración y revisión de guías didácticas, el diseño de objetos de aprendizaje, la organización de eventos académicos centrados en la catálisis y la revisión final del informe.

Dr. Ricardo A. Peralta Ávila, Profesor Visitante adscrito al Departamento de Química UAM-I, especialista en Materiales y adscrito al área de Catálisis:

- Realización de los objetos digitales de aprendizaje en el laboratorio:
  - Investigar y recopilar información relevante sobre la química de mezclas, separaciones, catálisis, analítica y su aplicación en el laboratorio de química experimental
  - Contribuir en la elaboración de objetos digitales de aprendizaje que integren experimentos y prácticas relacionadas con la química general, catálisis, mezclas, química analítica entre otros utilizando recursos multimedia como videos, animaciones y simulaciones
  - Trabajar en colaboración con el equipo de desarrollo multimedia para asegurar la calidad y precisión científica de los objetos digitales de aprendizaje.

- Formación de los recursos humanos mediante la dirección del proyecto terminal:
  - Supervisar y dirigir a estudiantes que estén realizando proyectos terminales relacionados con la enseñanza de química experimental en el laboratorio
  - Brindar orientación y asesoramiento a los estudiantes en la planificación, diseño y ejecución de los proyectos terminales, asegurando su relevancia y coherencia con los objetivos del proyecto
  - Evaluar y proporcionar retroalimentación a los estudiantes en el desarrollo de sus proyectos terminales, fomentando el aprendizaje y la adquisición de habilidades en el campo de la catálisis.

- Elaboración del material audiovisual, así como la edición de este:

- Participar en la elaboración y producción de material audiovisual relacionado con la enseñanza de la química experimental, que pueda ser utilizado en los objetos digitales de aprendizaje
- Realizar la grabación de experimentos y prácticas en el laboratorio, asegurando la captura de imágenes y vídeos de alta calidad
- Llevar a cabo la edición y postproducción de los materiales audiovisuales, asegurando su coherencia, claridad y adecuación a los objetivos de aprendizaje.

- Desarrollo del seminario y coloquio del proyecto:
  - Participar en la planificación y organización de un seminario y coloquio centrado en la química experimental y su aplicación en el contexto de química cotidiana.
  - Contribuir en el diseño del programa, la logística y la promoción del seminario y coloquio, buscando la participación activa de estudiantes, profesores e investigadores interesados en el tema.

- Redacción del informe final del proyecto:
  - Recopilar y analizar los resultados obtenidos a lo largo del proyecto, considerando los objetivos, la problemática abordada y los impactos esperados.
  - Redactar el informe final del proyecto, en el cual se documenten de manera clara y precisa las actividades realizadas, los resultados alcanzados y las conclusiones obtenidas.
  - Revisar y asegurar la calidad y rigurosidad científica del informe final, incluyendo referencias bibliográficas pertinentes y recomendaciones para futuras investigaciones.

Estas actividades permitirán al ***Dr. Peralta*** contribuir de manera significativa al desarrollo del proyecto, aplicando sus conocimientos y experiencia en catálisis para la realización de objetos digitales de

Dr. Leonardo David Herrera Zuñiga, Profesor Curricular adscrito al Departamento de Química UAM-I, Especialista en Biofisicoquímica:

- Realización de los objetos digitales de aprendizaje en el laboratorio:
  - Investigar y recopilar información relevante sobre biofisicoquímica, procesos industriales, química teórica y su aplicación en el laboratorio de química experimental.
  - Contribuir en la elaboración de objetos digitales de aprendizaje que integren experimentos y prácticas relacionadas con la biofisicoquímica, procesos industriales y química teórica, utilizando recursos multimedia como videos, animaciones y simulaciones.
  - Trabajar en colaboración con el equipo de desarrollo multimedia para asegurar la calidad y precisión científica de los objetos digitales de aprendizaje.

- Formación de los recursos humanos mediante la dirección del proyecto terminal:
    - Supervisar y dirigir a estudiantes que estén realizando proyectos terminales relacionados con la enseñanza de la química experimental en el laboratorio.
    - Brindar orientación y asesoramiento a los estudiantes en la planificación, diseño y ejecución de los proyectos terminales, asegurando su relevancia y coherencia con los objetivos del proyecto.
    - Evaluar y proporcionar retroalimentación a los estudiantes en el desarrollo de sus proyectos terminales, fomentando el aprendizaje y la adquisición de habilidades en el campo de la biofisicoquímica.

- Elaboración del material audiovisual, así como la edición de este:
    - Participar en la elaboración y producción de material audiovisual relacionado con la biofisicoquimica, procesos industriales, química teórica y su aplicación en el laboratorio de química experimental que pueda ser utilizado en los objetos digitales de aprendizaje
    - Realizar la grabación de experimentos y prácticas en el laboratorio, asegurando la captura de imágenes y vídeos de alta calidad
    - Llevar a cabo la edición y postproducción de los materiales audiovisuales, asegurando su coherencia, claridad y adecuación a los objetivos de aprendizaje.

- Desarrollo del seminario y coloquio del proyecto:
    - Participar en la planificación y organización de un seminario y coloquio centrado en la biofisicoquímica, procesos industriales, química teórica y su aplicación en el contexto de química experimental.
    - Colaborar en la selección de expertos en la enseñanza de la química experimental para participar como ponentes en el seminario y coloquio.
    - Contribuir en el diseño del programa, la logística y la promoción del seminario y coloquio, buscando la participación activa de estudiantes, profesores e investigadores interesados en el tema.

- Redacción del informe final del proyecto:
    - Recopilar y analizar los resultados obtenidos a lo largo del proyecto, considerando los objetivos, la problemática abordada y los impactos esperados.
    - Redactar el informe final del proyecto, en el cual se documenten de manera clara y precisa las actividades realizadas, los resultados alcanzados y las conclusiones obtenidas.
    - Revisar y asegurar la calidad y rigurosidad científica del informe final, incluyendo referencias bibliográficas pertinentes y recomendaciones para futuras investigaciones.

Estas actividades permitirán al ***Dr. Herrera*** contribuir de manera significativa al desarrollo del proyecto, aplicando sus conocimientos y experiencia en biofisicoquímica para la realización de objetos digitales de aprendizaje.

Dra. Nora S. Portillo Vélez, Posdoctorante adscrita al Departamento de Química UAM-I Especialista en Fotocatálisis:

- Realización de los objetos digitales de aprendizaje en el laboratorio:
  - Investigar y recopilar información relevante sobre la catálisis química, química medioambiental, química de materiales, entre otros y su aplicación en el laboratorio de química experimental.
  - Contribuir en la elaboración de objetos digitales de aprendizaje que integren experimentos y prácticas relacionadas con la catálisis química, química medioambiental, química de materiales, utilizando recursos multimedia como videos, animaciones y simulaciones.
  - Trabajar en colaboración con el equipo de desarrollo multimedia para asegurar la calidad y precisión científica de los objetos digitales de aprendizaje.

- Formación de los recursos humanos mediante la dirección del proyecto terminal:
  - Supervisar y dirigir a estudiantes que estén realizando proyectos terminales relacionados con la catálisis en el laboratorio de química experimental.
  - Brindar orientación y asesoramiento a los estudiantes en la planificación, diseño y ejecución de los proyectos terminales, asegurando su relevancia y coherencia con los objetivos del proyecto.
  - Evaluar y proporcionar retroalimentación a los estudiantes en el desarrollo de sus proyectos terminales, fomentando el aprendizaje y la adquisición de habilidades en el campo de la catálisis.

- Elaboración del material audiovisual, así como la edición de este:
  - Participar en la elaboración y producción de material audiovisual relacionado con la catálisis química, química medioambiental, química de materiales, que pueda ser utilizado en los objetos digitales de aprendizaje.
  - Realizar la grabación de experimentos y prácticas en el laboratorio, asegurando la captura de imágenes y vídeos de alta calidad.
  - Llevar a cabo la edición y postproducción de los materiales audiovisuales, asegurando su coherencia, claridad y adecuación a los objetivos de aprendizaje.

- Desarrollo del seminario y coloquio del proyecto:
  - Participar en la planificación y organización de un seminario y coloquio centrado en la enseñanza de la química y su aplicación en el contexto de química experimental.

- Colaborar en la selección de expertos en la enseñanza de la química experimental para participar como ponentes en el seminario y coloquio.
- Contribuir en el diseño del programa, la logística y la promoción del seminario y coloquio, buscando la participación activa de estudiantes, profesores e investigadores interesados en el tema.

- Redacción del informe final del proyecto:
  - Recopilar y analizar los resultados obtenidos a lo largo del proyecto, considerando los objetivos, la problemática abordada y los impactos esperados.
  - Redactar el informe final del proyecto, en el cual se documenten de manera clara y precisa las actividades realizadas, los resultados alcanzados y las conclusiones obtenidas.
  - Revisar y asegurar la calidad y rigurosidad científica del informe final, incluyendo referencias bibliográficas pertinentes y recomendaciones para futuras investigaciones.

Estas actividades permitirán a la ***Dra. Portillo*** contribuir de manera significativa al desarrollo del proyecto, aplicando sus conocimientos y experiencia en catálisis para la realización de objetos digitales de aprendizaje y la formación de recursos humanos en el área.

10. POSIBLES USUARIOS DE LA CIUDAD DE MÉXICO

Los posibles usuarios de este proyecto en la Ciudad de México son docentes y estudiantes de bachillerato que se encuentren cursando asignaturas de Química Teórica y Experimental en instituciones educativas de la región. Específicamente, se dirige a aquellos usuarios que enfrentan limitaciones en cuanto a la disponibilidad de recursos materiales e infraestructura adecuada para llevar a cabo de manera óptima las prácticas experimentales necesarias para la comprensión y aplicación de los conceptos teóricos.

Estos usuarios incluyen, pero no se limitan a:

1. Docentes de Química Experimental:
   a. Profesores de bachillerato en la Ciudad de México que imparten la asignatura de Química Experimental.
   b. Docentes interesados en enriquecer y actualizar sus métodos de enseñanza, incorporando recursos digitales y objetos de aprendizaje para mejorar la comprensión de los conceptos teóricos y diseño experimental.

2. Estudiantes de bachillerato:
   a. Estudiantes de instituciones educativas de la Ciudad de México que estén cursando la asignatura de Química Experimental.

b. Estudiantes que deseen fortalecer sus conocimientos y habilidades prácticas en química, complementando los aspectos teóricos con experiencias de laboratorio virtuales interactivas.

3. Instituciones educativas:
    a. Instituciones de bachillerato en la Ciudad de México que enfrentan limitaciones en cuanto a infraestructura y recursos materiales para llevar a cabo prácticas experimentales de calidad en el área de química.
    b. Directivos y administradores educativos interesados en buscar soluciones innovadoras y accesibles para mejorar la formación en química experimental en sus instituciones.

Estos posibles usuarios se beneficiarán del proyecto al contar con objetos digitales de aprendizaje interactivos, autocontenidos y de alta calidad, que les permitirán desarrollar habilidades prácticas en química experimental, comprender y aplicar los conceptos teóricos de manera más efectiva, y superar las limitaciones de infraestructura y recursos materiales en sus instituciones educativas.

REFERENCIAS

Callejas-Cuervo, M., Hernández Niño E. J. y Pinzón-Villamil, J. N. (2011) Objetos de aprendizaje: Un estado del arte. *Entramado*, 7(1), 177-189.

Díaz-Barriga, A. (2013) Guía para la elaboración de una secuencia didáctica. *Comunidad de conocimiento UNAM*. UNAM. México.

Garritz, A. y Trinidad-Velasco, R. (2004) El conocimiento pedagógico del contenido. *Educación Química*, 15(2), 2-6.

Nakhleh, M.B., Polles, J., Malina, E. (2002). Learning Chemistry in a Laboratory Environment. In: Gilbert, J.K., De Jong, O., Justi, R., Treagust, D.F., Van Driel, J.H. (eds) Chemical Education: Towards Research-based Practice. Science & Technology Education Library, vol 17. Springer, Dordrecht. https://doi.org/10.1007/0-306-47977-X_4

Olubu, Odutuyi Musili. (2015) Effects of Laboratory Learning Environment On Students' Learning Outcomes In Secondary School Chemistry. International Journal of Arts & Sciences; Cumberland 8, Nº 2, 507-525.

6. Otras actividades académicas

Notificación de Reconocimiento y vigencia del Perfil Deseable, PRODEP 2024

Ciudad de México, 16 de abril de 2025

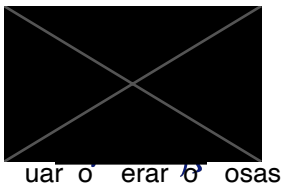
PERALTA AVILA RICARDO ATAHUALPA
UNIVERSIDAD AUTÓNOMA METROPOLITANA
PRESENTE

Anteponiendo un cordial saludo y de conformidad con lo señalado en el punto II.9, de la sección II, sobre el procedimiento de las solicitudes y su evaluación de la convocatoria Reconocimiento a Profesores/as de Tiempo Completo (PTC) con Perfil Deseable, referida en el Anexo 3a Modelo de Convocatorias de las Reglas de Operación 2024 (RO2024) del Programa para el Desarrollo Profesional Docente (PRODEP), Tipo Superior, me permito comunicar a usted que se ha dictaminado favorablemente su solicitud de reconocimiento al perfil deseable que presentó la institución a la que se encuentra actualmente adscrito/a.

Con base en lo anterior, la Dirección General de Educación Superior Universitaria e Intercultural (DGESUI), a través de esta Dirección de Fortalecimiento Institucional (DFI), en el marco del PRODEP, Tipo Superior, le otorga el Reconocimiento como Profesor/a de Tiempo Completo con Perfil Deseable, por un período de 3 años, contados a partir del 01 de Diciembre de 2024, siempre y cuando, durante el periodo de vigencia indicado, continúe laborando en la institución.

Sin otro particular, me reitero a sus órdenes.

Atentamente.



Dr. uar o erar o osas González.
Director de Fortalecimiento Institucional

"Este programa es pùblico, ajeno a cualquier partido político. Queda prohibido el uso para fines distintos a los establecidos en el programa."

México, ciudad de México a 10 de febrero de 2025

Casa abierta al tiempo

UNIVERSIDAD
AUTÓNOMA
METROPOLITANA
Iztapalapa

LA DIVISIÓN DE CIENCIAS BÁSICAS E INGENIERÍA DE LA
UNIVERSIDAD AUTÓNOMA METROPOLITANA IZTAPALAPA

Otorga el presente

Certificado

A: *Dr. Ricardo A. Peralta Ávila*

Por formar parte del comité organizador de los “Talleres colaborativos entre profesores del Colegio de Bachilleres y la UAM Iztapalapa”, con una duración de 30 horas, realizado los días 4, 6 y 7 de febrero de 2025 en la Casa de la Primera Imprenta de América, como parte de las actividades del proyecto “Jóvenes hacia la ciencia: vinculación entre la Universidad Autónoma Metropolitana Iztapalapa y El Colegio de Bachilleres”, Sectei/154/2023.

[redacted]

Dr. Carlos Andrés Escobar Ruiz
Responsable técnico

[redacted]

Dr. Román Linares Romero
Director de la División de CBI Iztapalapa

Subsecretaría de Ciencia y Humanidades
Dirección General de Investigación Científica y Humanística
Dirección de Investigación Científica Básica y de Frontera

Ciudad de México, a 23 de mayo de 2025

CONSTANCIA

Dr. Ricardo Atahualpa Peralta Avíla
Universidad Autónoma Metropolitana
Presente

La Secretaría de Ciencia, Humanidades, Tecnología e Innovación agradece su importante colaboración como **evaluador del Informe Técnico Etapa 2 de un proyecto**, apoyado en el marco de la convocatoria **"Ciencia de Frontera 2023"**.

Su participación en dicho proceso ha sido un apoyo decidido y fundamental en el compromiso compartido por impulsar el desarrollo de la investigación científica en nuestro país. La Secretaría de Ciencia, Humanidades, Tecnología e Innovación le hace un reconocimiento por el apoyo brindado y expresa su deseo de seguir contando con su apreciable aporte académico en las tareas de evaluación.

Sin otro particular, aprovecho la ocasión para enviarle un cordial saludo.

Atentamente

[redacted]

Lic. Andrea Judith Suárez López
Subdirectora de Evaluación y Seguimiento de Proyectos de Investigación Científica Básica y de Frontera

Ciencia y Tecnología

Secretaría de Ciencia, Humanidades, Tecnología e Innovación

CIENCIA DE FRONTERA 2023

Cuestionario de evaluación del Informe Técnico Etapa 2

Datos generales de la propuesta	
Proyecto No:	2143
Nombre del proyecto:	Materiales magnetocalóricos anisotrópicos para la licuefacción de hidrógeno.

1. Antes de proceder con el llenado de su evaluación, lea con atención y seleccione las tres casillas de confirmación.

Confirmo que he revisado con atención el Informe Técnico de Etapa 2 del presente proyecto, así como los documentos probatorios de los productos reportados en este.	(X)
Confirmo que he revisado las secciones del Convenio de Asignación de Recursos (CAR) asociadas al Informe Técnico de Etapa 2.	(X)
Confirmo que cuento con acceso al documento Guía de Usuario correspondiente al presente documento.	(X)

2. Seleccione la opción que mejor represente su juicio sobre el cumplimiento de las ACTIVIDADES COMPROMETIDAS del proyecto en la presente etapa. Fundamente su respuesta.

Se cumplió con la totalidad de las actividades comprometidas.	( )
Se cumplió con un porcentaje importante de las actividades comprometidas.	(X)
Se cumplió con un porcentaje moderado de las actividades comprometidas.	( )
Se cumplió con un porcentaje muy bajo de las actividades comprometidas.	( )

El proyecto está dividido en tres etapas. En esta segunda fase, se presentaron dificultades técnicas que limitaron la obtención de resultados más satisfactorios. No obstante, se logró la caracterización de las propiedades estructurales, magnéticas y magnetocalóricas de los materiales mencionados en el proyecto. Los resultados obtenidos cumplen con el objetivo general y con las metas planteadas. Además, se avanzó en diversos compromisos del proyecto, incluyendo la publicación de un artículo, la participación en congresos, actividades de retribución social y la formación de recursos humanos.

3. Seleccione la o las opciones que mejor representen su juicio sobre las ACTIVIDADES ADICIONALES del proyecto realizadas en la presente etapa. Fundamente su respuesta.

Brindan valor agregado a lo esperado del proyecto.	(X)
Compensan la falta de cumplimiento de las actividades comprometidas.	( )
Subsanan la falta de cumplimiento de actividades comprometidas en la etapa anterior.	( )
Carecen de valor.	( )

No aplica, ya que no se realizaron actividades adicionales.	( )

Se han tenido actividades adiciones que brindan un valor agregado al proyecto. Producto de ellos es que se tiene un artículo publicado en la revista Journal of Alloys and Compounds (Q1, factor de impacto: 6.2). Además de un segundo artículo en la revista Materials Chemistry and Physics (Q1, factor de impacto: 4.3) y un tercero en la revista del área de ingeniería y aplicaciones IEEE Transactions on Magnetics (Q2, factor de impacto: 2.1). En cuanto a la formación de recursos humanos, se tiene como producto la tesis de ingeniería desarrollada y presentada, que constituye una contribución importante al desarrollo del proyecto. Por último, se ha realizado cálculos, que se hacen desde primeros principios, contribuyen a comprender mejor su estructura electrónica así como sus propiedades magnéticas y térmicas de los materiales que se estudian en el proyecto.

4. Basándose en los logros humanísticos, científicos y/o tecnológicos reportados y los documentos probatorios presentados de los productos reportados como realizados, ¿considera que el desarrollo humanístico, científico y/o tecnológico de la presente etapa es relevante y acorde al tema? Seleccione la opción que mejor represente su juicio. Fundamente su respuesta.

Sí, totalmente de acuerdo.	(X)
Parcialmente de acuerdo.	( )
No, en desacuerdo.	( )

Compromiso de la etapa 2: graduar 1 maestro en Nanociencias y Materiales e iniciar una segunda tesis doctoral. Ambos se cumplieron.

TÍTULO DE LA TESIS DE MAESTRÍA PRESENTADA. Síntesis y caracterización de aleaciones magnetocalóricas HoB2 y Ho0.8Gd0.2B2 para la licuefacción de hidrógeno. ALUMNO: Lic. Luis Guillermo Escobedo Valadez. PROGRAMA AL QUE PERTENECE: Maestría en Nanociencias y Materiales, DMAv-IPICyT, San Luis Potosí, México. Fecha de defensa: Julio 5 de 2024. // REALIZADA //

TESIS DOCTORAL EN PROCESO. TÍTULO (tentativo): Sinterización por chispa y plasma de compuestos intermetálicos magnetocalóricos R-Ni para la licuefacción de hidrógeno (R= tierra rara". ALUMNO: M.C. Rubén Uziel Pérez Batalla. PROGRAMA DE POSGRADO: Doctorado en Nanociencias y Materiales, DMAv-IPICyT. Fecha de presentación: julio de 2026. //EN PROCESO //

TESIS DOCTORAL INICIADA. TÍTULO (tentativo): "Aleaciones magnetocalóricas basadas en elementos de tierra rara para la licuefacción de hidrógeno". ALUMNO: M.C. Luis Guillermo Escobedo Valadez. PROGRAMA AL QUE PERTENECE: Doctorado en Nanociencias y Materiales, DMA-IPICyT, San Luis Potosí, México. Fecha de defensa: julio de 2028. // EN PROCESO //

TESIS MAESTRÍA INICIADA: "Método para realizar mediciones directas de ΔTad(T) utilizando la opción de resistividad en el PPMS Dynacool". ALUMNO: Ing. Milton Uriel Treviño Calderón. PROGRAMA AL QUE PERTENECE: Maestría en Nanociencias y Materiales, DMAv-IPICyT, San Luis Potosí, México. Fecha de defensa: Julio de 2025. // EN PROCESO //

5. Basándose en la formación de recursos humanos, participación en congresos y organización de eventos para la comunidad científica reportados como realizados, y los documentos probatorios presentados sobre estos, ¿considera que lo realizado en la presente etapa ha coadyuvado al fortalecimiento de la comunidad académica? Seleccione la opción que mejor represente su juicio. Fundamente su respuesta.

Sí, totalmente de acuerdo.	(X)

Parcialmente de acuerdo.	( )
No, en desacuerdo.	( )

Compromiso de la etapa 2: graduar 1 maestro en Nanociencias y Materiales e iniciar una segunda tesis doctoral. Ambos se cumplieron.

Compromiso de la etapa 2 en PARTICIPACIÓN EN CONGRESOS: presentar 2 trabajos. Se presentaron 5 trabajos, con lo cual se sobrecumplió este rubro.

Compromiso de la etapa 2 en ACCESO UNIVERSAL AL CONOCIMIENTO. Impartir 1 charla divulgativa. // REALIZADA //

Los datos de la charla divulgativa impartida son los siguientes:
XXVI Semana de la Ciencia, Cultura y Salud, Instituto Cervantes, Apostólica, San Luis Potosí, SLP. Audiencia: estudiantes de primaria y Charla divulgativa "Magnetismo e hidrógeno (H2): dos aliados

6. Basándose en los aportes sociales de la etapa y los productos de acceso universal al conocimiento reportados, ¿considera que durante el desarrollo del proyecto se estableció vinculación con algunos de los siguientes actores: gobierno, empresa, sociedad y/o medio ambiente? Fundamente su respuesta.

Absolutamente, el proyecto impacta los cuatro actores (gobierno, empresa, sociedad y medio ambiente).	( )
En buena medida, el proyecto impacta tres o dos actores.	( )
Aceptablemente, el proyecto impacta un actor.	( )
No, el proyecto solo impacta a la comunidad académica.	(X)

No Aplica, No Aplica, No Aplica,

sintetizar por solidificación rápida cintas de DyNi5, TbNi5 y de otros compuestos RX2 (R= tierra rara; X= Ni, Al). Se consiguió obtener cintas con granos parcialmente orientados de los compuestos DyNi5 y TbNi5. Por su parte, de los compuestos RX2 (R= tierra rara; X= Ni, Al; estructura cúbica) se consiguió obtener cintas monofásicas con propiedades magnetocalóricas óptimas; en este caso, a sus propiedades magnetocalóricas óptimas también contribuye la orientación parcial de los granos con respecto a las caras de las cintas.

(b) Se han obtenido consolidados por SPS de varias aleaciones con una densidad relativa de igual no menor del 95 % y con propiedades magnetocalóricas iguales o superiores a los mejores valores reportados en la literatura (HoNi2, DyNi2, ErAl2, DyAl2, DyNi5, y TbNi5). Todos estos consolidados se obtuvieron utilizando como precursor las cintas monofásicas.

(c) Según se indicó en el informe técnico del año 1, al proyecto se incorporó la síntesis y estudio de aleaciones magnetocalóricas en bulto HoB2, que fueron decubiertas recientemente y que poseen excepcionales propiedades magnetocalóricas en el rango de temperatura de la licuefacción de hidrógeno. Dada la importancia de este tema, se desarrolló exitosamente una tesis de maestría cuyo examen de posgrado se presentó el 5 julio de 2024 (Estudiante: L.G. Escobedo Valadez; el estudiante forma parte del proyecto). Actualmente, ya se sintetizaron barras por solidificación rápida con excelentes propiedades mediante la técnica de fundición por succión (suction casting).

(d) Aún cuando la caracterización de las propiedades estructurales, magnéticas y magnetocalóricas de los materiales mencionados en (a), (b) y (c) tienen diferentes grados de avance, los resultados que hemos obtenido dan cumplimiento satisfactorio tanto al objetivo general como a la meta del proyecto.

8. Seleccione los objetivos de la convocatoria en los que considera el proyecto ha obtenido un impacto importante en la presente etapa. Fundamente su respuesta.

Generar conocimiento nuevo.	( )
Favorecer el cambio en el entendimiento de conceptos científicos existentes.	(X)
Abordar cuestiones sobre las que existe alguna controversia en la comunidad científica del ámbito en el que se desarrolla.	( )
Abordar cuestiones de difícil respuesta, al menos con las aproximaciones metodológicas actuales y, por tanto, utilizan metodologías y conceptos atípicos o novedosos en su ámbito de conocimiento.	( )
Promover la formación de nuevos científicos, capaces de emprender un ejercicio independiente.	( )

El impacto de estas actividades adicionales es esencialmente en Academia.

INSTITUCIONES/ ORGANISMOS QUE PARTICIPARON. Participaron junto con el IPICYT, la Universidad Autónoma de Ciudad Juárez (UACJ), la Universidad Autónoma de San luis Potosí (UASLP), Institut Laue-Langevin (ILL, Grenoble, Francia) y la Universidad de Oviedo (Uniovi, España); aunque en menor grado han participado otras instituciones.

SOBRE LOS ARTíCULOS CIENTÍFICOS.

ARTÍCULO 1. En el primero de estos trabajo se hace, por primera vez, un estudio de la transición magnetoelastica de aleaciones magnetocalóricas FeRh mediante la técnica de análisis llamada T-FORC. El mismo se complementa con un análisis por difracción de neutrones de la evolución con la temperatura de estructura magnética y cristalina de estas aleaciones. El artículo fue publicado en la pretigiosa revista Journal of Alloys and Compounds (Q1, factor de impacto: 6.2).

ARTÍCULO 2. En el segundo artículo se demuestra experimentalmente haciendo uso de las técnicas de difracción de neutrones y mediciones de magnetización en función de la temperatura y el campo magnético que, contrario a lo que muchos autores reportan, la difracción de rayos X no es una técnica adecuada para determinar la composición de fases en aleaciones FeRh con composición cercana a la equiatómica. Esto se debe a que la deformación plástica trasforma la

estructura cúbica B2 en la llamada fase gamma que es paramagnética y en otras fases no reportadas hasta el momento en el sistema FeRh. Esta aleación es tanto refrigerante magnetocalórico como mecanocalórico (elastocalórico y barocalórico). El artículo fue publicado en la pretigiosa revista Materials Chemistry and Physics (Q1, factor de impacto: 4.3).

ARTÍCULO 3. En el tercer artículo se sintetizan hilos de la aleación Heusler Ni50Mn37Sb13 y se reporta su caracterización estrucural, magnética y magnetocalórica. El artículo fue publicado en la tradicional y pretigiosa revista del área de ingeniería y aplicaciones IEEE Transactions on Magnetics (Q2, factor de impacto: 2.1).

SOBRE LA TESIS DE INGENIERÍA. La tesis de ingeniería desarrollada y presentada constituye una contribución importante al desarrollo del proyecto ya se enfocó en desarrollar un método experimental novedoso para medir de manera directa la variación de temperatura adiabática para materiales magnetocalóricos en el rango de las temperaturas criogénicas.

SOBRE LOS CÁLCULOS SOBRE LAS PROPIEDADES MAGNÉTICAS DE FASES DE LAVES. Estos cálculos, que se hacen desde primeros principios, contribuyen a comprender mejor su estructura electrónica así como sus propiedades magnéticas y térmicas de los materiales que se estudian en el proyecto. Los resultados obtenidos se concretaron en 2 trabajos presentados en un congreso científico internacional (IMRC 2024).

9. Seleccione el porcentaje que, en su opinión, y con base en lo establecido en el CAR y lo reportado en el Informe Técnico de Etapa 2, considera se ha avanzado en los objetivos del proyecto. Fundamente su respuesta.

0%	( )
25%	( )
50%	(X)
70%	( )
90%	( )
100%	( )

En el avance del proyecto ha influenciado negativamente la rotura de la fuente de radio frecuencia (RF; Radyne RF Power Supply Modelo VERSAPOWER XTREME) que permite fundir las aleaciones en el sistema de temple rotatorio para obtenerlas en forma de cintas por solidificación rápida. Durante todo el año 2024 y hasta el día de hoy los autores afirman que este equipo ha estado fuera de operación.
Las aleaciones objeto de estudio son RX2 (R= tierra rara; X= Ni, Al; estructura cristalina cúbica), y RNi5 (R= Dy, Tb; estructura cristalina hexagonal). Las mismas se deben obtener primero en forma de cintas (por solidificación rápida) para ser posteriormente consolidadas por sinterización mediante la técnica de SPS.

10. ¿Considera que lo hecho hasta ahora llevará al responsable técnico al logro total del (de los) objetivo(s) y el alcance de la meta del proyecto? Seleccione la opción que mejor represente su juicio. Fundamente su respuesta.

Sí, totalmente de acuerdo.	( )
Posiblemente, ya que reporta retrasos y/o dificultades para lograrlo.	(X)
No, ya que reporta severos retrasos y/o dificultades para lograrlo.	( )

Si no se repara el equipo de rotura de la fuente de radio frecuencia (RF; Radyne RF Power Supply Modelo VERSAPOWER

XTREME) que permite fundir las aleaciones en el sistema de temple rotatorio para obtenerlas en forma de cintas por solidificación rápida, el proyecto puede dificultarse en terminarse. Los autores afirman que durante todo el año 2024 y hasta el día de hoy los autores afirman que este equipo ha estado fuera de operación. Sin embargo, se han realizados avances importantes en otros puntos:

(a) Revisión y análisis bibliográfico. Adquisición de consumibles de lab. //REALIZADA//
(b) Sinterización por SPS de aleaciones en bulto RM2 y RNi5 (R= Tb, Dy, Ho, Er; M= Ni, Al). //REALIZADA//
(c) Caracterización magnetoestructural y magnetocalórica de aleaciones los sinterizados. Ajuste parámetros de síntesis proceso del SPS. //EN PROCESO// y // REALIZADA //
(d) Análisis de resultados, envío de 2 artículos y asistencia a 2 congresos. //EN PROCESO// y // REALIZADA //
(d) Defensa de maestría y seguimiento a tesis doctoral. Elaboración cápsula divulgativa .// REALIZADA //
(e) Informe técnico y financiero año 2. // REALIZADA //

Por lo tanto, sugiero a los autores tener una alternativa si el equipo no logra repararse.

11. Tomando en cuenta los resultados de la presente etapa del proyecto, ¿cómo calificaría usted el desarrollo de la misma? Fundamente su respuesta, y en caso de tener recomendaciones favor de incluirlas.

Excelente (el desarrollo de esta etapa ha sido extraordinario).	( )
Bueno (cumplió con lo comprometido).	(X)
Aprobada con recomendaciones.	( )
No aceptable.	( )

Remiendo a los autores tener un plan por si el equipo no logra repararse, quizá una colaboración.

No Aplica, No Aplica, No Aplica,

Casa abierta al tiempo
UNIVERSIDAD AUTÓNOMA METROPOLITANA

DIVISIÓN DE CIENCIAS BÁSICAS E INGENIERÍA
COORDINACIÓN DIVISIONAL DE DOCENCIA Y ATENCIÓN A ALUMNOS

A QUIEN CORRESPONDA:

Por este medio informo a usted que la **Dr. Ricardo Atahualpa Peralta,** con número económico **45029** y adscrito al Departamento de Química de la División de Ciencias Básicas eIngeniería de la UAM, Unidad Iztapalapa, realizó la labor tutorial con los siguientes alumnos de licenciatura:

Matrícula	Alumno(a)	Licenciatura
2223008840	ALEXIS RAFAEL LUCIO	LICENCIATURA EN QUÍMICA
2223009267	RODRIGO GARRIDO RAMIREZ	LICENCIATURA EN QUÍMICA
2223010911	BRENDA ESTHER BAUTISTA RAMIREZ	LICENCIATURA EN QUÍMICA
2223011409	SOFIA GUADALUPE ALVAREZ SALINAS	LICENCIATURA EN QUÍMICA
2223011427	OSCAR EMILIO GUZMAN OROZCO	LICENCIATURA EN QUÍMICA
2223011749	MARIANA MARTINEZ JIMENEZ	LICENCIATURA EN QUÍMICA
2223012068	JUAN ANTONIO MENDOZA CETINA	LICENCIATURA EN QUÍMICA
2223044140	GIBRAN YAIR ESTRADA RICALDE	LICENCIATURA EN QUÍMICA
2223044613	JORGE DIAZ MEDINA	LICENCIATURA EN QUÍMICA
2223045245	VALENTINA GONGORA LOPEZ	LICENCIATURA EN QUÍMICA
2233050472	HANNA FERNANDA SALAZAR NAVARRO	LICENCIATURA EN QUÍMICA
2233050623	DEIVY EUSEBIO AMARO MARTINEZ	LICENCIATURA EN QUÍMICA

Las fechas en las que realizó tutorías grupales fueron:

Fecha
11 de agosto 2023 12:00 p.m.
17 de noviembre 2023 12:00 p.m.
08 de marzo 2024 12:00 p.m.
26 de julio 2024 12:00 p.m.
16 de agosto 2024 12:00 p.m.

A petición de la persona interesada y para los fines que a esta convengan, se extiende la presente a los 20 días del mes de agosto de 2024.

A T E N T A M E N T E
“CASA ABIERTA AL TIEMPO”

Dra. Claudia Rojas Serna
Coordinadora Divisional de Docencia y Atención a Alumnos
División de Ciencias Básicas e Ingeniería

c.c.p. Coordinación Divisional de Docencia y Atención a Alumnos
c.c.p. Expediente Oficina de Tutorías y Apoyo a la Docencia

UNIDAD IZTAPALAPA
Edificio Carlos Graeff (T) cubículo 133.
Av. Ferrocarril San Rafael Atlixco No. 186,
Col. Leyes de Reforma 1ª sección,
C.P. 09310, México, CDMX.
Email: cdcbi@xanum.uam.mx

Casa abierta al tiempo
UNIVERSIDAD AUTÓNOMA METROPOLITANA

Departamento de Química
División de Ciencias Básicas e Ingeniería

CDMX a 25 noviembre del 2024

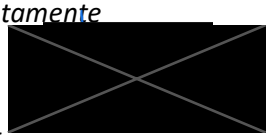
ASUNTO
Constancia de realización de videos para el ingreso al Posgrado de Química
A quien corresponda
P R E S E N TE

Por este medio les comunico que el Dr. Ricardo A. Peralta Ávila, el cual se desempeña como profesor visitante del Departamento de Química, ha venido realizando actividades en la elaboración y organización de videos de preparación para estudiantes que deseen ingresar al posgrado del Departamento de Química. Dichos videos tienen como finalidad ser una ayuda a los posibles aspirantes para ingresar al posgrado además de tengan un mejor desempeño en el examen de ingreso al posgrado. Estos videos son base para la creación de un aula virtual propedéutica y pilar del ingreso a nuestro Posgrado de Química en la UAM-Iztapalapa en un futuro próximo.

Sin más por el momento, quedando de ustedes para cualquier comentario.
Reciban un Cordial Saludo

"Casa Abierta al Tiempo"

Atentamente



Dr. Francisco Javier Tzompantzi Morales
Coordinador de Posgrado en Química
Laboratorio R-201, Departamento de Química
Universidad Autónoma Metropolitana-Iztapalapa
Email: fjtz@xanum.uam.mx

SPRINGER NATURE

REVIEWER CERTIFICATE

This certificate is awarded to

Ricardo Peralta

in recognition of their contribution to

1 manuscript in 2025 for

Scientific Reports

02 May 2025

Springer nature portfolio BMC Discover palgrave macmillan Birkhäuser Adis

WILEY

Reviewer Certificate

This certificate is awarded to

RICARDO PERALTA

for serving as a reviewer for

Applied Organometallic Chemistry



Thank you for reviewing 2 manuscripts in 2024

7 March 2025

David Morales-Morales
Editor-in-Chief

CODAI

Casa abierta al tiempo

UNIVERSIDAD AUTÓNOMA METROPOLITANA
Unidad Iztapalapa

Ciudad de México, a 16 de mayo de 2025

LA COORDINACIÓN DE DESARROLLO ACADÉMICO E INSTITUCIONAL UNIDAD IZTAPALAPA

A través de la oficina de Innovación Educativa y Desarrollo Pedagógico, otorga la presente constancia a:

Ricardo Atahualpa Peralta Avila

Por participar en el curso de formación docente

Prevención y Erradicación de Machismos Cotidianos en el Ámbito Escolar

Realizado en modalidad presencial los días 12, 13 y 14 de mayo del 2025, con duración de 9 horas.

[redacted]

Dra. Mercedes Jatziri Gaitán González
Coordinación de Desarrollo Académico
e Institucional

Temachtiani
Sistema de Formación Docente
UAM IZTAPALAPA

INNOVACIÓN EDUCATIVA
DESARROLLO PEDAGÓGICO